PNC ZJ1579 97—001·VOL, 1

Report to:
PNC Power Reactor and Nuclear Fuel Development Corporation
Tokyo, Japan

Discrete Fracture Network Code Development

Heisei-8 Progress Report Volume I

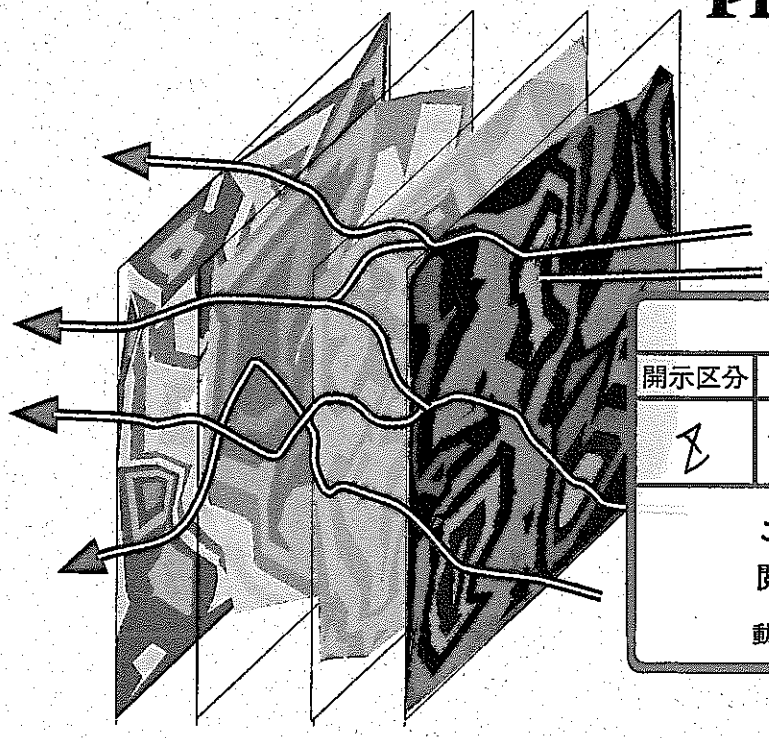

Golder Associates

PNC ZJ1579 97—001·VOL, 1

Report to:

PNC Power Reactor and Nuclear Fuel Development Corporation
Tokyo, Japan

Discrete Fracture Network Code Development

Heisei-8 Progress Report

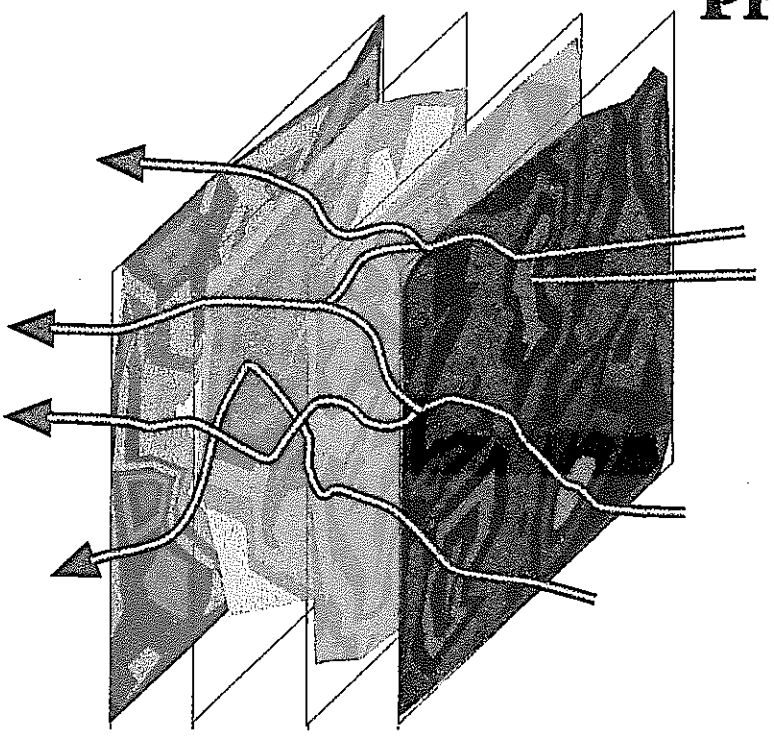

Golder Associates

Report to:

Power Reactor and Nuclear Fuel Development Corporation (PNC)
Tokyo, Japan
Tokai, Japan

Discrete Fracture Network Code Development

Heisei-8
Progress Report
Version 1.0

William Dershowitz
Thomas Doe
Glori Lee
Peter Wallmann
Ed Sudicky
Dawn Shuttle
Todd Foxford
Thorsten Eiben

March 31, 1997

923-1089.800
h-8rept1.doc

ABSTRACT

This report presents the results of fracture flow model development and application performed by Golder Associates Inc. during the Heisei-8 (1996-1997) fiscal year. The major goals of Heisei-8 were to develop FracMan technologies to support the PNC HY-12 performance assessment effort, and to provide technical support the PNC for the Äspö and Kamaishi projects.

The software developed during HY-8 included improvements to pathways analysis and radionuclide transport, stochastic continuum pre-processing, and analyses for fracture size. Verification cases and user documentation are provided for all software features.

Scoping calculations of flow and transport were carried out in support of repository performance assessment using and comparing three approaches: discrete fracture network finite element modeling (MAFIC), Laplace Transform Galerkin methods (PAWorks/LTG), and cell based PA (RIP-5). Simulations and analyses were also carried out within the Äspö Tracer Retention and Understanding Experiments ("TRUE-1", "TRUE-1/RC" and "TRUE-1/Dipole), and within the Kamaishi mine.

TABLE OF CONTENTS Page No.

LIST OF FIGURES

LIST OF TABLES

LIST OF APPENDICES

1. INTRODUCTION

The primary objective of the Golder Associates work scope during HY-8 was to prepare the numerical tools necessary for the PNC's H-12 repository development report. In addition to code development, Golder Associates provided technical support for the PNC HY-12 performance assessment project, the "Site Generic Project", the Kamaishi experimental program, and PNC participation in the Äspö Modeling Task Force (AMTF).

The project focus during HY-8 was on development of fracture flow and transport features necessary for repository performance assessment for both fractured rock and sedimentary sequences. Developments included:

- Improvements to pathways analysis for repository performance assessment;
- Improvements for geostatistical and fractal analysis of fractured and sedimentary rock site characterization data;
- 3D stochastic continuum field generation for sedimentary rocks;
- Support to PNC HY-11 performance assessment activities;
- Support to the PNC "Site Generic" project;
- Support to the PNC "ENTRY-2" project;
- Support to PNC experimental programs at Kamaishi; and
- Support to PNC international cooperation projects at the Äspö hard rock laboratory.

This report is organized according to the tasks as defined in the project scope of work. The work is divided into three major task areas: code development (Chapter 2), applications (Chapter 3), and international programs (Chapter 4). Conclusions are presented in Chapter 5.

2. TASK 1: CODE DEVELOPMENT

Table 2-1 provides the version numbers for FracMan software developed during HY-8. These code versions provide unique capabilities which will directly support the PNC performance assessment effort for HY-12, experimental activities at ENTRY-2, and field activities at Kamaishi and Äspö. Where possible, HY-8 software has been implemented in Windows 95, Windows NT, and Unix versions.

Table 2-1 H-8 Software Versions

Software	Version	OS	Platform
FracMan	2.6	DOS	PC
FracSys/FracSize	1.1	Win95, WinNT	PC-Pentium
FracSys/Fractal	1.1	Win95, WinNT	PC-Pentium
PipeTrans (LTG)	NA		Incorporated to PAWorks and PAWorks/U
PAWorks	1.4	Win95, WinNT	PC-Pentium
PAWorks/U	1.4	Unix	RS/6k, DEC Alpha
EdMesh	1.4	Unix	RS/6k, DEC Alpha
MeshMaster	1.5	Unix	RS/6k, DEC Alpha
MAFIC	1.62	Unix	RS/6k, DEC Alpha

2.1 Task 1.1.1: Crosshole Conditioning: Preliminary Development

The fundamental philosophy of FracMan is forward modeling. In forward modeling, we start with field measurements of fracture geometry and hydraulic properties, and use these to build the three dimensional model for flow and transport. This approach avoids problems of calibration and conditioning by tying the hydrogeologic model directly to a statistical description of site geology and hydrogeology.

While this purely stochastic approach is appropriate for describing the rock mass at large, or the uncharacterized portion of the rock mass, it has limitations when used for modeling testing boreholes where the fracture intersections and the properties of intersecting fractures are known deterministically.

During HY-6 and HY-7, FracMan was upgraded to include an ability to condition individual boreholes to match the geometric properties of fractures as they intersect boreholes and tunnel walls. Thus, FracMan can now condition fracture realizations to fracture geometry as encountered in borehole and flow logging (Figure 2-1).

The implementation of an ability to condition fracture realizations to cross-hole hydraulic response is expected to be a major, multi-year effort. This feature will condition the properties of fracture networks to match steady state pressure responses to hydraulic signals such as flow to pumping wells, drainage to tunnels, and other hydraulic signals. During HY-8, preliminary work was carried out to support the development of a cross-hole conditioning feature within FracMan. The following activities were carried out to support the future implementation of cross-hole conditioning within FracMan:

- Algorithm development; and
- Improvements to approximate flow solution within PAWorks.

These activities are described in the following sections.

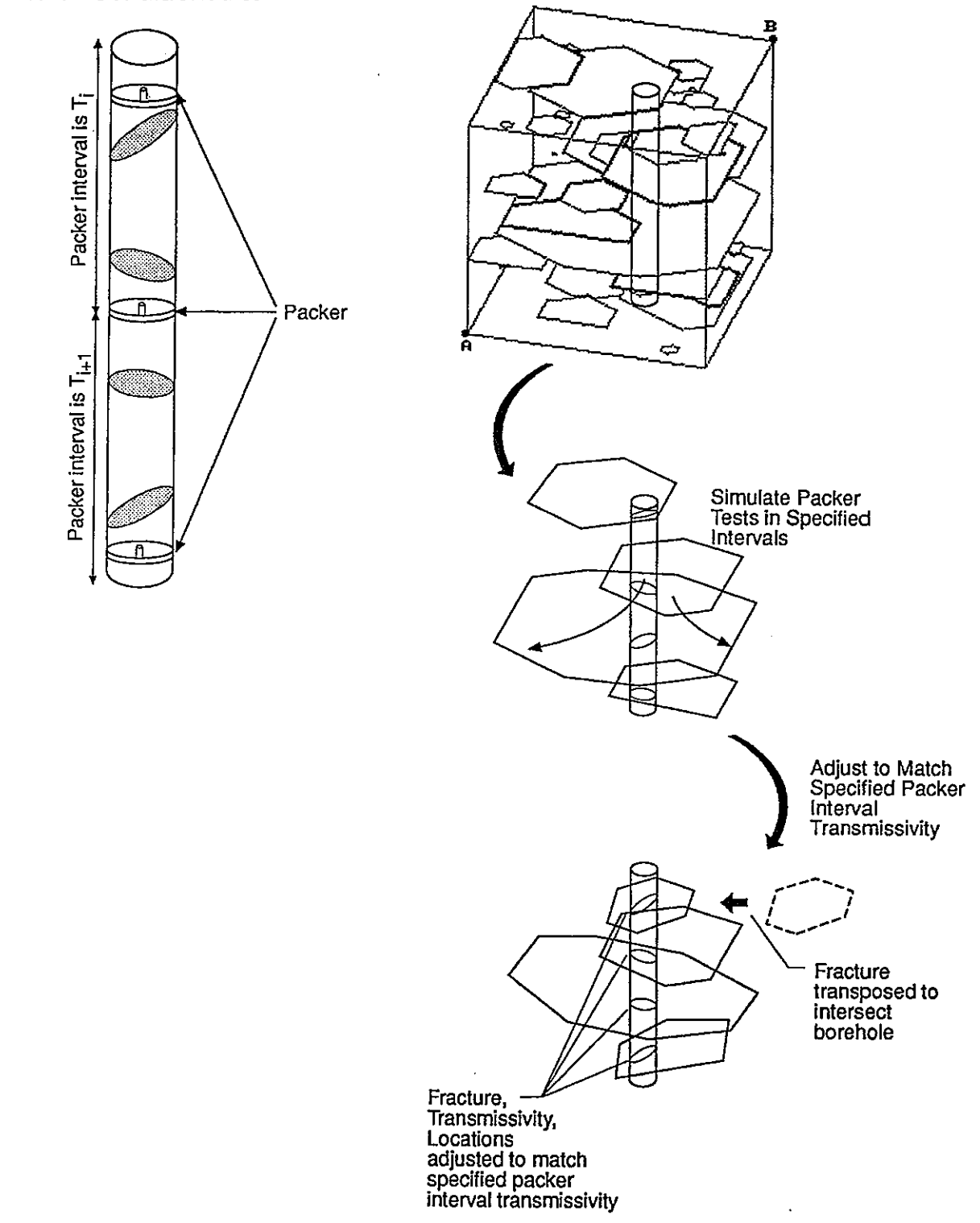

FIGURE **2-1**
FracMan/FracWorks
CONDITIONAL SIMULATION
PNC/H8

PROJECT NO. 923 1089.800 DRAWING NO. 73167 DATE 5/9/97 DRAWN BY EA

Golder Associates

2.1.1 Crosshole Conditioning Algorithm

The basic algorithm for cross-hole conditioning will calibrate the effective properties of pathways between measurement points, hydraulic sources, and boundary conditions. By concentrating on the few key pathways within a realistic fracture network, this cross-hole conditioning approach will be significantly more efficient than methods based on random pipe networks.

The cross-hole conditioning algorithm is illustrated in Figure 2-2. The algorithm starts with:

- A realization of the fracture network being evaluated (conditioned to packer tests, flow logging, and BHTV as appropriate);
- Calibration criteria (allowable difference between measurements and simulations);
- The initial (BC-1) and modified (BC-2) boundary conditions; and
- The head measurement values under initial (BC-1) and modified (BC-2) boundary conditions.

First, PAWorks will determine the primary pathways (1) between the measurement points and the hydraulic source, (2) among the measurement points, and (3) between the measurement points and the boundaries. The PAWorks approximate (finite element) flow solution will then be run to calculate the head field both with and without the hydraulic disturbance. These simulations will determine the sensitivity of the simulated drawdowns to the hydraulic properties of the key pathways. The properties of the key pathways will then be adjusted using an optimization technique to determine sets of pathway properties which simulate the pressure responses within acceptable accuracy.

Once the one-dimensional PAWorks pathways provide acceptable pressure values, the properties of the fractures which make up the pathways will be adjusted to match the conditioned pathway effective properties. At the end of this process, the PAWorks pathway geometry and flow solutions for initial and modified boundary conditions will

be repeated to determine the accuracy of the conditioning based on key pathways. If necessary, additional rounds of pathway conditioning and reallocation of properties to fractures will be carried out. Alternatively, different realization of the conditioned DFN might be used as the basis for the analysis.

2.1.2 Software Development in Support of Cross-hole Conditioning

The use of an approximate one-dimensional pipe solution for head is the key aspect of the proposed cross-hole conditioning algorithm. The major developments in preparation for implementation of cross-hole conditioning therefore focused on improvements to the generation of pipe networks from fracture networks, and improvements to the approximate head solutions.

2.1.2.1 MAFIC 1D Approximate Head Solution

The approximate 1-D flow solution implemented within PAWorks during HY-7 was based on a complete Cholesky solution, with a variable bandwidth option. The code was implemented in C++ to facilitate direct linking into PAWorks.

During HY-8, this code was incorporated into MAFIC to provide a more efficient flow solution. The resulting MAFIC code can solve flow for 3-D networks of both 1-D pipe flow elements and 2-D triangular elements. The solution within MAFIC is more efficient because it takes advantage of Incomplete Cholesky Decomposition, while the flow solver in PAWorks 1.1 used Complete Cholesky Decomposition. In addition, improved node-renumbering algorithms provides an increase in computational efficiency and a decrease in memory requirements.

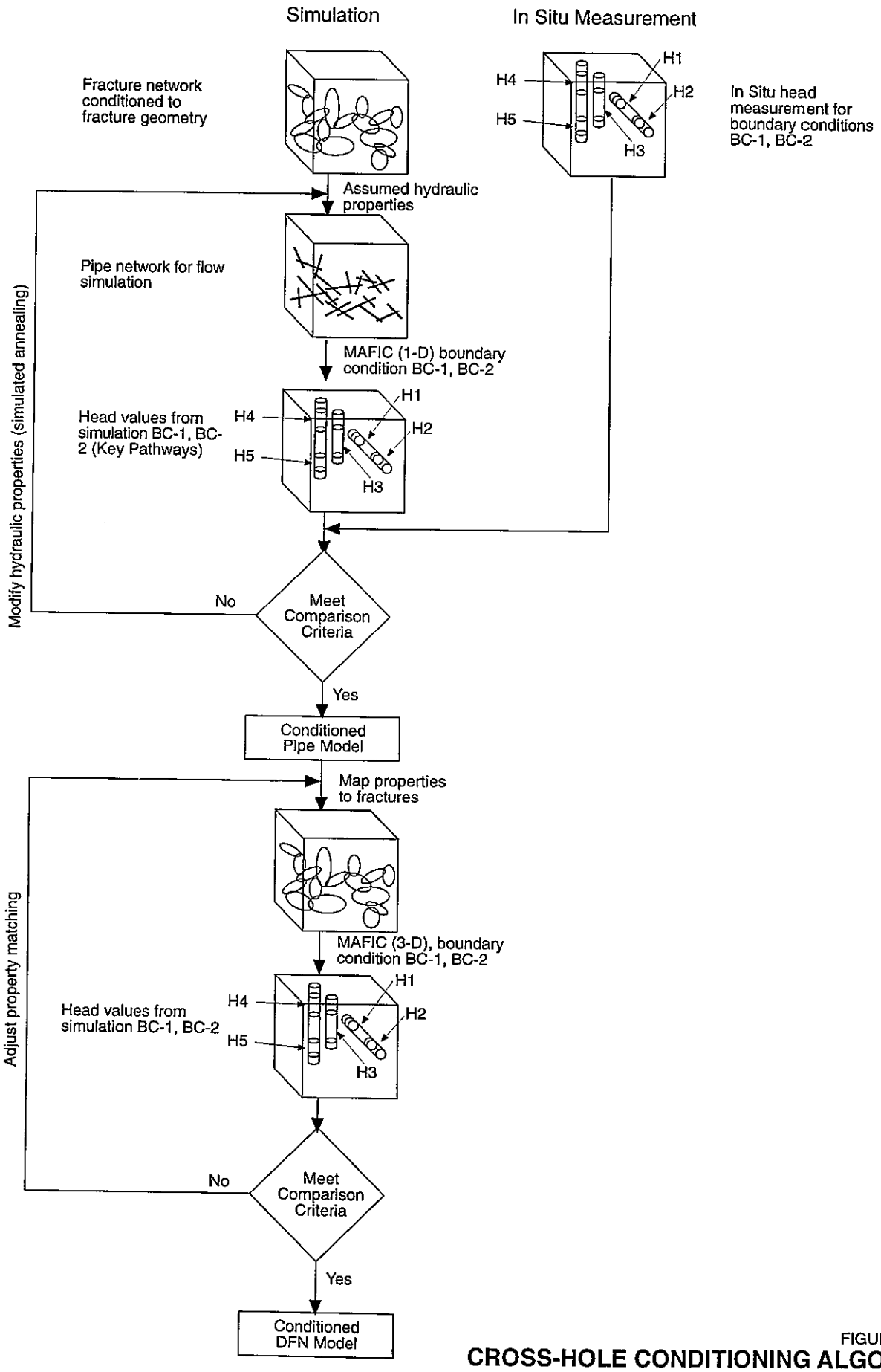

FIGURE **2-2**

CROSS-HOLE CONDITIONING ALGORITHM

PNC/H8

PROJECT NO. 923 1089.800 DRAWING NO. 73112 DATE 5/9/97 DRAWN BY EA

Golder Associates

The optimized node renumbering algorithm works as follows:

1. Count the connections to each node, and store.
2. Assign new numbers to fixed head boundary condition nodes and linked nodes.
3. Loop through nodes, starting at fixed head boundary condition nodes. Renumber the node connected to the lowest node number, previously renumbered node. In the case of a tie, renumber the node with the smallest number of connections. Continue recursively until all nodes are renumbered.
4. Compare the average bandwidth (matrix terms per row) of the renumbered system to the bandwidth before renumbering. If the bandwidth is not improved, restore the original numbering.

This optimized node renumbering scheme for 1-D pipe network flow solutions resulted in dramatic performance improvements, including most importantly the ability to solve large fracture networks, which previously required more memory for the 1-D solution than for the 3-D solution.

This performance improvement was necessary to facilitate cross-hole conditioning. For example, a steady state flow solution for a network of 1,000 fractures with MAFIC using triangular elements required 791 seconds on a 100MHz Pentium 100 computer. With the code improvements during HY-8, the same case based on the pipe network required only 2 seconds on a 100MHz Pentium 100 computer. The memory requirements for the pipe flow solution are less than 20% of those for the comparable DFN model using triangular elements.

This improvement was due primarily to more efficient node renumbering - the improvement in the solver is estimated to have improve the solution times by 30 to 50 percent.

Comparison of flow rates indicate that the solution is identical for Cholesky and Incomplete Cholesky solver formulations, and the node renumbering does not effect solution accuracy.

The improvement in flow solution speed and memory requirements is considered sufficient for the current 1-D pipe flow solution to provide the basis for the cross-hole conditioning algorithm.

2.1.2.2 GenPipe Pipe Generation Module

HY-8 improvements to algorithms for transformation of fracture networks to approximately equivalent pipe networks were initially carried out to support crosshole conditioning. These improvements are described in detail in Section 2.4.1.1 below. The major improvements which facilitate cross-hole conditioning simulation include:

Pipe Generation Options

1. All possible pipes that can be formed from the midpoints of traces. The only restriction is that the newly formed pipes cannot cross the existing pipes.
2. Pipes from (1) with two more restrictions: (i) pipes cannot cross traces (intersection line segments of two fractures); (ii) each node (midpoint of the trace) must have at least one pipe connected.
3. Pipes from (2), supplemented by pipes which ensure that every node in each fracture has at least one connection through pipes in that fracture. These supplementary pipes can violate condition (i) of option (2).
4. Pipes from (3) supplemented by pipe which ensure that the distance between traces through the pipe network in any given fracture is not greater than a factor N times the Cartesian distance between two nodes. The factor, N, must be provided by the user for this option.

Pipe Width Options

Pipe width is calculated from the size of the two traces that form the pipe. GenPipes program first asks the user to choose the correlation formula:

(1). $W = W_{min} * L_{min} + W_{max} * L_{max}$

(2). $W = W_{area} * (W_{min} * L_{min} + W_{max} * L_{max})$

where: L_{min} = the length of the shorter trace;

L_{max} = the length of the longer trace;

W_{min} = the input parameter associated with L_{min}, usually on [0,1];

W_{min} = the input parameter associated with L_{min}, usually on [0,1];

The selection of (2) means that the pipe width of each pipe on the same fracture must be correlated to the fracture area. The parameter W_{area} is defined as

$W_{area} = \Sigma \{W_i * L_i\} / A_f$

where: W_i = width of the pipe i on the fracture,

$W_i = W_{min} * L_{min} + W_{max} * L_{max}$, [m] ;

L_i = Length of the pipe I on the fracture, [m];

A_f = fracture area, [m^2].

The recommended value for W_{area} is a number close to one.

Transport Aperture Options

1. Transport aperture, e, can be based on the aperture in the fracture data file (.FAB)
2. Transport aperture, e, an be derived from a formula, $e = a_1 * T^{a2}$, where T is the fracture transmissivity. This formula can be used for either the Doe Law or the Cubic Law.
3. Transport aperture e can be derived from the aperture in the fracture data file as,

   $e = a_1 e$, where a_1 is a user specified constant.

Input/Output Options

Pipe Generation using the FracMan 2.60 fracture data format .FAB. Alternatively, pipe generation speed can be increased by approximately 60% by using a special file format which contains fracture intersection data. These files are binary, direct-access, with fixed record length. These files are listed in Table 2-2.

Table 2-2 Pipe Generation Input Files

File Name	Record Length	Data type	Variables
interxs.xyz	32	(2I*4,6R*4)	NF1,NF2,XX1,XX2 -- two intersection points
trasfm.mtx	72	(9Dbl*8)	A(3,3) -- fracture transformation matrix
farea.bin	24	(1I*4,3R*4)	NSET,Area,Trans, Storf -- fracture prop.

Each pipe produced by the pipe generation algorithm has three hydrological properties, three geometric properties, and two nodes defining the beginning and ending pipe coordinates. These pipe properties are provided in Table 2-3.

Table 2-3 Pipe Properties from Pipe Generation

Column	Property
1	Transmissivity [m^2/s],
2	Storativity [-],
3	Transport aperture [m],
4	Pipe width [m],
5	Trace length 1 [m],
6	Trace length 2 [m].

The nodal specifications are provided in Table 2-4. The input file for control of pipe generation is presented in Table 2-5.

Table 2-4 Node Definitions from Pipe Generation

Parameter	Explanation
J	Node Number
Xj,Yj,Zj	Nodal Coordinates
NTYPj	Node Type (see MAFIC Manual)
Hj	Assigned Head (if head boundary node)
Qj	Assigned Flux (if flux boundary node)
NGRPj	Nodal Group
NF1,NF2	Fracture Numbers

Table 2-5 Control file for Pipe Generation

Record Number	Parameter	Example	Explanation
1	INFILE	tst	[header file]
2	OUTFILE	tst	[output file]
3	FTYPE	2	[(1) .FAB file (2 intersection]
4	NFILES	1	[# of frac. file]
5	FRACFILE	f100bab	[frac. file name]
6	PIPEOPT	4	[option for generation of pipe network]
7	WFACT	1.2	[Factor for effective pipe pathway]
8	MERGE	1.e-3	[Merge distance]
9	TCUTOFF	1.e-18	[Min. T]
10	APERFLAG	1	[(1) from .FAB file (2) from transmissivity, T]
11	A1,A2	1.0 2.0	[(a1,a2) (1)A=a1*S (2) A= a1*T**a2]
12	WIDFLAG	1	[(1) W=w1*W_min+w2*W_max, (2) W=(w1*W_min+w2*W_max)*w3]
13	LENFLAG	1	[(1) length (2) projected length]
14	WIDFACT	0.5 0.5 1.0	[(w1,w2,w3)]

2.2 Task 1.1.3: Sampling/Header Structures

During HY-8, the FracMan/MAFIC software programs were upgraded to use new "sampling object" .SAB sampling and boundary condition structures. The use of .SAB files is summarized in Table 2-6.

Sampling object files (.SAB) contain the following information:

- Geometry: boreholes, traceplanes, multiplanes, and tunnels;
- Boundary conditions: pressure, flux, and solute transport;
- Time step: time step values; and
- Analysis control: MAFIC simulation control parameters from current .HDR files.

The structure of .SAB files is illustrated in Tables 2-7 through 2-10.

Table 2-6 .SAB (Sampling Object) Features

Module	Feature	Current File	HY-8 Implementation
FracWorks	Trace Plane Conditioning	.SAM File	.SAB Object File
FracWorks	Borehole Conditioning	.SAM File	.SAB Object File
FracSys	OxFilet	.SVY File	.SAB Object File
FracSys	FracSize	.SVY File	.SAB Object File
FracSys	HeterFrac	.SVY File	.SAB Object File
MeshMaker	Header File	.HDR File	.SAB Object File
MeshMaster	Header File	.HDR File	.SAB Object File
EdMesh	Check Boundary Conditions	.HDR File	.SAB Object File
MAFIC	Header Information portion	.MAF File	.SAB Object File (as option)
PAWorks	Sampling File	.SAM Object File	.SAB Object File
PAWorks	LTG	N/A	.SAB Object File

Table 2-7 Sampling Object for Simulated Exploration (FracWorks/FracSys)

```
######
# Define Sampling structures:
#

#----
# Generic properties of sampling structures:
#
#----
# name                                  "Whatever you like"
# source_type                   source | sink | not_specified


#----
#       Simple boreholes are simple because they have one and only one segment.
#       Simple boreholes are defined by an origin, trend, plunge, length and radius,
# as well as the generic properties.
#----
BEGIN borehole_simple
        #csys = gbl             #what to do about Csys

        #Specifiy generic properties
                name            = "Borehole Bob"
                source_type = source

        #Specify geometric properties
                #origin x    y   z
                #------ --   --  --
                origin =1.      2.      3.309

                trend  = 0.
                plunge = 90.
                radius = 5.
                length = 20.

        #specify boundary conditions
                boundary_condition = Nirvana
END


#-----
# Traceplanes
#-----
BEGIN traceplane
        #Specify generic properties
                name            = "Tracy Traceplane"
                source_type = sink

        #Specify geometric properties
                #origin         x   y   z
                #------         --  --  --
                origin =        0.      0.      0.

                #define scan vector
                scan_trend      = 90.
                scan_plunge     = 90.
                scan_length = 10.

                #define transverse vector
                tran_trend      = 90.
                tran_plunge     = 60.
                tran_width      = 15.

        #specify boundary conditions
                boundary_condition = HeadStand
END


#----
#       Simple boreholes are simple because they have one and only one segment.
#       Simple boreholes are defined by an origin, trend, plunge, length and radius,
# as well as the generic properties.
```

```
#----
BEGIN borehole_simple
        #csys = gbl             #what to do about Csys

        #Specify generic properties
                name            = "Borehole Bob"
                source_type = source

        #Specify geometric properties
                #origin x    y   z
                #------ --   --  --
                origin = 1E+03 20.     33

                trend  = 22.5
                plunge = 73
                radius = 0.05
                length = 19.

        #specify boundary conditions
                boundary_condition = Nirvana
END

#-----
# Box regions
#-----
BEGIN box_region
        #Specify generic properties
                name            = "big_box"
                source_type = not_specified

        #Specify geometric properties
                #                       x       y       z
                #------         --  --  --
                center  =       1.      3.      5.
                length  =       15      20      40

                # all faces have the same boundary
                boundary_condition = foo
END


BEGIN box_region
        #Specify generic properties
                name            = "Ms. Cube"
                source_type = not_specified

        #Specify geometric properties
                #                       x       y       z
                #------         --  --  --
                center  =       0.      0.      0.
                length  =       15      20      40

                #each face can have a different boundary condition
        #                                               x+      y+      z+      x-      y-
        z-
                #-----------------              ---     ---     ---     ---     ---     ---
                boundary_condition =    foo     bar     foo     bar     foo bar
END


#----
#multi-planes
#----
#still under development
BEGIN multi_plane
        number_of_planes
        BEGIN plane
        END
        BEGIN plane
        END
        BEGIN plane
        END
END


#-----
```

```
#circular-tunnels
#-----
BEGIN circular_tunnel
        #Specify generic properties
                name           = "BH1"
                source_type = not_specified

        #Specify geometric properties

                #                              x   y   z
                #-----                    --- --- ---
                origin =                 0.      0.      0.
                axis_trend = 30
                axis_plunge = 90.0

                length  =  50.
                radius  =  30.
                panels  =  4

        #specify boundary conditions
                boundary_condition = FluxStand
END


BEGIN circular_tunnel
        #Specify generic properties
                name           = "Pete R. Pipe"
                source_type = not_specified

        #Specify geometric properties

                #                              x   y   z
                #-----                    --- --- ---
                origin =    0.  0.  -100.
                axis_trend = 30
                axis_plunge = 90.0

                length  =  50.
                radius  =  30.
                panels  =  4

        #specify boundary conditions
                boundary_condition = FluxStand
END


#-----
#horseshoe-tunnels
#-----
BEGIN horseshoe_tunnel
        #Specify generic properties
                name           = "Mrs. Ed"
                source_type = not_specified

        #Specify geometric properties
                #                              x   y   z
                #-----                    --- --- ---
                origin =                 20.     20.     20.
                axis   =                 0.      1.      0.
                trans_axis =   1.        0.      0.

                width          = 40.
                length         = 60.
                wall_height    = 30.
                radius         = 30.
                panels         = 4

        #specify boundary conditions
                boundary_condition = FluxTick
END
#----
#       Simple boreholes are simple because they have one and only one segment.
#       Simple boreholes are defined by an origin, trend, plunge, length and radius,
# as well as the generic properties.
#----
BEGIN borehole_simple
```

```
        #csys = gbl             #what to do about Csys

        #Specify generic properties
                name            = "Borehole Bob"
                source_type = source

        #Specify geometric properties
                #origin x    y   z
                #------ --   --  --
                origin =9.      1.2E+01,        113

                trend  = 45.
                plunge = 90.
                radius = 5.e-02
                length = 20.

        #specify boundary conditions
                boundary_condition = Nirvana
END

BEGIN slab_region
        name            = "slab_2"

        #Specify geometric properties

                #             x   y   z
                #-----       --- --- ---
                center =     40.  0.  -100.
                scan_trend = 30
                scan_plunge = 90

                tran_trend = 30
                tran_plunge = 90

                high_trend = 30
                high_plunge = 90

                #           scan_len transv_len  height
                #-----      --- --- ---
                length =  50. 60   80

END

#-----
# prism region:
#-----
# keywords: name, origin, axis_trend , axis_plunge
#           axis_length, cross_polygon

BEGIN prism_region
        name            = "peter 2"

        #Specify geometric properties

                #             x   y   z
                #-----       --- --- ---
                origin =     0.  -100.  30.
                axis_trend = 90
                axis_plunge = 0

                axis_length     =  150.

                cross_polygon   = "pentagon"

END


#-----
# 2D polygon:
#-----
# keywords: name, BEGIN 2d_data, END
#-----
BEGIN polygon_2D

        name    = "pentagon"
```

```
        BEGIN 2d_data
        #       x   y
        #-----  --- ---
                50   -50
                50   0
                25   50
                10   0
                10   -50
        END
END
```

Table 2-8 Sampling Object for Specification of Boreholes and Traceplanes

```
BEGIN borehole_simple
    origin =    .000    .000 100.000
    trend  =  90.000
    plunge =  90.000
    radius =    .015
    length = 200.000
END

BEGIN borehole_simple
    origin =  30.000 -50.000 100.000
    trend  =  90.000
    plunge =  90.000
    radius =    .010
    length = 100.000
END

BEGIN traceplane
    origin =      .000  -100.000      .000
    scan_trend  =  90.000
    scan_plunge =    .000
    scan_length = 200.000
    tran_trend  =    .000
    tran_plunge =  90.000
    tran_width  = 200.000
END

BEGIN traceplane
    origin =      .000  -100.000      .000
    scan_trend  =  90.000
    scan_plunge =    .000
    scan_length = 200.000
    tran_trend  =    .000
    tran_plunge =  45.000
    tran_width  = 200.000
END

BEGIN traceplane
    origin =      .000  -100.000      .000
    scan_trend  =  90.000
    scan_plunge =    .000
    scan_length = 200.000
    tran_trend  = 180.000
    tran_plunge =  45.000
    tran_width  = 200.000
END

BEGIN traceplane
    origin =      .000  -100.000      .000
    scan_trend  =  90.000
    scan_plunge =    .000
    scan_length = 200.000
    tran_trend  =    .000
    tran_plunge =    .000
    tran_width  = 200.000
END
```

Table 2-9 Sampling Object for Specification of Boundary Conditions (EdMesh/MeshMaster/MAFIC)

```
#*****
# FILE: MAFIC.SAB
# DATE: SEP-1996
# BY:   Glori Lee
#       Golder Associates
#
# Sampling structures file format
#*****

BEGIN mafic_header
       name = 'PNC_97'
     mafic_namelist = 'PNC_list_1'
     mafic_parameter= 'PNC_par_1'
     mafic_title    = 'Cross-hole Simulation'
     boundary_group_number = 7
     BEGIN time_step
               # time     output flag     nSteps
               #------    ------------          ------
                 1.           1           1
                25.           6           2
                50.           6           1
               100.           1           1
     END
     solute_parameter= 'particle_ABC'
     data_file = 'f100.dat'
END


BEGIN mafic_namelist
      name = "PNC_list_1"
        debug=F
         InFill = 2
END


#-----
# mafic_parameter :
#-----
# keywords: name,
#           data for mafic flow solver and plot file
#-----
BEGIN mafic_parameter
       name = 'PNC_par_1'

       iplot   = 3
       ielem   = 1
       restart = 1
       mtype   = 3
       proj    = 0.5
       output_type =1
       itrans  = 0
       I2D     = 1
       tolerance  = 1.E-08
       iteration_no = 1
       solute_mode = 1

        # if iplot is not zero the following data line is required :
       # Node Numbers for head values in plot.dat

       BEGIN plot_data
         10, 34
         126
       END
END

#-----
# solute_parameter :
#-----
# keywords: name, source_group
#           parameteres for mafic solute transport simulation
```

```
#-----
BEGIN solute_parameter
        name = 'particle_ABC'
        ISEED=12321
        DISPL = 1.0
        DISPT = 0.0
        diffusion = 1.E-09
        PM=1E-2
        RHOW = 1000.0
        RSink = 0.01
        NPTRAK = -1
        No_Source_Groups = 2

        BEGIN source_group_name
        'Source_A'
        'Source_B'
        END
END

#-----
# solute_parameter :
#-----
# keywords: name, chemical_name, boundary_group, solute_concentration
#-----
BEGIN solute_group
        name = 'Source_A'
        # No_of_Data_Pairs  Boundary_Group_No.
        chemical_name = "A"
        boundary_group = 1
        BEGIN solute_concentration
            # time   concentration
                0.0     1.0
                50.0    1.0
                50.001  0.0
                100     0.0
        END
END

BEGIN solute_group
        name = 'Source_B'
        chemical_name = "B"
        boundary_group = 2
        BEGIN solute_concentration
            # time   concentration
                0.0     1.0
                25.0    1.0
                25.001  0.0
        END
END


#####
# Define boundary conditions:
#
# boundary_cond_type    = constant_head | constant_flux | time_vary_head | time_vary_flux |
interior | nodal_group
# boundary_group_numbers = integer numbers separated by blank spaces,
#                          tabs or commas.
# boundary_values


BEGIN flow_boundary
        name = 'PNC_Outer'
        region_type = box
        region_name = 'big_box'
        BEGIN boundary_groups
                up = 2
                down = 1
                wall_1 = 4
                wall_2 = 4
                wall_3 = 3
                wall_4 = 3
        END
END

BEGIN flow_boundary
```

```
        name = 'inner1'
        region_type = circular_tube
        region_name = 'BH1'
        BEGIN boundary_groups
                up = 6
                down = 6
                all_walls = 5
        END
END

BEGIN flow_boundary
        name = 'Hello 2'
        region_name = 'Peter 2'
        region_type = prism
        BEGIN boundary_groups
                all = 7
        END
END

BEGIN boundary_condition
        name = "init_H"
        boundary_condition_type = constant_head
        boundary_group_numbers  = 1-2
        BEGIN boundary_values
                h0 = 0.1
                hx = 0.2
                hy = 0.3
                hz = 0.4
        END
END

BEGIN boundary_condition
        boundary_condition_type = constant_head
        boundary_group_numbers  = 1-2
        BEGIN boundary_values
                h0 = 0.1
                hx = 0.2
                hy = 0.3
                hz = 0.4
        END
END

BEGIN traceplane
        #Specify generic properties
                name           = "Tracy Traceplane"
                source_type = sink

        #Specify geometric properties
                #origin        x   y   z
                #------        --  --  --
                origin  = -3.E+01,     0.2E-01 10.

                #define scan vector
                scan_trend     = 9.
                scan_plunge    = 10.
                scan_length = 10.

                #define transverse vector
                tran_trend     = 20.
                tran_plunge    = 60.
                tran_width     = 15.

        #specify boundary conditions
                boundary_condition = HeadStand
END

BEGIN boundary_condition HeadTick
        boundary_condition_type = time_vary_head
        BEGIN boundary_values
                # time  h0
                #------ ----
                1.              1.
                5.              4.
        END
END
```

```
BEGIN boundary_condition FluxStand
        name = "init_Q"
       boundary_condition_type = constant_flux
       boundary_group_numbers  = 3,6-9
       BEGIN boundary_values
              q0 = 2.
              qx = 4.
              qy = 0.
              qz = 6.
       END
END

BEGIN boundary_condition FluxTick
       boundary_condition_type = time_vary_flux
       boundary_group_numbers  = 4
       BEGIN boundary_values
              # time  q0      qx
              #------ ----    ----
              1.              1.E-2
              2.5             2.E-3
       END
END


BEGIN boundary_condition Nirvana
       boundary_condition_type = nodal_group_flux
       boundary_group_numbers  = 5
       BEGIN boundary_values
              # time  q0      qx
              #------ ----    ----
              0.              1.
              5.0             2
       END
END
```

Table 2-10 Sampling Object for Pathway Search (PAWorks)

```
#############################################################################
#tst.sab
#-- test file for paworks command line interface
#############################################################################
BEGIN paworks_runtime
   ###
   # List fracture files (.BAB only) to process here
   # one per line please...
   ###
   BEGIN frac_files
      ltg1
   END

   ###
   # The sab file that GenPipes will use
   # Usually this will be the same file PAWorks will use
   # but it doesn't necessarily have to be.
   ###
   BEGIN sab_file
      tst
   END

   ###
   # These are the runtime parameters GenPipes requires.
   #    sab_transfer: the transfer file (.sab) that GenPipes will generate
   #    mafic_output: the output file mafic will generate
   #    frac_area_file: the file for fracture areas
   #    min_T: minimum transmissivity cuttoff for fractures
   #    merge_factor: factor used in merging 2 nodes
   #    Fd: kludge factor
   ###
   BEGIN gen_pipes_parameters
      sab_transfer = pawxfer
      mafic_output = pawmfc
      frac_area_file = farea.bin
      min_T = 1.E-10
      merge_factor = 0.
      Fd = 1.
   END

   ###
   #Head calculation options:
   #    head_calc_type = linear
   #    head_calc_type = mafic
   #    head_calc_type = file
   #    maf_file = restart.maf
   ###
   BEGIN head_calc
      head_calc_type = mafic
      maf_file = restart.maf
   END

   ###
   #Aperture calculation options:
   #    apert_calc_type = weighted
   #    apert_calc_type = use_T
   #    apert_calc_type = use_Q
   #    apert_calc_type = use_Qout
   ###
   BEGIN aperture_calc
         apert_calc_type = weighted
   END

   ###
   #Graph traversal options:
   #    path_weights = none
   #    path_weights = transmissivity
   #    path_weights = flux
   #    path_weights = resistance
   #    path_weights = travel_time
   #    path_search = simple
```

```
#    path_search = weight_larger
#    path_search = weight_smaller
#    path_search = minimize_weight
#    depth_option = fracs
#    depth_option = one_dim
#    depth_fracs = all_fracs
#    depth_fracs = path_fracs
#    depth_fracs = damk_fracs
#    depth_fracs = one_dim
###
BEGIN path_search_options
   path_weights = travel_time
   path_search  = weight_smaller
   max_num_paths = 100000
      max_branches  = 20
      compute_penetration = FALSE
      depth_option = fracs
      depth_fracs = all_fracs
      depth_samples = 50
      damk_thresh = 1.
   Fa = 1.
END

###
#Representative path generation options:
#    path_option = travel_time
#    path_option = source
#    path_option = exit
###
BEGIN rep_path_generation
   path_option  = source
   max_roots    = 5
   max_branches = 5
      weight_fraction = 1.
END

###
# Boundary definition
#    define sources and sinks for PAWorks graph traversals.
#    you can define boundary pipes as coming from either a
#           - boundary group
#           - owner fracture fracture set
#           - owner fracture index
#
# Specify numeric ranges as comma delimited numbers with
# ranges specified using hyphens, eg. 1,2,3,5,7-12,15,18
# Multilines are ok just remember the comma.
#
# It's also okay to remove the empty BEGIN/END blocks.
###
BEGIN source_def
   BEGIN bdry_groups
      7
   END
   BEGIN frac_sets
         1
   END
   BEGIN frac_ids
   END
END

BEGIN sink_def
   BEGIN bdry_groups
      1-6
   END
   BEGIN frac_sets
   END
   BEGIN frac_ids
   END
END

###
#Output options
#  If an output option is missing you won't get it.
#
###
```

```
BEGIN pa_output
   ###
   # root name for rip files (*.RIP, *.RIP2)
   ###
   rip_file = pa

   ###
   # root name for stats files (root_01.sts, etc.)
   ###
   sts_root = pa

   ###
   # view dec alpha output (GeomView)
   ###
   view_transfer = paw.list

   ###
   # controls for diagnostic output
   ###
   diag_file = paw.dig
   dump_runtime = TRUE
   dump_nodes = TRUE
   dump_pipes = TRUE
   dump_adjacency = TRUE
   dump_paths = TRUE
   dump_reppaths = TRUE
END


    BEGIN LTG_options
                ###
                # input files
                ###
          RunOut =       UNIT5.LTG
          PipeOut =      UNIT77.LTG
          PipePropOut =  UNIT99.LTG
          RetardOut =    UNIT88.LTG
          ImmobileOut =  UNIT111.LTG
          FluxOut =      UNIT32.LTG

                ###
                ## path_selection = real
                ## path_selection = representative
                ###
          path_selection = real

                ###
                # floating parameters
                ###
          title = "PAWorks-LTG test sab"
          logprt = .TRUE.
          bctype = .TRUE.
          peclet_threshold = 2.0
          dispersion_length = 5.E-1

          infill_density = 2.4E3
          infill_thickness = 2.E-2

          BEGIN immobile_zones
                n_zones = 2
                      #              tortuosity,    porosity,      density,
diffusion distance
                zone_data =    1              0.1                    2.5E3    0.01
                zone_data = 1                 0.1                    2.5E3    0.02
          END

          BEGIN radio_nuclides
                number_of_species = 2
                BEGIN nuclide
                            # species 1
                      Kd =                    0.25
                      diffusivity =  1.e-9
                      lambda =                9.390E-15
                      nparent =               0

                      n_czero_nodes =               1
```

```
                        BEGIN c_zero_data
                                c_zero_node =           1
                                c_zero_times =          3#
                                                                species 1
                                #                               czero_times czero
                                c_zero_data =   0.0             1.0
                                c_zero_data =   1000000.0       1.0
                                c_zero_data =   1000001.0       1.0
                        END
                        #optionally more c_zero_data blocks
                END

                BEGIN nuclide
                        #species 2
                        Kd =                    3.56            #kd (m3/kg)
                        diffusivity =  1.5E-9                   #free water
diffusivity
                        diffusion =             8.114E-3        #diffusion for species
                        lambda =                9.390E-15       #lamda for species
                        nparent =               1
        #nparents for species
                        kparent =               1
        #species number of parent
                        aparent =               1. #all of species 1 decayusto species 2

                        n_czero_nodes =         1
                        BEGIN c_zero_data
                                c_zero_node  = 1
                                c_zero_times = 3
                                #species 2
                                #                               czero_times czero
                                c_zero_data =   0.0                     1.0
                                c_zero_data =   1000000.0       1.0
                                c_zero_data =   1000001.0       1.0
                        END
                        #optionally more c_zero_data blocks
                END
        END

        BEGIN output
                output_spacing = 5.                             #meters
                n_output_times = 10
                output_time = 20000                             #years
                output_time = 30000
                output_time = 40000
                output_time = 50000
                output_time = 60000
                output_time = 70000
                output_time = 80000
                output_time = 90000
                output_time = 100000
                output_time = 200000
        END

        deltol = 1.E-12
        level = 0
        nitmax = 500
        order = .TRUE.
        reduce = .TRUE.
        nterm = 5
        relerr = 1.E-09

END

END
# This is the end of the road for PAWorks runtime parameters                #
#########################################################################

#########################################################################
# Genpipes parameters
#
# From this point on is the sab file that GenPipes would expect
# to see. Defines boundaries, boundary conditions and header for
# mafic run.
#
# Mafic reads the output from GenPipes.
```

```
########################################################################
BEGIN mesh_header
   mafic_header   = "MAF_Head.maf"
   outer_boundary = "out_bnd"
   inner_boundary = "inner_1"
   initial_head = "init_H"
   initial_flux = "init_Q"
END

BEGIN boundary_condition
   name ="init_H"
   boundary_condition_type = constant_head
   BEGIN boundary_values
      Hx =   0.000E+00
      Hy =   0.000E+00
      Hz =   0.000E+00
      Ho =   0.000E+00
   END
END


BEGIN boundary_condition
    name ="init_Q"
    boundary_condition_type = constant_flux
    BEGIN boundary_values
       Qx =   0.000E+00
       Qy =   0.000E+00
       Qz =   0.000E+00
       Qo =   0.000E+00
    END
END


BEGIN flow_boundary
    name = "out_bnd"
    region_type = prism
    region_name = "out_bnd"

    BEGIN boundary_groups
         up =   1
       down =   2
       wall_1 =  3
       wall_2 =  5
       wall_3 =  4
       wall_4 =  6
    END
END


BEGIN prism_region
    name ="out_bnd"
    origin =   0.000E+00    100.       0.000E+00
    axis_trend  =      270.00
    axis_plunge =        0.00
    axis_length =      200.00
    cross_polygon = "out_bnd"
END

BEGIN polygon_2D
    name ="out_bnd"

    BEGIN 2d_data
          #    x           y
          # ----    --------
       -100.0000    100.0000
       -100.0000   -100.0000
        100.0000   -100.0000
        100.0000    100.0000
    END
END


BEGIN flow_boundary
    name = "inner_1"
    region_type = prism
    region_name = "inner_1"
```

```
    BEGIN boundary_groups
       all =   7
    END
END


BEGIN prism_region
    name ="inner_1"
    origin =   0.001E+00    0.       0.000E+00
    axis_trend  =        0.00
    axis_plunge =        0.00
    axis_length =        1.00
    cross_polygon = "inner_1"
END

BEGIN polygon_2D
    name ="inner_1"

    BEGIN 2d_data
          #    x           y
          # ----    --------
         -.97000      .97000
         -.97000     -.97000
          .97000     -.97000
          .97000      .97000
    END
END


BEGIN MAF_Head.maf
Benchmark Test Case Header # 1
 $MAFIC  $END
 Proj     iOut   iPlot  iEtype   iStart  iMtype  iTrans  I2D
 .900        0       0       1        1       1       0    1
 Tolerance   MaxIter
  1.000E-08   1000
  Time Steps      Output Flag   nSteps
      1.0000          1            1
      .00000          0            0
 NODAL GROUPS
     7
 Data Pairs for Nodal Group   1        BND-TYPE=  1
   0       0.000E+00  0.000E+00  0.000E+00  0.000E+00      [Hx,Hy,Hz,Ho]
 Data Pairs for Nodal Group   2        BND-TYPE=  1
   0       0.000E+00  0.000E+00  0.000E+00  0.000E+00      [Hx,Hy,Hz,Ho]
 Data Pairs for Nodal Group   3        BND-TYPE=  1
   0       0.000E+00  0.000E+00  0.000E+00  0.000E+00      [Hx,Hy,Hz,Ho]
 Data Pairs for Nodal Group   4        BND-TYPE=  1
   0       0.000E+00  0.000E+00  0.000E+00  0.000E+00      [Hx,Hy,Hz,Ho]
 Data Pairs for Nodal Group   5        BND-TYPE=  1
   0       0.000E+00  0.000E+00  0.000E+00  0.000E+00      [Hx,Hy,Hz,Ho]
 Data Pairs for Nodal Group   6        BND-TYPE=  1
   0       0.000E+00  0.000E+00  0.000E+00  0.000E+00      [Hx,Hy,Hz,Ho]
 Data Pairs for Nodal Group   7        BND-TYPE=  1
   0       0.000E+00  0.000E+00  0.000E+00  1.000E+00      [Hx,Hy,Hz,Ho]
 Solute Transport Mode
    0
*** HEADER
END
```

2.3 Task 1.1.6: PAWorks User Improvements

During HY-8, significant improvements were made to the PAWorks user interface. The improvements incorporated to PAWorks 1.4 under the scope of this task included:

- **Unification of PAWorks/Win32:** A single version of PAWorks containing all the features developed for PNC, SKB, and Enresa was implemented for Win/32. This version includes the following features: (a) breadth first, depth first searches, and flux following searches, (b) specification of fractures (e.g., EDZ) as sources and sinks, and (c) the ability to visualize the results of PAWorks/Unix simulations.
- **PAWorks/Unix:** PAWorks/Unix, developed for Enresa, was extended to include all of the features of PNC PAWorks/Win32. New simulation control features based on .SAB files were added to provide the same functionality for PAWorks/Unix as for PAWorks/Win32.
- **PAWorks Documentation:** A complete set of documentation was developed for both PAWorks/Win32 and PAWorks/Unix.

PAWorks version 1.4 incorporates the features of:

- PNC PAWorks (HY-7),
- SKB PAWorks (1994),
- Enresa PAWorks (Win32),
- Enresa PAWorks (Unix), and
- PAView.

To maintain compatibility between Unix and Windows version of PAWorks, the algorithms of PAWorks were divided into four separately callable programs:

GenPipe: Generation of 1D Pipe Networks from 3D Fracture Networks

MAFIC: Approximate 1D Pipe Network Flow Solution

PAW: Pathways Analysis in 3D Networks of 1D Pipes

LTG: Laplace Transform Galerkin Transport Solution for 3D Networks of 1D Pipes.

PAWorks Version 1.4 capabilities include:

- Use of MAFIC (1D) output, MAFIC (3D) output, or the linear circuit approximation to solve the head field;
- Use of .SAB sampling object files (See Section 2.2);
- Output files for CRYSTAL (See Section 2.4.2);
- Ability to define sources as fractures or as sampling objects;
- Link to GeomView for visualization on workstations;
- Ability to define equivalent pathways based on either the highest common source or common sink locations; and
- Ability to calculate the Peclet and Damköhler number for every.

PAWorks Version 1.4 documentation is provided as Appendix E. PAWorks Algorithms are summarized in Section 2.4 below. The following sections summarize the algorithms and user interface of Unix and Win32 implementations of PAWorks Version 1.4.

2.3.1 PAWorks User Interface: Unix

The implementation of PAWorks on Unix is comparable to the implementation of MAFIC. PAWorks on Unix is actually a series of independent programs, run by a common script. The modeling sequence on Unix is:

1. FracWorks (PC) fracture generation as ASCII or Babylonian .FAB file.
2. PAWorks (PC) generate .SAB files to control PAWorks, MAFIC and PAWorks/LTG execution.
3. Transfer .FAB and .SAB files to workstation.
4. GenPipes (Unix) transform fracture network to network of 1D pipes.
5. EdPipes (Unix) ensures that the pipe network is suitable for finite element modeling.

6. MAFIC (Unix) calculates head field for given boundary conditions, and output as .RST restart file.
7. PAW (Unix) transforms MAFIC restart file and .SAB files to LTG input files.
8. LTG (Unix) calculates concentration as a function of time for specific time points and locations.

For more information on the operation of PAWorks under Unix, see Appendix E.

2.3.2 PAWorks User Interface: Win32

Figures 2-3 through 2-6 illustrate the PAWorks user interface for Windows 95 and Windows NT. The user interface for PAWorks was completely rebuilt during HY-8 to make it compatible with the new Unix version. The analysis sequence for PAWorks for Windows 95 and Windows NT is follows:

1. Begin a new analysis and load input fracture network, source/sink and analysis parameter files.

   File|New

   File|Open

2. Define Analysis Parameters and define boundary conditions.

   Edit|Exploration

   Edit|Analysis Parameters

3. Perform PAWorks analyses to determine fracture intersections, pipe networks, head drops, and flow patterns.

   Analysis|Pipe Generation

   Analysis|Calculate Heads

   Analysis|Pathways Analysis

   Analysis|Penetration Depth

   Analysis|LTG Transport

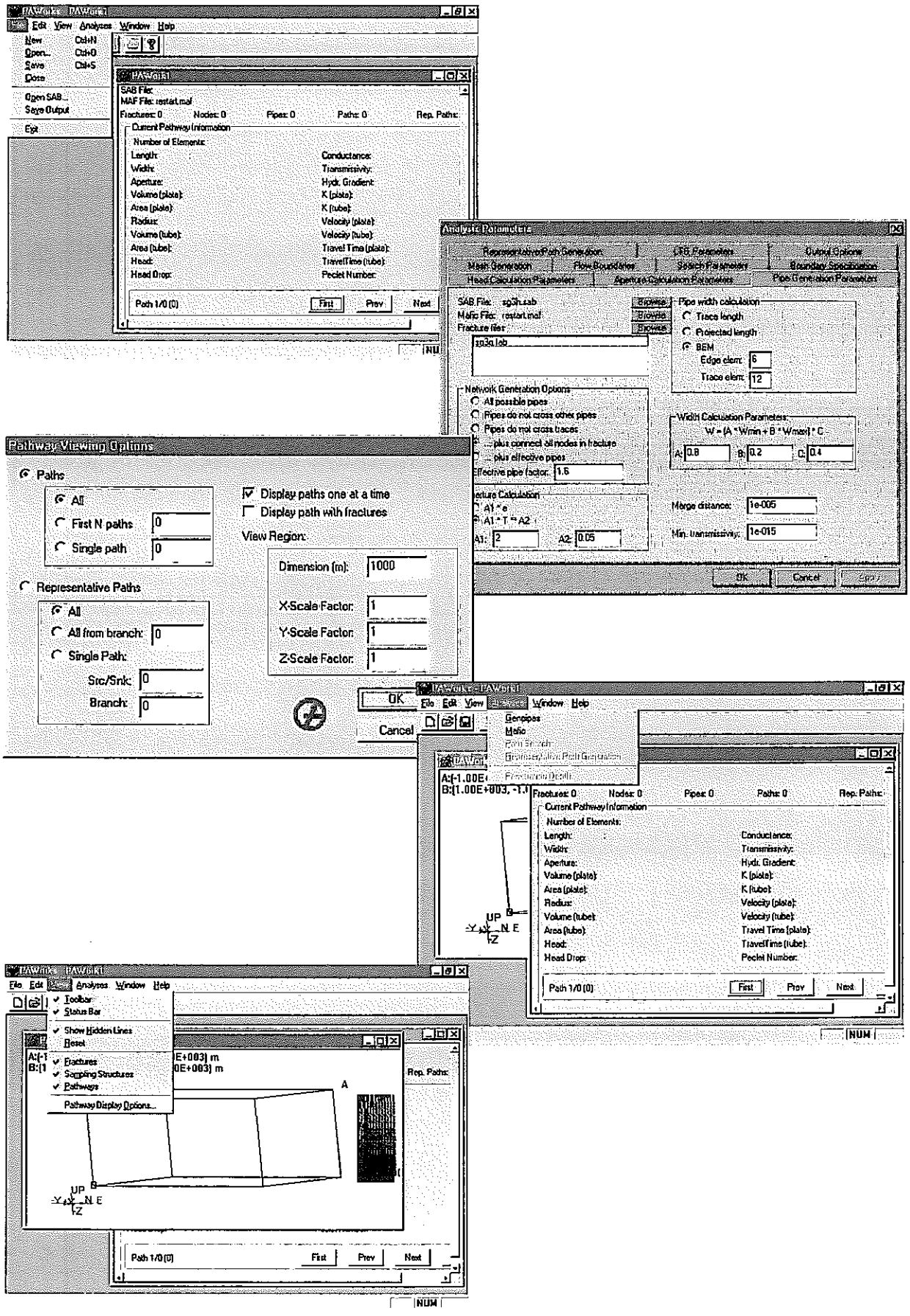

FIGURE **2-3**

PAWorks USER INTERFACE

PNC/H8

PROJECT NO. 923 1089.800 DRAWING NO. 77049 DATE 2/20/98 DRAWN BY EA

Golder Associates

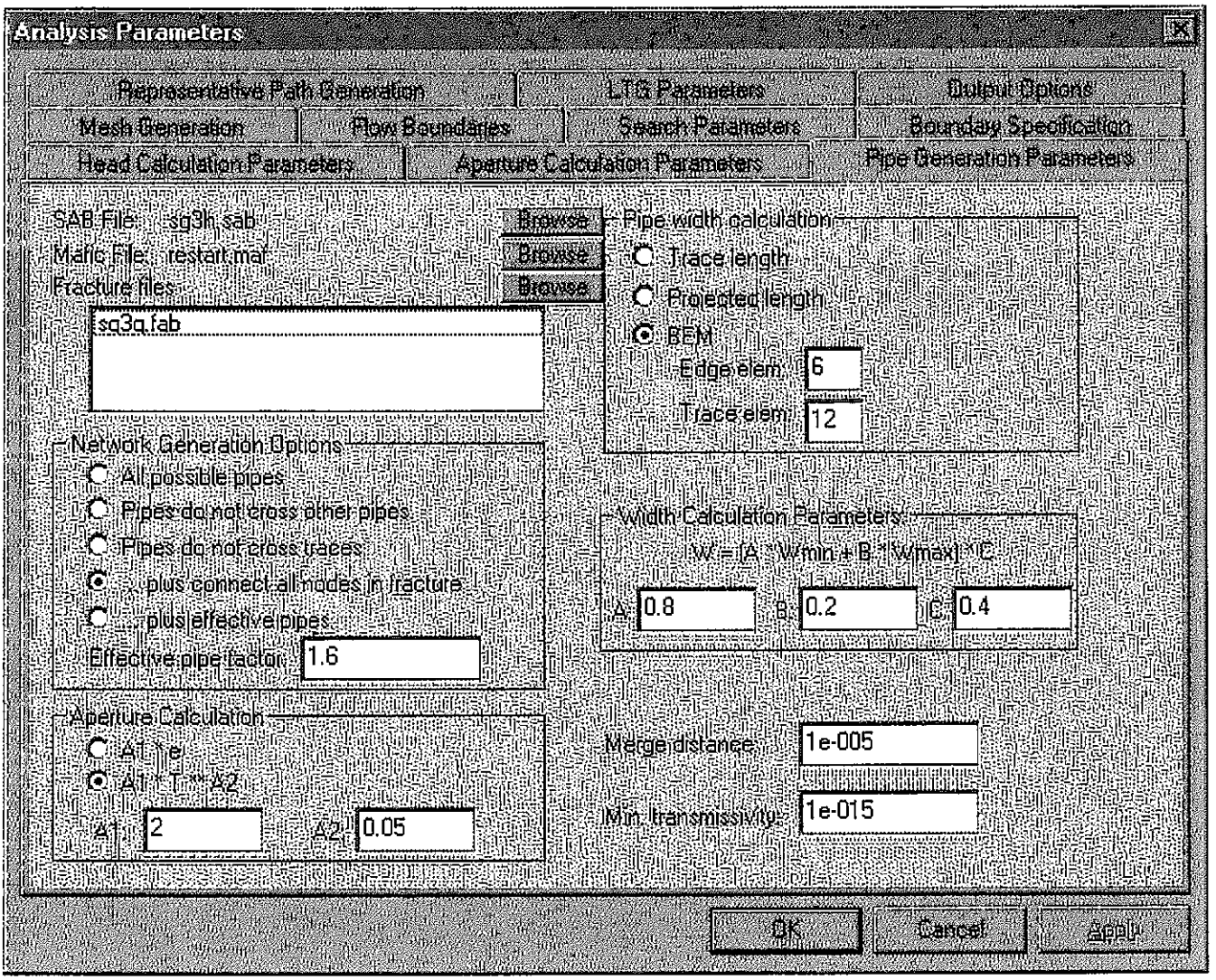

FIGURE **2-4**
PAWorks ANALYSIS CONTROL
PNC/H8

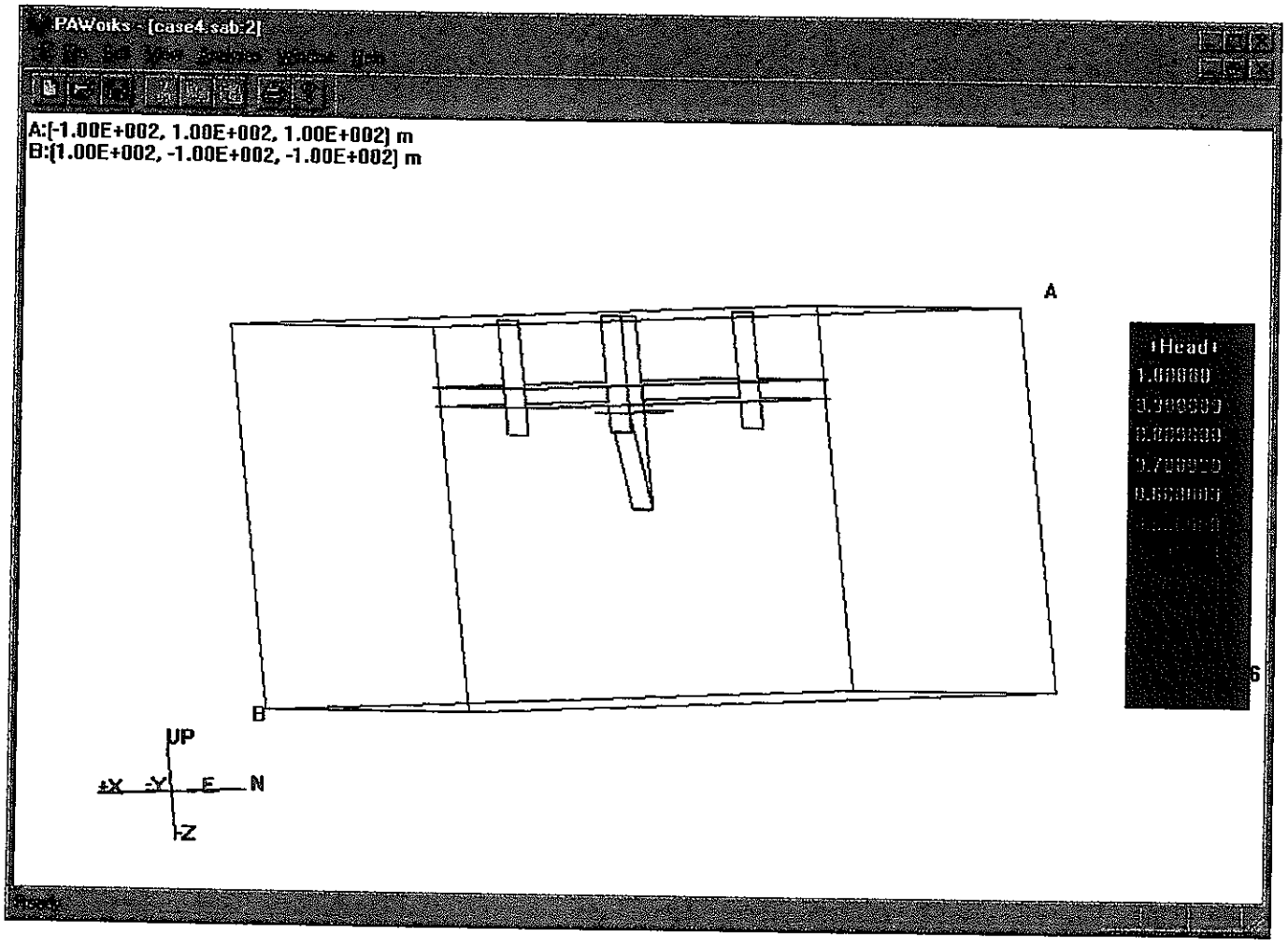

FIGURE **2-5**
PAWorks FRACTURE DISPLAY
PNC/H8

PROJECT NO. 923 1089.800 DRAWING NO. 73164 DATE 5/13/97 DRAWN BY EA

Golder Associates

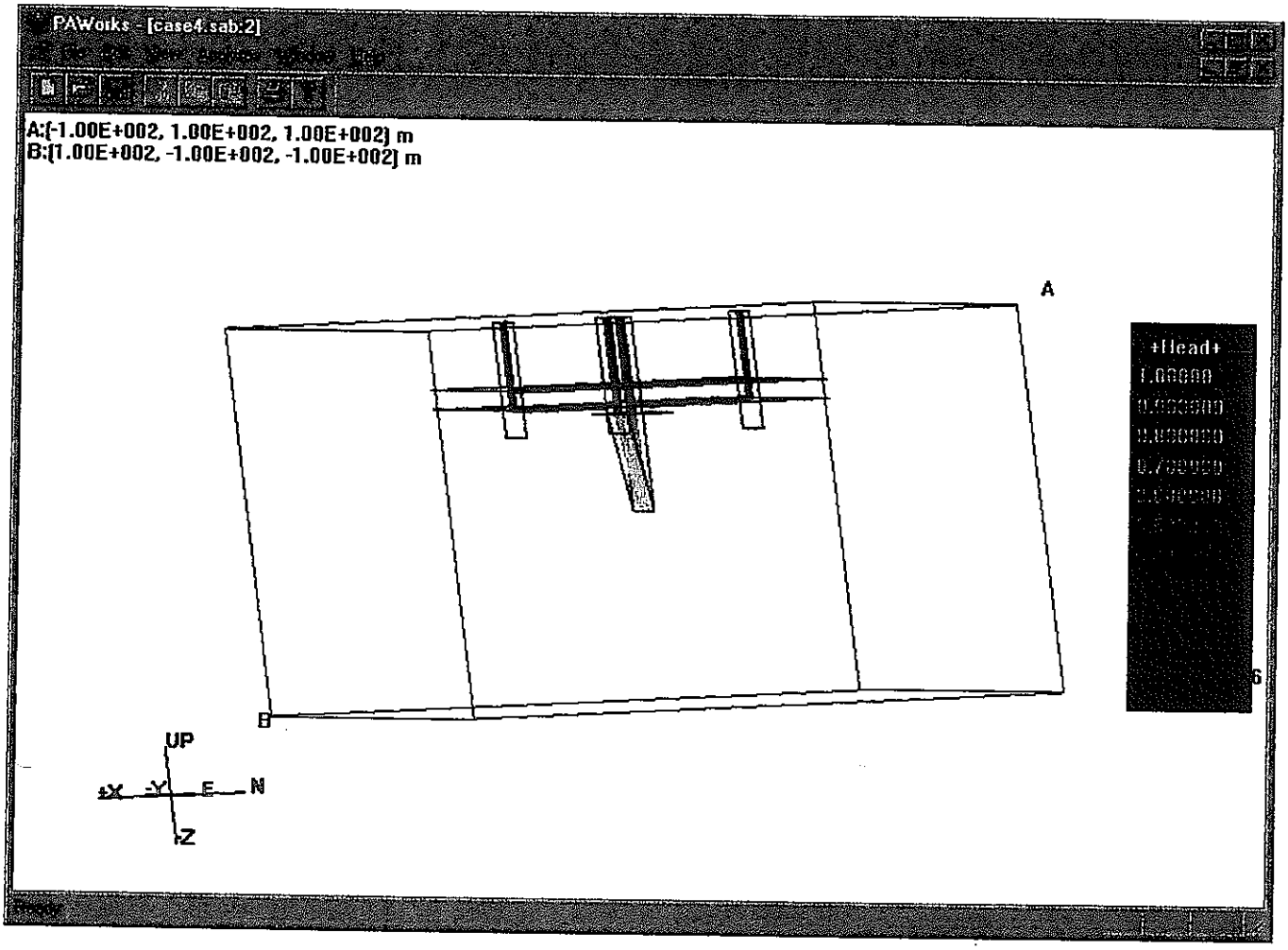

FIGURE **2-6**
PAWorks PATHWAY DISPLAY
PNC/H8

PROJECT NO. 923 1089.800 DRAWING NO. 73165 DATE 5/13/97 DRAWN BY EA

Golder Associates

4. View and save the results.

   Window|3D View

   File|Save

For more information on the operation of PAWorks under Unix, see Appendix E.

2.4 Task 1.1.10: PAWorks Development for Fractured Rock

PAWorks is expected to play a key role in supporting the PNC performance assessment effort for HY-12. During HY-8, PNC specified the following upgrades for PAWorks, consistent with PNC priorities:

- **Pipe Generation Algorithm:** Increase flexibility in generation of pipes to improve topological match between 3-D fracture networks (MAFIC) and 3-D pipe networks (PAWorks),
- **Pathway Property Assignment:** Increased flexibility in assignment of pathway properties,
- **Diffusive Fracture Identification:** Add the ability to identify and filter out fractures in which diffusive transport dominates,
- **Crystal Interface:** Derive equivalent homogeneous pipe properties for Crystal according to agreed specifications,
- **Confirmation:** Carry out sensitivity studies to confirm the scope of the PAWorks approximation by comparison to MAFIC simulations.

These issues are dealt with in the following sections. For discussion of other PAWorks related HY-8 activities, please see:

- PAWorks Calculation Efficiency (Section 2.1.2.2)
- PAWorks Pipe Generation (Section 2.1.2.1)
- PAWorks User Interface Development (Section 2.3)
- PA Scoping Calculations (Section 3.3)

2.4.1 Pipe Generation Algorithm

The transformation of 3D fracture networks to 3D networks of 1D pipes requires,

- the definition of pipes between fracture intersections to maintain connection and connectivity within fractures, without generating excessive numbers of pipes or over-counting fracture transmissivity, and
- calculation of the effective width of pipe elements, which reflects the average or effective cross-sectional area available for flow between each of the fracture intersections.

During HY-8, PAWorks was extended to provide a variety of options for pipe generation and for calculation of effective width. A sensitivity study was carried out comparing MAFIC and PAWorks results to determine the range of pipe assumptions which produce reasonable results. These features are implemented in the GenPipe module of PAWorks.

2.4.1.1 Pipe Geometry

The problems which arise in generation of pipe elements to topologically match the connectivity of 3D fracture networks are illustrated in Figure 2-7. In HY-7 PAWorks, pipes were only generated when they did not cross fracture intersections traces (Figure 2-7a). This is necessary to avoid the double generation of pipes as in Figure 2-7b. However, this algorithm can also result in incomplete connection across the fracture plane (Figure 2-7c), and excessively tortuous paths (Figure 2-7d).

During HY-8, a series of alternative pipe generation algorithms were implemented, as options in PAWorks version 1.4 (Figure 2-8, Table 2-11).

Table 2-11 Pipe Generation Options

Option	Generation Option	Algorithm
1	Pipe Generation Maximum	Generate all pipes which do not cross each other
2	Minimum Pipe Generation	Remove pipes from (1) which cross traces
3	Connectivity Conserved	Add pipes to (2) to ensure that no portions of any fracture are disconnected from other portions of the fracture
4	Pathlength Conserved	Add pipes to (3) to ensure that the tortuous distance between traces through pipes is never greater than a specified percentage longer than the Cartesian distance

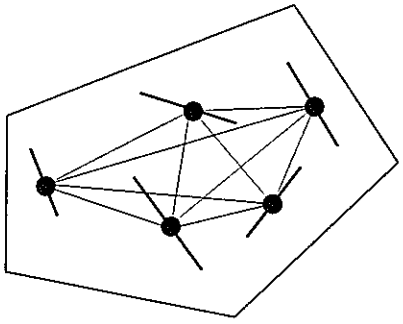

(a) Pipes crossing traces over connect fracture

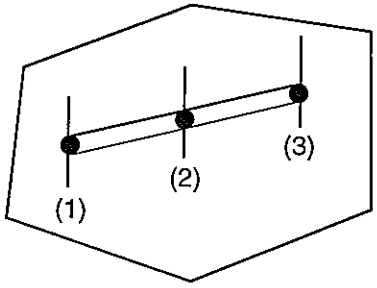

Pipe between (1) and (3)
crosses trace (2), duplicates

(b) Double generation of pipe

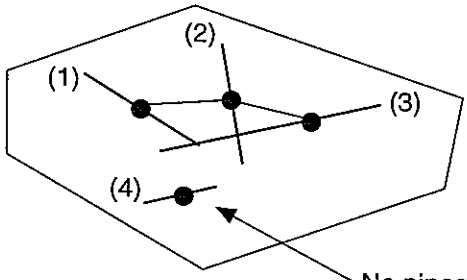

(c) Incomplete connectivity of fracture

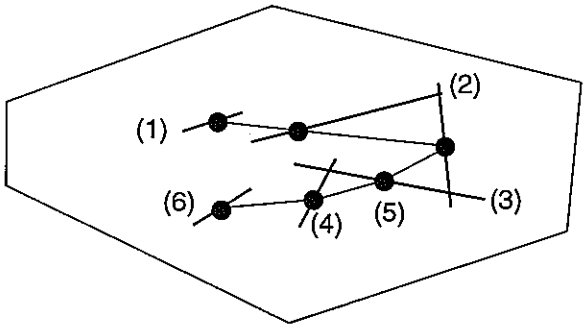

(d) Tortuous paths

FIGURE **2-7**
PIPE GENERATION ISSUES
PNC/H8

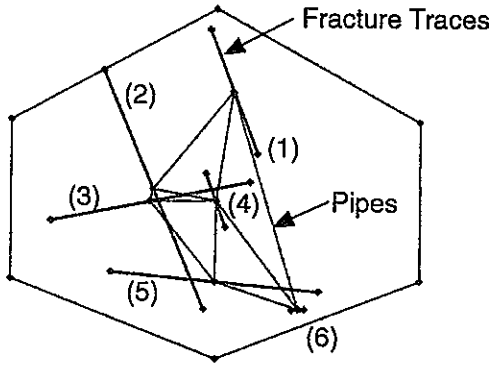

(a) Option 1 - All pipes not crossing each other

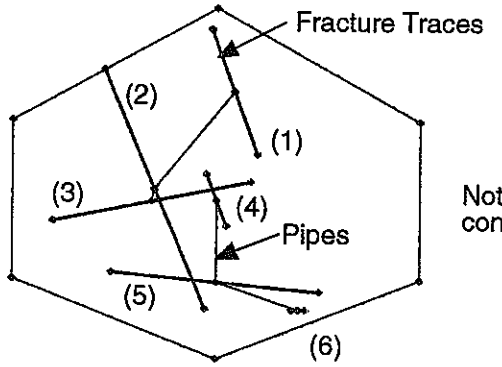

Note: (4), (5) and (6) have no connection to (1), (2), and (3)

(b) Option 2 - Remove pipes which cross traces

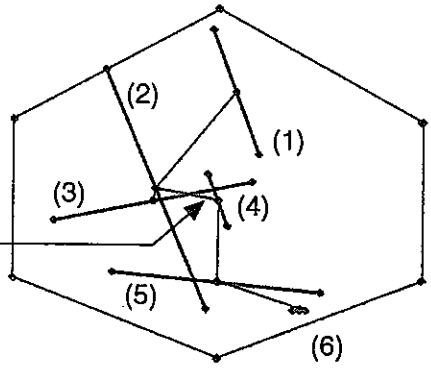

Pipe added to connect (4), (5) and (6) to (1), (2), and (3)

(c) Option 3 - Additional pipes to connect all nodes on fracture

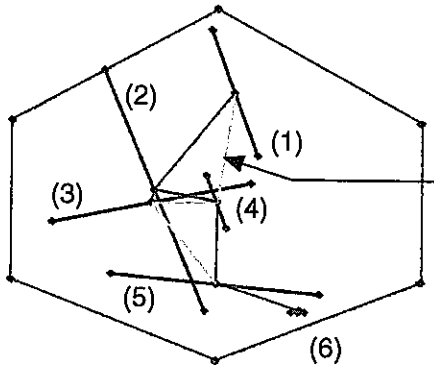

(Effective Factor 1.4)

Pipe added to ensure no tortuous paths greater than 140% of the cartesian distance

(d) Option 4 - Additional pipes to prevent excessively tortuous path

FIGURE **2-8**
PIPE GENERATION OPTIONS
PNC/H8

Of these options, the "connectivity conserved" algorithm is generally preferred, since it avoids adding too many additional pipes, and does not require the level of computation necessary for the tortuous path length calculation of the "path-length conserved" algorithm.

2.4.1.2 Pipe Properties

The fundamental properties assigned to individual pipes are (Figure 2-9):

- Effective Pipe Circumference F_i
- Effective Pipe Cross-Sectional Area A_i
- Effective Pipe Conductance C_i
- Effective Pipe Transport Aperture e_i

Previous versions of PAWorks assumed either slab or circular pipe geometries to derive these values from fracture transmissivity T_i, transport aperture e_i and the average width of the pipe W_i.

PAWorks 1.4 provides additional flexibility in calculation of both flow width and in the use of flow width for transport calculations.

1. Different values of width W_i can be calculated for flux, advective transport, and reactive transport, flow wetted area.
2. Width W_i can be calculated as, $W_i = c_1 \text{ Min } [L_1,L_2] + c_2 \text{ Max } [L_1,L_2]$ where L_1 and L_2 are the widths of the traces defining the ends of the fractures, and c_1,c_2 are user specified constants. If $c_1=c_2,=0.5$, then W_i is based on the average trace length, as in previous versions of PAWorks.
3. Transport aperture (e_i) can be calculated as a function of the form: $a_1 T^{a_2}$, where a_1 and a_2 are user specified values, and T_i is the fracture transmissivity. Alternatively, e_i can be defined using the "fracture thickness" value provided in the fracture file.

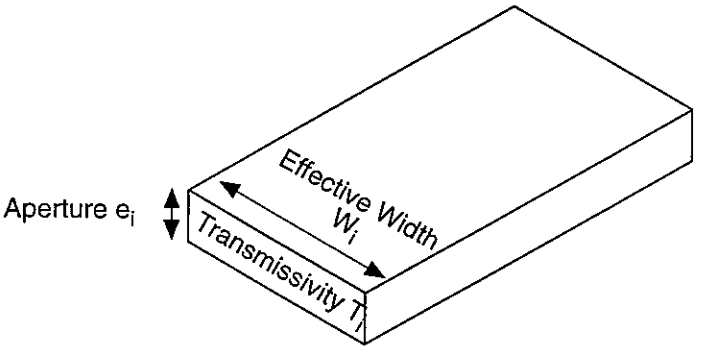

Circumference $S = 2(e_i+W_i)$

Cross-Sectional Area $A_i = e_i\ W_i$

Conductance $C_i = T_iW_i$

FIGURE **2-9**
PIPE PROPERTIES
PNC/H8

PROJECT NO. 923 1089.800 DRAWING NO. 73115 DATE 5/9/97 DRAWN BY EA

Golder Associates

4. The available flow wetted surface for a pipe can be defined as
   $W_i = c_1*A_1+c_2*A_2+c_3*A_3$ where
   c_1, c_2, and c_3 are user specified constants,
   $A_1 = L_i W_i$, the area of the pipe expressed as a channel,
   A_2 = the total area of the fracture "touched" weighted by the flux in the pipes, and
   A_3 = the total area of connected "diffusive fractures", weighted by the flux in the pipes.

5. Pipes dominated by adjective and diffusive transport can be distinguished by the Peclet number Pe_i, calculated as, $Pe_i = v\ L/D_e$ where
   v is the advective velocity (m/s) , L is the pipe length, and D_e is the diffusion rate (m^2/s). In PAWorks, the pathway search can be implemented to ignore diffusively dominated fractures below a user specified Peclet number.

6. Damköhler Type I number, DaI_{im}, where the Damköhler indicates the relative importance of diffusion and advection in fractured systems. Damköhler numbers greater than about 100 indicate that transport is dominated by diffusion. Damköhler numbers less than 0.01 are indicative of advective transport. For DaI_{im} values between 0.01 and 100 the time for diffusion is of about the same order as for advection, and double porosity behavior is to be expected.

   For each immobile zone (non-advective fracture) the Damköhler number is given by:

$$DaI_{im} = \frac{\pi^2}{4}\frac{\theta_{im}}{R_{im}}\frac{D_0\tau}{d^2}(\beta_{im}+1)\frac{LR_m}{V} \qquad \text{(Equation 2-1)}$$

   D_0 = coefficient of molecular diffusion [L^2/T]

   θ_{im} = porosity of immobile zone [-] defined as the volume of pores in the immobile zone divided by the volume of the immobile zone.

   L/V = travel time for the pipe [T]

   d = thickness of diffusive zone [L]

τ = tortuosity (smaller number is more tortuous) [-]

R_m = mobile zone retardation factor [-]

$$R_m = 1 + \frac{K_{d,m} f_m \rho_m}{\theta_m^*}$$

$K_{d,m}$ = distribution coefficient of the mobile zone [L^3/M]

ρ_m = bulk density of the infill in the mobile zone [M/L^3]

f_m = volume of the infill in the mobile zone divided by the total volume [-]

$$= \frac{t_{\inf ill}}{(2.d + e)}$$

θ_m^* = volume of voids in the mobile zone divided by the total volume [-]

$$\theta_m^* = \frac{e}{(2.d + e)}$$

e = aperture [L]

R_{im} = immobile zone retardation factor [-]

$$R_{im} = 1 + \frac{K_{d,im} f_{im} \rho_{im}}{\theta_{im}^*}$$

$K_{d,im}$ = distribution coefficient of the immobile zone [L^3/M]

ρ_{im} = bulk density of the immobile zone [M/L^3]

f_{im} = volume of the immobile zone divided by the total volume [-]

$$= \frac{2.d}{(2.d + e)}$$

θ_{im}^* = volume of voids in the immobile zone divided by the total volume [-]

$$\theta_{im}^* = \theta_{im} \cdot \frac{V_{im}}{V_T}$$

for the case of only one immobile zone (assumed for the Damköhler pruning)

$$\theta_{im}^* = \theta_{im} \cdot \frac{2.d}{(2.d + e)}$$

β_{im} = "capacity ratio" [-]

$$= \frac{\textit{total contaminant mass in the immobile zone at equilibruim}}{\textit{total contaminant mass in the mobile zone at equilibruim}}$$

$$\beta_{im} = \frac{\theta^*_{im} R_{im}}{\theta^*_m R_m}$$

2.4.2 Effective Pathway Properties

To facilitate safety assessment, PAWorks incorporates a number of algorithms to transform the full three-dimensional network of pipe elements to a simplified pipe network with approximately equivalent properties. This is necessary because performance assessment codes such as CRYSTAL can only handle simple series pipe networks, and even RIP can only handle networks on the order of 10 to 200 pipe elements.

The generation of effective pathways requires decisions concerning the approximations which are acceptable. During HY-8, we developed an effective pathway algorithm in cooperation with PNC to ensure that PAWorks effective pathways are consistent with PNC performance assessment goals.

The PNC effective pathway algorithm is based on a matrix of alternative algorithms such that the user would have the choice for pathway generation, pathway properties, and pathway searches. The following alternatives have been implemented for the PNC effective pathway calculations. In the discussion below, the actual pathways through the pipe networks will be referred to as "branches", while the effective pathways will be referred to as "pathways".

1. Branches are identified by following the flux through the pipe network from a predefined "source" location to a "sink" location.
2. Branches are grouped and combined to pathways according to common sources (at specific emplacement drifts).
3. Each pathway is represented by either a single effective pipe or a simplified series pipe network.
4. Flux through the branch is computed from the branch aperture.

5. Flux through the pathway is calculated for the pathway source (initiation) and sink (discharge) locations. The pathway input flux assigned to the P.A. files is calculated as the sums of all of the source fluxes for the individual branches assigned to the pathway. Pathway discharge flux is calculated as the sums of all of the sink fluxes for the individual branches assigned to the pathway
6. Branch travel time is calculated as the sum of the travel times of all the pipes in the branch.
7. Pathway travel time is calculated as the weighted average of the travel time of all of the branches assigned to the pathway. Weighting can be made according to
    - the incoming flux associated with the branch, or
    - the conductance of the branch
8. The reactive surface area of each branch can be calculated for a flux weighted traversal as (Figure 2-10):
    - The total area of all of the pipes along, $A_i = 2\Sigma W_i L_i$,
    - The total area of all fractures touched by the branch $2\Sigma A_f$
    - The total area of all fractures touched by the branch, weighted by the percentage of the flux through that fracture which is related to the branch, $A = 2\, W_{branch} L_{branch}$
9. The reactive surface area of each pathway is calculated as either
    - the total reactive surface area of all of the related branches,
    - the branch reactive surface area, weighted by the branch travel time
    - the branch reactive surface area, weighted by the branch flux
    - the branch reactive surface area, weighted by the branch transmissivity
    - the branch reactive surface area, weighted by the branch resistance (=1/conductive)

(a) Sum of True Fracture Areas on Path

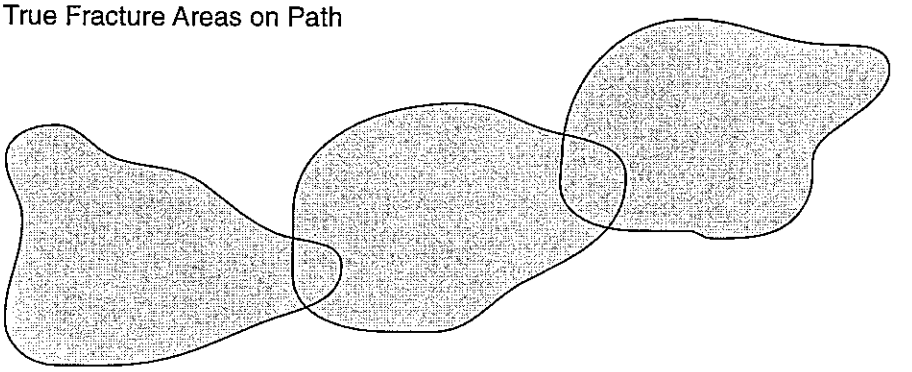

(b) Sum of L_i*W_i

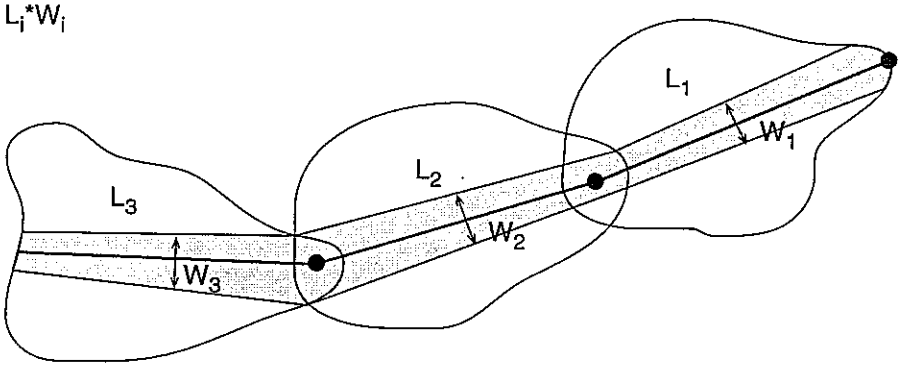

(c) Weighted Width * L

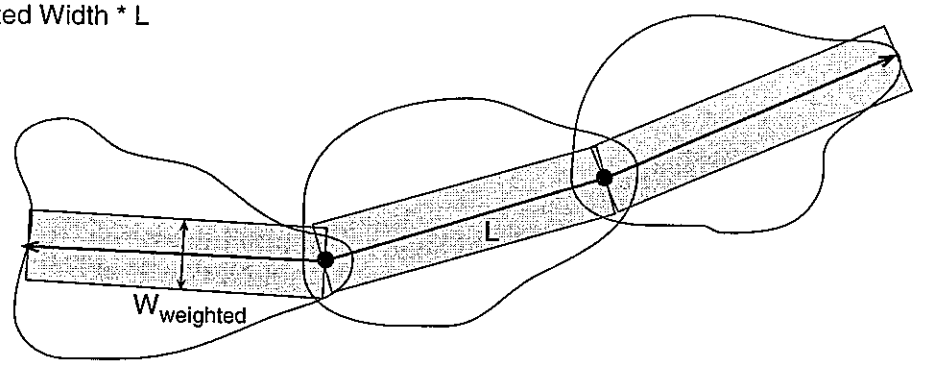

FIGURE **2-10**
REACTIVE SURFACE AREA OPTIONS
PNC/H8

PROJECT NO. 923 1089.800 DRAWING NO. 73116 DATE 5/8/97 DRAWN BY EA

Golder Associates

10. The "aperture" e_i associated with each branch is calculated either,

    - from the pathway transmissivity T, e_i

      $$e_i = \frac{T}{K}$$

    - from branch weighted flux Q, $e_i = e_i = Q/K_iW$
    - from branch output flux Q_{out} $e_i = Q_{out}/K_iW$
    - from weighting the aperture using the weighting used to determine the branches

11. The aperture associated with each pathway is computed from the branch aperture and the weighting parameter,

    $$e_i = \frac{\Sigma(e_i + weight\ function\ branch\ i)}{\Sigma(weight\ function\ branch\ i)}$$

12. The "spacing" between branches can be calculated as either,

    - the number of pathways
    - the mean spacing between fractures along a vertical borehole
    - the mean spacing between fractures perpendicular to the fractures
    - the rock block volume defined by advective fractures.

2.4.3 CRYSTAL Interface:

PNC has specified that the linkage between PAWorks and CRYSTAL will be provided through a table containing the following values for effective pathways.

- A: Block Area/Unit Volume (m^2/m^3). This value is provided as the fracture intensity P_{32}
- l: Path Length (m), defined as tortuous distance through the fracture network along a pipe.
- L: Distance to downstream boundary (generally infinite)
- q: Average velocity in the fracture (m/yr), calculated as the advective travel time t_{50} divided by the tortuous path length l

- d: Slab thickness (m), calculated as the mean spacing between advective fractures for a vertical borehole
- Θ: Advective fracture porosity (-), calculated as the total volume of advective fractures divided by the rock mass volume.

The CRYSTAL interface was implemented to PNC specifications during HY-8. Example pathway property calculations were carried out for the Kamaishi prototype rock block (Figure 2-11; Table 2-12). Results were obtained assuming (Figure 2-12):

1. Properties for the single pathway with the fastest advective travel time;
2. Effective properties for all pathways from a single emplacement room;
3. Effective properties for pathway accounting for 90% of the flux from a single emplacement room.

Results from these simulations are provided in Table 2-13 and visualized in Figure 2-13.

Table 2-12 Kamaishi Rock Block for Crystal Calculations

Property	Set 1	Set 2	Source
Location Model	Levy-Lee	Levy-Lee	Spatial fracture location analysis using data from boreholes and drifts
Exponent	2.4	2.4	Doe et al. (1996)
Min Step Size	8 m	8 m	
Generation Mode	Surface Points	Surface Points	
No. Fracture Sides	6	6	
Generation Region	Box	Box	
Center	0, 0, 0 m	0, 0, 0 m	
Dimensions	225, 225, 225 m	225, 225, 225 m	
Orientation Model	Bivariate Bingham	Bivariate Bingham	ISIS analysis of orientation data from boreholes and drifts
Mean Pole	133.2, 17.6 deg	176.4, 24.1 deg	Doe et al. (1996)
K1, K2	-12.69, -4.23	-4.92, -3.25	
Size (Radius) Distribution	Truncated LogNormal	Truncated LogNormal	Heisei-4 analysis of KD-90 censoring statistics
Mean, StdDev.	7, 1.25 m	7, 1.25 m	Doe et al. (1993)
Lower Bound	none	none	
Upper Bound	25 m	25 m	*(Note: Truncates less than 0.1% of the distribution)*
Elongation	none	none	
Transmissivity Distrib.	Truncated LogNormal	Truncated LogNormal	KH-5 interval transmissivities
Mean, StdDev.	1.1×10^{-7}, 3.85×10^{-4} m^2/m^3	1.1×10^{-7}, 3.85×10^{-4} m^2/m^3	
Lower Bound	10^{-6} to 10^{-12} use 3×10^{-9} m^2/s	10^{-6} to 10^{-12} use 3×10^{-9} m^2/s	Doe et al. (1996)
Upper Bound	none	none	
Storativity	$= 5.0\times10^{-5} \times T^{1/2}$	$= 5.0\times10^{-5} \times T^{1/2}$	Empirical relationship (Doe, 1993); calibration
P_{32} Fracture Intensity	use 0.149 m^2/m^3	use 0.302 m^2/m^3	P_{10} conductive fracture depending on transmissivity cutoff

Table 2-13 Options Considered for PAWorks Crystal Demonstration Application

Parameter	Options Calculated
Fracture pruning for representative path	Single least resistive pathway
	All advective pathways
	Pathways with 90% of outflow flux
Fracture area	Sum of true fracture areas (A_f)
	0.2 * Sum of true fracture areas (A_f)
Pathway length	Tortuous length
Aperture	Based on flux
Weighting for pathway	Flux
Pathway option	Common source
Number of representative pathways	Single pathway
	One for each cluster
Pathway spacing	From PAW pathway spacing

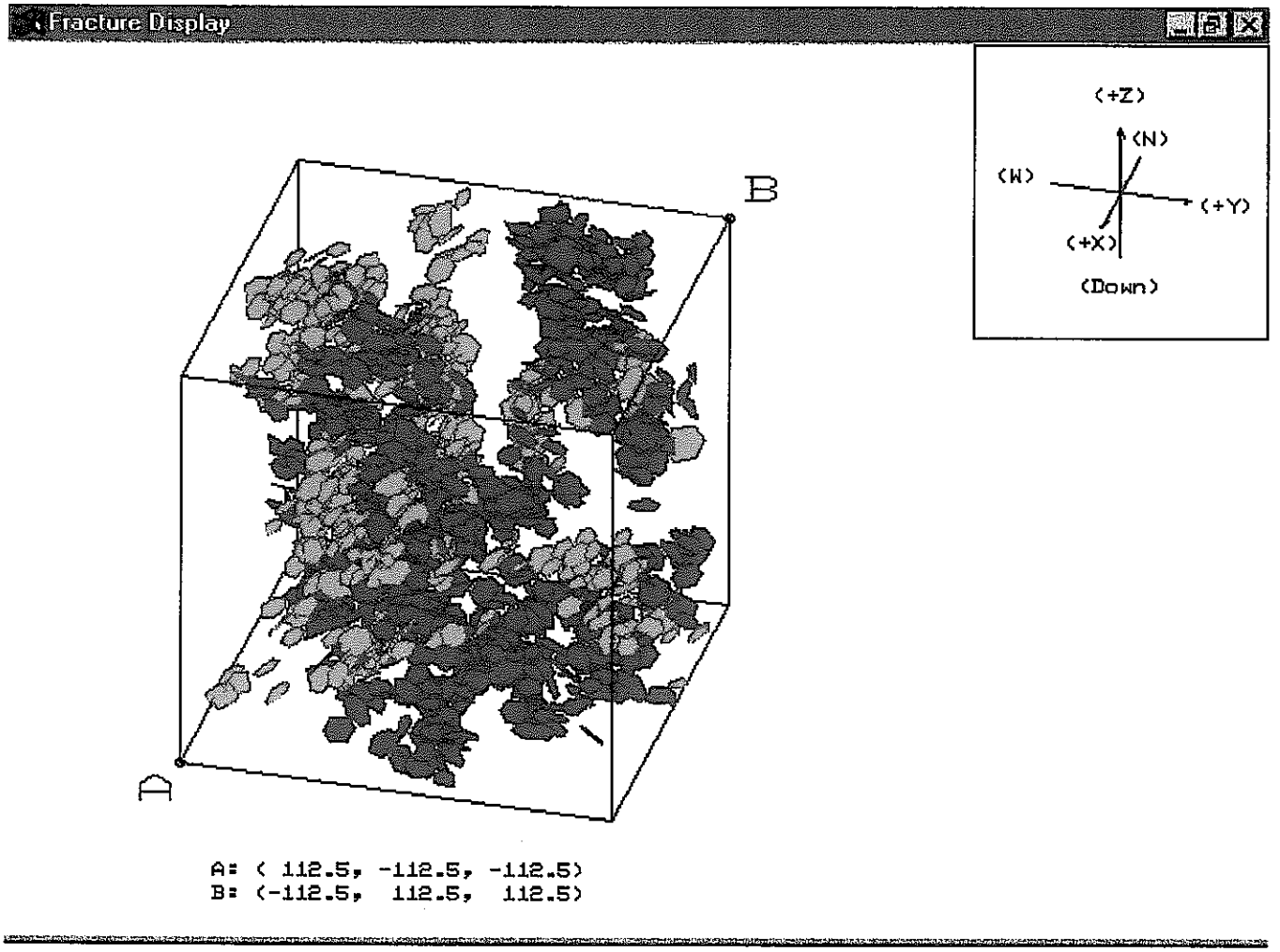

FIGURE **2-11**
KAMAISHI ROCK BLOCK
PNC/H8

PROJECT NO. 923 1089.800 DRAWING NO. 73117 DATE 5/8/97 DRAWN BY EA

Golder Associates

Fracture Area = true fracture area (A_f)
or 0.2 x A_f

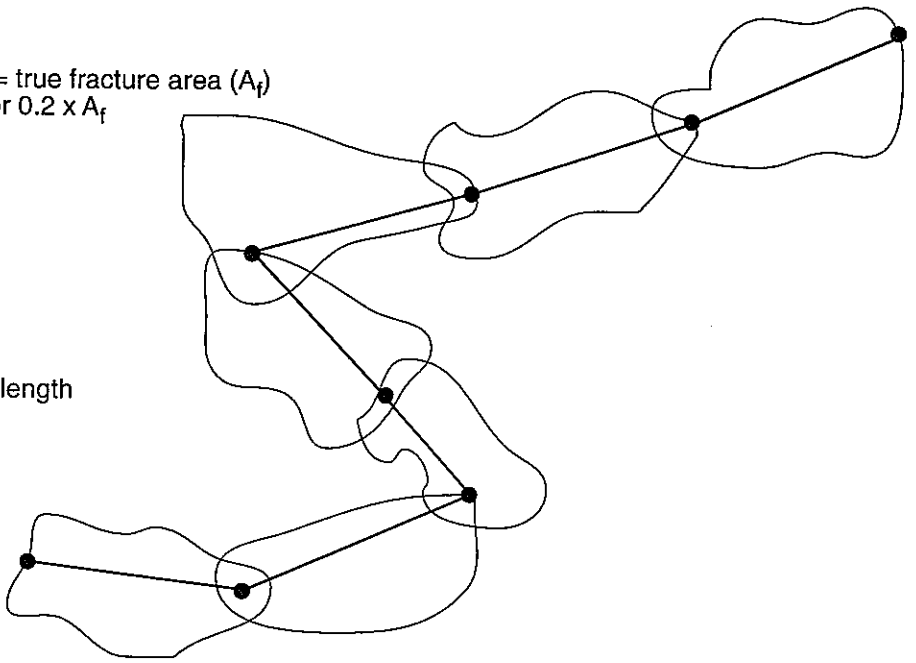

Length = tortuous length

Flux weighting search for paths

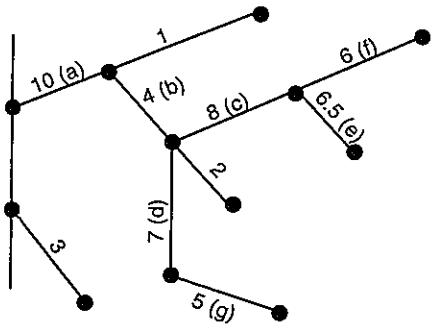

Scaled flux given on pipes
pipe, followed in ( ) in alphabetical order

Pathway Option = common source
Spacing based on PAW pathways

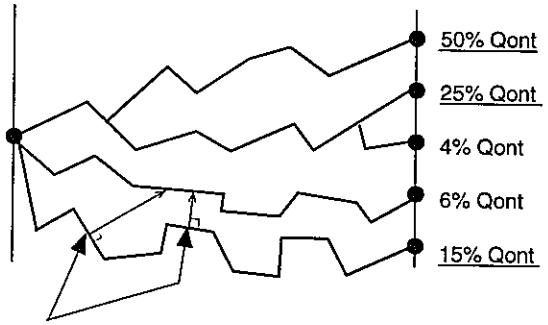

Pathway spacing as perpendicular distance to nearest PAWorks selected pipe

Aperture = $\frac{\text{Qweighted}}{K_i \text{ Wweighted}}$

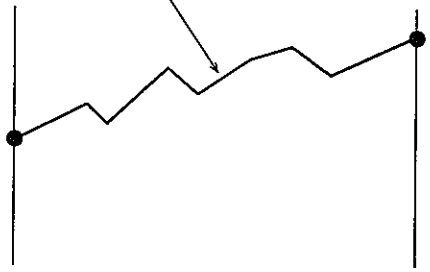

Representative pathway creating using
(1) all representative pathways;
(2) pathways with 90% of flux
(only underlined PAW pathways)

FIGURE **2-12**
ASSUMPTIONS FOR CRYSTAL INPUT
PNC/H8

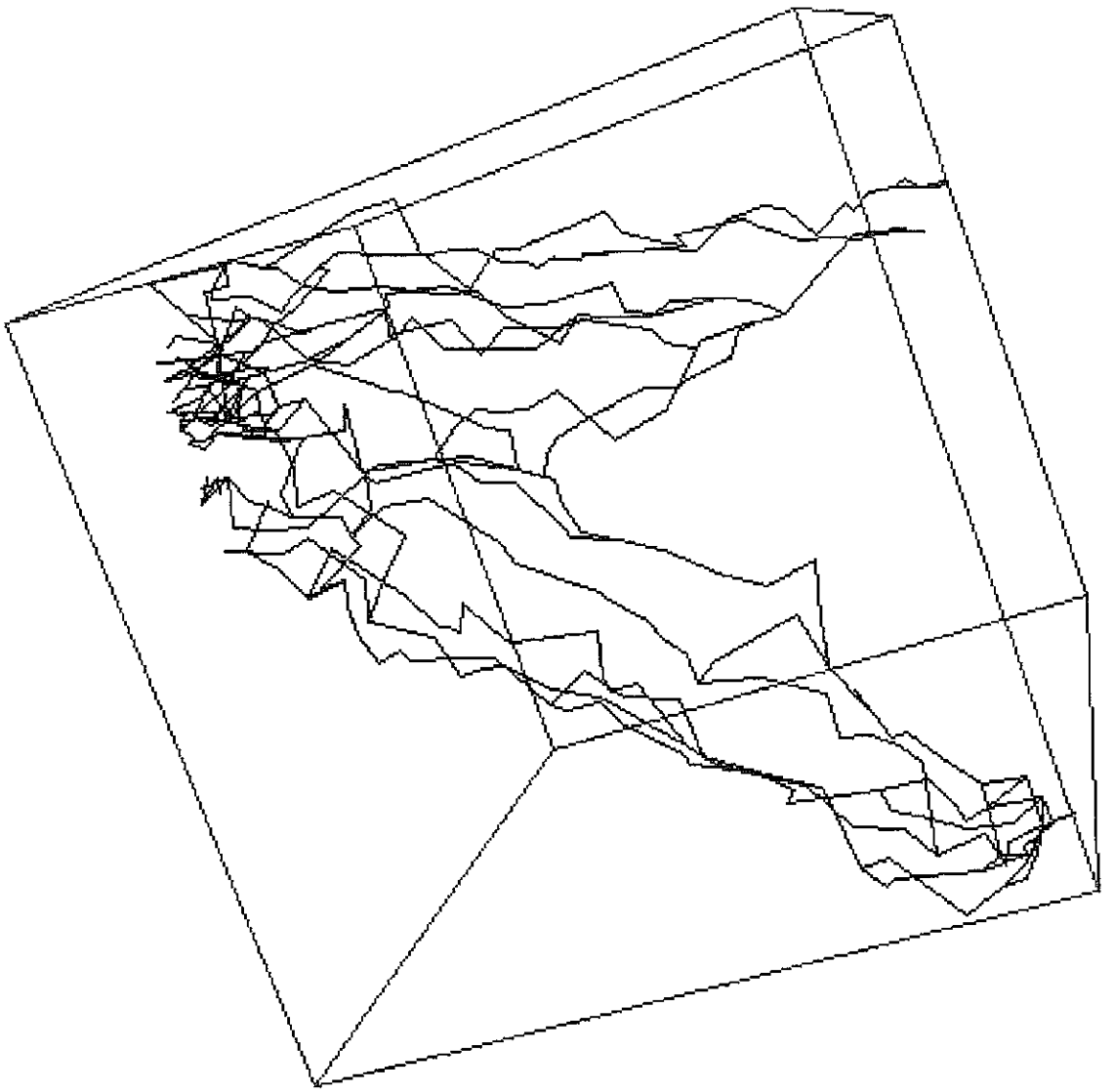

FIGURE **2-13**
PAWorks PATHWAYS FOR CRYSTAL
PNC/H8

PROJECT NO. 923 1089.800 DRAWING NO. 73119b DATE 5/21/98 DRAWN BY EA

Golder Associates

2.4.4 PAWorks Performance Enhancements

Previous versions of PAWorks suffered from several performance problems and accuracy limitations related to pipe generation. The performance problems arise in large (>1000 fracture) cases, due to the use of a direct flow solver, rather than the pre-conditioned solver used in MAFIC. The accuracy problems are described in the HY-7 Progress Report (Dershowitz et al., 1996). During HY-8, the performance and accuracy of the pipe generation and flow solver were significantly improved. Test cases have been run on the order of 10^5 fractures. Performance improvements are as follows:

- improvements to the efficiency of the pipe generation algorithm
- improvements to the efficiency of the approximate head solution in MAFIC1D
- improvements to the efficiency of adjacency list generation in PAWorks

2.4.5 PAWorks Verification

PAWorks requires a series of calculations to describe the geometry and properties of the fracture network and calculate pathways. Each of these algorithms is verified separately in the eight verification cases defined below.

- Case 1: Verification of the algorithm for calculating fracture intersections,
- Case 2: Verification of the algorithm for defining pipes based on fracture intersections,
- Case 3: Verification of the algorithm for calculating heads based on linear interpolation,
- Case 4: Verification of the algorithm for calculating heads based on the finite element method,
- Case 5: Verification of the algorithm for calculating heads based on MAFIC output files,
- Case 6: Verification of the depth-first algorithm for identifying pathways,

- Case 7: Verification of the breadth-first algorithm for identifying pathways, and

- Case 8: Verification of the algorithms for defining the properties of the pathways.

The results of the verification can be found in the PAWorks user documentation attached as Appendix E to this report.

2.5 Task 1.1.12: FracMan 1 MegaFrac Feature

Previous versions of FracMan have used integer*2 fracture indices, and have therefore been limited to 32,768 fractures. During HY-8, FracWorks Version 2.6 was implemented with the ability to handle up to approximately 16 million fractures in a single simulation. This required extensive changes to the FracWorks code, and revision to the fracture file format. The revised .FAB file format can be used for both decimal and "babylonian" data. The file format is presented in Table 2-14.

Table 2-14 .FAB File Format

```
.FAB files contains three data objects: Format, Properties,
and Fracture data.  All text is case-insensitive in a .FAB file.
Each data object begins with the
key word "BEGIN" followed by the object name.  The data block
ends with the keyword "END".

(1) Format :

The format data object contains five items:

  Format = either "Babylonian" or "Ascii"
  Scale =  FMeter value in meters.
  No_Fractures = total # of fractures
  No_Nodes =     total # of nodes excluding fracture normal vectors
  No_Properties =   # of fracture properties associated with each fracture

(1A). Example:

BEGIN FORMAT
  Format = Ascii
  Scale =    125.
  No_Fractures =       93
  No_Nodes =          563
  No_Properties =       3
END


(2) Properties

     Each property definition starts with "Prop#", where # is an integer index.
     The  data type is specified in a parenthesize, can be
     real, Integer, or percentage.  The memory size of each data that will
     be allocated in the program is specified in bytes
     followed by the character "*".  For example, (Real*4) represents
     four-byte real number.  The property name is specified
     inside a pair of double-quotes.


(2A). Example:

BEGIN Properties
  Prop1  = (Real*4)        "Transmissivity"
  Prop2  = (Real*4)        "Storativity"
  Prop3  = (Real*4)        "Frac Thickness"
  Prop4  = (Percentage*4)  "Iron Oxide"
  Prop5  = (Percentage*4)  "Permeability"
END Properties


(3) Fracture data:

The beginning of this data block is "BEGIN Fracture".  Each fracture
is defined by (NSIDES+2) consecutive lines, where NSIDES is the number of sides of
the polygonal fracture.

The fracture data in an ascii file (Format = Ascii) is free format. Each
data field is separated by one or more blank spaces.  For the Babylonian
format (Format = Babylonian) the format is fixed: a real number takes
5 characters (5C), a long integer takes 4 characters (4C) and
one-byte integer occupies one character (1C) such as NSIDES.

(3A). Babylonian Fracture Data:

The following show the contents of a Babylonian fracture data block:

Line 1:   NSIDES, NSET, Prop1,Prop2,Prop....,Prop#    (1C4C5C5C....5C)

          where, NSET is the number of set,
          Prop#, #=1, No_Properties are the property values.

Line 2:   X-Coord., Y-Coord, Z-Coord    (5C5C5C)
```

```
          The coordinates of NODE 1 in meters

Line 3:   X-Coord., Y-Coord, Z-Coord    (5C5C5C)
          The coordinates of NODE 2 in meters
:::::
:::::
Line NSIDE+1:   X-Coord., Y-Coord, Z-Coord    (5C5C5C)
          The coordinates of the last NODE on this fracture.

Line NSIDE+2:   X-Coord., Y-Coord, Z-Coord    (5C5C5C)
          The fracture orientation, a unit vector, normal to frac. plane.

Example:

600017T29JaHFOJfFv5I       ! NSIDES=6,NSET=1,PROP1=6.109E-07,PROP2=8.278E-07,PROP3=2.018E-
08
1XNMo1hN9o1GNbO            ! X=-1.198300E+02,Y=-7.781917E+01,Z=1.028197E+02
1XEyo1pRJo1bKnO
1w3do1xohoVhjJN
14z7o1wOco1dP6O
14Ilo1oJAo1IRSO
1wlFo1hf5o1XmVO


(3B). ASCII Fracture Data:

Line 1:   NF, NSIDES, NSET, Prop1,Prop2,Prop....,Prop#

          where, NF is the number of fracture.

Line 2:   N, X-Coord., Y-Coord, Z-Coord

          where, N is the nodal index.  In this line,
          N is 1 to indicate the first node of the fracture
          The coordinates of NODE 1 in meters

Line 3:   N, X-Coord., Y-Coord, Z-Coord
          where, N=2 to indicate the second node of the fracture
          The coordinates of NODE 2 in meters
:::::
:::::
Line NSIDE+1:   N, X-Coord., Y-Coord, Z-Coord
          The coordinates of the last NODE on this fracture.

Line NSIDE+2:   N, X-Coord., Y-Coord, Z-Coord    (5C5C5C)
          where, N=0 to indicate the fracture orientation,
          a unit vector, normal to frac. plane.

Example,

     1   6   1   6.109E-07   8.278E-07   2.018E-08
     1  -1.198300E+02  -7.781917E+01   1.028197E+02
     2  -1.196761E+02  -8.589584E+01   7.177306E+01
     3  -9.205361E+01  -9.340472E+01   5.728882E+01
     4  -6.458528E+01  -9.283667E+01   7.385167E+01
     5  -6.473917E+01  -8.476000E+01   1.048983E+02
     6  -9.236139E+01  -7.725139E+01   1.193825E+02
     0  -1.303074E-01  -9.596937E-01   2.490140E-01
```

The number of fractures generated by FracWorks Version 2.6 is limited by the amount of space available on the caching directory device. Approximately 1 Megabyte is required per 4000 fractures. Thus, 200,000 fractures requires 50 Megabytes of available space on the caching directory device.

Table 2-15 presents parameters for a test problem requiring generation of approximately 200,000 fractures, based on the Doe et al (1996) Kamaishi rock block model, without truncation based on fracture transmissivity. A total of 203,688 fractures were generated in 5 minutes on Pentium/100 MHz PC.

The statistics for the fracture population are provided in Figure 2-14a. Borehole sampling statistics for a vertical borehole are provided in Figure 2-14b.

As part of this task, MeshMaster Version 1.4 and EdMesh 1.5 were also updated to work with the .FAB file format.

2.6 Task 1.2.1: FracSize Tunnel Size Derivation

During HY-8, a new Windows 95 program "FracSize" was implemented to provide for automatic, optimized calculation of fracture size from fracture trace measurements on tunnel walls (multi-plane traces). This program provides an extension to previous FracSize algorithms which derived fracture size estimates based on fracture trace measurements on a single plane.

Table 2-15 MegaFrac Test Case

Property	Set 1	Source
Location Model	Levy-Lee	Spatial fracture location analysis using data from boreholes and drifts
Exponent	2.4	
Min Step Size	8 m	Simulated KD-90 trace maps
Generation Mode	Surface Points	
No. Fracture Sides	6	
Generation Region	Box	
Center	0, 0, 0 m	
Dimensions	225, 225, 225 m	
Orientation Model	Bootstrap from KD-90 allwet.ors	ISIS analysis of orientation data from boreholes and drifts
Dispersion K	200	
Size (Radius) Distribution	Truncated LogNormal	Heisei-4 analysis of KD-90 censoring statistics
Mean, StdDev.	7, 1.25 m	
Lower Bound	none	
Upper Bound	25 m	*(Note: Truncates less than 0.1% of the distribution)*
Elongation	none	
Transmissivity Distrib.	Truncated LogNormal	KH-5 interval transmissivities
Mean, StdDev.	1.1×10^{-7}, 3.85×10^{-4} m^2/s	
Lower Bound	10^{-12} m^2/s	
Upper Bound	none	
Storativity	$= 5.0 \times 10^{-5} \times T^{1/2}$	Empirical relationship (Doe, 1995); calibration
P_{32} Fracture Intensity	2.803 m^2/m^3	P_{10} conductive fracture frequency in boreholes KH-4 through 18

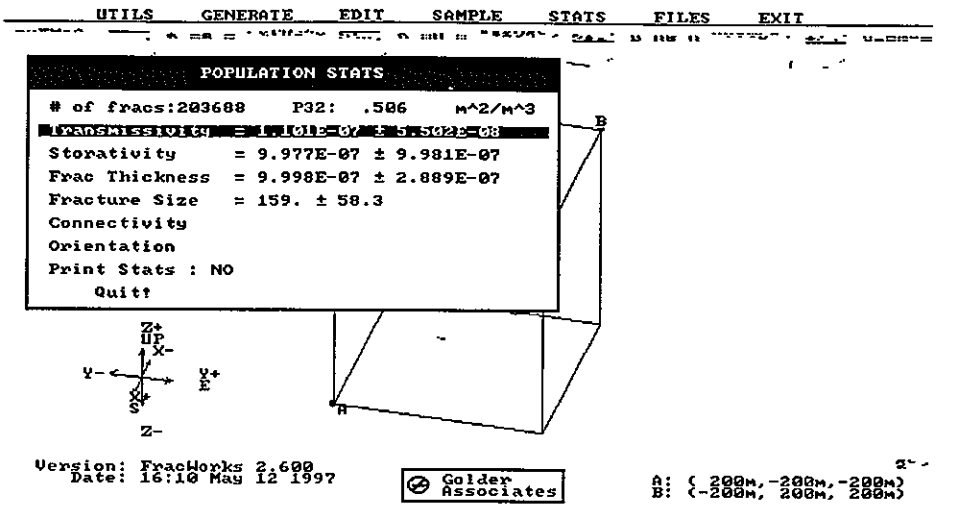

(a) Fracture population statistics

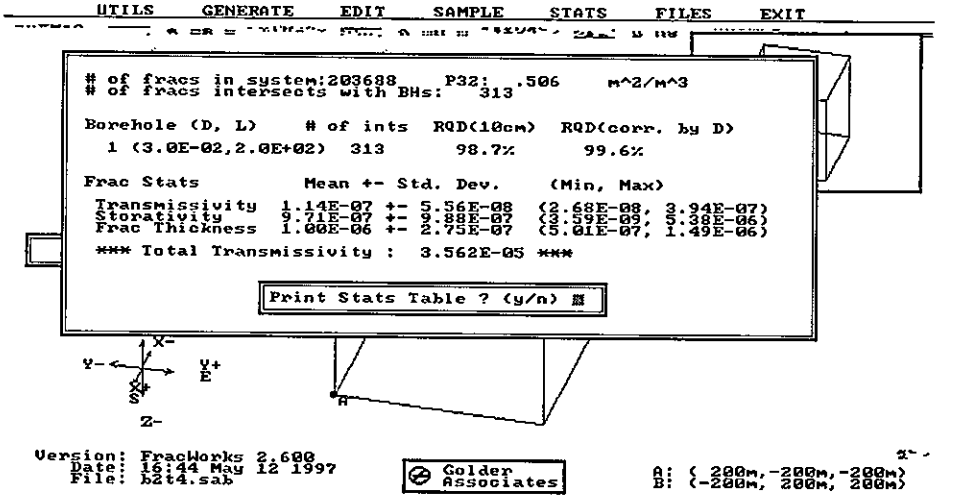

(b) Borehole Sampling Statistics

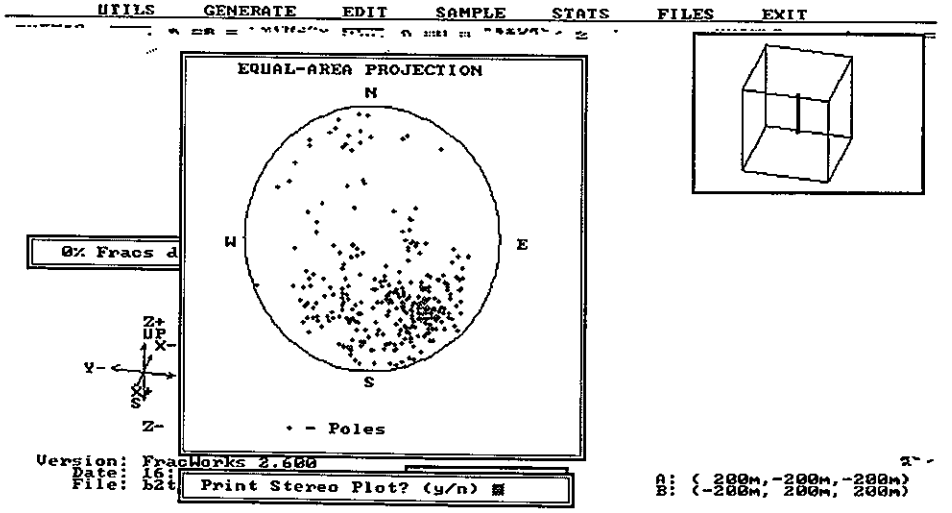

(c) Vertical Borehole

FIGURE **2-14**
FRACTURE POPULATION STATISTICS
PNC/H8

2.6.1 FracSize Algorithm

The algorithm for HY-8 FracSize is based on the approach of LaPointe et al. (1993). The algorithm is illustrated in Figure 2-15.

The input for the FracSize algorithm consists of a file providing the geometry of the tunnel on which the data was collected, in .SAB file format (Table 2-4). and a .DAB file containing the fracture trace lengths and the percentages of length on each of the tunnel panels. The .DAB file can also contain the fracture orientations, if available. The format of the .DAB file is provided in Table 2-16.

If it is desired to calculate fracture size separately by site, the fractures in the .FAB file should be separated into separate .DAB files by set using for example, FracSys/ISIS.

Based on the fracture trace information in the .DAB file, FracSize calculates the following fracture trace statistics:

1. Trace length mean, standard deviation, skewness, and kurtosis;
2. Percentage of fractures spanning one panel, two panels, etc. up to the number of panels defined on the tunnel; and
3. The fracture trace intensity (P_{21}) on the mapped panels.

The user then specifies the assumed fracture population orientation (Fisher, Bingham, bootstrap, etc.) and size distribution (log normal, power law, exponential, etc.). The user must also specify the minimum fracture trace length mapped.

The following parameters are required for analysis control:

4. The minimum fracture trace length mapped;
5. The search space maximum, minimum, and step size for fracture radius mean and standard deviation;
6. The number of realizations to be combined to calculate the trace length and panel percentage statistics for a given fracture radius assumption;

Table 2-16 .DAB File Format for FracSize Analysis

```
#*****
# FILE: FSIZE.dab
# DATE: Mar.-1997
# BY:   Glori Lee
#      Golder Associates
#
# Sampling structures file format
#*****


BEGIN survey_ids

       no_surveys = 1

       #Specify survey names:
              ID1 = "circular-tunnels" "Tunnel_A"
END


#-----
#circular-tunnels
#-----
BEGIN circular-tunnel
       #Specifiy generic properties
              name = "Tunnel_A"

       #Specify geometric properties

              #                      x   y   z
              #-----                --- --- ---
              origin =   40.     0.       0.
              axis_trend = 0
              axis_plunge = 0.0

              length =  80.
              radius =  10.
              panels =  6

END


BEGIN traces
       #Specifiy generic properties
              name = "fsize.ors"

       #Specify colmn name:
              Col1 = trend
              Col2 = plunge
              Col3 = survey_id
              Col4 = trace_length
              Col5 = No_panels

       BEGIN data
       # Col1 Col2   Col3   Col4   Col5
       #trend plunge s_ID   length no_panels
        211     29     1    3.96   1
        224     34     1    7.05   2
        201     13     1    2.22   3
        221     40     1    7.95   1
        252     37     1    4.00   1
        221     35     1    1.13   2
        220     10     1    1.78   3
        208     41     1    3.70   1
```

```
        10      20      1   3.48   4
       344      38      1   2.29   5
       341      36      1   4.73   1
       314      31      1   7.73   1
      END data
END


BEGIN traceplane
      #Specifiy generic properties
            name = "ABC"

      #Specify geometric properties
            #origin      x   y  z
            #------      --  --  --
            origin = 290  1000 300

            #define scan vector
            scan_trend   = 90.
            scan_plunge  = 90.
            scan_length = 100.

            #define transverse vector
            tran_trend   = 180.
            tran_plunge  =  00.
            tran_width   = 100.

END

######
# Define Sampling structures:
######

BEGIN traceplane
      #Specifiy generic properties
            name = "Tracy"

      #Specify geometric properties
            #origin      x   y  z
            #------      --  --  --
            origin = 345   1083      353

            #define scan vector
            scan_trend   = 90.
            scan_plunge  =  0.
            scan_length = 100.

            #define transverse vector
            tran_trend   = 180.
            tran_plunge  =  0.
            tran_width   = 100.

END


#----
#multi-planes
#----
BEGIN multi-plane

      name   = "Z-shape"

      panels =  3

      BEGIN plane
            origin = 50  -50  0
```

```
            #define scan vector
            scan_trend    = 90.
            scan_plunge   =  0.
            scan_length = 100.

            #define transverse vector
            tran_trend    = 0.
            tran_plunge   = 90.
            tran_width    = 40
      END

      BEGIN plane
            origin = 50   50   0

            #define scan vector
            scan_trend    = 315.
            scan_plunge   = 0
            scan_length = 75.

            #define transverse vector
            tran_trend    = 180.
            tran_plunge   =  0.
            tran_width    = 40
      END

      BEGIN plane
            origin = -20.7   -20.7   0

            #define scan vector
            scan_trend    = 270.
            scan_plunge   =  0.
            scan_length = 60.

            #define transverse vector
            tran_trend    =   0.
            tran_plunge   =  90.
            tran_width    = 40
      END
END

#-----
#horseshoe-tunnels
#-----
BEGIN horseshoe_tunnel
      #Specifiy generic properties
            name          = "Mr_Ed"

      #Specify geometric properties
            #                              x   y   z
            #-----                     --- --- ---
            origin =                  20.   20.   20.
            axis   =                  0.    1.    0.
            trans_axis = 1.           0.    0.

            width         = 40.
            length        = 60.
            wall_height   = 30.
            radius        = 30.
            panels        = 4

END
```

7. The type of search (single point, grid search, conjugate gradient search, or simulated annealing search);
8. The search criteria (Kolmogorov-Smirnov or Chi-Squared Statistic); and
9. The maximum number of iterations, parameter temperature, and jumping scale (for a simulated annealing search), or the damping factor (for a conjugate gradient search).

Based on the parameters provided, FracSize then generates stochastic fracture realizations, and calculates the trace statistics and panel percentages for intersections with the specified traceplane or tunnel. In a change from previous versions of FracSys/FracSize, FracSize now generates fractures in each realization up to the calculated value of intensity P_{21}. This ensures that the standard deviation and panel percentage statistics of simulations and field measurements are strictly comparable.

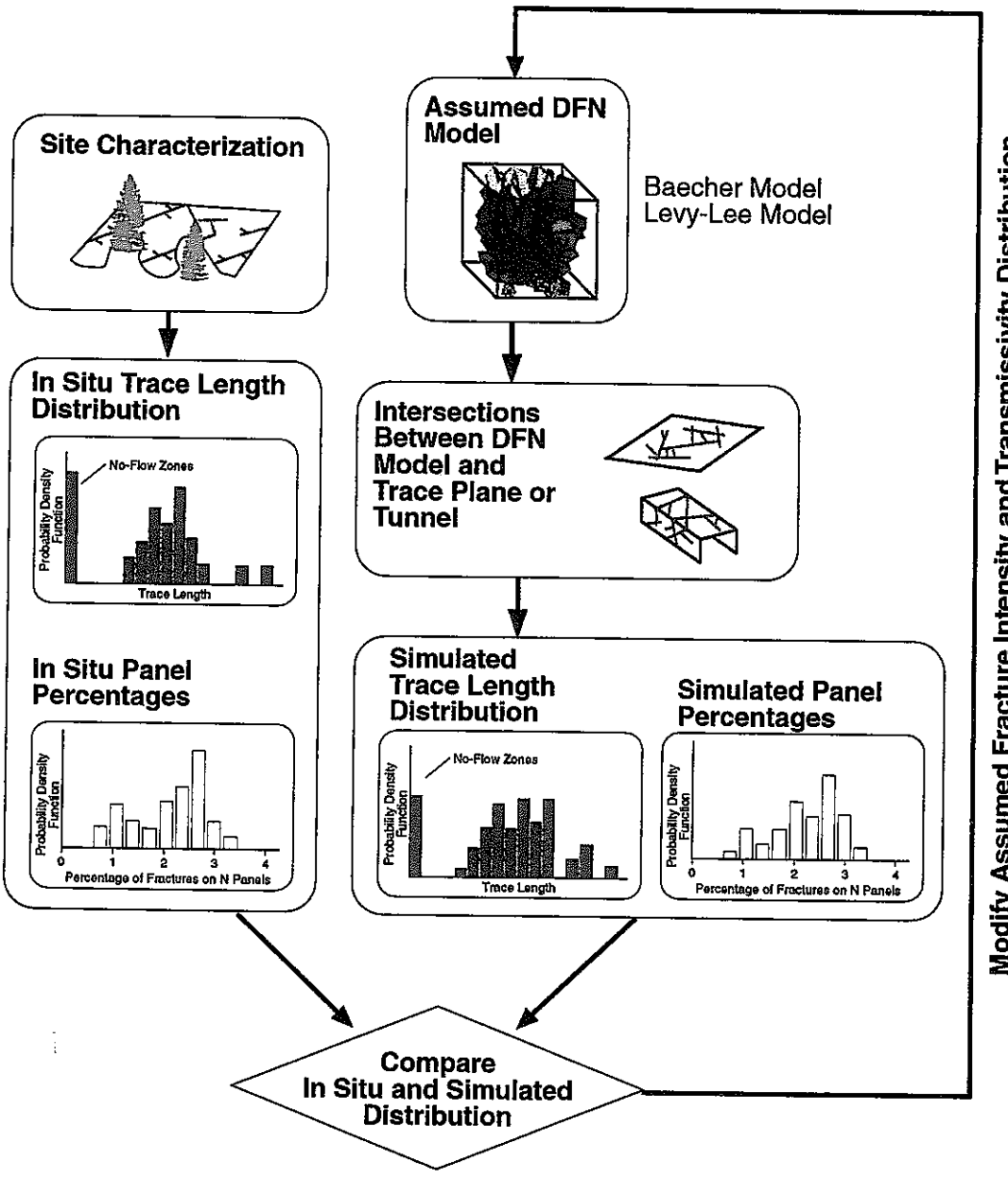

FIGURE **2-15**
FracSize ALGORITHM
PNC/H8

PROJECT NO. 923 1089.800 DRAWING NO. 73121 DATE 5/9/97 DRAWN BY EA

Golder Associates

2.6.2 FracSize User Interface

The FracSize user interface is illustrated in Figures 2-16 through 2-18. The user interface complies with Windows 95 user interface standards. To execute FracSize, select the FracSize icon, and double click with the mouse. The operation of the individual FracSize menu items are described in Section 2.6.3 below. The general procedure for analysis is summarized in Table 2-17.

Navigation through FracSize is done using Microsoft windows mouse conventions. In general, the left hand mouse button is used for making selections.

2.6.3 Command Summary

2.6.3.1 File Menu

New: Begin a new analysis, without closing the current analysis. Opens a window for the new analysis.

Open: Open fracture trace (.DAB format) and sampling object (.SAB) files. Uses the standard Microsoft Windows File Open menu syntax and assumptions.

Close: Close the current active analysis and all windows related to that analysis.

Save As: Saves statistical analysis .STS and graphical display .JPG files for current analysis.

Exit: Exit FracSize. Warns the user if statistical reports have not been saved.

Table 2-17 FracSize Analysis Sequence

	Command	Action
1.		Collect fracture trace data and prepare fracture trace file in .DAB format.
2.	File/Open Fracture Trace*.FAB	Load the *.DAB format fracture trace data file, which incorporates the sampling structure .SAB data.
2a.	(optional) File/Open Sampling Files .SAB	Load a sampling .SAB object containing geometries for trace mapping surfaces (if not contained in .DAB file)
3.	Edit/Analysis Structures	Define and modify the analysis parameters: - Fracture Assumptions - Trace Mapping Assumptions - Search Assumptions
3a.	Edit/Sampling Structures	Modify the geometry of the boreholes and analysis regions as necessary
4.	Analyses/Single Iteration Analyses/Grid Search Analyses/Conjugate Gradient Analyses/Simulated Analyzing Search	Realize the fracture populations and calculate the fracture trace statistics and panel percentages. Histogram pdf and cdf displays and statistical results will be displayed
5.	File/Save As	Save .STS file containing selected statistical results and assumptions
6.	File/Save As	Save .JPG file containing selected graphical displays
7.	File/Print	Print selected analysis statistics and graphical displays
8.	File/Exit	Leave FracSize

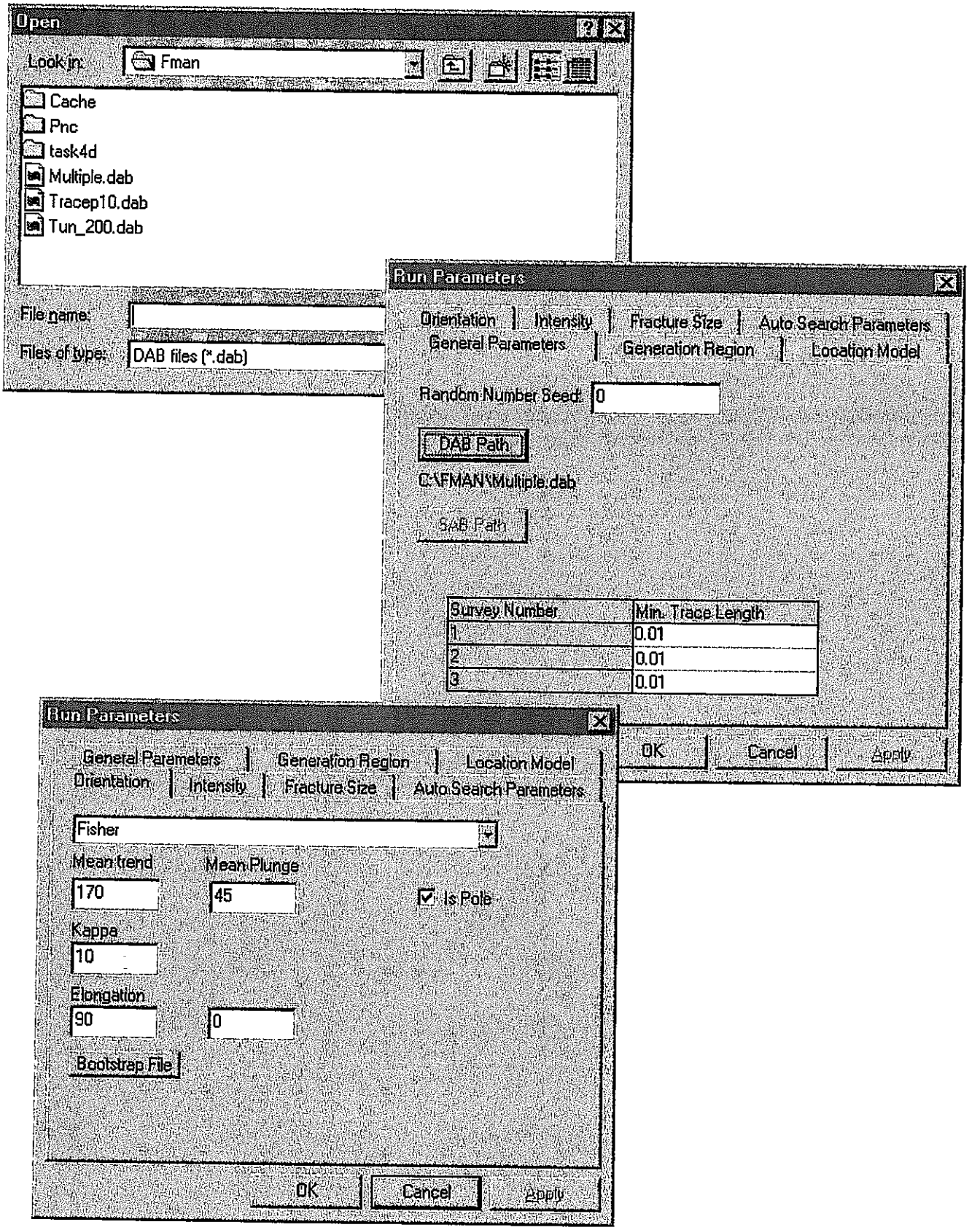

FIGURE **2-16**
FracSize USER INTERFACE
PNC/H8

PROJECT NO. 923 1089.800 DRAWING NO. 73122 DATE 5/13/97 DRAWN BY EA

Golder Associates

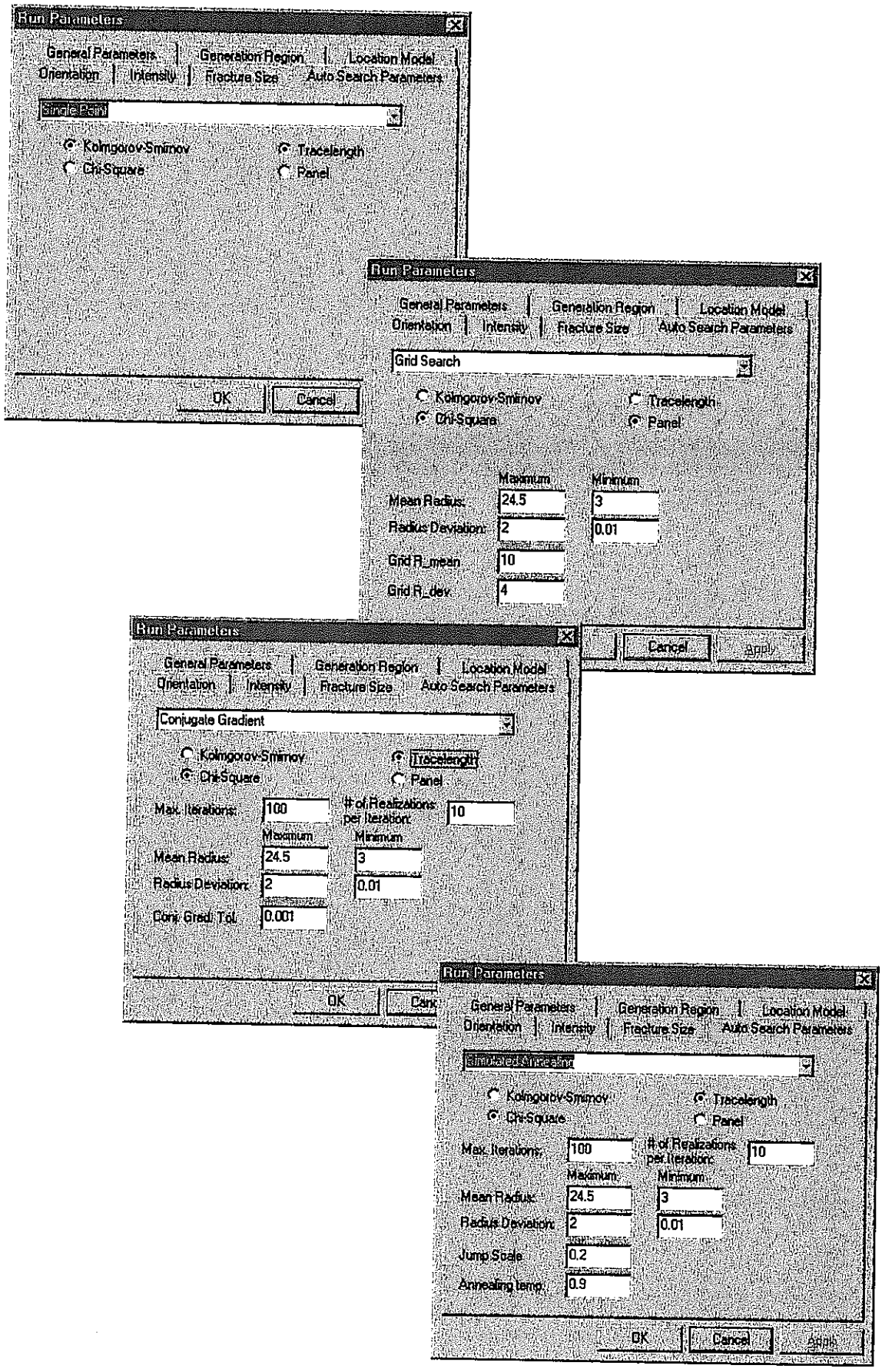

FIGURE **2-17**
FracSize SEARCH
PNC/H8

PROJECT NO. 923 1089.800 DRAWING NO. 73123 DATE 5/13/97 DRAWN BY EA

Golder Associates

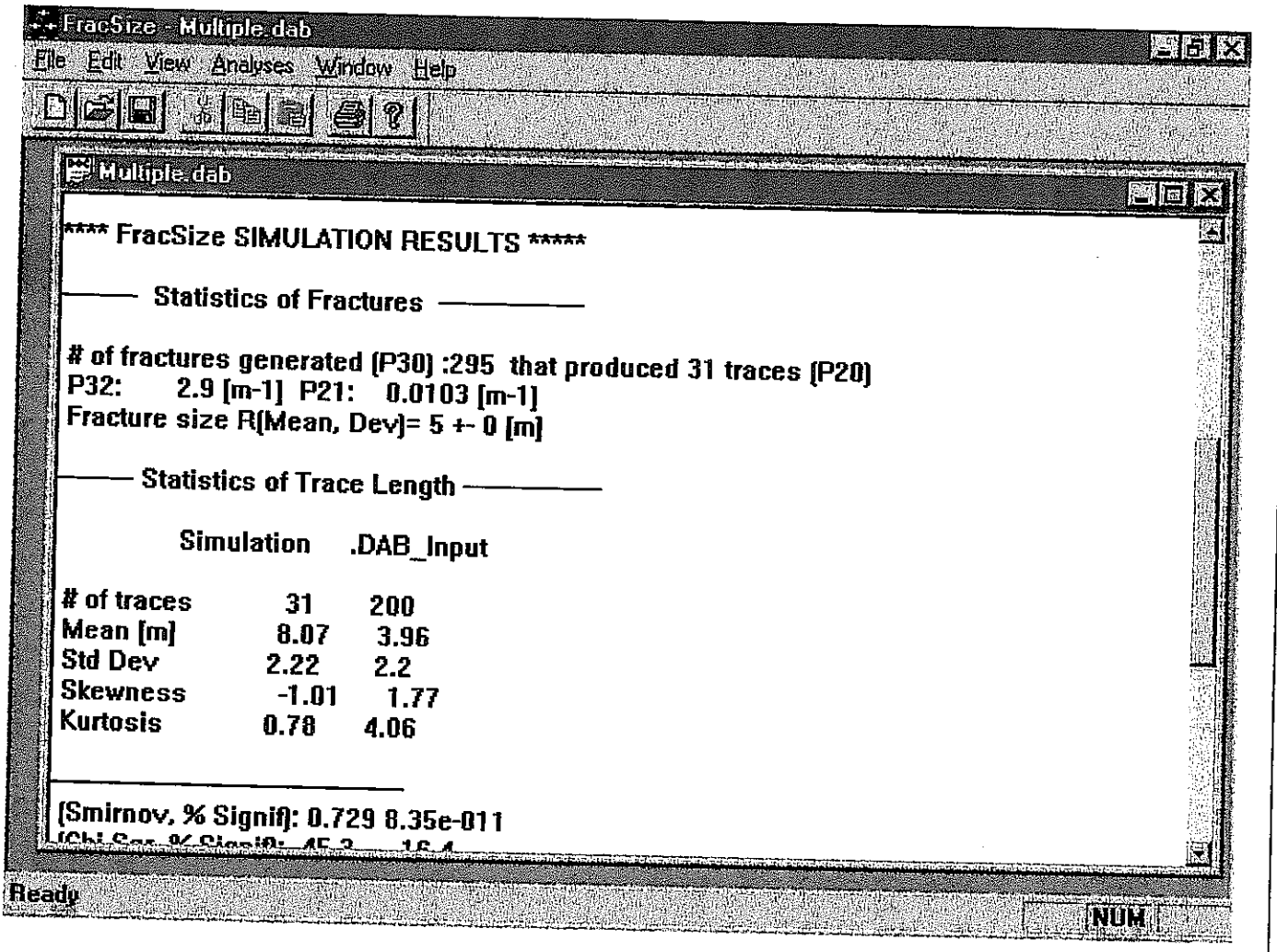

FIGURE **2-18**
FracSize OUTPUT
PNC/H8

2.6.3.2 Edit Menu

Undo: Not currently implemented

Cut: Not currently implemented

Copy: Not currently implemented

Paste: Not currently implemented

Analysis: Select parameters for the fracture geometric assumptions, traceplane sampling, and analysis specification. Each Analysis is assigned a unique name, and is assigned a serial number when "Analysis/Simulate" is selected. Analysis includes the following tabs:

General Parameters: Random number seed and number of realizations to be averaged for each search step

Generation Region: Size of region for fracture generations as either a CDF value for the distance from the traceplane(s) or the dimensions of a region centered on the traceplane(s)

Location Model: Baecher or Levy-Lee spatial models and model parameters

Orientation: Assumed fracture orientation distribution (Bootstrap, Fisher, Bivariate Fisher, Bingham, Bivariate normal, or constant) and associated parameters

Intensity: Intensity for fracture to be generated as either number of traces or trace intensity, P_{21}

Fracture Size: Size distribution assumption (Exponential, Normal, Log Normal, or Power Law/Pareto) and associated parameters

Autosearch: Provides the specifications for the search: (single value, grid, simulated annealing, or conjugate gradient.

Sampling Structures: Edit the currently active sampling program.

Add: Add an additional exploration object. A submenu provides the option to select the type of tunnel object.

Remove: Remove the selected object

+ : Expand the current selection to display specific objects

- : Collapse the display to show only object types

Edit: Double click on a selected object to edit its properties.

When editing or adding an object, three property tabs are available. The *General* tab always provides the object name. The *Geometry* tab requires different input for each object type. . The ***Boundary Conditions*** tab is not active for FracSize.

2.6.3.3 View Menu

Toolbar: Display or hide the toolbar display

Statusbar: Display or hide the line providing status information.

2.6.3.4 Analysis Menu

Single Iteration: Generate fracture realizations according to specification provide and calculate statistics

Grid Search: Carry out a grid search and report results

Conjugate Gradient Search: Carry our a conjugate gradient search and report results

Simulated Annealing Search: Carry out a simulated annealing search and report results

2.6.3.5 Windows Menu

New Window: Open a new window for the current analysis

Cascade: Cascade currently open windows

Tile: Tile currently open windows

Arrange Icons: Neatly arrange icons for minimized windows

Close: Close the current window

Close All: Close all the windows in the current analysis.

2.6.3.6 Help Menu

Help Index: Not currently implemented

Using Help: Not currently implemented

About FracSize: FracSize QA, copyright, and license information.

2.6.4 FracSize Walk-through

This section describes an example user session with FracSize.

FracSize is run by clicking on the "FracSize" icon. Under the Files menu, the user should use the mouse to highlight the data object (.DAB) files to be processed. If no traceplane geometry data is included in the .DAB file, the user will also be prompted for a .SAB file. The formats for the .DAB and .SAB files are described in Tables 2-19 and 2-4 above.

Returning to the main menu, the user next selects Edit, to define the assumptions to be used in the FracSize simulation and analysis. Remember that FracSize is actually carrying out discrete fracture stochastic simulations.

Once these have been set, the user can continue to Analysis to carry out the actual FracSize simulation. Each simulation is assigned a unique number, relating the values set under Edit/Analysis, and the windows displaying statistical and graphical results. To carry out additional analyses, return to the Edit/Analysis window and modify the parameters. Use the update button on the toolbar to place the results form the previous search into the fracture radius assumption fields for the next analysis.

To choose alternative views of the results, the user should select View from the main menu. From this menu, the user can select the results.

2.6.5 FracSize Verification

Two examples of software verification of FracSize are show in Figures 2-19 and 2-20. The probability distribution functions qualitatively compare the tracelength data and simulated data. In the statistics window the best fit model is displayed as well as the two goodness of fit measures (Kolmogorov-Smirnov or Chi-Squared Statistic). Table 2-18 lists the other verification case for FracSize.

Table 2-18 FracSize Verification Cases

Verification Case	Size Distribution Model	Mean	Standard Deviation	Sampling Objects(s)
1.1: STP_Const	Constant	3	0	1 2x180 TP
1.2: STP_Unif	Uniform	2.5	2	1 2x180 TP
1.3: STP_Norm	Normal	8	4	1 2x180 TP
1.4: STP_LogN	LogNormal	4	2	1 2x180 TP
1.5: STP_Expo	Exponential	3	-	1 2x180 TP
1.6: STP_Power	Power Law	0.5 (min)	2.4 (D)	1 2x180 TP
2.1: MTP_LogN	LogNormal	4	2	3 2x180 TPs (tunnel)
2.2: MTP_Expo	Exponential	3	-	3 2x180 TPs (tunnel)
3.1: STP_SA	LogNormal	4	2	1 2x180 TP
3.1: STP_CG	LogNormal	4	2	1 2x180 TP

2.7 Task 1.2.5 Geostatistical Analysis: Borehole Location and 2D POCS

During HY-8, the geostatistical analysis features of FracSys were upgraded to include two additional features:

- Fractal and geostatistical analysis of fracture aperture based on 2-D surfaces, linear cross sections, and point measurements from co-planar boreholes, with capacity for up to 300,000 measurements and 1000 boreholes; and

Fracture intersections with boreholes (.DAB files), to derive fractal dimension, spherical, exponential, and power law variograms of fracture location.

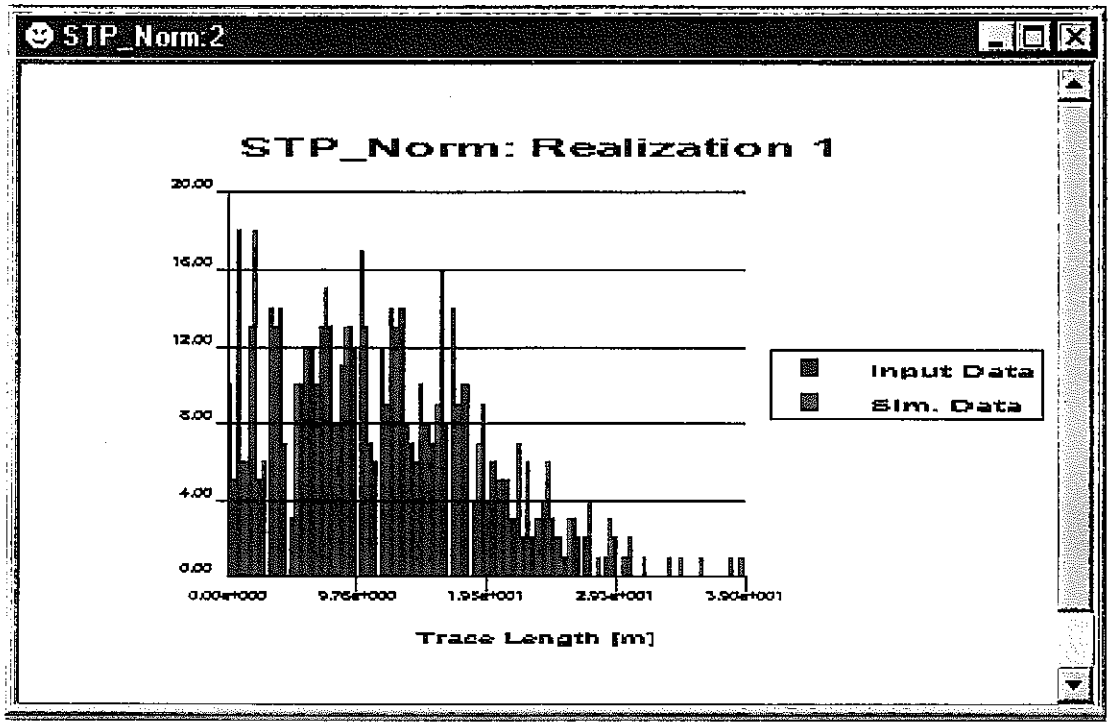

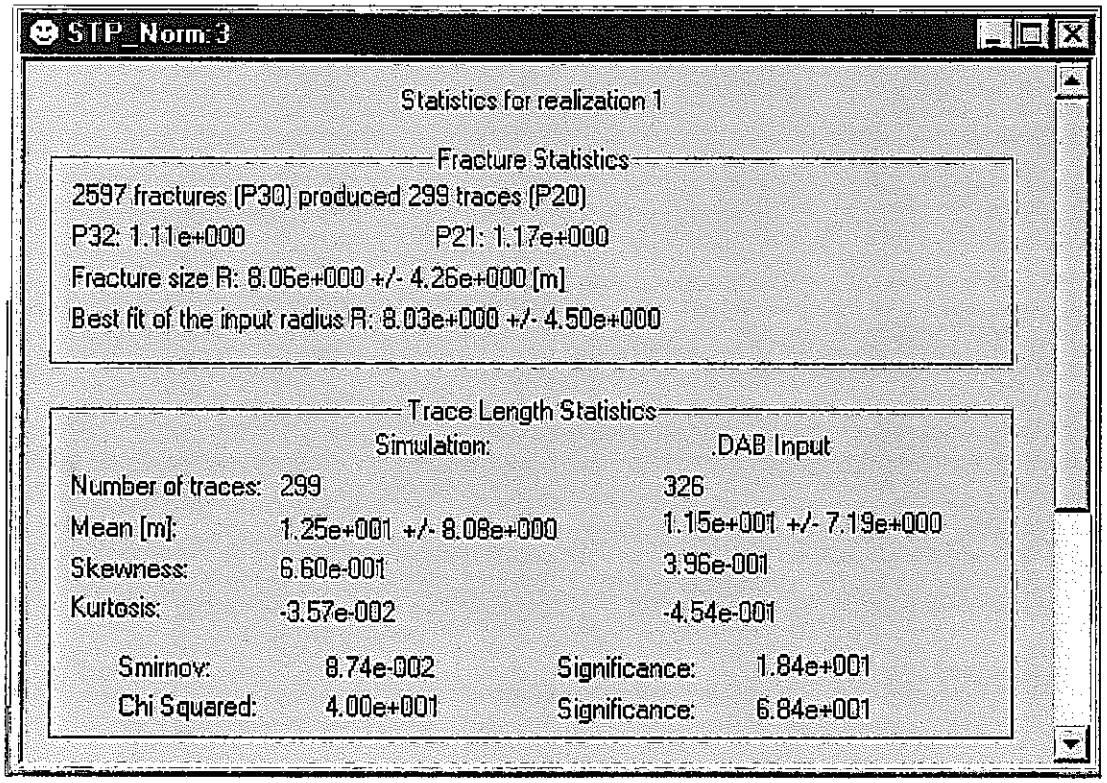

FIGURE **2-19**
FracSize VERIFICATION
EXAMPLE: NORMAL DISTRIBUTION,
MEAN = 8 M, STDEV = 4.0 M
PNC/H8

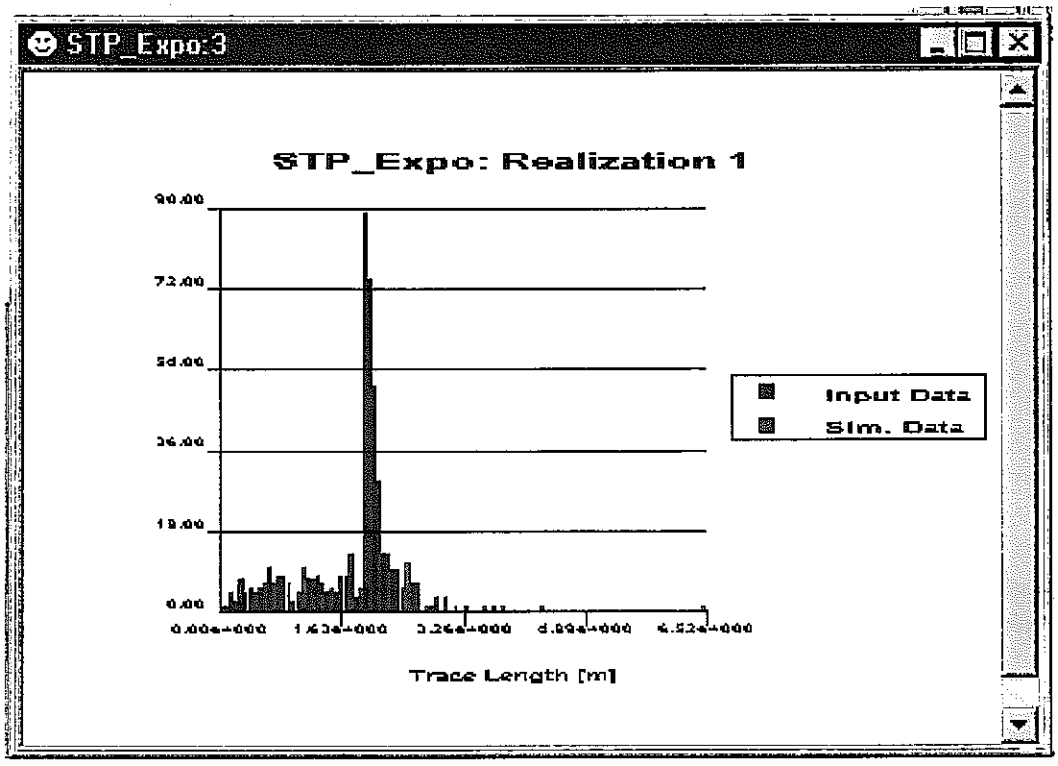

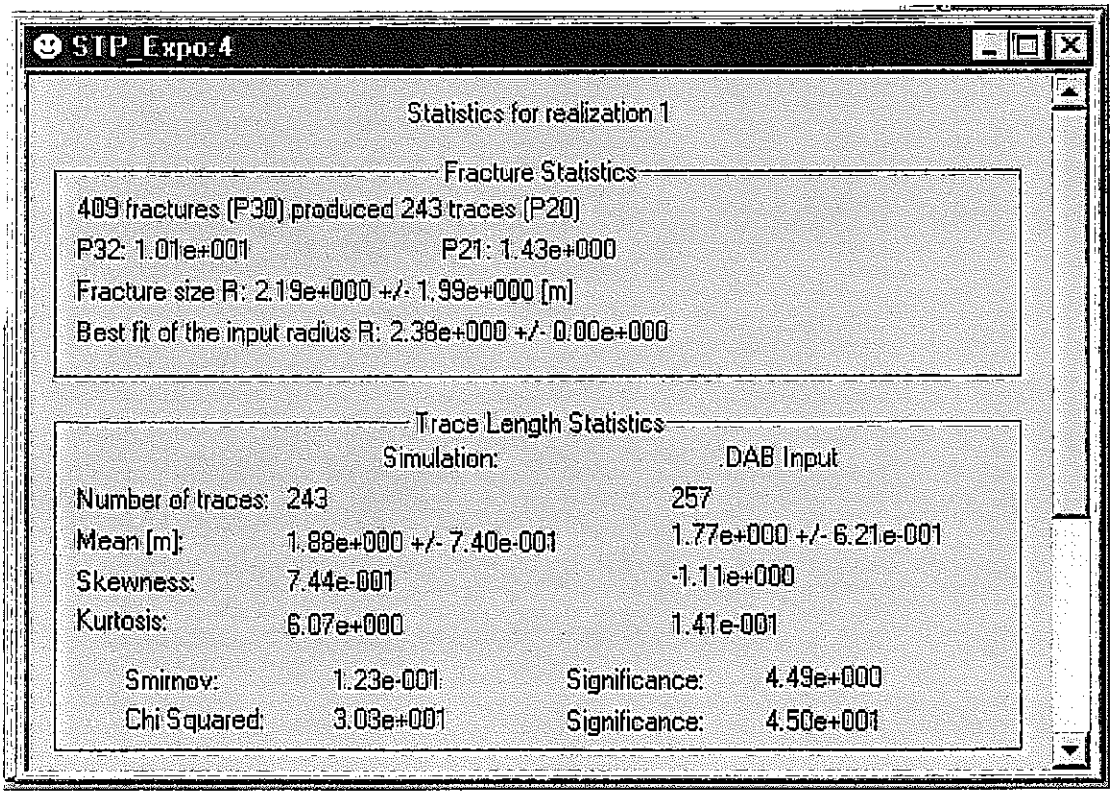

FIGURE **2-20**
FracSize VERIFICATION EXAMPLE: EXPONENTIAL DISTRIBUTION, MEAN = 3 M
PNC/H8

These additional features were implemented to facilitate the kinds of analysis carried out for evaluation of Kamaishi site data during HY-7 (Doe et al, 1997). The algorithms implemented are described in Sections 2.7.1 and 2.7.2. The program Fractal, which consolidates all of the geostatistical features of FracSys within a Windows 95 user environment is described in Section 2.7.3. Verification cases are presented in Section 2.7.4.

2.7.1 Algorithm for Analysis of 2-D Data

Variogram analysis is implemented to calculate the parameters of spherical and exponential correlation structures. The equations for these models are:

SPHERICAL MODEL: (Equation 2-2)

$$\gamma(h) = C\left(\frac{3h}{2\alpha} - \frac{h^3}{2\alpha^3}\right) \text{ for } h \leq \alpha$$

$$\gamma(h) = C \text{ for } h \geq \alpha$$

EXPONENTIAL MODEL: $$\gamma(h) = C\left(1 - e^{\frac{-h}{\alpha}}\right)$$ (Equation 2-3)

where

h is the lag distance,

α is the range or correlation length

C is the sill, and

γ**(h)** is the semivariance.

The variogram analysis implemented for up to 300,000 measurements are illustrated in Figure 2-21.

The analysis as implemented includes nested variograms,

$$\gamma(h) = a_1\gamma_1(h) + a_2\gamma_2(h) + a_3\gamma_3(h)$$ (Equation 2-4)

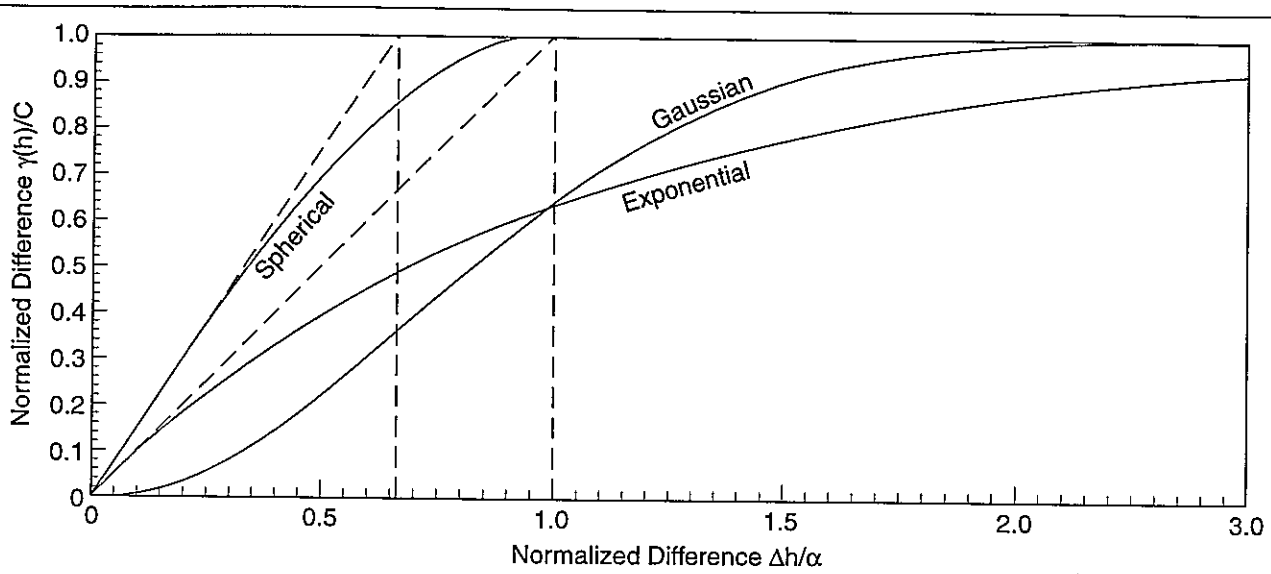

Δh = Lag distance between measurements

α = Range or correlation length

γ(h) = Semivariance

C = Variogram sill

(a) Standard Variograms

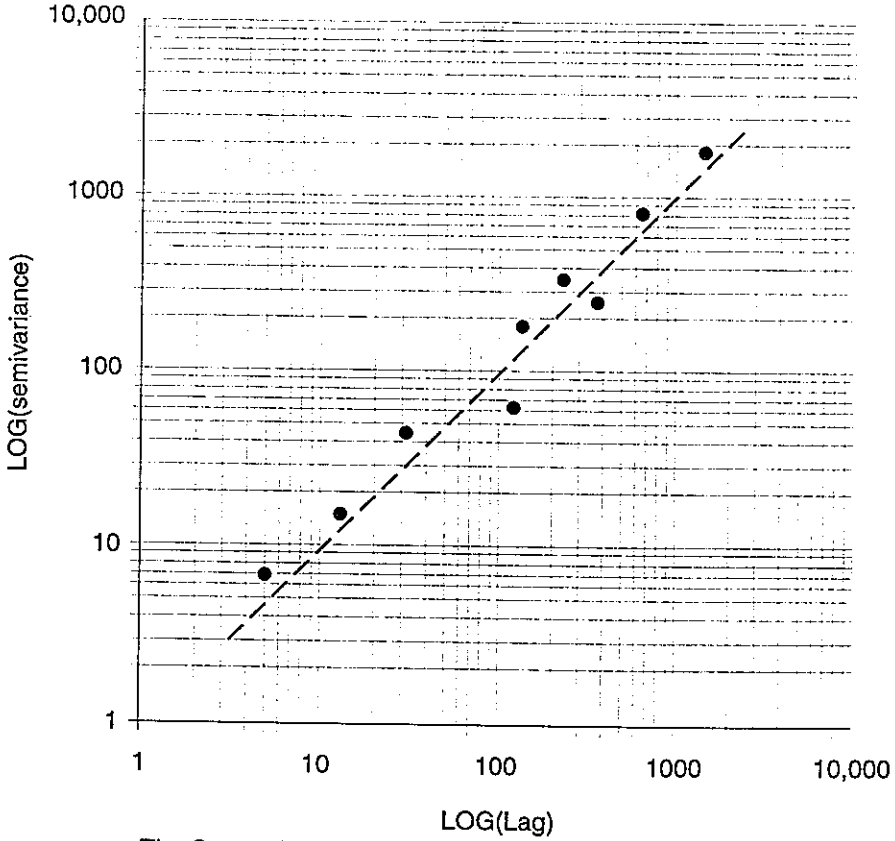

The Spectral Fractal Dimension (D_S) relates to the slope of the semivariogram (θ):

(b) Powerlaw Fractal Variograms

$$D_S = 2 - \frac{\theta}{2}$$

FIGURE **2-21**
GEOSTATISTICAL VARIOGRAMS
PNC/H8

2.7.2 Algorithm for Analysis of 1-D Data

Previous versions of PNC FracMan have provided spatial data analysis of 2-D trace data. However, for many sites, the best available data is distributed along boreholes or trace-lines, and spatial analyses of these features are therefore essential. The analyses implemented during HY-8 include:

- Box Fractal Analysis
- Levy-flight Analysis
- Power-law Fractal Analysis
- Spherical and Exponential Variogram Analysis

The Box fractal analysis is illustrated in Figure 2-22.

The box fractal dimension measures the scaling behavior of the distance between one fracture and the next one encountered. It is calculated by overlaying a series of boxes or intervals of constant length λ and counting the number of boxes that contain one or more conductive fractures (Figure 2-22). This calculation is repeated for a series of different interval lengths. The results are plotted on a logarithmic graph as the number of boxes containing fractures vs. the box size, as in Figure 2-22. If the fracture spacing is well described by a fractal Box model, then these points should be described by the equation:

$$N_{boxes}(\lambda) \propto \lambda^{-D} \qquad \text{(Equation 2-5)}$$

which plots as a straight line on logarithmic axes with slope D, the Box fractal dimension.

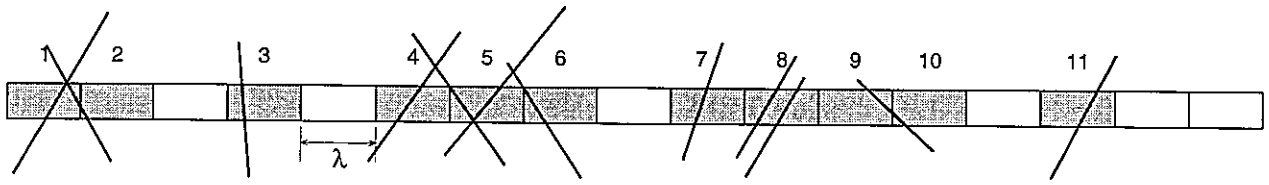

11 Filled Boxes

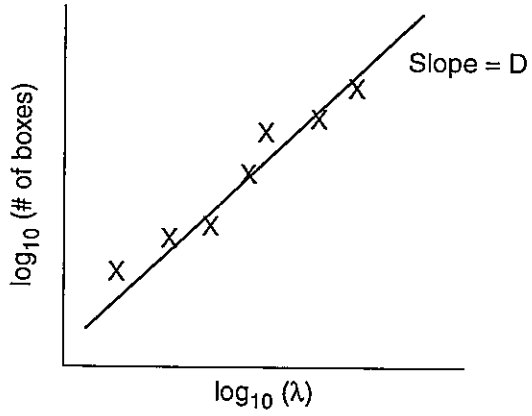

FIGURE **2-22**
BOX FRACTAL DIMENSION FROM BOREHOLE FRACTURE DATA
PNC/H8

PROJECT NO. 923 1089.800 DRAWING NO. 73128 DATE 5/8/97 DRAWN BY EA

Golder Associates

The Lévy flight fractal analysis is similar to the procedure used to calculate the Box fractal dimension. A series of boxes or intervals of a fixed length are overlaid on the core, and the *number* of conductive fractures in each interval that contains one or more fractures is recorded. This differs from the box dimension calculation in that, instead of counting *how many boxes contain fracturing*, the mass dimension estimates the *mass* or *amount* of fracturing in a box of a particular size. If the conductive fracture locations in a core or well log follow a Lévy flight model, then the number of fractures, $N(\lambda)$, found in an interval of size λ is expressed by the equation:

$$N_{fractures}(\lambda) \propto \lambda^{D} \qquad \text{(Equation 2-6)}$$

which plots as a straight line on a logarithmic plot of $N(\lambda)$ vs. λ, with the slope equal to the mass fractal dimension, D. The Lévy flight analysis is illustrated in Figure 2-23.

Stationary geostatistical and self-affine fractal models can also be evaluated. This evaluation is carried out by computing semivariograms for the fractures. A self-affine fractal has a power law semivariogram $\lambda(h)$ given by the equation:

$$\gamma(h) = h^{\theta} \qquad \text{(Equation 2-7)}$$

where h is the distance between intervals, θ is an exponent related to the self-affine fractal dimension, and $\gamma(h)$ is the averaged squared difference in fracture intensity between the intervals.

The relation between the self-affine fractal dimension and the exponent is given as:

$$D = E + 1 - \frac{\theta}{2} \qquad \text{(Equation 2-8)}$$

where E is the Euclidean dimension of the space of interest. θ must be between 0.0 and 2.0 (e.g., Matheron, 1988). For a volume of rock, the value of E is 3, so a self-affine fractal dimension for fracture intensity will have a dimension ranging between 3.0 and 4.0.

Equation for spherical and exponential variograms are given in Equation 2-2 and 2-3 above in Section 2.7.1.

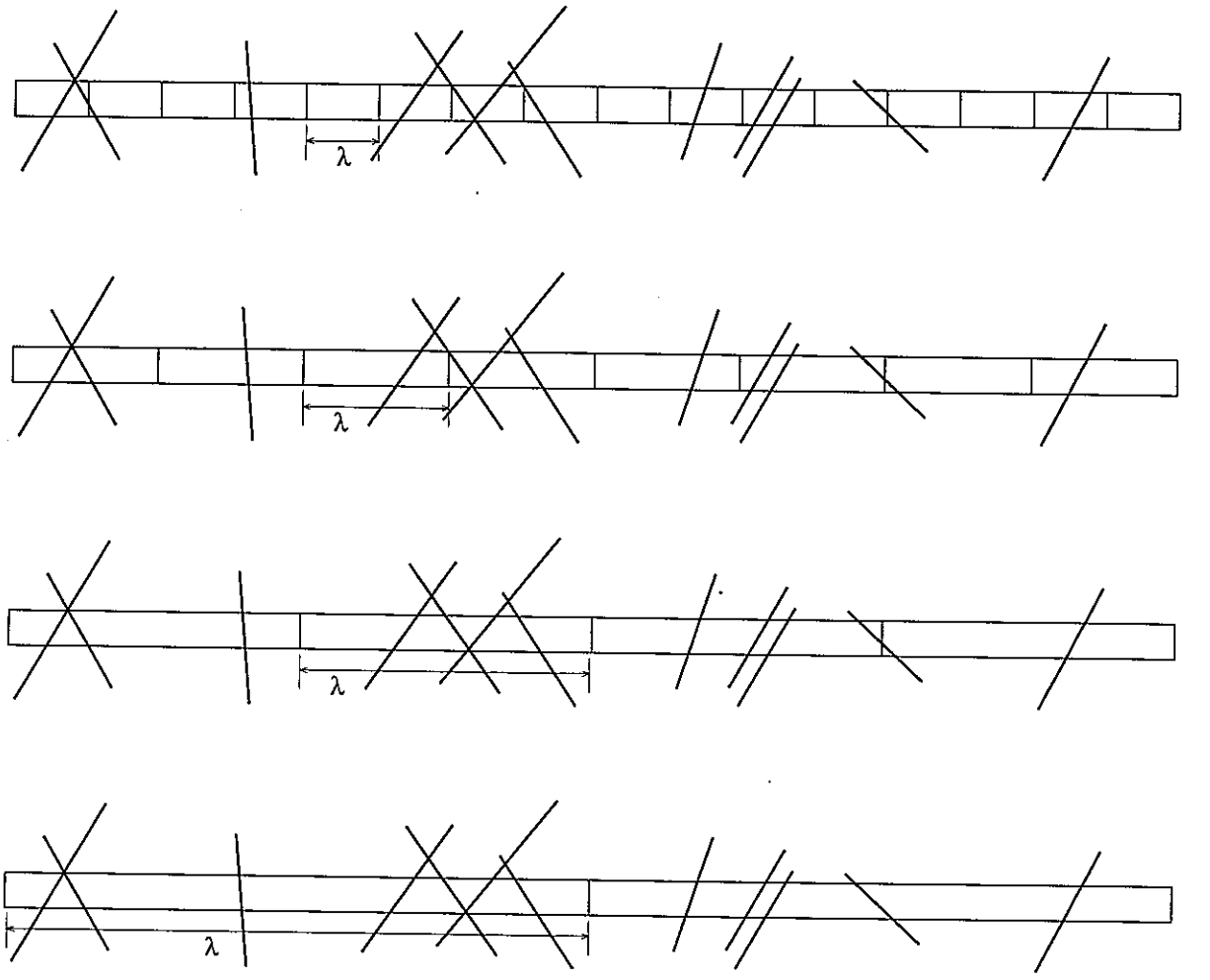

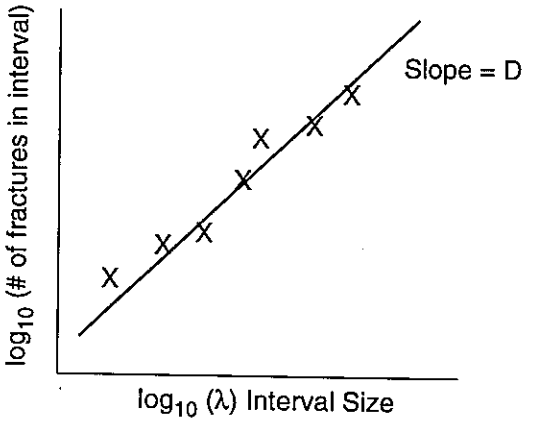

FIGURE **2-23**
LEVY-FLIGHT FRACTAL MASS DIMENSION FROM BOREHOLE FRACTURE DATA
PNC/H8

PROJECT NO. 923 1089.800 DRAWING NO. 73129 DATE 5/9/97 DRAWN BY EA

2.7.3 Fractal 1.0

The user interface for Fractal 1.0 is illustrated in Figures 2-24 through 2-26. Fractal 1.0 uses input files in .DAB format, as described in Table 2-19. User instructions for Fractal 1.0 are summarized in Table 2-20.

Table 2-19 Fractal 1.0 Data Objects

```
1. Data tables

#----
#       Data tables
#
#       A data table is characterized by its structure and entity.
#       The table structure must be defined within the definition block,
#       the data entity can appear in a separate ASCII file.
#
#----
BEGIN   data_table
        name =  "Example data table"
        location_col =  1,3             # column containing data
                                            # location (x,y,z)
        data_col =      4,6-8           # column containing data
        data_label =    4,"porosity"    # label for column# 4
        data_label =    6,"aperture"
                                        # any unnamed label will default
                                            # to data_n
        missing_value_char =    "*"     # "*" is default, include this
                                            # only if other characters such
                                            # as "-" is used.
        BEGIN   data_entity
                #       x       y       z       Data_1  Data_2  . . .
                0       0       0       1       1.1     1.2     ...
        END
        # Alterntively, specify file where data can be read.
        # If a data_tabel block contains more than one data_entity
        # block, then the data from the blocks will be joined.
        BEGIN   data_entity
                data_file =     "filename.dat"
        END
END
```

Table 2-19 (continued)

```
2. Borehole data

#----
#
#   borehole data
#
#   borehole measurements contains both borehole and data measured
#
#   IMPORTANT NOTES ON CONFLICT RESOLUTION:
#   1.  If the same object (such as a borehole_simple) is specified more
#       than once either within the same block, in the same file, or in
#       the same group of files within the same project, the MORE RECENT
#       definitions will overwrite the earlier definitions. As each
#       object is identified by name, make sure the names are unique.
#   2.  If more than one data table definition exists within the same
#       block, the data will be joined unless the data structure in the
#       different blocks has changed. In that case, the MORE RECENT
#       definition will overwrite the earlier ones.
#
#----
BEGIN   borehole_data
    name =  "unique_borehole_id"
    #
    # borehole info
    #
    # either include the info in the block
    BEGIN   borehole_simple
        # use existing borehole_simple object
    END
    # or point to a file where the borehole object can be found
    borehole_name = "BH_1"          # must provide name in case the file
    data_file =     "borehole.dat"  # contains more than one borehole
                                        # object
    #
    # data type, point measurement of interval measurement
    # the location of point measurement is specified in one column
    # the location of interval measurement must be specified in two
    # columns (x1,x2)
    #
    point_measurement = 1           # 0 if interval measurement
    #
    # data block
    #
    # again, either include the data_table object in the block
    BEGIN   data_table
            # ........
    END
    # or point to a file where the data table can be found
    data_table_name =   "Example data table"    # must provide name to
                                                    # aid search
    data_file =         "filename.dat"          # note that both
                                                    # "borehole.dat" and
                                                # "filename.dat" will
                                                    # both on the search
                                                # path and will be
                                                    # searched in order of
                                                # their presence in the
                                                    # block. In this
                                                    # example,"borehole.dat" #
                                                    will be searched
                                                # first.
END
```

Table 2-19 (continued)

```
3. Surface data

#----
#   surface data
#
#   surface measurement contains both surface description and data
#
#   SEE NOTES ON CONFLICT RESOLUTION UNDER BOREHOLE DATA
#
#----
BEGIN   surface_data
    name =  "unique_surface"
    #
    #   surface info
    #
    # either include the info in the block
    BEGIN   traceplane
        # use existing traceplane object
    END
    # or point to a file where the object can be found
    traceplane_name = "TP_1"          # must provide name in case the
                                          # file contains more
    data_file =     "traceplane.dat"  # than one traceplane object
    #
    # data type, point measurement or interval measurement
    # the end points of an interval measurement are ends of fracture
    # trace and the data may contain orientation, aperture, and other
    # measurements or the data may be absent in the case of a simple
    # fracture trace plane.
    # the location of point measurement is specified in two columns
    # (x,y) the location of interval measurement must be specified in
    # four columns as (x1,y1,x2,y2), the order must be strictly observed
    #
    point_measurement = 1           # 0 if interval measurement
    #
    # data block
    #
    # again, either include the data_table object in the block
    BEGIN   data_table
            # ........
    END
    # or point to a file where the data table can be found
    data_table_name =   "Example data table"    # must provide name to
                                                    # aid search
    data_file =         "filename.dat"          # note that both
                                                    # "traceplane.dat" and
                                                # "filename.dat" will
                                                    # both on the search
                                                # path and will be
                                                    # searched in order of
                                                # their presence in the
                                                    #block. In this
                                                # example,
                                                    # "traceplane.dat" will
                                                    # be searched
                                                # first.
END
```

Table 2-20 User Instructions for Fractal 1.0

File Menu

New: start a new database with a new root folder
Load: load a different project database from disk
Save As: save the current project folder under a new name
Print: print the current object or branch
Preferences: set user preferences
Exit: end the current session

Edit menu

Undo, Cut, cOpy, Paste, and Delete objects.

Data menu

New: create a new object as a peer of the existing object
Add: add a new object as a child of the exiting object
Edit: change the attributes or contents of the existing object
Properties: inspect the attributes of the existing object
Import: import an object from an external SAB file as a peer
Export: export the objects and all child objects to an SAB file

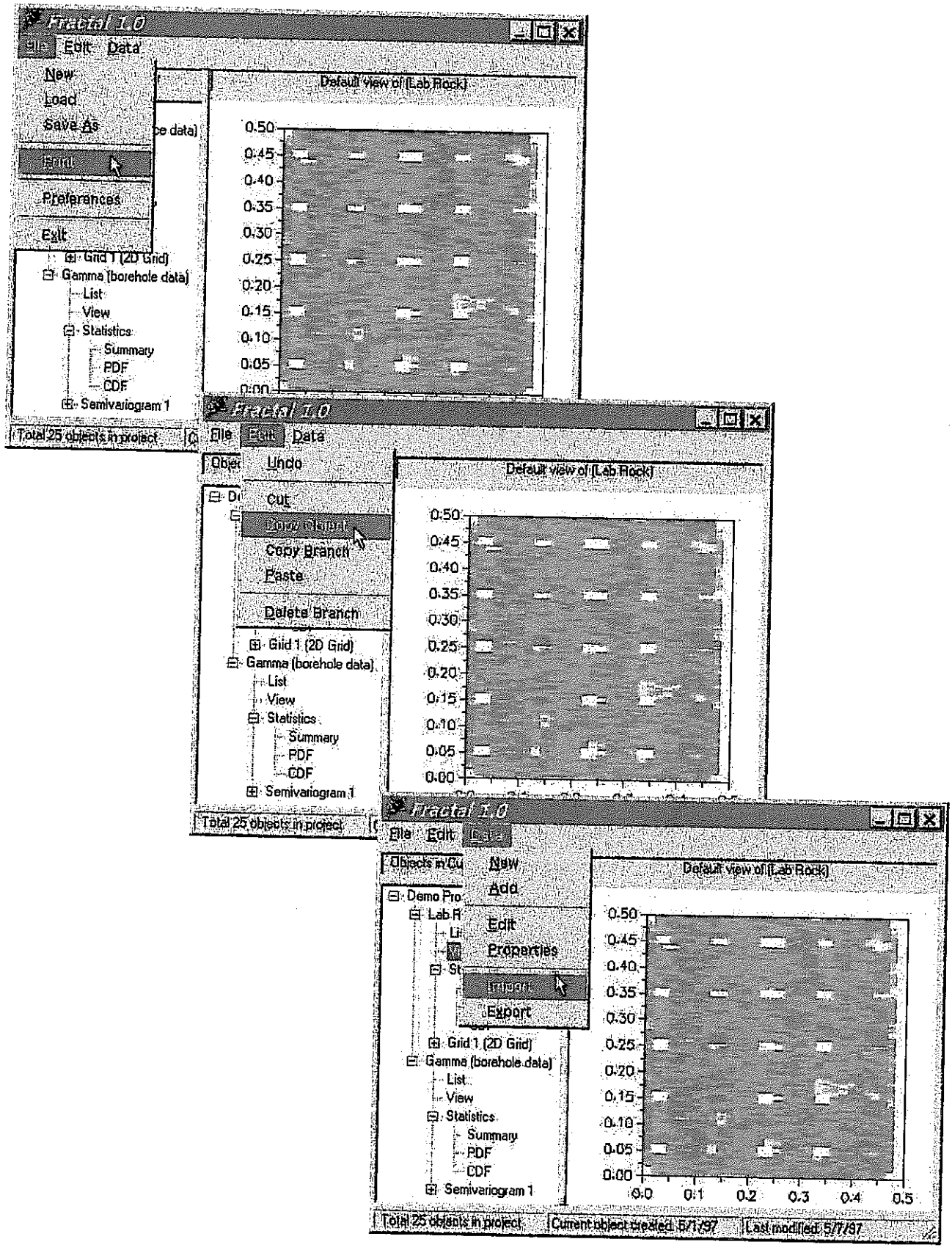

FIGURE **2-24**
FRACTAL 1.0 USER INTERFACE
PNC/H8

PROJECT NO. 923 1089.800 DRAWING NO. 73130 DATE 5/8/97 DRAWN BY EA

Golder Associates

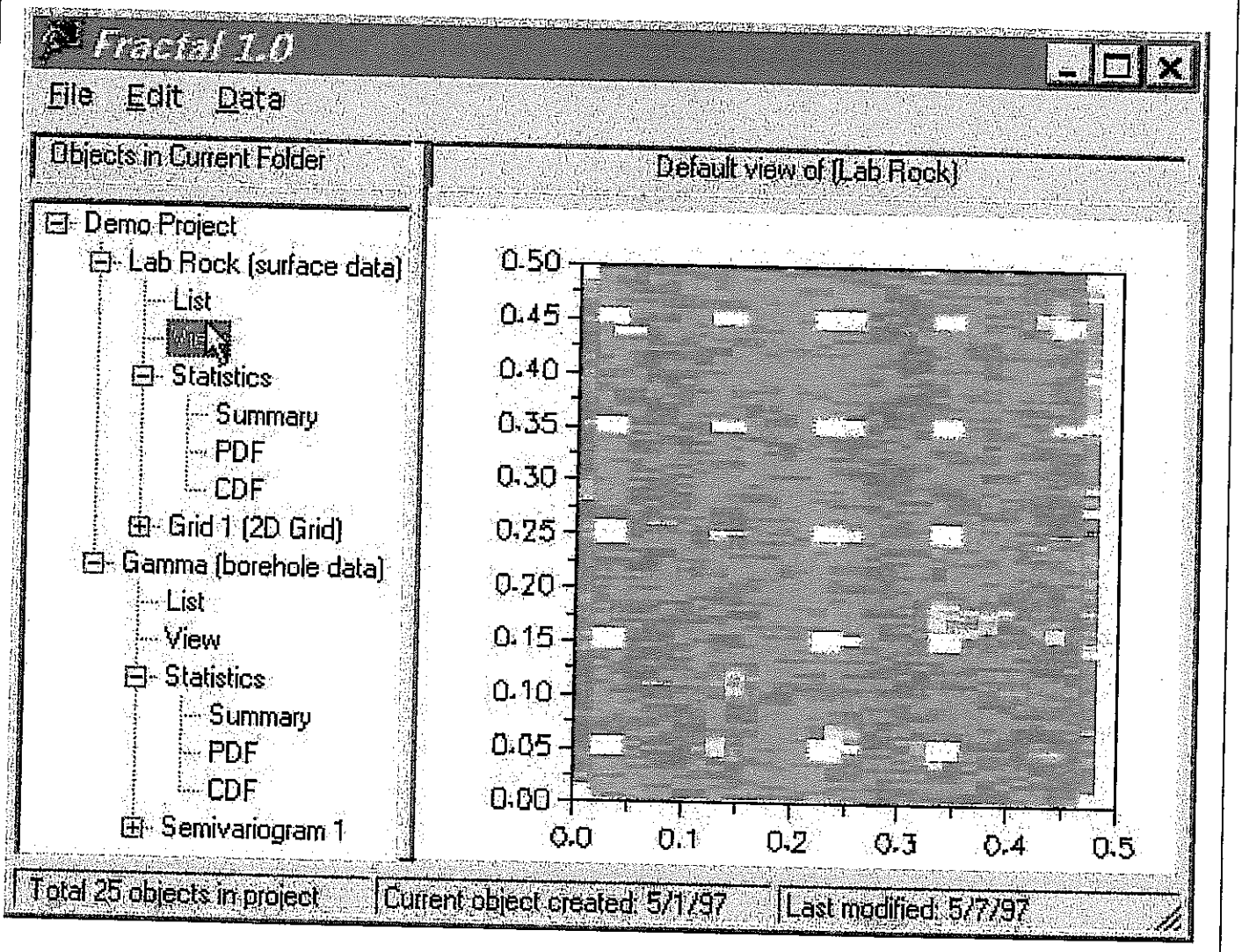

FIGURE **2-25**
ANALYSES OF 2-D DATA
PNC/H8

PROJECT NO. 923 1089.800 DRAWING NO. 73131 DATE 5/8/97 DRAWN BY EA

Golder Associates

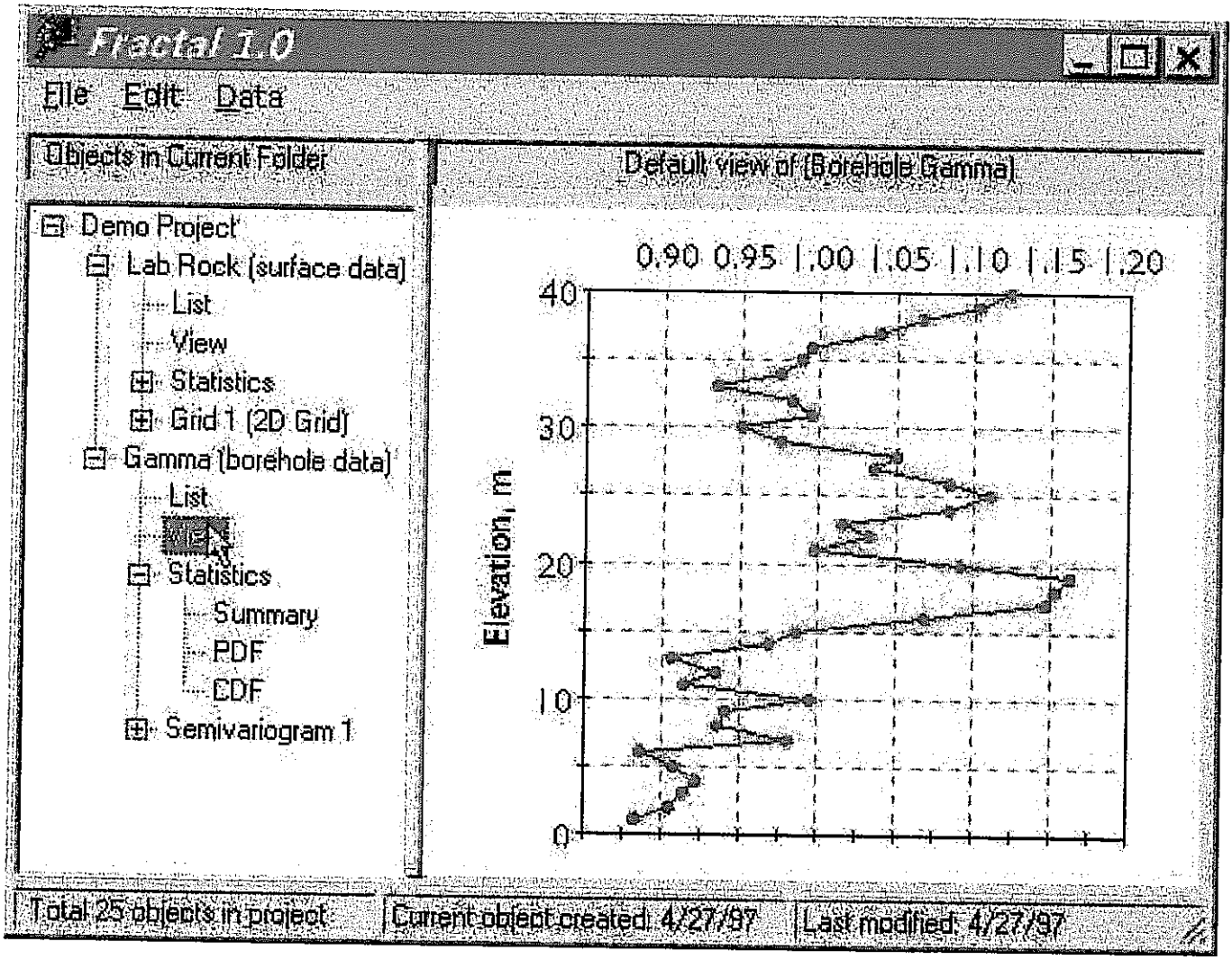

FIGURE **2-26**

ANALYSES OF 1-D FRACTURE LOCATION DATA

PNC/H8

PROJECT NO. 923 1089.800 DRAWING NO. 73132 DATE 5/8/97 DRAWN BY EA

Golder Associates

Fractal 1.0 is a Windows 95 program and follows the event-driven model of the Windows 95 operating system. Other than during the setup stage when the program first starts, the program waits and responds to the user's command. Figure 2-24 depicts a typical chain of events following a user's command.

Step 1: The user issues a command. Commonly such commands include the request to inspect (view), edit, create, or delete a data object. A data object may represent original field measurements (such as a trace map), or data derived from the field measurements (such as gridded measures), or characteristics of the original or the derived data (such as contours or semivariograms). In addition to the common commands, the user may also import, export, print, or copy the data object to the clipboard.

Step 2: The data object that is affected by the user's command then communicates with the central data vault to retrieve or store the data. If the object owns other (child) objects, it automatically initiates a chain reaction (as explained in the Data Flow Diagram) to update all the child objects. At the same time, the object hierarchy diagram on screen will be updated to highlight either the object that is being affected or to show the new hierarchy.

Step 3: When the data object completes updating, it submits a change request to the display manager. The display manager maintains a list of windows that are currently open, the object that is being displayed in the window, and the data associated with the object. An important function of the display manager is knowing how to display each type of object.

Step 4: Upon receiving the change request from the object, and if the change requires creating a new display or modifying an existing display, the display manager will submit a data request to the data vault to obtain a reference to the data associated with the object. If the change is for closing a display, the display manager will skip Steps 5 and 6, delete the display structure, and close the corresponding window on screen.

Step 5: The data vault responds to the request and pass a copy of the data to the display manager.

Step 6: The display manager processes the data and, in most cases, transform the data to a form suitable for display. It then prepare the display structure and update the display on screen. The updated display provides the user with the visual feedback.

When the user closes the program, the program will automatically store the data in an external database so these need not be generated again. The program will also store the object hierarchy into a control file on disk. If the user starts the program in the future, the program will read the control file to restore the objects and their hierarchy, the program will also initialize the data vault and connect the data vault to the external database. Finally, the program will restore the link between the objects and the data vault.

During a live session, data are retrieved from the external database into the data vault on demand. The data vault keeps a reference count of each piece of data and store the data back into the database when it is no longer used by any of the objects. This allows efficient use of memory and provides persistent data storage from one session to the next.

2.7.4 Fractal Verification

Three examples of the verification of Fractal are show in Figures 2-27, 2-28 and 2-29. Figure 2-27 demonstrates that Fractal properly calculates the power spectrum of arbitrary, gridded data (i.e. the top frame). The middle frame shows the Spectral Density of the data as calculated by Fractal. By exporting these calculated values to Microsoft Excel, it can be verified that Fractal determines the spectral characteristics of the anisotropic x,y data in the top frame which has a self-affine fractal dimension of 2.0. The bottom frame shows the analysis in Excel. For this example, the slope on the doubly logarithmic plot should be 0.0 and the actual values of each component should be near 320 (equal to the square root of the variance multiplied by the number of grid cells=sqrt(25*64*64)). Figures 2-28 and 2-29 demonstrate the calculation of box dimension and Levy-flight dimension by Fractal for the fracture tracemaps at the top of each figure.

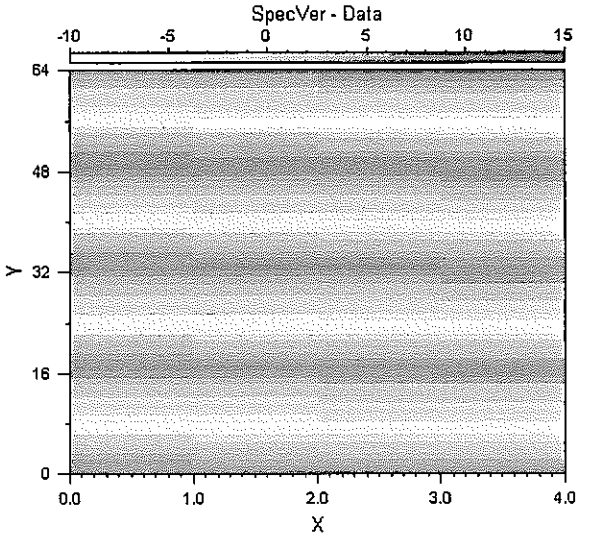

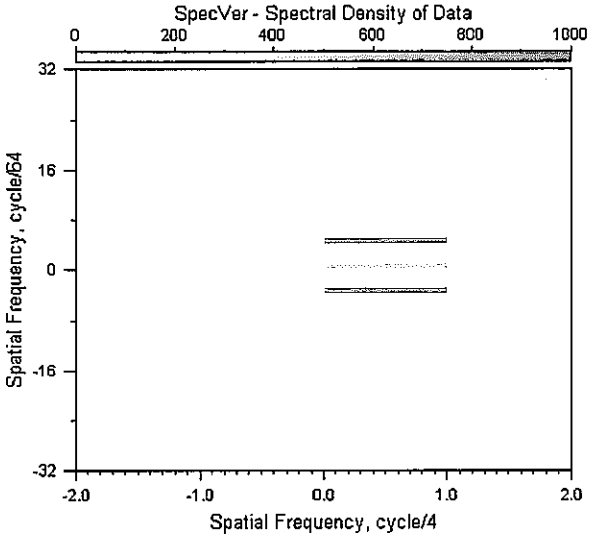

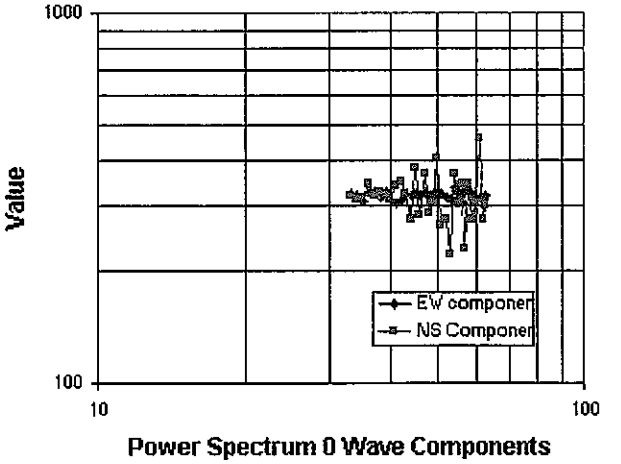

Power Spectrum 0 Wave Components

FIGURE **2-27**

VERIFICATION OF SPECTRAL FRACTAL ANALYSIS

PNC/H8

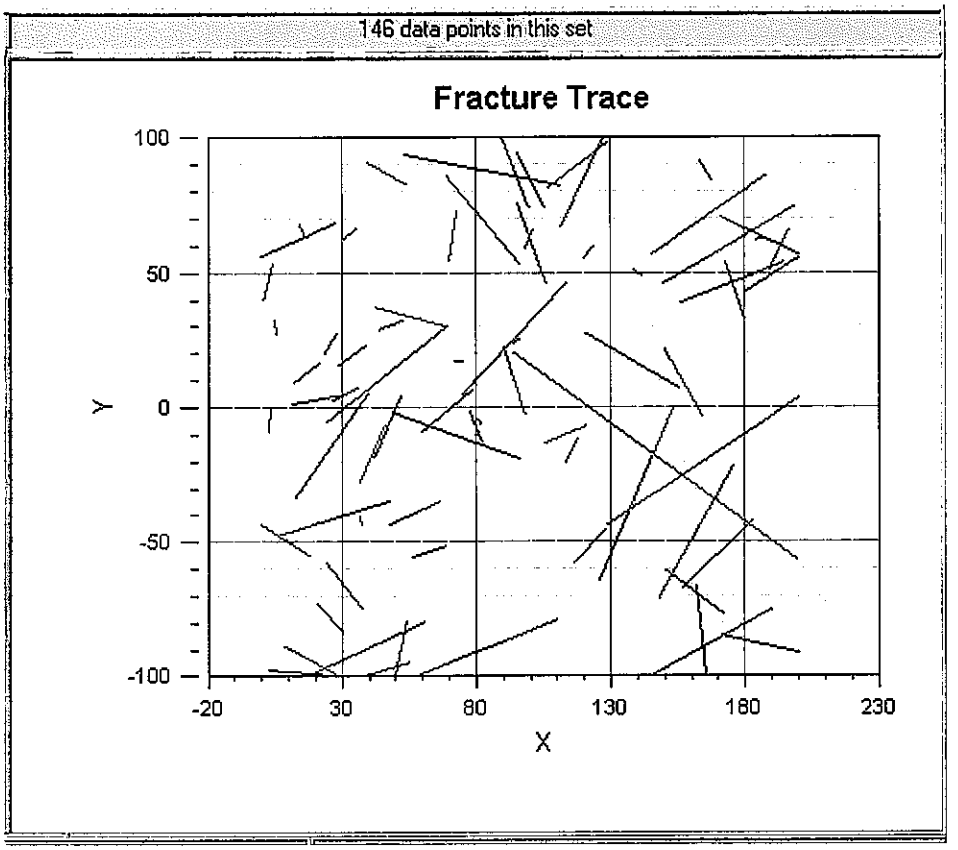

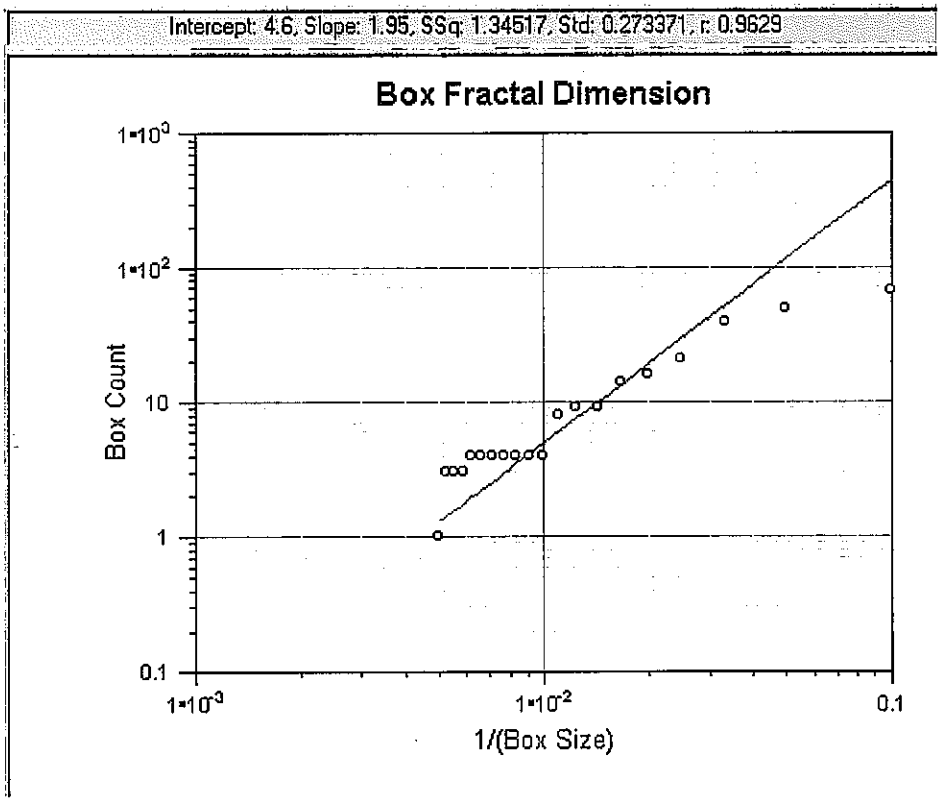

FIGURE **2-28**
VERIFICATION OF BOX FRACTAL ANALYSIS
PNC/H8

PROJECT NO. 923 1089.800 DRAWING NO. 76834 DATE 5/11/98 DRAWN BY TK

Golder Associates

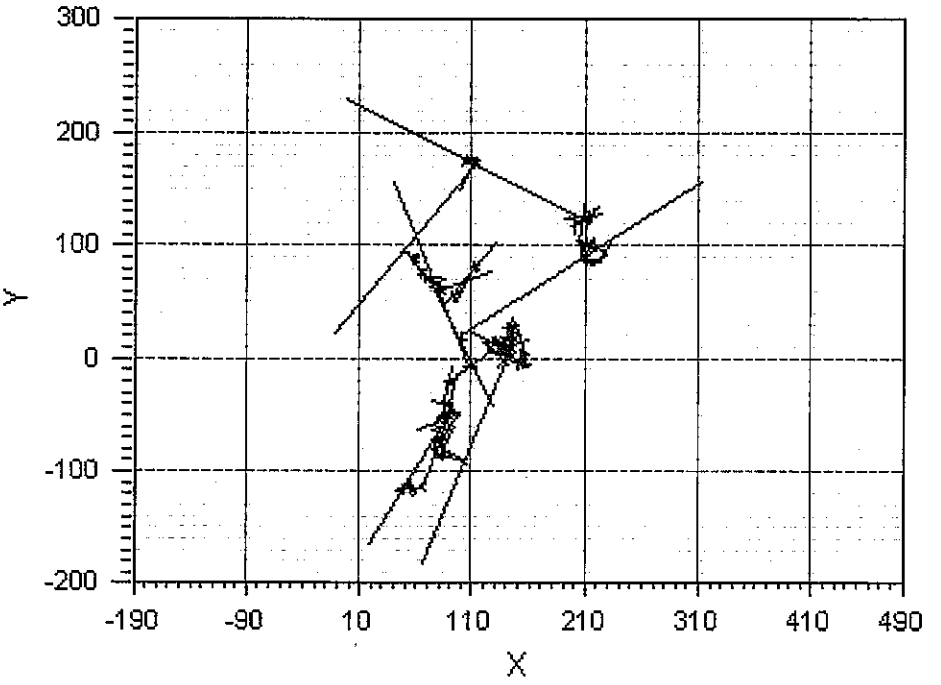

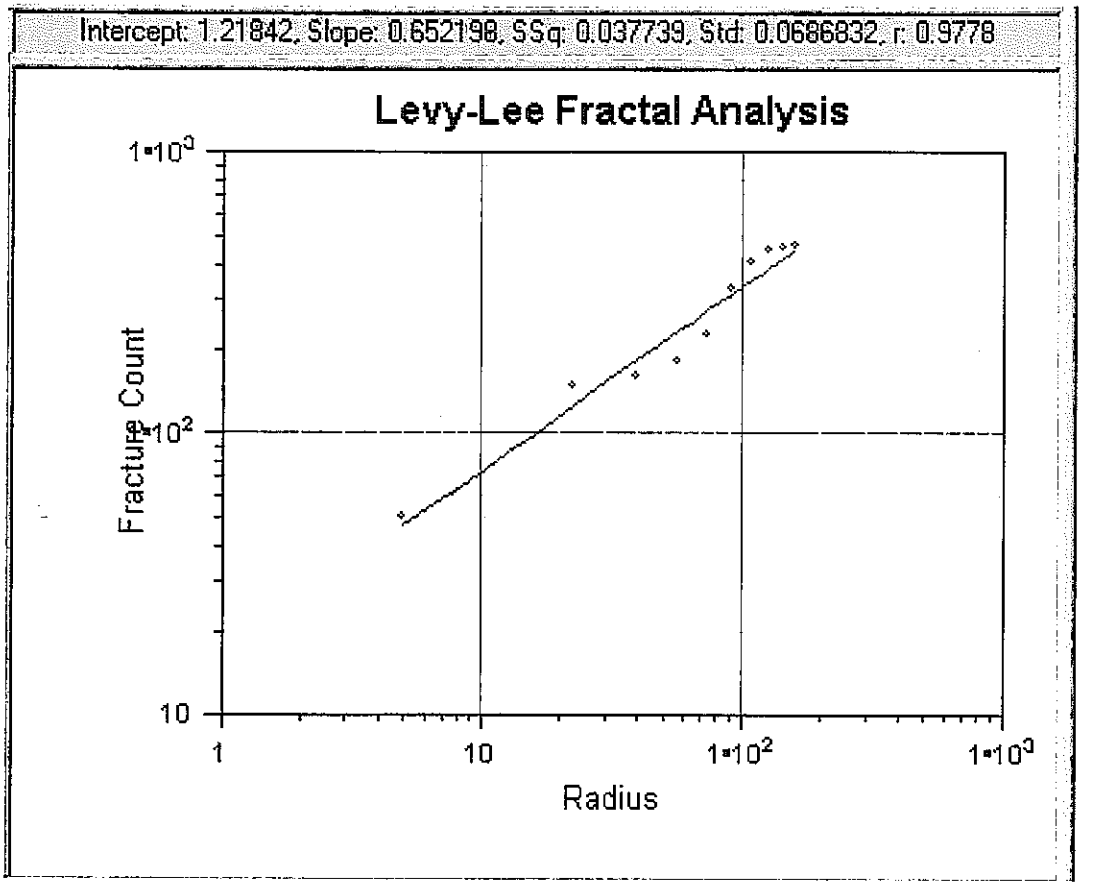

FIGURE **2-29**
VERIFICATION OF LEVY-FLIGHT FRACTAL ANALYSIS
PNC/H8

PROJECT NO. 923 1089.800 DRAWING NO. 76835 DATE 5/11/98 DRAWN BY TK

Golder Associates

2.8 Task 1.2.6: Geostatistical Analysis: Borehole, 2D, and Trace Spectral Analysis

In this task, the fractal analysis of borehole, 2D field (aperture), and fracture trace intensity (P_{21} or P_{20}) were extended to provide spectral analysis for calculation of the POCS fractal dimension. The algorithms implemented are described in Section 2.8.1 below. These analyses are included in Fractal 1.0, described in Section 2.7.3 above. Figures 2-30 and 2-31 illustrate the user interface for these analyses. Test cases are described in Section 2.8.2.

2.8.1 2D Data Analysis Algorithm

The algorithm for spectral analysis of 2D Data is based on the Fast Fourier Transform. The Fast Fourier Transform converts a regular grid of spatial data (position x,y) into a grid of frequency-domain data (wave number i,j) with the same dimensions. For a 64 × 64 grid, the wave numbers in each dimension range from -31 to +32 (excluding the (0,0) component).

The power spectrum is computed by averaging all of the J values for each I wave component, and then averaging all of the I values for each J wave component. The negative wave components should be exactly equal to their positive counterparts.

Calculation of the fractal dimension of 2-D Data is based on the fact that a self-affine fractal field has a spectral density that is in the form of a power law (see for example, Voss, 1986). This means that the power spectrum (positive wave numbers only), when plotted on logarithmic axes, appears as a straight line (Figure 2-32). The slope (θ) of this straight line relates to the fractal dimension, D:

$$D = 3 - \left(\frac{\theta}{3}\right) \quad in\ 2D \quad and$$
$$D = 4 - \left(\frac{\theta}{3}\right) \quad in\ 3D. \qquad \text{(Equation 2-9)}$$

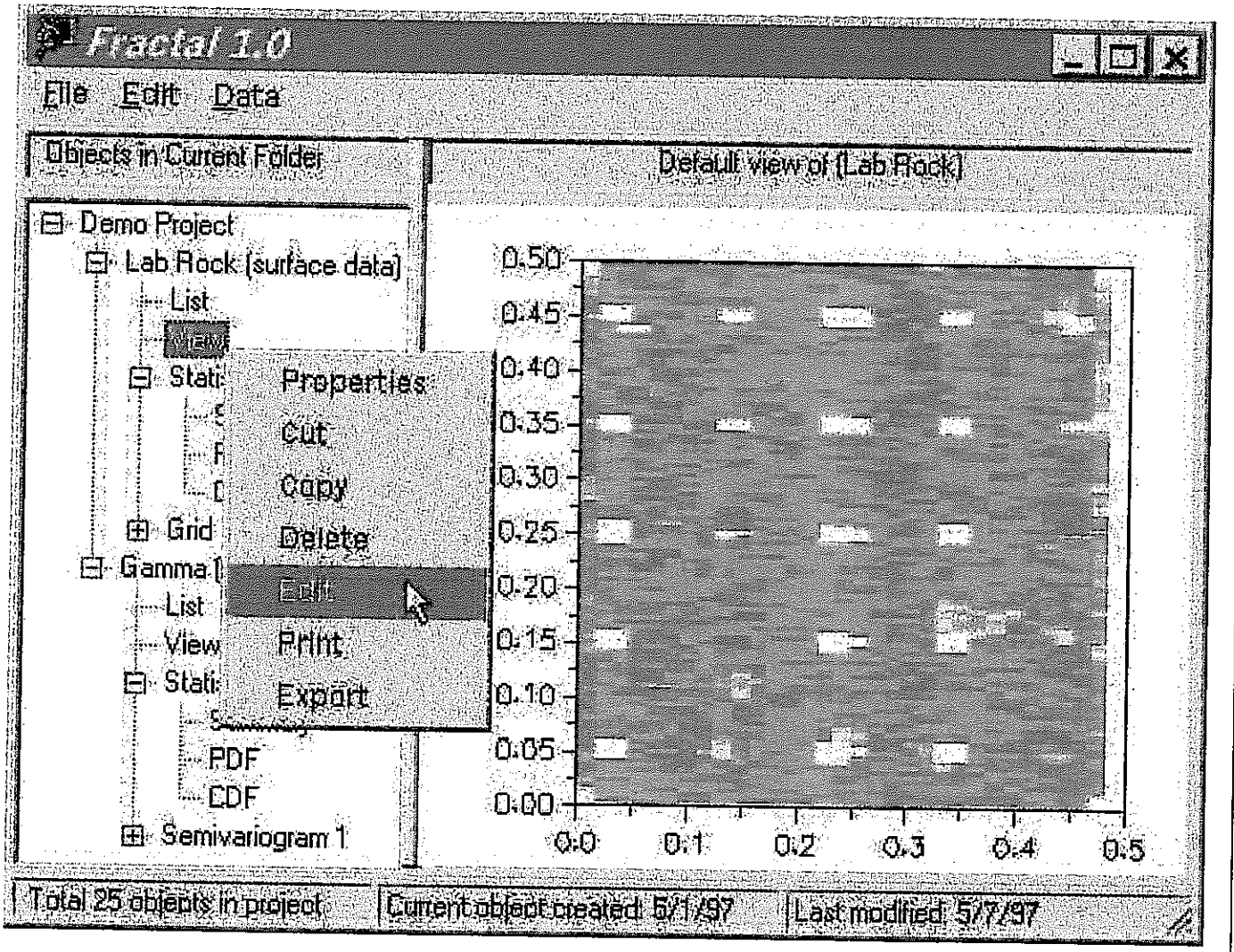

FIGURE **2-30**

USER INTERFACE FOR ANALYSIS OF 2-D DATA

PNC/H8

PROJECT NO. 923 1089.800 DRAWING NO. 73136 DATE 5/8/97 DRAWN BY EA

Golder Associates

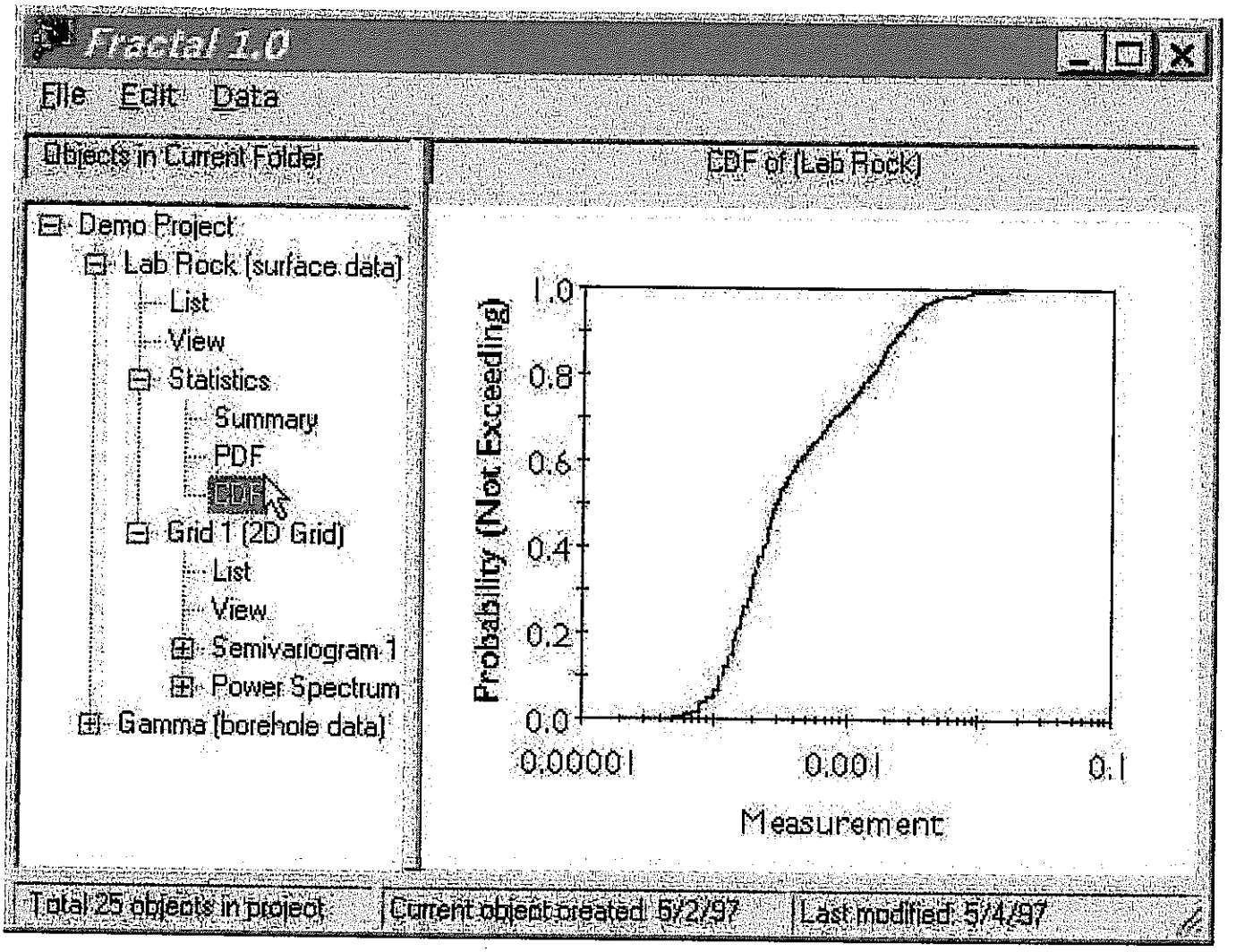

FIGURE **2-31**
USER INTERFACE FOR ANALYSIS OF 1-D DATA
PNC/H8

PROJECT NO. 923 1089.800 DRAWING NO. 73137 DATE 5/8/97 DRAWN BY EA

Golder Associates

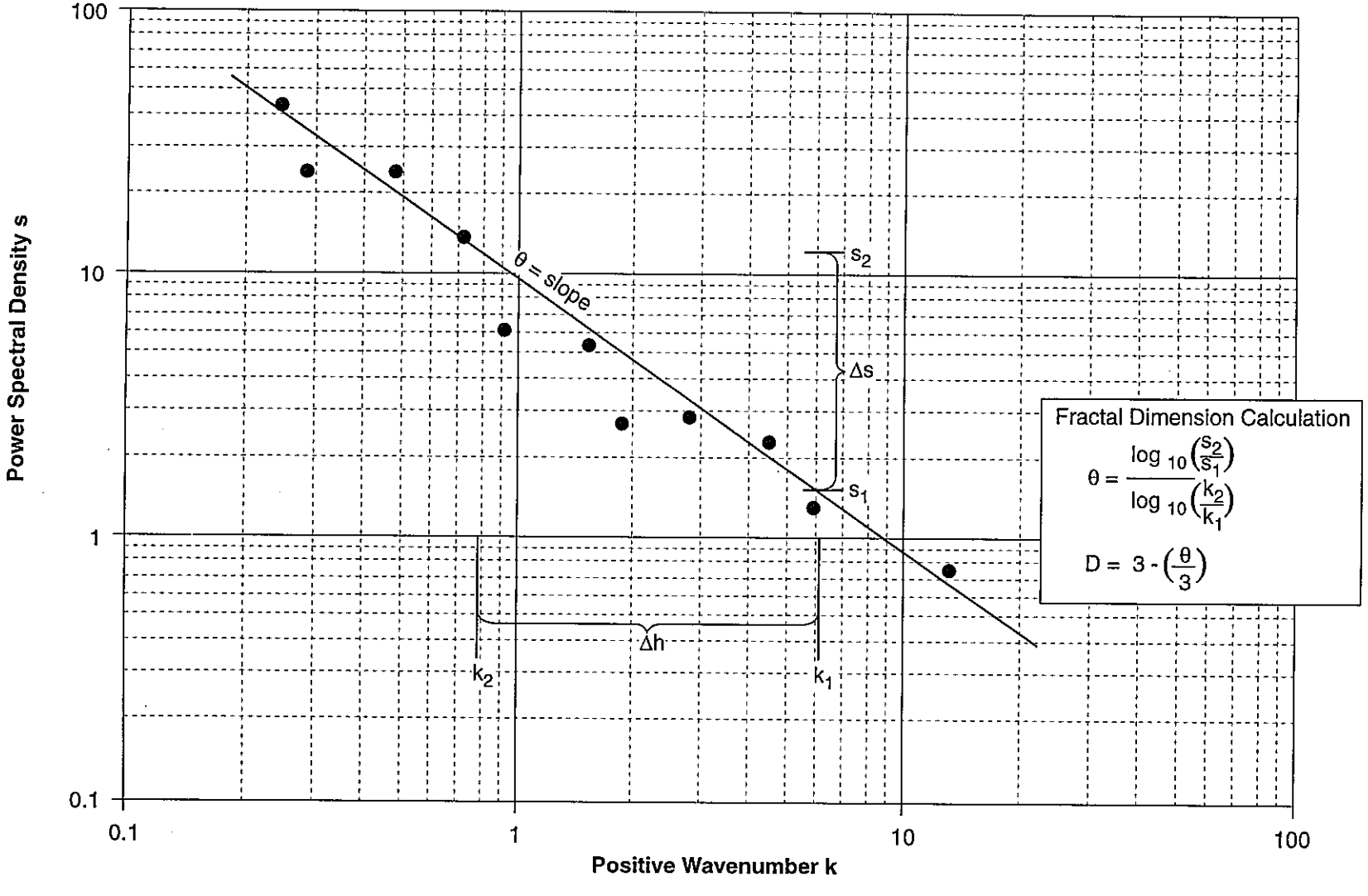

FIGURE **2-32**
SPECTRAL DENSITY CALCULATION OF FRACTAL DIMENSION
PNC/H8

PROJECT NO. 923 1089.800 DRAWING NO. 73138 DATE 5/8/97 DRAWN BY EA

Golder Associates

The anisotropy of a self-affine fractal field is calculated from the ratio of average anisotropy values in multiple, orthogonal directions (Figure 2-33). For a two dimensional field,

$$A = \frac{\overline{A_x}}{\overline{A_y}} \qquad \text{(Equation 2-10)}$$

The single-dimension anisotropy values (A_x, A_y) may be derived from the equation for the spectral component. The spectral component, S, for each (I,J) wave in an anisotropic self-affine fractal is related to anisotropy as :

$$S(I,J) = C\left(\left(\frac{2A_x I}{N_x}\right)^2 + \left(\frac{2A_y J}{N_y}\right)^2\right)^{-\beta} \qquad \text{(Equation 2-11)}$$

where C is a constant related to the energy of the stochastic field

A_i is the anisotropy in the i-th direction,

N_i is the number of grid cells in the i-th direction,

I (or J) is the wave number, and

β is the spectral exponent calculated from the fractal dimension:

$$\beta = 6 - 2D. \qquad \text{(Equation 2-12)}$$

If the J^{th} component is set to 0.0, then the spectral component is a function only of the number of grid cells in the X direction, the fractal dimension, the value of the I^{th} wave component, and the anisotropy factor. For all wave components in which J=0, the spectral value S(I,J) is:

$$A_x = C\frac{N_x(S(I,0))^{-\frac{1}{2\beta}}}{2I}. \qquad \text{(Equation 2-13)}$$

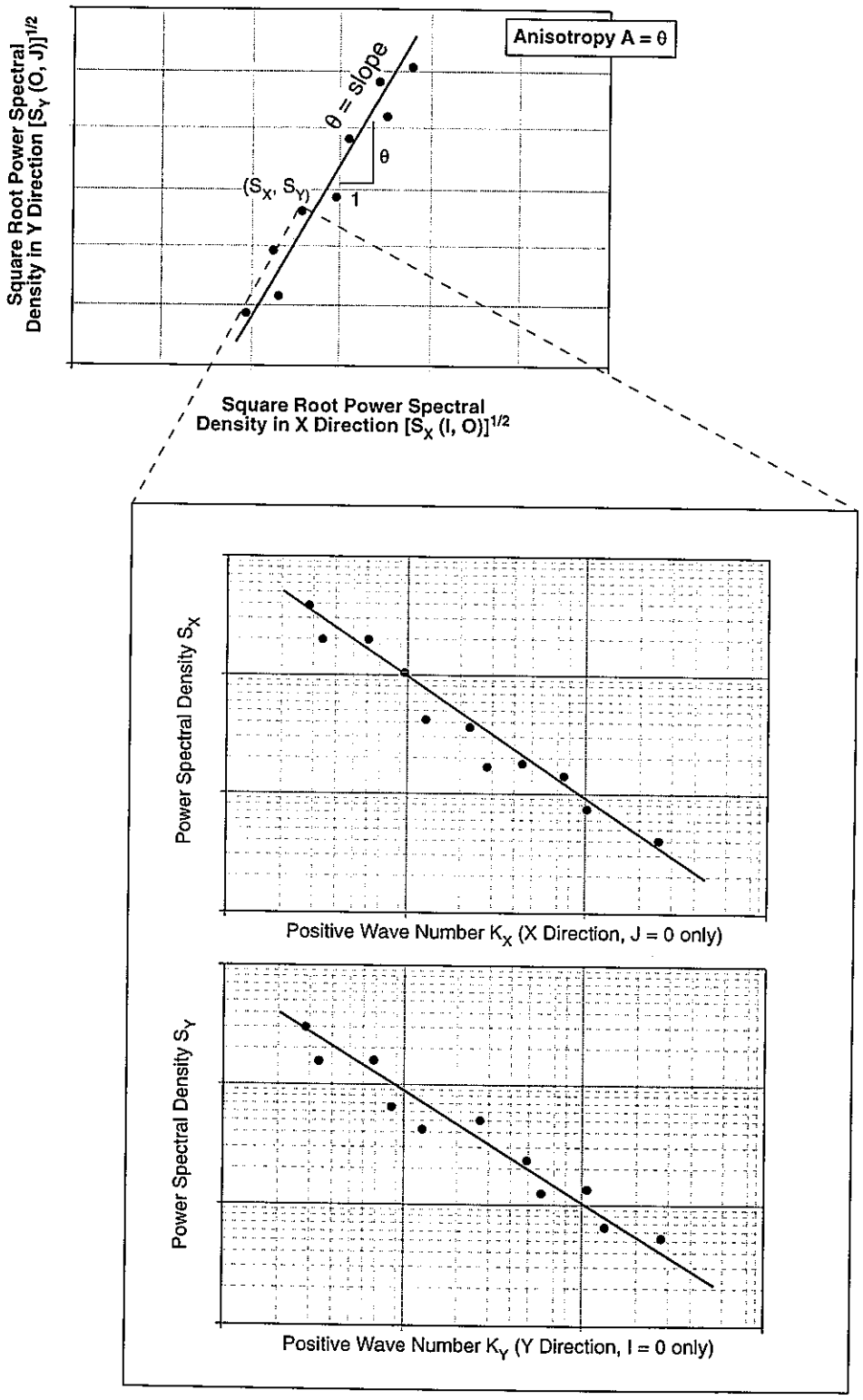

FIGURE **2-33**
SPECTRAL DENSITY
CALCULATION OF ANISTROPY
PNC/H8

PROJECT NO. 923 1089.800 DRAWING NO. 73139 DATE 5/8/97 DRAWN BY EA

Golder Associates

Likewise, for all wave components in which I=0,

$$A_y = C\frac{N_y(S(0,J))^{-\frac{1}{2\beta}}}{2J} \qquad \text{(Equation 2-14)}$$

A_x/C and A_y/C are averaged over N_x-1 and N_y-1 values of S(I,0) and S(0,J) respectively. The anisotropy can then be calculated according to Equations 2-13 and 2-14 above.

The fractal dimension and anisotropy may also be calculated by performing a variogram analysis, rather than a spectral analysis of the field. As with a spectral analysis, the triangular element mesh should be converted to a $N_x \times N_y$ field of square elements.

The fractal dimension of the field can be calculated from the semivariogram (e.g. Burrough, 1981). The semivariogram should be computed in two grid directions. Plotting the variogram using logarithmic axes for both lag and semivariance, the points should plot on a straight line whose slope θ (in log-space) relates to the fractal dimension D according to the equation (Figure 2-34):

$$4 - 2D = \theta \qquad \text{(Equation 2-15)}$$

$$D = 2 - \left(\frac{\theta}{2}\right). \qquad \text{(Equation 2-16)}$$

Note that the semivariogram cannot be robustly estimated for lags much greater than half the domain width, so points representing lag classes that are greater than half the domain width should be ignored.

Anisotropy is calculated by plotting the east-west and the north-south variograms on the same plot, and determining h_{shift}, the ratio of the east-west to the north-south direction lag values for equal semivariance values (Figure 2-35):

$$h_{shift} = \frac{dh_{NS}}{dh_{EW}} \qquad \text{(Equation 2-17)}$$

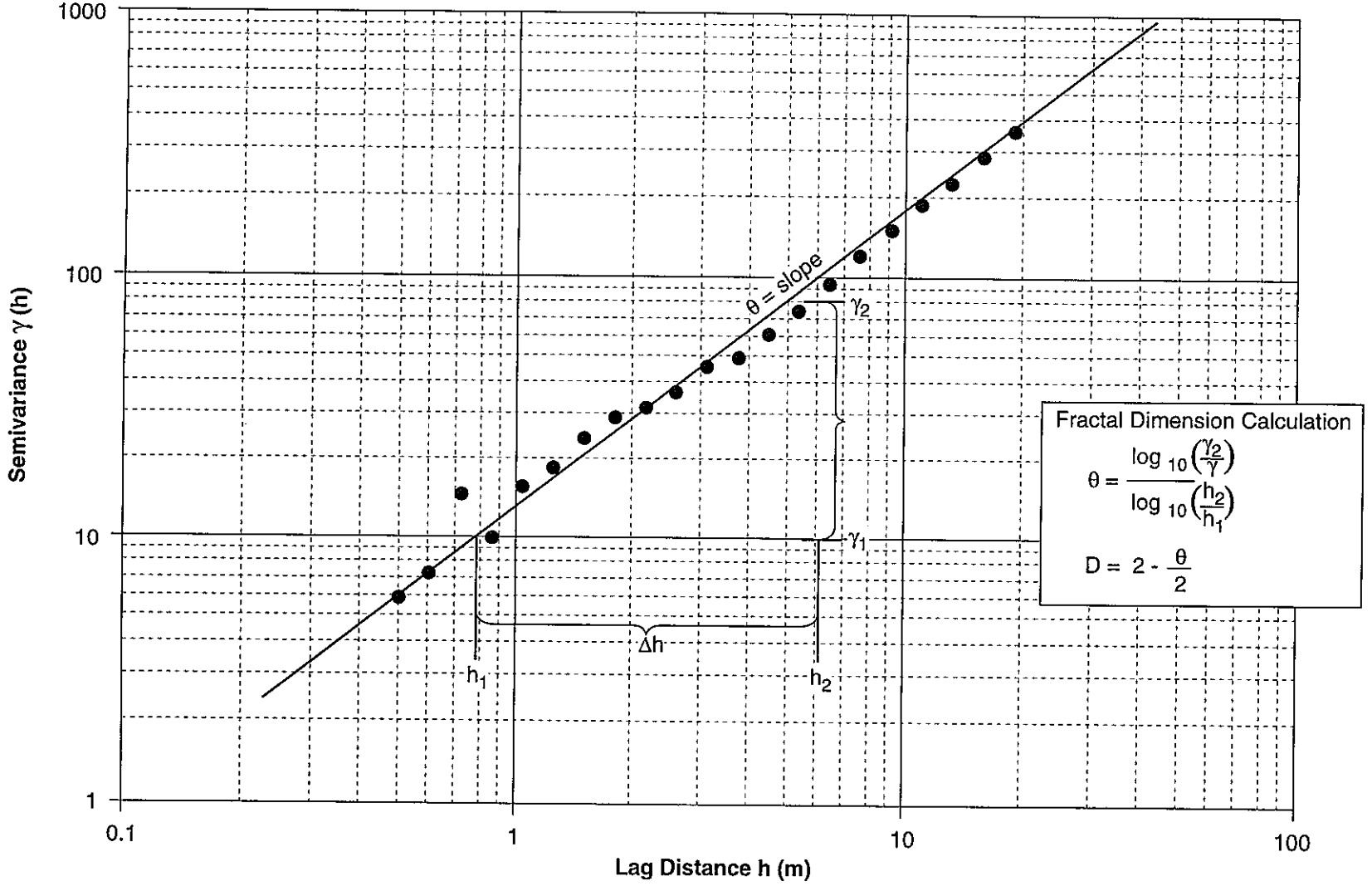

FIGURE **2-34**
SEMIVARIOGRAM CALCULATION OF FRACTAL DIMENSION
PNC/H8

PROJECT NO. 923 1089.800 DRAWING NO. 73140 DATE 5/8/97 DRAWN BY EA

Golder Associates

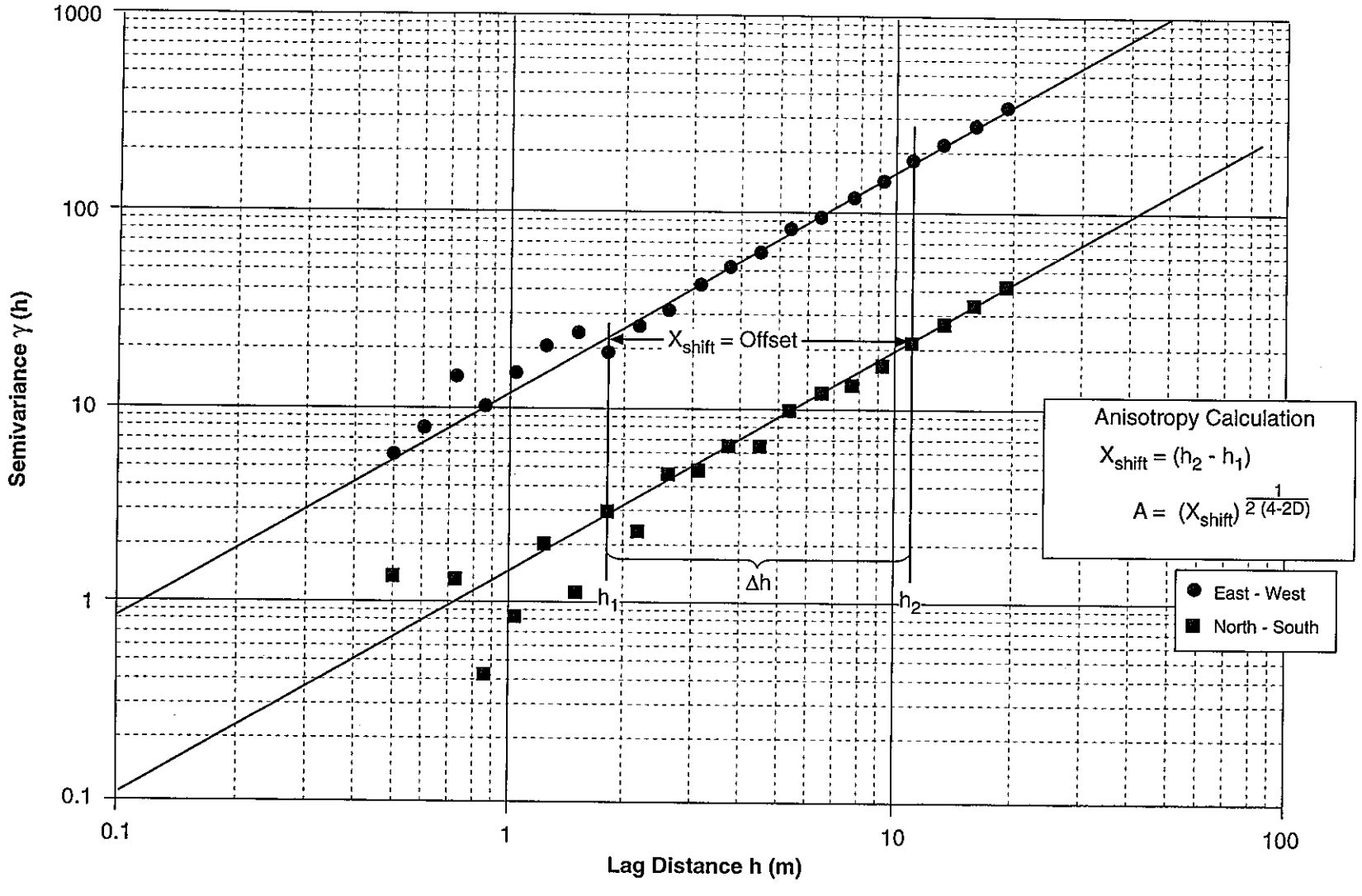

FIGURE **2-35**
SEMIVARIOGRAM CALCULATION OF ANISOTROPY
PNC/H8

PROJECT NO. 923 1089.800 DRAWING NO. 3141 DATE 5/8/97 DRAWN BY EA

Golder Associates

when dh_{NS} is the lag for a given semivariance value calculated in the north-south direction, and dh_{EW} is the lag for the same semivariance calculated in the east-west direction.

The anisotropy A can be calculated from X_{shift} as

$$h_{shift} = \left(A^2\right)^{4-2D} \quad \text{(Equation 2-18)}$$

$$A = (h_{shift})^{\frac{1}{2(4-2D)}}. \quad \text{(Equation 2-19)}$$

2.9 Task 1.3.12: Laplace Transform Galerkin (LTG) Implementation

During H8, the Laplace Transform Galerkin method was implemented to provide solute transport for PAWorks pipe networks. Solute transport modeling includes the following (Figure 2-36):

- Heads are calculated at nodes based on 1-D pipe flow solutions;
- Source terms are expressed as radionuclide concentrations over time for up to 10 radionuclides; and
- Each pipe allows for transport by the following processes:
    1. Advective transport,
    2. Matrix diffusion (from the fracture pathway into the surrounding rock);
    3. Sorption (from the fracture pathway onto the fracture surfaces on the pathway);
    4. Dead pore diffusion (from the fracture pathway into "dead" porosity of the fracture and fracture filling);
    5. Dead pore sorption (from the "dead" porosity onto the fracture surface);

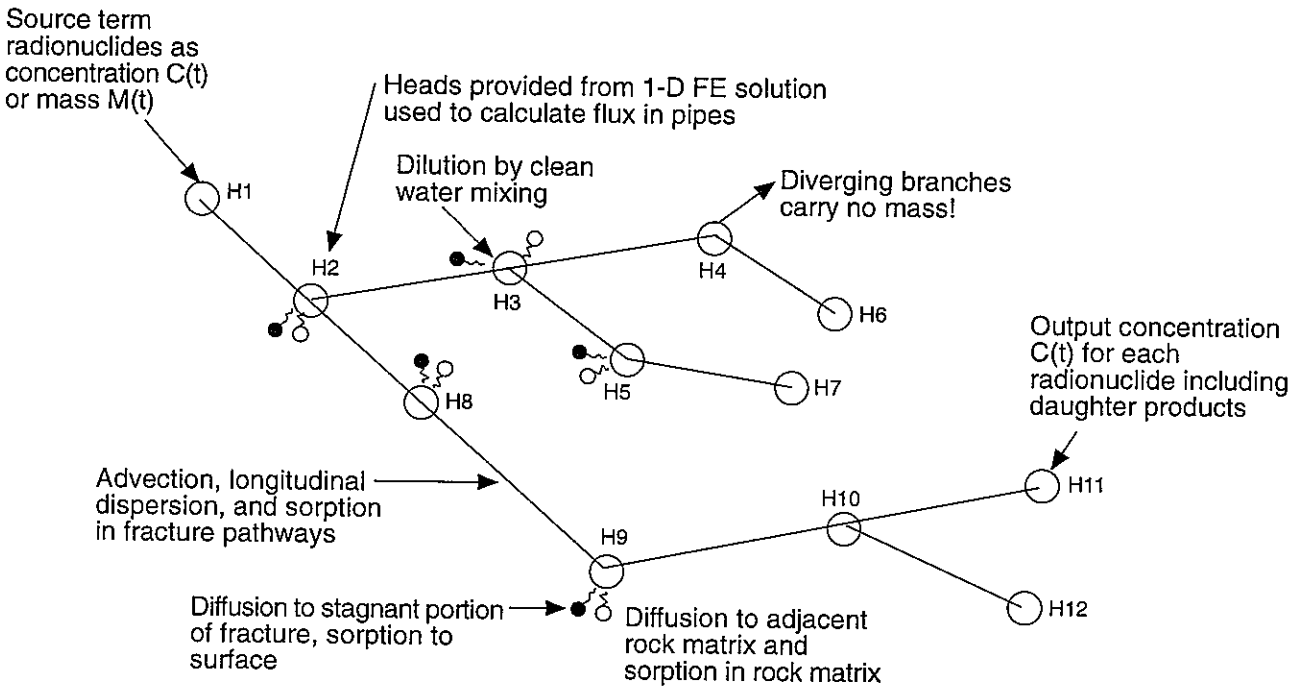

FIGURE **2-36**

TRANSPORT FEATURES OF PAWorks/LTG

PNC/H8

PROJECT NO. 923 1089.800 DRAWING NO. 73142 DATE 5/9/97 DRAWN BY EA

Golder Associates

6. Dead pore matrix diffusion (from the "dead" porosity into the rock matrix);

7. Connected fracture diffusion (from the "dead" porosity into connected fracture networks);

8. Connected fracture sorption (from connected fracture networks onto the fracture surface);

9. Connected fracture matrix diffusion (from connected fracture networks into the rock matrix);

10. Longitudinal dispersion within pipes;

11. Complete mixing at intersections;

12. Dilution and divergence at intersecting pipes (pure water); and

13. Radioactive decay.

PAWorks/LTG was implemented to simulate the advective-dispersive transport of multi-species decay chain through an arbitrarily structured network of interconnected one-dimensional pipes in three-dimensional space. For generality, the decay chain can be either straight or it can be comprised of a complex branching network where each daughter species can have multiple parent species. In essence, PAWorks/LTG is based on a conceptualization that flow and transport in a three-dimensional rock mass containing a network of interconnected fracture planes can be reduced to that in a network of pipes, where the pipes represent the primary flow conduits through the fracture planes. The model can also accommodate processes known to be important in the context of radionuclide transport in the subsurface such as 1) diffusion from the pipes containing mobile groundwater into the surrounding rock matrix containing immobile groundwater, 2) diffusion into the immobile porewater within the fracture "plane" attached to a pipe containing the flowing groundwater, 3) diffusion from the mobile groundwater in a pipe to attached "dead-end" pipes that contain immobile groundwater and 4) diffusion into fracture infilling or surface-coating material. Thus, in general, each

pipe containing the flowing groundwater can be connected to multiple interacting immobile porosity zones. The model also allows for the sorption of the solutes onto the geologic materials within each immobile zone, including sorption onto the surfaces of the pipes in the network. Sorption is described by a linear Freundlich isotherm such that a retardation factor can be defined for each solute for each pipe and each immobile porewater zone.

In order to achieve a high degree of computational efficiency, especially for cases involving very large pipe networks and long simulation time frames, the governing transport equations are solved using the Laplace Transform Galerkin (LTG) finite element method (Sudicky, 1989; Sudicky, 1990, Sudicky and McLaren 1992). The primary advantages of the LTG method are that it avoids time stepping and it is more resistant to numerical dispersion artifacts that conventional time-marching numerical schemes are prone to. It is, however, restricted to linear problems and the flow must be steady state. Further computational efficiency is achieved through the use of an advanced iterative sparse matrix equation solver, WatSolv (VanderKwaak et al., 1997), which only stores and operates on the non-zero terms appearing in the finite element coefficient matrix, it employs ILU factorization with a user-defined level of infill and several re-ordering options including Red/Black system reduction, and it uses CGSTAB (van der Vorst, 1992) acceleration to solve the complex-arithmetic system that arises from the LTG discretization.

2.9.1 Governing Equations

In this section, the governing transport equations are presented based on the pipe network conceptualization to describe solute migration through a fractured rock mass. First, the equations as they exist in the time domain are given, followed by their corresponding forms in Laplace transform space which are the forms that are solved numerically according to the LTG method.

2.9.1.1 Pipe Transport

The conceptual model used for transport in an individual pipe is illustrated in Figure 2-37. PAWorks/LTG assumes steady-state flow and a first-order approach to describe the diffusive mass transfer of a solute between the groundwater in a pipe and the multiple immobile porosity zones attached to it (see, e.g., Sudicky, 1990), the advective-dispersive transport of solute species k in a pipe network is given by:

$$A(\ell)\left[R_k(\ell)\frac{\partial C_k}{\partial t}+q(\ell)\frac{\partial C_k}{\partial \ell}-\frac{\partial}{\partial \ell}D_{\ell_k}(\ell)\frac{\partial C_k}{\partial \ell}+R_k(\ell)\lambda_k C_k-\sum_{j=1}^{m_k,k>1}\eta_{kj}R_j(\ell)\lambda_j C_j\right]$$
$$\pm\sum_{\ell'}\dot{M}\,\delta(\ell-\ell')+\sum_{\ell^*}Q(C_k-C_k^*)\delta(\ell-\ell^*)+\sum_{im=1}^{IM}P(im,\ell)\alpha_k(im,\ell)(C_k-C_k')=0$$

(Equation 2-20)

where:

$A(\ell)$ = Pipe cross-sectional area [L^2]

$R_k(\ell)$ = Retardation factor [-]

$q_\ell(\ell)$ = Specific discharge (≡ Pipe velocity v) [L/T]

$D_{\ell_k}(\ell)$ = Dispersion coefficient = $\alpha v + D_k^o$ [L^2/T]

α = Pipe longitudinal dispersivity [L],

D_k^o = Free-solution diffusion coefficient [L^2/T]

λ_k = Decay constant [1/T]

m_k = Number of parents for species k (=1 for straight chain)

η_{kj} = Stoichiometric constant indicating fraction of parent species j that decays to daughter species k

= 1.0 for straight decay chain; ($0.0 < \eta_{kj} < 1.0$ for branching chain)

$\dot{M}(t)$ = Internal solute mass source/sink [M/T]

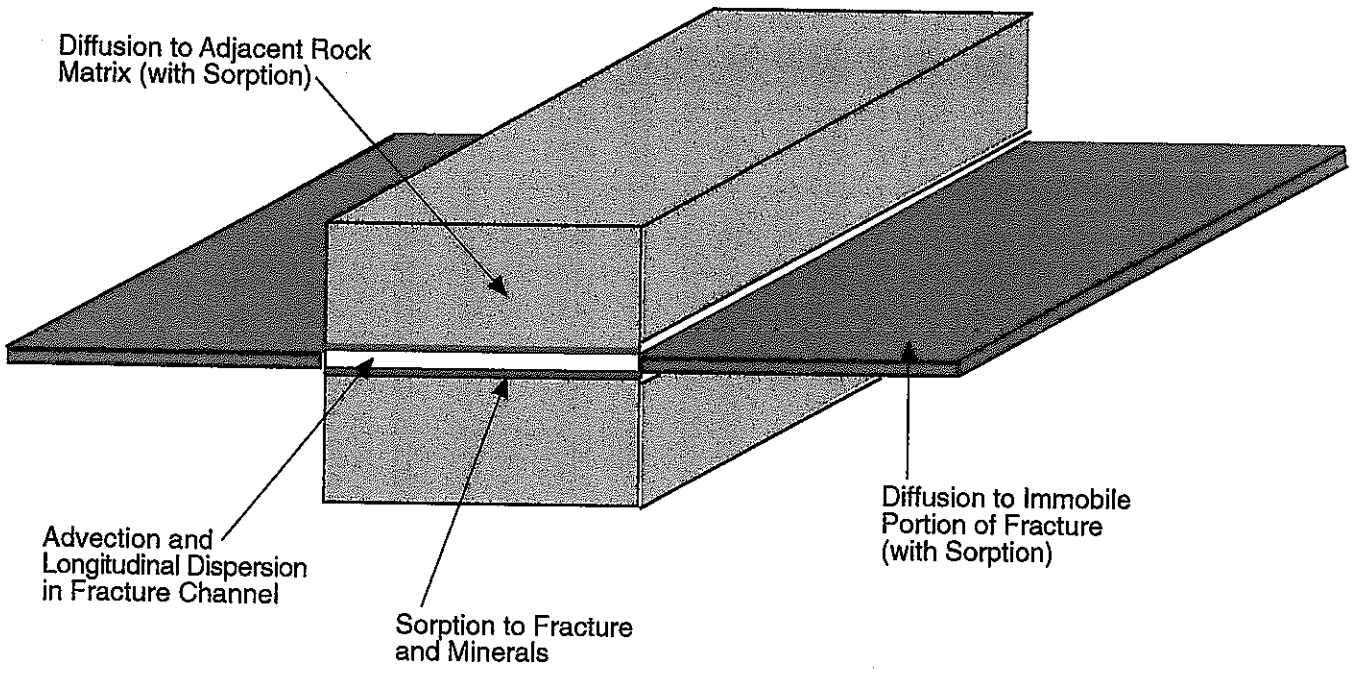

FIGURE **2-37**
CONCEPTUAL MODEL OF PIPE TRANSPORT
PNC/H8

PROJECT NO. 923 1089.800 DRAWING NO. 73143 DATE 5/9/97 DRAWN BY EA

Golder Associates

Q = External fluid source/sink [L^3/T]

$\delta(\ell - \ell')$ = Dirac delta [1/L]

$P(im, \ell)$ = Immobile zone wetted perimeter for immobile zone "im" attached to pipe "ℓ" [L]

$\alpha_k(im, \ell)$ = Pipe/immobile zone transfer coefficient for immobile zone "im" attached to pipe "ℓ" [L/T]

C_k = Pipe concentration [M/L^3]

C_k' = Immobile zone concentration [M/L^3]

C_k^* = Concentration of injectate in external fluid source [M/L^3]

ℓ = Distance along interconnected pipe network [L]

ℓ' = Location of solute mass source/sink [L]

ℓ^* = Location of external fluid source/sink

im = Immobile zone class number (note: if desired im can equal 0) [-]

$IM(\ell)$ = Total number of immobile zones attached to pipe ℓ [-]

k = Species number [-]

m_k = Number of parent species decaying to species k [-]

t = time [T]

It should be noted that if there is no flow along a particular pipe within the network (i.e. $q_\ell(\ell) = 0$), then the model allows for diffusive transport along the length of this pipe. It should also be pointed out that if fluid is withdrawn at a resident concentration $C_k^* = C_k'$ then the term involving Q in Equation 2-20 vanishes. If the injectate concentration $C_k^* = 0.0$, then this term accounts for the dilution effect of the injection of solute-free water.

The initial concentrations of all species within the domain are assumed to be zero in the current version of PAWorks/LTG. For boundary conditions, they can be either of the Dirichlet-type where the input concentration history of each species is a specified function of time, or of the Cauchy-type where the advective input mass flux can be prescribed as a function of time at the origin of a pipe on the boundary of the domain. Mathematically, these boundary conditions are described by:

Dirichlet: $C_k = C_k^o(t)$ on Γ (Equation 2-21a)

Cauchy: $A(\ell)q(\ell)C_k^o(t) = A(\ell)\left[q(\ell)C_k(\ell,t) - D_\ell(\ell)\frac{\partial C_k}{\partial \ell}\right]$ on Γ (Equation 2-21b)

where $C_k^o(t)$ is the specified concentration for species k. PAWorks/LTG also allows the concentration at an interior point to be specified as a Dirichlet condition.

2.9.1.2 Immobile Zone

In order to represent the diffusive exchange of solute mass between the pipes and any of the *im* immobile zones attached to them, PAWorks/LTG uses an established first-order approach (see e.g. Sudicky, 1990, among others). Accordingly, the governing equation for the im^{th} immobile zone, allowing for chain decay and sorption according to a linear equilibrium Freundlich isotherm is described by:

$$\theta_{im}(im,\ell)V_{im}(im,\ell)\left[R_k'(im,\ell)\frac{\partial C_k'}{\partial t} + R_k'(im,\ell)\lambda_k C_k' - \sum_{j=1}^{m_k,k>1}\eta_{kj}\lambda_j R_j'(im,\ell)C_j'\right] = P(im,\ell)\alpha_k(im,\ell)[C_k - C_k'] \quad \text{(Equation 2-22)}$$

where:

$\theta_{im}(im,\ell)$ = Immobile zone porosity for immobile zone "*im*" attached to pipe "ℓ" [-]

$V_{im}(im,\ell)$ = Immobile zone volume/unit pipe length for immobile zone "*im*" attached to pipe "ℓ" [L^2]

$R_k'(im,\ell)$ = Immobile zone retardation factor for immobile zone "*im*" attached to pipe "ℓ" [-]

Note that PAWorks/LTG assumes the initial condition $C_k'(\ell,0) = 0$. With the formulation given by Equations 2-20 and 2-22, the mass transfer coefficient α_k is interpreted to be:

$$\alpha_k = \frac{\theta_{im}D_k^o\tau}{d}; \quad \text{(Equation 2-23)}$$

where:

τ = Tortuosity [-]

d = Diffusion distance [L]

If a particular immobile zone is fluid-filled, such as within an immobile water zone attached to a pipe within a fracture plane, then the immobile zone porosity, θ_{im}, would equal 1.0. Note that the definition of α_k given above differs from that used by Sudicky (1990) in that he uses d^2 in the denominator of Equation 2-23.

2.9.2 Laplace-transform Domain Transport Equations

The LTG method (Sudicky, 1989; Sudicky, 1990; Sudicky and McLaren, 1992) is a numerical solution procedure where the Laplace transform is first applied to the governing equation, and the transformed equation is then solved numerically using the Galerkin finite element procedure (or alternatively any other discretization method such as finite differences). Finally, upon a solution for the nodal Laplace-space solution, the time-domain solution is recovered by a numerical inversion of the Laplace transformed nodal solution.

Let the Laplace transform of a function $f(t)$ be defined according to:

$$\bar{f}(p) = \int_0^\infty f(t)\, e^{-pt}\, dt \qquad \text{(Equation 2-24)}$$

where p is the Laplace-transform parameter and first apply it to Equation 2-22 for the im^{th} immobile zone. Upon it's application and following algebraic manipulations, one obtains:

$$\overline{C}'_k = \frac{P\alpha_k \overline{C}_k + \theta_{im} V_{im} \sum_{j=1}^{m_k, k>1} \eta_{kj} \lambda_j R'_j \overline{C}'_j}{\theta_{im} V_{im} R'_k \mathcal{P}_k + P\alpha_k} \qquad \text{(Equation 2-25)}$$

where $\mathcal{P}_k = p + \lambda_k$ is the shifted Laplace parameter.

The next step involves application of the Laplace transform to the pipe transport equation Equation 2-20, followed by substitution of Equation 2-25 for the transformed immobile-zone concentration into the term involving the mobile-immobile zone solute transfer process appearing in Equation 2-20. After algebraic manipulations, one obtains the following for the Laplace transform of the pipe transport equation:

$$A(\ell)\left[\{R_k(\ell)\mathcal{P}_k+\frac{1}{A(\ell)}\bar{g}\}\bar{C}_k+q(\ell)\frac{\partial\bar{C}_k}{\partial\ell}-\frac{\partial}{\partial\ell}D_{\ell_k}(\ell)\frac{\partial\bar{C}_k}{\partial\ell}\right]\pm\sum_{\ell'}\dot{M}\delta(\ell-\ell')+\sum_{\ell^*}Q(\bar{C}_k-\bar{C}_k^*)\delta(\ell-\ell^*)$$

$$=A(\ell)\sum_{j=1}^{m_k,k>1}\eta_{kj}R_j(\ell)\lambda_j\bar{C}_j+\sum_{im=1}^{IM}\frac{P\alpha_k\theta_{im}V_{im}\sum_{j=1}^{m_k,k>1}\eta_{kj}\lambda_j\bar{R}_j'\bar{C}_j'}{\theta_{im}V_{im}\bar{R}_k'\mathcal{P}_k+P\alpha_k}$$

(Equation 2-26)

where:

$$\bar{g}=\sum_{im=1}^{IM}\frac{\theta_{im}V_{im}R_k'\mathcal{P}_kP\alpha_k}{\theta_{im}V_{im}R_k'\mathcal{P}_k+P\alpha_k}$$

It can be seen that the application of the Laplace transformation to the governing equations describing transport in the pipe network and each of the multiple immobile zones, followed by algebraic manipulations, has acted as a form of preconditioning in that the primary variable in Equation 2-26 is now restricted to that of the Laplace transform of the pipe network concentrations. This implies further savings in computational efficiency in that only one unknown, the Laplace transform of the nodal pipe concentrations, need be solved for implicitly. Once the transform of the nodal pipe concentrations is solved for, Equation 2-25 can be used to compute the immobile-zone concentrations as a flash calculation.

2.9.3 Numerical Solution Procedure

The numerical solution of the primary governing Equation 2-26 is obtained using a standard Galerkin finite element procedure with linear interpolation functions used for each one-dimensional pipe finite element, and a consistent mass matrix formulation

applied to the accumulation terms arising from the Laplace transform of the temporal derivative and decay terms. Details concerning the application of the Galerkin finite element method in the context of the LTG algorithm can be found elsewhere (e.g. Sudicky, 1989; Sudicky, 1990; Sudicky and McLaren, 1992) and will not be repeated here. Inversion of the nodal Laplace-transformed concentrations is achieved using the discrete Fourier series methodology provided by de Hoog et al. (1982) which employs an efficient quotient-difference algorithm to enhance convergence of the inversion process, thus yielding a high degree of accuracy with relatively few discrete $p = p_n$ Laplace p-space vectors. Details concerning the implementation and performance of the de Hoog et al. scheme when applied to the inversion of nodal Laplace-transformed concentrations that arise from an application of the LTG method to solve for transport in fractured geologic media can be found in Sudicky and McLaren (1992).

The matrix equations arising from the LTG algorithm when used in conjunction with the de Hoog et al. (1982) Laplace inversion scheme are complex-valued, and the coefficient matrix is sparsely populated for an arbitrary network of interconnected pipes. Thus, the WatSolv iterative sparse-matrix solver library (VanderKwaak et al., 1997) was adapted to handle the complex system of matrix equations. The WatSolv library is based on an ILU factorization of the non-symmetric coefficient matrix with user-defined levels of infill and several alternative re-ordering methods, including Red/Black system reduction, and employs CGSTAB (van der Vorst, 1992) acceleration to solve the preconditioned system of matrix equations. It also uses a compact ia-ja data storage structure such that only the non-zero terms in the matrix equations are stored and operated on. Further details on the capabilities of WatSolv can be found in VanderKwaak et al. (1997). The WatSolv library is designed to solve systems of equations arising from finite element, finite difference or finite volume discretizations using either single- or double-precision real, or single- or double-precision complex arithmetic.

2.9.4 PAWorks/LTG Test Cases

The examples presented here are intended to serve as test cases to ensure that PAWorks/LTG correctly solves the governing equations. Thus, the test problems all involve transport along a one-dimensional flow path for which exact analytic solutions

exist in most cases. The results from these analytic solutions will therefore be compared to those obtained from PAWorks/LTG. The test cases were designed to test a hierarchy of transport processes represented in PAWorks/LTG, and range in complexity from strictly one-dimensional advective-dispersive transport of a single, nonreactive solute, to the migration of a three-member decay chain comprised of sorbing radionuclides in a system of parallel fractures.

2.9.4.1 Single-porosity Test Problems 1 & 2: Transport of a Nonreactive Solute

This test case consists of the transport a single nonreactive solute (retardation $R = 1.0$, decay constant $\lambda = 0.0$) by advection and dispersion in a single-porosity domain. The input Darcy flux, q, is 1.0 m/day, the pipe area, A, equals 1.0 and the longitudinal dispersivity, α, is 1.0 m. Diffusion along the flow direction is neglected for simplicity. The domain is 100m in length and the spatial discretization is 2.0 m. This grid spacing, combined with an input dispersivity equal to 1.0 m, yields a grid Peclet number, Pe, equal to 2.0. A Dirichlet boundary condition was specified at the inflow end of the physical system in which the concentration was set to 1.0. At the outflow boundary, the concentration gradient was held at 0.0.

The PAWorks/LTG results are shown in Figure 2-38 for transport times equal to 25, 50, and 75 days, and they are compared to those obtained with the well-known Ogata-Banks analytic solution (Ogata and Banks, 1961). It can be seen that for $Pe = 2.0$, the PAWorks/LTG results are essentially identical to the analytical solution. The test problem was also repeated using a coarser grid spacing equal to 10.0 m ($Pe = 10.0$). The PAWorks/LTG results obtained with the coarse grid also compare very well with those calculated using the analytic solution. This demonstrates the effectiveness of the LTG scheme to resist unwanted numerical dispersion.

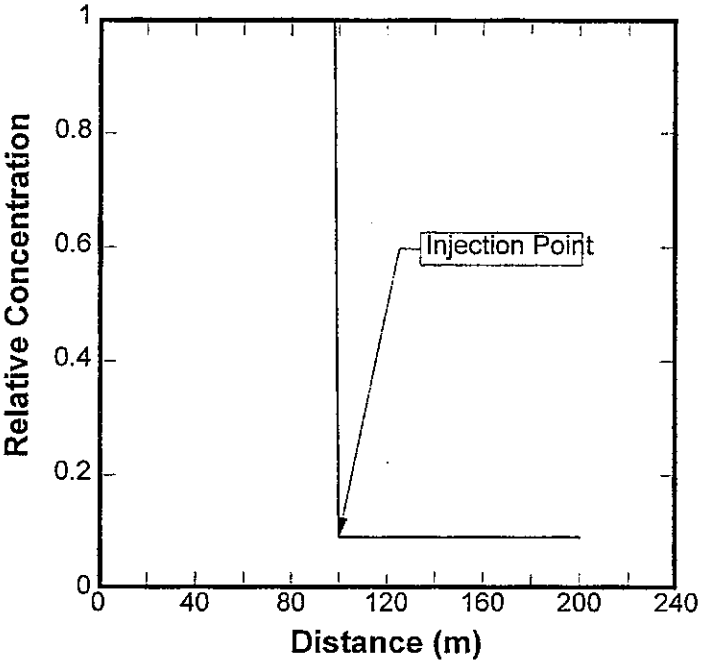

Comparison of PAWorks/LTG results to those from Ogata-Banks analytic solution for the case of one-dimensional advective-dispersive transport of a nonreactive solute

FIGURE **2-38**
TEST PROBLEM 1
PNC/H8

PROJECT NO. 923 1089.800 DRAWING NO. 73147 DATE 5/9/97 DRAWN BY EA

Golder Associates

In order to test the effect of the injection of a solute-free (i.e., $C^* = 0.0$) groundwater, the problem described above was repeated ($Pe = 2.0$ case) using a flow system of length 200m and with groundwater injected at the rate of $Q = 10$ m^3/day at a point 100m from the inlet boundary. Thus, the Darcy flux, q, is 1.0 m/day at the inlet and abruptly increases to 11.0 m^3/day at distance of 100 m. Figure 2-39 shows the PAWorks/LTG results at a time equal to 150 days. The reduction in the concentration at the injection point agrees closely with that calculated analytically based on mass balance considerations.

2.9.4.2 *Test Problem 3: Transport of Tritium in a System of Parallel Fractures*

This test case is concerned with the transport of a decaying, non-sorbing (i.e., $R = 1.0$) solute in a double-porosity system comprised of parallel fractures embedded in low-permeability, low-porosity rock matrix. The solute is tritium which has a half-life of 12.35 years ($\lambda = 1.54 \times 10^{-4}$ days^{-1}). The flow system is 300 m in length and the aperture of the parallel fractures, spaced at 0.1 m, is 100 μm. With this setting, the pipe area, A, is interpreted to equal the fracture porosity [-], which is 10^{-3}. The Darcy flux, q, is 0.1 m/day in the fractures and the longitudinal dispersivity of the fractures, α, is 0.1 m. The free-water diffusion coefficient for tritium, D^o, equals 1.38×10^{-4} m^2/day. The matrix porosity, θ_{im}, and tortuosity, τ, are 0.01 and 0.1, respectively. In order to facilitate a comparison with the exact analytic solution of Sudicky and Frind (1982), the mobile/immobile zone mass transfer coefficient was computed using d^2 instead of d in (4). A value of d equal to the half-spacing of the fractures (0.05 m) was used. This yields a modified mass transfer coefficient equal to 1.656×10^{-4} days^{-1}. The mesh spacing used is 10.0 m which yields a grid Pe number equal to about 100. The concentration was fixed at 1.0 at the inlet boundary and the concentration gradient equals 0.0 at the outflow end.

Figure 2-40 compares the PAWorks/LTG results with those obtained with the analytic solution of Sudicky and Frind (1982) at times equal to 1,000, 10,000 days and at steady-state. It can be seen that PAWorks/LTG yields highly-accurate results even though a coarse grid is used. Indeed, at 1,000 days, only the first node within the domain has a non-zero concentration and the concentration at this node agrees with the analytic solution.

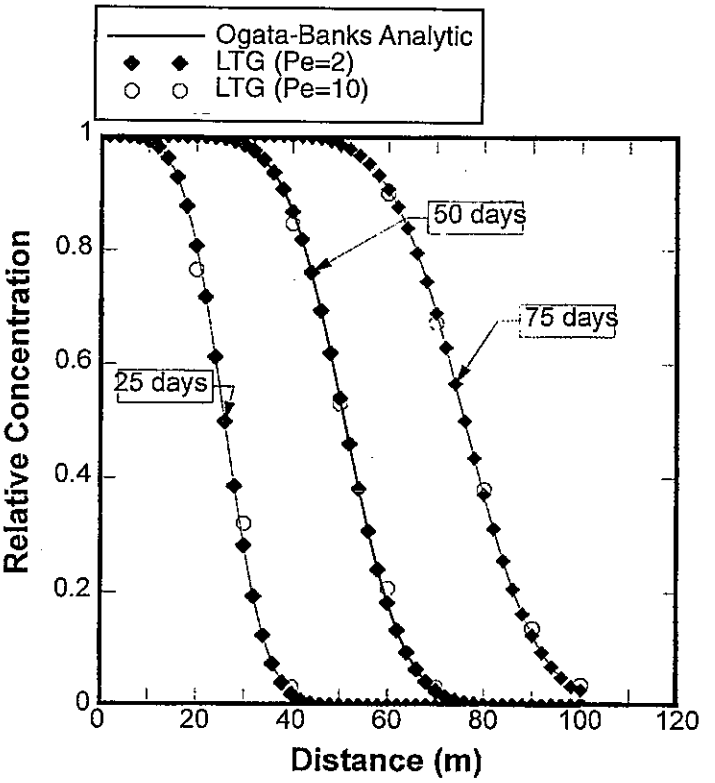

PAWorks/LTG results for injection of solute-free groundwater at x = 100m

FIGURE **2-39**
TEST PROBLEM 2
PNC/H8

PROJECT NO. 923 1089.800 DRAWING NO. 73148 DATE 5/9/97 DRAWN BY EA

Golder Associates

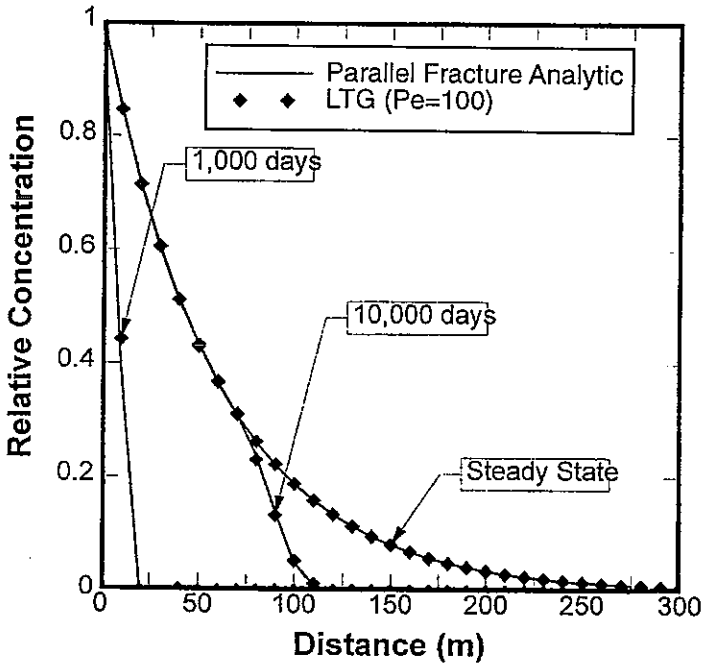

Transport of tritium in a system of parallel fractures

FIGURE **2-40**
TEST PROBLEM 3
PNC/H8

PROJECT NO. 923 1089.800 DRAWING NO. 73149 DATE 5/9/97 DRAWN BY EA

Golder Associates

2.9.4.3 *Test Problem 4: Decay Chain Transport in a System of Parallel Fractures*

The fourth test case involves the transport of the decay chain Uranium 234 → Thorium 230 → Radium 226 in a system of parallel fractures and is designed to verify many of the processes represented in PAWorks/LTG. The fracture aperture, fracture spacing and matrix porosity values are identical to those used for test problem 3 described above; however, for this example the Darcy flux, q, in the fractures is 100 m/year and the longitudinal dispersivity of the fractures, α, is 10.0 m. The flow system is 500 m in length and a grid spacing of 10 m was used. The matrix (i.e., immobile zone) retardation factors for U^{234}, Th^{230} and Ra^{226} were assigned values equal to 1.43×10^4, 5.00×10^4 and 5.00×10^2, respectively, and the decay constants equal 2.83×10^{-6}, 9.00×10^{-6} and 4.33×10^{-6} $year^{-1}$, respectively. For simplicity, retardation on the surfaces of the fractures (i.e., pipes) was neglected. The effective diffusion coefficients for each of the species, τD^o, were assigned identical values equal to 3.154×10^{-2} m^2/year. Once again, to facilitate comparison to the analytic solution of Hodgkinson and Maul (1985) for chain-decay transport in a system of parallel fractures, d^2 instead of d was used in (4) to compute the mobile/immobile zone mass transfer coefficient. Values assigned for each species is 3.78×10^{-2} $year^{-1}$. A prescribed concentration of 1.0 was assigned for U^{234} at the fracture inlet, but 0.0 was used as the inlet concentration for Th^{230} and Ra^{226}. Once again, the concentration gradient at the outflow boundary was taken to equal 0.0.

Figure 2-41 compares the PAWorks/LTG results to those obtained with the analytic solution of Hodgkinson and Maul (1985) at a time equal to 100,000 years. It can be seen from the results that PAWorks/LTG is capable of accurately representing the transport of a reactive decay chain in a double porosity-medium. While all of the examples involved a flow system that is essentially one-dimensional, it should be kept in mind that the code is structured to handle an arbitrary network of interconnected pipes in three-dimensional space; however, exact analytic solutions for such a setting are unavailable for comparison to PAWorks/LTG. It should also be mentioned that PAWorks/LTG has been coded to achieve a high degree of efficiency. For example, the 100,000 year simulation involving test problem 4 required only 0.22 seconds of CPU time on a 200 *Mhz* Pentium PC.

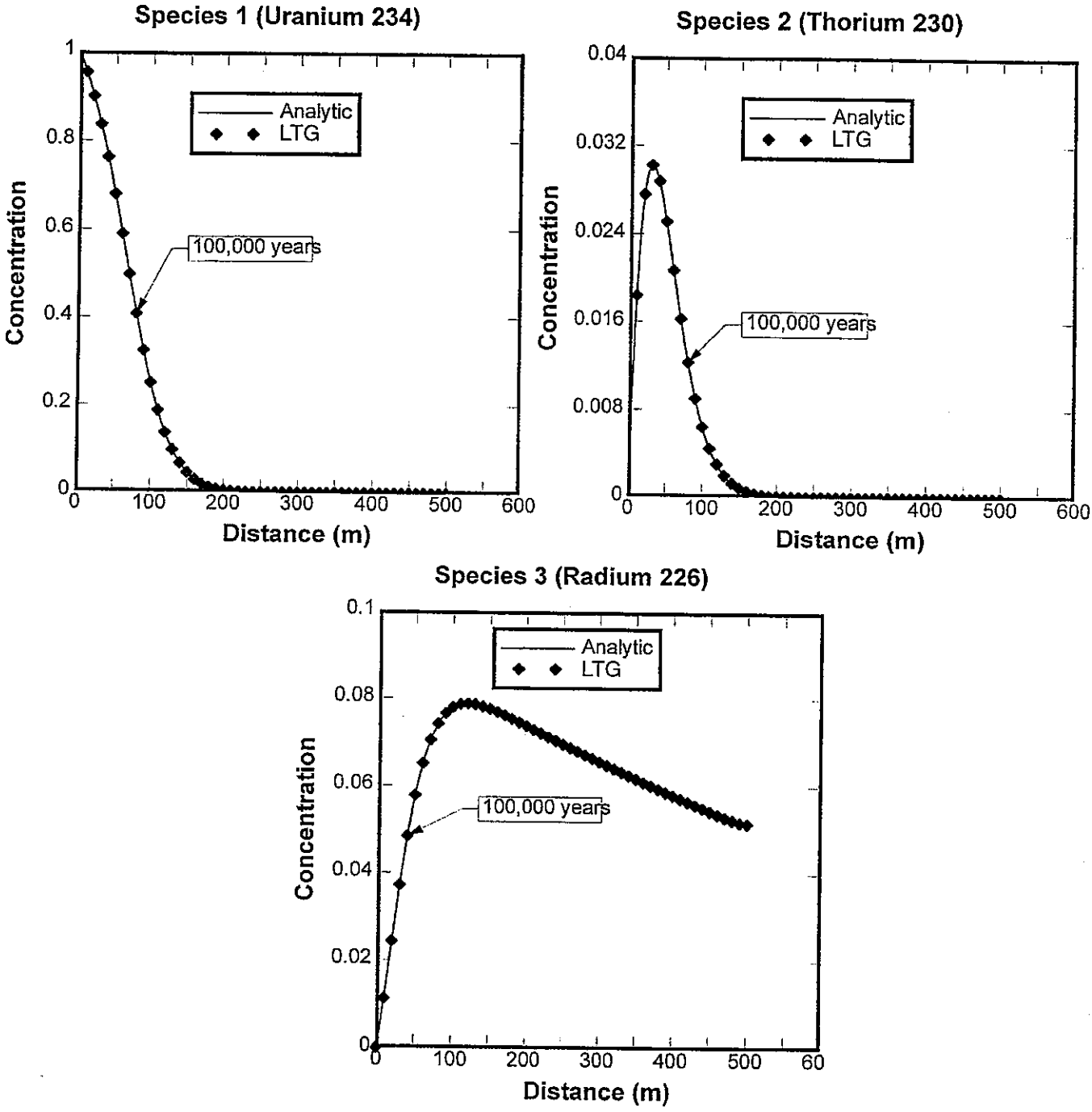

Decay chain transport in a system of parallel fractures

FIGURE **2-41**
TEST PROBLEM 4
PNC/H8

PROJECT NO. 923 1089.800 DRAWING NO. 73150 DATE 5/9/97 DRAWN BY EA

Golder Associates

2.10 Task 1.4.2: Stochastic Continuum Interface (EdMesh)

In this task, the EdMesh three dimensional stochastic field generator was modified to serve as a stochastic field generation pre-processor for the TAGSAC continuum code. EdMesh 1.4 is able to accept both MAFIC and TAGSAC meshes as input files, producing MAFIC and TAGSAC meshes as output files. All fractal, geostatistical, and empirical stochastic fields currently supported by EdMesh are available for use in generating stochastic continuum fields for assignment of properties to TAGSAC mesh elements. The EdMesh/TAGSAC feature is specified as follows:

- EdMesh reads TAGSAC fields and produces .SAB files containing either 1 point per element or n-nodes points per element, where n-nodes is the number of nodes on the element. Each point consists of x,y,z and property values from the TAGSAC files;
- EdMesh stochastic continuum and property assignment features are available to assign values to points in an .SAB file, using all of the existing EdMesh property assignment features, including stochastic continuum and correlated properties, and to specify assignment regions; and
- EdMesh writes TAGSAC files to assign properties to elements based on a .SAB file. The element assignment is based on the geometric or arithmetic mean of the values at points inside the elements, as a user option.
- The following sections describe the algorithm and file formats, present user instructions and a test case.

2.10.1 Algorithm

The modified version of EdMesh assigns or modifies continuum properties of any specified region within the TAGSAC model domain. Figure 2-42 presents a flowchart of the general EdMesh/TAGSAC interface. A TAGSAC mesh file "geometry file" and optionally the TAGSAC material property file, are read and translated into an .SAB file to allow linking with the EdMesh property generation routines. The EdMesh routines are used to generate material properties and assign regions for their application. A new

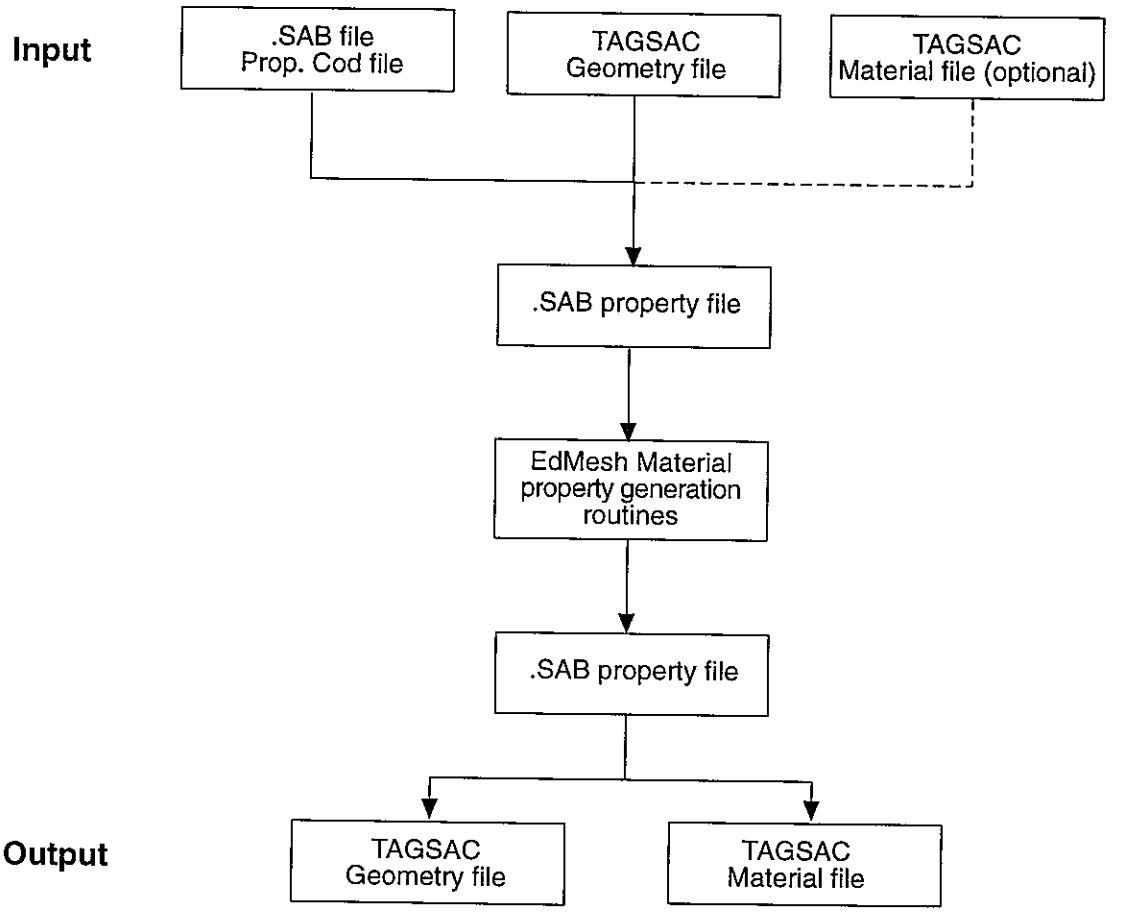

FIGURE **2-42**
EdMesh/TAGSAC INTERFACE FLOWCHART
PNC/H8

PROJECT NO. 923 1089.800 DRAWING NO. 73144 DATE 5/9/97 DRAWN BY EA

Golder Associates

.SAB file is then generated, and translated back into TAGSAC geometry-file and material-file format.

The TAGSAC geometry file contains mesh design information, including nodal coordinates, element configuration, and element material types. The element material types are linked to the TAGSAC material file (.MAT), that specifies the element material properties. As illustrated in Figure 2-42, the .MAT file is an optional input file. Input and output file formats are described in the following section.

TAGSAC elements may occur in five different two-dimensional or three-dimensional configurations, as shown in Figure 2-43. Each TAGSAC element is represented in the .SAB file either as a single point at the centroid of the element, or as n-nodes points per element, where n-nodes is the number of nodes comprising the element. In the latter case, the points are located halfway between each element node and the element centroid. Figure 2-44 illustrates the two options available for representing the elements as points within the .SAB file. The resulting translated .SAB file contains point x,y,z coordinates and, if a .MAT file exists, property values consistent with the original TAGSAC element property values. The PROPCOD.SAB input file shown in Table 2-21 specifies the property types to be generated in the EdMesh property generation routines.

Table 2-21 Example .SAB File Containing "PROP.COD"
Data Object: PROPCOD.SAB

```
begin prop.cod
MENU 0   :  items = 4
title    =  "FRACTURE PROPERTIES"          Null
item 1   =  "Permeability"                 Percentage   1
item 2   =  "Suction"                      Real
item 3   =  "Porosity"                     Real
item 4   =  "Storativity"                  Real
end
```

Two-Dimensional

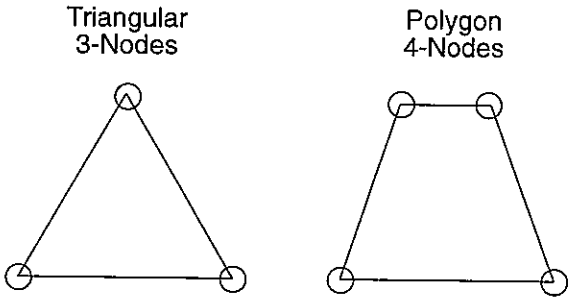

Three-Dimensional

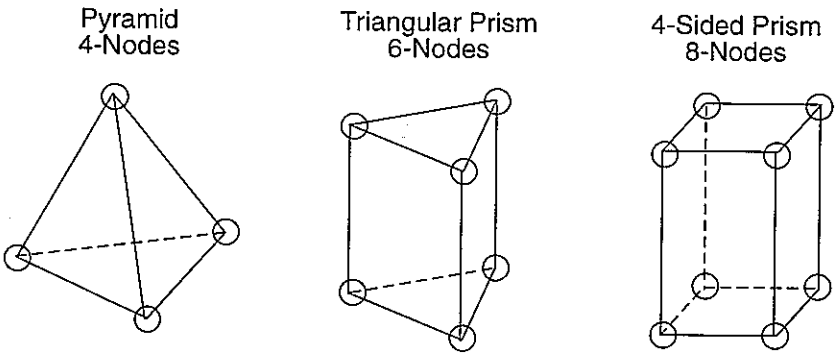

FIGURE **2-43**
TAGSAC ELEMENT CONFIGURATIONS
PNC/H8

PROJECT NO. 923 1089.800 DRAWING NO. 73145 DATE 5/8/97 DRAWN BY EA

Golder Associates

Two-Dimensional

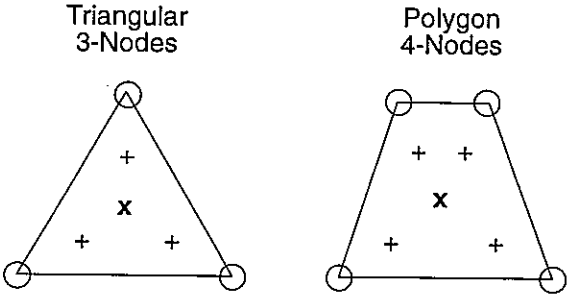

Three-Dimensional

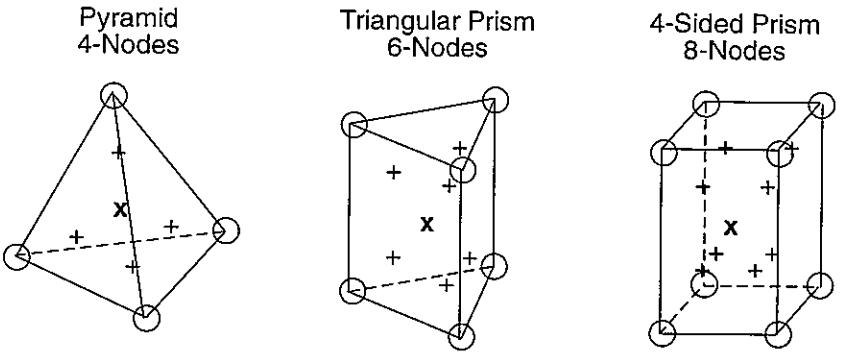

LEGEND

- x Element Centroid - Option 1 in representing element in .SAB file
- \+ Option 2 in representing element in .SAB file (points located halfway between centroid and element nodes)

FIGURE **2-44**
POINT REPRESENTATION OPTIONS IN .SAB FILE OF TAGSAC ELEMENTS
PNC/H8

PROJECT NO. 923 1089.800 DRAWING NO. 73146 DATE 5/9/97 DRAWN BY EA

Golder Associates

The EdMesh routines are then used to assign material properties, including permeability, suction, porosity, and storativity as specified in PROP.COD for each of the points in the .SAB file. Further, they can be repeatedly correlated to the previous values, or other parameters. The new values can be generated using any one of the following ten ways:

1. Geostatistical process,
2. Fractal Model,
3. Power-Law Correlation,
4. Linear Correlation;
5. Correlated to the distance from a plane
6. Uncorrelated to original property
7. Non-stationary Spatial Process
8. Conditional Field Process
9. POCS Process; or
10. Response surface

Methods (8) and (10) are newly added features specifically for use in interfacing with TAGSAC. These two methods are described below. The other methods have been previously described in the EdMesh users manual.

When method (8) is selected, EdMesh will ask for the conditioned data object name. The input conditioned field data, which consists of x,y,z coordinates followed by saturation values, must be specified as one of the data objects in the .SAB file. When (10) is selected, the response surface data object name is also required by EdMesh. All data objects used in a simulation must be included in a single .SAB file. The response surface data consists of several independent variables and one dependent variable. For example, the independent variables might be defined as Saturation (S), and Aperture (A) and the dependent variable as Relative Permeability (K). The input surface data define a response relationship: K = F(S,A).

The saturation S(i) for element i was assigned from the "Sat_Field" according to,

S(i) = S(closest X,Y,Z) point in "Sat_Field" .

Or, in general S(i) can be assigned by the N closest X,Y,Z points in "Sat_Field" based on the weighted average distance:

$$S(i) = \frac{\sum_{j=1}^{j=N} \frac{S_j}{D_j^P}}{\sum_{j=1}^{j=N} \frac{1}{D_j^P}} \qquad \text{(Equation 2-27)}$$

where, D_j is the distance from the centroid of element I to the closest point j; S_j, the saturation value of field point j; and P, the user specified constant.

The users have several options in selection of response functions:

(1) Point Response: The dependent value, K, is assigned from the closest surface point that has the closest saturation value to S(i).

$$K(i) = K_j \qquad \text{(Equation 2-28)}$$

where, K_j is the relative permeability value of the surface point j that has the closest saturation value to the element I.

(2) Linear Response: The dependent value, K, is assigned from the linear interpolation of two closest surface points: (S_1, K_1) and (S_2, K_2).

$$K(i) = K_1 + (K_2 - K_1)\frac{S(i) - S_1}{S_2 - S_1} \qquad \text{(Equation 2-29)}$$

(3) Quadratic Response: K is assigned from a quadratic formula:

$$K(i) = aS(i)^2 + bS(i) + c \qquad \text{(Equation 2-30)}$$

where, the coefficients: a, b, and c are determined from three closest surface points: (S_1, K_1), (S_2, K_2) and (S_3, K_3).

The above response Equations 2-27 and 2-28 can be applied in arithmetic domain, semi-log or in logrithmatic domain. When the menu item (10): response surface is chosen, EdMesh offers the following options on screen for the user to choose:

1 -- X_log, Y_log

2 -- X_log, Y_linear

3 -- X_linear, Y_log

4 -- X_linear, Y_linear

The input surface data specified in arithmetic values .SAB are converted to log-values before the linear or quadratic relationship in equations 2-27 and 2-28 is applied to obtain K(i) value when log or semi-log is chosen.

Verification cases are provided to test these surface function options. These verification cases are provided in the file ED_VERIF.ZIP.

When the number of independent variables (n) is more than one the dependent value V is calculated from a linear combination of the univariate response functions:

$$V = F(X_1, X_2, \ldots, X_n) = \frac{1}{n}(F(X_1)_{\text{fixed } X_j, j \neq 1} + F(X_2)_{\text{fixed } X_j, j \neq 2} + \ldots + F(X_n)_{\text{fixed } X_j, j \neq n})$$

(Equation 2-31))

The maximal dimensions of n is limited to 3 in this version of EdMesh. The univariate function $F(X_i)$ describes the response values with respect to one independent variable X_i at a time. The univariate function can be a point, linear or quadratic response as described in Equations 2-28 to 2-30. Before Equation 2-31 is applied to obtain V, the mean $(\overline{X}_i)$ and the standard deviation of each independent variable are calculated. When the standard deviation is smaller than 4% of the mean, the response is treated

invariable with respect to this independent variable. Thereby, the response surface dimensions, N, is reduced by one. The data file "K_Sat" in "usgs.sab" is one of these kinds.

For multi-dimensional response surface analysis, the input surface points must be grouped into several categories, before they are considered in Equation 2-31. The group number M is determined from:

$$M = \text{Min}\ (\ NPTS/4,\ 10) \qquad \text{(Equation 2-32)}$$

Where, NPTS is the total number surface points in .sab, and M is at least 1.

The data points that can be considered in the univariate function, $F(X_i)_{\text{fixed } X_j, j \neq i}$ must have $X_{j, j \neq i}$ values in the same category as the input data. The grouping process of the surface points is repeated for each input data. The input data is such as the fracture properties of each element in EdMesh. The grouping process ensures only the surface points in the vicinity of the input point are considered in the function $F(X_i)_{\text{fixed } X_j, j \neq i}$. For example, the input dimension of the response surface is N=2 and the input independent value $X_2 = 4.5$. When consider the univariate function : $F(X_1)_{\text{fixed } X2}$ only the surface points that have X_2 in (4.5-dx, 4.5+dx) are considered, where

$$dx = \frac{(X_{max} - X_{min})}{2M} \qquad \text{(Equation 2-33)}$$

where, Xmax and Xmin are the maximum and minimum values of X_2 among data in .SAB file.

After generation of the property values is complete, the region in which the properties are adjusted is selected by the user. There are five options for the selection of regions:

- All 3-D space,
- Box region
- Cylinder region

- Slab region
- Prism region

A new .SAB file is generated containing the new property values, which is then translated back into TAGSAC geometry and material file formats. The point property values contained in the .SAB file are translated back into element property values for TAGSAC in one of three ways, as specified by the user: 1)Arithmetic average, 2) Geometric mean, or 3) Harmonic mean of points inside the element. If none of the points occur inside the element, the property of the point closest to the element's centroid will be used for the element. This latter case can occur if the input .SAB file was not generated by translating the original TAGSAC input geometry file.

2.10.2 Input/Output File Formats

This section briefly describes the pertinent aspects of the contents of the input and output files, and presents simple examples of the files.

Table 2-22 presents a sample TAGSAC geometry file. The first line (record) is a file description. The second line contains several flags. The two flags of concern in this application are in the 6th and 7th positions. The 6th flag is the number of nodes (37), and the 7th is the number of elements (5). The third line is irrelevant to EdMesh. The next data block contains node numbers, flags, and corresponding x,y,z coordinates. The final block contains element numbers in the first column, property type (linked to the .MAT file) in the third column, the number of nodes per element in the 6th column, and following the 6th column, the node numbers comprising the element.

Table 2-23 presents a simple TAGSAC material file. The first flag represents the number of material blocks (5). Then there are two lines for each material, the first line has the material number only, and the next line has the material number and material properties.

Table 2-22 Example TAGSAC Geometry Input File: TAG_SMP.INP

```
TAGSAC input file
   0     0     0     0     0    37     5     0     0     0     0
       1.0
   1     0  0.0000000E+00  0.0000000E+00  0.0000000E+00
   2     0  1.0000000E+01  0.0000000E+00  0.0000000E+00
   3     0  2.0000000E+01  0.0000000E+00  0.0000000E+00
   4     0  3.0000000E+01  0.0000000E+00  0.0000000E+00
   5     0  4.0000000E+01  0.0000000E+00  0.0000000E+00
   6     0  5.0000000E+01  0.0000000E+00  0.0000000E+00
   7     0  6.0000000E+01  0.0000000E+00  0.0000000E+00
   8     0  7.0000000E+01  0.0000000E+00  0.0000000E+00
   9     0  8.0000000E+01  0.0000000E+00  0.0000000E+00
  10     0  9.0000000E+01  0.0000000E+00  0.0000000E+00
  11     0  1.0000000E+02  0.0000000E+00  0.0000000E+00
  12     0  0.0000000E+00  1.0000000E+01  0.0000000E+00
  13     0  1.0000000E+01  1.0000000E+01  0.0000000E+00
  14     0  2.0000000E+01  1.0000000E+01  0.0000000E+00
  15     0  3.0000000E+01  1.0000000E+01  0.0000000E+00
  16     0  4.0000000E+01  1.0000000E+01  0.0000000E+00
  17     0  5.0000000E+01  1.0000000E+01  0.0000000E+00
  18     0  6.0000000E+01  1.0000000E+01  0.0000000E+00
  19     0  7.0000000E+01  1.0000000E+01  0.0000000E+00
  20     0  8.0000000E+01  1.0000000E+01  0.0000000E+00
  21     0  0.0000000E+00  0.0000000E+00  1.0000000E+01
  22     0  1.0000000E+01  0.0000000E+00  1.0000000E+01
  23     0  2.0000000E+01  0.0000000E+00  1.0000000E+01
  24     0  3.0000000E+01  0.0000000E+00  1.0000000E+01
  25     0  4.0000000E+01  0.0000000E+00  1.0000000E+01
  26     0  5.0000000E+01  0.0000000E+00  1.0000000E+01
  27     0  6.0000000E+01  0.0000000E+00  1.0000000E+01
  28     0  7.0000000E+01  0.0000000E+00  1.0000000E+01
  29     0  8.0000000E+01  0.0000000E+00  1.0000000E+01
  30     0  9.0000000E+01  0.0000000E+00  1.0000000E+01
  31     0  1.0000000E+02  0.0000000E+00  1.0000000E+01
  32     0  0.0000000E+00  1.0000000E+01  1.0000000E+01
  33     0  1.0000000E+01  1.0000000E+01  1.0000000E+01
  34     0  2.0000000E+01  1.0000000E+01  1.0000000E+01
  35     0  3.0000000E+01  1.0000000E+01  1.0000000E+01
  36     0  4.0000000E+01  1.0000000E+01  1.0000000E+01
  37     0  5.0000000E+01  1.0000000E+01  1.0000000E+01
   1     0     1     0     0     8     1     2    13    12    21    22    33    32
   2     0     1     0     0     8     2     3    14    13    22    23    34    33
   3     0     1     0     0     8     3     4    15    14    23    24    35    34
   4     0     1     0     0     8     4     5    16    15    24    25    36    35
   5     0     1     0     0     8     5     6    17    16    25    26    37    36
```

Table 2-23 Example TAGSAC Material File: TAG_SMP.MAT

```
5
1
1   1.939E-08  -1.000E+03   7.576E-01   1.968E-05
2
2   5.066E-08  -1.000E+03   4.274E-01   6.455E-08
3
3   2.368E-07  -1.000E+03   5.300E-01   1.938E-06
4
4   4.510E-06  -1.000E+03   3.550E-01   4.771E-07
5
5   1.966E-06  -1.000E+03   4.136E-01   1.902E-08
```

Table 2-21 presents a .SAB file with the "PROP.COD" data object. This file names the properties that will be manipulated and assigned in the EdMesh/TAGSAC sessions. The first line names the data object "PROP.COD". The second line lists the number of items in the following list, and the remaining lines name the material types, and specify the data type (i.e. "Real"). The PROP.COD data object is required to name the properties of concern in the EdMesh/TAGSAC routines, and to specify the order in which the property values will appear in the .SAB files and the output TAGSAC .MAT file. It should be placed in the first .SAB file entered for EdMesh.

Table 2-24 shows a typical .SAB property file. Note that the first data block is the "PROP.COD" data object described above, separated by a blank line from the remainder of the file. Lines beginning with # are comment lines. The third line in the second data block specifies the data object type "tabular_data", and the forth line names the data object "tagout1.sab". The tabular data comprising the "tagout1.sab" data object begins with the keyword "begin data", followed by a variable label line. The property names in the label line correspond with those specified in the PROP.COD data object. Each line in the tabular data set presents point coordinates and corresponding property values. Each .SAB file may contain several data objects.

2.10.3 Running EdMesh

EdMesh is designed as an interactive program in which the user responds to a series of prompts generated from series of menus. EdMesh is also easily operated in batch-mode, as explained later in this section.

To run EdMesh in interactive mode for manipulating TAGSAC files, type the name of the EdMesh executable file from the command prompt >edmesh

EdMesh responds by requesting which file type, MAFIC or TAGSAC you wish to work with.

Input file type (1=.maf, 2=.sab) >

Table 2-24 Example .SAB File Translated From TAGSAC Geometry File: TAG_S1.SAB

```
begin prop.cod
MENU 0  :  items = 4
title   =  "FRACTURE PROPERTIES"          Null
item  1 =  "permeability"                 Real
item  2 =  "suction"                      Real
item  3 =  "porosity"                     Real
item  4 =  "storativity"                  Real
end

# File converted from TAGSAC:tag_smp.inp
# nnode, nelem in TAGSAC file =  37   5
begin tabular_data
  name=tagout1.sab
  begin data
  X  Y  Z  permeabil   suction     porosity    storativi
   5.000E+00   5.000E+00   5.000E+00   0.000E+00   0.000E+00   0.000E+00   0.000E+00
   1.500E+01   5.000E+00   5.000E+00   0.000E+00   0.000E+00   0.000E+00   0.000E+00
   2.500E+01   5.000E+00   5.000E+00   0.000E+00   0.000E+00   0.000E+00   0.000E+00
   3.500E+01   5.000E+00   5.000E+00   0.000E+00   0.000E+00   0.000E+00   0.000E+00
   4.500E+01   5.000E+00   5.000E+00   0.000E+00   0.000E+00   0.000E+00   0.000E+00
  end
end
```

Enter 2 to work with a TAGSAC files. EdMesh responds by requesting the name of the .SAB file containing the "PROP.COD" data object.

Enter name of .SAB file containing PROP.COD object >

EdMesh then opens the main menu for the EdMesh/TAGSAC interface.

```
**** MAIN MENU ****
  (0) Quit without saving changes!
  (1) Create continuum file
  (2) Assign continuum properties
  (3) Modify TAGSAC file
  (4) Save EdMesh file
  (5) Run EdMesh
```

Option (1) is used to create a new .SAB continuum file from an existing .SAB continuum file. Option (2) assigns stochastic continuum or correlated property values to points in the .SAB file, and specifies the assignment region. Option (3) creates an .SAB file from TAGSAC files to allow interfacing with the EdMesh property assignment routines, and when property assignments have been made, writes TAGSAC files from the new .SAB files. Option (4) saves all key-entries recorded during the interactive session for documentation purposes, and possible later use as input in batch-mode sessions. Option (5) creates a log file, performs the selected property value calculations on the selected .SIP and TAGSAC files, and terminates the program.

The order of execution of the above main menu items will vary depending on the particular application. For example, for the general EdMesh/TAGSAC interface described in Section 2.10.1, Option (3) may be selected first to translate TAGSAC files to .SAB format, followed by (1) to create a new .SAB file, (2) to set parameters for generating properties and assign regions to the new .SAB file, (3) again to translate the new .SAB file back to TAGSAC format, and (5) to execute the commands and terminate the session.

Submenus for each of the five main menu options are described as follows:

Option (0) - Quit without saving changes

This option is self explanatory.

Option (1) Create continuum file

EdMesh prompts the user to enter the name of an existing .SAB file containing continuum data, the continuum data object name, and the name of the .SAB file to be created.

Enter input .SAB filenames for continuum properties :

Enter continuum data object name >

Enter output SAB file name >

EdMesh then returns you to the main menu.

Option (2) Assign continuum properties

Option (2) is used to assign continuum properties to the points in the continuum data file. EdMesh responds with the following menu.

```
**** ELEMENT PROPERTIES ****
     ( 0) Quit, return to main menu
     ( 1) Assign permeability
     ( 2) Assign suction
     ( 3) Assign porosity
     ( 4) Assign storativity
```

After selecting the element property you wish to work with, EdMesh responds with another menu specific to the property chosen. An example for permeability is as follows:

```
****  permeability  Options: ****
   ( 0) Quit, return to previous menu
   ( 1) Geostatistical process
   ( 2) Fractal Model
   ( 3) Power-Law Correlation
   ( 4) Linear    Correlation
   ( 5) Correlated to the distance from a plane
   ( 6) Uncorrelated to original permeability□
```

```
( 7) Non-stationary Spatial Process
( 8) Conditioned Field Process
( 9) POCS Process
(10) Response Surface
```

After a selection is made, EdMesh displays the corresponding formulation and prompts the user for parameter values to be used in the equation, or prompts the user for additional input files, as required. For example, if (6) was selected, the following formula and prompt for input would be displayed:

Formula: P_1 = Xo + 10^[bX + N(0,eX)]

Enter parameters (Xo, bX, eX) >

After entering the requested values, EdMesh prompts the user to select the region for which the properties are to be assigned.

```
**** SELECT REGION ****
      (0) Back to previous menu
      (1) All 3-D space
      (2) Box
      (3) Cylinder
      (4) Slab
      (5) Prism
```

Depending on the type of region selected, the user will be further prompted for additional coordinate information. When the region has been assigned, the algorithm returns to the ELEMENT PROPERTIES menu, and the user repeats the above general procedure to assign suction, porosity, storativity properties, or permeability properties to another region, at the users option. After completing the property assignment, the user will return to the main menu.

Option (3) Modify TAGSAC file

This option creates an .SAB file from TAGSAC files to interface with the EdMesh property assignment routines, and when property assignments have been made, writes TAGSAC files from the new .SAB files.

The submenu for this option is as follows:

```
****  Get TagSac I/O File Names ****
  (0) Quit,  return to main menu
  (1) Create SAB file from TagSac
  (2) Create TagSac file from SAB
```

If (1) is selected, the user will be prompted for an .SAB output file, a TAGSAC input geometry file, and a TAGSAC material file.

SAB output file name >

Enter TagSac input geometry file name >

Do you have an existing .MAT file ? 1=Yes, 2=No >

As suggested by the last prompt, a TAGSAC material file (.MAT) is not required. If a .MAT file is provided, however, the new properties can be generated from correlation with the existing data. EdMesh then prompts the user to specify the number of internal points per element to be included in the .SAB file.

Select number of internal points:

1 for one point per element; 2 for No. Points=No. Nodes

Enter 1 or 2 >

If (1) is selected, each element in the TAGSAC geometry file will be represented in the .SAB file with a single centroid point. If (2) is selected, each element in the TAGSAC geometry file will be represented by n-node points, as described in Section 2.10.1.

If menu option (2) "Create TagSac file from SAB" is selected, the user will be prompted for input and output .SAB and TAGSAC files, similar to that above. In addition, the user must chose an option to calculate the property value for each element from the point values in the .SAB file. Options for calculating the property value for each element include :

1=Arithmetic, 2=Geometric, 3=Harmonic mean from points inside element

If none of the points are inside the element, the property of the point closest to the element's centroid will be used for the element.

Option (4) Save EdMesh file

This options saves the key-entered data during the interactive session to a file called "edmesh.set". The primary function of this file is to provide a record of changes to a mesh file. However, since this file contains all commands given to the program EdMesh (except for the name of the input file), it may be used to run EdMesh in batch mode. The file includes descriptive text associated with the key-entered data to facilitate understanding of the file, and to allow for easy modification for future batch mode sessions.

After saving edmesh.set, rename it to record the run and to avoid overwriting of the file later. For later runs of EdMesh, append this file to a file containing the name of the next file you wish to edit. An example of an "edmesh.set" file is presented in Table 2-25. After renaming edmesh.set to "run1.in", for example, the EdMesh session can be rerun by typing edmesh <run1.in at the command prompt.

Option (5) Run EdMesh

Option (5) creates a log file, performs the selected property value calculations on the selected .SAB files, and modifies the TAGSAC files as specified. Before exiting, EdMesh will request any additional information needed for calculations. This information may include a random number seed to initialize a Monte Carlo routine; minimum and maximum parameter values, or the data file name for the fractal model (if used). The EdMesh session is then terminated.

2.10.4 Test Case

A simple example of an EdMesh/TAGSAC session is presented in Tables 2-26. Table 2-27 presents the input TAGSAC geometry file. Note that the material property codes (third column of the last data block) are all set to 1. Table 2-24 presents the PROPCOD.SAB file. For this example, an input TAGSAC .MAT file is not used. Table 2-26 presents the

EdMesh menus and prompts, and corresponding key entries recorded during the test session.

The .SAB file translated from the input TAGSAC file was previously presented in Table 2-24. Note that the material properties in this file appear as zeros, because an input TAGSAC .MAT file was not used during the translation. The output .SAB file stemming from the execution of EdMesh is presented in Table 2-27. Note that material properties are now present for permeability, suction, porosity, and storativity, consistent with the parameters used in the EdMesh session.

Table 2-28 presents the output TAGSAC geometry file. Note now that the material property codes (third column of the last data block) have been modified. Table 2-23 presents the output TAGSAC .MAT file, with element material properties translated from the output .SAB file (Table 2-24), and material flags corresponding to those in the TAGSAC geometry file.

This simple test case demonstrates the correct operation of the EdMesh/TAGSAC interface.

Table 2-25 Example EDMESH.SET Output

```
   2     [ input  type ]
propcod.sab□                              [ input file name ]
   3     [ Modify TAGSAC file ]
   1     [ 1-TagSac to SAB, 2-SAB to TagSac ]
tagout1□                                  [ SAB output name converted from
TagSac file ]
tag_smp.inp□                              [ TagSac input geom. name ]
   2                                      [ 1=yes,  2=no .mat file ]
   1                                      [ 1=centroid, 2=No. Nodes ]
   1     [ Create continuum file ]
tagout1□                                  [ SAB input filename ]
tagout1.sab□                              [ SAB data object name ]
tagout2.sab□                              [ SAB output name ]
   1     [ Assign fracture property # ]
   6     [ model option ]
   .0000      -6.000       2.000          [ Xo, bX, eX ]
   1                                      [ All 3-D space ]
   2     [ Assign continuum properties ]
   2     [ Assign fracture property # ]
   6     [ model option ]
  -1001.       .0000       .0000          [ Xo, bX, eX ]
   1                                      [ All 3-D space ]
   2     [ Assign continuum properties ]
   3     [ Assign fracture property # ]
   1     [ model option ]
   0                                        [ Geostatistics option ]
   .5000       .1500       .0000          [ xmean, stddev, cov_par ]
   1                                      [ All 3-D space ]
   2     [ Assign continuum properties ]
   4     [ Assign fracture property # ]
   6     [ model option ]
   .0000      -6.000       2.000          [ Xo, bX, eX ]
   1                                      [ All 3-D space ]
   3     [ Modify TAGSAC file ]
   2     [ 1-TagSac to SAB, 2-SAB to TagSac ]
tagout2□                                  [ SAB input name containing prop.cod]
tagout2.sab□                              [ SAB data object name ]
   1                                      [ 1=yes,  2=no geometry file ]
tag_smp.inp□                              [ TagSac input geom. name ]
tag_smpo.inp□                             [ TagSac output geom. name ]
tag_smp.mat□                              [ TagSac material name ]
   1                                      [ 1=Arithmetic, 2=Geometric,
3=Harmonic mean ]
   5     [ Run ]
        20357                             [ seed ]
    .100E-09    .100E+01                  [ min, max of permeability ]
   -.200E+04    .000E+00                  [ min, max of suction ]
    .000E+00    .100E+01                  [ min, max of porosity ]
    .100E-09    .100E-01                  [ min, max of storativity ]
```

Table 2-26 Example EDMESH/TAGSAC Interactive Session

```
C>edmesh

Input file type (1=.maf, 2=.sab) >  2

**** MAIN MENU ****
      (0) Quit without saving changes!
      (1) Create continuum file
      (2) Assign continuum properties
      (3) Modify TAGSAC file
      (4) Save EdMesh file
      (5) Run  EdMesh

Selections >  3

    ****  Get TagSac I/O File Names ****
      (0) Quit,  return to main menu
      (1) Create SAB file from TagSac
      (2) Create TagSac file from SAB

Selection >  1
       Selected: (1) Create SAB file from TagSac

SAB input file name containing prop.cod object > propcod.sab
    SAB output file name > tago_s1
    Enter TagSac input geometry file name >  tag_smp.inp
      Do you have an existing .MAT file ?  1=Yes, 2=No >  2

Select number of internal points:

     1 for one point per element; 2 for No. Points=No. Nodes

Enter 1 or 2 >  1

**** MAIN MENU ****
      (0) Quit without saving changes!
      (1) Create continuum file
      (2) Assign continuum properties
      (3) Modify TAGSAC file
      (4) Save EdMesh file
      (5) Run  EdMesh

Selections >  1
    Enter input .sab filenames for continuum properties :

Enter .sab file name  > tago_s1
    Enter continuum data object name >  tagout1.sab
    Enter output SAB file name >  tagout2.sab


    **** ELEMENT PROPERTIES ****
     ( 0) Quit, return to main menu
     ( 1) Assign permeability
     ( 2) Assign suction
     ( 3) Assign porosity
     ( 4) Assign storativity

Selection >  1

****  permeability□  Options: ****
   ( 0) Quit, return to previous menu
   ( 1) Geostatistical process
   ( 2) Fractal Model
   ( 3) Power-Law Correlation
   ( 4) Linear    Correlation
   ( 5) Correlated to the distance from a plane
   ( 6) Uncorrelated to original permeability□
   ( 7) Non-stationary Spatial Process
   ( 8) Conditioned Field Process
   ( 9) POCS Process
   (10) Response Surface
```

Table 2-26 (continued)

```
Selection > 6

Formula:  P_1 = Xo + 10^[ bX + N(0,eX)]

 Enter parameters (Xo, bX, eX) > 0,-6,2

    **** SELECT REGION ****
      (0) Back to previous menu
      (1) All 3-D space
      (2) Box
      (3) Cylinder
      (4) Slab
      (5) Prism

Selection Region >  1

**** MAIN MENU ****
      (0) Quit without saving changes!
      (1) Create continuum file
      (2) Assign continuum properties
      (3) Modify TAGSAC file
      (4) Save EdMesh file
      (5) Run  EdMesh

Selections >  2

    **** ELEMENT PROPERTIES ****
     ( 0) Quit, return to main menu
     ( 1) Assign permeability
     ( 2) Assign suction
     ( 3) Assign porosity
     ( 4) Assign storativity

Selection >  2

****  suction□  Options: ****
   ( 0) Quit, return to previous menu
   ( 1) Geostatistical process
   ( 2) Fractal Model
   ( 3) Power-Law Correlation
   ( 4) Linear    Correlation
   ( 5) Correlated to the distance from a plane
   ( 6) Uncorrelated to original suction□
   ( 7) Non-stationary Spatial Process
   ( 8) Conditioned Field Process
   ( 9) POCS Process
   (10) Response Surface

Selection >   6

Formula:  P_1 = Xo + 10^[ bX + N(0,eX)]

 Enter parameters (Xo, bX, eX) > -1001,0,0

    **** SELECT REGION ****
      (0) Back to previous menu
      (1) All 3-D space
      (2) Box
      (3) Cylinder
      (4) Slab
      (5) Prism

Selection Region >  1

**** MAIN MENU ****
      (0) Quit without saving changes!
      (1) Create continuum file
      (2) Assign continuum properties
      (3) Modify TAGSAC file
      (4) Save EdMesh file
      (5) Run  EdMesh

Selections >  2
```

Table 2-26 (continued)

```
**** ELEMENT PROPERTIES ****
     ( 0) Quit, return to main menu
     ( 1) Assign permeability
     ( 2) Assign suction
     ( 3) Assign porosity
     ( 4) Assign storativity

Selection >  3

   ****  porosity□  Options: ****
   ( 0) Quit, return to previous menu
   ( 1) Geostatistical process
   ( 2) Fractal Model
   ( 3) Power-Law Correlation
   ( 4) Linear    Correlation
   ( 5) Correlated to the distance from a plane
   ( 6) Uncorrelated to original porosity□
   ( 7) Non-stationary Spatial Process
   ( 8) Conditioned Field Process
   ( 9) POCS Process
   (10) Response Surface

Selection >  1

   Select Covariance Function Type :

       0) Null  1) Exponential  2) Spherical > 0

 !=!=!=!==!=!=!=!=!=!=!=!=!=!=!=!=!=!=!=!=!=!=!=!=!=!=!=!=!=!=!=
 When a negative mean value is specified below
 and a range of fracture numbers or sets is
 selected EdMesh uses original fracture (T,S,A)
 as the mean value for elements on this fracture;
 and the std. dev. of (T,S,A) of the elements on
 this fracture is calculated from the input
 deviation factor multiplied by (T,S,A).
 !=!=!=!==!=!=!=!=!=!=!=!=!=!=!=!=!=!=!=!=!=!=!=!=!=!=!=!=!=!=!=

 Enter mean, std. dev. (factor) >  .5,.15,0

**** SELECT REGION ****
      (0) Back to previous menu
      (1) All 3-D space
      (2) Box
      (3) Cylinder
      (4) Slab
      (5) Prism

Selection Region >  1

**** MAIN MENU ****
      (0) Quit without saving changes!
      (1) Create continuum file
      (2) Assign continuum properties
      (3) Modify TAGSAC file
      (4) Save EdMesh file
      (5) Run  EdMesh

Selections >  3

**** ELEMENT PROPERTIES ****
     ( 0) Quit, return to main menu
     ( 1) Assign permeability
     ( 2) Assign suction
     ( 3) Assign porosity
     ( 4) Assign storativity

Selection >

****  storativity□  Options: ****
   ( 0) Quit, return to previous menu
   ( 1) Geostatistical process
   ( 2) Fractal Model
   ( 3) Power-Law Correlation
   ( 4) Linear    Correlation
```

Table 2-26 (continued)

```
    ( 5) Correlated to the distance from a plane
    ( 6) Uncorrelated to original storativity□
    ( 7) Non-stationary Spatial Process
    ( 8) Conditioned Field Process
    ( 9) POCS Process
    (10) Response Surface

 Selection >

 Formula:  P_1 = Xo + 10^[ bX + N(0,eX)]

  Enter parameters (Xo, bX, eX) >

     **** SELECT REGION ****
       (0) Back to previous menu
       (1) All 3-D space
       (2) Box
       (3) Cylinder
       (4) Slab
       (5) Prism

 Selection Region >

     **** MAIN MENU ****
       (0) Quit without saving changes!
       (1) Create continuum file
       (2) Assign continuum properties
       (3) Modify TAGSAC file
       (4) Save EdMesh file
       (5) Run  EdMesh

 Selections >

     ****  Get TagSac I/O File Names ****
       (0) Quit,  return to main menu
       (1) Create SAB file from TagSac
       (2) Create TagSac file from SAB

 Selection >  2
        Selected: (2) Create TagSac file from SAB

     SAB input file name >
     Enter data object name in SAB file >
       Do you want to modify material index in geomery file
       while .MAT file is created ?   1=Yes, 2=No >
     Enter TagSac input geometry file name >
     Enter TagSac output geometry file name >
     Enter TagSac output material file name >
 Options for calculation of property value for each element :

    1=Arithmetic, 2=Geometric, 3=Harmonic      mean from points inside element

 Enter 1, 2, or 3 >

 **** MAIN MENU ****
       (0) Quit without saving changes!
       (1) Create continuum file
       (2) Assign continuum properties
       (3) Modify TAGSAC file
       (4) Save EdMesh file
       (5) Run  EdMesh

 Selections >  5

 Seed value for random numbers >

     **** Set lower and upper bounds for fracture properties ****
       Enter min. and max. values for permeability >
       Enter min. and max. values for suction >
       Enter min. and max. values for porosity >
       Enter min. and max. values for storativity >
    Running EdMesh
 Stop - Program terminated.
```

Table 2-27 Example .SAB File Used to Generate Final TAGSAC Files: TAG_S2.SAB

```
begin prop.cod
MENU 0  :  items = 4
title   =  "FRACTURE PROPERTIES"          Null
item  1 =  "permeability"                 Real
item  2 =  "suction"                      Real
item  3 =  "porosity"                     Real
item  4 =  "storativity"                  Real
end

# Input continuum file:tagout1.sab
# npts, nprops=   5   4
begin tabular_data
  name=tagout2.sab□
  begin data
  X  Y  Z  permeabil   suction     porosity    storativi   □
   5.000E+00   5.000E+00   5.000E+00     1.939E-08  -1.000E+03   7.576E-01   1.968E-05
   1.500E+01   5.000E+00   5.000E+00     5.066E-08  -1.000E+03   4.274E-01   6.455E-08
   2.500E+01   5.000E+00   5.000E+00     2.368E-07  -1.000E+03   5.300E-01   1.938E-06
   3.500E+01   5.000E+00   5.000E+00     4.510E-06  -1.000E+03   3.550E-01   4.771E-07
   4.500E+01   5.000E+00   5.000E+00     1.966E-06  -1.000E+03   4.136E-01   1.902E-08
end
```

Table 2-28 Example TAGSAC Geometry Output File: TAG_SMP.OUT

```
TAGSAC output file
   0     0     0     0     0    37     5     0     0     0     0
    1.000
   1     0  0.0000000E+00  0.0000000E+00  0.0000000E+00
   2     0  1.0000000E+01  0.0000000E+00  0.0000000E+00
   3     0  2.0000000E+01  0.0000000E+00  0.0000000E+00
   4     0  3.0000000E+01  0.0000000E+00  0.0000000E+00
   5     0  4.0000000E+01  0.0000000E+00  0.0000000E+00
   6     0  5.0000000E+01  0.0000000E+00  0.0000000E+00
   7     0  6.0000000E+01  0.0000000E+00  0.0000000E+00
   8     0  7.0000000E+01  0.0000000E+00  0.0000000E+00
   9     0  8.0000000E+01  0.0000000E+00  0.0000000E+00
  10     0  9.0000000E+01  0.0000000E+00  0.0000000E+00
  11     0  1.0000000E+02  0.0000000E+00  0.0000000E+00
  12     0  0.0000000E+00  1.0000000E+01  0.0000000E+00
  13     0  1.0000000E+01  1.0000000E+01  0.0000000E+00
  14     0  2.0000000E+01  1.0000000E+01  0.0000000E+00
  15     0  3.0000000E+01  1.0000000E+01  0.0000000E+00
  16     0  4.0000000E+01  1.0000000E+01  0.0000000E+00
  17     0  5.0000000E+01  1.0000000E+01  0.0000000E+00
  18     0  6.0000000E+01  1.0000000E+01  0.0000000E+00
  19     0  7.0000000E+01  1.0000000E+01  0.0000000E+00
  20     0  8.0000000E+01  1.0000000E+01  0.0000000E+00
  21     0  0.0000000E+00  0.0000000E+00  1.0000000E+01
  22     0  1.0000000E+01  0.0000000E+00  1.0000000E+01
  23     0  2.0000000E+01  0.0000000E+00  1.0000000E+01
  24     0  3.0000000E+01  0.0000000E+00  1.0000000E+01
  25     0  4.0000000E+01  0.0000000E+00  1.0000000E+01
  26     0  5.0000000E+01  0.0000000E+00  1.0000000E+01
  27     0  6.0000000E+01  0.0000000E+00  1.0000000E+01
  28     0  7.0000000E+01  0.0000000E+00  1.0000000E+01
  29     0  8.0000000E+01  0.0000000E+00  1.0000000E+01
  30     0  9.0000000E+01  0.0000000E+00  1.0000000E+01
  31     0  1.0000000E+02  0.0000000E+00  1.0000000E+01
  32     0  0.0000000E+00  1.0000000E+01  1.0000000E+01
  33     0  1.0000000E+01  1.0000000E+01  1.0000000E+01
  34     0  2.0000000E+01  1.0000000E+01  1.0000000E+01
  35     0  3.0000000E+01  1.0000000E+01  1.0000000E+01
  36     0  4.0000000E+01  1.0000000E+01  1.0000000E+01
  37     0  5.0000000E+01  1.0000000E+01  1.0000000E+01
   1     0     1     0     0     8     1     2    13    12    21    22    33    32
   2     0     2     0     0     8     2     3    14    13    22    23    34    33
   3     0     3     0     0     8     3     4    15    14    23    24    35    34
   4     0     4     0     0     8     4     5    16    15    24    25    36    35
   5     0     5     0     0     8     5     6    17    16    25    26    37    36
```

3. TASK 2: APPLICATION SUPPORT

Application support during HY-8 consisted of 4 tasks: Kamaishi analysis, site generic analysis, performance assessment, and fracture network literature survey. The first two application support tasks are described in Sections 3.1 and 3.2 below. The final two application support tasks are summarized in Sections 3.3 and 3.4 below, and are described in Appendices A and F.

3.1 Task 2.1: Kamaishi Analysis Support

During HY-7, Golder Associates reviewed fracture and hydrological data from the Task 3-2 area and developed a preliminary FracMan model for the Task 3-2 area. The H-7 model used hydraulically-based definitions of the fracture network clusters with properties obtained from the build-up testing in KH-25. The model successfully modeled the steady heads using non-unique sets of property values for the fracture networks between the fracture network clusters.

HY-8 activities related to Kamaishi analysis support were limited to:

- Assembly and analysis of fracture data gathering during the past 3 years as input to the Task 3-2 area model, to facilitate future development of the hydrogeologic discrete fracture conceptual model;
- Further development of the Task 3-2 area fracture network model using new information; and
- Simulation of Tracer Tests using the Task 3-2 area model.

Future development of the Kamaishi FracMan model was deferred until HY-9.

3.1.1 Tracer Test Modeling

This section presents scoping calculations for tracer tests in the Kamaishi Task 3-2 block. These calculations, which employ the FracMan/MAFIC software suite, will provide guidance for setting actual test parameters such as the pumping and injection rates and the duration of injection, pumping, and monitoring. The FracMan/MAFIC software allows a variety of simulation options including:

1. variable transmissivity and aperture,
2. matrix diffusion,
3. sorption, and
4. particle tracking.

The tracer test simulations discussed in this report incorporate various combinations of these options. Thus, the potential power of the discrete feature/finite element approach possible with FracMan/MAFIC is demonstrated.

3.1.1.1 Mesh Generation

The first step in the modeling is to generate a finite element mesh of a single fracture penetrated by two wells. Three different well spacings were simulated: 2 m, 5 m, and 10 m (Table 3-1). In each case, the mesh around the well pairs was discretized at a finer scale than the area away from the wells. For the 2 and 5 m spacings, the wells were simulated by hexagonal prisms with diameters of 0.08 m. For the 10 m spacing, the wells were simulated by square prisms with diameters of 0.08 m. Figures 3-1 to 3-6 show each of the three meshes at different scales. Near the simulated boreholes all three meshes (Figures 3-3, 3-4, 3-5, and 3-7) contain skinny elements which could introduce problems to the particle tracking algorithms in MAFIC; however, as long as lateral dispersion was non-zero those problems were scarcely evident. Better meshes (Figures 3-1b and 3-3b) were also created by selecting the borehole refinement option in MeshMonster with no fracture predivision, then using EdMesh to refine the mesh.

Table 3-1 The finite element meshes.

Mesh #	Interwell distance	Fracture radius	Max area of element	# nodes before refine	Refined zone dim	Max area of element	# nodes after refine
PNC005x	2 m	15 m	0.25 m^2	8515	4x4	0.1 m^2	11319
PNC004x	5 m	30 m	1.0 m^2	8513	10x10	0.2 m^2	12721
PNC006x	10 m	50 m	2.0 m^2	8499	20x20	0.4 m^2	12673

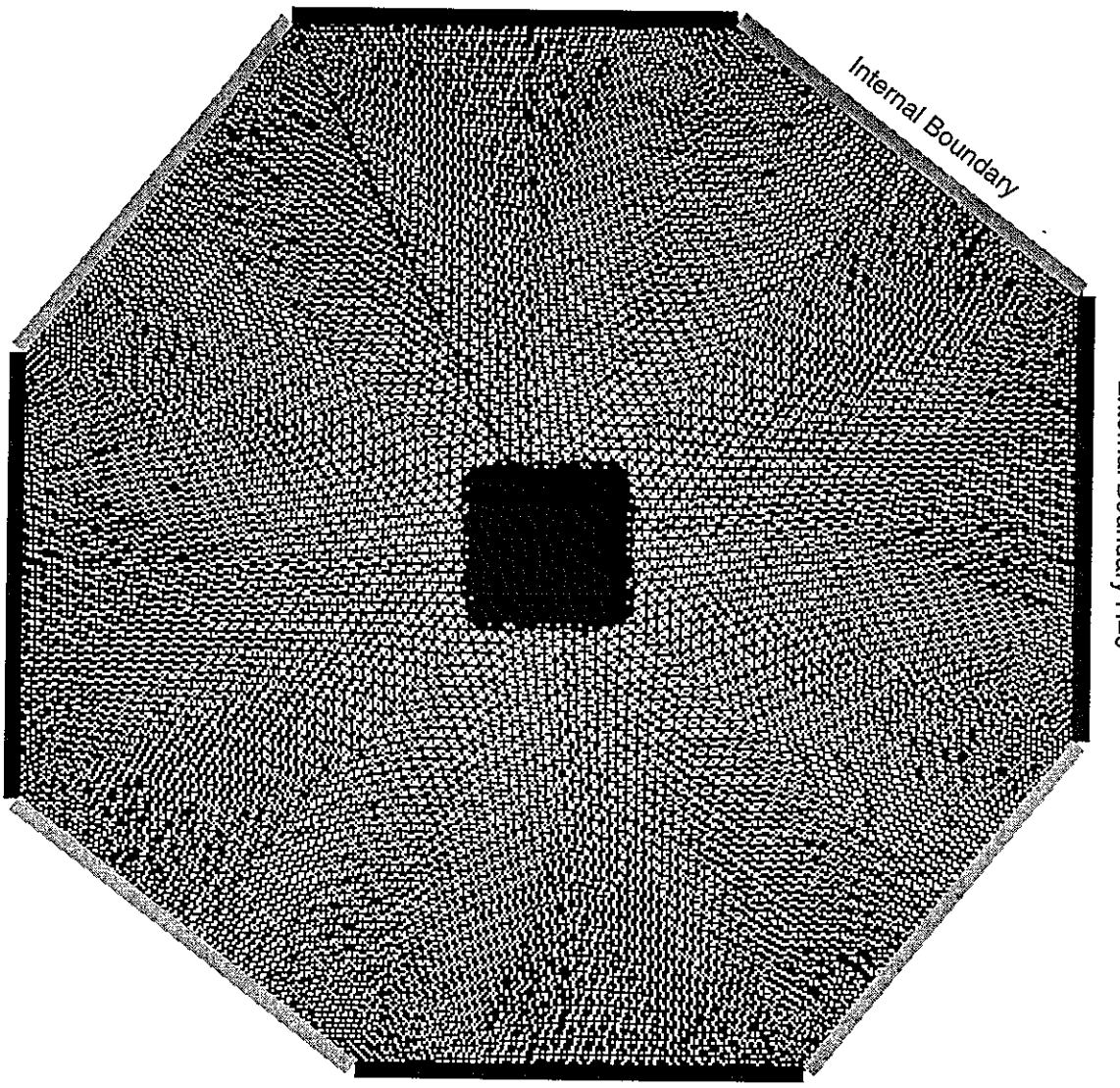

FIGURE **3-1**
PNC0050a MESH
PNC-KAMAISHI/H8 REPORT

PROJECT NO. 923 1089.921 DRAWING NO. 72877 DATE 6/25/97 DRAWN BY CB

Golder Associates

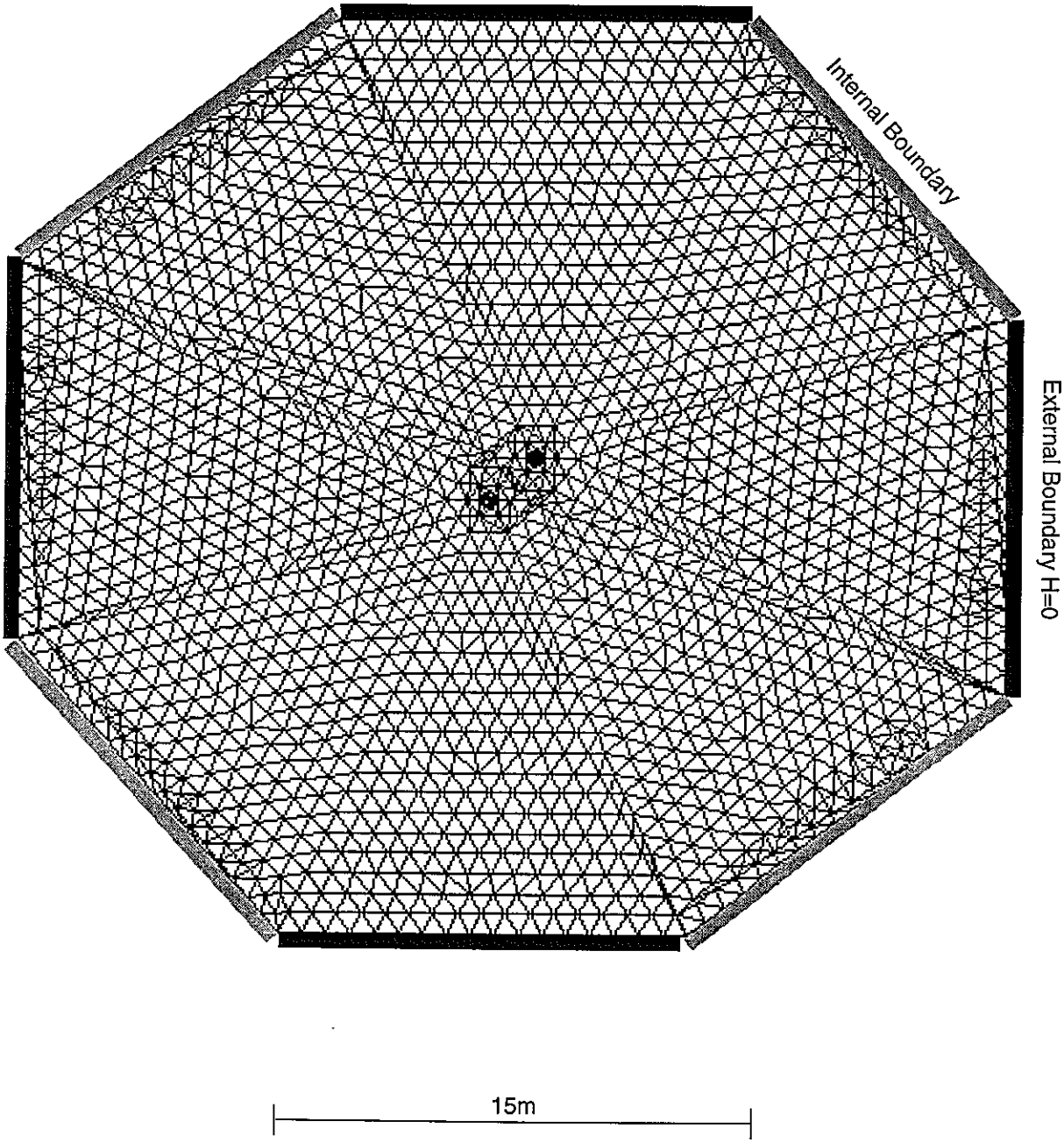

FIGURE **3-1b**
ALTERNATE 1:1 DIPOLE MESH
PNC-KAMAISHI/H8 REPORT

PROJECT NO. 923 1089.921 DRAWING NO. 77043 DATE 2/20/98 DRAWN BY EA

Golder Associates

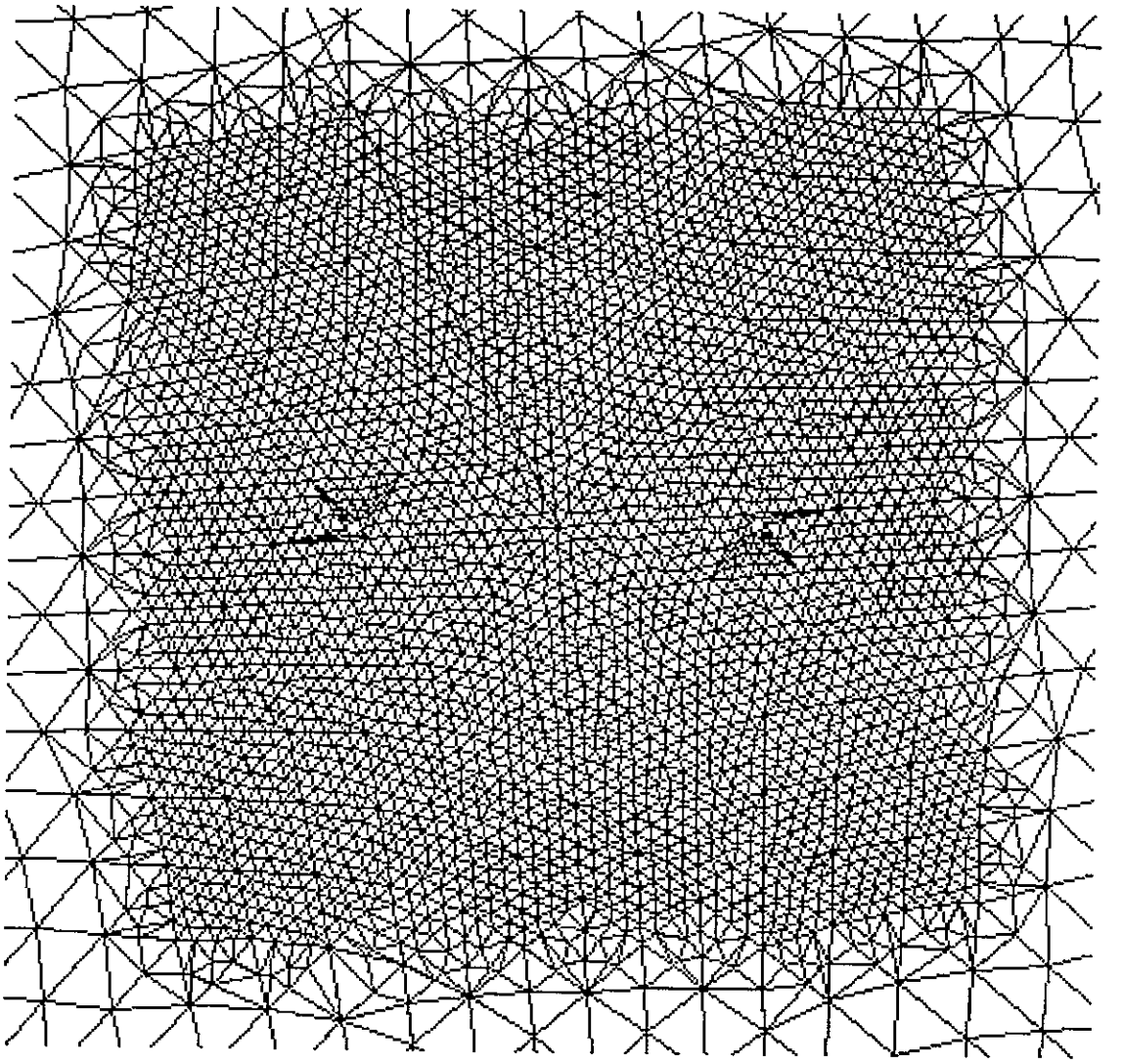

FIGURE **3-2**
PNC005X MESH
PNC-KAMAISHI/H8 REPORT

PROJECT NO. 923 1089.921 DRAWING NO. 72878 DATE 6/25/97 DRAWN BY CB

Golder Associates

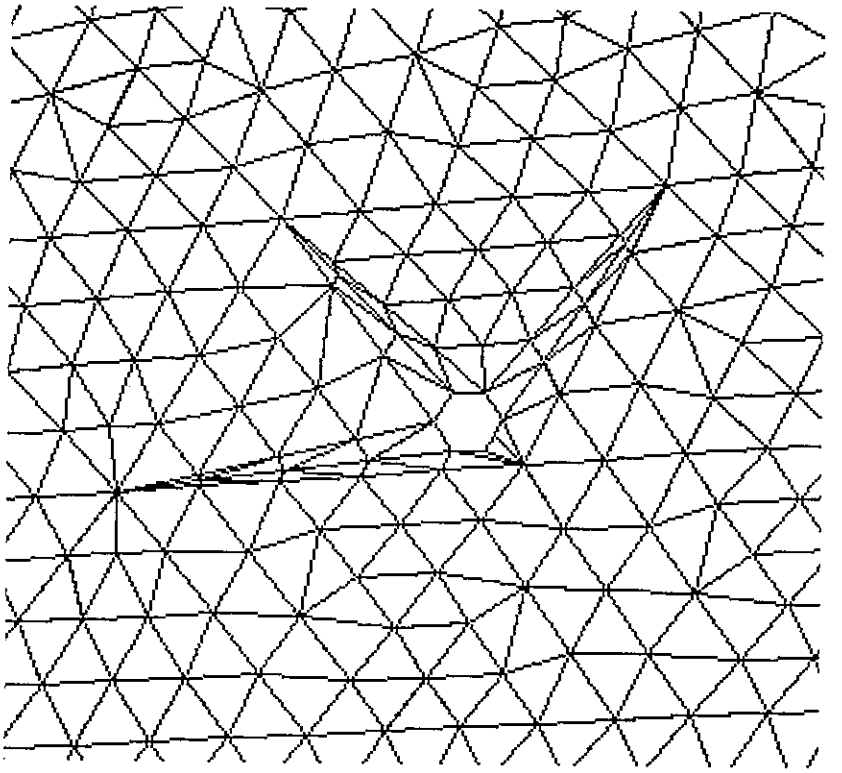

0.1m

FIGURE **3-3**
PNC005X MESH NEAR WELL
PNC-KAMAISHI/H8 REPORT

PROJECT NO. 923 1089.921 DRAWING NO. 72879 DATE 6/25/97 DRAWN BY CB

Golder Associates

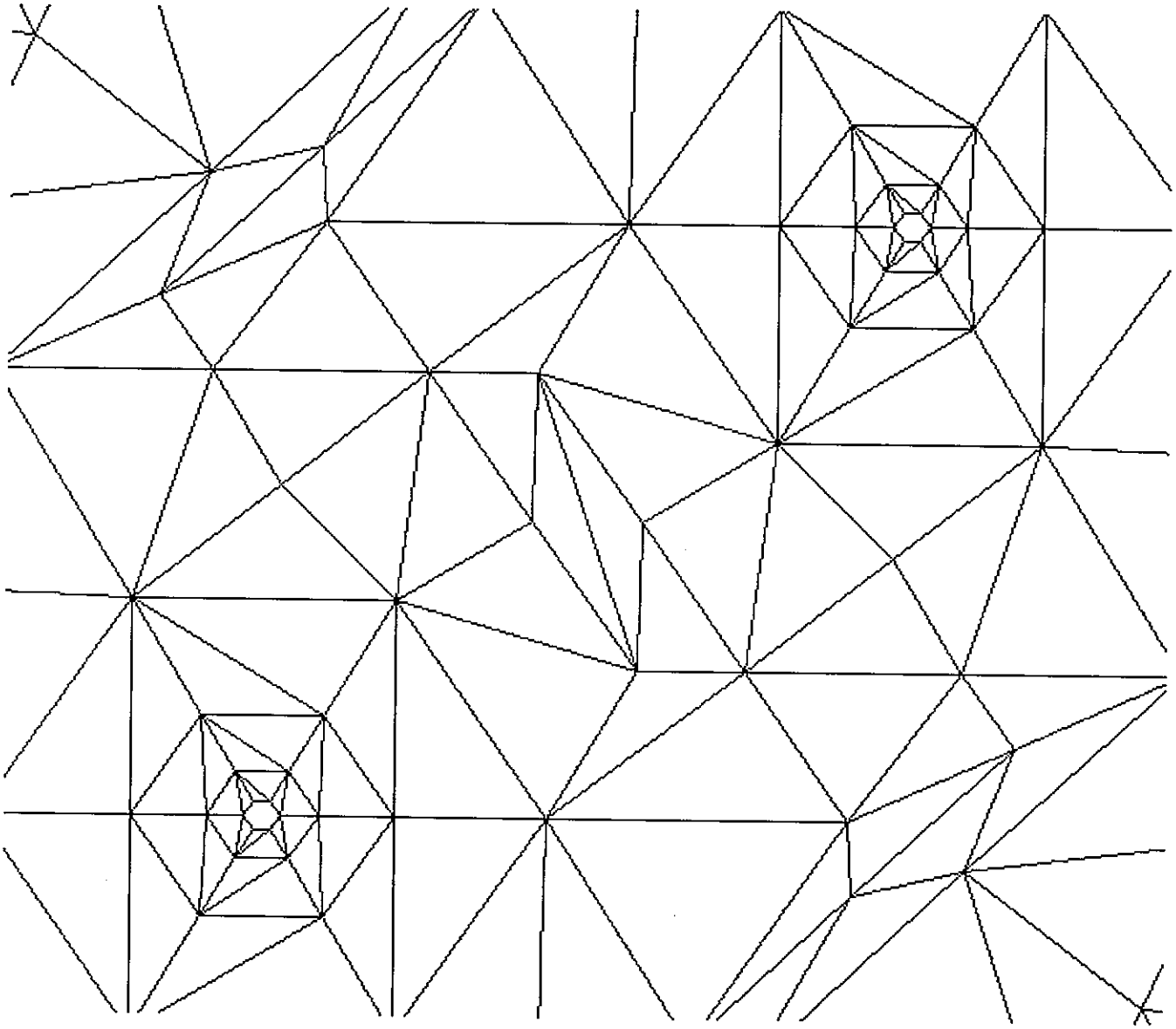

FIGURE **3-3b**

ALTERNATE 1:1 DIPOLE MESH NEAR WELLS

PNC-KAMAISHI/H8 REPORT

PROJECT NO. 923 1089.921 DRAWING NO. 77044 DATE 2/20/98 DRAWN BY EA

Golder Associates

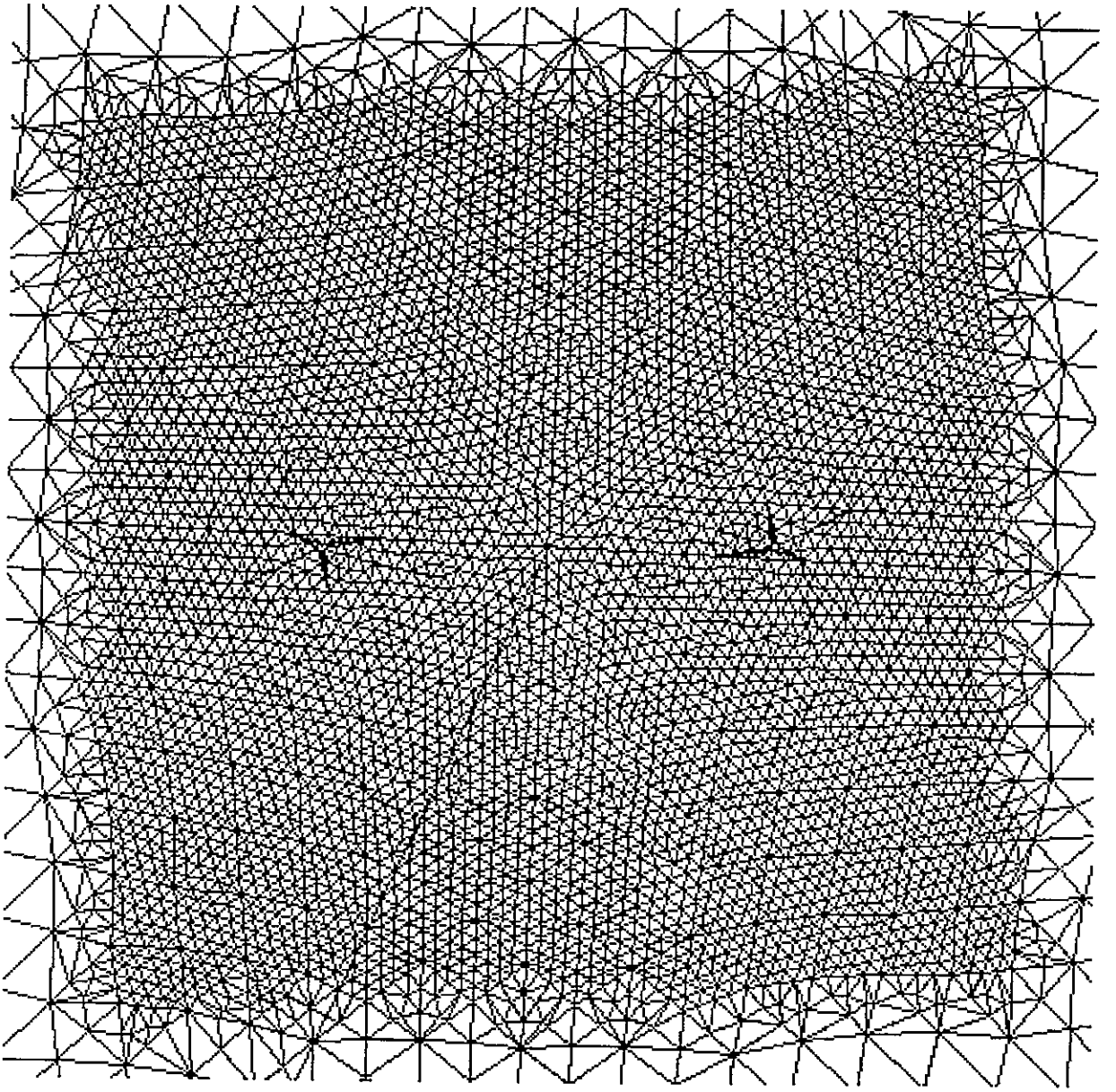

FIGURE **3-4**
PNC004X MESH
PNC-KAMAISHI/H8 REPORT

PROJECT NO. 923 1089.921 DRAWING NO. 72880 DATE 6/25/97 DRAWN BY CB

Golder Associates

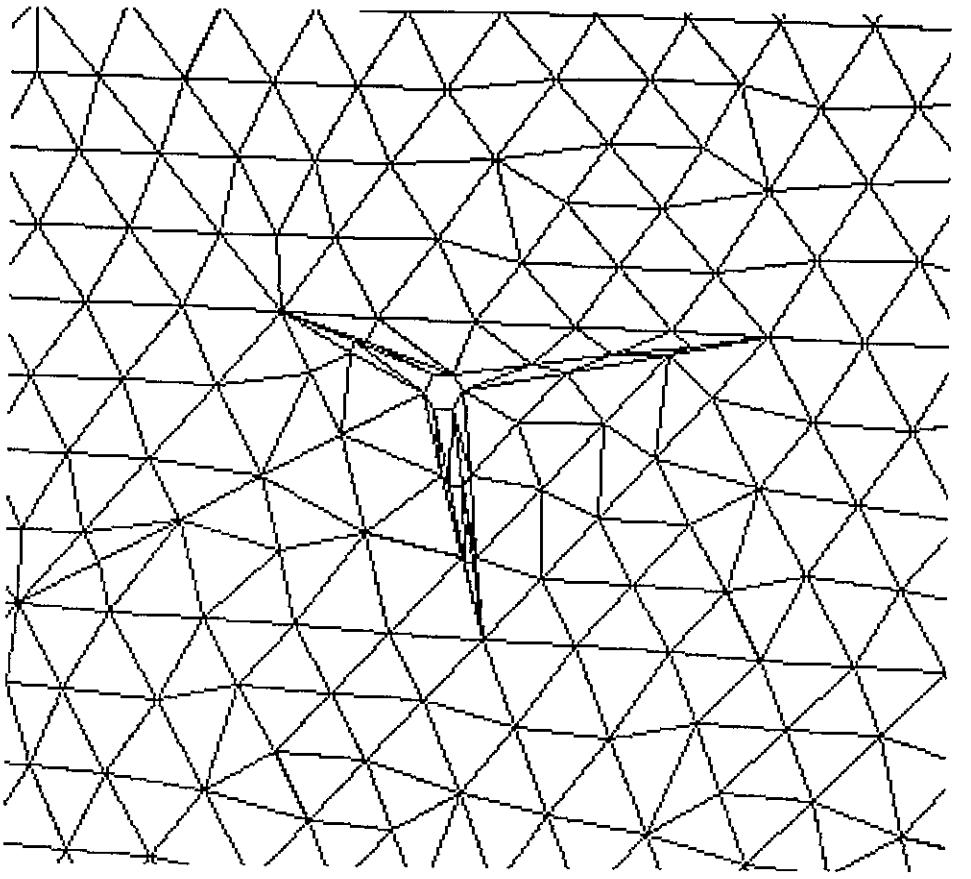

0.1m

FIGURE **3-5**
PNC004X MESH NEAR WELL
PNC-KAMAISHI/H8 REPORT

PROJECT NO. 923 1089.921 DRAWING NO. 72881 DATE 6/25/97 DRAWN BY CB

Golder Associates

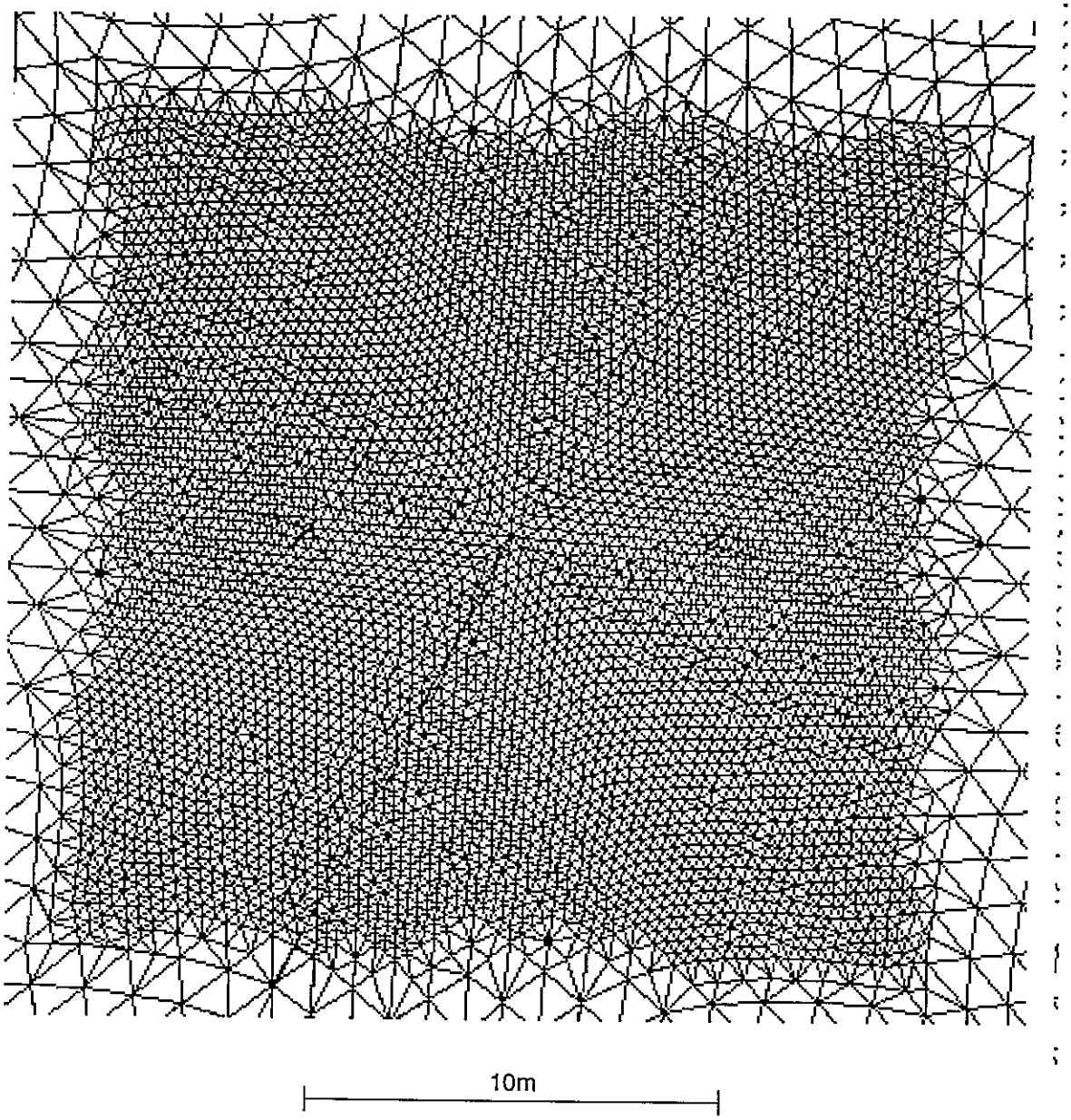

FIGURE **3-6**
PNC006X MESH
PNC-KAMAISHI/H8 REPORT

PROJECT NO. 923 1089.921 DRAWING NO. 72882 DATE 6/25/97 DRAWN BY CB

Golder Associates

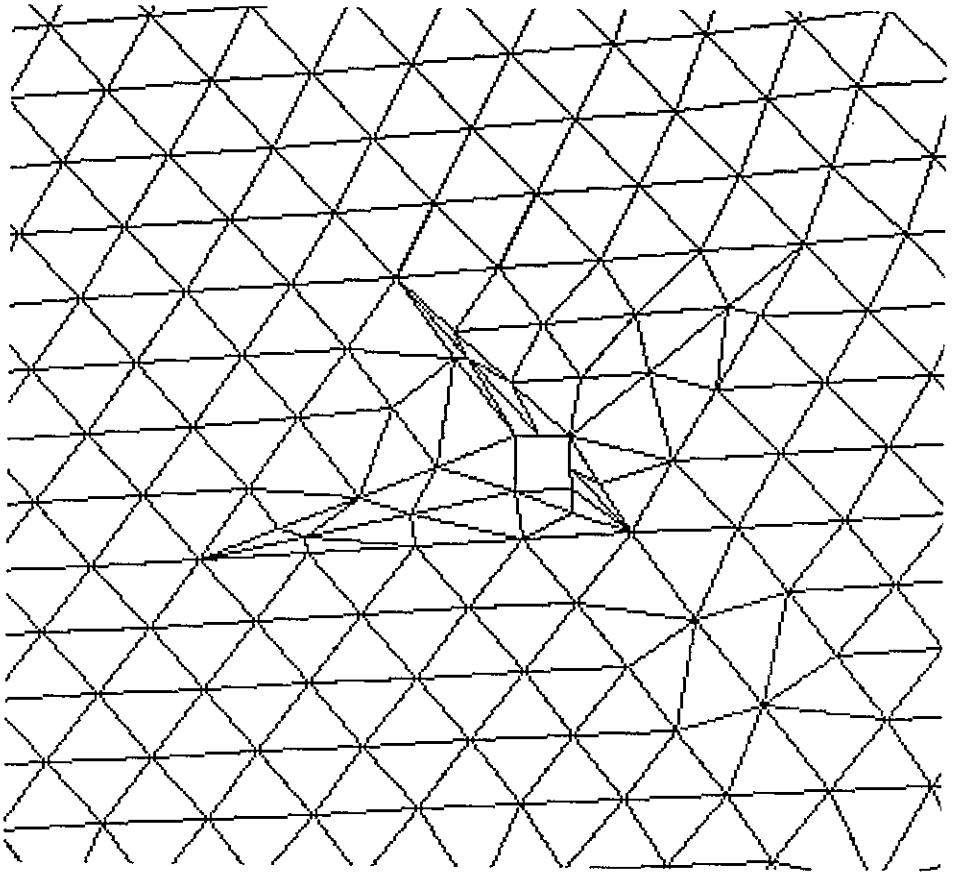

0.1m

FIGURE **3-7**

PNC006X MESH NEAR WELL

PNC-KAMAISHI/H8 REPORT

PROJECT NO. 923 1089.921 DRAWING NO. 72883 DATE 6/27/97 DRAWN BY CB

Golder Associates

3.1.1.2 Flow Parameters

The flow parameters used in the tracer test studies are provided in Table 3-2. Transmissivity distribution, dipole strength, and pumping rate were varied as part of the scoping calculations.

External boundary conditions – The fracture was modeled as an octagonal plate. To simulate a single fracture with good connection (no flux limit) to its surrounding, a constant head boundary was set at four of the fracture edges (Figure 3-1). Along those boundaries the head was arbitrarily set to zero. The other four edges are internal boundaries with no specified condition.

Internal boundary conditions – Internal boundary conditions were defined at the two wells. At the pumping well the flux was set equal to the pumping rate (Table 3-2). At the tracer and chase fluid injection well the flux was set equal to the pumping rate multiplied by the dipole ratio.

Table 3-2 Flow parameters set with EdMesh

Run #	T mean (m^2/s)	T st. dev	e mean (mm)	Pump Rate (m^3/s)	Dipole Strength	Individual particle mass (kg)	L and T dispersion	Other feature
PNC0050a	2.3e-7	2.0e-7	0.98	2.3e-6	1:1	1e-4	0.5 / 0.05	
PNC0051	3.6e-7	3.0e-7	1.2	3.3e-6	1:1	1e-4	0.5 / 0.05	
PNC0052	2.3e-7	0	0.98	2.3e-6	1:1	1e-4	0.5 / 0.05	No diffusion
PNC0053	2.3e-7	0	0.98	2.3e-6	1:1	1e-4	0.5 / 0.05	
PNC0054	2.3e-7	0	0.98	2.3e-6	1:1	1e-4	0.5 / 0.05	Retard=3
PNC0040a	2.3e-7	2.0e-7	0.98	2.3e-6	1:2	5e-5	0.1/0.01	
PNC0041	3.6e-7	3.0e-7	1.2	3.3e-6	1:2	5e-5	0.1/0.01	
PNC0042	2.3e-7	0	0.98	2.3e-6	1:2	5e-5	0.1/0.01	No diffusion
PNC0060a	2.3e-7	2.0e-7	0.98	2.3e-6	1:10	1e-5	0.01/.001	
PNC0061	3.6e-7	3.0e-7	1.2	3.3e-6	1:10	1e-5	0.01/.001	

Transmissivity – Three flow simulations were done with a constant transmissivity field in the fracture. Six simulations were run using a spatially uncorrelated transmissivity field with a lognormal distribution of transmissivity values (Figure 3-8). Table 3-2 lists the transmissivity mean and standard deviation used in each test. In order to test the sensitivity of the system to the mean transmissivity simulations PNC00X0a and PNC00X1 used different mean transmissivity values.

Flow aperture – For the purpose of the modeling, aperture (e) was calculated from the transmissivity (T):

$$e = 2\text{sqrt}(T). \qquad \text{(Equation 3-1)}$$

Using this relation, a geometric mean aperture of about 1 mm resulted from a geometric mean transmissivity of 2.3e-7 m^2s^{-1}.

Dipole Strengths – Three different dipole strengths were modeled. For the 2 m spaced wells (PNC005X) an equal dipole (1:1) was simulated. For the 5 m spaced wells (PNC004X) a 1:2 dipole was simulated and for the 10 m spacing (PNC006X), an almost radially convergent dipole (1:10) was simulated. Head contour maps (Figures 3-9, 3-10 and 3-11) demonstrate the different flow regimes represented by the three different dipole strengths. Table 3-3 shows the change in heads due to pumping and injection at the two wells.

Table 3-3 Heads at wells

Head change in m	**PNC0050a (1:1)**	**PNC0040a (1:2)**	**PNC0060a (1:10)**
at injection well	4.55	1.70	-1.61
at withdrawal well	-5.34	-7.44	-8.28

Duration of tracer injection – For the purposes of the flow modeling an injection period of 1000 seconds was chosen. During this time period 500-1000 particles were released into the injection well at one of the six nodes along the well wall. A constant flux condition at the well resulted in roughly equal numbers of particles departing from each node.

Figure 3-7a: Transmissivity distribution for Pnc0050a

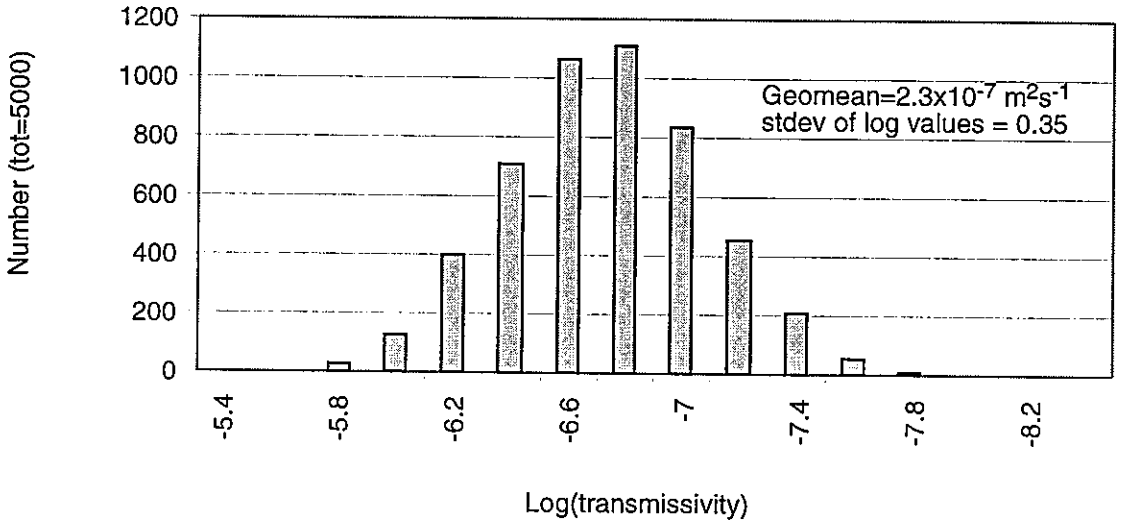

Figure 3-7b: Aperture distribution of Pnc0050a

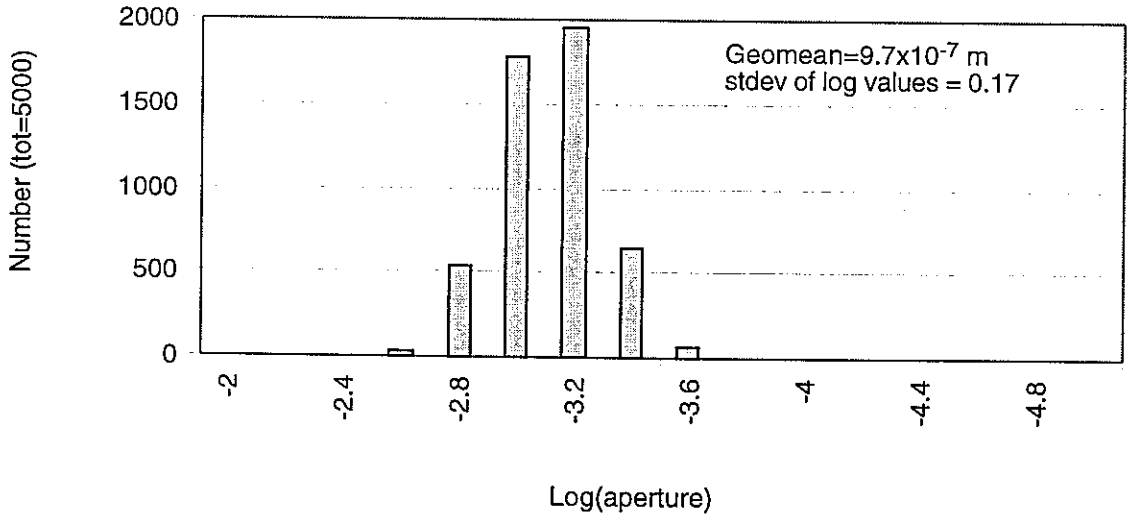

FIGURE **3-8**
TRANSMISSIVITY AND APERTURE DISTRIBUTIONS FOR PNC0050a
PNC KAMAISHI/H8 REPORT/JAPAN

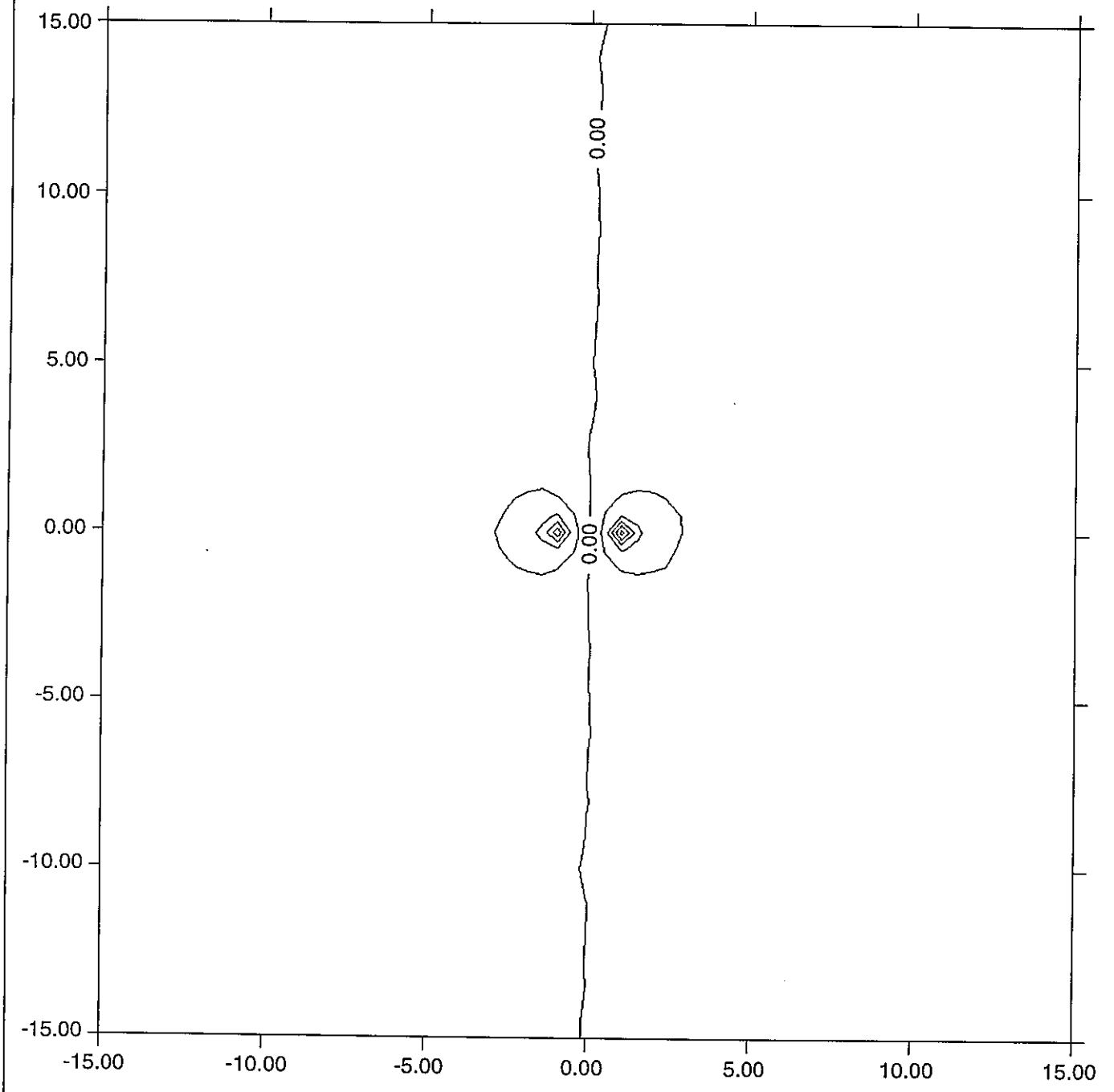

FIGURE **3-9**
PNC0050a, 1:1 DIPOLE
PNC-KAMAISHI/H8 REPORT

PROJECT NO. 923 1089.921 DRAWING NO. 72884 DATE 6/27/97 DRAWN BY CB

Golder Associates

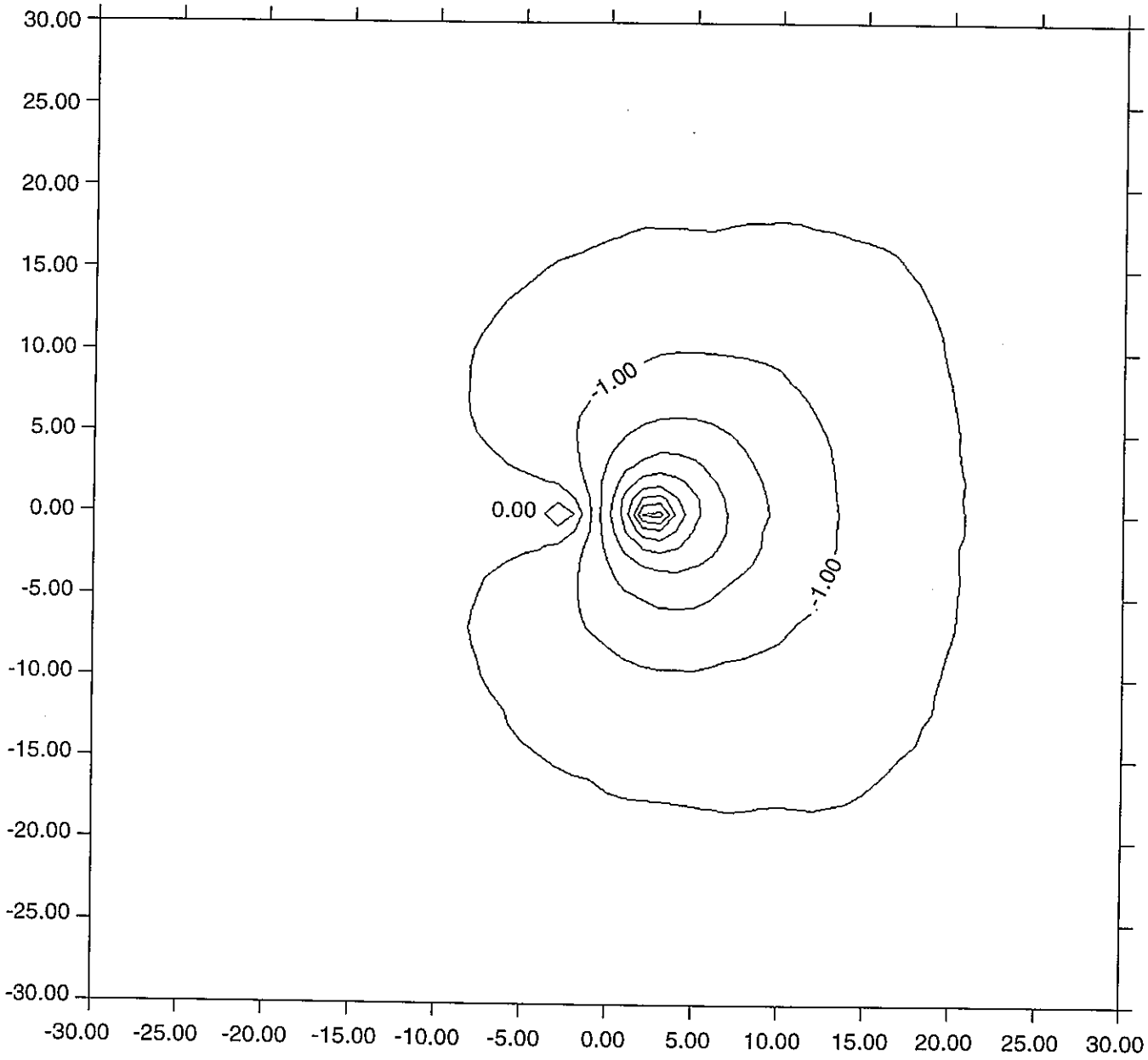

FIGURE **3-10**
PNC0040a, 1:2 DIPOLE
PNC-KAMAISHI/H8 REPORT

PROJECT NO. 923 1089.921 DRAWING NO. 72885 DATE 6/27/97 DRAWN BY CB

Golder Associates

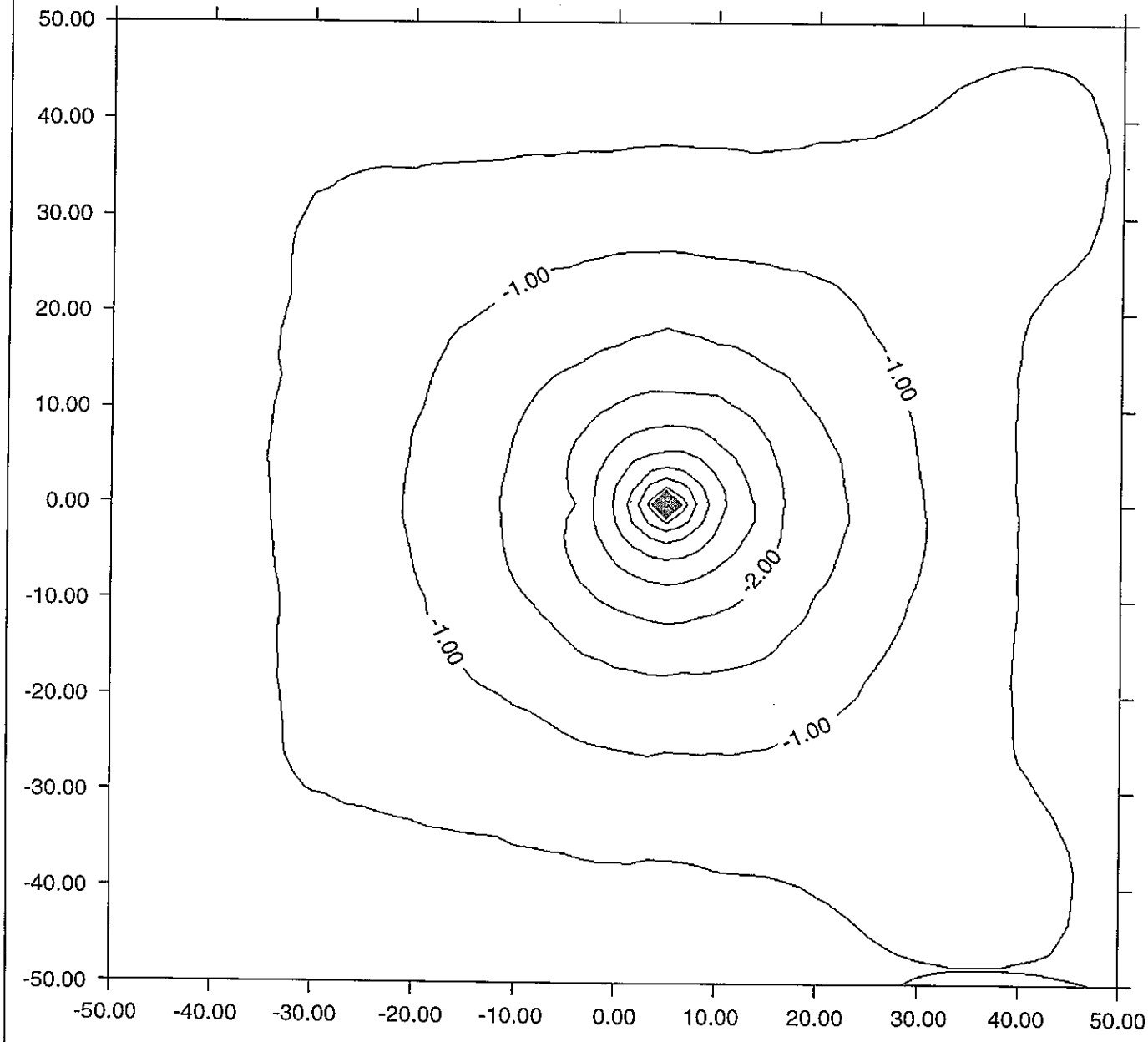

FIGURE **3-11**
PNC0060a, 1:10 DIPOLE
PNC-KAMAISHI/H8 REPORT

PROJECT NO. 923 1089.921 DRAWING NO. 72886 DATE 6/27/97 DRAWN BY CB

Golder Associates

Matrix diffusion – MAFIC allows simulation of tracer particles diffusing from the fracture opening into the rock matrix and eventually back into the fracture opening. However, for the desired matrix diffusion conceptual model, it was necessary to set matrix porosity to 100%. To simulate a matrix porosity of 0.1% (a reasonable value for granite), the free water diffusivity was lowered from 1e-9 to 1e-12 m^2s^{-1}.

Sorption – In one flow simulation (PNC0054) the retardation factor was set to 3.0. In all other cases the retardation was set to 1.00 (no retardation).

3.1.1.3 Transport Results

MAFIC particle tracking transport output includes the time of departure from the injection well and time of arrival at the pumping well for each particle. In addition, the particle track or path of each particle can be recorded. The following discussion summarizes MAFIC transport results for the simulation described above.

Single Slug – Figure 3-12 shows the breakthrough curve for dipole strengths of 1:1, 1:2, and 1:10. These curves were created by counting the number of particles arriving during consecutive 5000 second intervals and then dividing the number of particles by 5 to renormalize to the same time period (1000 second) as the tracer release. The vertical scale was normalized to the total number of particles that arrived at the pumping well.

Slug Superposition – In order to simulate longer injection periods of length Nx1000 seconds, the single slugs shown in Figure 3-12 were superposed. This was done by adding 1000, 2000, 3000, …. , (N-1)x1000 seconds to the arrival time of each particle in the original slug, and then combining all N columns into one breakthrough curve. Using this technique three different injection periods were simulated:

5 superpositions = 1.4 hour injection (Figure 3-13),

13 superpositions = 3.6 hour injection (Figure 3-14), and

90 superpositions = 25 hour injection (Figure 3-15).

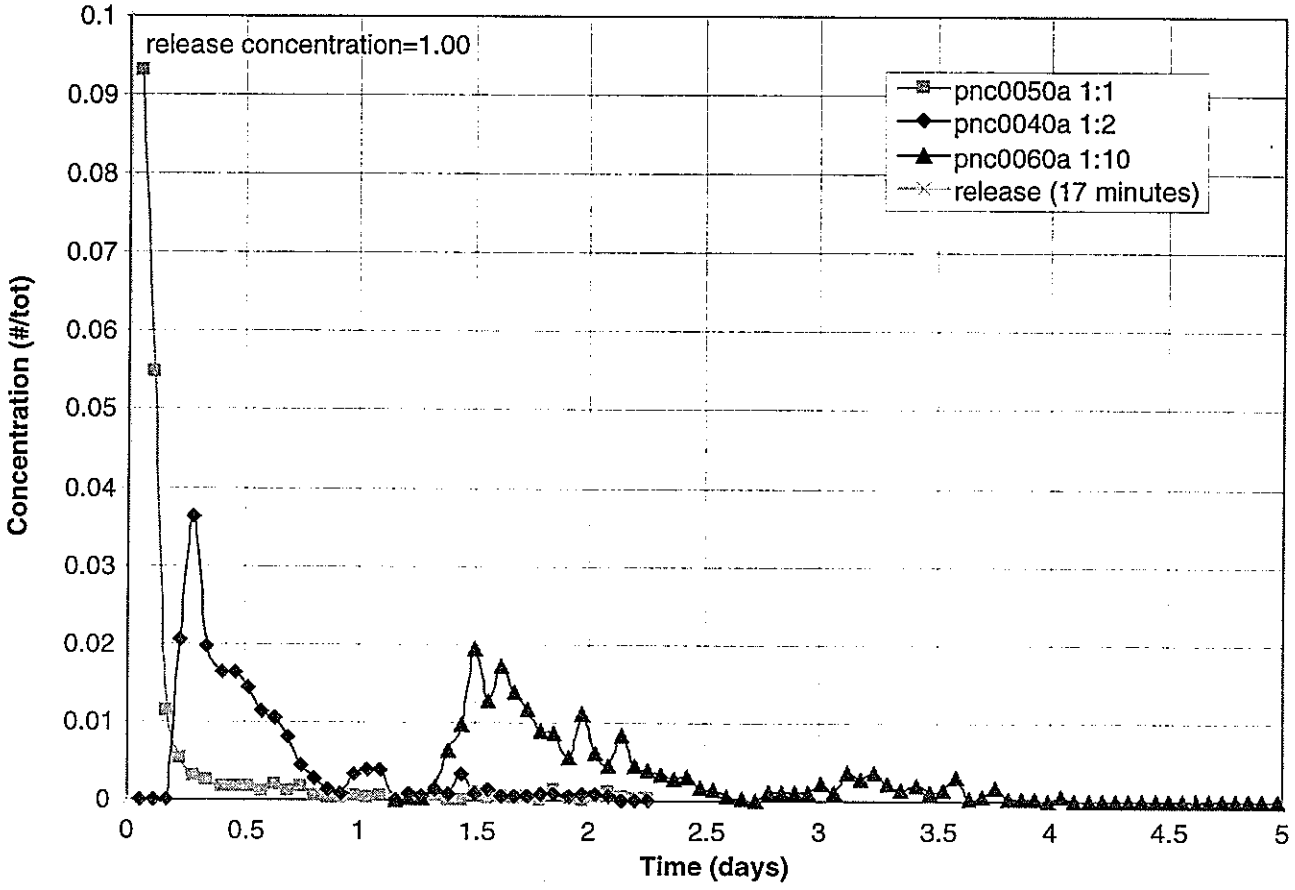

FIGURE **3-12**
BREAKTHROUGH CURVE FOR SINGLE 1000 SECOND TRACER INJECTION
PNC KAMAISHI/H8 REPORT/JAPAN

PROJECT NO. 923 1089.921 DRAWING NO. 73399 DATE 6/26/97 DRAWN BY EA

Golder Associates

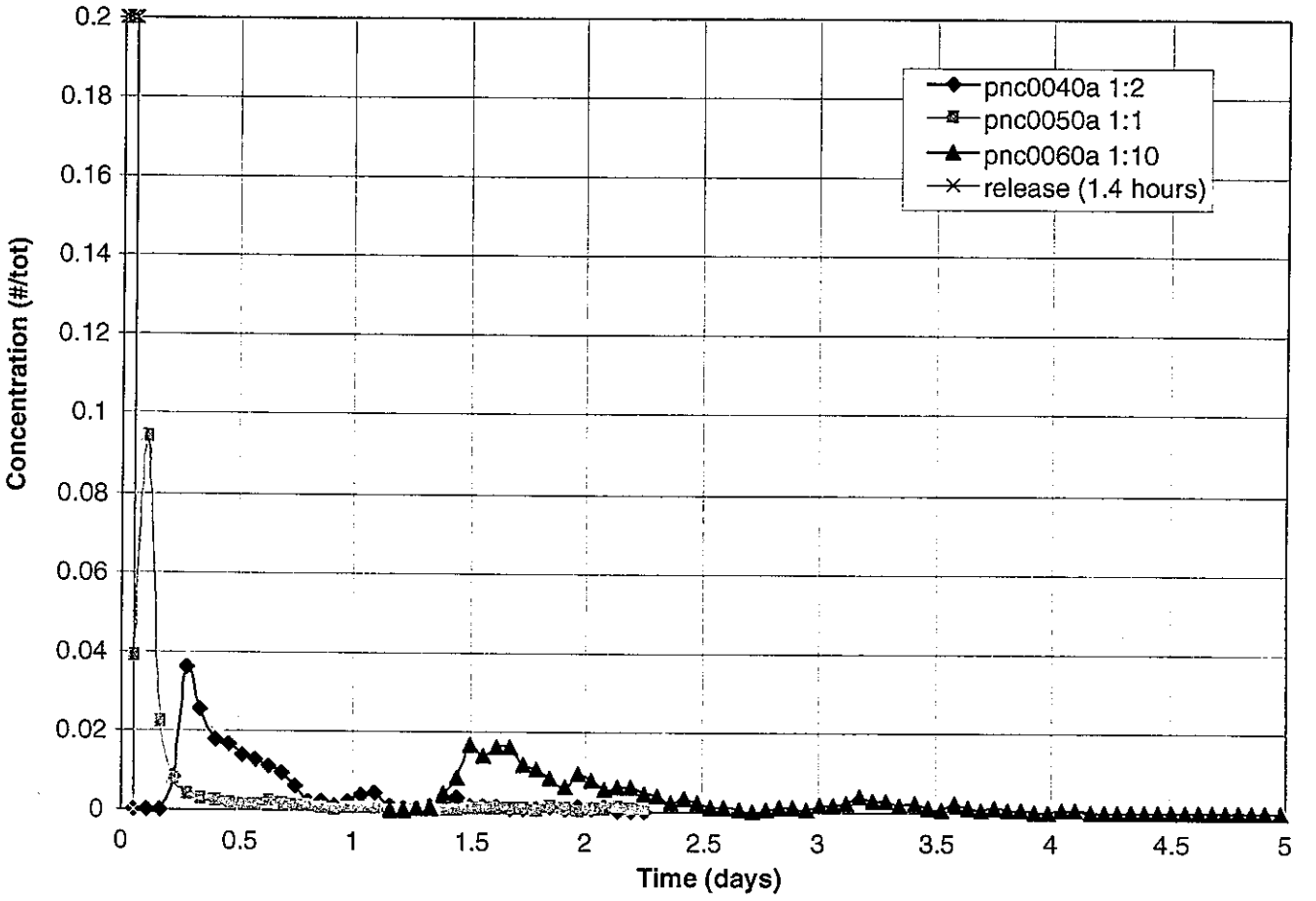

FIGURE **3-13**
BREAKTHROUGH CURVE FOR 5x1000 SECOND TRACER INJECTION
PNC KAMAISHI/H8 REPORT/JAPAN

PROJECT NO. 923 1089.921 DRAWING NO. 73400 DATE 6/11/98 DRAWN BY EA

Golder Associates

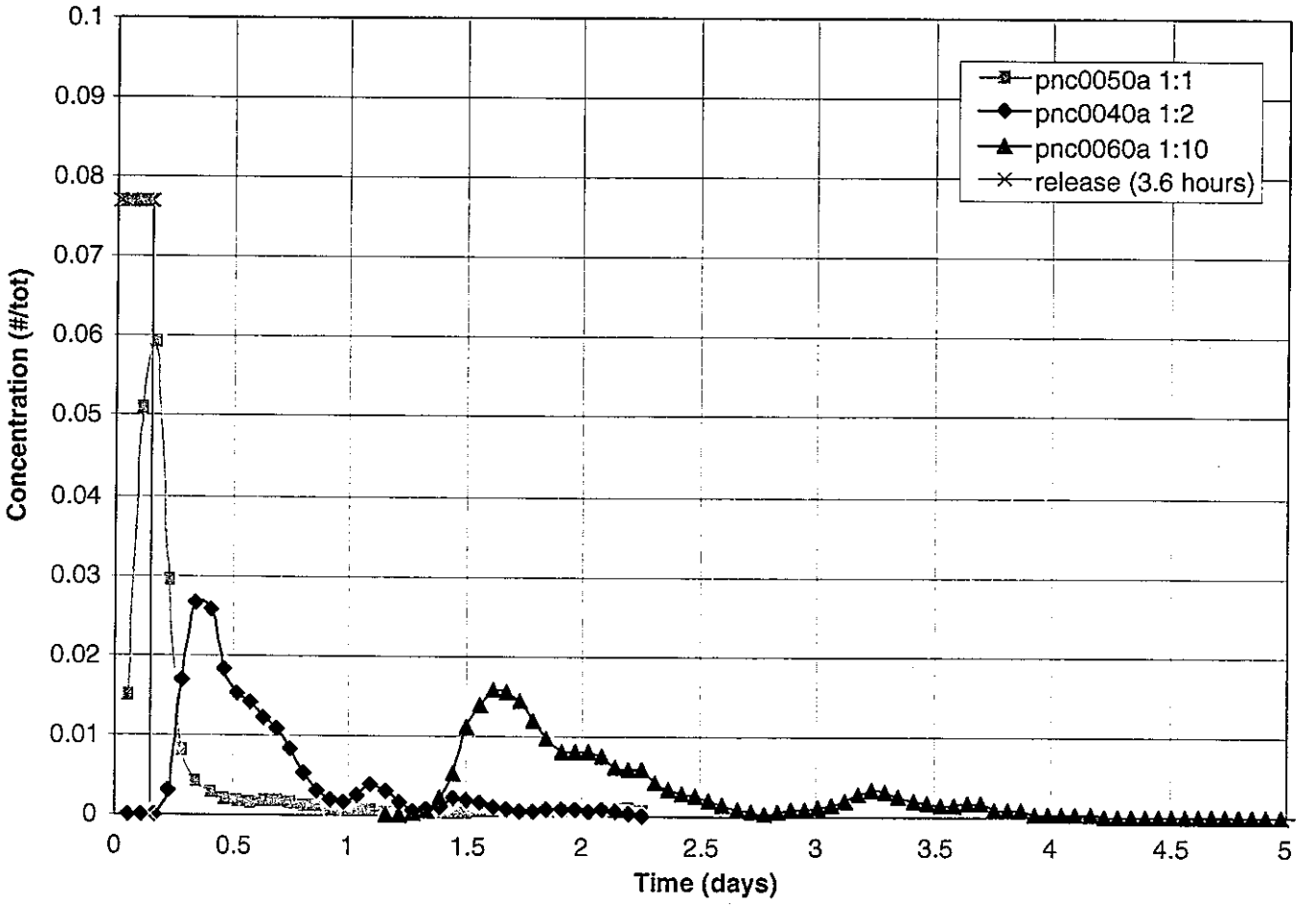

FIGURE **3-14**
BREAKTHROUGH CURVE FOR 13x1000 SECOND INJECTION
PNC KAMAISHI/H8 REPORT/JAPAN

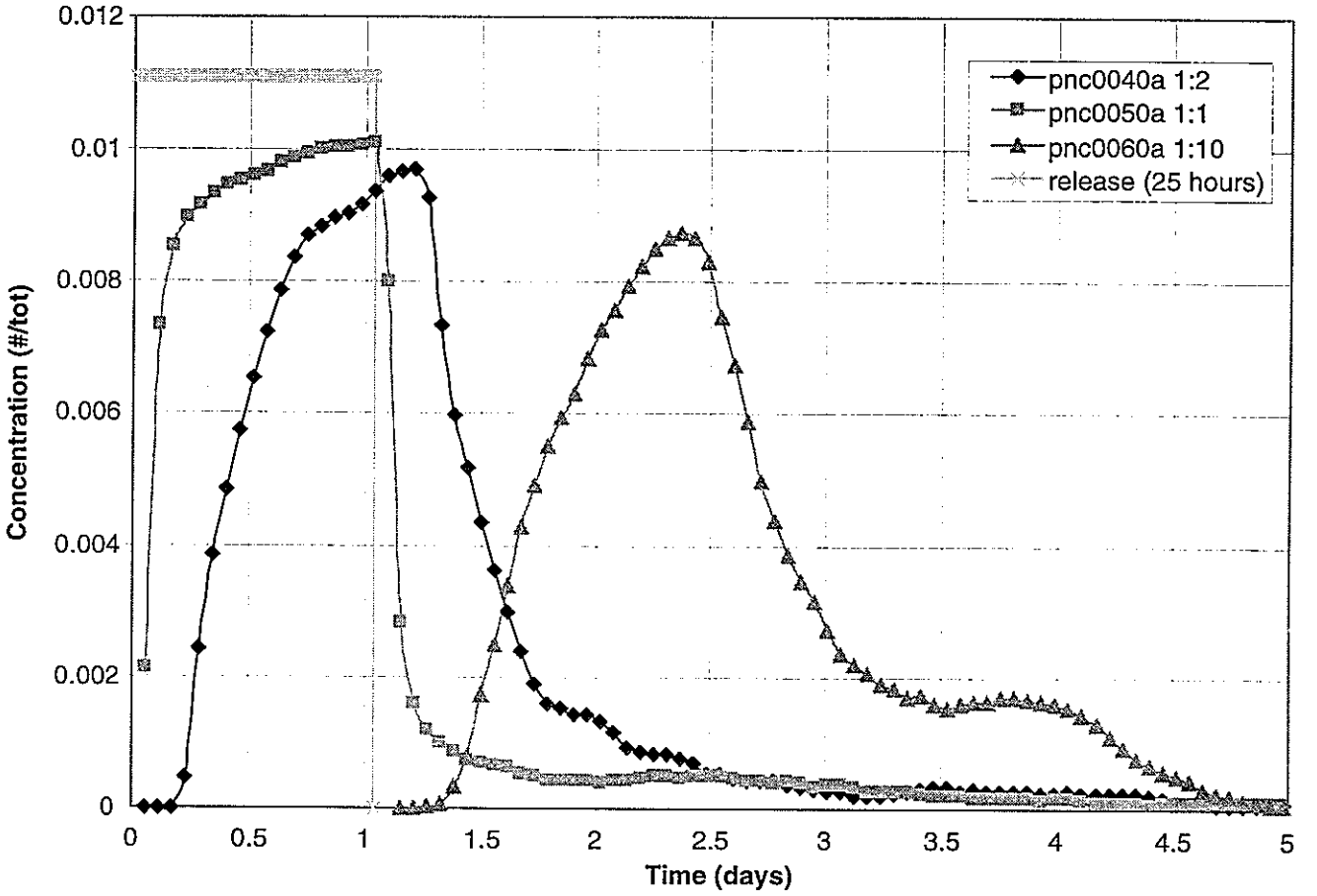

FIGURE **3-15**
BREAKTHROUGH CURVES FOR 90X1000 SECOND TRACER INJECTION
PNC KAMAISHI/H8 REPORT/JAPAN

PROJECT NO. 923 1089.921 DRAWING NO. 73402 DATE 6/26/97 DRAWN BY EA

Golder Associates

Slug superposition has two major advantages. First, it reduces the computational time necessary to simulate a great number of particles. In this experiment the transport of ~500 particles were modeled, yet slug superposition allowed breakthrough curves based on ~45,000 particles to be constructed. Second, slug superposition smoothes out spikes in the breakthrough curves caused by the arrival of relatively few particles in a given time interval.

3.1.1.4 Steady State Concentrations

Even with 90 superpositions (Figure 3-15), none of the simulations reached a true steady state concentration at the pumping well (injection concentration equaling withdrawal concentration). However, after a 25 hour injection period the output concentration reached 80% or more of the input concentration for all three dipoles (Table 3-4). To reach a true steady state concentration at the pumping well, the release period needs to last as long as the travel time of the slowest particles from the first slug to arrive at the pumping well. This means that tracer chemical injection would have to last for more than 3 days (>80 hours) for all three well spacings in order to achieve a true steady state concentration (i.e. last row of Table 3-5). However, if 80% of the input concentration is allowed to represent a steady state condition, much shorter injection periods are required: ~3.7 hours for the 1:1 dipole, ~17.1 hours for the 1:2 dipole and ~52.4 hours for the 1:10 dipole (i.e. the penultimate row of Table 3-5).

Table 3-4 Asymptotic approach to steady-state concentration at the withdrawal well.

Maximum concentration as percent of release concentration	**PNC0050a (2m/1:1)**	**PNC0040a (5m/1:2)**	**PNC0060a (10m/1:10)**
Single slug	9.3%	3.6%	1.9%
5 superpositions	47%	18%	8%
13 superpositions	77%	35%	21%
90 superpositions	91%	87%	79%

Table 3-5 Travel times in hours (single slug)

Average Time of	PNC0050a (2m/1:1)	PNC0040a (5m/1:2)	PNC0060a (10m/1:10)
first 5%	0.6	4.9	32.5
middle 5%	1.5	10.2	42.5
75-80%	3.7	17.1	54.2
last 5%	81.0	84.6	88.8

3.1.1.5 Effect of variable transmissivity and aperture, matrix diffusion, and sorption

Three simulations (PNC0052, PNC0053, PNC0054) were run to investigate the effect of matrix diffusion, variable transmissivity and aperture, and sorption on the breakthrough curves. The breakthrough curves of these transport simulations, along with the standard curve (PNC0050a) are shown on Figure 3-16.

Matrix diffusion – Compared to the PNC0053 (matrix diffusion) curve, the PNC0052 (no diffusion) curve is more symmetric, has less of a tail, and has a shorter lag time to the peak concentration. These are all changes to be expected between a model without diffusion and a model with diffusion.

Variable vs. constant transmissivity and aperture – Compared to the PNC0053 (constant T and e field) curve, the PNC0050a (variable T and e field) curve has a shorter lag time and narrower peak. Because smaller transport apertures require higher fluid velocities for the same flux rate, these characteristics indicate that the controlling apertures are smaller in the variable aperture case. Thus, even though the mean apertures are the same for both tests, particles are preferentially finding higher velocity (smaller aperture) paths between the two wells. This may be due to the choice of a lognormal distribution which would assign apertures smaller than the mean more often than apertures larger than the mean.

Soprtion – Compared to the PNC0053 (no sorption) curve, the PNC0054 (retardation =3.0) curve is stretched out in the time direction by a factor of about three and reduced in the concentration direction by about a third. This is entirely consistent with a model of sorption with a retardation value of 3.

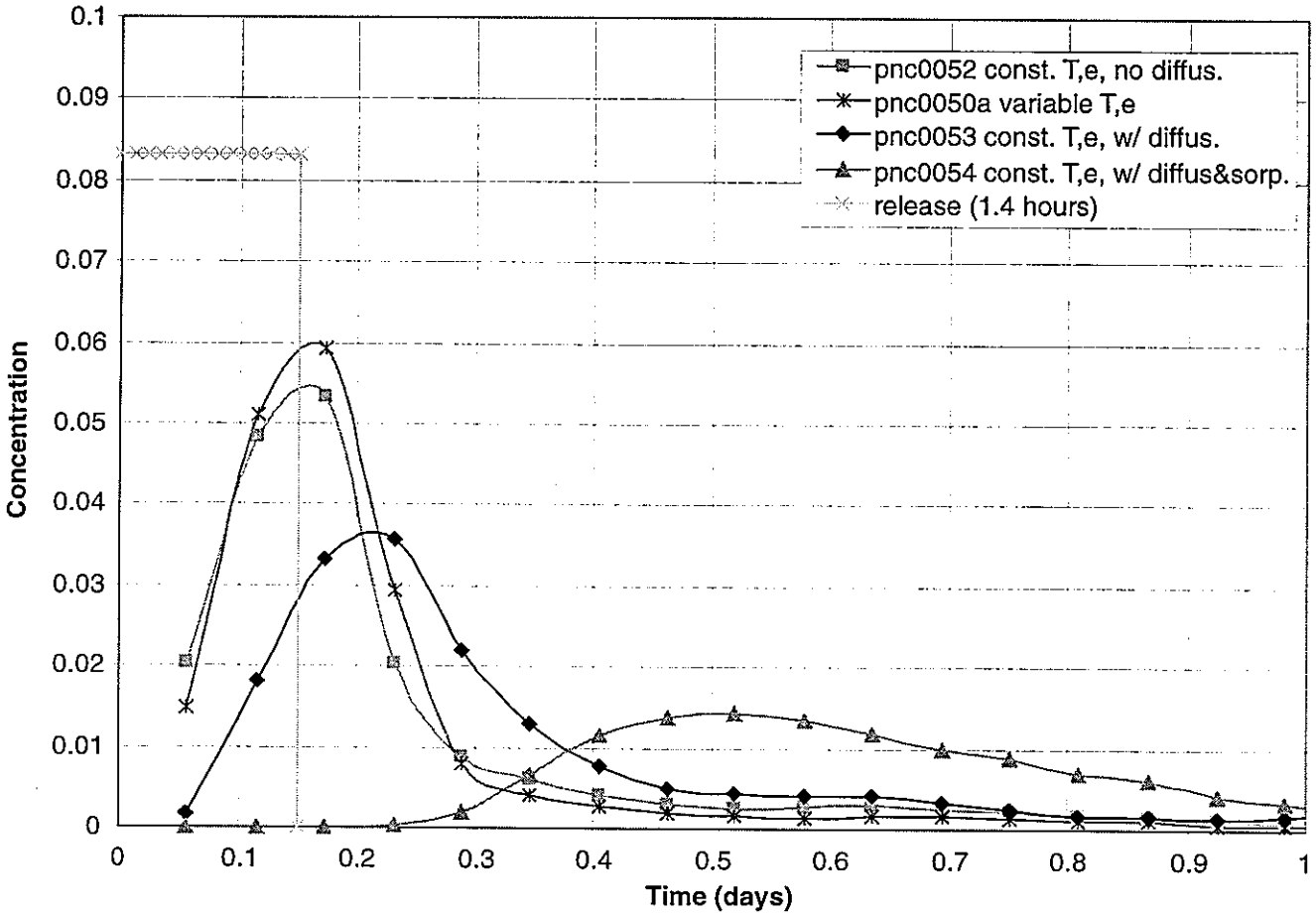

FIGURE **3-16**
BREAKTHROUGH CURVES
COMPARISON OF TRANSPORT PARAMETERS
PNC KAMAISHI/H8 REPORT/JAPAN

3.1.1.6 Effect of the mean value of Transmissivity

Scoping studies for increased transmissivity ($4.5x10^{-7}$ vs. $3.2x10^{-7}$ m^2/s) were run at increased pumping rates ($3.3x10^{-6}$ m^3/s vs. $2.3x10^{-6}$ m^2/s) to compensate for aperture increase due to the greater transmissivity. Two scenarios for each dipole ratio were tested (Table 3-2). Figures 3-17, 3-18, and 3-19 show that the breakthrough curves of the higher transmissivity simulations (PNC0051, PNC0041, and PNC0061) are quite similar to the primary set of simulations (PNC0050a, PNC0040a, and PNC0060a). This indicates that the larger transport mean transport apertures of the PNC00X1 simulations (1.2 mm rather than 1.0 mm) could be compensated for by the higher pumping rate.

3.1.1.7 Concentration inflection at late times

A distinctive feature of all the breakthrough curves is the inflections near 200,000 seconds. We believe that this may be a result of the constant flux condition at the injection wells. The constant flux condition means that equal numbers of particles depart from each of the 6 nodes in the finite element mesh that define the injection well. Because, each of those nodes is connected to 4-5 elements, there are ~25 initial paths that a particle can take. Paths that initially lead away from the pumping well will result in very long travel times. In Figure 3-20 a clock position of 3:00 is the node closest to the pumping well, and a clock position of 9:00 is the opposite node. This figure shows that the large number of late-arriving particles (creating an inflection on the breakthrough curves) exited from the injection well on the node opposite of the pumping well (9:00).

3.1.1.8 Particle Tracking

FracMan/MAFIC allows the user to track particle paths. Figures 3-21, 3-22, and 3-23 show the paths of several particles from the injection well (on the left) to the pumping well (on the right). The particle paths are overlain on contour maps of the head at the same scale. As expected, these particle paths remain perpendicular to the head contour lines throughout the journey of the particles--slight deviations in the paths were caused by the variable aperture field within the fracture. Notice that some paths did not finish at the pumping well. Those particles were still moving when the simulation stopped.

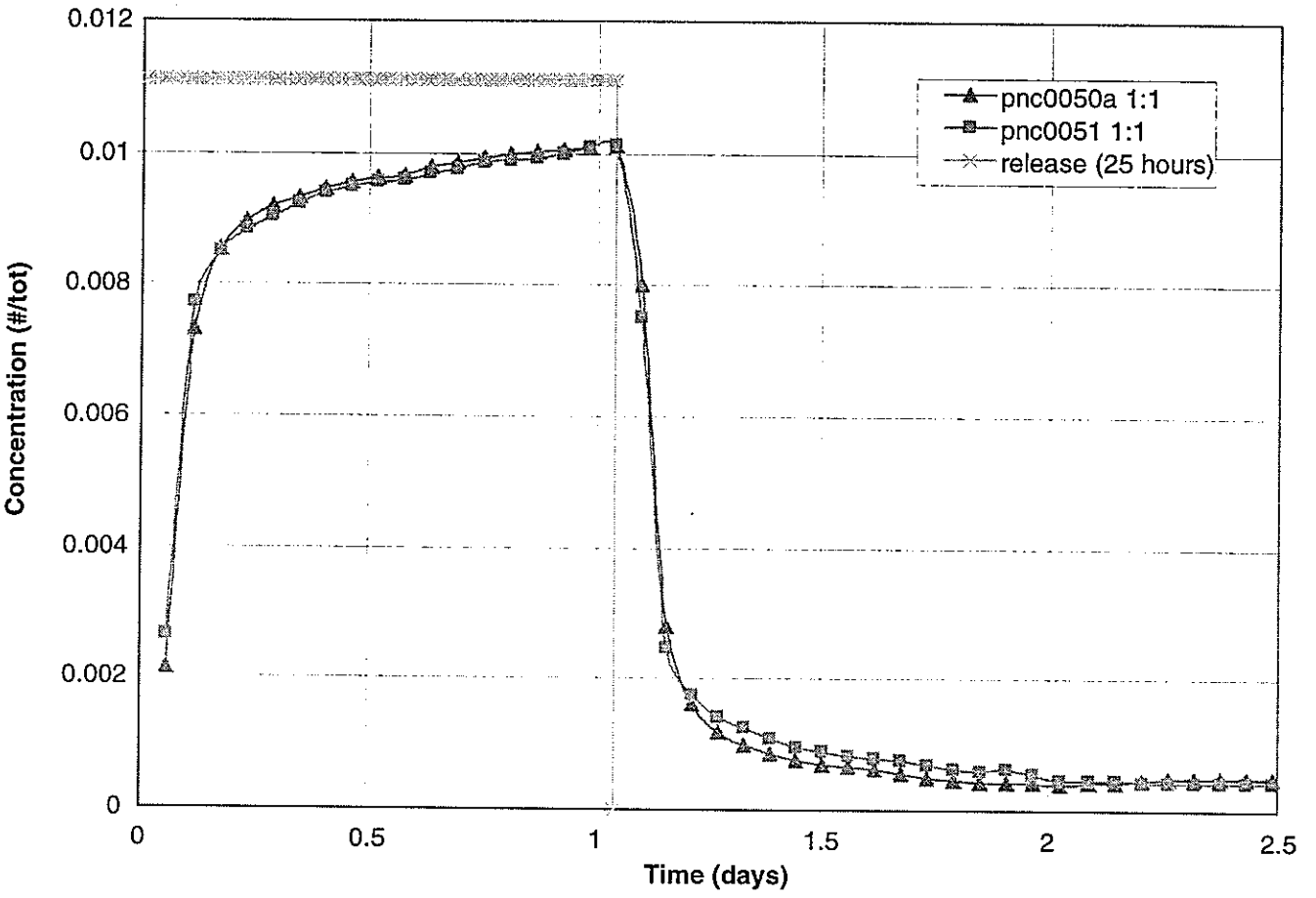

FIGURE **3-17**
BREAKTHROUGH CURVES FOR 1:1 DIPOLE PUMPING RATE AND TRANSMISSIVITY COMPARISON
PNC KAMAISHI/H8 REPORT/JAPAN

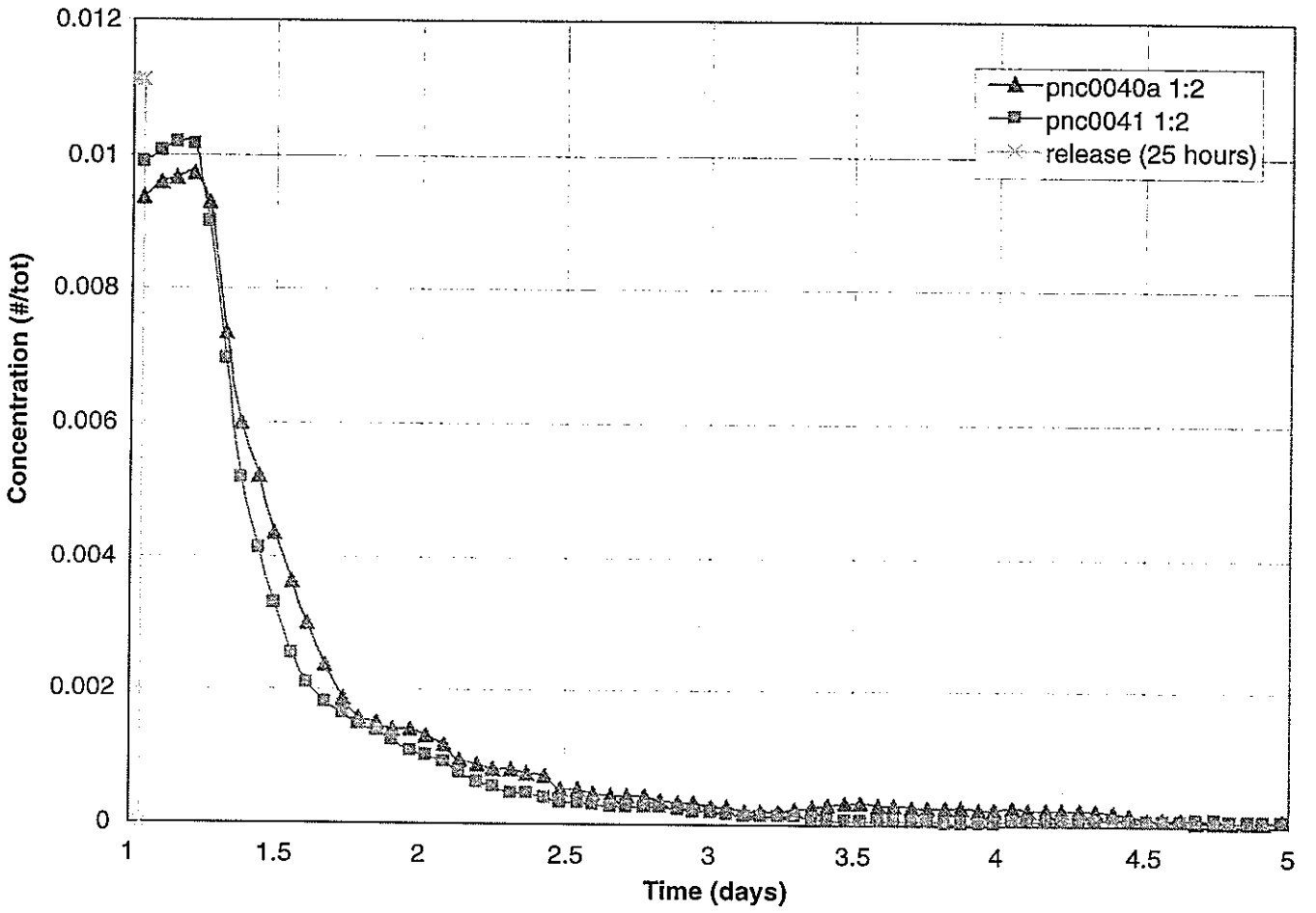

FIGURE **3-18**
BREAKTHROUGH CURVES FOR 1:2 DIPOLE PUMPING RATE AND TRANSMISSIVITY COMPARISON
PNC KAMAISHI/H8 REPORT/JAPAN

PROJECT NO. 923 1089.921 DRAWING NO. 73405 DATE 6/26/97 DRAWN BY EA

Golder Associates

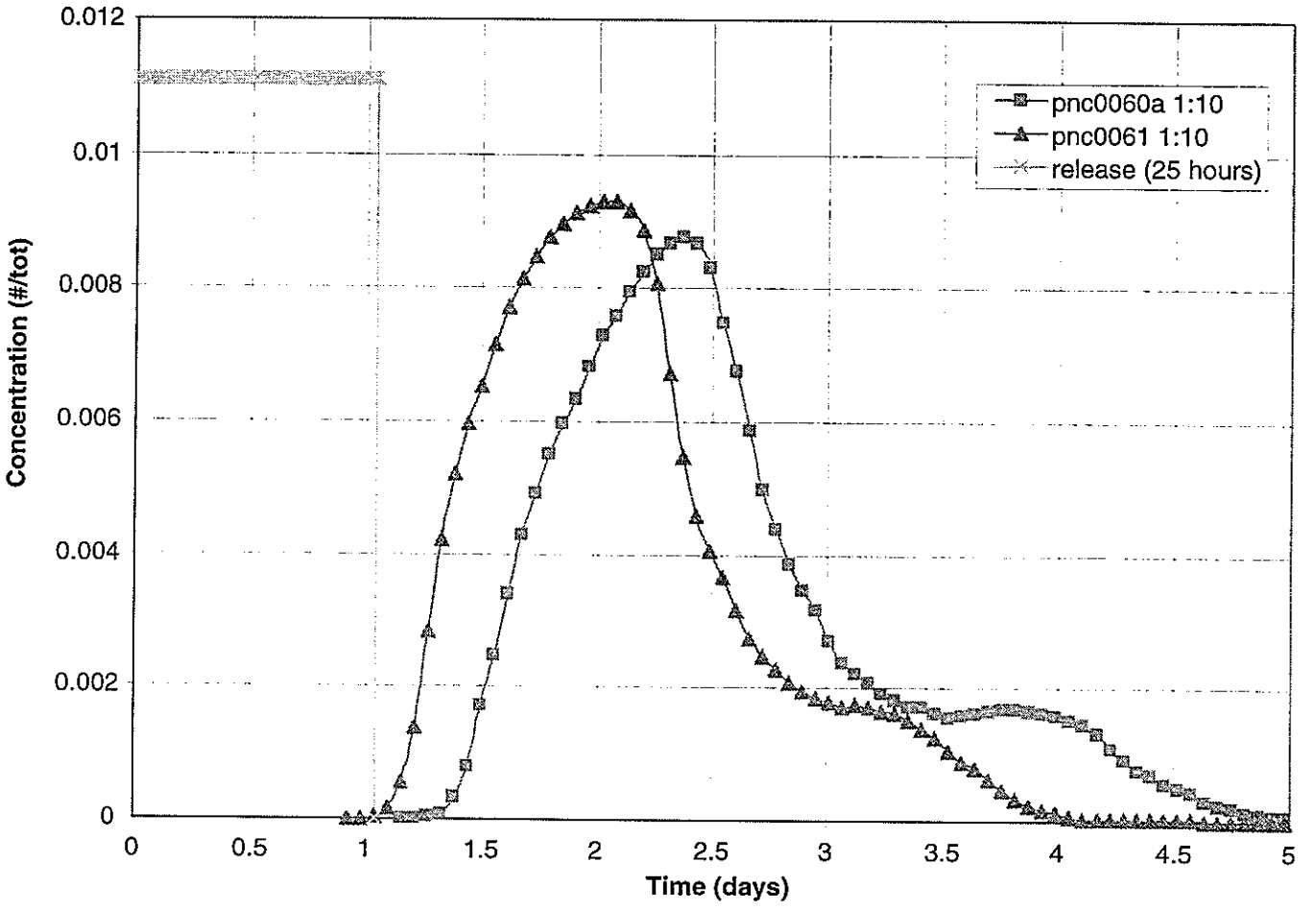

FIGURE **3-19**

BREAKTHROUGH CURVES FOR 1:10 DIPOLE PUMPING RATE AND TRANSMISSIVITY COMPARISON

PNC KAMAISHI/H8 REPORT/JAPAN

PROJECT NO. 923 1089.921 DRAWING NO. 73406 DATE 6/26/97 DRAWN BY EA

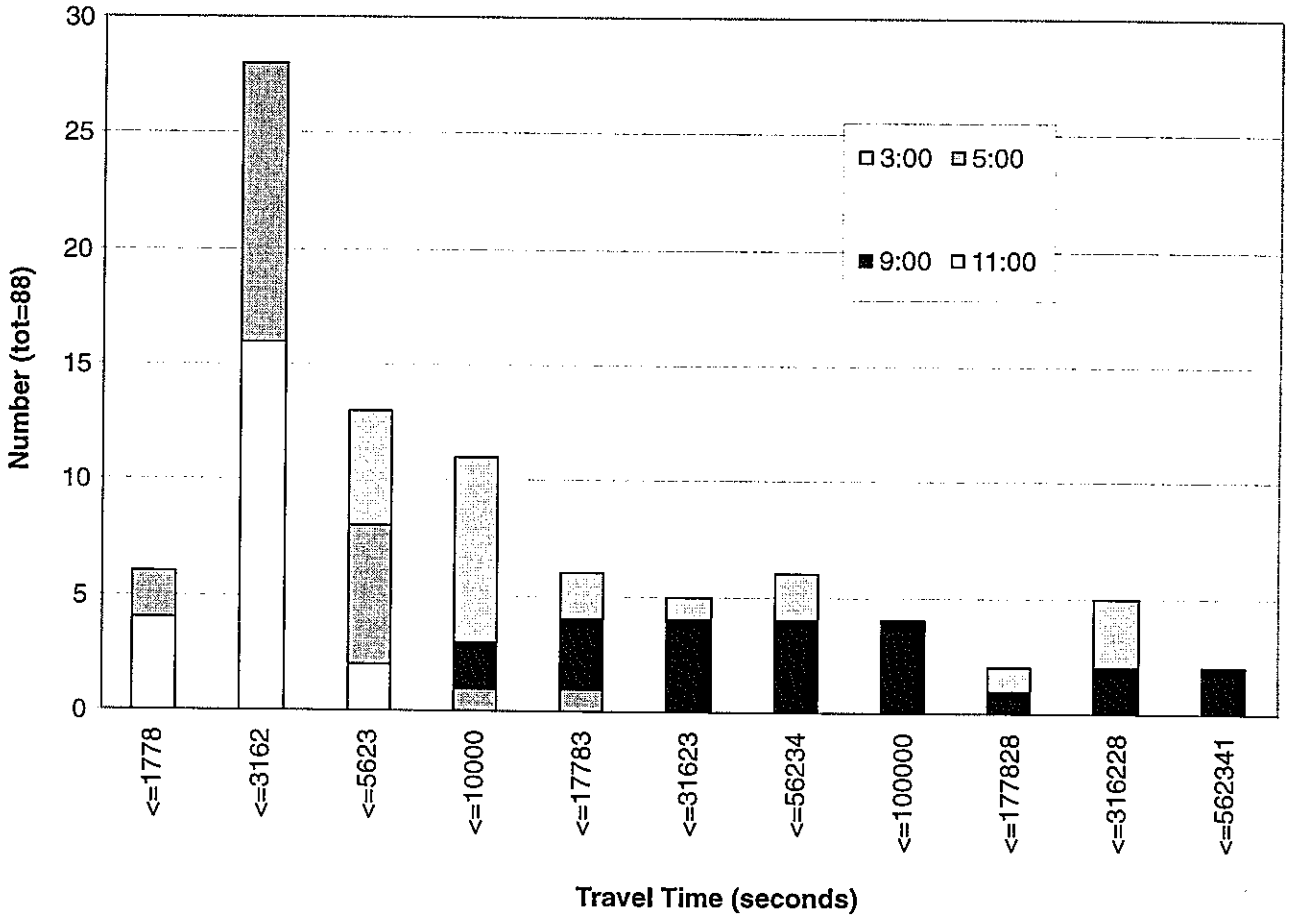

FIGURE **3-20**
TRAVEL TIME DEPENDENCE ON POSITION OF RELEASE NODE IN BH
PNC KAMAISHI/H8 REPORT/JAPAN

PNC0050a

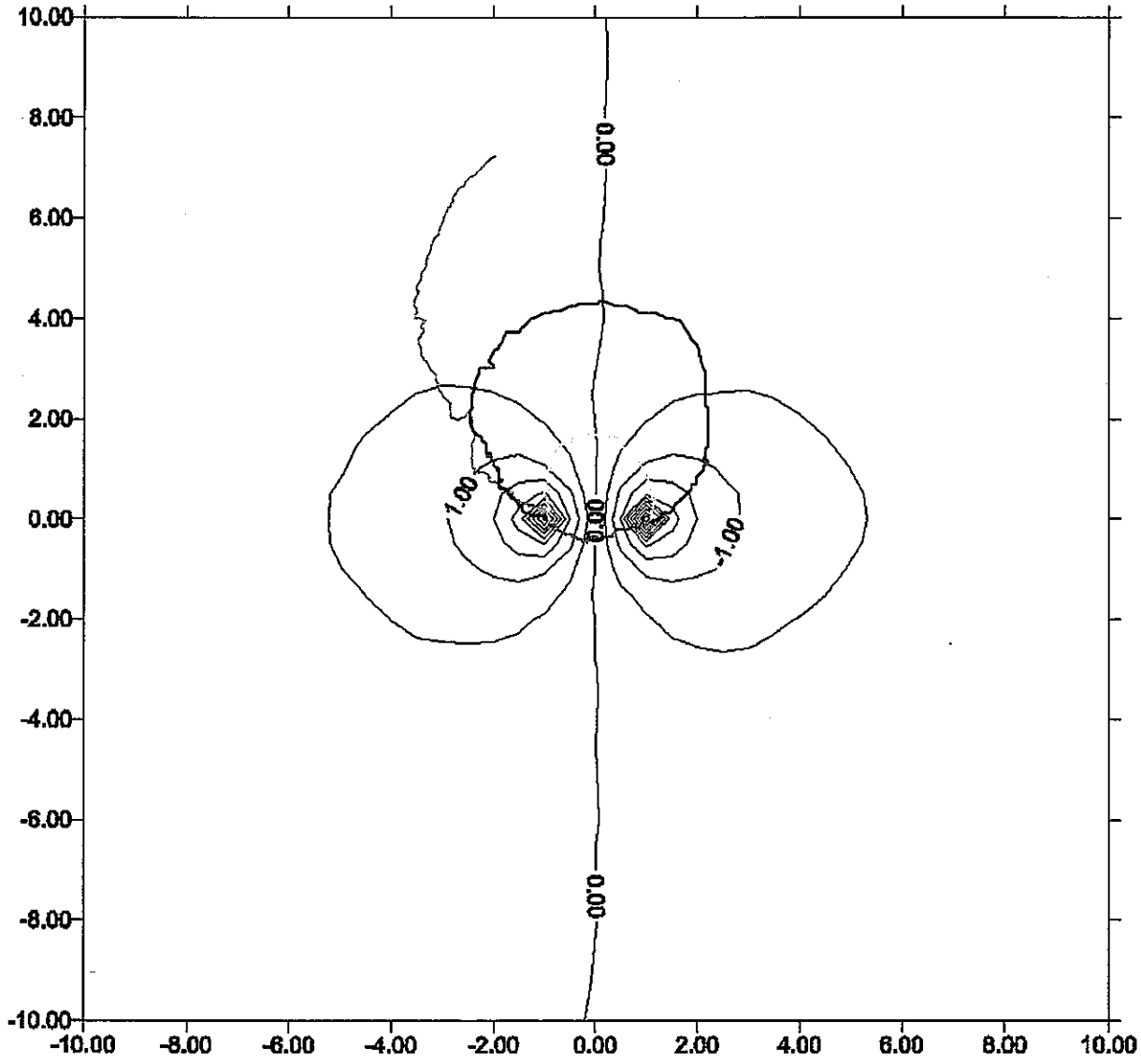

FIGURE **3-21**

PARTICLE PATHS FOR EQUAL DIPOLE (PNC0050a)

PNC KAMAISHI/H8 REPORT/JAPAN

PROJECT NO. 923 1089.921 DRAWING NO. 73408 DATE 6/26/97 DRAWN BY EA

Golder Associates

PNC0040a

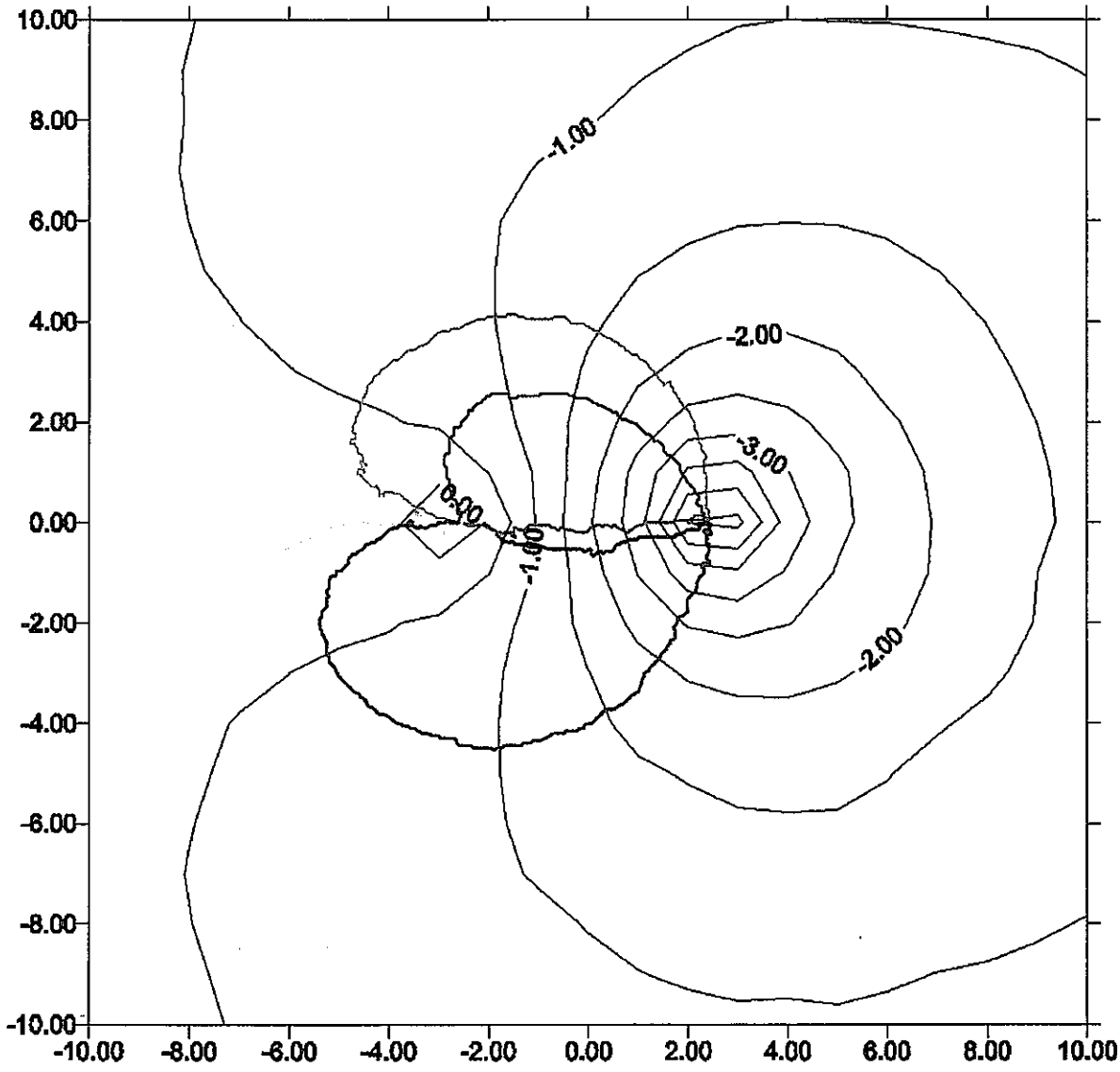

FIGURE **3-22**

PARTICLE PATHS FOR 1:2 DIPOLE (PNC0040a)

PNC KAMAISHI/H8 REPORT/JAPAN

PROJECT NO. 923 1089.921 DRAWING NO. 73409 DATE 6/26/97 DRAWN BY EA

Golder Associates

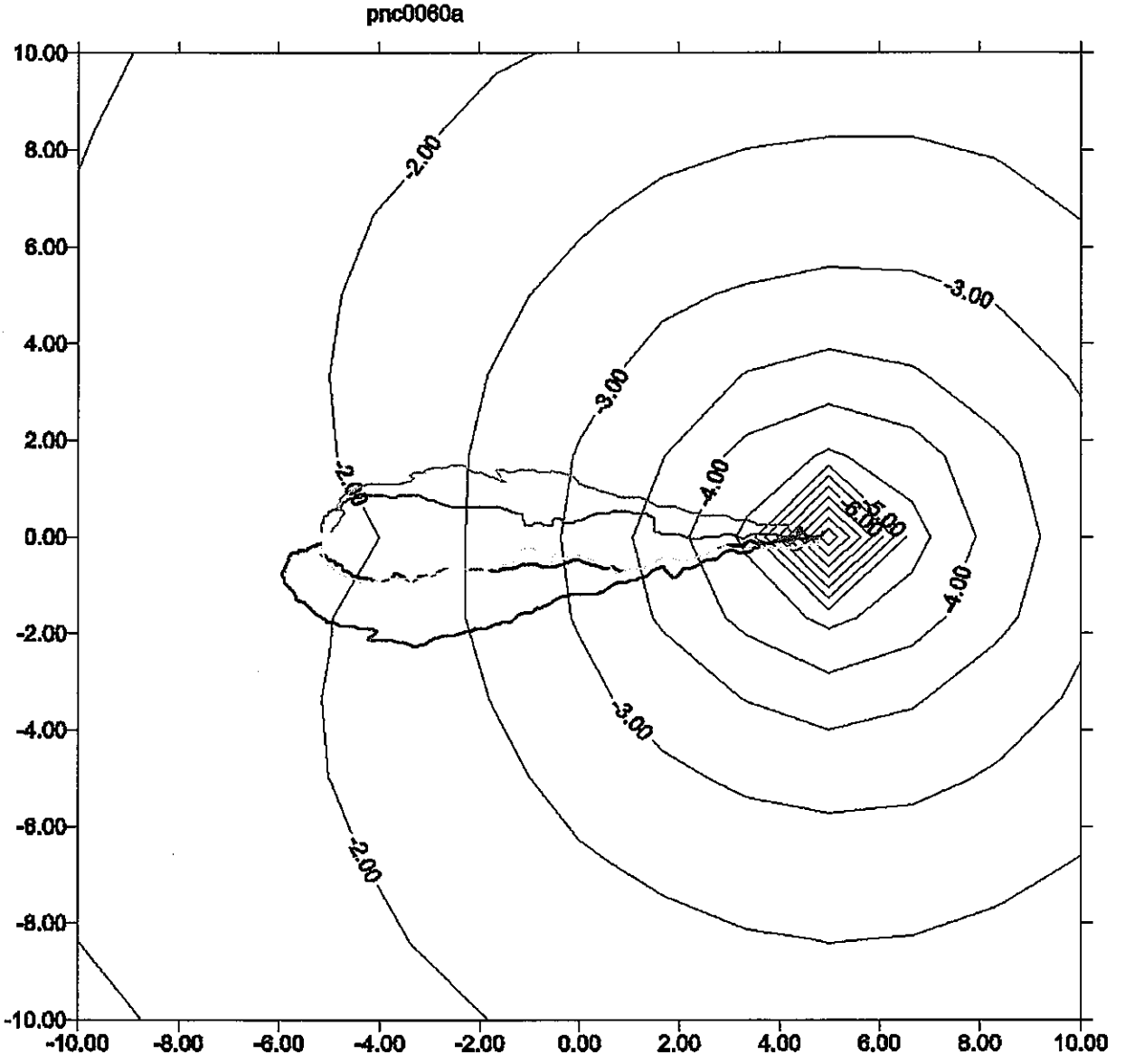

FIGURE **3-23**

PARTICLE PATHS FOR 1:10 DIPOLE (PNC0060a)

PNC KAMAISHI/H8 REPORT/JAPAN

PROJECT NO. 923 1089.921 DRAWING NO. 73410 DATE 6/26/97 DRAWN BY EA

Golder Associates

3.1.1.9 Breakthrough curves compared to analytical solution

FracMan/MAFIC breakthrough curves were compared to the analytical solution developed by Gelhar (1977). Gelhar's (1977) solution was originally developed for 1:1 dipoles only. Gelhar's approach was extended to any dipole ratio using the dipole flow field equations of Heer and Hadermann(1994).

Table 3-6 provides the parameters used to compare the analytical solution to FracMan/MAFIC. Output from the analytical solution is provided as dimensionless time and dimensionless concentration. To convert dimensionless time to time in hours multiply by

$$24 \times \text{aperture} \times (\text{dipole spacing})^2 / V_{out} . \qquad \text{(Equation 3-2)}$$

To find concentration in kg/m^3 multiply dimensionless concentration by

$$\text{tracer mass}/(\text{aperture} \times (\text{dipole spacing})^2). \qquad \text{(Equation 3-3)}$$

Table 3-6 GELHAR and DIPOLE Inputs

	Number of stream tubes	points per tube	Well spacing, Ro (m)	Injection rate, Vin (m^3/d)	Pumping rate, Vout (m^3/d)	Aperture	Dispersion	Tracer mass* (kg)
tst1-1	20	100	2	0.2016	0.2016	0.001	0.5	0.0588
tst2-1	20	100	5	0.1008	0.2016	0.001	0.1	0.0209
tst10-1	20	100	10	0.02016	0.2016	0.001	0.1	0.00602

** Tracer mass is equivalent to the mass (# of particles x mass per particle) arriving at the pumping well in MAFIC simulation.*

To compare these results and the MAFIC results, both must be converted to a mass rate (kg/hr). For the analytical results this is done by multiplying by V_{out} (in m^3/hr). For the MAFIC results this is done by multiplying the number of particles arriving in a time interval by the mass of each particle and then dividing by the length of the time interval.

Figures 3-24 and 3-25 compare the breakthrough curves produced by MAFIC to those found analytically. Agreement between the analytical results and the MAFIC results are good. In all three cases, the analytical solution predicts a peak solute arrival rate earlier than the MAFIC simulation. This can be explained by two input factors which differ between the two curves: 1. the aperture in the MAFIC simulation is lognormally distributed but constant in the analytical solution, and 2. matrix diffusion is simulated in the MAFIC simulation but not the analytical solution. Section 3.3.4 discusses the effects of these parameters on the breakthrough curves (also see Figure 3-16).

3.1.1.10 Conclusions

Based on simulations carried out, the Task 3-2 area tracer tests should not be expected to reach a true steady state within the anticipated time frames. True steady state is nearly impossible to achieve due to the long travel times of the slowest particles. However, for an equal dipole test and 2 m spaced wells an injection period of ~4 hours and pumping period of one day should give good results (i.e. Figure 3-13).

Table 3-7 summarizes the main findings of the scoping calculations. For a 3.6 hour tracer release period, the peak concentrations will occur between 4.2 hours and 1.5 days after the beginning of the test, depending on the strength of the dipole. For the same release period, 1% recovery will occur between 5.3 hours and 1.8 days after the beginning of the test. These calculations confirm that a total test length of 4-5 days will be more than sufficient to achieve the desired results.

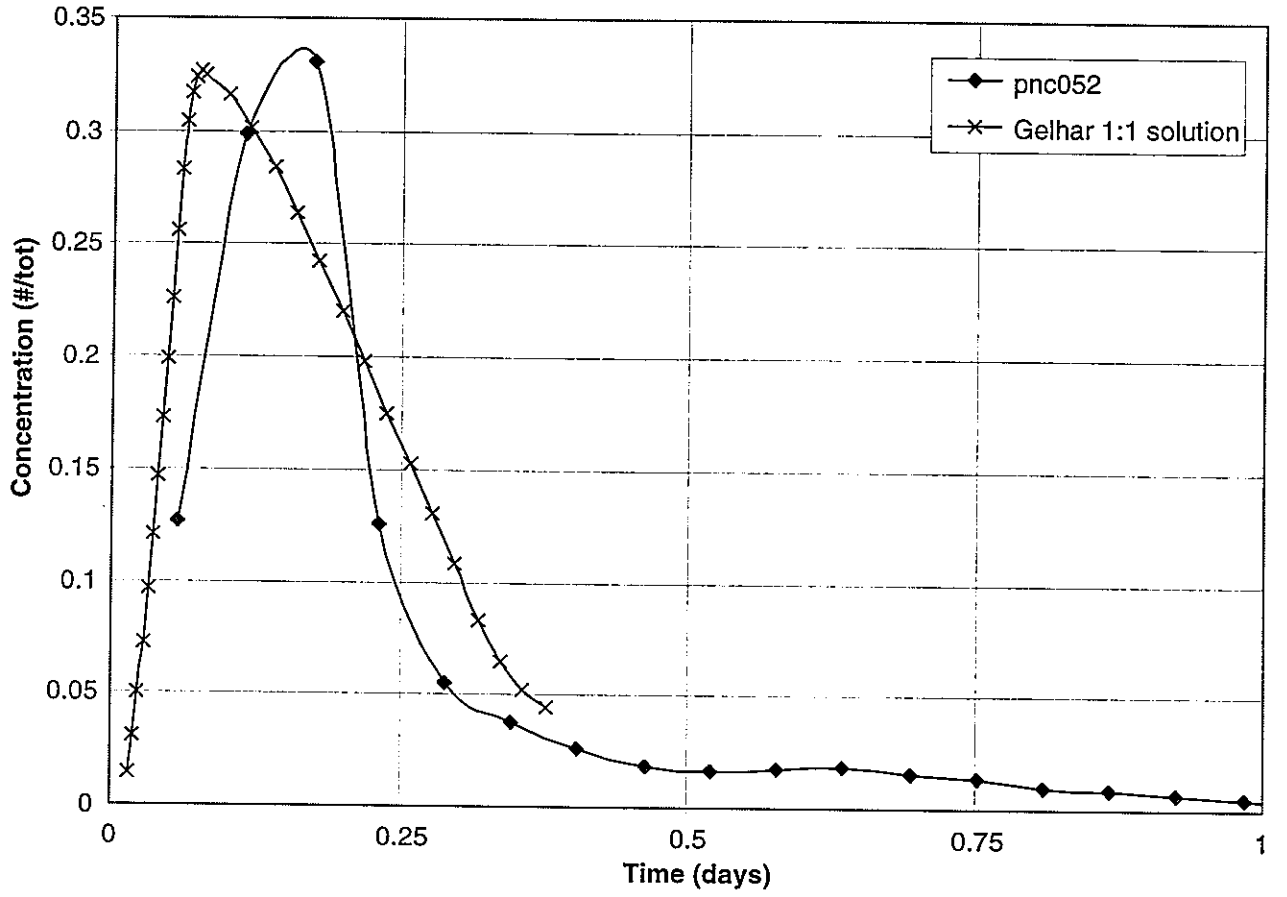

FIGURE **3-24**
1:1 DIPOLE SIMULATION - MAFIC VS. ANALYTICAL SOLUTION
PNC-KAMAISHI/H8 REPORT

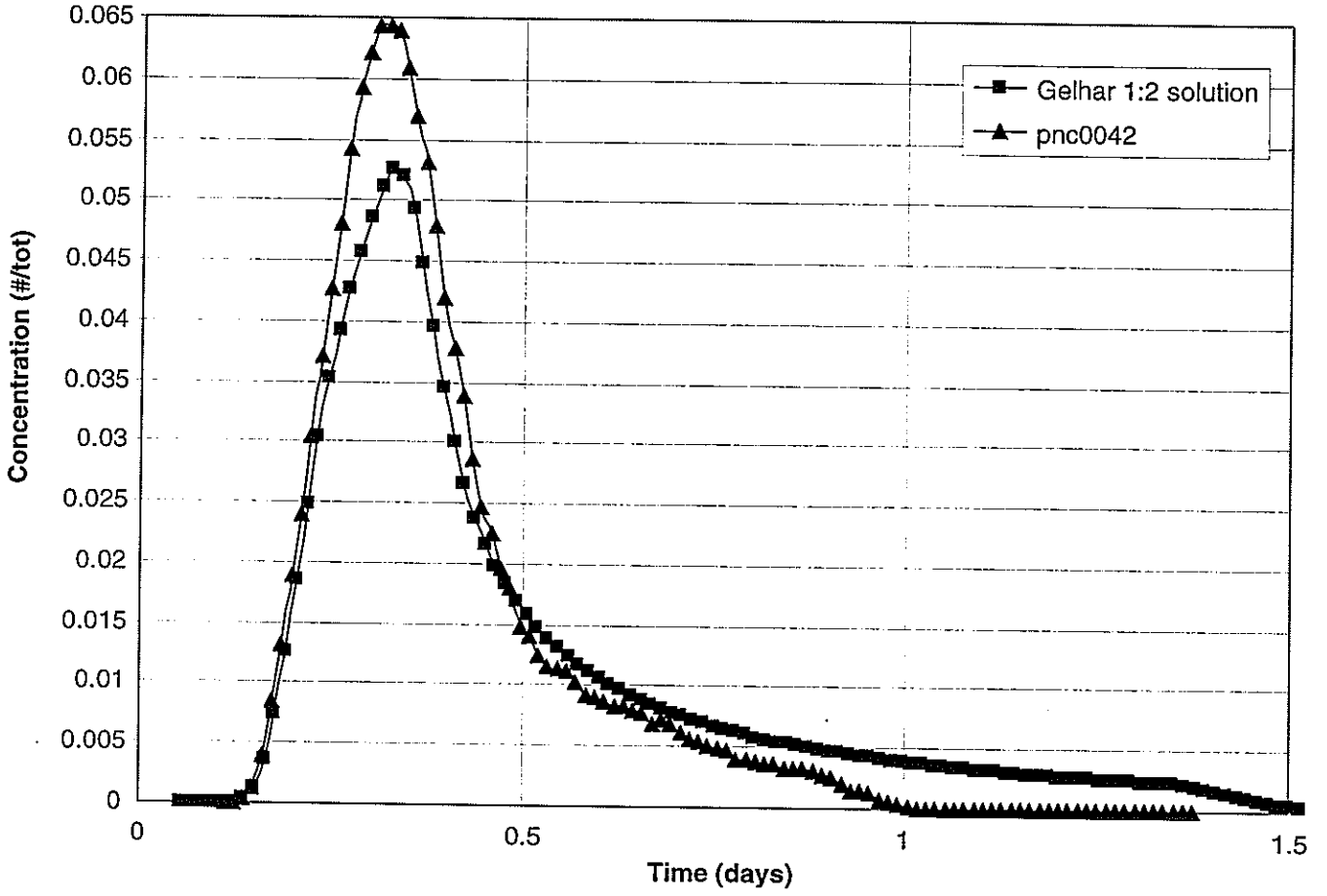

FIGURE **3-25**
1:2 DIPOLE SIMULATION - MAFIC VS. ANALYTICAL SOLUTION
PNC-KAMAISHI/H8 REPORT

PROJECT NO. 923 1089.921 DRAWING NO. 77046 DATE 2/20/98 DRAWN BY EA

Golder Associates

Table 3-7 Summary of breakthrough curve results

	Time to Peak	Time to 1% recovery	Time to 0.1% recovery
1.4 hour injection			
1:1	2.8 hours	5.3 hours	18 hours
1:2	6.9 hours	15.8 hours	27.8 hours
1:10	1.5 days	1.8 days	2.6 days
3.6 hour injection			
1:1	4.2 hours	6.9 hours	20.8 hours
1:2	8.3 hours	16.6 hours	30 hours
1:10	1.6 days	1.8 days	3.7 days
25 hour injection			
1:1	25.1 hours	not reached	31.9 hours
1:2	29.2 hours	not reached	51 hours
1:10	2.4 days	not reached	4.2 days

3.1.2 Overview of neural network investigations

3.1.2.1 Identifying Conductive Features for Nuclear Waste Repositories

The performance of a nuclear waste repository depends upon the existence and transport properties of pathways from the canisters to the accessible environment. Identification of these pathways during site selection or characterization would improve the success of selecting a suitable repository site.

The relation between mappable geological features and the flow and transport through fractures is problematic. Decades of work in the petroleum industry have repeatedly shown that the production of oil from a fractured rock mass often comes from a few zones. In these zones there are fractures which appear indistinguishable from other fractures that contribute little, if anything, to production. This is because there are two essential components that both must exist for there to be a conductive pathway. These components are:

1. The network must be well connected on a regional basis; and
2. The network must be conductive.

While these two properties may seem self-evident, they are very difficult to assess from the geological data that can be gathered. Clearly, for a regionally-connected, conductive pathway to exist between a canister or underground drift, the fractures that intersect the

underground opening or canister hole must themselves be conductive. Likewise, some fractures are more likely to intersect a canister or other subsurface feature because of their favorable orientations. These observations suggest that fracture orientation and transmissivity should be important. However, even perfect knowledge of the transmissivity or orientation of fractures that intersect a well or underground opening do not clarify whether these fractures are part of a conductive, regional fracture network, and thus a pathway to the accessible environment. Transient well testing of long-term duration may improve understanding of how well individual fractures form part of larger networks. However, even in the best of circumstances, well tests can only test the fracture flow network tens or perhaps a few hundreds of meters from the well, and such tests may not be economic for testing the cubic kilometers of rock in which a repository may be situated.

Licensing of a repository requires demonstration that the flow and transport properties of the proposed site are well understood. This implies that it is possible to put forth and defend a model for regional transport pathways.

It is unlikely that any current technology can identify all of the actual significant transport pathways within a large volume of fractured rock. However, a defensible performance calculation can be made by considering stochastic realizations of possible pathways that approximately match the actual (unknown) number of pathways and their transport properties. The strategy is to generate realizations of the fracture pattern in a rock mass, conditioning the pattern not only to statistical distributions but to the local geology as well. The realizations may then be tested against transient well tests or multiwell tests to determine whether the stochastic patterns respond like the actual fracture networks.

What factors characterize a conductive fracture pathway? First, fractures intersecting the well or underground opening must be conductive, and must have a geometry that makes it likely that it will intersect other fractures and also the opening. These are necessary conditions, but are not sufficient. Are there others, which taken together, would make it easier to identify conductive pathways? By definition, fractures that are part of a regionally conductive network conduct fluids. This suggests that fractures

forming part of the conductive pathways may have particular alteration characteristics. Likewise, fractures that are large are more likely to intersect other fractures and form part of regional networks. Although fracture size cannot be directly measured from well data or even from most underground openings, due to their small size relative to the fracture size, large fractures often have diagnostic morphological characteristics, such as planarity and smooth walls.

Taking all of these geological parameters into account and relating them to whether a fracture is part of a conductive pathway is a complex pattern recognition problem. It is not straightforward, as demonstrated in Doe et al. (1993, 1994).

Many fields not related to earth science have encountered similar complex pattern recognition problems. These include automatic fingerprint identification, computer voice recognition, handwriting recognition, stock market trading and income tax audits. Neural networks of various types have been devised to recognize complex patterns in these fields. They are also well-suited to identifying conductive pathways from geological attributes.

3.1.2.2 Different Types of Neural Networks

Neural networks are a sophisticated form of non-linear pattern recognition that are used in such diverse areas as stock market analysis, loan application screening, voice recognition, disease diagnosis, and medical expert systems (Eberhart and Dobbins, 1990). They are particularly well-suited for problems in which the input and output variables are of different mathematical types (e.g. class, ordinal, and continuous variables) and are potentially correlated. Neural network have found geologic application in a variety of areas including slope stability analysis (Xu and Huang, 1994), rock and soil mechanics (Lee and Sterling, 1992; Ellis, 1995; Feng, 1995), fracture network hydrology (La Pointe et al., 1995; Thomas and La Pointe, 1995), prediction of earthquake intensity and liquefaction (Goh, 1994; Tung et al. 1994), and petroleum geology (Baldwin et al., 1989, 1990; Raiche, 1991; Weiner et al., 1991; Osborne, 1992; Rogers et al., 1992, 1995). The most common type of neural network used in published geological applications is the *Back-Propagation* network (e.g., Rogers et al., 1992). This type of net has proven useful for

classifying data, for example, looking at the parameter values of a series of wireline logs for each 1-foot interval and classifying the interval as sandstone, shale, etc. These nets are similar in function to classical *discriminant analysis* (Davis, 1973).

There are other types of neural nets as well, designed to solve problems other than the classification problem. Classification involves placing an unknown observation into one of two or more categories based upon measured parameters. Classifying fractures as conductive or non-conductive based upon measured geological parameters is a classification problem. The two principal types of nueral networks that are used for classification problems are the Back-Propagation Nets (BPN), and the Probabilistic Neural Nets (PNN).

Sometimes the output categories are unknown, and the goal is to define meaningful output classes or categories. This is the purpose for which classical *cluster analysis* is used (Davis, 1973). An example of a cluster analysis problem in fracture characterization is to determine if there are any *domains* with similar geological characteristics, which could mean either contiguous spatial regions of the rock mass, or could be an effort to define the number of fracture sets and their distinguishing characteristics. Neural nets that try to determine natural groupings within data are termed self-organizing. A successful architecture for solving cluster analysis-type problems has proven to be the Kohonen net.

A final type of problem that neural nets have been able to successfully solve is to predict the value of a continuous output variable. This type of problem is the goal of *multivariate regression analysis* in classical statistics. BPN's can be used for this purpose; recent work (Ward, 1996) suggests, however, that Generalized Regression Neural Nets (GRNN) out perform BPN's in many applications. Table 3-8 summarizes the three different classes of neural nets.

Table 3-8 Alternative Neural Net Architectures and Their Applications

Type of Problem	Classical Statistical Approach	Neural Net Architectures	Example Applications
Classification	*Discriminant Analysis*	*Back-Propagation, Probabilistic Neural Net*	*Conductive Fracture Recognition, Lithologic Classification*
Identification of Groups	*Cluster Analysis, K-Nearest neighbor*	*Kohonen Self-Organizing Map*	*Fracture Set Identification, Geological Domain Identification*
Prediction of Continuous Variable	*Linear, Non-Linear Regression*	*Back-Propagation, Generalized Regression Neural Net*	*Fracture T, Interval T*

3.1.2.3 Neural Net Terminology

There are many types of neural networks, but all share a common architecture consisting of *neurons* and *synapses* (Figure 3-26). A neuron is simply a node in the network which uses a non-linear transfer function to convert an input signal (value) to an output signal. Neurons are connected by synapses. A synapse takes the output signal from one neuron, multiplies it by a *synaptic weight*, and passes the modified signal to an adjacent neuron as input. Depending on the number of incoming and outgoing synapses connected to it, a neuron can be classified into one of three categories:

1. *Input neurons* have zero incoming synapses and one or more outgoing synapses. They represent input variables, and take the variable value as their output.
2. *Output neurons* have one or more incoming synapses and zero outgoing synapses. They represent output variables, and produce an output signal which equals the predicted variable value.
3. *Hidden neurons* have one or more incoming synapses and one or more outgoing synapses. They sit between the input and output neurons and pass signals through the network.

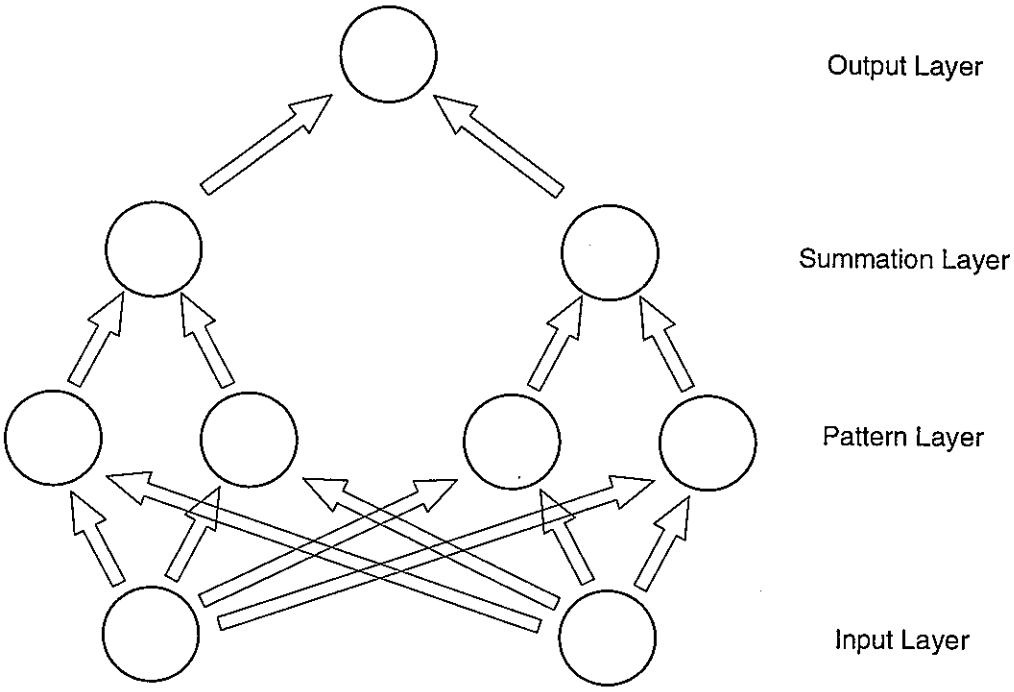

After Masters, 1995.

FIGURE **3-26**
PNN ARCHITECTURE
PNC-KAMAISHI/H8 REPORT

PROJECT NO. 923 1089.921 DRAWING NO. 77074 DATE 2/20/98 DRAWN BY EA

Golder Associates

A distinct advantage of neural networks over other classification methods is their ability to learn the relative importance and complex interrelations among input and output variables. By changing the neuron transfer functions, the synaptic weights, and the network connectivity, a neural network can be conditioned to provide the expected response for a given input pattern. Once trained, a neural network can then be used to make predictions for input patterns whose correct classification is unknown.

3.1.2.4 Networks for Classifying Fractures as Conductive or Non-Conductive

Determination of whether a fracture is likely to be conductive or not based upon measured geological parameters is a classification problem. The two alternative neural networks for solving classification problems are BPN's and PNN's. BPN's are the most widely used, and many different variations in their architecture have been developed to solve specialized problems. In general, BPN's are less sensitive to local "noise", and thus may generalize better than PNN's. However, PNN's are superior when the training data is sparse.

The PNN (Specht, 1990) is a combination of probability theory and Bayesian statistics, and was developed primarily for solving multivariate classification problems (Masters, 1993, 1995). The probabilistic neural network algorithm is designed to provide a classification which minimizes misclassification of fractures to the wrong set. The classification system which has the minimum "cost" of misclassification is termed "Bayes Optimal" (Parzan, 1962). For treatment of fracture data, it is assumed that the cost of misclassification is equal for all fractures. This means that it is no worse to misclassify any particular fracture in the fracture population; all misclassifications are equally bad. The major advantages of using a PNN is that it can account for data "shape", overlap, outliers, and multiple modes with a high degree of classification accuracy (Figure 3-26). The question mark symbol in Figure 3-27 illustrates the problem of correctly classifying an unknown observation at that location. In Figure 3-27a, the new point is much closer to the set shown by lines, yet it belongs to the set shown as open circles. Computing a "distance" measure alone will lead to incorrect classification. Figure 3-27b shows an example of a bimodal distribution, and the problems encountered in this situation. Figure 3-27c illustrates how nearest-neighbor methods can fail when distributions have overlap and different densities.

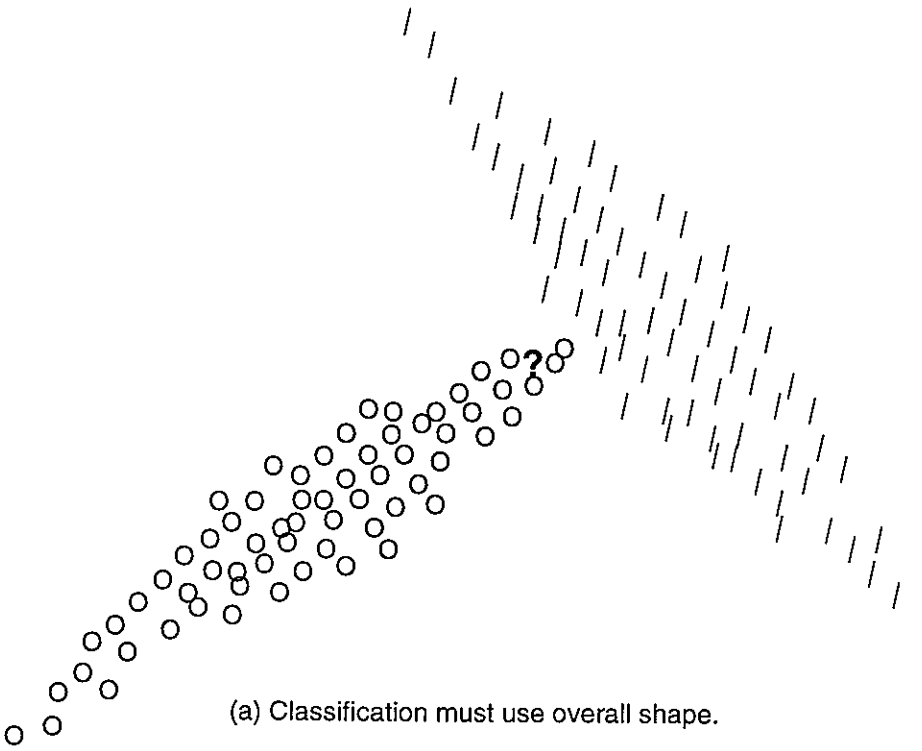

(a) Classification must use overall shape.

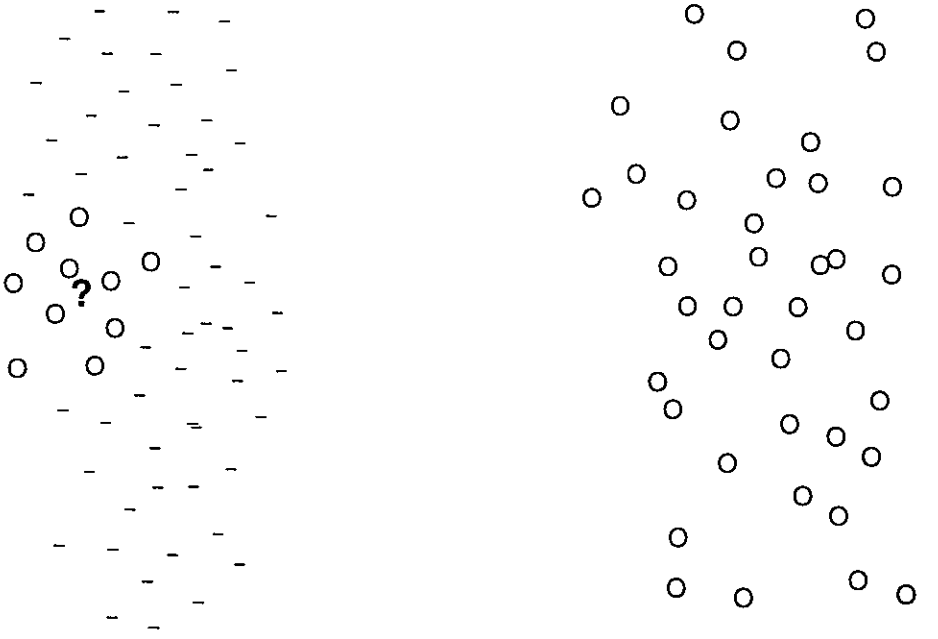

(b) Classes may have multiple modes.

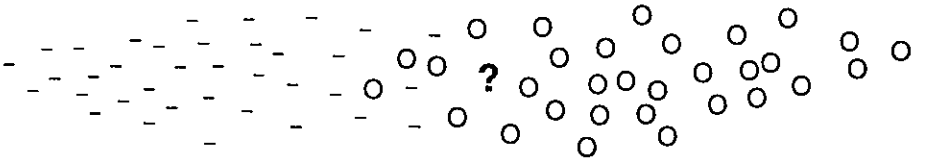

(c) Nearest-neighbor methods can fail.

After Masters, 1995.

FIGURE **3-27**
PNN CLASSIFICATION
PNC-KAMAISHI/H8 REPORT

PROJECT NO. 923 1089.921 DRAWING NO. 77074 DATE 2/20/98 DRAWN BY EA

Golder Associates

For example, the U.S. National Institute of Standards & Technology carried out two studies comparing several popular traditional and neural network classification techniques. The PNN gave the lowest error rate on very complicated databases (Candela and Chellappa, 1993; Grother and Candela, 1993). In addition, the ability of a PNN to minimize the cost of misclassification and provide mathematically rigorous confidence levels for decision analysis make PNN's the preferred neural net algorithm for a variety of military applications (Masters, 1995). The major drawback of PNN's are that they require very large amounts of memory and computational speed, which were not widely and cheaply available for realistically-sized problems until the 1990's.

The basic architecture of a PNN is illustrated in Figure 3-26. It consists of four layers: an Input layer, a Pattern layer, a Summation layer, and the Output layer. The Input layer has the same number of neurons as there are input parameters. The number of neurons in the Pattern layer is equal to the number of training cases used for each class. In the figure, there are two classes and two training sets for each class, producing a total of 4 neurons in the Pattern layer. There is one Summation layer neuron for each class. The Output layer consists of a very simple single neuron which determines which Summation layer neuron is producing the maximum signal.

This type of network is often superior to back-propagation networks in classification accuracy (Candela and Chellappa, 1993; Grother and Candela, 1993), such as the one tested on Kamaishi data by Doe et al. (1994). To see if they would perform better than back-propagation nets on the type of data typically gathered during site investigations, and also if they provide deeper insight into the geology of conductive pathways, a PNN was run on the data from Kamaishi previously analyzed with a back-propagation net (Doe et al., 1994).

3.1.2.5 Performance of PNN

The PNN software used for analysis consisted of a module of the commercial neural net package, NeuroShell II (Ward Systems Group, 1996). In all, 2107 observations from the KD-90, KD-88, Northeast and Northwest drifts was used. Approximately two thirds of

this data consisted of fractures classified as "dry". The remainder consisted of fractures were combined into a single set termed "conductive" or "wet".

These 2107 observations were separated into three groups at random. Group 1 (termed the Training set) consisted of 250 dry and 250 conductive fractures. Group 2 (termed the Test set) consisted of 250 dry and 250 conductive fractures. Group 3 (termed the Production set) consisted of the remaining 1107 fractures. The prediction of the Production set is the key test of the predictive accuracy of the network, since none of this data is used in the training or calibration of the net. The Training and Test sets were given equal numbers of dry and conductive fractures so that the network would focus on recognizing patterns in the data, rather than being biased by the predominance of dry fractures. For example, one could arbitrarily classify all fractures as dry and be correct two thirds of the time! However, this would not accomplish the goal of accurately predicting the number of conductive pathways. Constructing training and testing sets with equal numbers of dry and conductive fractures forces the net to use patterns in the data, rather than prior probabilities, for making predictions.

The network was trained using the genetic adaptive method and the Euclidean distance metric options (Ward Systems Group, 1996). Training continued with different random number seeds until the mean-squared error for the Test set did not improve after 1000 training epochs. Table 3-9 summarizes the classification performance for each of the data sets.

Table 3-9 Results of PNN training and application

Parameter	Training Set		Test Set		Production Set	
Fractures classified:	500		500		1107	
Fractures classified correctly:	408		329		735	
Fractures classified incorrectly:	92		171		372	
Smoothing factor:	0.8447059		0.8447059		0.8447059	
Categories:	Dry	Wet	Dry	Wet	Dry	Wet
Actual winners:	250	250	250	250	878	229
Classified winners:	296	204	289	211	722	385
Global Performance	+18%	-18%	+16%	-16%	-18%	+40%
True positives:	227	181	184	145	614	121
False positives:	69	23	105	66	108	264
True positive proportion:	0.908	0.724	0.736	0.58	0.6993	0.5284
False positive proportion:	0.276	0.092	0.42	0.264	0.4716	0.3007

Table 3-9 can be interpreted as follows. The results have been divided into three categories. The categories are for the Training Set, the Test Set and the Production Set. The first four lines of the table shows how many fractures were classified correctly out of all the fracture classified, and also the smoothing factor that the PNN used for classification. The classification accuracy is described in greater detail in the bottom portion of the Table. In this portion, each of the three fracture data sets is further divided into "Dry" and "Wet", where Dry means non-conductive, and Wet mean conductive. As an example to what the numbers in the Table mean, consider the results for the Training set. The actual winners correspond to the actual number of fractures that are have been measured in the drifts and determined to be dry or wet. There were 250 dry fractures and 250 wet fractures in the Training set. "Classified winners" refers to the number of fractures that the PNN classified as wet or dry. For the Training set, the PNN classified 296 fractures as dry and 204 fractures as wet.

These two lines do not describe the *local* performance of the net, only the *global* performance. The global performance does not record whether every dry fracture is correctly classified as dry, and every wet fracture is correctly classified as wet. For the example in Table 3-9, the 204 fractures classified as wet could, theoretically, all have been actually dry. Globally accurate classifications are useful when the a global measure is required, such as the conductive P_{10} in a well.

Local performance means that a fracture classified as wet is actually wet, while a fracture classified as dry is actually dry. The next four lines of the table show the local performance.

True positives refer to the number of dry fractures correctly classified as dry, and the number of wet fractures correctly classified as wet. False negatives are the errors in local classification. Table 3-9 shows that 227 dry fractures were correctly classified as dry, while 181 wet fractures were correctly classified as wet. The proportion of correct and incorrect local classification are calculated and shown in the last two lines. The true positive proportion for dry fractures represents the number of correctly classified dry fractures (227) divided by the total number of dry fractures (250). The false positive proportion represents the number of wet fractures incorrectly classified as dry (69)

divided by the number of actual wet fractures (250). Analogous calculations are shown for the wet fractures. The local performance is best summarized by the second-to-last row that has been highlighted. The closer that the numbers in this row are to 1.0, the better the local and global classification accuracy.

These results can be compared to the previous results, and also to random guessing. Table 3-10 summarizes the results that would be obtained from random guessing.

Random guessing is analogous to flipping a coin that had two sides; a "wet" side and a "dry" side. The coin could land with the wet or dry side showing with probability proportional to the ratio of dry to wet fractures. For the data considered, the dry side of the coin would come up about two-thirds of the time, since 65.4% of the fracture data is classified as dry. If this coin were used to classify fractures, about one-third of the wet fractures would be correctly classified as wet, and about two-thirds of the wet fractures would be incorrectly classified as dry. Likewise, about two-thirds of the dry fractures would be correctly classified as dry, while one-third of the dry fractures would be incorrectly classified as wet. Thus, the global performance for the Training and Test sets is about a 31% misclassification; for the Production set, there is approximately a 67% overestimation of the number of wet fractures. The local performance is, as expected, a 65.4% correct classification of dry fractures and a 34.6% correct classification of weet fractures.

Table 3-10 Results for random guessing

	Training and Testing Sets		Production Set	
Categories:	**Dry**	**Wet**	**Dry**	**Wet**
Actual winners:	250	250	878	229
Classified winners:	327.0052	172.9948	723.9896	383.0104
Global Performance	30.80%	-30.80%	-17.54%	67.25%
True positives:	163.5026	86.49739	574.2212	79.23161
False positives:	163.5026	86.49739	149.7684	303.7788
True positive proportion:	0.65401	0.34599	0.65401	0.34599
False positive proportion:	0.65401	0.34599	0.65401	0.34599

A comparison of Tables 3-9 and 3-10 shows that the PNN has improved both the global and local classification performance measures. The global errors for random guessing decreased from around 31% to 18% for the training and test sets, and decreased from 67% to 40% for the Production set wet fractures (the errors for the Production set dry fractures was virtually unchanged). A comparison in the true positive proportion for the wet fractures shows that the PNN greatly improves the identification of conductive fractures over random guessing. Conductive fractures would only be correctly identified as conductive 35% of the time by guessing at random. However, the PNN identifies the conductive fractures correctly 72% of the time in the Training set, 58% of the time in the Test set, and 52% of the time in the Production set. The fact that the PNN predicts conductive fractures at 52% accuracy shows that the net has uncovered a useful pattern in the data, since the production set is not used in any way for calibration of the net, and has very different prior probabilities for conductive and dry than the Test and Training sets.

When these results are compared to the previous results using a 3-layer Back-Propagation net, the PNN shows better performance. The equivalent measure of "True Positive Proportion" for conductive fractures in the Back-Propagation net is the parameter **MPc** for wet fractures. For the test sets considered, the value of **MPc** is typically in the range 0.28 to 0.35 (Doe et al., 1994, Table 2-9). The PNN represents about a 60% improvement over the back-propagation results.

In addition, other types of nets including a Generalized Regression Neural Net (GRNN) and several more complex back-propagation nets were tried. These nets typically had a correct classification of conductive fractures for the Production set in the 0.40 to 0.45 range.

3.1.2.6 Geological Parameters Important to the PNN's Classification

Table 3-11 shows which parameters had the most importance for the trained PNN. These parameters could be considered as the most important properties to measure in order to distinguish between fractures that are likely to be conductive and those that are likely to be non-conductive. The importance of a parameter in a PNN is a function of its

smoothing factor. Smoothing factors may vary from 0.0 (no importance) to 3.0 (very important). A discussion of smoothing factors is beyond the scope of this report; details can be found in Specht (1990) or Masters (1993; 1995). Table 3-11 shows that epidote and apatite in the fillings of fractures is important. White, green and brown fracture coatings and fillings are important. Alteration degree is important, but not alteration width. Likewise, dip direction is important, but not the amount of dip. Fracture aperture and openness are also important.

Table 3-11 Smoothing factors for the trained PNN

Parameter	Smoothing Factor
Epidote-1	2.98824
Apatite-1	2.90588
Aperture	2.8
White	2.78824
Dip Direction	2.76471
Alteration Degree	2.70588
Openess	2.56471
Green	2.28235
DGM	2.27059
Brown	2.23529
Laumontite-1	1.91765
GNM	1.70588
Grey	1.69412
CAL	1.50588
Calcite-1	1.31765
ST	1.21176
Stilbite-1	1.17647
Dip	0.74118
Pink	0.72941
YGM	0.62353
GYM	0.56471
L	0.56471
QZ	0.50588
BKM	0.42353
S-Scale R.	0.4
Quartz-1	0.4
Alteration Width	0.21176
Plagioclase-1	0.07059

Smoothing factors do not describe whether the conductivity of a fracture is positively or negatively correlated with a factor. The correlation coefficients for conductivity shown

in Table 3-12 provide some additional insight. They are ranked from most positive to most negative.

Table 3-12 Correlation coefficients for conductive fractures

	Correlation Coefficient
Openness	0.275173
Aperture	0.133002
CAL	0.088556
Dip Direction	0.072119
Green	0.063209
Alteration Width	0.063103
Calcite-1	0.062832
Alteration Degree	0.056119
Brown	0.031436
Epidote-2	0.027133
Stilbite-1	0.026771
ST	0.024846
Epidote-1	0.020751
Laumontite-2	0.017895
Dip	0.016288
Stilbite-2	0.014487
Quartz-2	0.012247
BKM	0.00891
Calcite-2	0.002018
S-Scale R.	-0.00184
Grey	-0.00562
DGM	-0.00874
White	-0.01479
QZ	-0.01908
Plagioclase-1	-0.02242
Laumontite-1	-0.02418
Quartz-1	-0.02684
Apatite-1	-0.02746
Location	-0.02982
GYM	-0.03504
GNM	-0.038
YGM	-0.03891
Pink	-0.04109
Plagioclase-2	-0.04205
L	-0.05937

This table shows that epidote is positively correlated with conductive fractures, while apatite is negatively correlated. Openness, aperture and dip direction are all positively correlated with conductivity, as are alteration degree and width. Brown and green

fracture coatings and fillings are positively correlated, while white colored fracture coatings and fillings are associated with non-conductive fractures, as is the DGM mixed mineral group.

Table 3-12 shows the correlation matrix for a number of input parameters. These correlations suggest the existence of certain mineral assemblages and associated colors that might provide a geological basis for interpreting the pattern uncovered by the PNN.

One of the associations that emerges from study of Table 3-12 is that epidote-1 (epidote the most abundant mineral filling) is associated with lesser amounts of calcite and quartz (calcite-2 and quartz-2). One possibility for this association is the breakdown of epidote in the presence of groundwater into calcite, quartz and iron-bearing minerals such as hematite. Presumably the hematite would impart a brown coloration to the filling material or the surrounding rock. The green coloration might be due to a ferrous compound, or perhaps reflects the color of the epidote itself. Brown and green colors are also associated with increased fracture aperture, though they have a negative correlation with alteration degree.

This model is not entirely self-consistent, however, since brown and green colors and the occurrence of epidote fillings are negatively correlated with dip direction, while fracture conductivity is positively correlated. Also, brown and green coloration is not correlated with epidote-1, but only with epidote-2. Pink is positively correlated with epidote-1, which might have something to do with associated quartz or clay by-products. Thin section analysis of the petrology of the fractures might clarify these statistical relations. It would be worthwhile to try to relate the correlations and patterns found in this study to any existing petrological studies of the fractures and their fillings, or to undertake such studies if they have not been carried out.

3.1.2.7 Conclusions and Recommendations

1. A probabilistic neural net was designed for the Kamaishi data used in a previous study (Doe et al., 1994). The PNN successfully predicted conductive fractures in data set withheld from all training and calibration about 52% of the time. This is

about 60% better than random guessing, and about 25% better than the back-propagation network used previously.

2. The PNN did not include censoring information, as it was not available for much of the data set. However, previous back-propagation network studies of the KD-90 drift data showed that censoring information was among the most useful information. Inclusion of this data would likely have improved the classification accuracy.

3. Examination of the smoothing factors and the correlation coefficients suggests that certain measured geological parameters are important for identifying conductive fractures. The presence of epidote, brown or green coloration, dip direction, openness, larger aperture and higher alteration degree are positively correlated. The presence of apatite and white coloration characterize dry fractures.

4. A geological model to explain these results has been proposed. The model is speculative and needs to be based upon petrologic examination of the fractures and their fillings, which was not part of this study. The model is that fractures filled with epidote have partially broken down into calcite, an iron-rich constituent, and perhaps some other silicates minerals, imparting a brown or green coloration to the fracture. This degeneration may have created a secondary porosity, leading to more open, wider aperture fractures. The fractures that tend to have epidote may also have a preferred orientation.

5. It would be useful to include censoring information in future neural net work. It is recommended that this data be routinely gathered in fracture studies. However, if predictions are to be made from borehole data, this information cannot be collected, and so a PNN similar to the current one in which censoring information is neglected must be used.

6. The PNN should be tested against data from wells or drifts elsewhere in the Kamaishi mine or its immediate vicinity, to evaluate whether the pattern defined by the PNN to classify fractures generally applies to the Kamaishi rock mass. However, the same data parameters used in the PNN must be collected. If a

different set are collected, then the PNN must be re-trained, and perhaps additional data will need to be collected in the KD-90, KD-88 Northeast or Northwest drifts.

7. PNN's or other types of neural nets could be used for other purposes in siting a nuclear waste repository. For example, self-organizing Kohonen nets could be used to identify fracture sets or identify geological domains at any rock mass scale. Identifying and characterizing geological domains is essential for any large scale performance modeling. Once recognized, the nets could then be used to classify new observations into their correct geological domain.

3.2 Task 2.3: Site Generic Analysis Support

During HY-6, Golder Associates developed a methodology for analysis of generic sites based on fracture mapping. During HY-8, PNC will apply these methodologies to a variety of sites in Japan. In this task, Golder Associates provided technical support services to site generic analyses to be carried out by PNC, including trace plane fracture location model analysis, DFN flow modeling, and PAWorks pathways analysis.

To facilitate this analysis, Golder provided .F2D files of the 10 digitized maps to PNC. These files are illustrated in Figure 3-28. Site generic analysis will be carried out by building 200 m scale models using fracture geometric statistics derived from the .F2D file trace analysis. Constant fracture transmissivity will be used. The sites will be compared based on a single measure, the conductance (flux) from a canister at the center of the model to the edges of the model. For each site, 100 to 1000 Monte Carlo simulations are expected to be carried out by PNC, with Golder support.

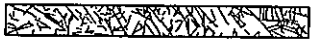

TRACE MAP A-1

TRACE MAP A-2

TRACE MAP A-3

TRACE MAP A-4

FIGURE 3-28a

FRACTURES ON TRACE MAPS A-1, A-2, A-3, A-4

PNC/H8/JAPAN

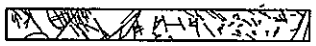

TRACE MAP H-1

TRACE MAP H-2

TRACE MAP I-1

TRACE MAP I-2

FIGURE **3-28b**

FRACTURES ON TRACE MAPS H-1, H-2, I-1, I-2

PNC/H8/JAPAN

TRACE MAP I-3

TRACE MAP I-4

TRACE MAP M-1

TRACE MAP M-2

FIGURE 3-28c
FRACTURES ON TRACE MAPS I-3, I-4, M-1, M-2
PNC/H8/JAPAN

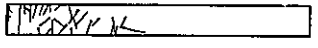

TRACE MAP N-1

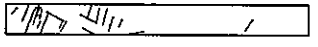

TRACE MAP N-2

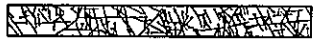

TRACE MAP O-2

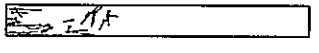

TRACE MAP O-3

FIGURE 3-28d

FRACTURES ON TRACE MAPS N-1, N-2, O-2, O-3

PNC/H8/JAPAN

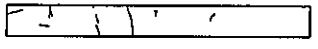

TRACE MAP O-4

TRACE MAP S-1

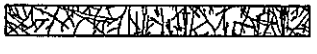

TRACE MAP S-2

TRACE MAP SB-1-A

FIGURE 3-28e

FRACTURES ON TRACE MAPS O-4, S-1, S-2, SB-1-A

PNC/H8/JAPAN

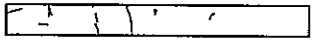

TRACE MAP SB-1-B

TRACE MAP SB-2

TRACE MAP ST-1

TRACE MAP ST-2

FIGURE 3-28f

FRACTURES ON TRACE MAPS SB-1-B, SB-2, ST-1, ST-2

PNC/H8/JAPAN

TRACE MAP T-1

TRACE MAP T-2

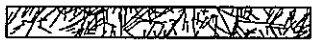

TRACE MAP X-1

TRACE MAP X-2

FIGURE 3-28g

FRACTURES ON TRACE MAPS T-1, T-2, X-1, X-2

PNC/H8/JAPAN

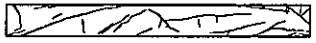

TRACE MAP Y-1

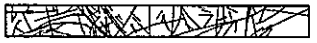

TRACE MAP Y-2

FIGURE **3-28h**

FRACTURES ON TRACE MAPS Y-1, Y-2

PNC/H8/JAPAN

3.3 Task 2.4: Performance Assessment Support

The major calculation for the PNC HY-12 performance assessment report will be carried out during HY-9. In this task, Golder Associates provided technical support to PNC for performance assessment calculations. Specific support activities included:

- Scoping calculations to determine to scale of models which can be run for different levels of fracture intensity, and the level of uncertainty introduced by simplifications of the fracture network;
- Preliminary applications of the PAWorks/LTG approach for PA;
- Preliminary applications of PAWorks to provide input for CRYSTAL PA;
- Prototype PA calculations using RIP (Miller, 1996);
- MAFIC truncation cutoff studies to study the effect of the truncation of the fracture population by minimum fracture size and transmissions; and
- PAWorks algorithm confirmation studies to demonstrate the validity of the PAWorks pipe approach by comparison to the 3D MAFIC DFN approach.

These studies are described in Appendix A.

3.4 Task 2.7: Fracture Network Literature Survey

During this task, Golder Associates carried out a state of the art review of laboratory testing of fracture networks, and participated in ENTRY project meetings in Tokai. The state of the art review is provided as Appendix F.

4. TASK 3: INTERNATIONAL PROGRAMS

4.1 Task 3.1: Äspö Project

During HY-8, Golder Associates provided support to PNC's analysis, simulation, presentation, and report presentation for the Äspö modeling task force. Golder Associates assisted PNC in carrying out analyses and preparing reports and presentations of Task 4C, the Tracer Retention Understanding Experiments (TRUE-1) and the TRUE-Block Scale experiments. Reports were prepared for publication as SKB ICR series reports.

Äspö related issues are as follows:

- Reporting;
- TRUE-Radial Converging Tracer Prediction;
- TRUE-Dipole Tracer Prediction; and
- TRUE-Block Scale Experiment.

4.1.1 Reports

During HY-8, Golder produced the following draft reports:

- the TRUE-1 Radially Converging Tracer;
- the TRUE-1 Dipole Tracer Prediction; and
- the Tunnel Drawdown Prediction ("TASK 3").

Draft TRUE-1 reports are attached in Appendices B and C. The Tunnel Drawdown report was previously provided to PNC.

4.1.2 TRUE-1 Radially Converging Tracer Prediction

During HY-8, Golder Associates supported PNC by carrying out an extensive series of simulations for the Äspö TRUE-1 radially converging tracer prediction, presented at the Äspö Modeling Task Force in June, 1996. The radially converging tracer experiment was carried out by SKB in a single identified relatively high transmissivity discrete feature,

"Feature A," within the "TRUE-1" rock block at the northern end of the Äspö Hard Rock Laboratory (Figure 4-1). The boreholes configuration in "Feature A" is illustrated in Figure 4-2. The report summarizing HY-8 modeling and analysis for the TRUE-1 radially converging tracer experiment is provided as Appendix B.

Three models were implemented and used in predictive simulations:

Model #1: **Moench:** An analytical solution for radially converging flow in a confined aquifer by Moench (1995). This solution requires simple boundary condition assumptions. The advantage of this model is in its simplicity (Figure 4-3).

Model #2: **SEEP/W**: A two dimensional finite element model, capable of modeling heterogeneity and more complex boundary conditions. This model is more powerful than analytical solutions (Figure 4-4).

Model #3: **FracMan**: The discrete fracture model provides a more realistic model for the TRUE-1 rock block. However, definition of geometry and properties is significantly more difficult (Figure 4-5).

The PNC/Golder team placed considerable emphasis on understanding boundary conditions for these simulations. PNC/Golder team recognizes that a proper understanding of boundary conditions is the key to prediction of tracer tests, and without proper boundary conditions, no experiment can be successful. The boundary conditions are designated as follows:

A: **Hydrostatic:** Constant head on the boundaries of the model such that the only hydraulic sink is provided by the pumping well.

B: **Point Dilution**: Boundary conditions consistent with the a point dilution interpretation of the tracer time histories in the injection boreholes.

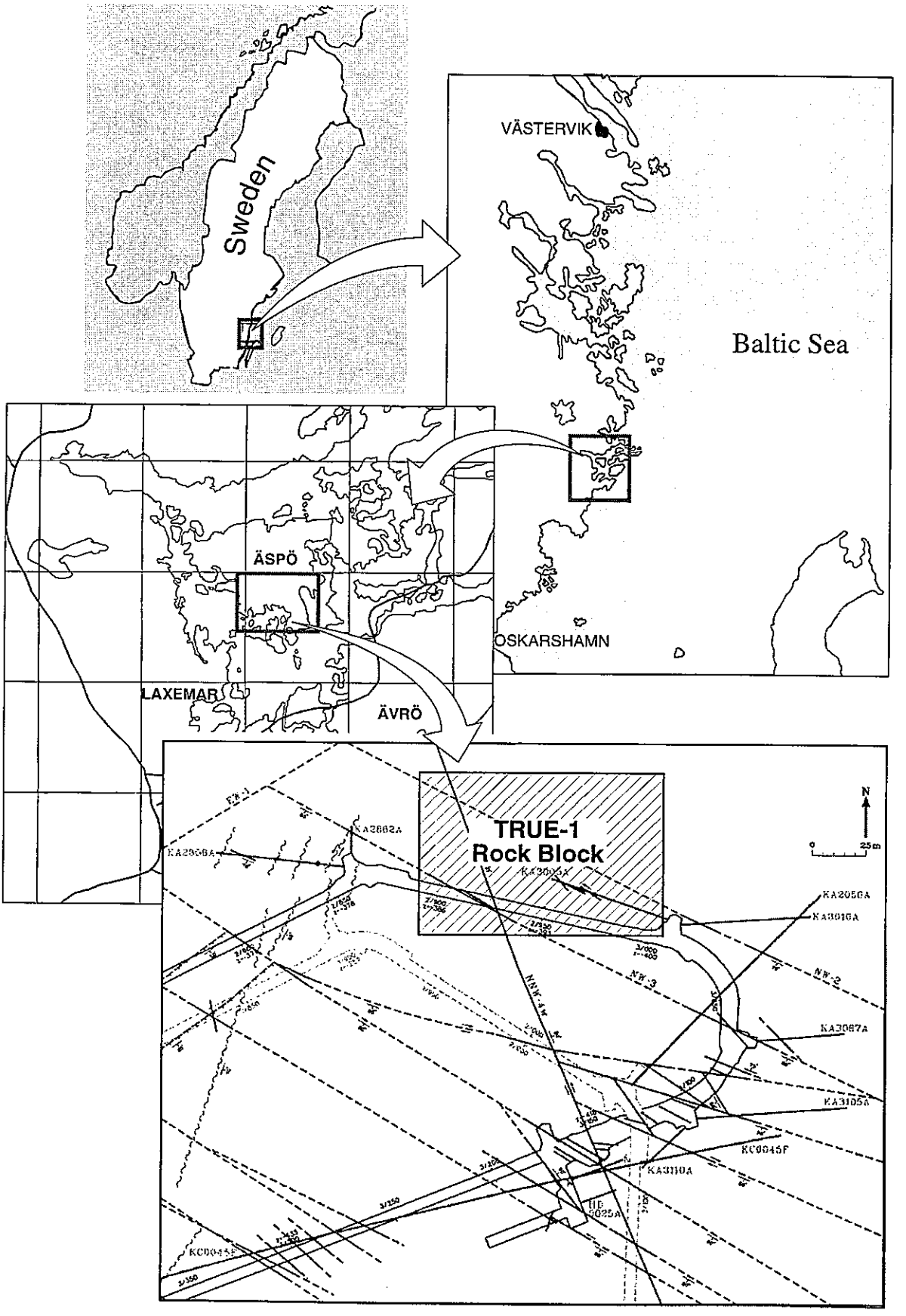

FIGURE **4-1**
TRUE-1 EXPERIMENT SITE
PNC/H8

PROJECT NO. 923 1089.800 DRAWING NO. 73158 DATE 5/9/97 DRAWN BY EA

Golder Associates

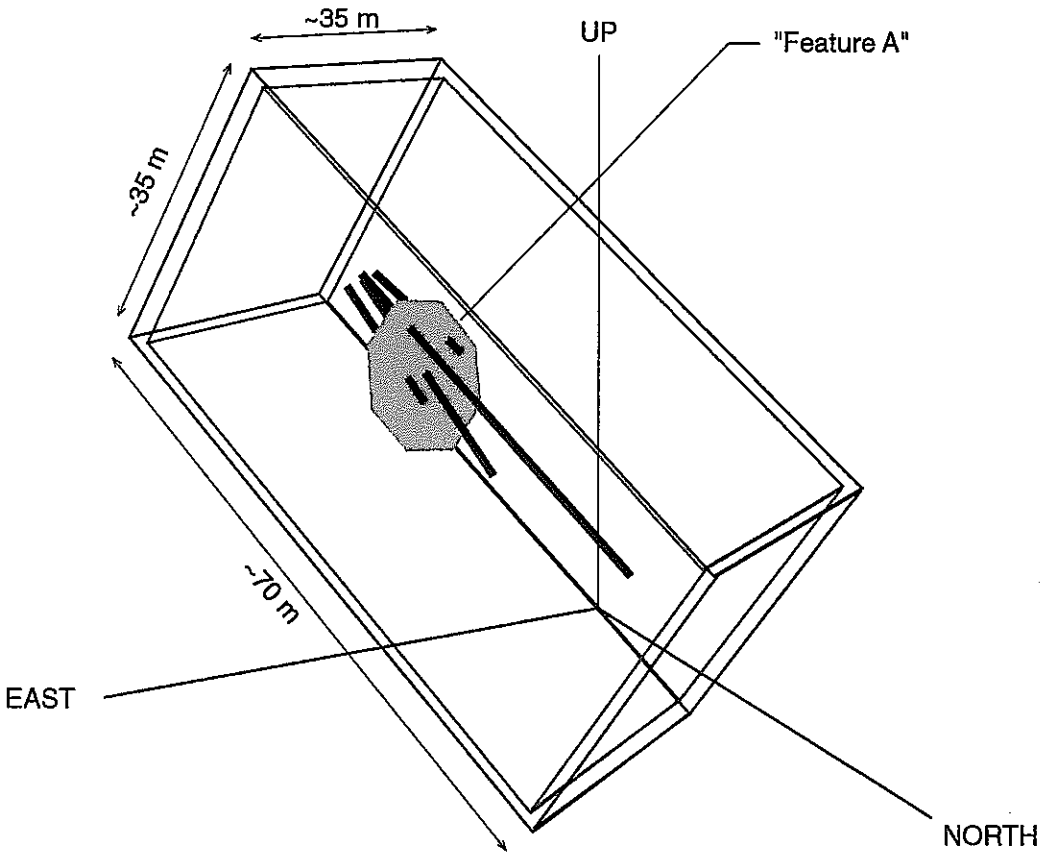

(a) View including boreholes.

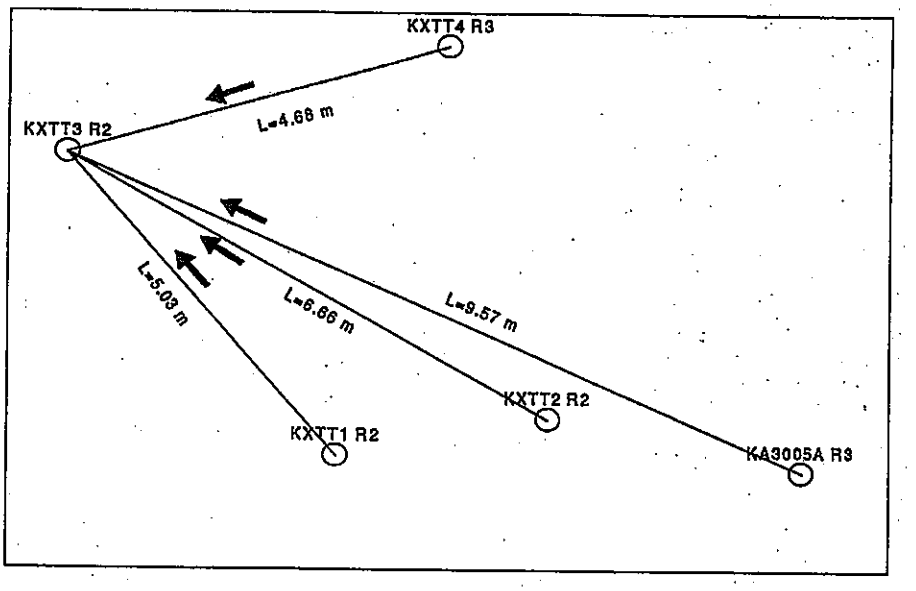

(b) True-1 radially converging tracer test RC-1. Test geometry in the plane of Feature A.

FIGURE **4-2**
TRUE-1 ROCK BLOCK
PNC/H8

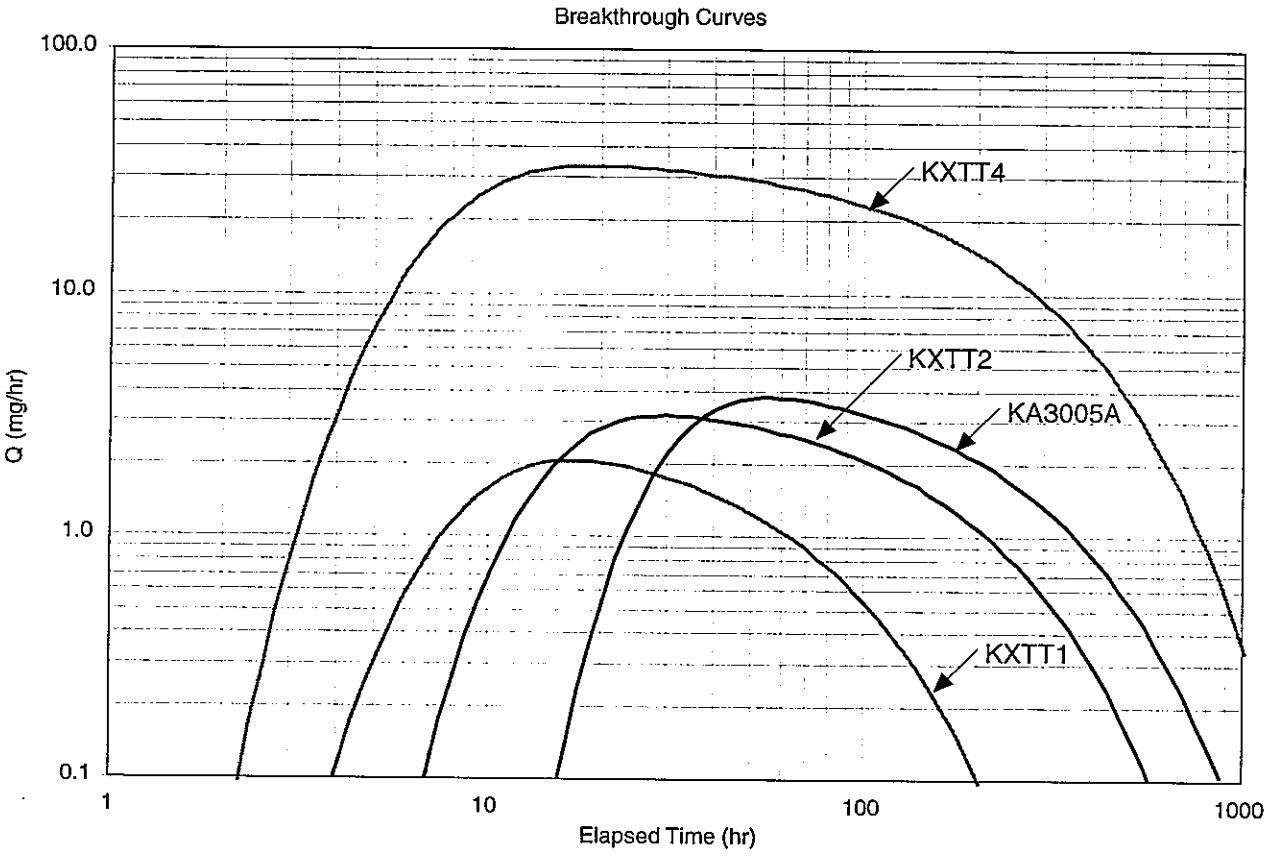

FIGURE **4-3**
MOENCH (1995) BREAKTHROUGH CURVES
PNC/H8

PROJECT NO. 923 1089.800 DRAWING NO. 73159 DATE 5/9/97 DRAWN BY EA

Golder Associates

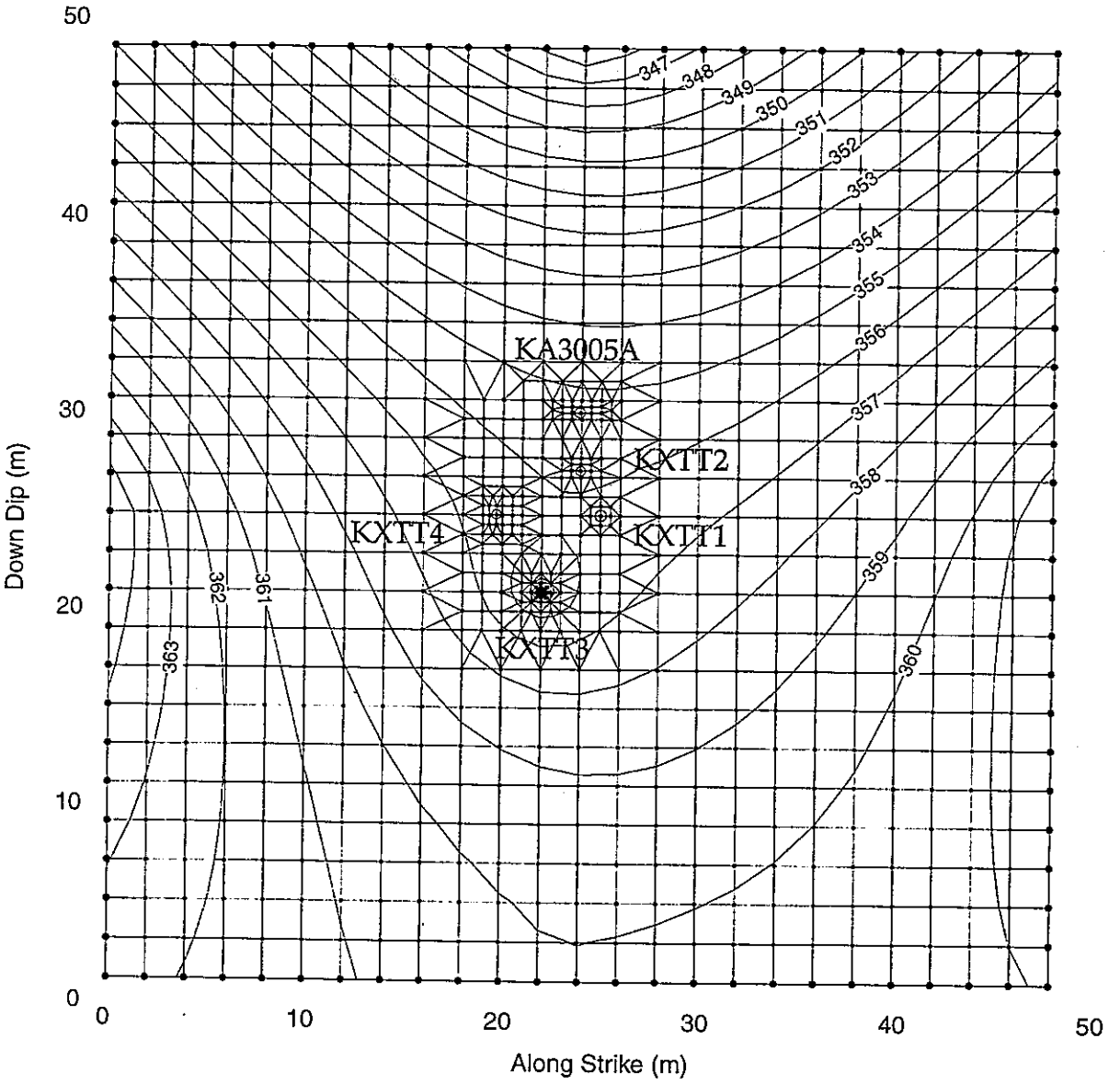

FIGURE **4-4**

SEEP/W HEAD FIELDS FOR BOUNDARY CONDITION "C"

PNC/H8

PROJECT NO. 923 1089.800 DRAWING NO. 73166 DATE 5/9/97 DRAWN BY EA

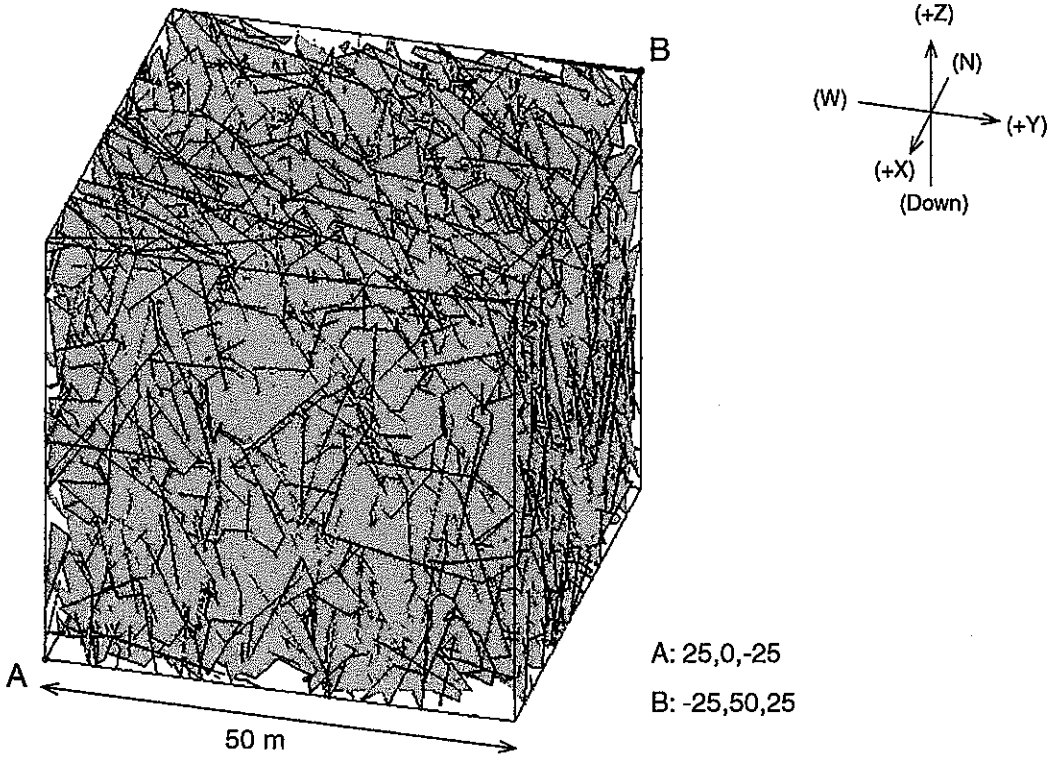

FIGURE **4-5**
FRACMAN MODEL FOR TRUE-1/RC
PNC/H8

C: **Local Head:** Boundary conditions consistent with the heads measured in the injection and withdrawal boreholes before initiation of the experiment.

D: **TRUE-1 Block Heads:** Boundary conditions consistent with the heads measured in all of the boreholes of the TRUE-1 block.

All of these boundary conditions have a theoretical basis, and each provided different insights into the behavior of the 50 m scale rock mass being studied.

Conclusions from preliminary modeling of the Äspö TRUE-1/RC radially converging tracer experiment include the following:

- The fractures intersecting "Feature A" create a complex boundary condition on the experiment, such that flow at the experimental pumping rates can not be considered purely radially converging.
- The most likely pressure field interpretation for conditions during the experiment is that obtained by interpretation of the point dilution process of the injection concentrations. This pressure fields indicates a high probability that tracer would be not recovered from KXTT2 and KA3005A for the experiment as run.
- The Moench analytical solution appears to be adequate for describing the shape of the tracer breakthrough, which was expected to match that for the injection time histories, since this was the response observed in the preliminary tracer testing.
- The FracMan modeling appeared to have been useful primarily in terms of understanding the pressure field during the experiment. The low drawdowns from the FracMan model are consistent with a leaky aquifer interpretation, but are much lower than would be expected based on the response seen in the preliminary tracer test.

4.1.3 TRUE-1 Dipole Tracer Prediction

During HY-8, Golder Associates supported PNC by carrying out analyses and modeling for the Äspö TRUE-1 dipole tracer experiment prediction, presented at the Äspö Modeling Task Force in February, 1997. The dipole tracer experiment was carried out using the same boreholes used for the radially converging tracer experiment (Figure 4-6). The draft report summarizing these analyses is provided as Appendix C.

For the prediction, the PNC/Golder team implemented two of the three approaches used for the TRUE-RC experiment (Section 4.1.2):

- 30 meter scale FracMan DFN modeling conditioned to the TRUE-RC-1 experimental results (Figure 4-7), and
- analytical solutions for radially converging and tracer experiments, calibrated to the TRUE-RC-1 experimental results.

The use of the TRUE-RC as the basis for calibration and conditioning was made somewhat problematic by lack of recovery from KXTT2 and KA3005A, particularly considering the large drawdown response seen in KXTT2. This is particularly problematic for the analytical solutions, which use parameters derived solely by calibration from the TRUE-RC tracer breakthroughs, without considering the TRUE-RC head responses. KXTT2 will be used in three of the dipole experiments, but does not have any tracer transport information. However, the drawdown response indicates the KXTT2 is well connected to KXTT3 and less connected to KXTT1 and KXTT4, which are closer.

The approach taken for DFN modeling of Task 4d is summarized as follows:

1. Define "Feature A" and "NW-2*" deterministically within a 30m scale discrete fracture model, using material properties postulated by Winberg et al (ICR-96-04).
2. Generate 50 to 100 realizations of a population of stochastically generated background fractures based on the analysis of Dershowitz et al (ICR-96-05), using only fractures with a transmissivity greater than 10^{-8} m^2/s.

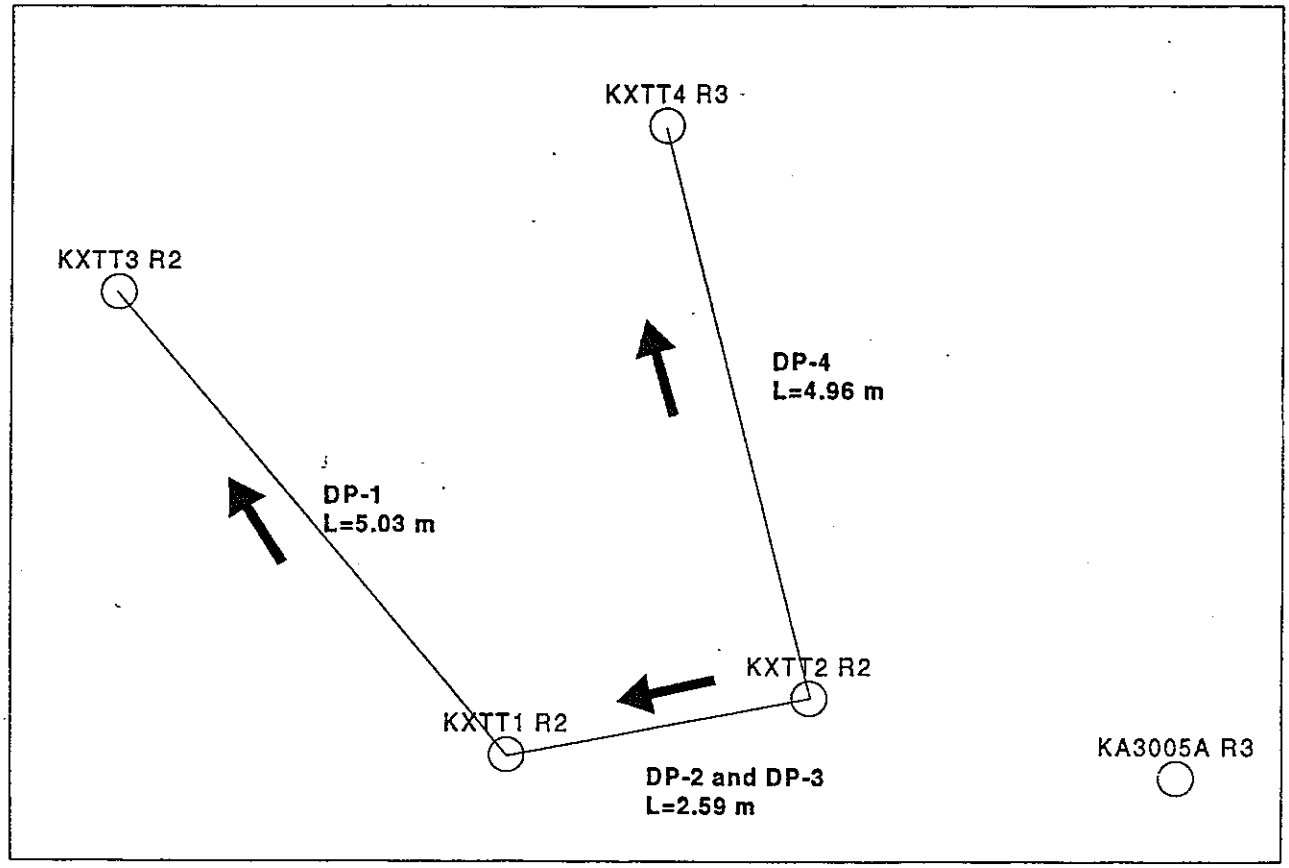

FIGURE **4-6**
TRUE-1 DIPOLE TRACER TESTS DP-1, DP-4 GEOMETRY
PNC/H8

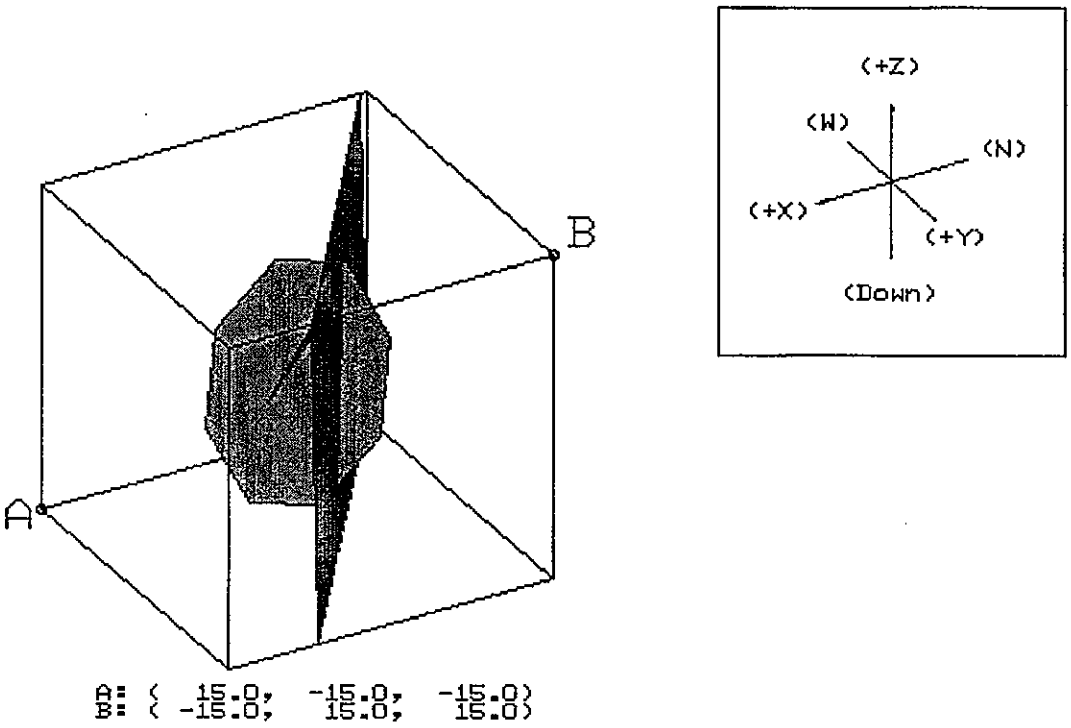

(a) 3D view of deterministic "Feature A", "Feature A*" and "NW-2*" in Discrete Fracture Network Model (30m rock block)

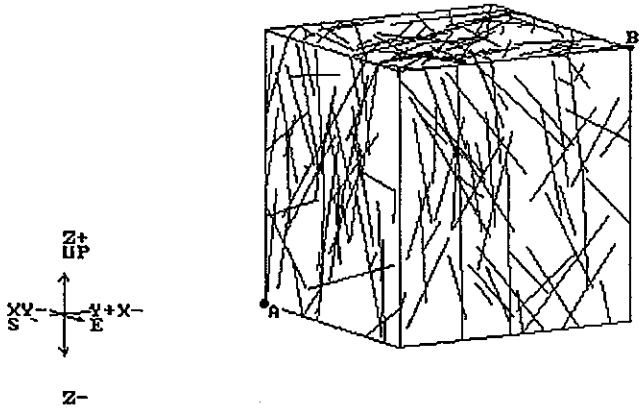

(b) 3D trace view of stochastic background fractures (30m rock block)

FIGURE **4-7**
FracMan MODEL USED FOR DIPOLE TRACER EXPERIMENT PREDICTION
PNC/H8

PROJECT NO. 923 1089.800 DRAWING NO. 73161 DATE 5/9/97 DRAWN BY EA

Golder Associates

3. Apply boundary conditions to the edges of the model to match the heads measured before TRUE-RC-1. Adjust these boundary conditions to obtain a head field which matches that before TRUE-RC-1 for a significant proportion of the realizations.
4. Simulate TRUE-RC-1 pumping from KXTT3, and calculate the drawdown in each of the five wells.
5. Implement a highly transmissive zone connecting KXTT2 and KXTT3 in order to reproduce the large observed drawdown response. Adjust transmissivities of "Feature A" and the channel between KXTT2 and KXTT3 to obtain a good match to the drawdown response for a significant portion of the realizations.
6. For realizations which reasonably match the drawdown responses of TRUE-RC-1, calculate tracer breakthrough for each of the four injection sections. Compare the simulated breakthrough curves to the measured breakthrough curves from TRUE-RC-1. Accept those realizations which have a reasonable match for breakthrough times t_5, t_{50}, t_{95}, and the mass recovery percentage from KXTT1->KXTT3 and KXTT4->KXTT3.
7. For realizations with a reasonable match to both drawdown response and tracer breakthrough, carry out simulations of the four TRUE-Dipole experiments. This requires modification of the external head boundary condition to account for the change in ambient pressure between TRUE-RC-1 and TRUE-Dipole.
8. Use the TRUE-Dipole simulations, conditioned to the TRUE-Radially converging experiment results to calculate probabilistic predictions for drawdown, breakthrough (t_5, t_{50}, t_{95}), and breakthrough.

4.1.4 TRUE-BS Block Scale Experiment

During HY-8, Golder Associates provided support to PNC in the planning of the TRUE-BS block scale experiment, to be carried out in the southern portion of the Äspö Hard Rock Laboratory. The rock block selected for the TRUE-BS experiment is illustrated in Figure 4-8. This experiment is expected to be a significant focus during HY-9.

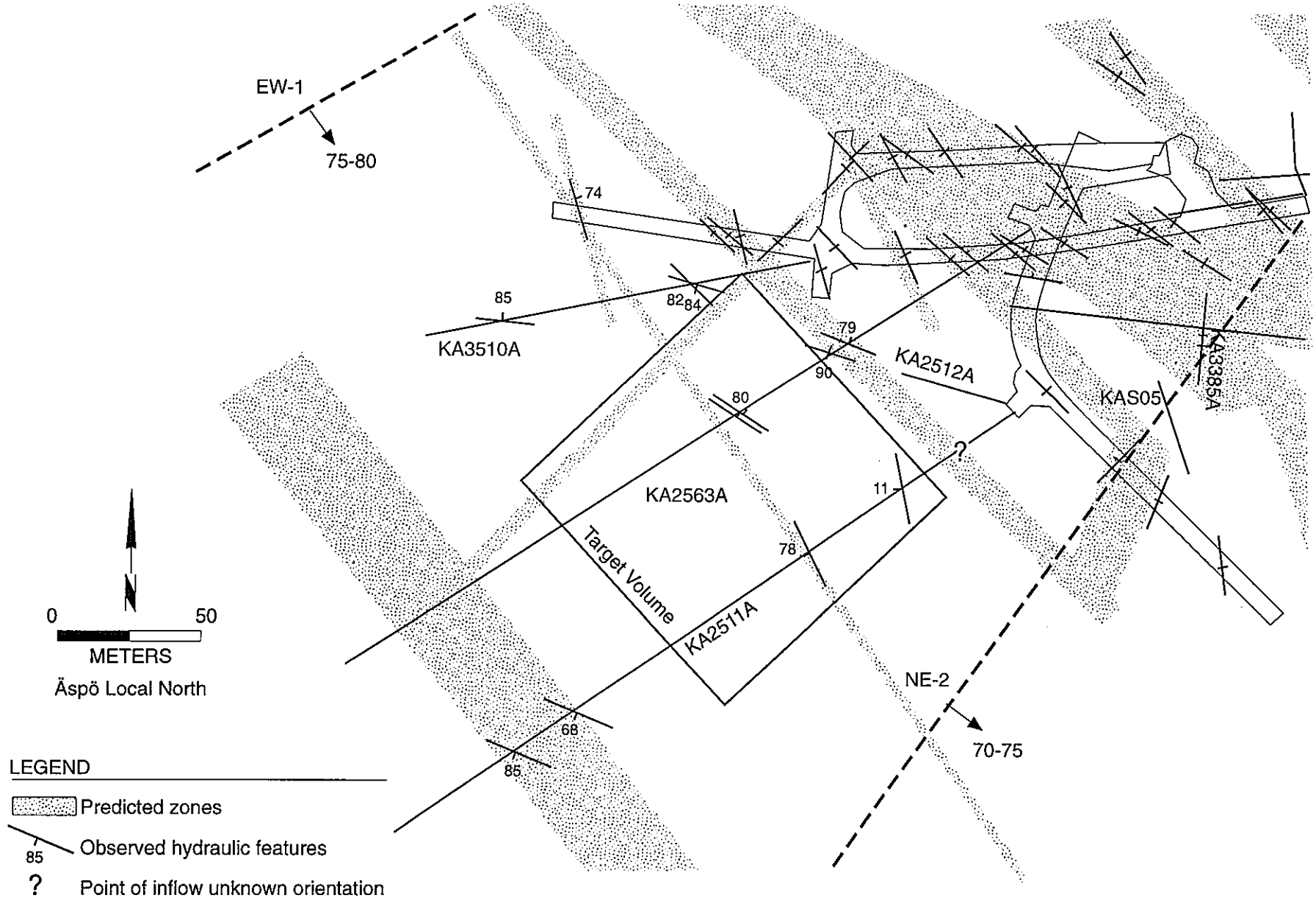

After Winberg (1996)

FIGURE **4-8**

TRUE-BS EXPERIMENT ROCK BLOCK

PNC/H8

PROJECT NO. 923 1089.800 DRAWING NO. 73168 DATE 5/12/97 DRAWN BY EA

Golder Associates

5. CONCLUSIONS

This section will briefly summarize the major accomplishments of the Discrete Fracture Network Code Development project during the Heisei-8 year:

- The PAWorks pathways analysis program was significantly improved, including improvements to the pathways analysis, interfaces to flow and transport codes, and interfaces for performance assessment. PAWorks was re-engineered to run equally on both Unix and Windows95 platforms.
- A Laplace transform Galerkin solute transport model was implemented for repository performance assessment. This model was linked directly to PAWorks. Solute transport is provided including the effects of advection, dispersion, sorption, and diffusion to multiple non-flowing porosities. These non-flowing porosities can include the rock matrix, intersecting fracture networks, and the stagnant portion of fracture planes containing flowing channels.
- Geostatistical and fractal analysis tools were developed to facilitate PNC laboratory testing and site characterization programs. Fractal is a Windows95 program for analysis of fracture roughness patterns from sectional analysis and borehole sampling of rock fractures, and for spatial analysis of data from borehole core logs.
- An interface was developed between the EdMesh stochastic continuum field generation code and PNC's TAGSAC hydraulic model. This interface will allow PNC to carry out stochastic continuum flow simulations with spherical, exponential variogram geostatistical fields, POCS fractal fields, and non-stationary fields.
- Sensitivity analyses were carried out to support the use of pathways analysis and truncated fracture populations in MAFIC and PAWorks simulations for repository performance assessment.
- Prototype performance assessment calculations were carried out using PAWorks/LTG and PAWorks/RIP to assist PNC in development of performance assessment strategies for HY-12.

- Support was provided to the PNC "Site Generic" project, the PNC "ENTRY-2", and the PNC experimental programs at Kamaishi.
- Successful predictive modeling was carried out for the SKB Äspö TRUE-1/Radially Converging (RC-1) and Dipole Tracer (DP-1) experiments, using PNC/FracMan discrete fracture modeling tools. This demonstrated the validity of the DFN approach, and the tools developed by PNC.

6. REFERENCES

Baldwin, J. L., D. N. Otte, and C. L. Wheatley, 1989, Computer emulation of human mental process: application of neural network simulation to problems in well log interpretation: Society of Petroleum Engineers SPE Paper 19619, p. 481-493.

Baldwin, J. L., A. R. M. Bateman, and C. L. Wheatley, 1990, Application of neural network to the problem of mineral identification from well logs: The Log Analyst, v. 3, p. 279-293.

Burrough, P., 1981. Fractal Dimensions of Landscape and other environmental data. Nature, Vol. 294 p. 240-242.

Candela, G. T. and R. Chellappa, 1993, Comparative performance of classification methods for fingerprints. National Inst. of Standards & Tech, NISTIR-5163.

de Hoog, F.R., J. H. Knight, and A. N. Stokes, 1982. An improved method for numerical inversion of Laplace transforms, SIAM J. Sci. Stat. Comput., 3(3), 357-366.

Dershowitz, W.S., T. Doe, G. Lee, P. Wallmann, A. Thomas, T. Foxford, R. Busse, P. LaPointe, 1996. Discrete Fracture network Code Development, Heisi-7 Progress Report. Golder Associates Inc., Seattle.

Doe, T., A. Thomas, P. LaPointe, and J. Thomas, 1996. Fracture Data Analysis and Flow Modeling of the Kamaishi KD-90 and Task 3-2 Experiments. Golder Associates Inc., Seattle.

Davis, J. C., 1973, Statistics and Data Analysis in Geology, John Wiley and Sons, Inc., New York.

Doe, T. W., W. Dershowitz, P. Wallmann, G. Lee, P. La Pointe, S. Hitchcock and C. Chakrbarty., 1993, Discrete fracture network code development, Heisei-4 progress report. PNC PJ 1579 93-001, chap. 1.3.

Doe, T. W., W. Dershowitz, G. Lee, P. La Pointe, P. Wallmann and A. Thomas, 1994, Discrete fracture network code development, Heisei-5 progress report. PNC PJ 1579 94-001, chap. 2.8.

Eberhart, R.C. and Dobbins, R.W., 1990. Neural Network PC Tools. Academic Press, London, 414p.

Ellis, G.W. 1995, Stress-strain modeling of sands using artificial neural networks: Journal of Geotechnical Engineering, v 121. p 429-435.

Feng, X., 1995. Neural network approach to comprehensive classification of rock stability, blastability and drillability: International Journal of Surface Mining, Reclamation and Environment, v. 9, no. 2, p 57-62.

Gelhar, L. W. (1977) Analysis of Two-Well Tracer Tests with a Pulse Input, Report prepared for USDOE, Rockwell International, Richland, WA, USA.

Goh, A.T.C.,1994, Seismic liquefaction potential assessed by neural networks: Journal of Geotechnical Engineering, v. 120, no. 9, p. 1467-1480.

Grother, P. J., and G. T. Candela, 1993. Comparison of handprinted digit classifiers. National Inst. of Standards & Tech., NISTIR-5209.

Heer, W., and Hadermann, J. (1994) Modelling Radionuclide Migration Field Experiments, Paul Scherrer Institut, Wurlenlingen, Switzerland.

Hodgkinson, D.P. and P. R. Maul, 1985. Harwell Laboratory of the United Kingdom Atomic Energy Authority report "One-dimensional modeling of radionuclide migration through permeable and fractured rock for arbitrary length decay chains using numerical inversion of Laplace transforms", September, 1985.

La Pointe, P. R., P.C. Wallmann, and S. Follin, 1995, Estimation of effective block conductivities based on discrete network analyses using data from the Äspö site: SKB Technical Report 95-15, Swedish Nuclear Fuel and Waste Management Co., Stockholm.

LaPointe, P., P. Wallmann, and W. Dershowitz, 1993. Stochastic estimation of fracture size through simulated sampling. Int. Jour. of Rock Mechanics, Mining Sciences, and Geomechanics Abstracts. Vol. 30, No. 7, pp. 1611-1617.

Lee, C., and R. Sterling, 1992, Identifying probable failure modes for underground openings using a neural network: International Journal of Rock Mechanics, Mining Sciences, and Geomechanics Abstracts, v. 29, no. 1, p 49-67.

Masters, T., 1993, Practical neural network recipes in C++: Academic Press, New York.

Masters, T., 1995, Advanced Algorithms for Neural Networks, A C++ Sourcebook: John Wiley & Sons, Inc., New York.

Matheron G., 1988. The internal consistency of models in geostatistics in proceedings, 3rd International Geostatistics Congress, Sept. 5-9, 1988, Auignon. Kluwer Academic Publishers, Dordrecht.

Miller, I., 1996. RIP: Performance Assessment and Strategy Evaluation. Theory Manual and Users Guide, Version 5.0. Golder Associates Inc., Seattle.

Ogata, A. and R.B. Banks, 1961. A solution of the differential equation of longitudinal dispersion in porous media. USGS Professional Paper 411-A.

Osborne, D. A., 1992, Neural networks provide more accurate reservoir permeability: Oil & Gas Journal, (Sept. 28), p. 80-87.

Parzan, E., 1962, On estimation of a probability density function and mode: Annals of Mathematical Statistics, v. 33, p. 1065-1076.

Raiche, A., 1991, A pattern recognition approach to geophysical inversion using neural nets: Geophysical Journal International, v. 105, p. 629-648.

Rogers, S. J., J. H. Fang, C. L. Karr, and D. A Stanley, 1992, Determination of lithology from well logs using a neural network: AAPG Bulletin, v. 76, p. 731-739.

Rogers, S. J., H. C. Chen, D. C. Kopaska-Merkel, and J. H. Fang, 1995, Predicting permeability from porosity using artificial neural networks: AAPG Bulletin, v. 79, p. 1786-1797.

Specht, D., 1990, Probabilistic neural networks: Neural Networks, v. 3, p. 109-118.

Sudicky, E.A. and R. G. McLaren, 1992. The Laplace transform Galerkin technique for large-scale simulation of mass transport in discretely fractured porous formations, Water Resour. Res., 28(2), 499-514.

Sudicky, E.A., 1990. The Laplace transform Galerkin technique for efficient time-continuous solution of solute transport in double-porosity media, Geoderma, 46, 209-232.

Sudicky, E.A., 1989. The Laplace transform Galerkin technique: A time-continuous finite element theory and application to mass transport in groundwater. Water Resour. Res., 25(8) ,1833-1846.

Sudicky, E.A. and Frind, E.O., 1982. Contaminant transport in fractured porous media: Analytical solutions for a system of parallel fractures. Water Resour. Res., 18(3), 1634-1642.

Thomas, A.L. and P. R. La Pointe, 1995. Conductive fracture identification using neural networks: Proceedings: 35th U.S. Rock Mechanics Symposium, University of Nevada, Reno, June 5-7, 1995, p. 627-632.

Tung, A.T., F. S. Wong, and W. Dong, 1994, Prediction of the spatial distribution of the modified Mercalli intensity using neural networks: Earthquake Engineering and Structural Dynamics, v. 23, n. 49, p. 62.

van der Vorst, H., 1992. Bi-CGSTAB: A fast and smoothly converging variant of Bi-CG for the solution of nonsymmetric linear systems, SIAM J. Sci. Stat. Comput., 13, 631-644.

VanderKwaak, J.E., P. A. Forsyth, K.T.B. MacQuarrie, and E.A. Sudicky, 1997. WatSolv: Sparse Matrix Iterative Solver, User's Guide for Version 2.16, Groundwater Simulations Group, Waterloo, Ontario, Canada.

Voss, R., 1986. Random Fractals: Characterization and Measurement. Physica Scripta T13, pp. 27-32.

Ward Systems Group, 1996, NeuroShell 2 User's Manual, 4th edition, Ward Systems Group, Inc., Frederick, MD.

Weiner, J. M., J. A. Rogers, J. R. Rogers, and R. F. Moll, 1991, Predicting carbonate permeabilities from wireline logs using a back-propagation neural network, CM1.1: Society of Exploration Geophysicists, Expanded Abstracts with Biographies, Technical Program, v. 1, p. 285-289.

Xu, Q., and R. Q. Huang, 1994, Artificial neural network methods for spatial prediction of slope stability: *in* Oliveira, R., L. F. Rodrigues, A. G. Coelho, and A. P. Cunha, (eds.), Seventh International Congress; International Association of Engineering Geology, v. 7, p. 4725-4728.

Report to:

PNC Power Reactor and Nuclear Fuel Development Corporation

Tokyo, Japan

Discrete Fracture Network Code Development

Heisei-8 Progress Report Volume 2 Appendices

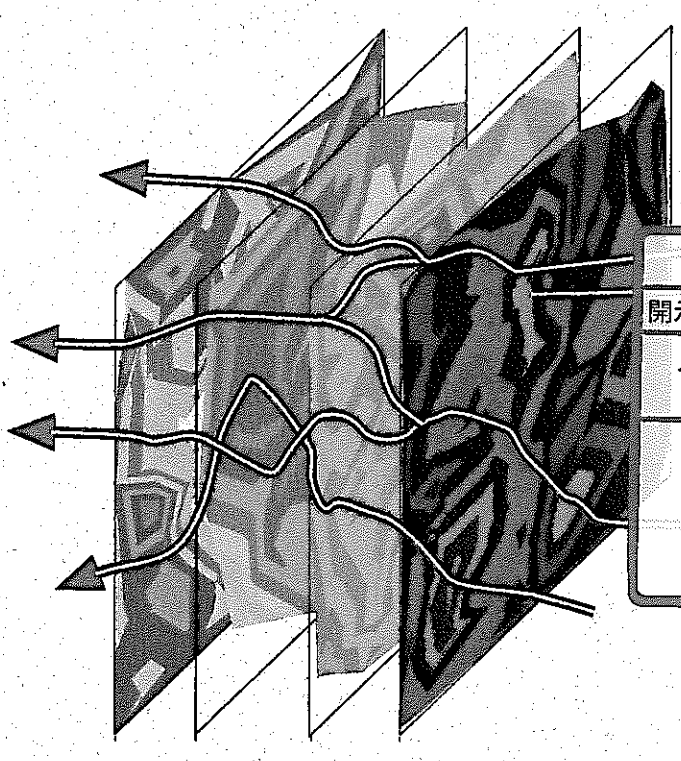

Golder Associates

Appendix A Analysis Support for Performance Assessment

Analysis in Support of Performance Assessment

Dawn Shuttle
William Dershowitz

Golder Associates Inc.
Seattle, WA

March 31, 1997

923-1089.800
hy8_paw.doc

TABLE OF CONTENTS

LIST OF FIGURES

LIST OF TABLES

1. INTRODUCTION

Accurate modeling of the hydrogeological regime in the vicinity of the radioactive waste repositories is critical to demonstrating site suitability. The PNC/FracMan suite of codes provides the ability to realistically model the local fracture network, generating representative flow and head fields, and, through PAWorks, providing critical pathways input into the Crystal performance assessment model.

This report describes a series of sensitivity studies and demonstration performance assessment calculations carried out to determine the feasibility of Discrete Fracture Network (DFN) analysis for performance assessment within the PNC repository project, using the PAWorks pipe-network approach, the MAFIC plate-fracture network approach, and the PAWorks/LTG pipe-solute transport approach.

1.1 Background

The PAWorks code is based on a pipe network representation of a fracture network. Fracture flow paths are idealized as tubes, as opposed to the triangular finite elements which discretize fractures in MAFIC. This simplification of the fracture network representation requires less computer memory and time than the corresponding plate fracture representation. This makes it possible to include more fractures in the simulated fracture network. Thus, PAWorks presents a compromise between the MAFIC approach which uses more realistic fractures and the need to represent a larger percentage of the fracture population.

Fractured rock masses contain fracture networks made up of a wide spectrum of fractures, varying from highly conductive faults, to background microfractures with low conductivity. Fracture network modeling depends on the fact that not every fracture is significant for repository performance. The key to the DFN approach is therefore to determine the portion of the fracture population which must be considered to accurately represent the flow and transport behavior in the vicinity of the repository and to represent the transport pathways from the repository to the accessible environment.

The purpose of the first part of this study is to determine

- the effect of truncation of the fracture population using transmissivity cutoffs on flow and transport behavior for both MAFIC and PAWorks approaches
- the maximum fracture network intensity that is feasible using current Unix workstation hardware for both the MAFIC and PAWorks approaches, and
- PAWorks assumptions which are appropriate to ensure that PAWorks produces flow and transport results comparable to those for the MAFIC approach.

This study has been carried out using the 200 meter scale Kamaishi rock block (Doe et al., 1996) as a reference case. The study will ultimately compare networks of between 1000 and 250,000 fractures, with truncations based on both size and transmissivity. For PAWorks, a range of assumptions for the conversion between plate fractures and pipes will be considered. The measures used for assessing and comparing simulation results are

- Effective block permeability (K_{eff}),
- Minimum and median transport time (t_0 and t_{50}),
- Effective network dispersion (t_{85} and t_{50}),
- Head distribution within the fracture network (H_{xyz})
- Computer resources (memory and CPU time)

Having determined an acceptable equivalence between the PAWorks (pipe) and MAFIC (plate) fracture networks, the final portion of this study illustrates how PAWorks can be effectively used for performance assessment, both independently and by providing input into the Crystal PA code.

1.2 Scope of Report

This report presents preliminary results for fracture networks of 1000 to 50,000 fractures, with differing transmissivity cutoffs. Section 2.0 describes the 200 meter scale Kamaishi

rock block used as the reference case, and the range of parameters simulated. MAFIC and PAWorks simulations are described in Sections 3.0 and 4.0, respectively. Section 5.0 presents the comparison of MAFIC and PAWorks, and highlights the areas where the codes do not produce the same result. Section 6.0 uses the full Kamaishi model assumptions and discusses the assumptions which need to be used in PAWorks to produce results comparable to those of MAFIC. Section 7 presents demonstration performance assessment calculations.

Future simulations will extend the range of PAWorks modeling to 250,000 fractures, will consider truncation by size as well as transmissivity, and will include additional PAWorks pipe generation models.

2. REFERENCE CASE

The 200 meter scale Kamaishi rock block model (Doe et al., 1996) was used as the reference case for these sensitivity studies, since it is also relevant for performance assessment scoping calculations. The 200m scale derives from the reported distance of 100m from the repository to the nearest fault with the repository located in the center of the modeled region.

The fracture geometry of this model is illustrated in Figure 2-1. Two sets of boundary conditions are simulated for the main sensitivity study and are illustrated in Figure 2-2. Both of these boundary conditions provide a 5% horizontal gradient. In boundary condition "A", the model results are affected by a symmetrical head distribution on the model sides parallel to the gradient. In boundary condition "B", model results are affected by the no-flow assumption on the model sides parallel to the gradient.

2.1 Fracture Geometry

The fracture geometry simulated was derived by Doe et al. (1996) to reflect conditions in the KD-90 area of the Kamaishi mine. The fracture statistics for this model are summarized in Table 2-1. The Kamaishi rock block contains two fracture sets with different orientation distributions and intensities. However, the two sets use the same transmissivity and size distribution. Because of this similarity between the fracture sets, truncation of fracture intensity through a minimum transmissivity cutoff is simple. It can be expressed in terms of the total fracture intensity for the combined sets .

The relationship between the number of fractures simulated and the transmissivity cutoff depends on the assumed transmissivity distribution. Assuming the transmissivity distribution of Table 2-1, the number of fractures in the Kamaishi block model for a range of transmissivity cutoff values is presented in Table 2-2 and illustrated in Figure 2-3.

Table 2-1 Fracture Properties Used for the KH-5/KD-90 Model

Property	Set 1	Set 2	Source
Location Model	Levy-Lee	Levy-Lee	Spatial fracture location analysis using data from boreholes and drifts
Exponent	2.4	2.4	
Min Step Size	8 m	8 m	Simulated KD-90 trace maps
Generation Mode	Surface Points	Surface Points	
No. Fracture Sides	6	6	
Generation Region	Box	Box	
Center	0, 0, 0 m	0, 0, 0 m	
Dimensions	225, 225, 225 m	225, 225, 225 m	
Orientation Model	Bivariate Bingham	Bivariate Bingham	ISIS analysis of orientation data from boreholes and drifts
Mean Pole	133.2, 17.6 deg	176.4, 24.1 deg	
K1, K2	-12.69, -4.23	-4.92, -3.25	
Size (Radius) Distribution	Truncated LogNormal	Truncated LogNormal	Heisei-4 analysis of KD-90 censoring statistics
Mean, StdDev.	7, 1.25 m	7, 1.25 m	
Lower Bound	none	none	
Upper Bound	25 m	25 m	*(Note: Truncates less than 0.1% of the distribution)*
Elongation	none	none	
Transmissivity Distribution	Truncated LogNormal	Truncated LogNormal	KH-5 interval transmissivities
Mean, StdDev.	1.1×10^{-7}, 3.85×10^{-4} m^2/s	1.1×10^{-7}, 3.85×10^{-4} m^2/s	
Lower Bound	User defined	User defined	
Upper Bound	none	none	
Storativity	$= 5.0 \times 10^{-5} \times T^{1/2}$	$= 5.0 \times 10^{-5} \times T^{1/2}$	Not used in computation
P_{32} Fracture Intensity	Dependent on T_{cutoff}	Dependent on T_{cutoff}	P_{10} conductive fracture frequency in boreholes KH-4 through 18
Aperture	$e = 2.0\ T^{1/2}$	$e = 2.0\ T^{1/2}$	Doe (1993)

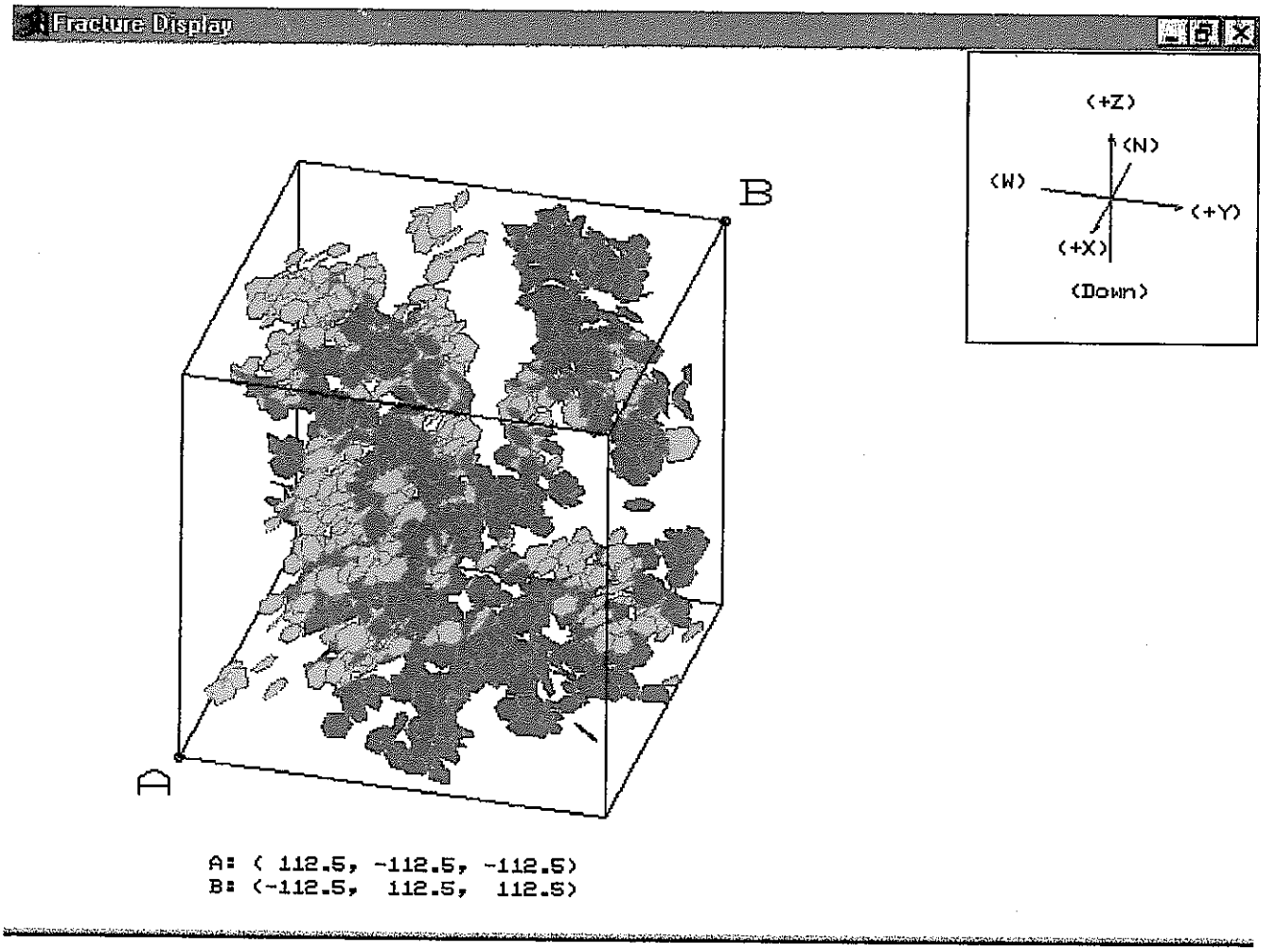

FIGURE **2-1**
FRACTURE GEOMETRY FOR THE KAMAISHI MODEL
PNC/PAW-LTG/JAPAN

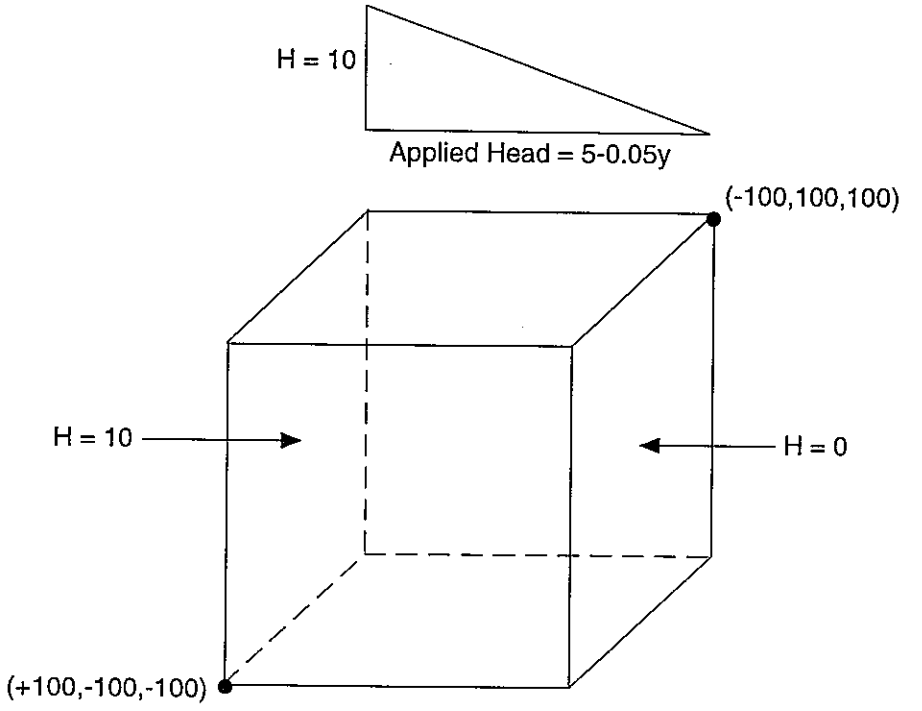

Boundary Condition A, "constant head" Configuration

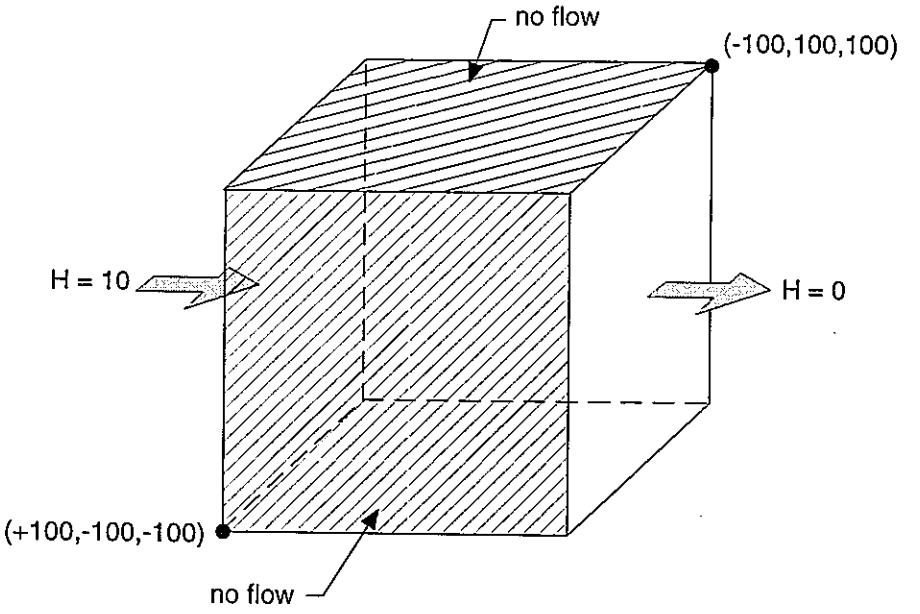

Boundary Condition B, "transport" Configuration

FIGURE **2-2**
BOUNDARY CONDITIONS FOR THE KAMAISHI SIMULATIONS
PNC/PAW-LTG/JAPAN

PROJECT NO. 923 1089.824 DRAWING NO. 72740 DATE 5/12/97 DRAWN BY CB

Golder Associates

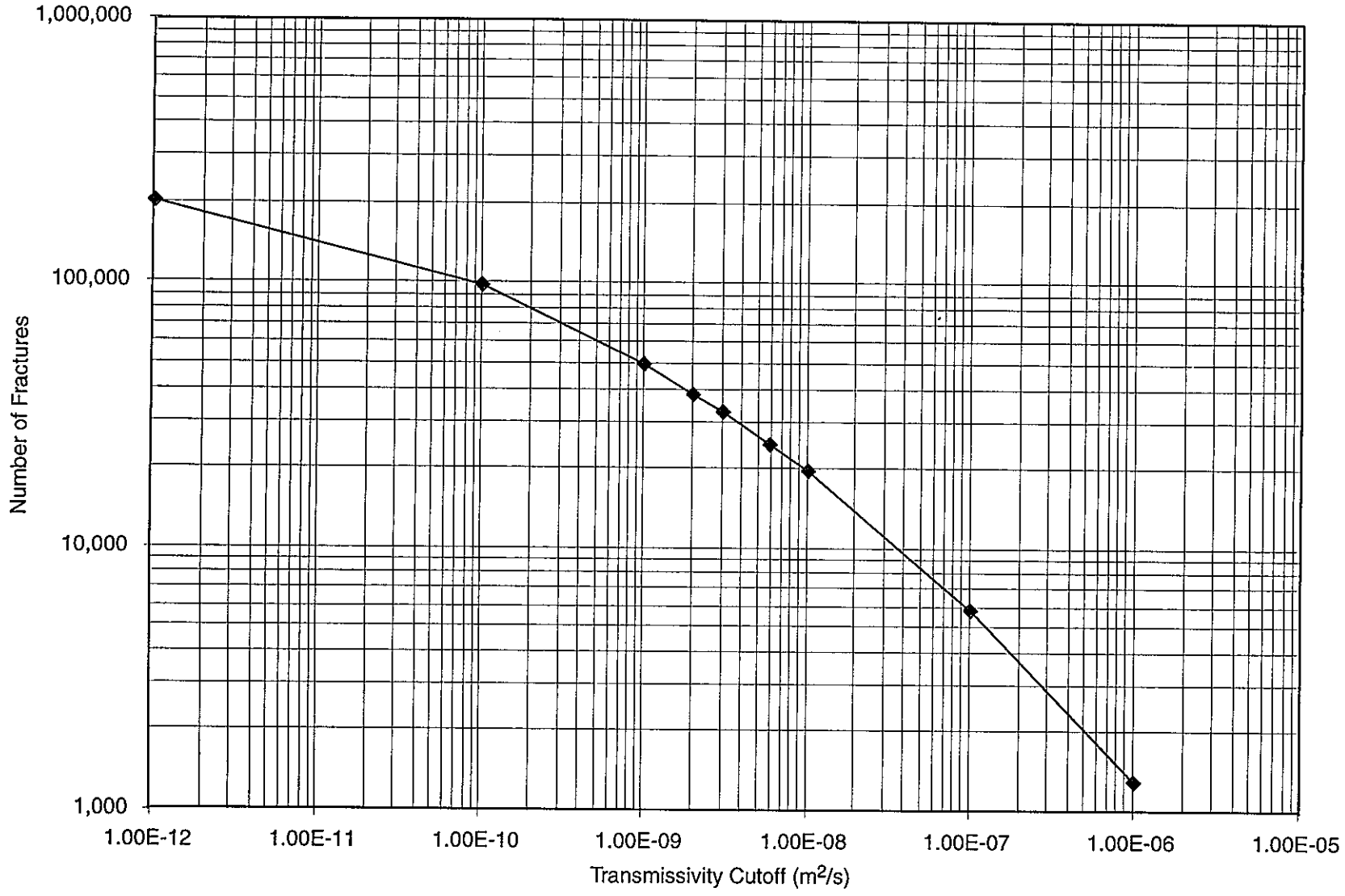

FIGURE **2-3**

NUMBER OF FRACTURES IN 225M CUBE VERSUS TRANSMISSIVITY CUTOFF

PNC/PAW-LTG/JAPAN

PROJECT NO. 923 1089.824 DRAWING NO. 72719 DATE 5/12/97 DRAWN BY CB

Golder Associates

Table 2-2 Transmissivity Cutoff and Fracture Intensity

Transmissivity Cutoff T_{cutoff} (m^2/s)	Total P_{32} Simulated (m^{-1})	Total Fractures Simulated (225 m Fracture Generation Region)
1.e-6	.018	1,305
1.e-7	.080	5,826
1.e-8	0.268	19,515
5.9e-9	0.339	24,754
3.e-9	0.451	32,889
2.e-9	0.530	38,571
1.e-9	0.684	49,711
1.e-10	1.35	98,252
1.e-12	2.797	203,688

2.2 Boundary Conditions

The two sets of boundary conditions used for the sensitivity calculations are illustrated in Figure 2-2. Both boundary conditions assume a 5% horizontal head gradient across a 200-m scale rock block, provided by constant heads on the eastern and western faces of the model.

For boundary condition "A", the four faces of the rock block parallel to the direction of flow are defined with the same 5% gradient varying head boundary condition used for the faces perpendicular to the gradient. Thus, for all faces, the head is defined by,

$$H(x,y,z) = H_x.x + H_y.y + H_z.z + H_0$$

where $H_x = H_z = 0.00$, $H_0 = 5.0$, $H_y = -0.05$ and y varies between $\pm$ 100.0.

These boundary conditions imply a head of 10m upgradient at y=-100m, and a head of 0.0m downgradient at y=+100m.

Boundary condition "A" provides a good basis for forming comparisons of the head variability within the rock block, because the flow is not truncated at the edge of the

model. However, the boundary condition does create a number of short flow paths between the western (source) boundary and the boundaries parallel to the gradient. These flow paths cut across the corners of the block, and may be strongly influenced by a single highly transmissive fracture. This may result in an exaggerated range of effective hydraulic conductivity, which can be problematic for the scoping calculations involving solute transport. However, this boundary condition does provide a useful basis for comparing the MAFIC and PAWorks approaches on the basis of head.

Boundary condition "B" is better suited for comparisons based on solute transport, since it provides for a no-flow boundary on all the faces parallel to the gradient. In this configuration the travel path is forced to flow from the release location to the downstream face of the cube.

The fluxes derived using boundary condition "B" are also easier to interpret in calculations of block scale effective permeability, since no flux occurs perpendicular to the gradient direction. Boundary condition "B" is therefore preferred for calculations of the effect of the truncation threshold T_{cutoff} on effective block permeability.

2.3 Simulations for determination of required tramsmissivity cutoff

An initial set of simulations were used to determine the sensitivity of the simulations to the transmissivity cutoff. These simulations did not incorporate the full variation of parameters required to map the MAFIC results to the PAWorks pipe network, but allow the determination of the fracture intensity at which the addition of more fractures has an insignificant effect on the measured model parameters (flux, head distribution, etc.). The final simulations, incorporating a mapping of MAFIC to PAWorks fracture representations, are discussed in Section 6 of the report.

Table 2-3 MAFIC & PAWorks Sensitivity: Simulations

Simulation Name	B.C.[1]	MAFIC (Plate) or PAWorks (Pipe)	T_{cutoff} (m^2/s)	Number of Fractures[2]	Flow Sim. Complete ?	Transport Sim Complete?
kamapa0	A	MAFIC	1.e-6	1,305	yes	N/A
kamapa1	A	MAFIC	1.e-7	5,826	yes	N/A
kamapa2	A	MAFIC	5.9e-9	24,754	yes	N/A
kamapa7a	A	MAFIC	3.e-9	32,889	yes	N/A
kamapa6	A	MAFIC	2.e-9	38,571	yes	N/A
kamapa3	A	MAFIC	1.e-9	49,711	no	N/A
kamapa4	A	MAFIC	1.e-10	98,252	no	N/A
kamapa5	A	MAFIC	1.e-12	203,688	no	N/A
kama0old	A	PAWorks	1.e-6	1,305	yes	yes
kama1old	A	PAWorks	1.e-7	5,826	yes	yes
kama2old	A	PAWorks	5.9e-9	24,754	yes	yes
kama7old	A	PAWorks	3.e-9	32,889	yes	yes
kama6old	A	PAWorks	2.e-9	38,571	yes	yes
kama3old	A	PAWorks	1.e-9	49,711	yes	no
kam3df11	B	MAFIC	1.e-7	5,826	yes	yes
kam3df12	B	MAFIC	5.9e-9	24,754	yes	yes
kam3df7a	B	MAFIC	3.e-9	32,889	yes	yes
kam3df16	B	MAFIC	2.e-9	38,571	yes	no
kam1df10	B	PAWorks	1.e-6	1,305	no conn.	N/A
kam1df11	B	PAWorks	1.e-7	5,826	yes	yes
kam1df18	B	PAWorks	1.e-8	19,515	yes	yes
kam1df12	B	PAWorks	5.9e-9	24,754	yes	yes
kam1df17	B	PAWorks	3.e-9	32,889	yes	yes
kam1df7a	B	PAWorks	3.e-9	32,889	yes	yes
kam1df16	B	PAWorks	2.e-9	38,571	yes	yes
kam1df13	B	PAWorks	1.e-9	49,711	yes	yes

[1] Boundary Condition A is the "constant head" assumption, "B" is the "pathway" assumption (see above)
[2] Number of fractures based on 225m cube within FracWorks

Table 2-3 describes the simulation parameters, the number of fractures associated with each simulation, and the corresponding value of T_{cutoff}. The notation "N/A" for the transport simulation column indicates that transport simulations were not undertaken for these cases.

2.4 Parameters for determination of required T_{cutoff}

The fracture model used for the transmissivity cutoff simulations was the same as that given by Doe et al. (1996) and summarized in Table 2-1 with the single exception that the aperture, e, was based on the cubic law [$e = (12\mu T_m/(\rho g))^{1/3}$] , rather than the equation, $e = 2.0\ T^{1/2}$, used for the final analyses. The aperture was changed to ensure equivalence between other performance assessment computations and the results of the demonstration PAWorks simulations presented in Section 7.

Aperture only affects the travel times. Flow and head distributions are unaffected by the aperture because fracture properties are specified in terms of transmissivity. In all simulations the same relationship between aperture and transmissivity was used for the corresponding MAFIC and PAWorks analyses.

For the T_{cutoff} sensitivity study, the pipes were generated assuming PAWorks pipe generation option 2, in which no pipes cross traces (Figure 2-4). The width of the pipe was derived from the geometry of the intersecting traces, as illustrated in Figure 2-5. These assumptions are investigated in Section 6 of this report, where these assumptions are varied to produce an equivalence of the MAFIC fracture and PAWorks pipe networks.

2.5 Models for Demonstration Applications

A series of PAWorks demonstration applications are presented in Section 7 of the report. The fracture geometry models used for these simulations are typically closely related to those described earlier. However, slight variations between the individual examples exist, and for clarity, these models are described in detail in Section 7.

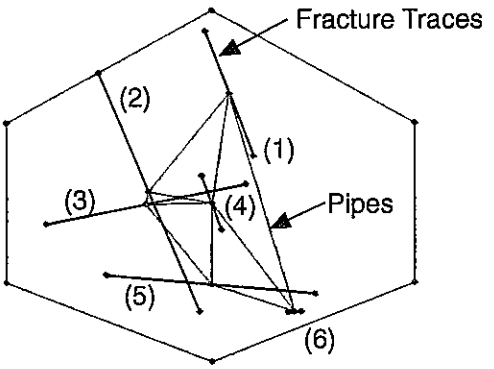

(a) Option 1 - All pipes not crossing each other

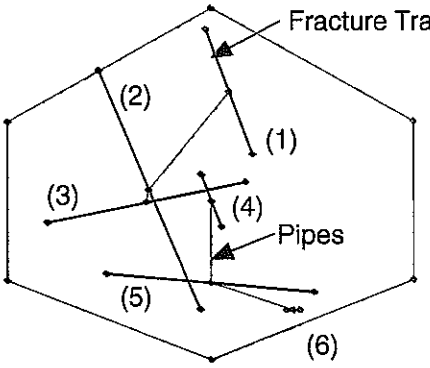

Note: (4), (5) and (6) have no connection to (1), (2), and (3)

(b) Option 2 - Remove pipes which cross traces

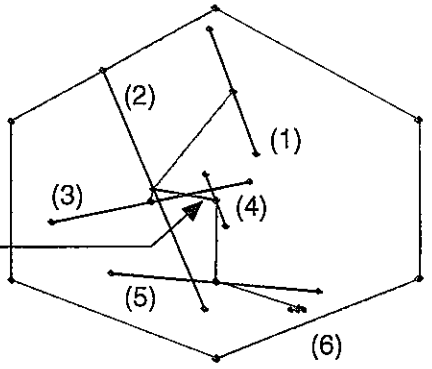

(c) Option 3 - Additional pipes to connect all nodes on fracture

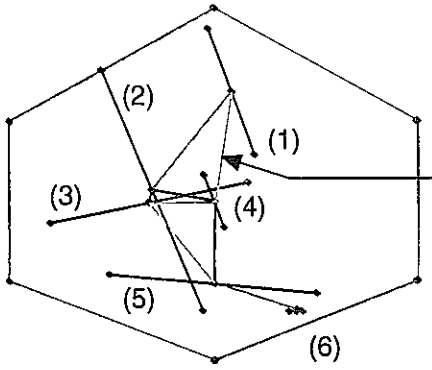

(Effective Factor 1.4)

Pipe added to ensure no tortuous paths greater than 140% of the cartesian distance

(d) Option 4 - Additional pipes to prevent excessively tortuous path

FIGURE **2-4**
PIPE GENERATION OPTIONS
PNC/PAW-LTG/JAPAN

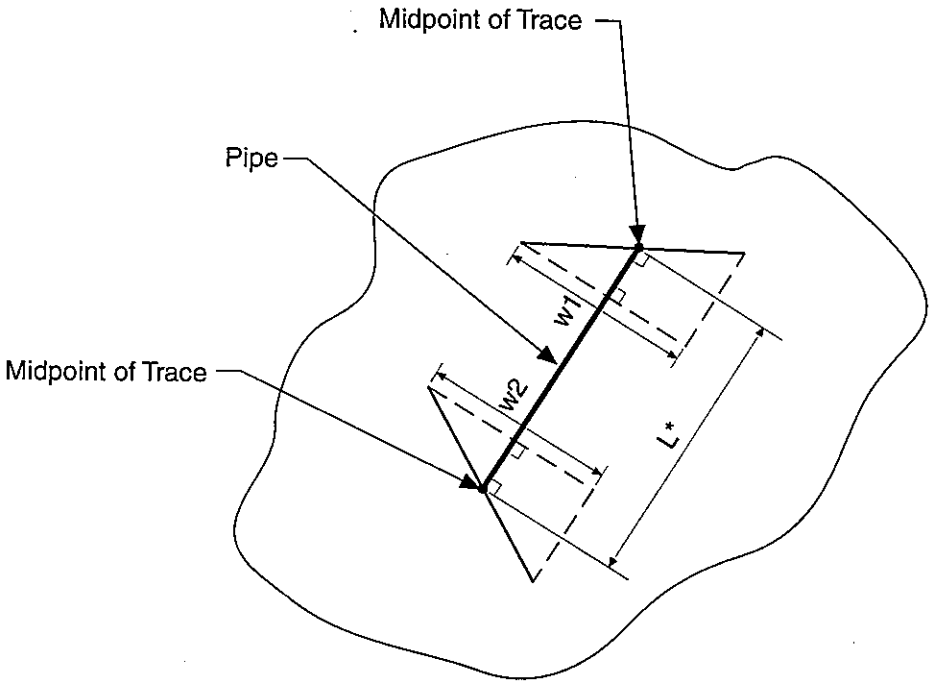

Pipe Width $W = 0.5w1 + 0.5\ w2$

Pipe Length $L = L^*$

FIGURE **2-5**
PIPE GEOMETRY FOR BASELINE SIMULATIONS
PNC/PAW-LTG/JAPAN

3. MAFIC SIMULATIONS (PLATE FRACTURE NETWORKS)

This section presents the results of MAFIC simulations of flow and transport in three dimensional networks of two dimensional triangular finite elements. Results are organized according to the comparative measures,

- Effective block hydraulic conductivity (K_{eff})
- Head distribution within the fracture network (H_{xyz})
- Minimum and median transport time (t_0 and t_{50})
- Effective network dispersion (t_{85} and t_{50})
- Computer resources (memory and CPU time)

3.1 Effective Hydraulic Conductivity

The variation of effective hydraulic conductivity versus the transmissivity cut-off and the number of generated fractures is shown in Figures 3-1 and 3-2 respectively. In these and subsequent figures, the legend "3-D Constant Head" refers to boundary condition A, and the legend "3-D Pathway" refers to boundary condition B. The effective hydraulic conductivity is computed for an assumed path length of 200m across the cube, from the face at a head of 10m to the opposite face of the cube at a head of 0m. This approximation reflects greater error for boundary condition "A", where flow may "shortcut" to the sides of the rock block.

The results of the simulations indicate the same trend in hydraulic conductivity for both boundary configurations, with a general rise in hydraulic conductivity being observed as the number of fractures increases. The simulation based on boundary condition "A" shows more variability in the block effective hydraulic conductivity, K_{eff}. Additionally, boundary condition "A" has a higher value of K_{eff} compared with boundary condition "B". This is to be expected as "A" includes flow across the corners of the cube which is biased by any local higher transmissivity fractures. Over longer distances, of the order of 100-200m, these higher transmissivity features are separated by lower conductivity fractures, lowering the overall flux.

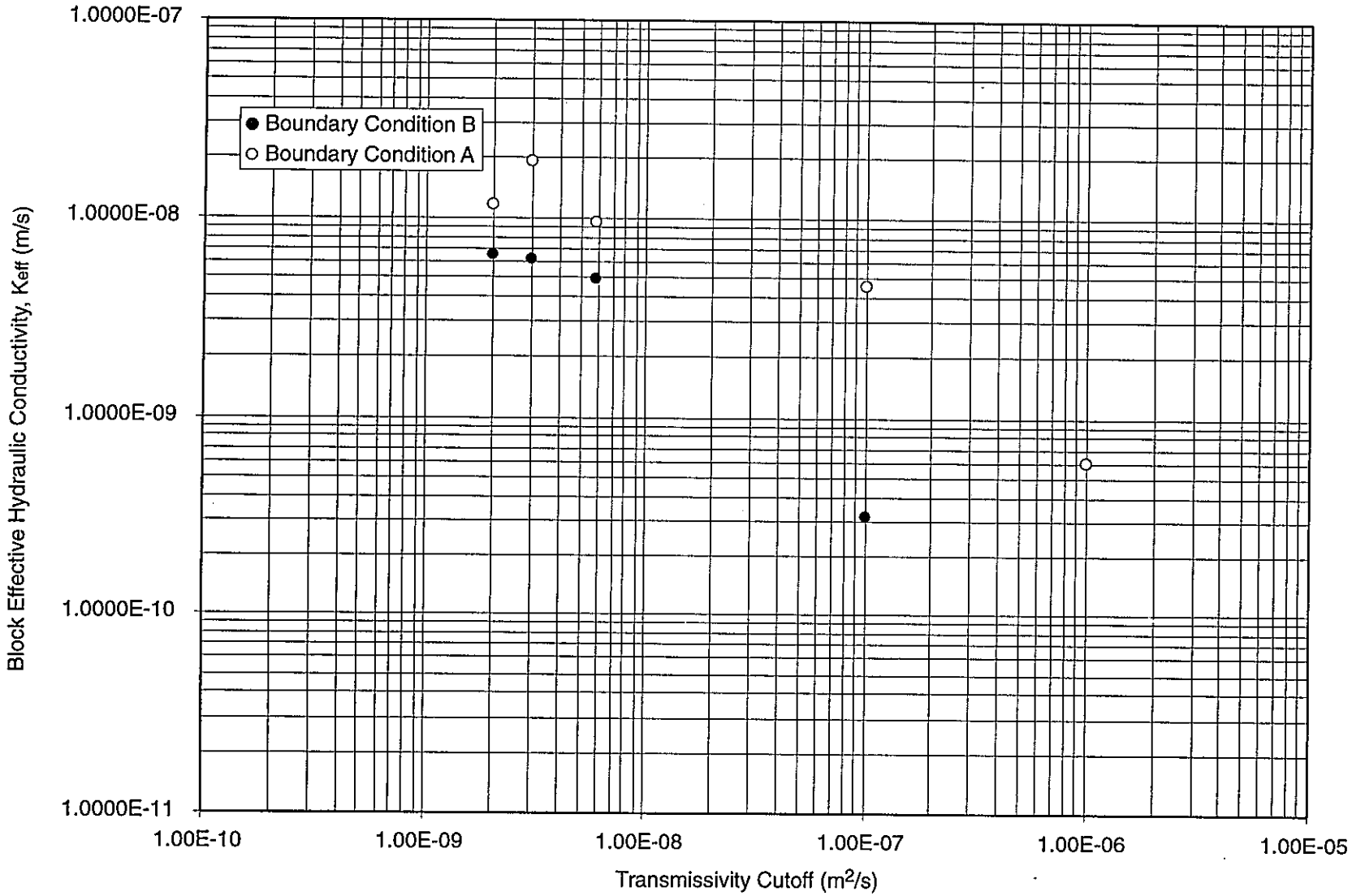

FIGURE **3-1**
MAFIC BLOCK EFFECTIVE HYDRAULIC CONDUCTIVITY VERSUS TRANSMISSIVITY CUTOFF
PNC/PAW-LTG/JAPAN

PROJECT NO. 923 1089.824 DRAWING NO. 72710 DATE 11/24/97 DRAWN BY CB

Golder Associates

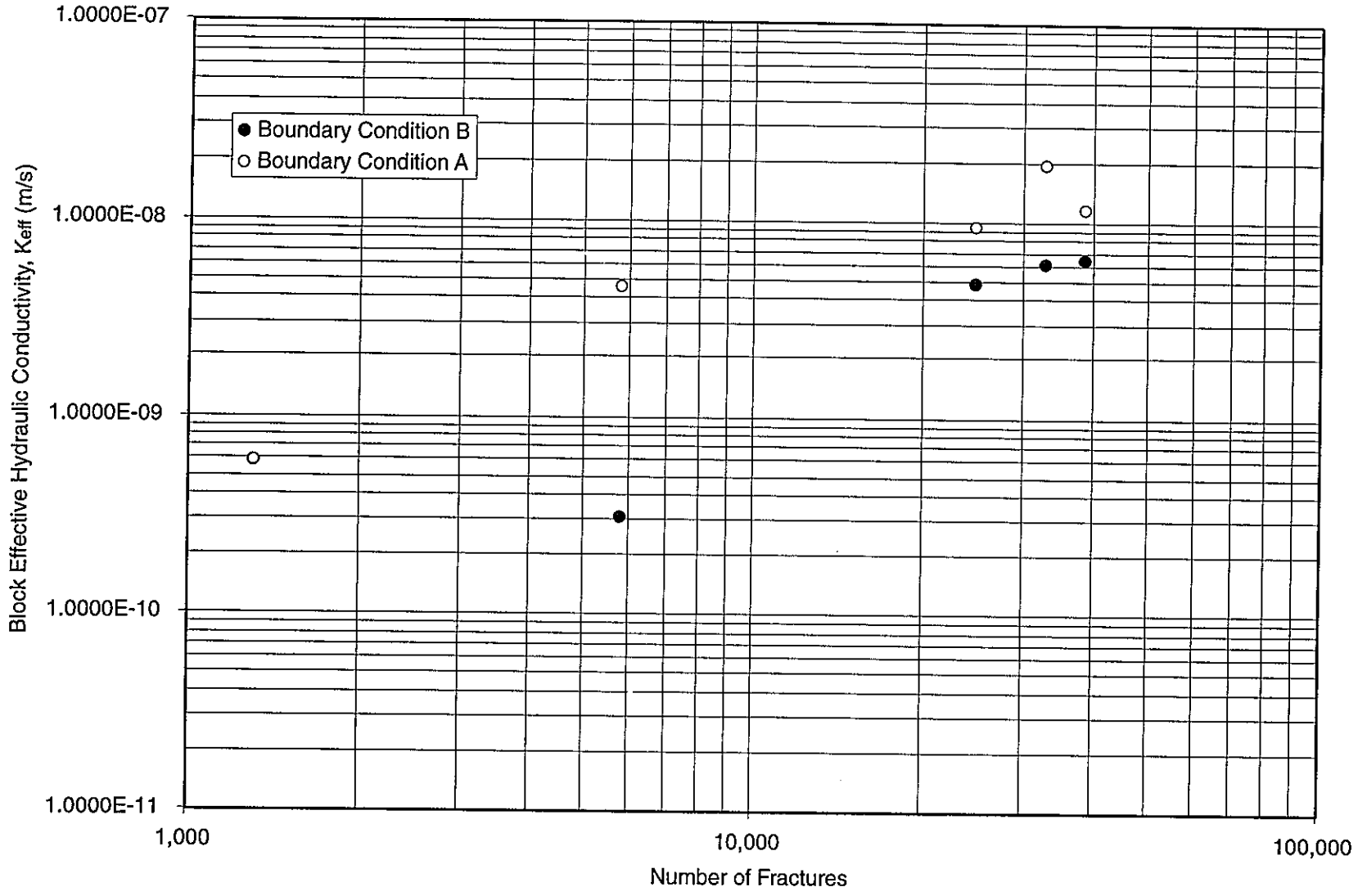

FIGURE **3-2**

MAFIC BLOCK EFFECTIVE HYDRAULIC CONDUCTIVITY VERSUS NUMBER OF FRACTURES

PNC/PAW-LTG/JAPAN

PROJECT NO. 923 1089.824 DRAWING NO. 72711 DATE 11/21/97 DRAWN BY CB

Golder Associates

The pathway simulation indicates a very distinct trend of K_{eff}, with the effective conductivity increasing with the number of fractures. The "pathway" simulations indicate a trend towards a constant value of K_{eff}, equal to approximately 6.5×10^{-9} m/s, reached at a transmissivity cutoff below approximately 2×10^{-9} m^2/s.

These results indicate that for T_{cutoff} below 3×10^{-9} m^2/s, or approximately 33,000 fractures in a 225m cube, the simulations are relatively insensitive to increased fracture density, although a small effect of T_{cutoff} on flux is still observed.

3.2 Head Variability across the Cube

The standard deviation of the computed head compared with the linear head distribution at the location x, y or z=±11m against the value of T_{cutoff} and the number of fractures is presented on Figure 3-3 and Figure 3-4 respectively. The standard deviation of the computed head compared with the linear head distribution at location x, y or z = ±30m against the value of T_{cutoff} and the number of fractures is shown on Figures 3-5 and 3-6. These locations were chosen as they were away from the boundary of the modeled region, and include variation both along, and perpendicular to the axis of applied head.

The figures show that the standard deviation of the head generally decreases with an increasing number of fractures (excluding the simulation with T_{cutoff} equal to 1.e-6 m^2/s). The standard deviation for the "pathway" network is consistently higher than for fracture network modelled with boundary condition "A", indicating the results are influenced by the greater distance to the source head in the case "B". However with additional fracture density the difference between the two boundary configurations diminishes.

Based on these analyses, the standard deviation of the linear head is relatively insensitive to the transmissivity cutoff at T_{cutoff} below 5.9×10^{-9} m^2/s.

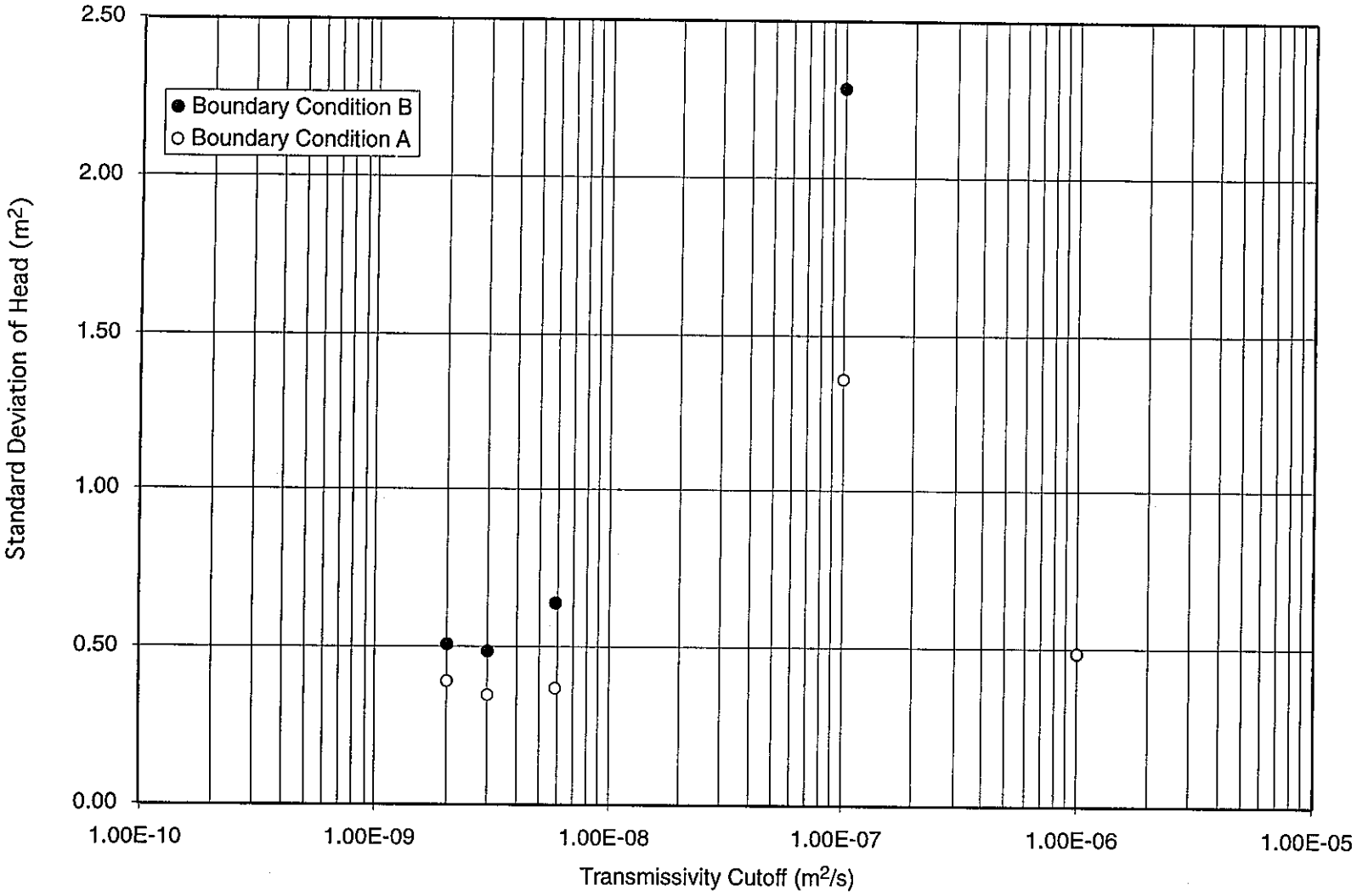

FIGURE **3-3**

STANDARD DEVIATION OF HEAD ABOUT LINEARLY INTERPOLATED VALUE AT x,y OR z=+-11 VERSUS TRANSMISSIVITY CUTOFF

PNC/PAW-LTG/JAPAN

PROJECT NO. 923 1089.824 DRAWING NO. 72712 DATE 11/21/97 DRAWN BY CB

Golder Associates

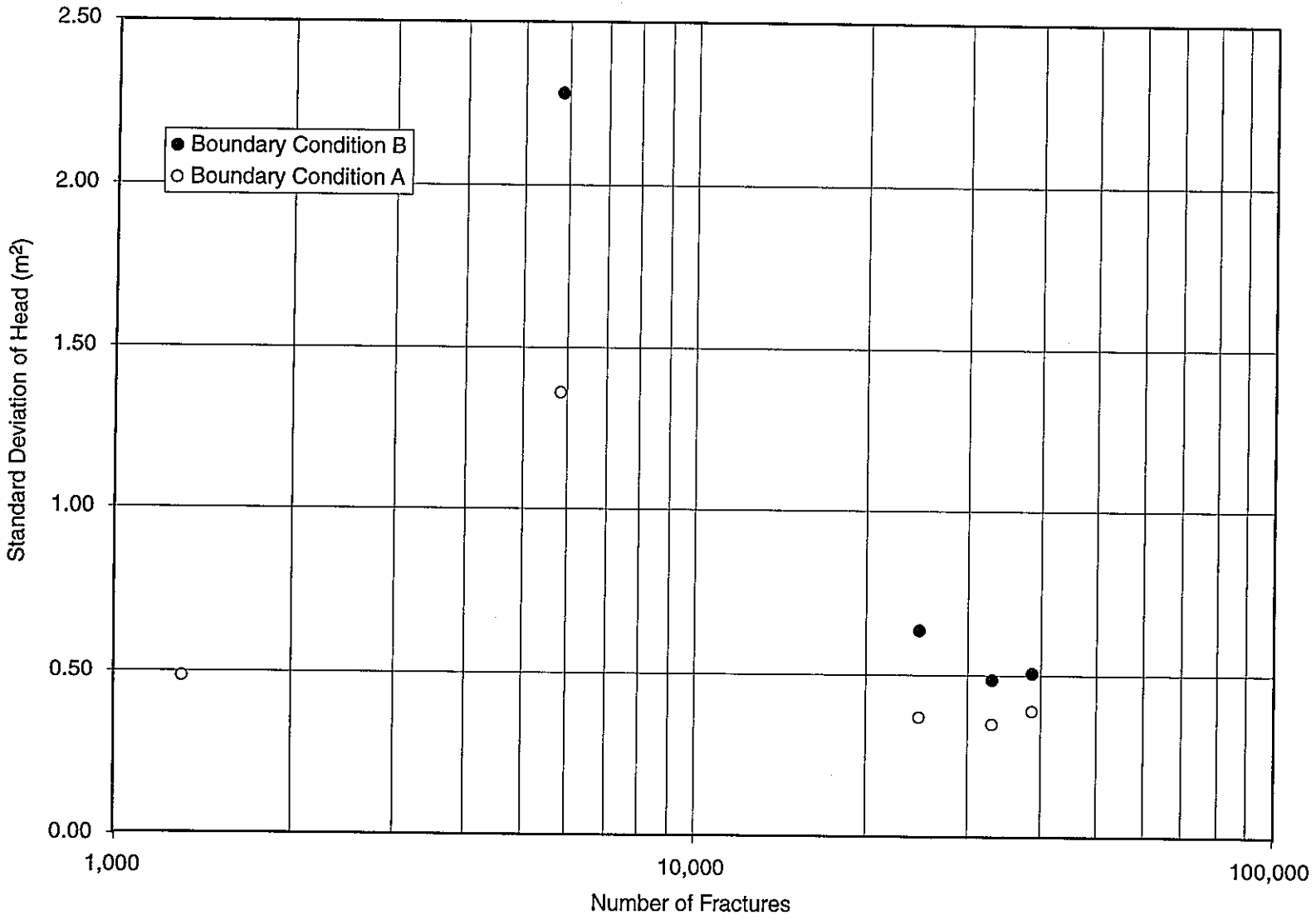

FIGURE **3-4**

STANDARD DEVIATION OF HEAD ABOUT LINEARLY INTERPOLATED VALUE AT x,y OR z=+-11 VERSUS NUMBER OF FRACTURES

PNC/PAW-LTG/JAPAN

PROJECT NO. 923 1089.824 DRAWING NO. 72713 DATE 11/21/97 DRAWN BY CB

Golder Associates

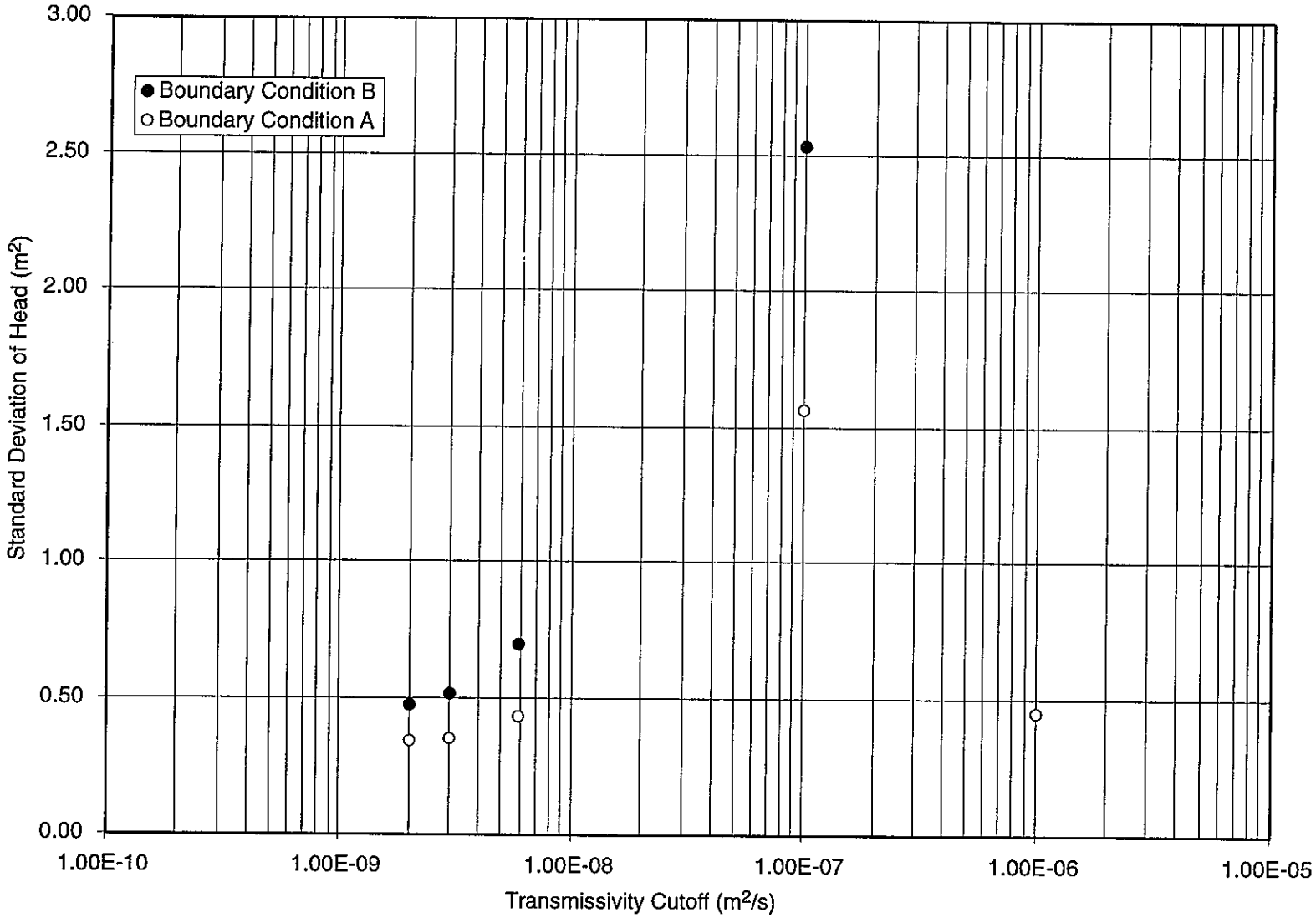

FIGURE **3-5**

STANDARD DEVIATION OF HEAD ABOUT LINEARLY INTERPOLATED VALUE AT x,y OR z=+-30 VERSUS TRANSMISSIVITY CUTOFF

PNC/PAW-LTG/JAPAN

PROJECT NO. 923 1089.824 DRAWING NO. 72714 DATE 11/24/97 DRAWN BY CB

Golder Associates

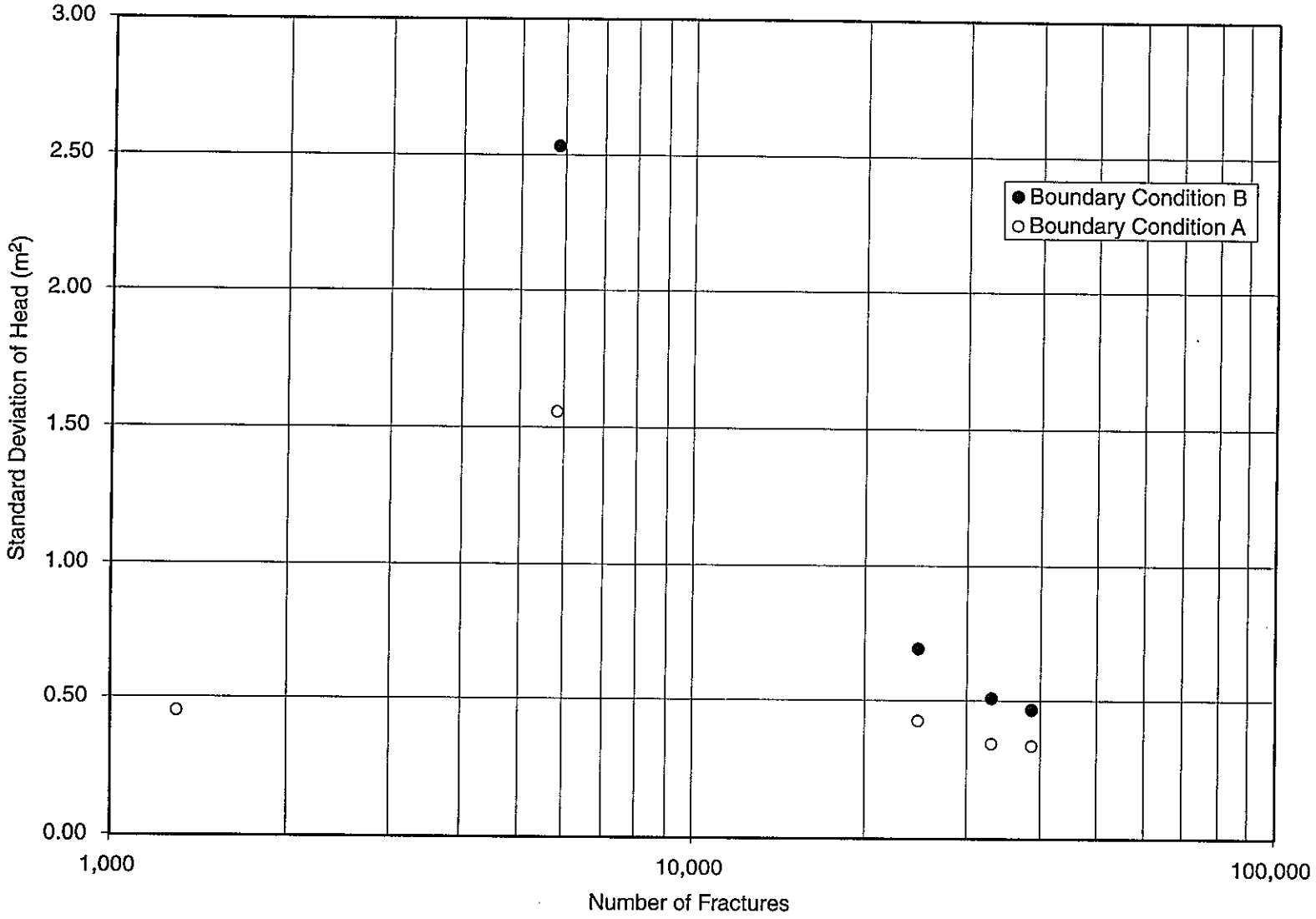

FIGURE **3-6**

STANDARD DEVIATION OF HEAD ABOUT LINEARLY INTERPOLATED VALUE AT x,y OR z=+-30 VERSUS NUMBER OF FRACTURES

PNC/PAW-LTG/JAPAN

PROJECT NO. 923 1089.824 DRAWING NO. 72715 DATE 11/21/97 DRAWN BY CB

Golder Associates

The results at the location of x=11m for boundary condition "B", for two separate values of T_{cutoff} have been processed to provide contour plots for visualization of the head field. Figure 3-7 shows the head distribution for a value of T_{cutoff} of 10^{-7} m^2/s, approximating to 6,000 fractures in a 225m cube. The figure shows that the fracture network is very localized, due to the FracMan codes deleting all fractures which are not connected to a head boundary (as the head in these fractures would be undefined). In addition to the lack of fracture connectivity the head distribution shows large deviation from the background applied head distribution. The head values are as much controlled by the tortuosity of the mesh connections as by the boundary conditions applied at y = ±100m.

Figure 3-8 shows the head distribution for a value of T_{cutoff} of 3×10^{-9} m^2/s, leading to approximately 33,000 fractures in a 225m cube. The fracture network is now more pervasively connected across the cube. The head distribution still shows about the applied gradient. However, there is now a much closer correlation between the applied and simulated distributions.

3.3 Travel Time

The MAFIC particle tracking algorithm releases particles into the fracture network at an upstream boundary and at each fracture intersection distributes the tracked particles to the connected fractures in proportion to the flow in those fractures. Hence, the higher flux pathways are more likely to transport the largest number of particles. However, this algorithm does not limit the traversed fracture network to only those fractures connected to the specified sink. Therefore if a type A boundary condition is used many particles exit before reaching the downstream face, and the algorithm is very inefficient. Therefore for the plate fracture transport calculations, only a type B boundary condition is considered. Travel times are recorded for transport from the upgradient boundary at y=-100m, to the downgradient boundary at y=+100m.

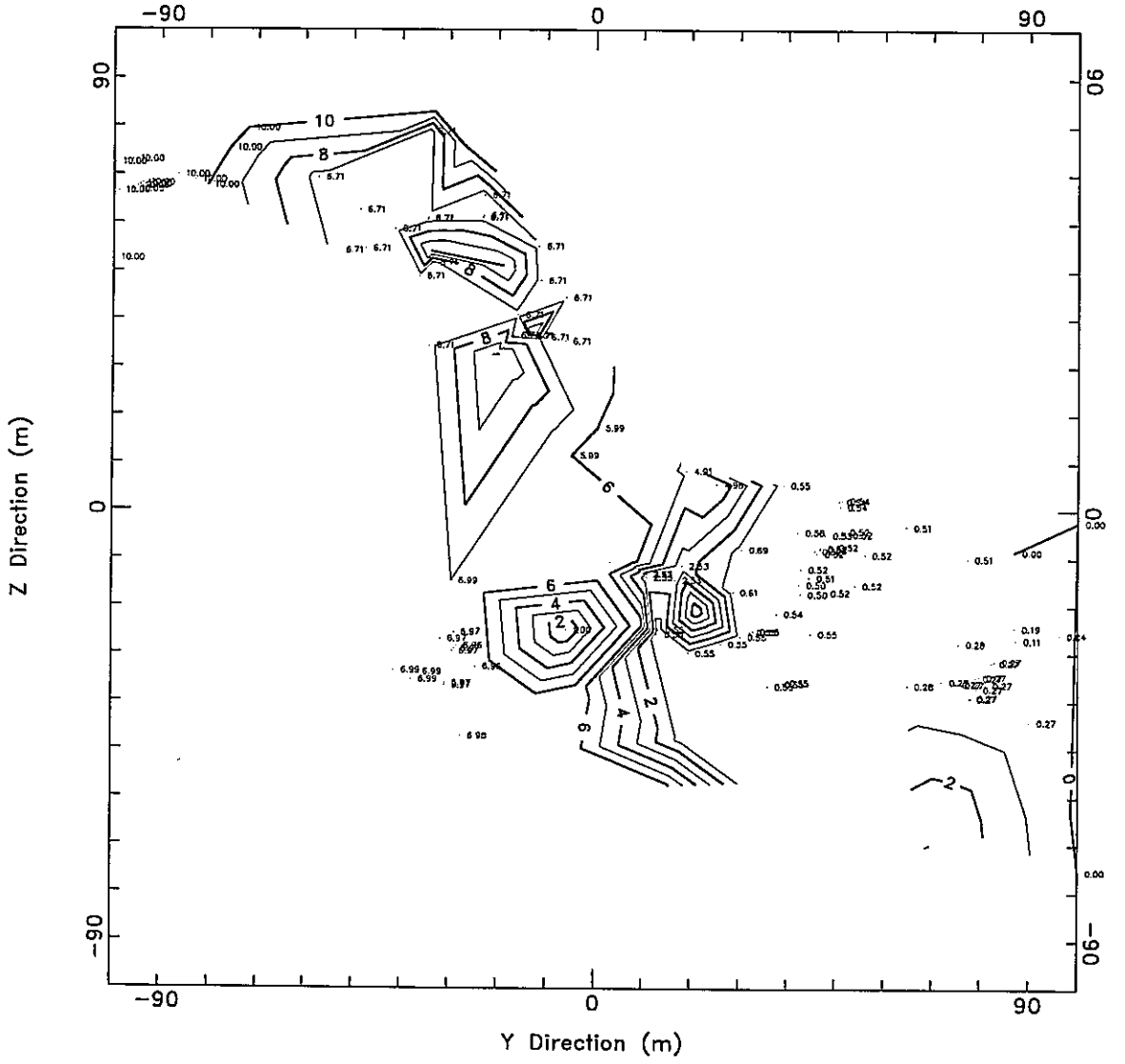

FIGURE **3-7**

HEAD DISTRIBUTION AT x=11 ACROSS MAFIC MESH WITH TRANSMISSIVITY CUTOFF = $10^{-7}m^2/s$

PNC/PAW & LTG/JAPAN

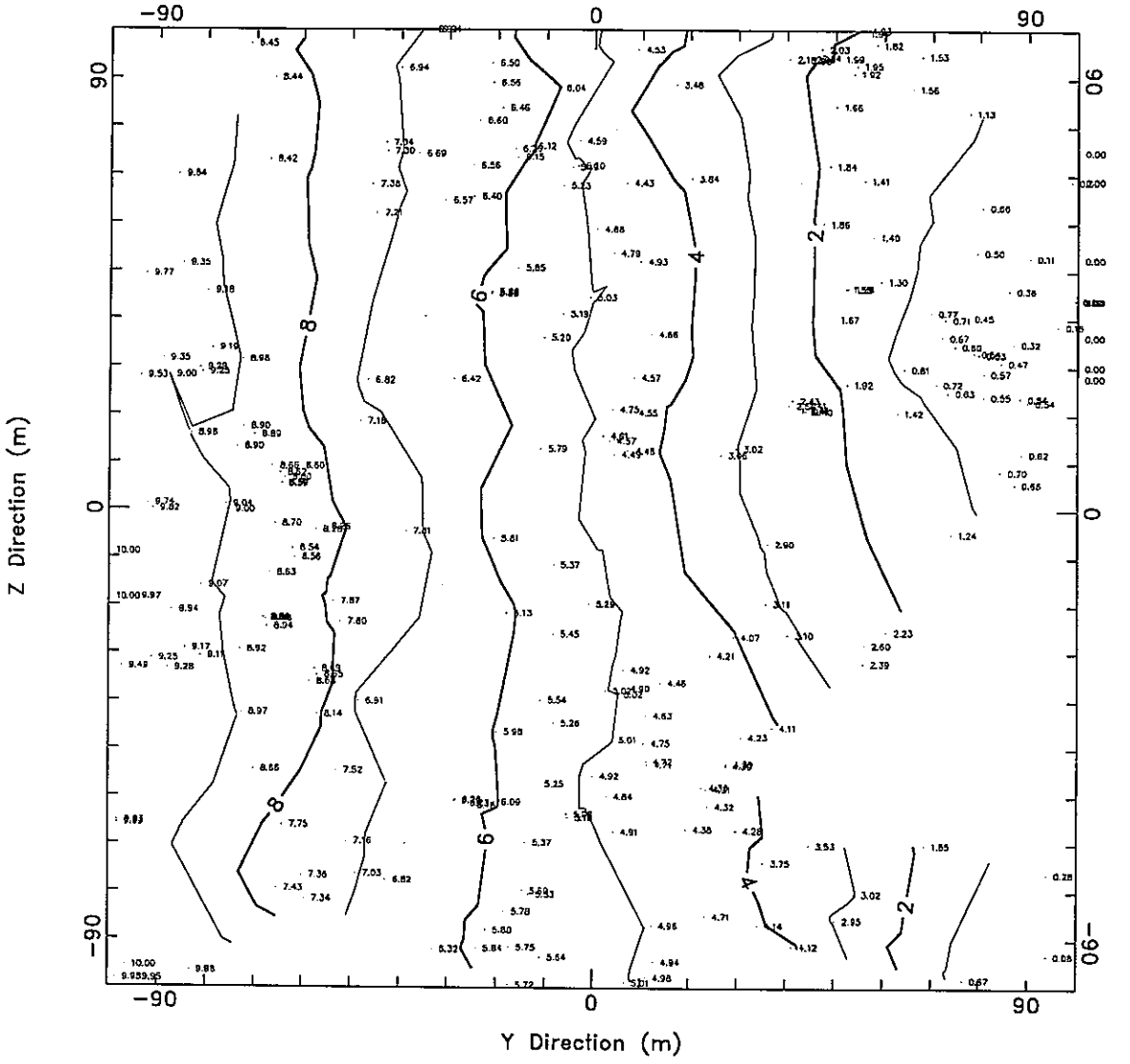

FIGURE **3-8**

HEAD DISTRIBUTION AT x=11 ACROSS MAFIC MESH WITH TRANSMISSIVITY CUTOFF = $3x10^{-9}m^2/s$

PNC/PAW & LTG/JAPAN

The minimum transport time for the MAFIC fracture network simulations plotted against the transmissivity cutoff are shown in Figure 3-9. The simulations indicate that the minimum transport time is of the order of 6×10^6 to 9×10^6 seconds (0.2 to 0.3 years). The median travel time for the simulations are shown in Figure 3-10. The median travel times all range between 2×10^7 and 3×10^7 seconds (0.69 to 0.79 years). The results indicate a reduction in both the minimum and median travel time with increasing numbers of fractures. This reduction may be due to increased connectivity between the fractures. However, for the median travel time this reduction is extremely small (2.5×10^7 to 2.2×10^7 seconds for a T_{cutoff} range from 1×10^{-7} to 3×10^{-9} m^2/s) and is expected to be within the variation between individual fracture realizations.

These computed travel times indicate that for T_{cutoff} below 10^{-7} m^2/s, or approximately 6,000 fractures in a 225m cube, the median travel time is relatively insensitive to increased fracture density.

3.4 Effective Dispersion

The effective dispersion in the transport simulations has been indicated by the difference in the median (t_{50}) and t_{85} travel time. The simulations presented on Figures 3-11 and 3-12 indicate that the t_{85} travel time is a factor of about 2.9 times greater than t_{50} at T_{cutoff} equal to 10^{-7} m^2/s. This factor reduces to 1.7 at T_{cutoff} equal to 3×10^{-9} m^2/s indicating a reduction in dispersion with increasing fracture density, perhaps due to increased mesh connectivity. However, it should be remembered that these differences are small and are within the expected variability of individual fracture networks.

3.5 Computer Resources (CPU Time and Memory)

The MAFIC CPU times are presented against T_{cutoff} and the number of fractures in Figures 3-13 and 3-14 respectively. In Figures 3-13 and 3-14, the legends "constant head" and "transport" refer to boundary conditions A and B respectively. The CPU time presented excludes the transport component of the simulations, since the number of tracked particles has a large influence on the total time required. However, as an example, tracking 175 particles requires approximately an additional 10% of the CPU time illustrated.

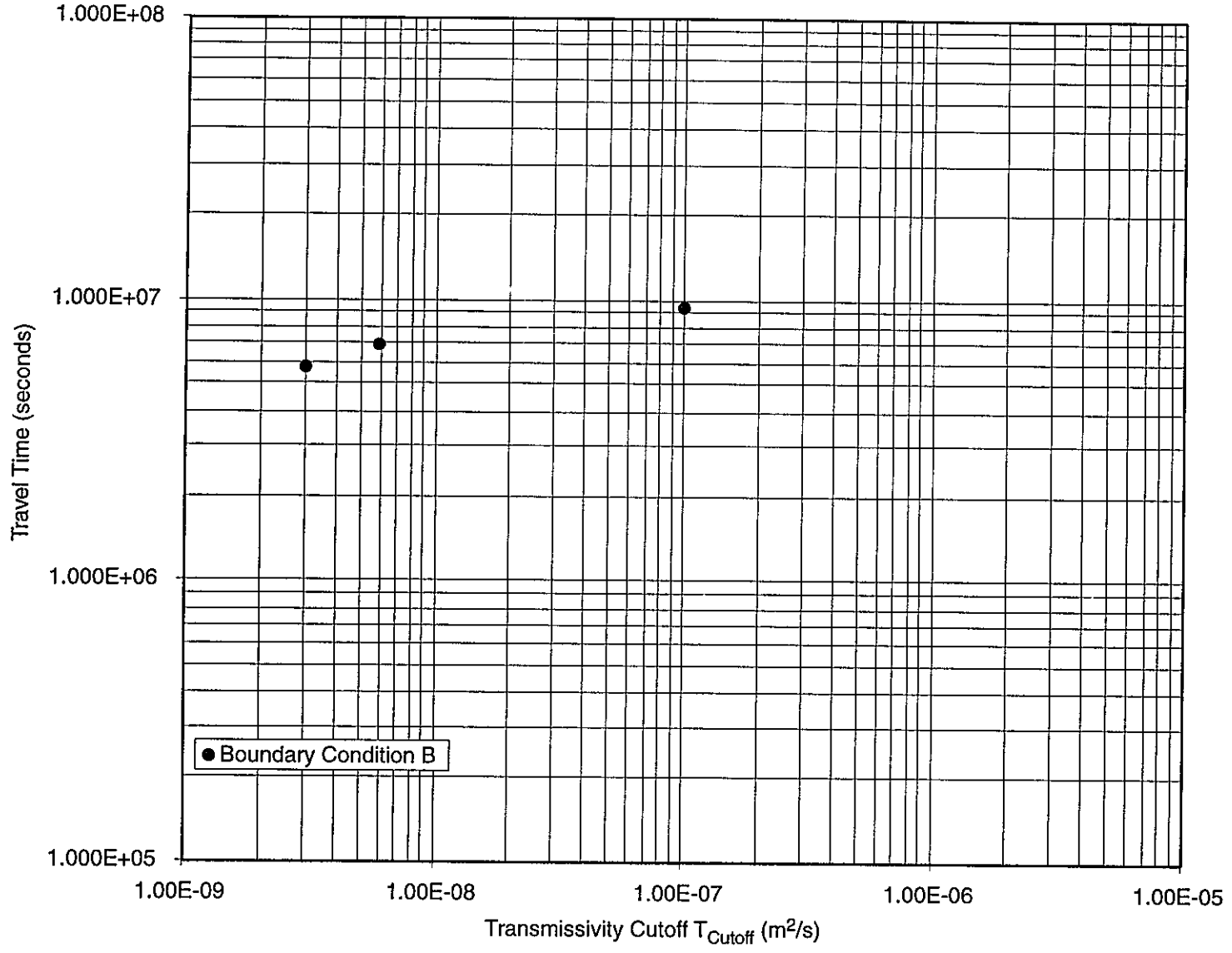

FIGURE **3-9**

MINIMUM TRAVEL TIME VERSUS TRANSMISSIVITY CUTOFF (MAFIC SIMULATIONS)

PNC/PAW-LTG/JAPAN

PROJECT NO. 923 1089.824 DRAWING NO. 72716 DATE 11/21/97 DRAWN BY CB

Golder Associates

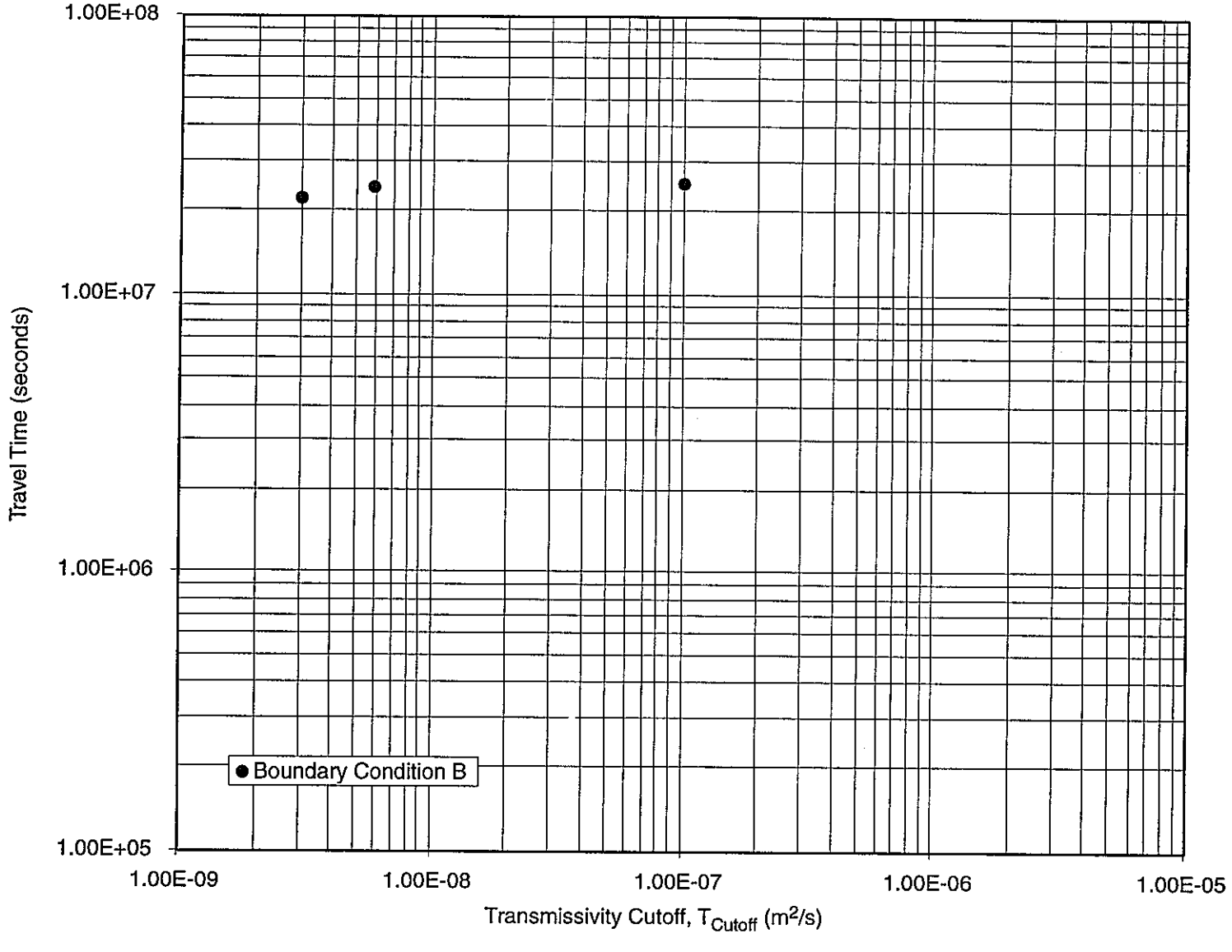

FIGURE **3-10**

MEDIAN TRAVEL TIME VERSUS TRANSMISSIVITY CUTOFF (MAFIC SIMULATIONS)

PNC/PAW-LTG/JAPAN

PROJECT NO. 923 1089.824 DRAWING NO. 72717 DATE 11/21/97 DRAWN BY CB

Golder Associates

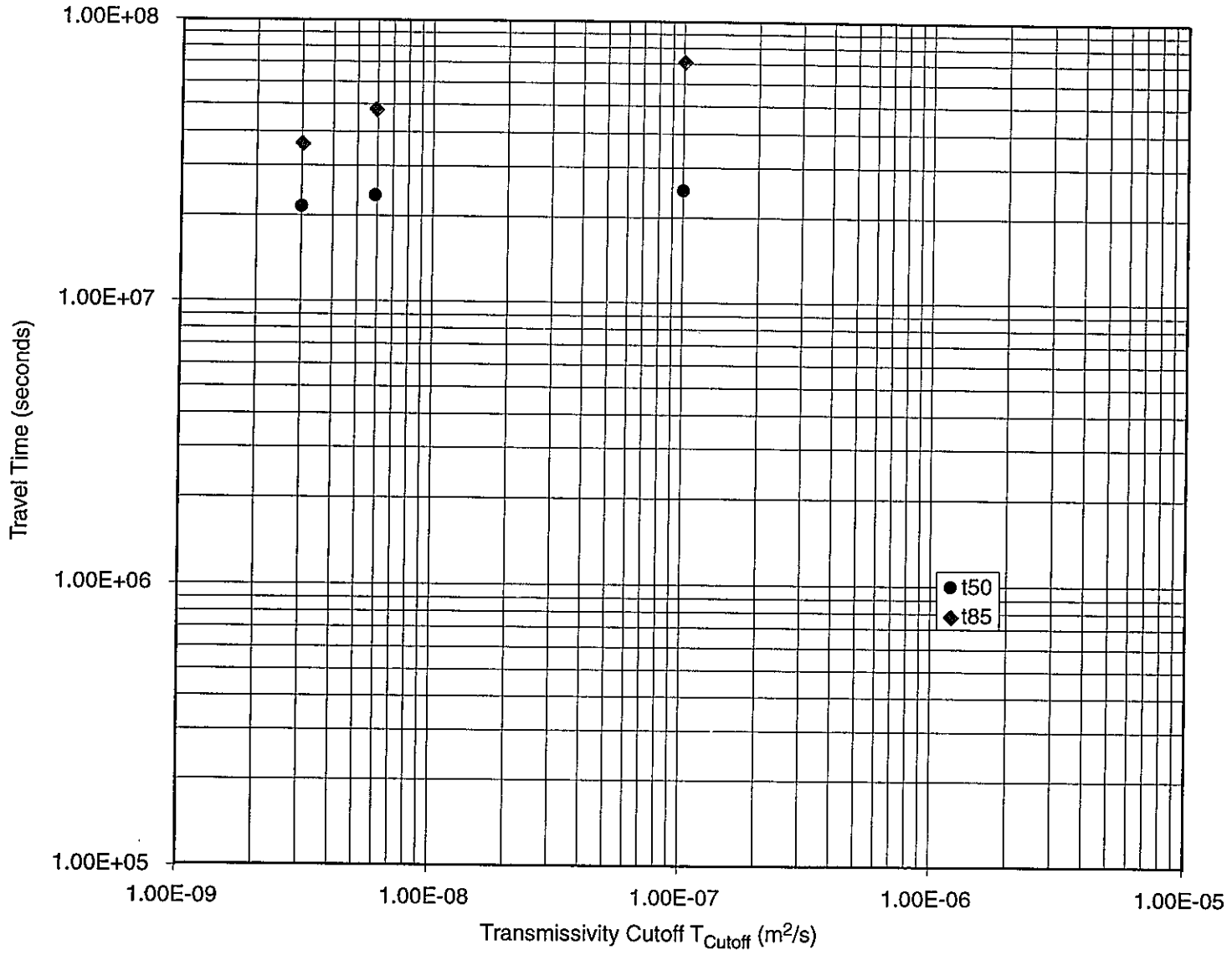

FIGURE **3-11**

EFFECTIVE DISPERSION IN TRAVEL TIME VERSUS TRANSMISSIVITY CUTOFF (MAFIC SIMULATIONS)

PNC/PAW-LTG/JAPAN

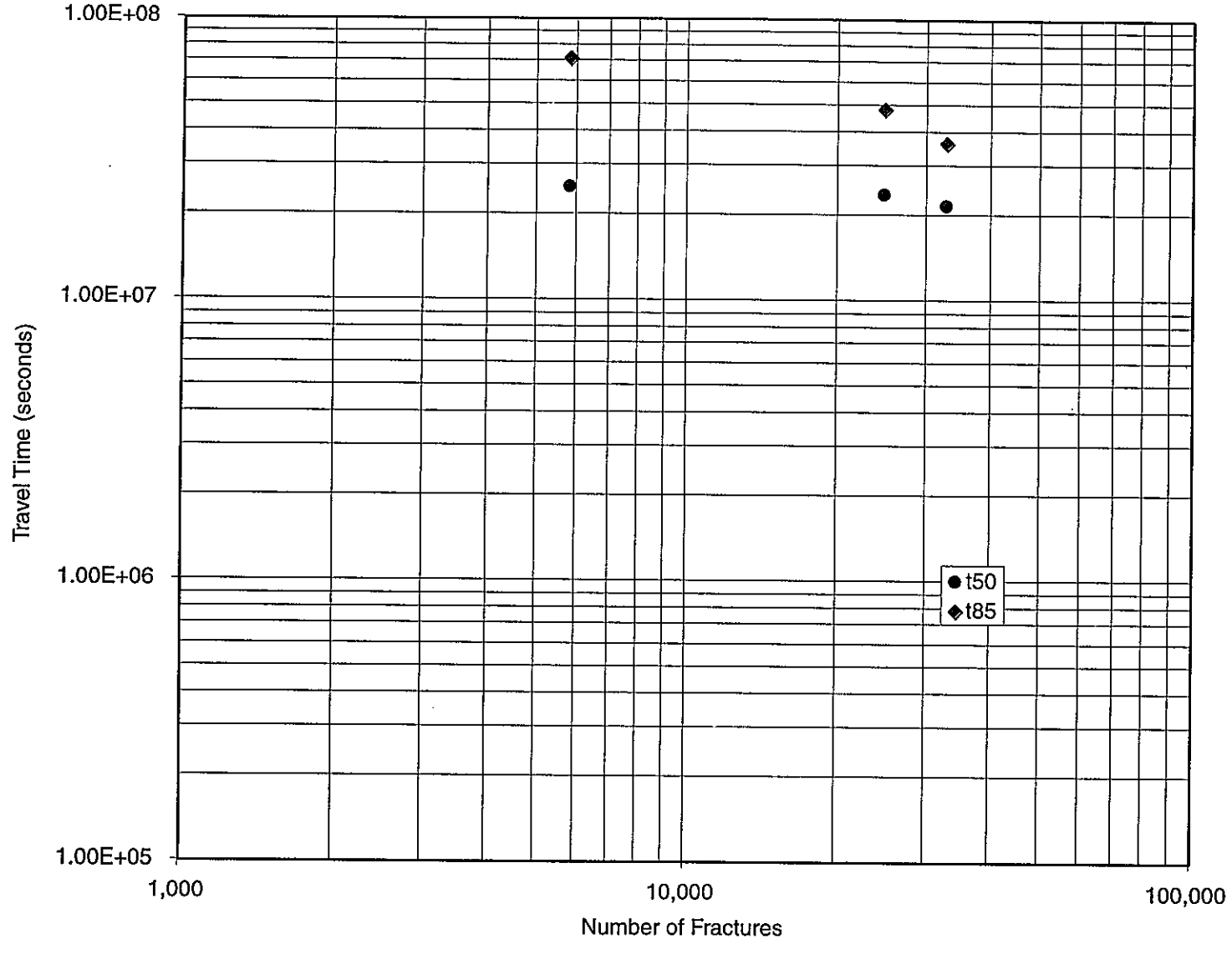

FIGURE **3-12**

EFFECTIVE DISPERSION IN TRAVEL TIME VERSUS NUMBER OF FRACTURES (MAFIC SIMULATIONS)

PNC/PAW-LTG/JAPAN

PROJECT NO. 923 1089.824 DRAWING NO. 72722 DATE 11/18/97 DRAWN BY CB

Golder Associates

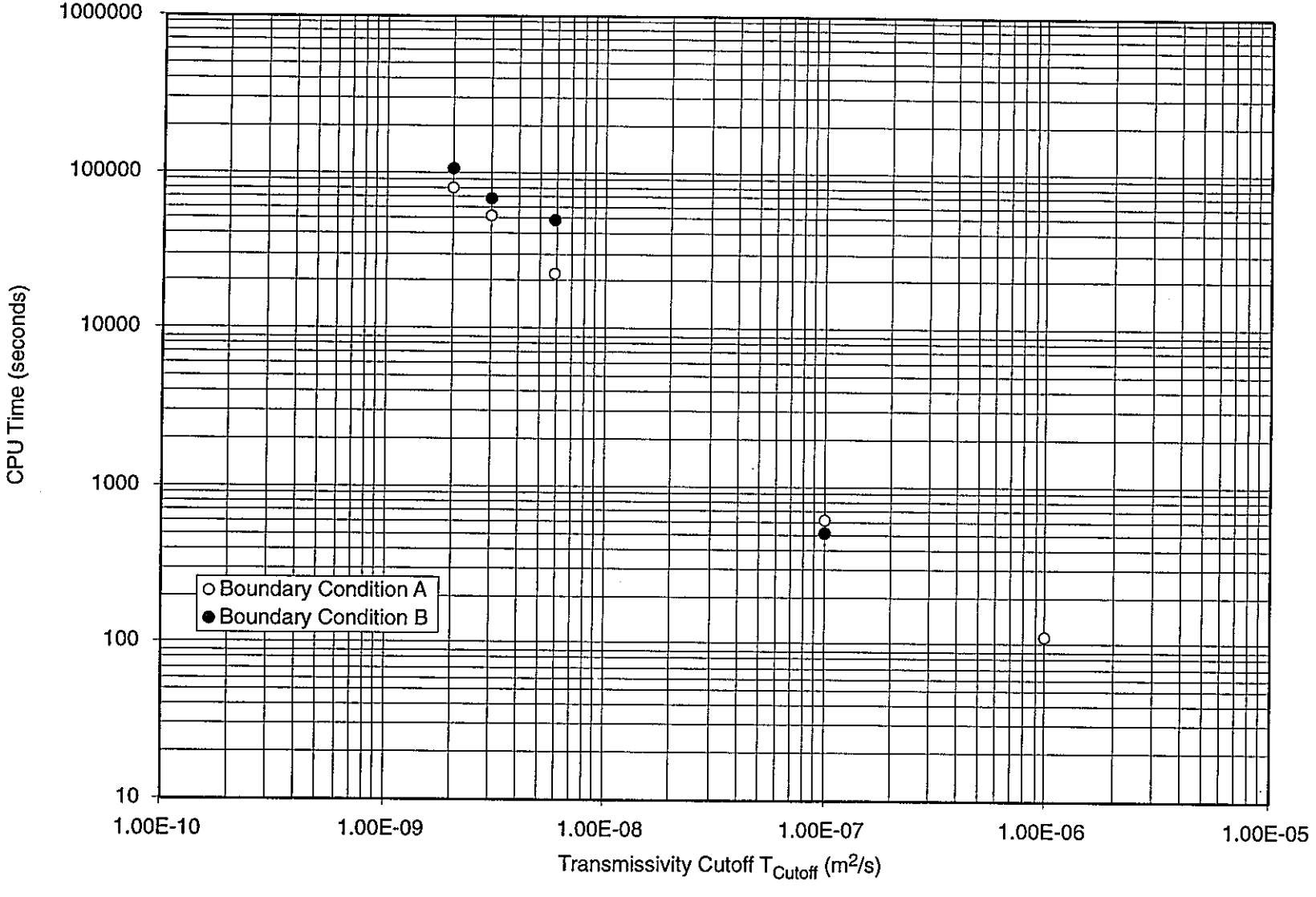

FIGURE **3-13**

REQUIRED CPU TIME VERSUS TRANSMISSIVITY CUTOFF, NO TRANSPORT (MAFIC SIMULATIONS)

PNC/PAW-LTG/JAPAN

PROJECT NO. 923 1089.824 DRAWING NO. 72723 DATE 11/21/97 DRAWN BY CB

Golder Associates

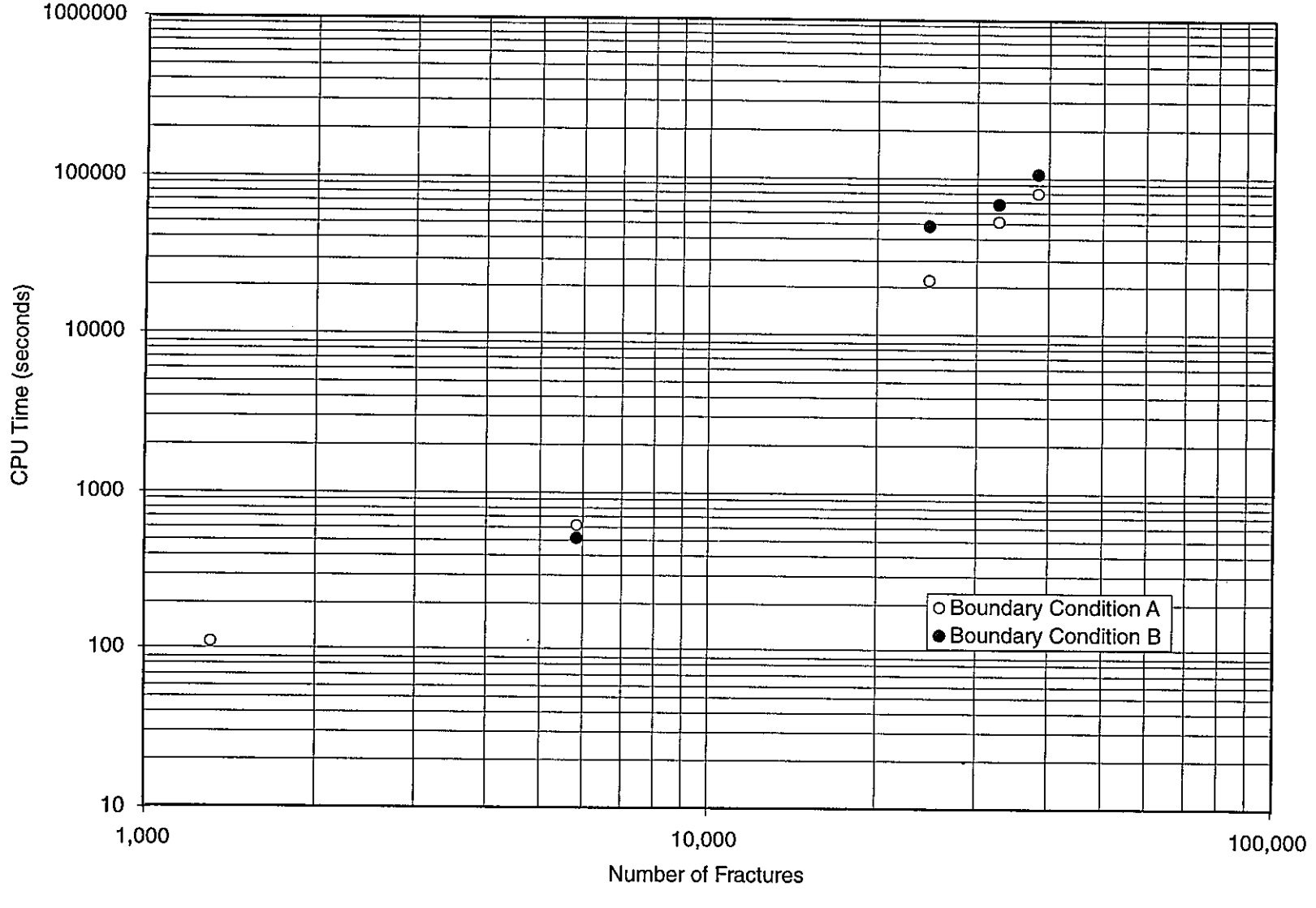

FIGURE **3-14**

REQUIRED CPU TIME VERSUS NUMBER OF FRACTURES, NO TRANSPORT (MAFIC SIMULATIONS)

PNC/PAW-LTG/JAPAN

PROJECT NO. 923 1089.824 DRAWING NO. 72724 DATE 11/21/97 DRAWN BY CB

Golder Associates

The results indicate a power-law trend of CPU time with T_{cutoff} or number of fractures. The figures show the boundary condition has little influence on the total CPU required. The simulations took between 100 seconds with T_{cutoff} equal to 10^{-6} m^2/s, to 104,000 seconds (28.9 hours) at T_{cutoff} equal to 2.e-9 m^2/s.

The memory requirement was tracked for the finite element solution of the flow equations, as this code required the largest memory. The MAFIC memory requirement (without transport calculation) is plotted against transmissivity cutoff and number of fractures in Figures 3-15 and 3-16 respectively. The transport simulations require additional memory depending on the number of particles tracked, and the number of output times.

The figures indicate a power law relationship between the required memory and T_{cutoff} (or number of fractures) for both boundary conditions. The memory requirement increases from 1.8 MB at T_{cutoff} equal to 10^{-6} m^2/s to 670 MB at T_{cutoff} equal to 2×10^{-9} m^2/s.

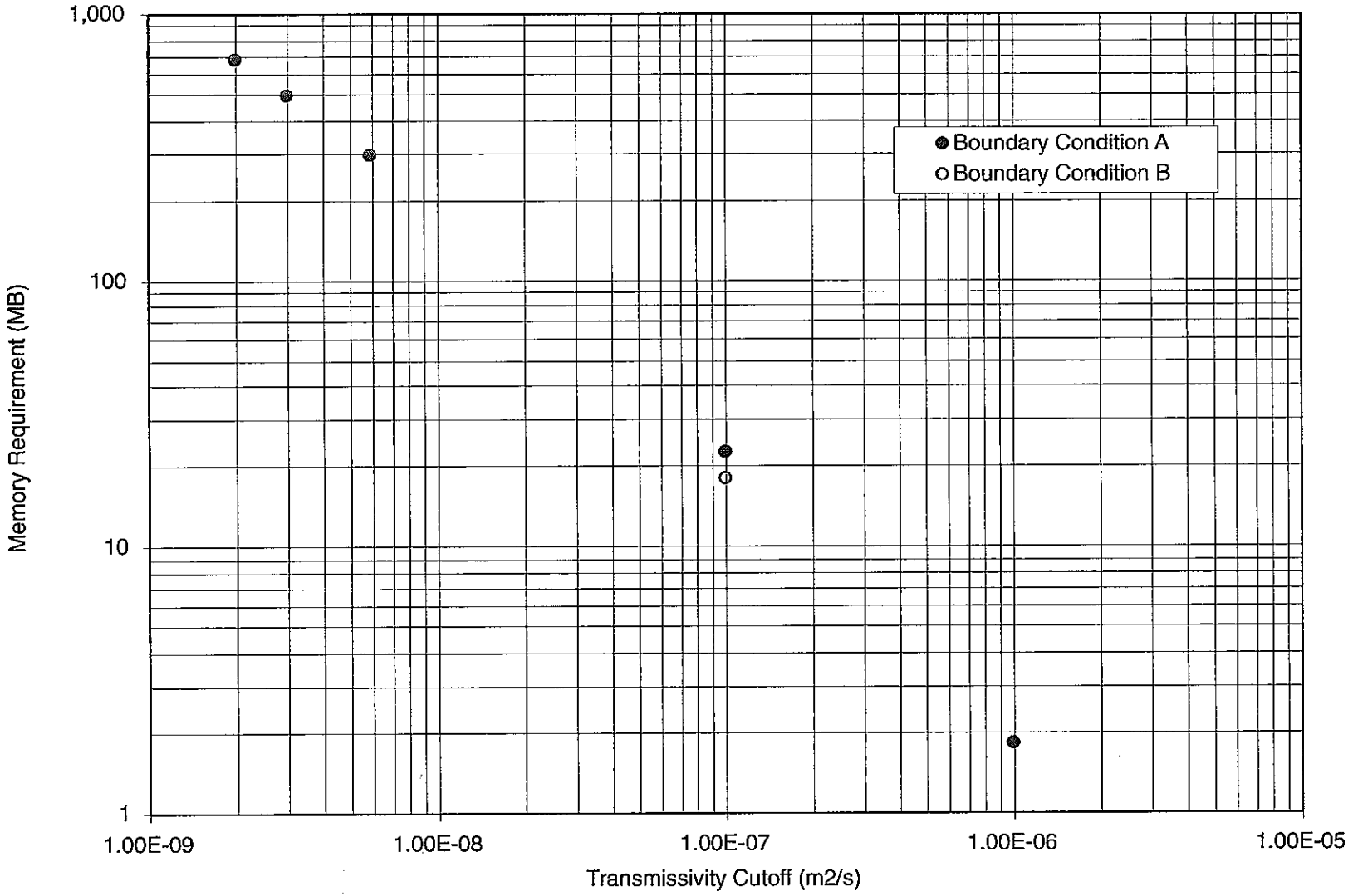

FIGURE **3-15**

MAFIC MEMORY REQUIREMENT VERSUS TRANSMISSIVITY CUTOFF (NO TRANSPORT)

PNC/PAW-LTG/JAPAN

PROJECT NO. 923 1089.824 DRAWING NO. 74771 DATE 11/24/97 DRAWN BY TK

Golder Associates

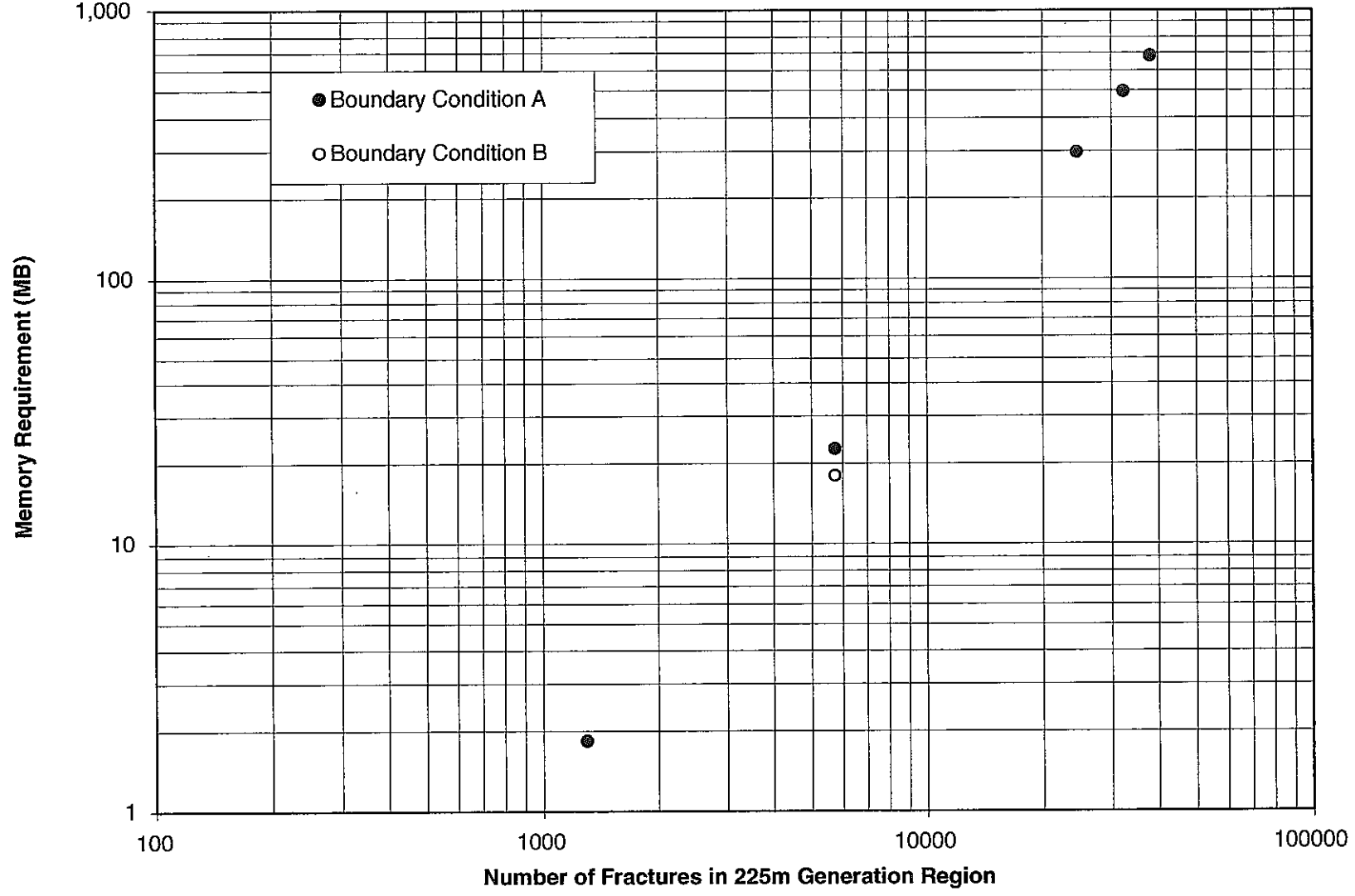

FIGURE **3-16**

MAFIC MEMORY REQUIREMENT VERSUS NUMBER OF FRACTURES CUTOFF (NO TRANSPORT)

PNC/PAW-LTG/JAPAN

4. PAWORKS PIPE NETWORKS

This section presents the results of PAWorks simulations of flow in three dimensional networks of one dimensional pipe elements, and pathway effective transport calculations in those networks. Results are organized according to the comparative measures,

- Effective block hydraulic conductivity (K_{eff}),
- Head distribution within the fracture network (H_{xyz})
- Pathway advective transport time (t_0 and t_{50}),
- Effective network dispersion (t_{50} and t_{85})
- Computer resources (memory and CPU time)

PAWorks flow calculations solve the full pipe network generated using Genpipes "Option 2" (Figure 2-5). Transport computations described in this section are based on transportation through the pipes sampled during a "maximum flux" network search (Foxford et al., 1997).

4.1 Effective Hydraulic Conductivity

The variation of effective hydraulic conductivity versus the transmissivity cut-off and the number of generated fractures is shown in Figures 4-1 and 4-2 respectively. Effective hydraulic conductivity is computed for an assumed Euclidean path length of 200m across the cube, from the face at a head of 10m to the opposite face of the cube at a head of 0m. As discussed in Section 3.1, this is an approximation for boundary condition "A" simulations, due to flow which "short cuts" across the corners of the block. The figures in this section use the legend "1-D transport" to refer to boundary condition B, and legend "1-D constant head" to refer to boundary condition A.

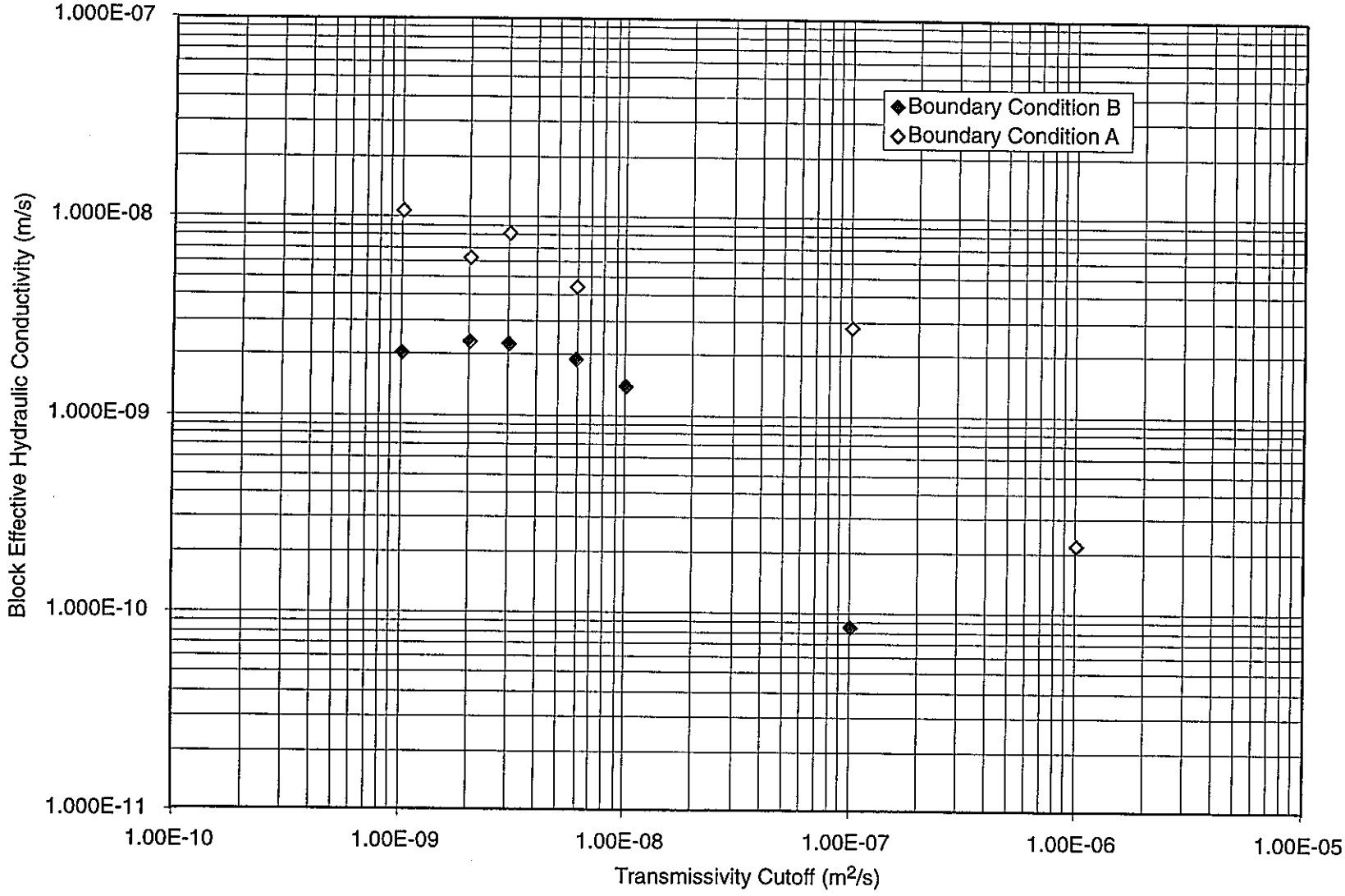

FIGURE **4-1**

BLOCK EFFECTIVE HYDRAULIC CONDUCTIVITY VERSUS TRANSMISSIVITY CUTOFF (PAWorks SIMULATIONS)

PNC/PAW-LTG/JAPAN

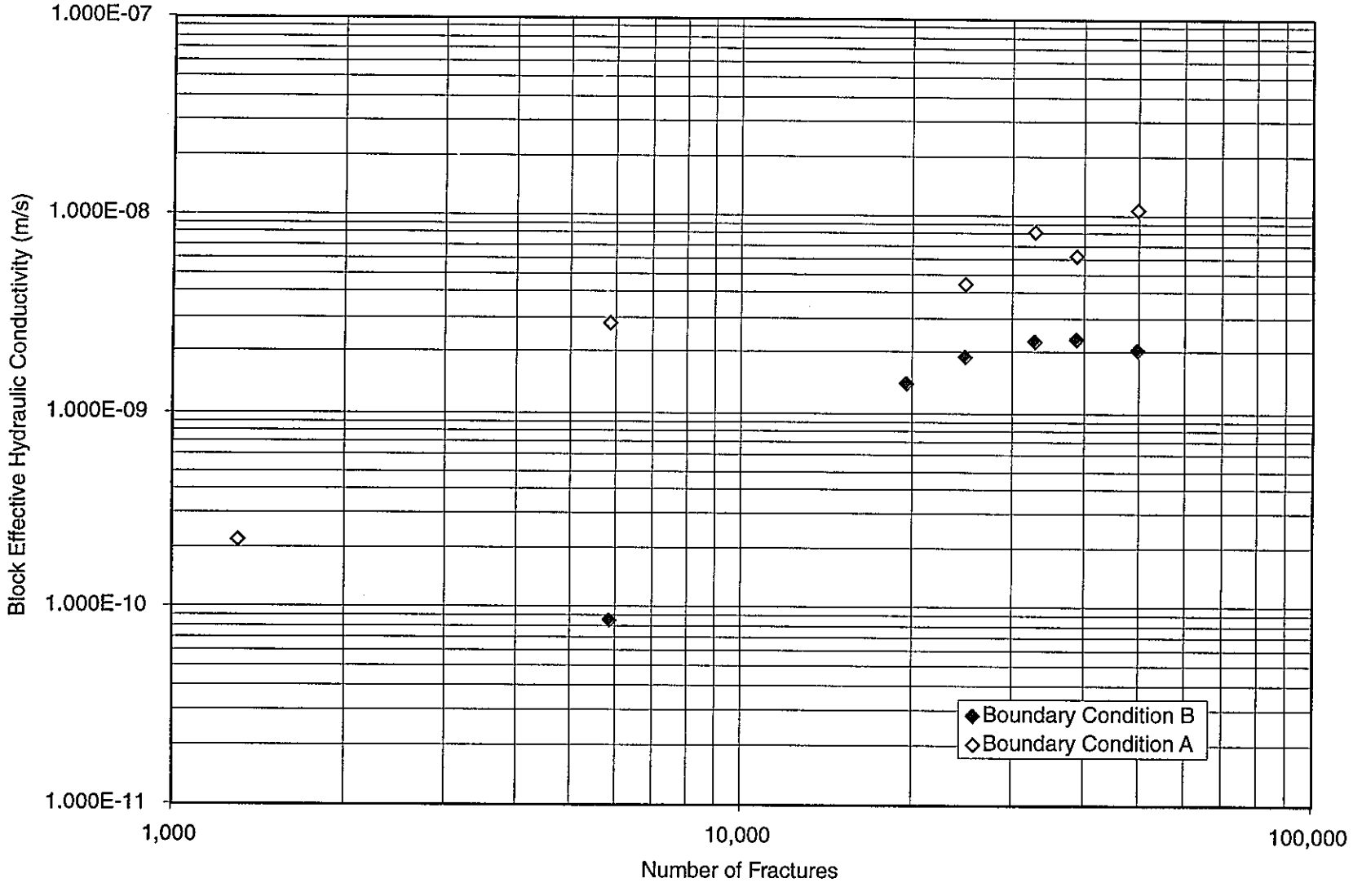

FIGURE **4-2**

BLOCK EFFECTIVE HYDRAULIC CONDUCTIVITY VERSUS NUMBER OF FRACTURES (PAWorks SIMULATIONS)

PNC/PAW-LTG/JAPAN

PROJECT NO. 923 1089.824 DRAWING NO. 72726 DATE 11/21/97 DRAWN BY CB

Golder Associates

The results of the simulations indicate that the hydraulic conductivity with boundary condition "A" show substantial variation between individual realizations compared to boundary condition B. This was also observed for the MAFIC simulations (Section 3.1), where local high conductivity features which "short cut" the edges of the block influence the results. However, there is an overall trend in the results. At T_{cutoff} below about 6×10^{-9} m^2/s (about 25,000 fractures in a 225m cube) the effective conductivity increases with increasing number of fractures. For the range of T_{cutoff} between 1×10^{-9} and 3×10^{-9} m^2/s (33,000 to 50,000 fractures in a 225m cube) the value of K_{eff} is approximately constant at 2 - 3×10^{-9} m/s for boundary condition "B". Boundary condition "A" shows more variability, but tends towards a K_{eff} of about 8×10^{-9} m/s.

Based on the more reliable boundary condition B simulations these results indicate that for T_{cutoff} below 3×10^{-9} m^2/s, or approximately 33,000 fractures in a 225m cube, the simulations are relatively insensitive to increased fracture density. For boundary type 'A' the results are less conclusive because the variation in K_{eff} between individual realizations is greater.

4.2 Head Variability across the Cube

The standard deviation of the computed head compared with the linear head distribution at x, y or z coordinates of ±11 against the value of T_{cutoff} and number of fractures in a 225m cube are indicated on Figures 4-3 and 4-4 respectively. These locations were chosen as they were away from the boundary of the modeled region, and include variation both along, and perpendicular to the axis of applied head. The results of the analyses indicate high variability in the measured head standard deviation for less than 20,000 fractures (T_{cutoff} of approximately 10^{-8} m^2/s). However, for transmissivity cutoff values below 10^{-8} m^2/s little change in the variability of measured head was observed. Interestingly, transport simulations using boundary condition "B" show more variability than those using boundary condition "A". This is probably a result of the closer proximity of the constant head boundary in the case boundary condition "A"; the closer proximity of the defined boundary resulting in less variability of head.

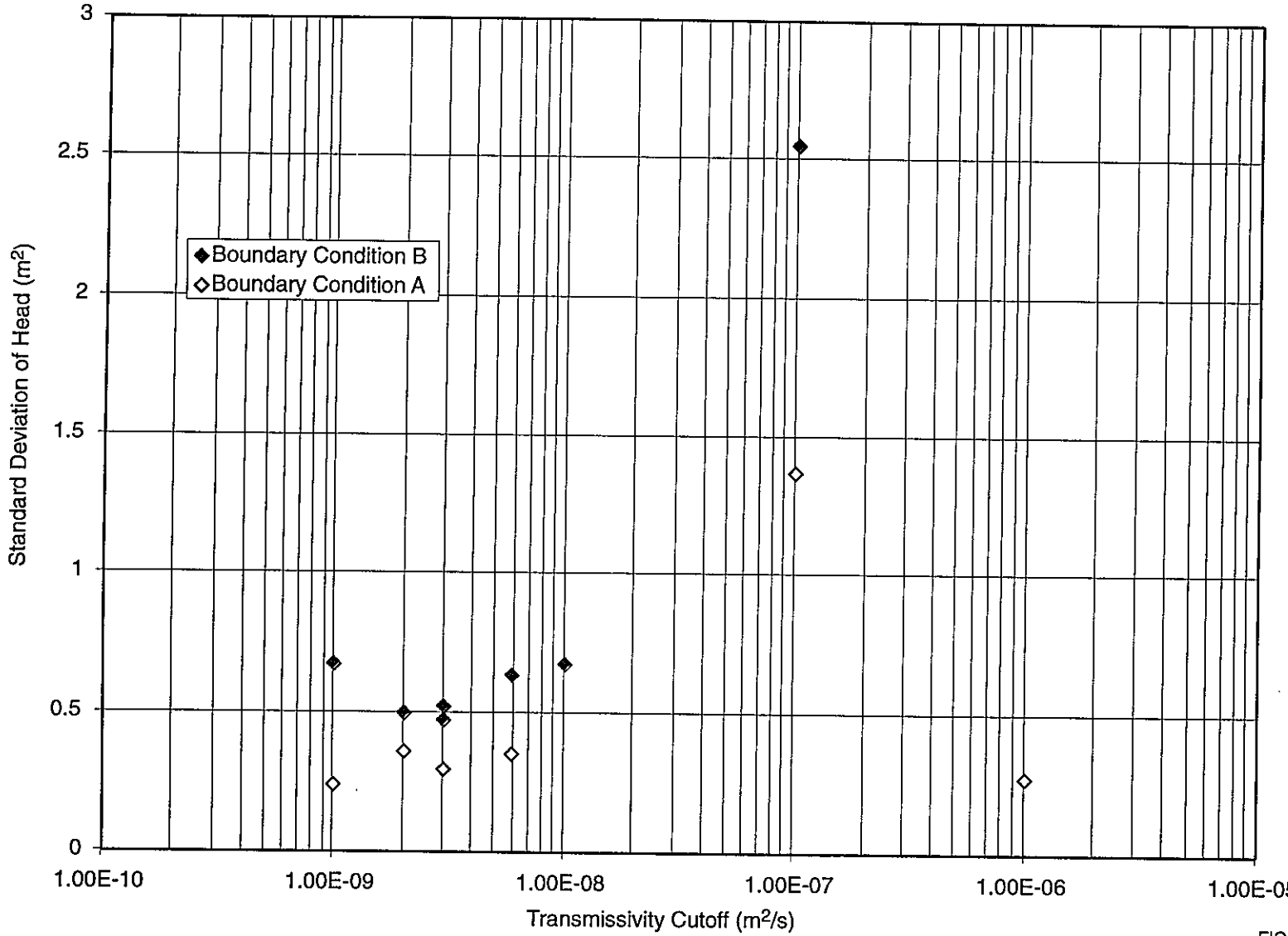

FIGURE **4-3**

STANDARD DEVIATION OF HEAD ABOUT LINEARLY INTERPOLATED VALUE FOR x,y OR z = +-11 VERSUS TRANSMISSIVITY CUTOFF (PAWorks SIMULATIONS)

PNC/PAW-LTG/JAPAN

PROJECT NO. 923 1089.824 DRAWING NO. 72727 DATE 11/21/97 DRAWN BY CB

Golder Associates

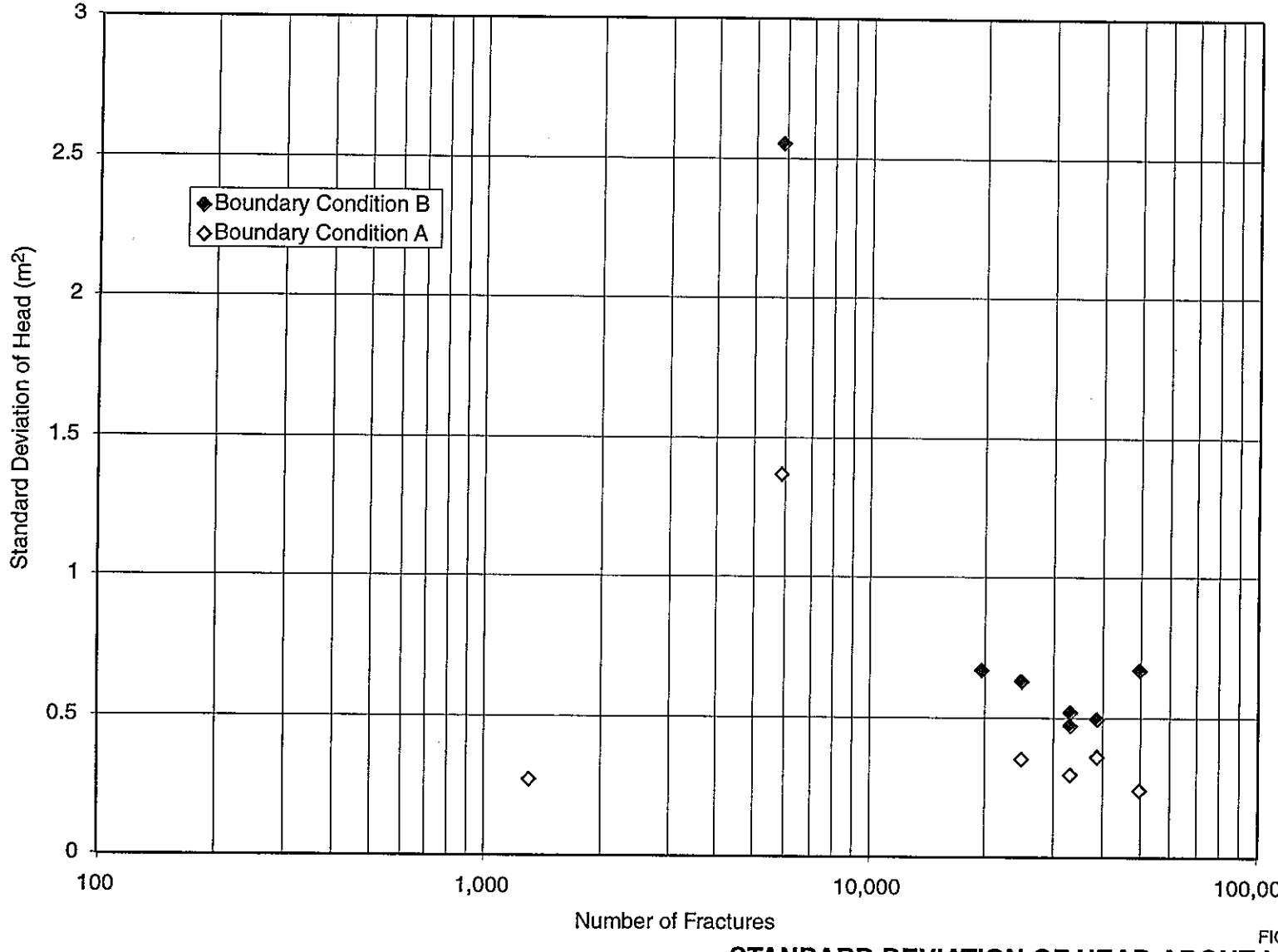

FIGURE **4-4**

STANDARD DEVIATION OF HEAD ABOUT LINEARLY INTERPOLATED VALUE FOR x,y OR z = +-11 VERSUS NUMBER OF FRACTURES (PAWorks SIMULATIONS)

PNC/PAW-LTG/JAPAN

PROJECT NO. 923 1089.824 DRAWING NO. 72728 DATE 11/21/97 DRAWN BY CB

Golder Associates

The results at the location of x=11m for boundary condition "B", for two separate values of T_{cutoff} have been processed to provide contour plots for visualization of the head field. Figure 4-5 shows the head distribution for a value of T_{cutoff} of 5.9×10^{-9} m^2/s, which leads to approximately 25,000 fractures in a 225m cube. The figure shows that the fracture network generally follows the head gradient applied at y = ±100m. However, locally higher and lower head gradients exist.

Figure 4-6 shows the head distribution for a value of T_{cutoff} of 3×10^{-9} m^2/s, which leads to approximately 33,000 fractures in a 225m cube. The head distribution still shows a slight variation of head about the applied gradient. However, there is now a much closer correlation between the initial distributions and the final head distributions.

4.3 Pathway Advective Travel Time

The transport computations in this section were based on the "maximum flux" search routine, which gives the transport time biased towards the maximum flux route through the network. These travel times are not necessarily the fastest, but tend to be faster than the average or median flux paths.

The minimum "follow the flux" traversal travel times for boundary configurations A and B are shown in Figures 4-7 and 4-8 against transmissivity cutoff and number of fractures respectively. At low T_{cutoff} the travel time for the simulations using boundary condition "A" is greater than for boundary conditions "B" by a factor of about 2, probably due to a more tortuous route to the downgradient boundary.

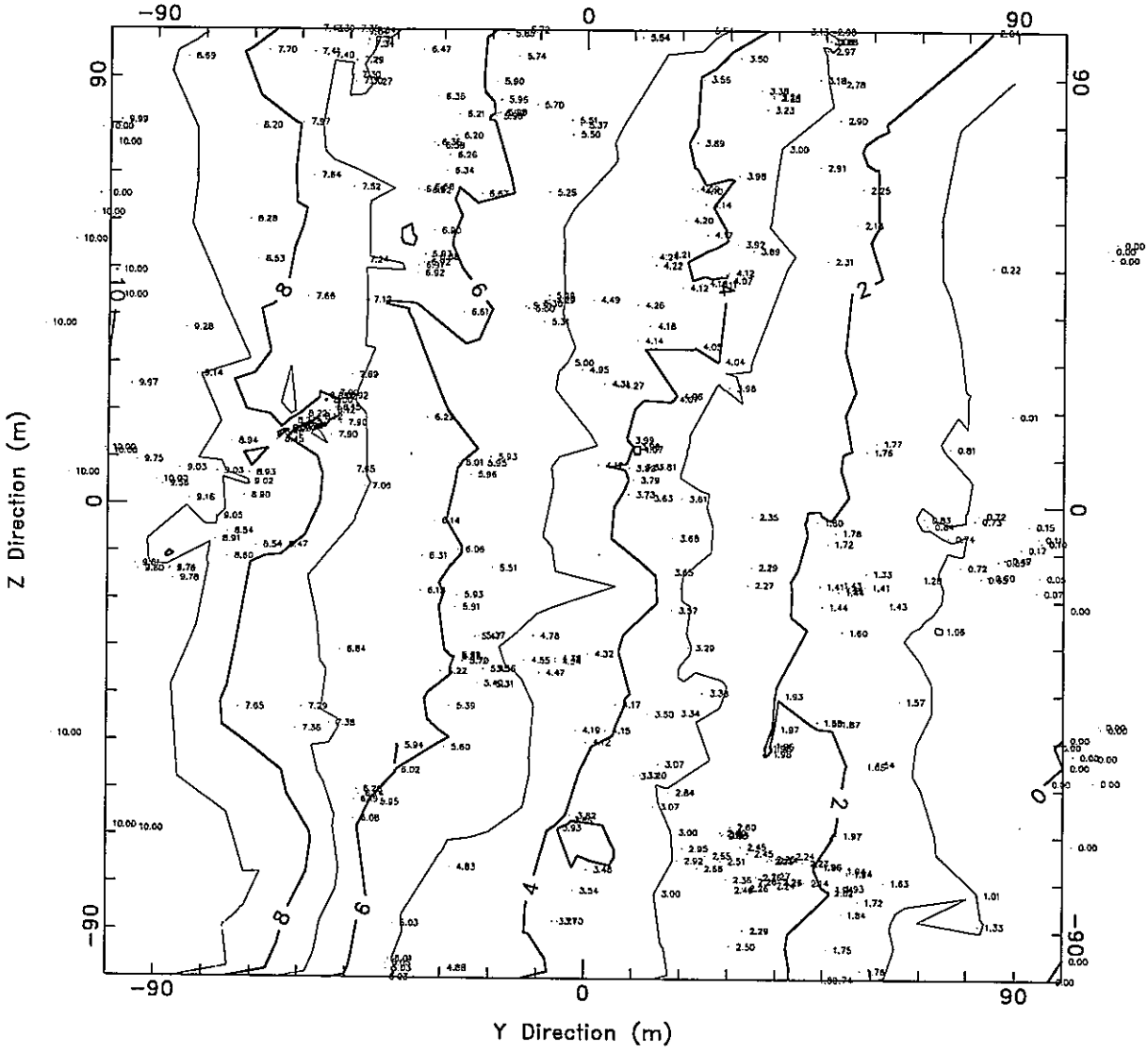

FIGURE **4-5**

HEAD DISTRIBUTION AT x=11 WITH TRANSMISSIVITY CUTOFF = $5.9 \times 10^{-9} m^2/s$ (PAWorks SIMULATIONS)

PNC/PAW & LTG/JAPAN

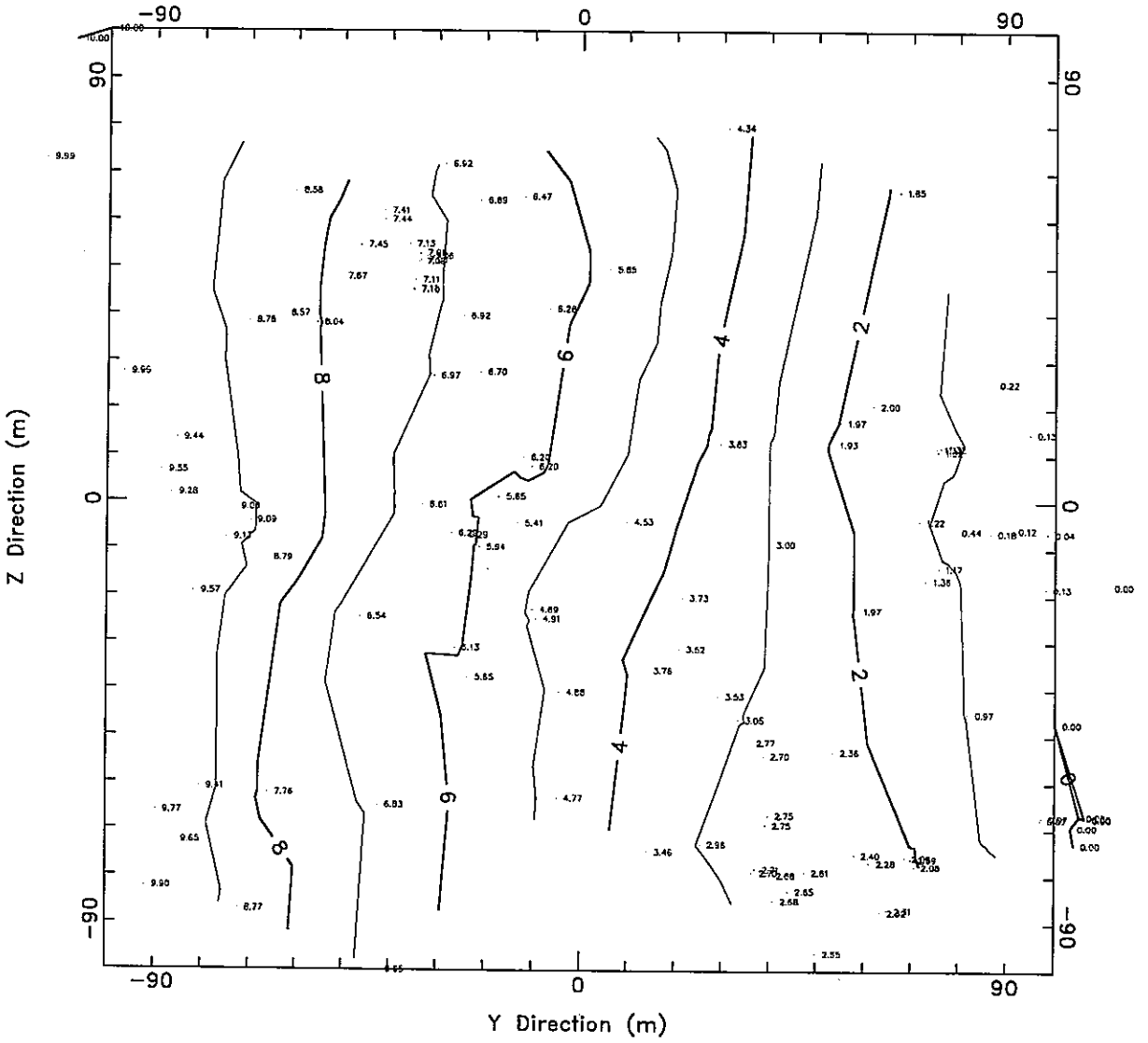

FIGURE **4-6**

HEAD DISTRIBUTION AT x=11 WITH TRANSMISSIVITY CUTOFF = $3x10^{-9}m^2/s$ (PAWorks SIMULATIONS)

PNC/PAW & LTG/JAPAN

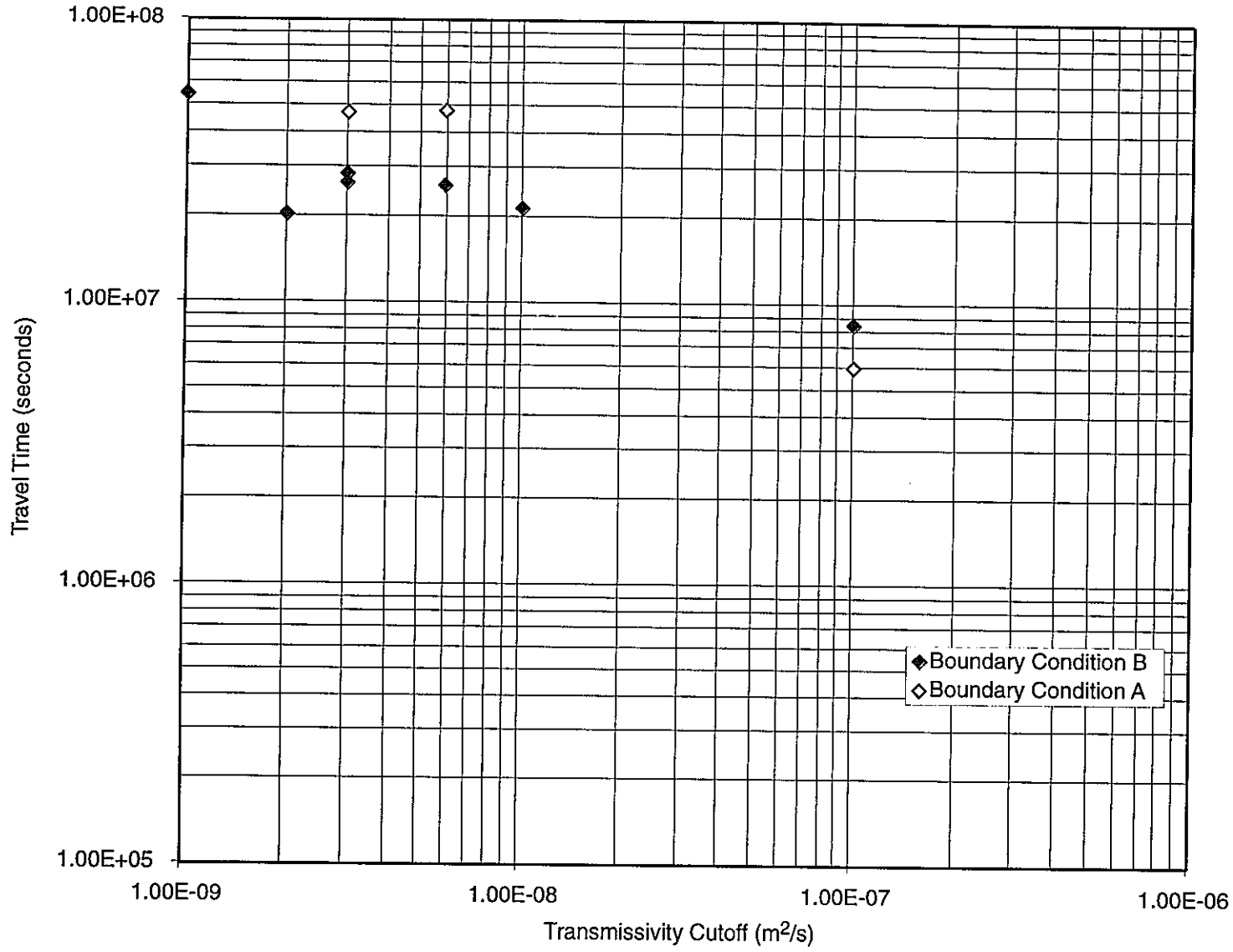

FIGURE **4-7**

MINIMUM TRAVEL TIME VERSUS TRANSMISSIVITY CUTOFF (PAWorks SIMULATIONS)

PNC/PAW-LTG/JAPAN

PROJECT NO. 923 1089.824 DRAWING NO. 72729 DATE 11/18/97 DRAWN BY CB

Golder Associates

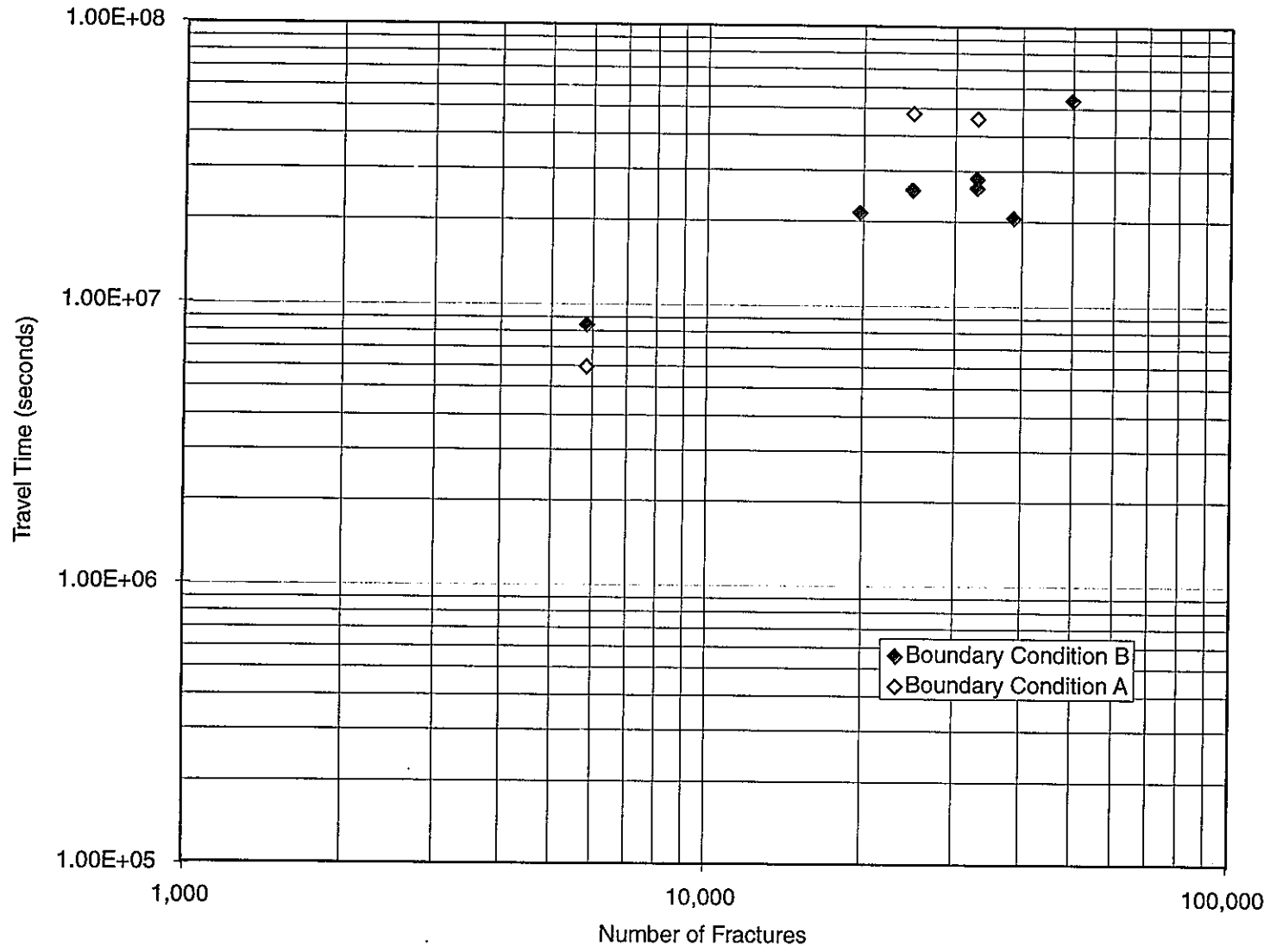

FIGURE **4-8**

MINIMUM TRAVEL TIME VERSUS NUMBER OF FRACTURES (PAWorks SIMULATIONS)

PNC/PAW-LTG/JAPAN

PROJECT NO. 923 1089.824 DRAWING NO. 72730 DATE 11/18/97 DRAWN BY CB

Golder Associates

If the single result at T_{cutoff} equal to 10^{-9} m^2/s is anomalous both boundary indicate the minimum advective travel is approximately constant for T_{cutoff} values below 1.0×10^{-8} m^2/s, corresponding to networks of greater than approximately 20,000 fractures. For the PAWorks model with boundary condition "B", which is directly comparable to the MAFIC transport calculations, the minimum travel time t_{min} converges at about 2.6×10^7 seconds (approximately 0.8 years). However, there is some variation within individual simulations, with the densest mesh having a longer minimum travel time of 5×10^7 seconds.

The median travel time for boundary condition "B" is shown in Figures 4-9 and 4-10 against T_{cutoff} and the number of fractures respectively. The figures indicate an increase in the median travel time with increasing fracture density. This is believed to occur due to increasing connectivity within the mesh, resulting in more possible choices of pathway at each intersection. With the inclusion of additional pathways, the probability of choosing the fastest route to the downgradient boundary diminishes. It should be remembered that these computations used a maximum flux traversal algorithm to select pathways with highest connected flux, rather than the minimum traversal time.

4.4 Effective Dispersion

The effective dispersion in the transport simulations has been indicated by the difference in the median (t_{50}) and t_{85} travel time. The simulations presented on Figures 4-11 and 4-12 indicate that the t_{85} travel time is a factor of about 1.7 times greater than t_{50} at T_{cutoff} equal to 10^{-7} m^2/s. This factor reduces to 1.2 at T_{cutoff} equal to 3×10^{-9} m^2/s indicating a general reduction in dispersion with increasing fracture density, perhaps due to increased mesh connectivity. However, the analyses indicate a variation in t_{85}/t_{50} between individual fracture realizations of the same order as the variation observed with increasing fracture density.

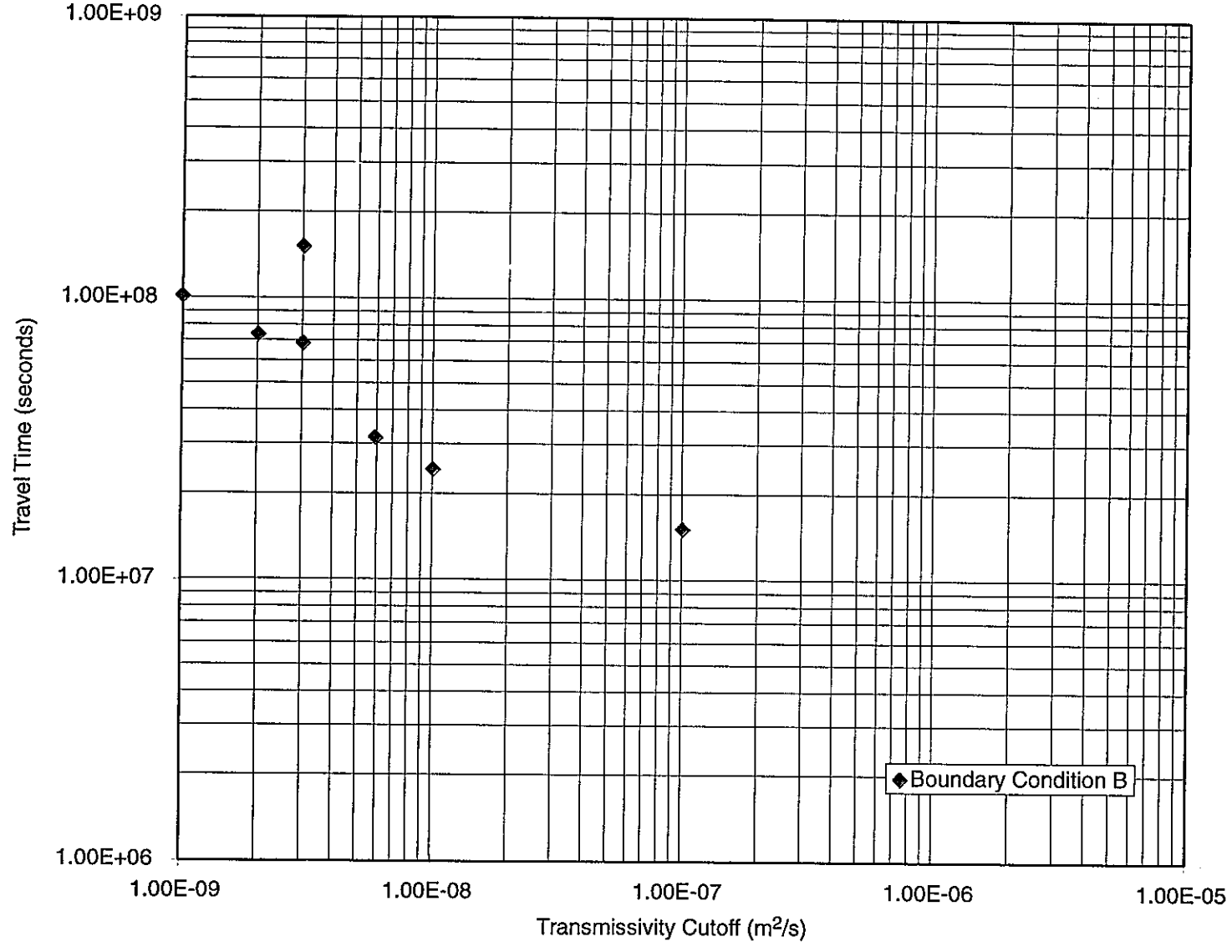

FIGURE **4-9**

T50 TRAVEL TIME VERSUS TRANSMISSIVITY CUTOFF (PAWorks SIMULATIONS)

PNC/PAW-LTG/JAPAN

PROJECT NO. 923 1089.824 DRAWING NO. 72731 DATE 11/21/97 DRAWN BY CB

Golder Associates

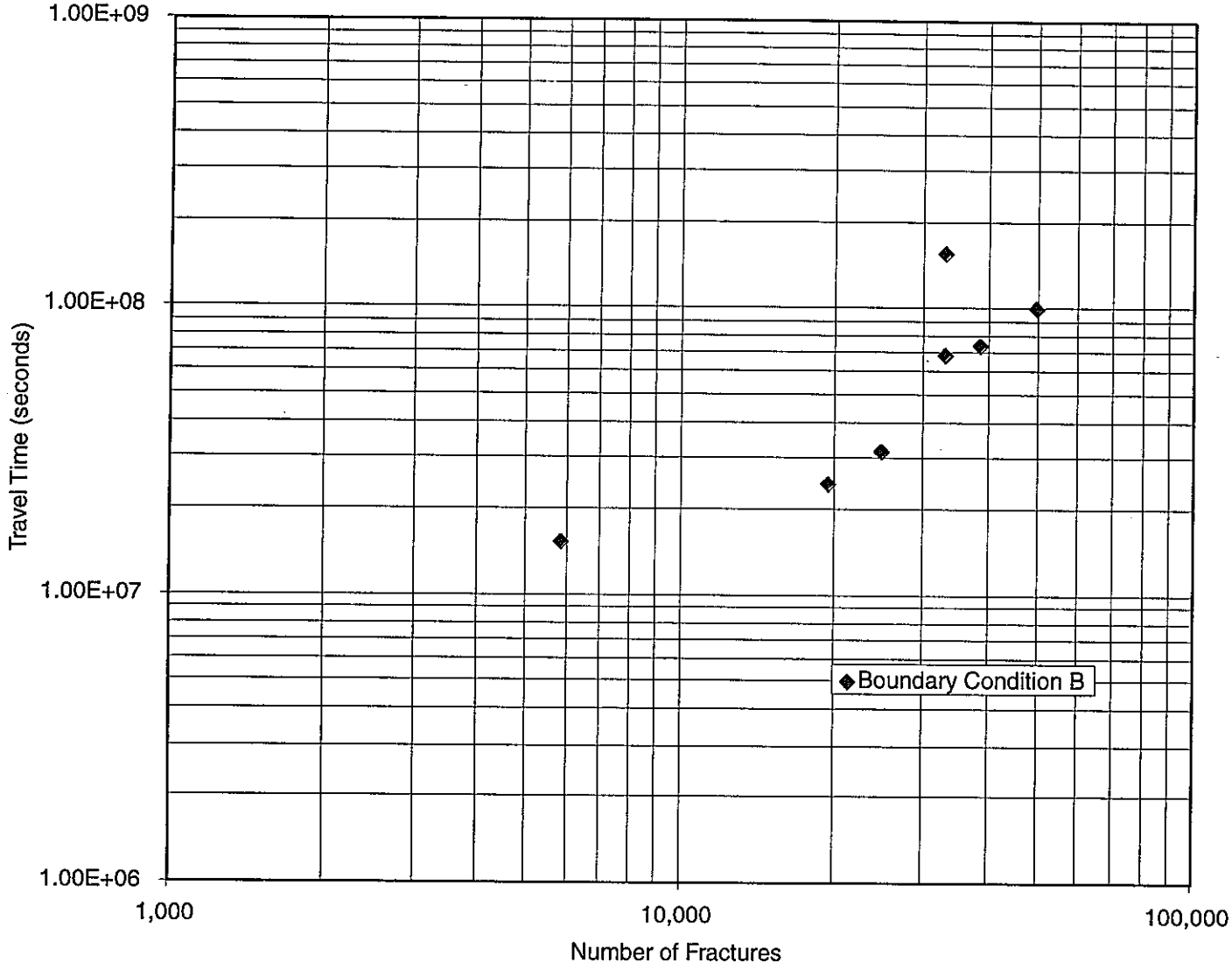

FIGURE **4-10**
T50 TRAVEL TIME VERSUS NUMBER OF FRACTURES (PAWorks SIMULATIONS)
PNC/PAW-LTG/JAPAN

PROJECT NO. 923 1089.824 DRAWING NO. 72732 DATE 11/21/97 DRAWN BY CB

Golder Associates

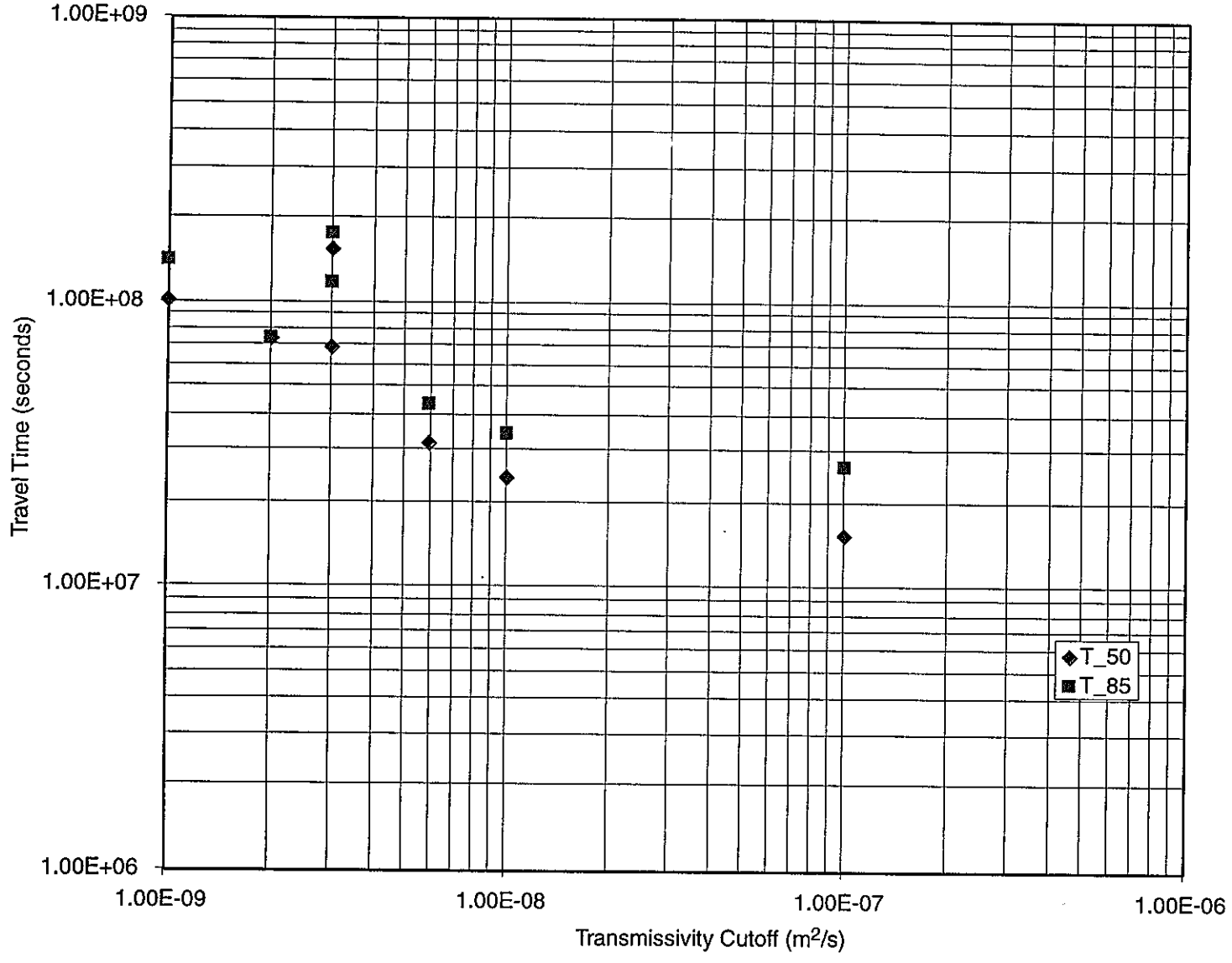

FIGURE **4-11**

T50 & T85 TRAVEL TIME VERSUS TRANSMISSIVITY CUTOFF (PAWorks SIMULATIONS)

PNC/PAW-LTG/JAPAN

PROJECT NO. 923 1089.824 DRAWING NO. 72733 DATE 11/21/97 DRAWN BY CB

Golder Associates

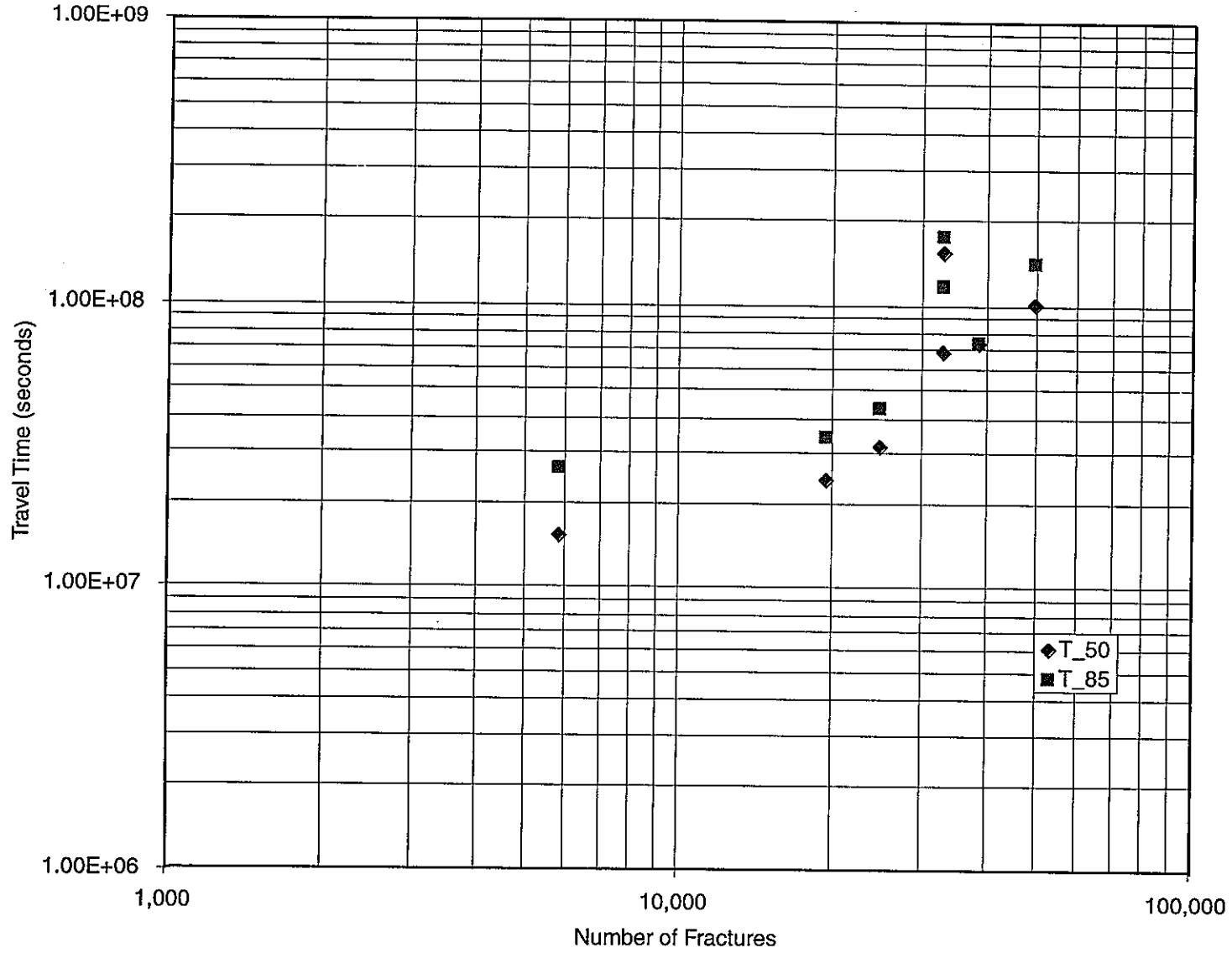

FIGURE **4-12**

T50 & T85 TRAVEL TIME VERSUS NUMBER OF FRACTURES (PAWorks SIMULATIONS)

PNC/PAW-LTG/JAPAN

PROJECT NO. 923 1089.824 DRAWING NO. 72734 DATE 11/18/97 DRAWN BY CB

Golder Associates

4.5 Computer Resources (CPU Time and Memory)

The PAWorks CPU times are presented against T_{cutoff} and the number of fractures in Figures 4-13 and 4-14 respectively. The CPU time presented excludes the transport component of the simulations, to be consistent with the results presented in Section 3. However, the transport component of the simulations typically takes about the same CPU as the flow solution, due to the large number of properties computed within PAWorks.

The results indicate power law trend of CPU time with T_{cutoff} or number of fractures. The simulations took between 45 seconds with T_{cutoff} equal to 10^{-7} m^2/s, to 7,000 seconds (1.94 hours) at T_{cutoff} equal to 10^{-9} m^2/s.

The memory requirement was tracked for the finite element solution of the flow equations, as this code required the largest memory within the PAWorks suite of codes. The required memory to run the PAWorks simulations are presented in Figures 4-15 and 4-16 against T_{cutoff} and number of fractures respectively. Similar to the MAFIC memory requirements, the variation of required memory and T_{cutoff} (or number of fractures) for both boundary conditions shows power law relationship. Figure 4-13 shows that the memory requirement increases from 3.5 MB at T_{cutoff} equal to 10^{-7} m^2/s to 220 MB at T_{cutoff} equal to 1×10^{-9} m^2/s.

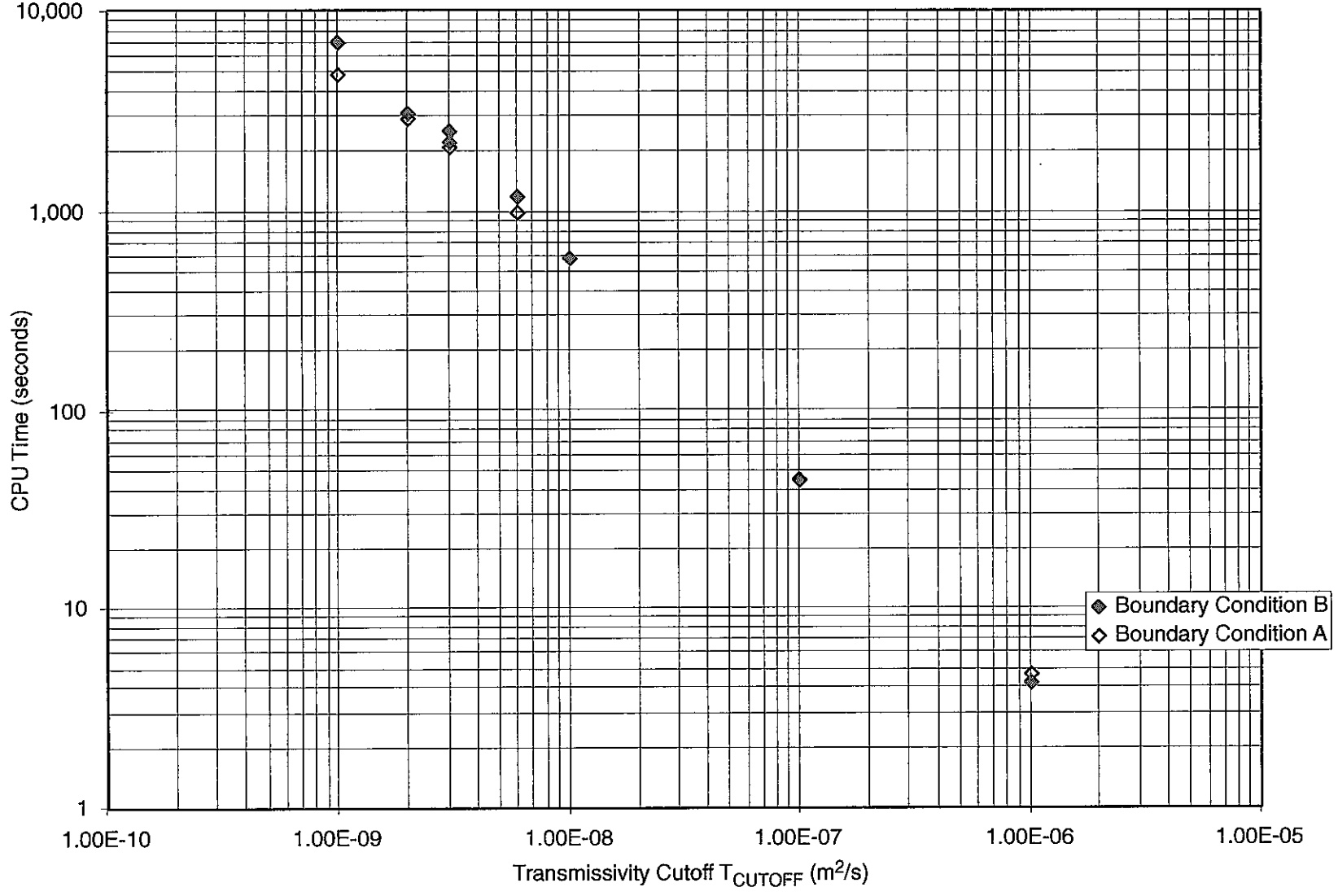

FIGURE **4-13**
REQUIRED PAWorks CPU TIME VERSUS T_{CUTOFF}, NO TRANSPORT
PNC/PAW-LTG/JAPAN

PROJECT NO. 923 1089.824 DRAWING NO. 72735 DATE 11/24/97 DRAWN BY CB

Golder Associates

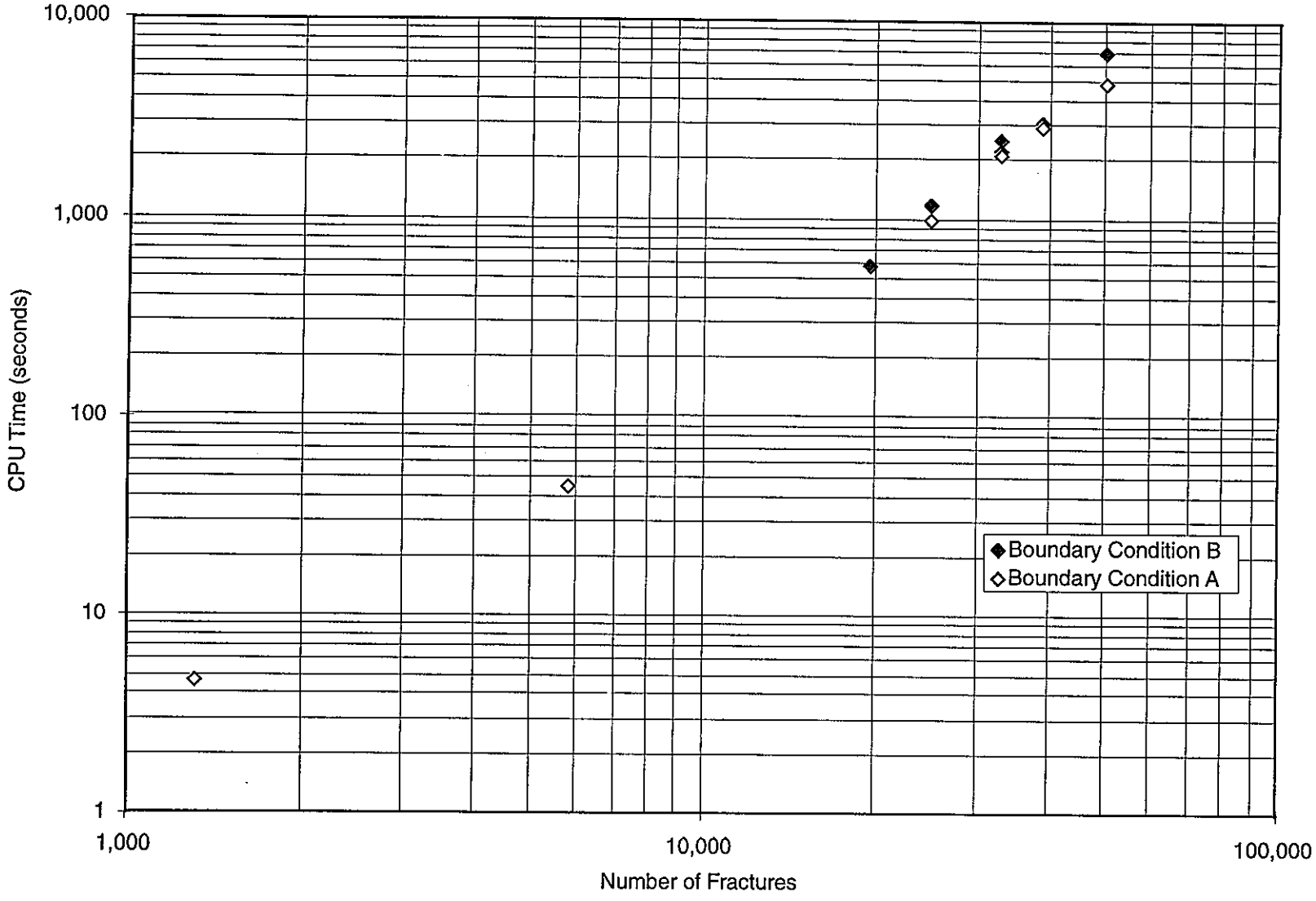

FIGURE **4-14**
REQUIRED CPU TIME VERSUS NUMBERS OF FRACTURES, NO TRANSPORT (PAWorks SIMULATIONS)
PNC/PAW-LTG/JAPAN

PROJECT NO. 923 1089.824 DRAWING NO. 72736 DATE 11/18/97 DRAWN BY CB

Golder Associates

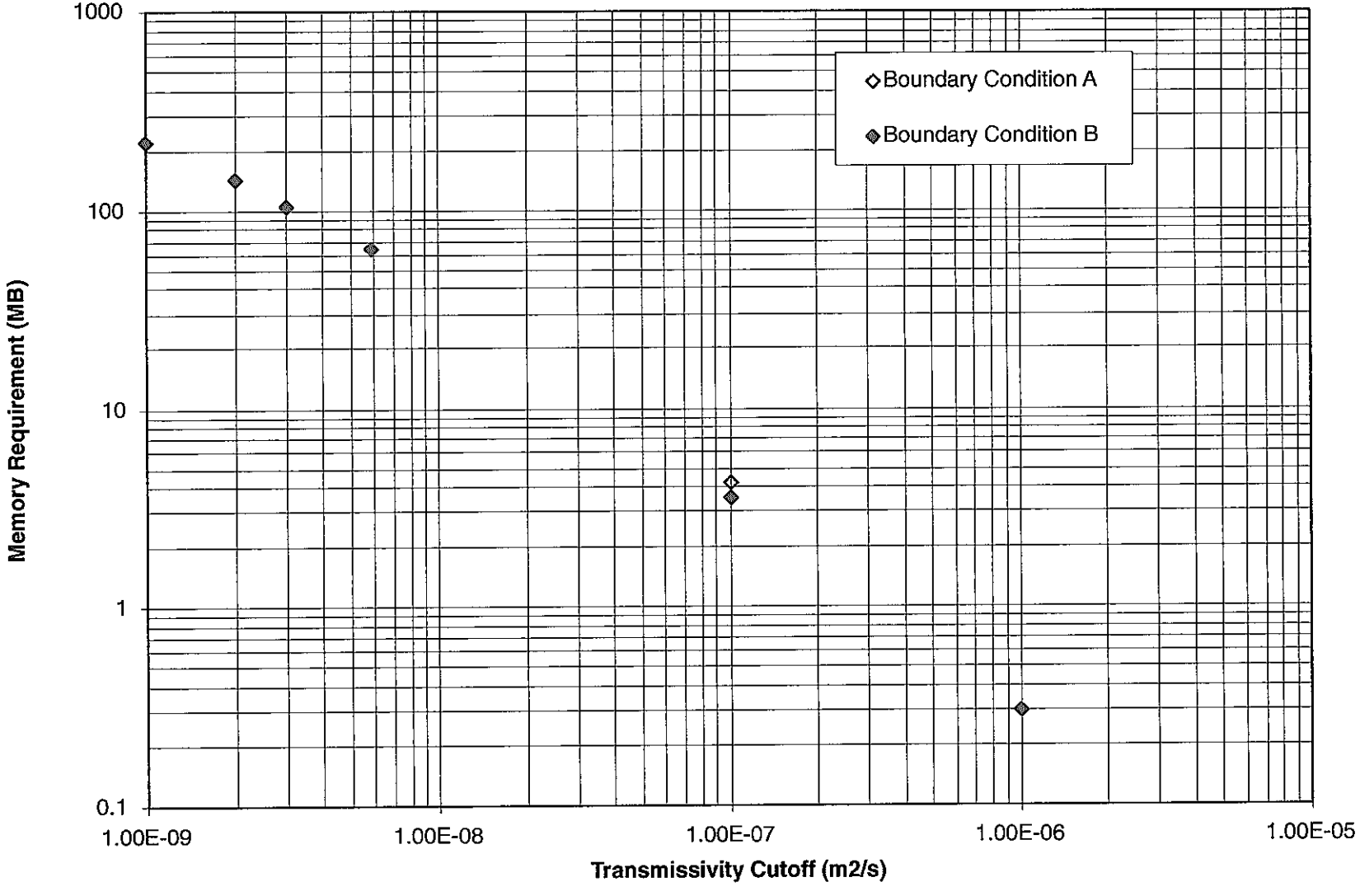

FIGURE **4-15**
PAWorks MEMORY REQUIREMENT VERSUS TRANSMISSIVITY CUTOFF
PNC/PAW-LTG/JAPAN

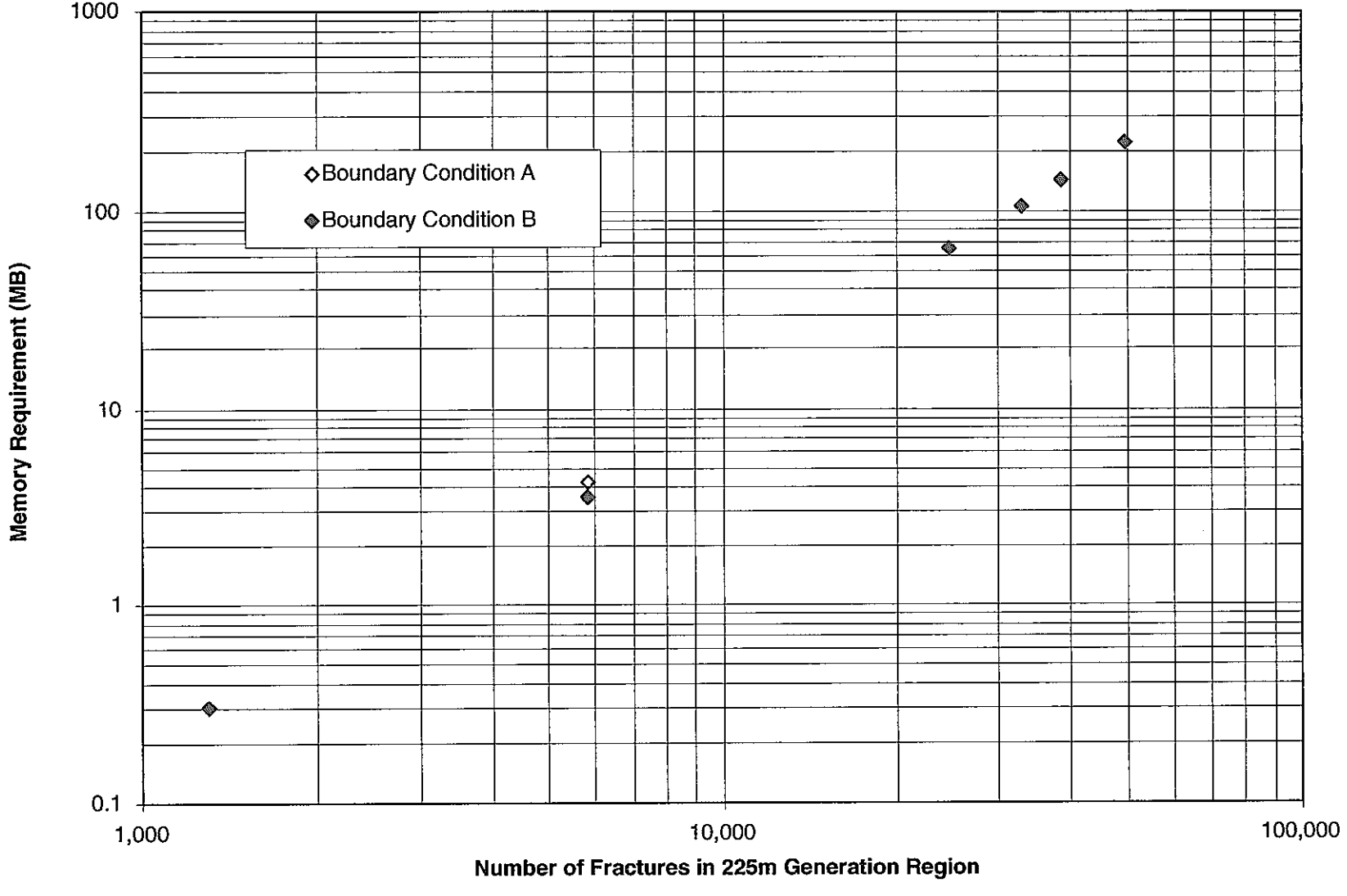

FIGURE **4-16**
PAWorks MEMORY REQUIREMENT VERSUS NUMBER OF FRACTURES
PNC/PAW-LTG/JAPAN

PROJECT NO. 923 1089.824 DRAWING NO. 74770 DATE 11/24/97 DRAWN BY TK

Golder Associates

5. COMPARISON OF MAFIC & PAWORKS SIMULATIONS

5.1 Scope of Comparison

This section provides a comparison between the MAFIC and PAWorks fracture networks using the original fracture model with aperture defined by the cubic law, and the pipe fracture width defined as $W = 0.5*(W_1 + W_2)$, where W_i is the trace length projected perpendicular to the pipe as shown on Figure 2-5.

The purpose of this comparison was to determine the differences between the MAFIC and PAWorks simulations undertaken in sections 5 and 6. In particular, this section discusses the relative CPU and memory requirements for PAWorks and MAFIC fracture representations, indicates the fracture density required to adequately model the Kamaishi 200m cube using pipe and plate fracture representations. These results have been used as our reference for the matching of the PAWorks and MAFIC models undertaken in Section 6.

The results of the comparison are set out under the headings used for the individual PAWorks and MAFIC fracture network result discussions, namely

- Effective block hydraulic conductivity (K_{eff}),
- Head distribution within the fracture network (H_{xyz})
- Pathway advective transport time (t_0 and t_{50}),
- Effective network dispersion (t_{50} and t_{85})
- Computer resources (memory and CPU time)

The final part of this section, Section 5.7, discusses the network density required to adequately model the fracture network at the Kamaishi site, for both PAWorks and MAFIC fracture networks.

For figures in this section, legends "1-D" refers to PAWorks, "2-D" refers to MAFIC, "transport" refers to boundary condition B, and "constant head" refers to boundary condition A.

5.2 Effective Hydraulic Conductivity

The variation of effective hydraulic conductivity for both the PAWorks and MAFIC fracture networks are shown in Figures 5-1 and 5-2 against the transmissivity cut-off and number of generated fractures respectively. These plots indicate that the effective hydraulic conductivity is essentially independent of T_{cutoff} for T_{cutoff} less than about 3 x 10^{-9} m^2/s (corresponding to more than approximately 33,000 fractures in a 225m cube) for both the PAWorks and MAFIC fracture networks.

The same simulations are plotted as the ratio (MAFIC K_{eff})/(PAWorks K_{eff}) on Figures 5-3 and 5-4. The figures indicate that the flux from the MAFIC fracture network is between 1.5 and 3 times larger than that obtained from the PAWorks pipe network. This suggests that the fracture width for the pipe fractures is underestimated at the Kamaishi site using the baseline equation for PAWorks pipe fracture width, $W = 0.5*(W_1 + W_2)$ or that pipe generation Option 2 underestimates the network connectivity. Varying these assumptions is investigated in Section 7.

5.3 Head Variability across the Cube

The standard deviation of the computed head compared for PAWorks and MAFIC fracture networks with the linear head distribution at x, y or z coordinates of ±11m against the value of T_{cutoff} and number of fractures in a 225m cube are indicated on Figures 5-5 and 5-6 respectively. The figures indicate that the difference in the standard deviation of head is essentially the same for PAWorks and MAFIC. The figures also indicate that below a transmissivity threshold of T_{cutoff} of about 10^{-8} m^2/s the PAWorks and MAFIC boundary conditions give approximately the same variation in head about the applied gradient.

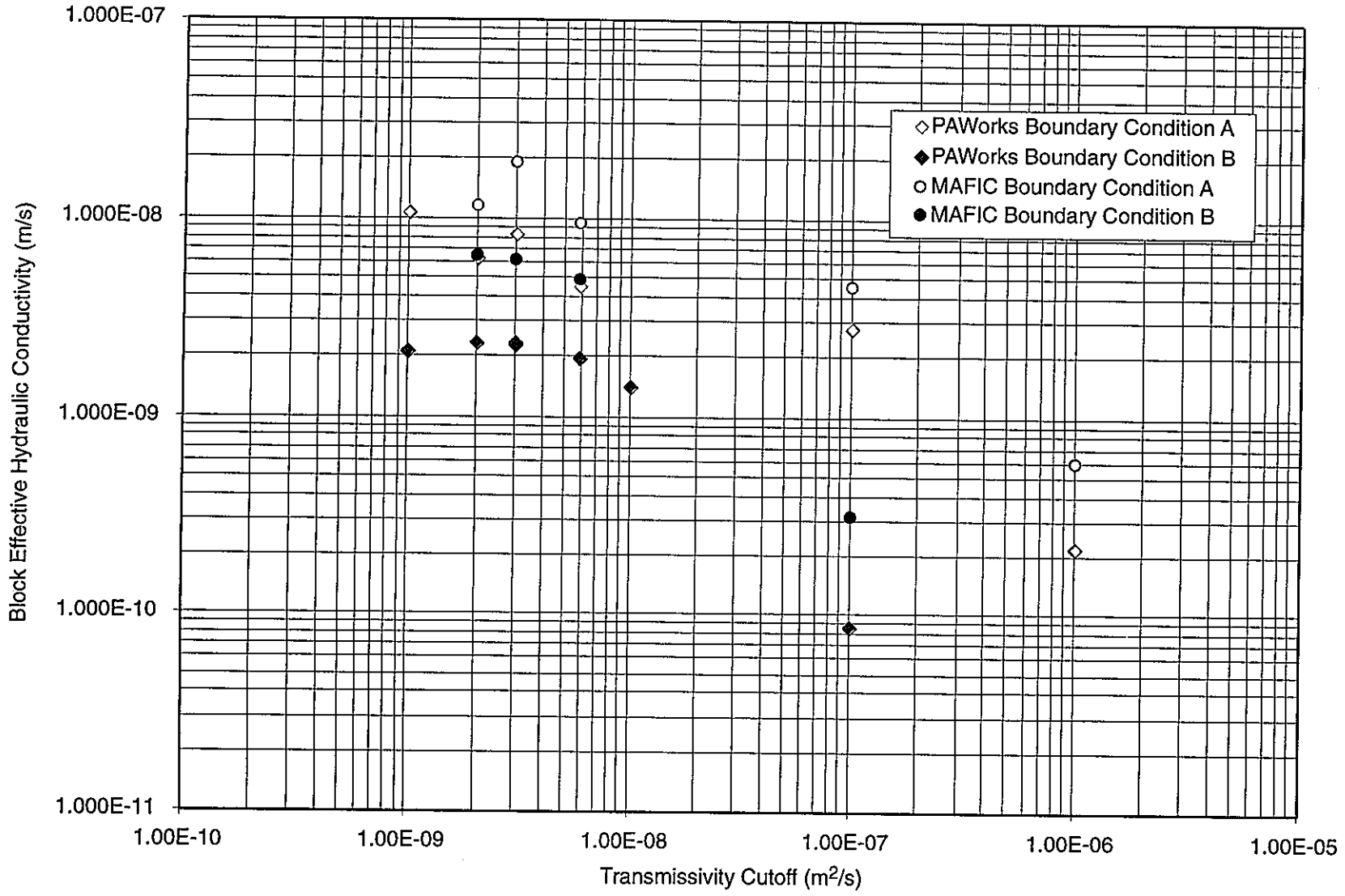

FIGURE **5-1**

BLOCK EFFECTIVE HYDRAULIC CONDUCTIVITY VERSUS TRANSMISSIVITY CUTOFF

PNC/PAW-LTG/JAPAN

PROJECT NO. 923 1089.824 DRAWING NO. 72741 DATE 11/24/97 DRAWN BY CB

Golder Associates

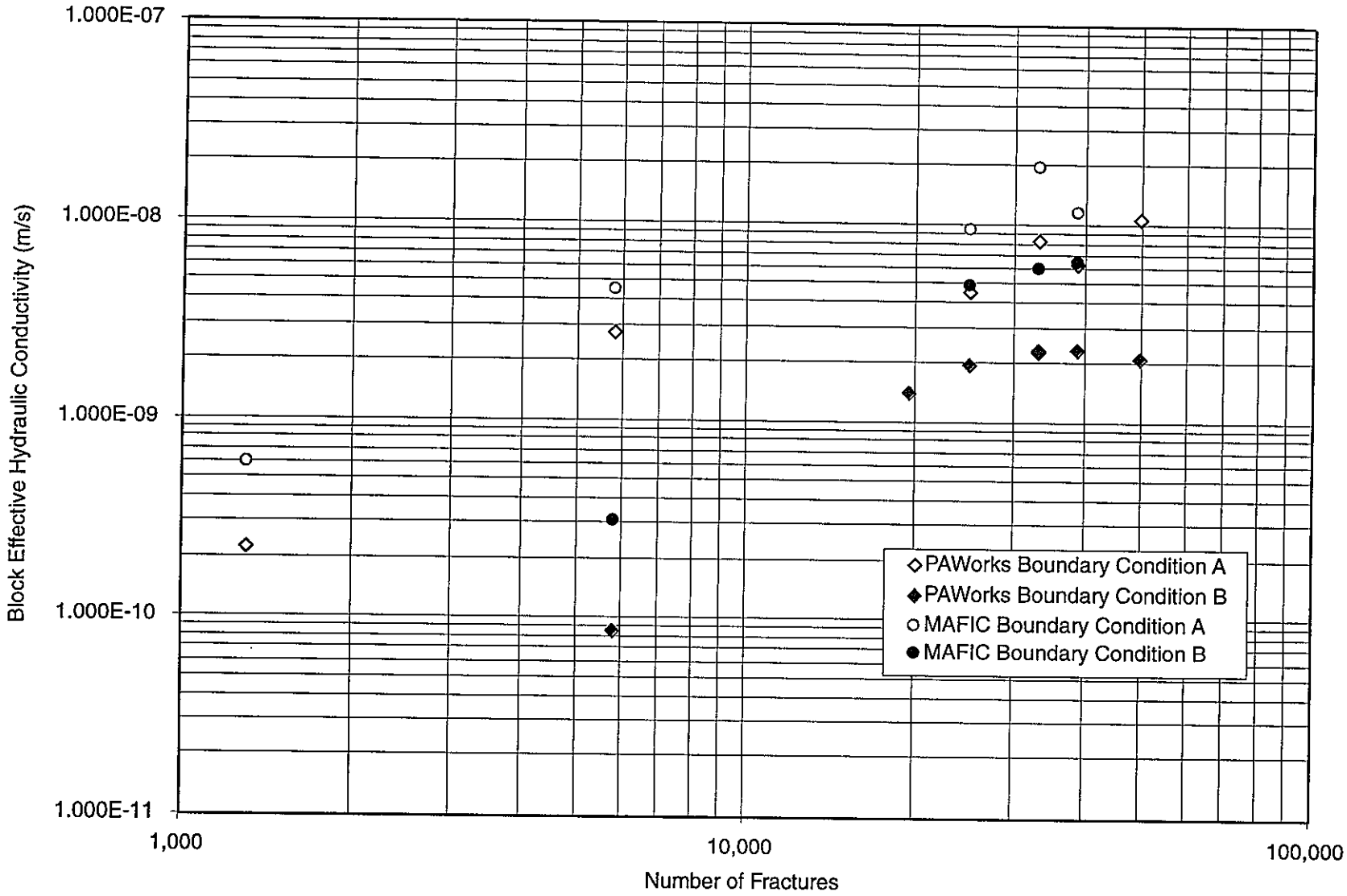

FIGURE **5-2**

BLOCK EFFECTIVE HYDRAULIC CONDUCTIVITY VERSUS NUMBER OF FRACTURES

PNC/PAW-LTG/JAPAN

PROJECT NO. 923 1089.824 DRAWING NO. 72742 DATE 11/21/97 DRAWN BY CB

Golder Associates

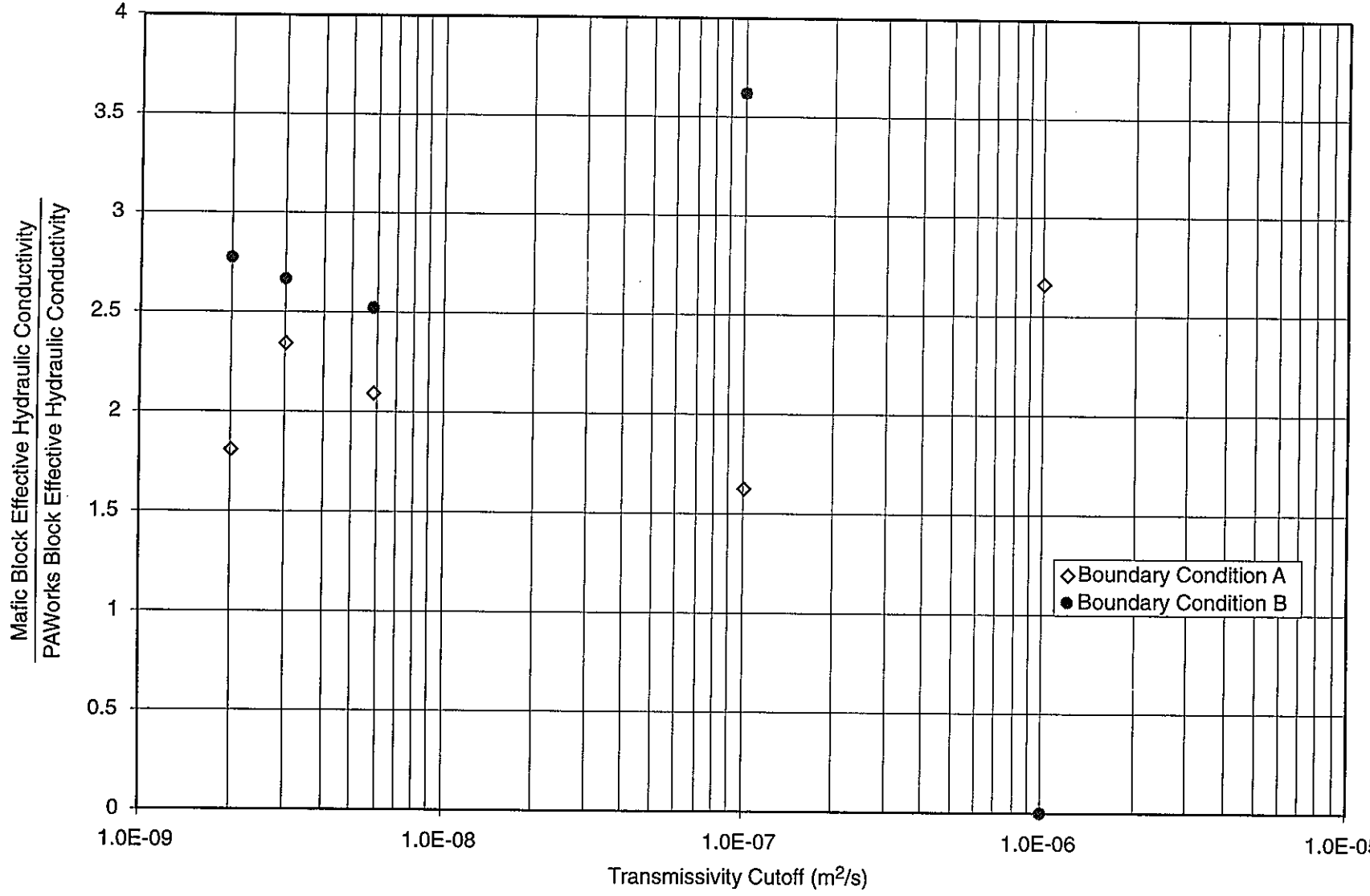

FIGURE **5-3**

MAFIC/PAWorks HYDRAULIC CONDUCTIVITY RATIO VERSUS TRANSMISSIVITY CUTOFF

PNC/PAW-LTG/JAPAN

PROJECT NO. 923 1089.824 DRAWING NO. 72744 DATE 11/21/97 DRAWN BY CB

Golder Associates

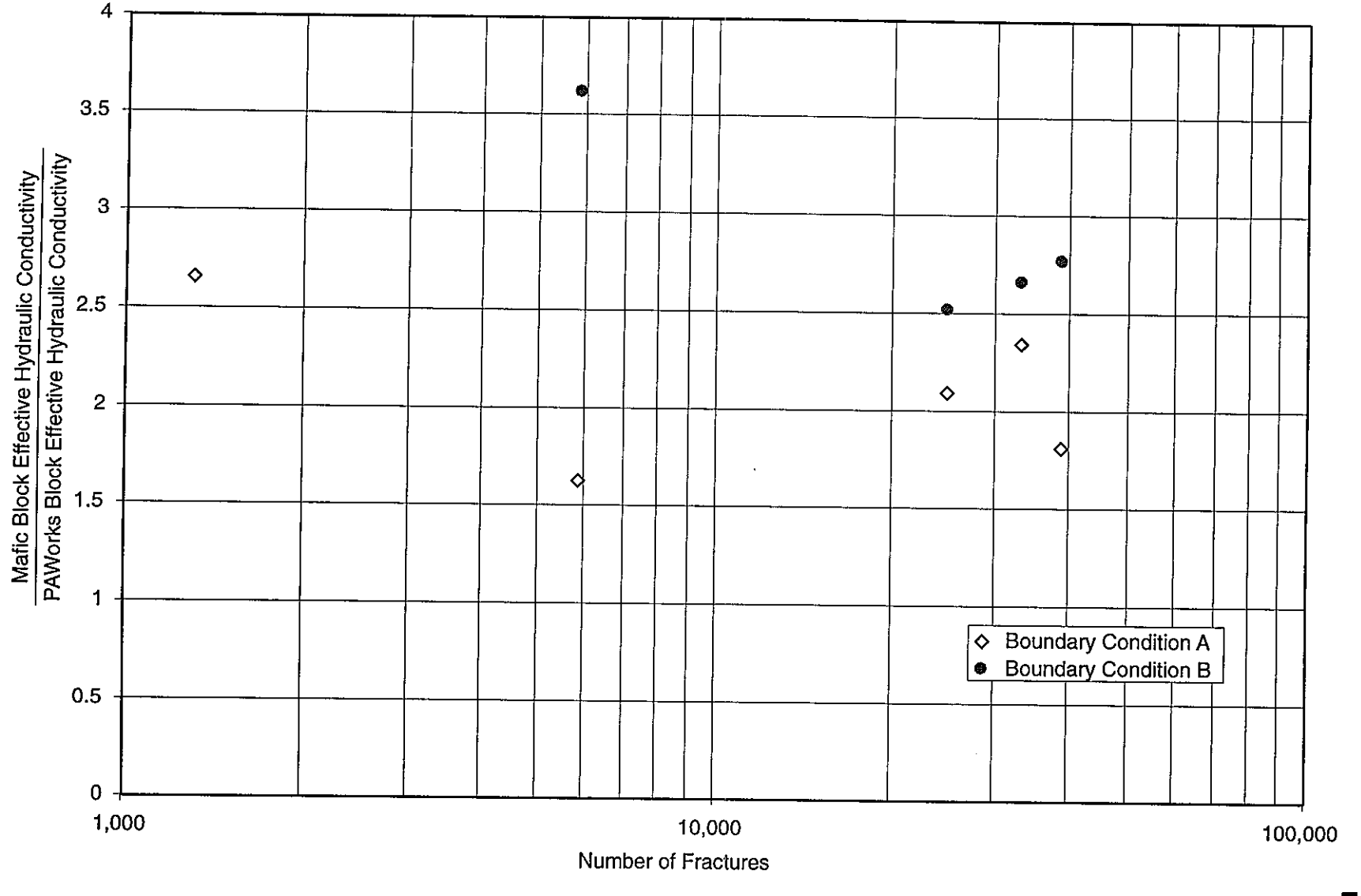

FIGURE **5-4**
MAFIC/PAWorks HYDRAULIC CONDUCTIVITY RATIO VERSUS NUMBER OF FRACTURES
PNC/PAW-LTG/JAPAN

PROJECT NO. 923 1089.824 DRAWING NO. 72743 DATE 11/21/97 DRAWN BY CB

Golder Associates

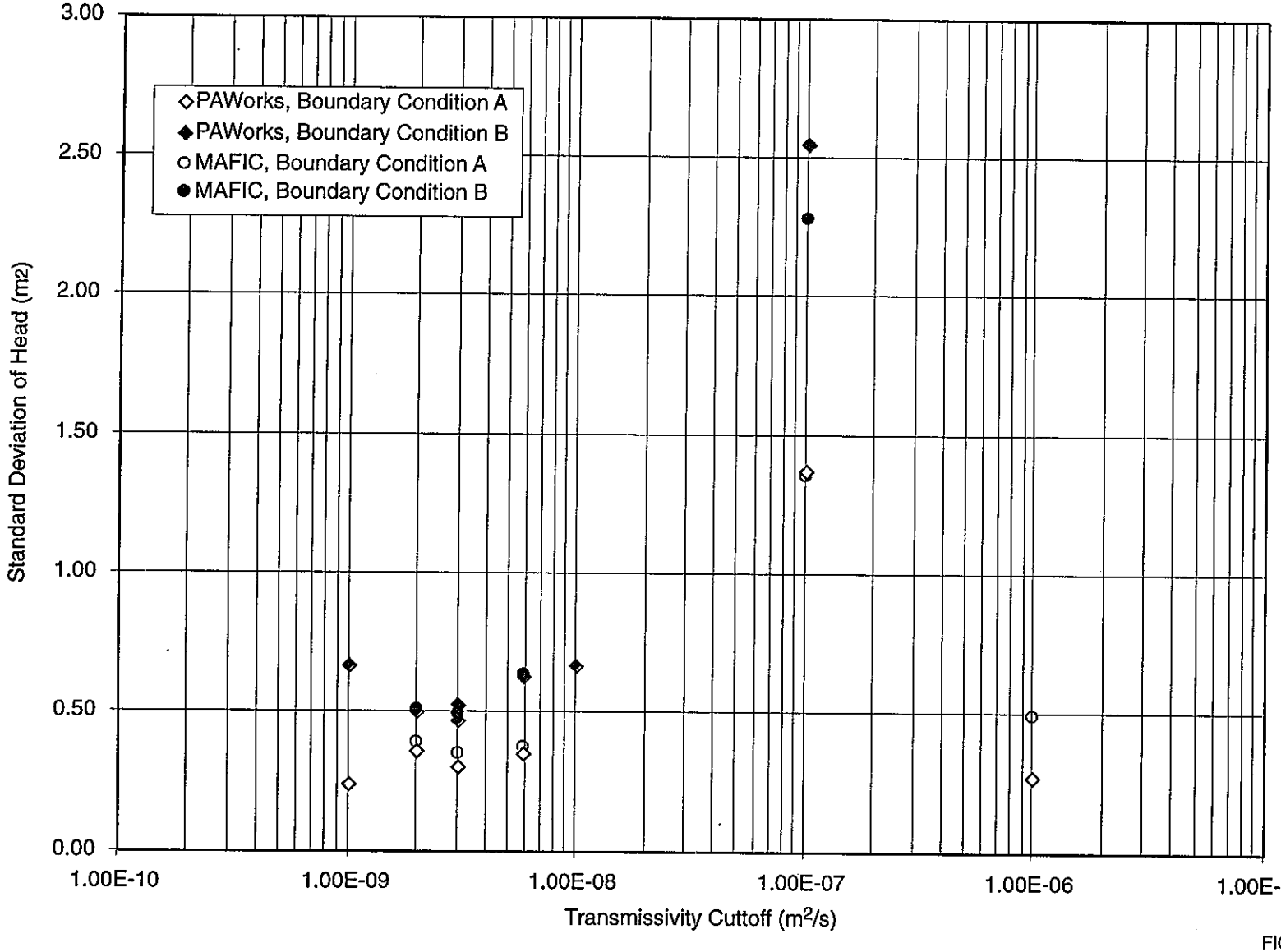

FIGURE **5-5**

STANDARD DEVIATION OF HEAD ABOUT LINEARLY INTERPOLATED VALUE AT x,y OR z = +-11 VERSUS TRANSMISSIVITY CUTOFF

PNC/PAW-LTG/JAPAN

PROJECT NO. 923 1089.824 DRAWING NO. 72745 DATE 11/21/97 DRAWN BY CB

Golder Associates

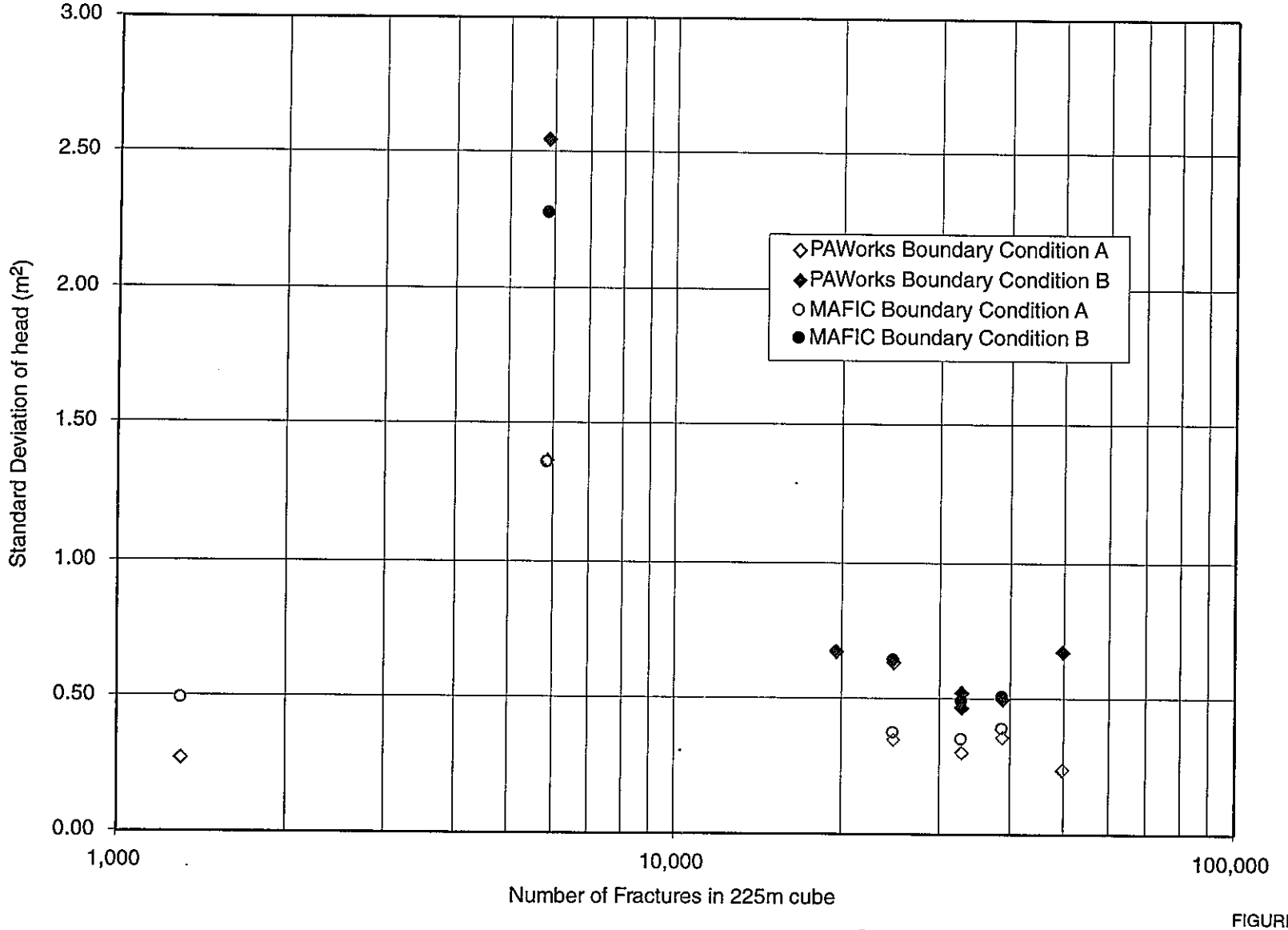

FIGURE **5-6**

STANDARD DEVIATION OF HEAD ABOUT LINEARLY INTERPOLATED VALUE AT x,y OR z = +-11 VERSUS NUMBER OF FRACTURES

PNC/PAW-LTG/JAPAN

PROJECT NO. 923 1089.824 DRAWING NO. 72746 DATE 11/21/97 DRAWN BY CB

Golder Associates

5.4 Pathway Advective Travel Time

The minimum travel time for the boundary condition "B" simulations are shown in Figures 5-7 and 5-8. The MAFIC fracture network shows a reduction in the minimum traversal travel time with increasing fracture density. However this reduction is very small; on the order of 0.3 years reduction for an additional 10,000 fractures. The results for the PAWorks simulations are inconclusive; it is uncertain whether the travel time at T_{cutoff} equal to 10^{-9} m^2/s is anomalous. Ignoring the T_{cutoff} equal to 10^{-9} m^2/s result the travel times are approximately constant below T_{cutoff} equal to 6×10^{-9} m^2/s.

Figures 5-7 and 5-8 also show the PAWorks pipe network travel times are typically about a factor of 4 higher than the MAFIC network values. This could be due to lack of connectivity between individual portions of a single fracture in the PAWorks fracture networks. The effect of varying fracture connectivity is investigated in Section 6.

5.5 Pathway Effective Dispersion

The effective dispersion in the transport simulations is indicated by the difference in the median (t_{50}) and t_{85} travel time. The simulations presented on Figure 5-9 indicate that although the effective travel times vary between the PAWorks and MAFIC fracture networks, the relative dispersion (T_{85}/T_{50}) is similar.

5.6 Computer Resources (CPU Time and Memory)

The PAWorks CPU times for both fracture networks are presented against T_{cutoff} and the number of fractures in Figures 5-10 and 5-11 respectively. The CPU time presented excludes the transport component of the simulations, due to the number of MAFIC tracked particles and PAWorks searched pathways having a large influence on the total CPU required.

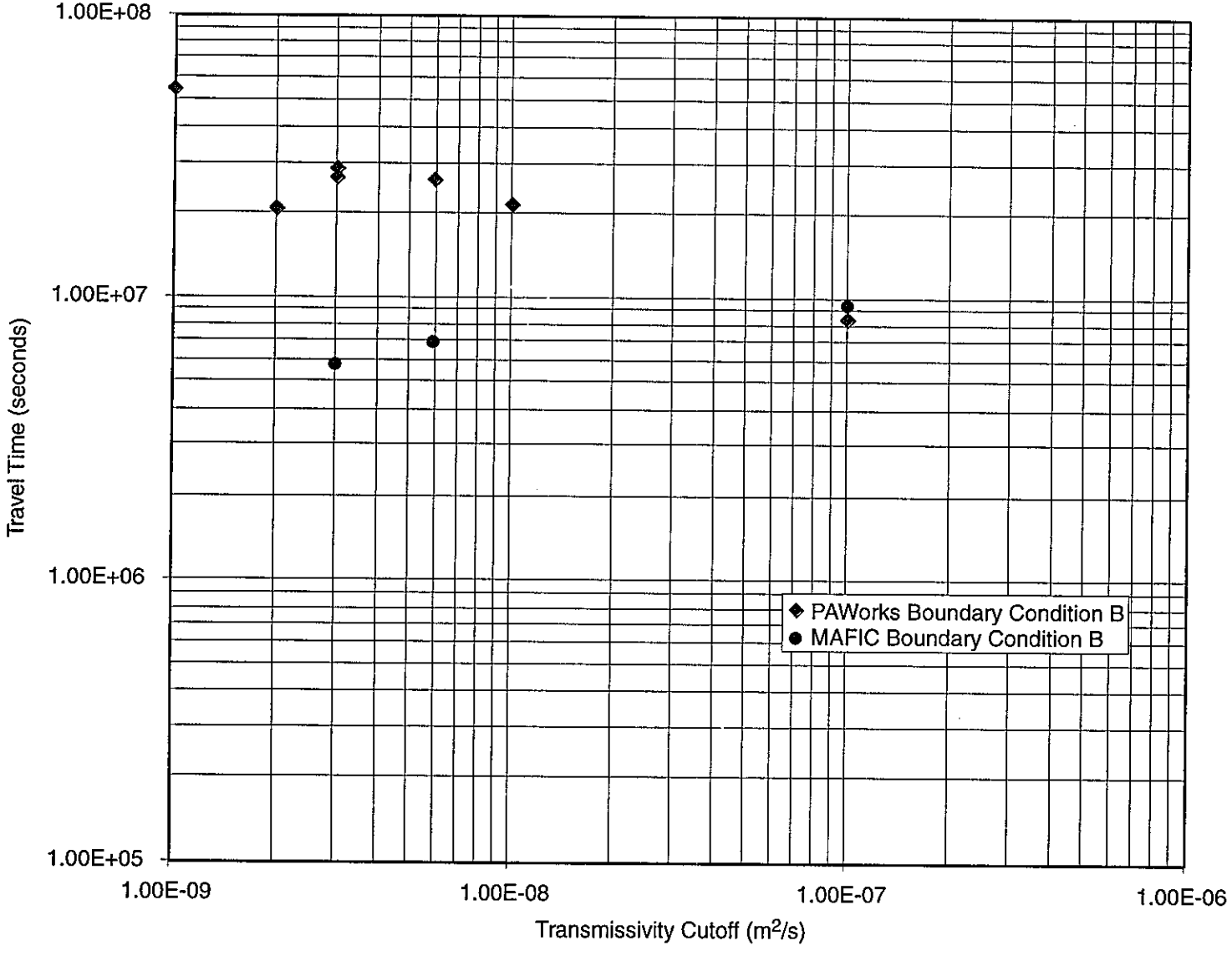

FIGURE **5-7**
MINIMUM TRAVEL TIME VERSUS TRANSMISSIVITY CUTOFF
PNC/PAW-LTG/JAPAN

PROJECT NO. 923 1089.824 DRAWING NO. 72747 DATE 11/21/97 DRAWN BY CB

Golder Associates

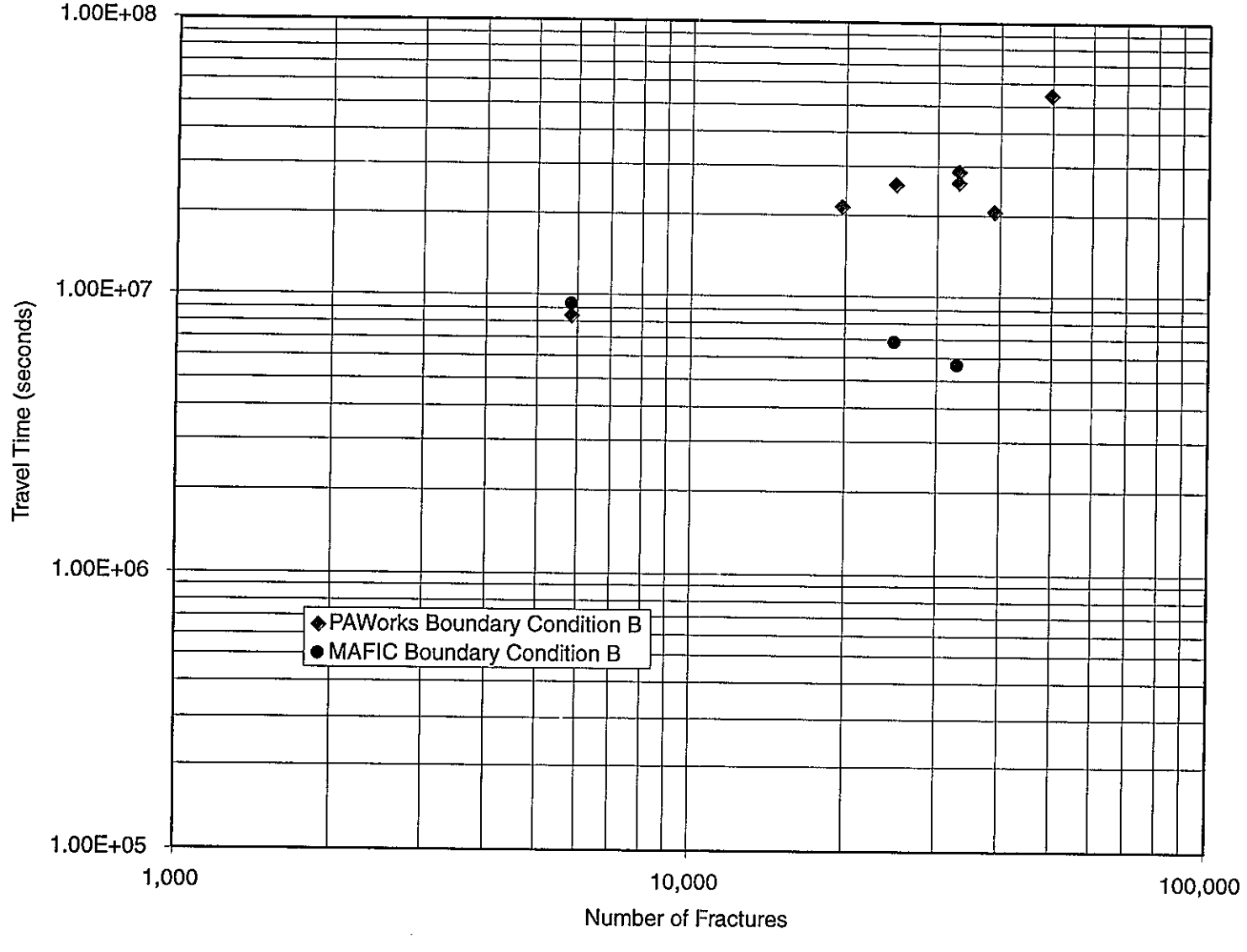

FIGURE **5-8**
MINIMUM TRAVEL TIME VERSUS NUMBER OF FRACTURES
PNC/PAW-LTG/JAPAN

PROJECT NO. 923 1089.824 DRAWING NO. 72748 DATE 11/17/97 DRAWN BY CB

Golder Associates

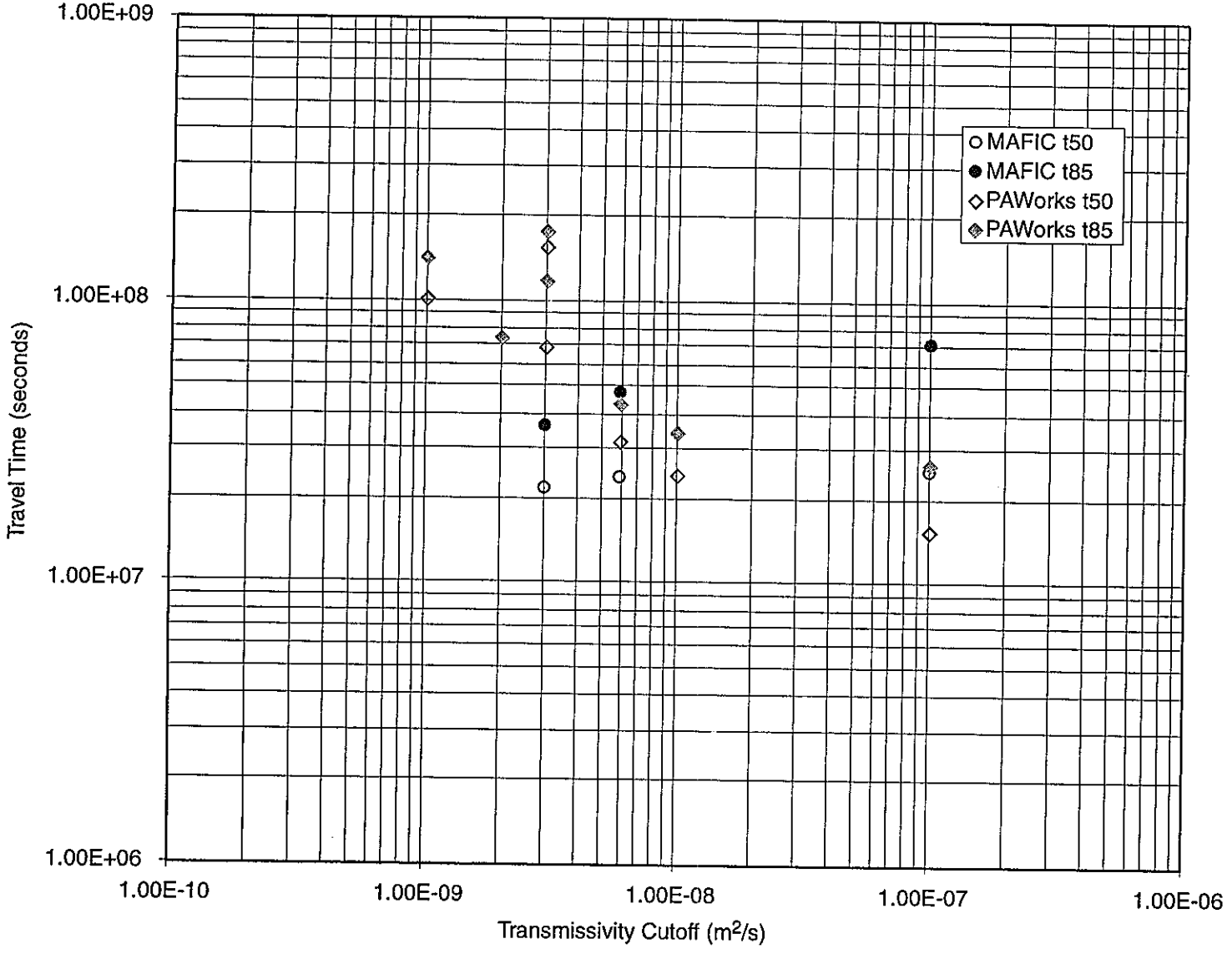

FIGURE **5-9**

EFFECTIVE DISPERSION IN TRAVEL TIME VERSUS TRANSMISSIVITY CUTOFF

PNC/PAW-LTG/JAPAN

PROJECT NO. 923 1089.824 DRAWING NO. 72739 DATE 11/24/97 DRAWN BY CB

Golder Associates

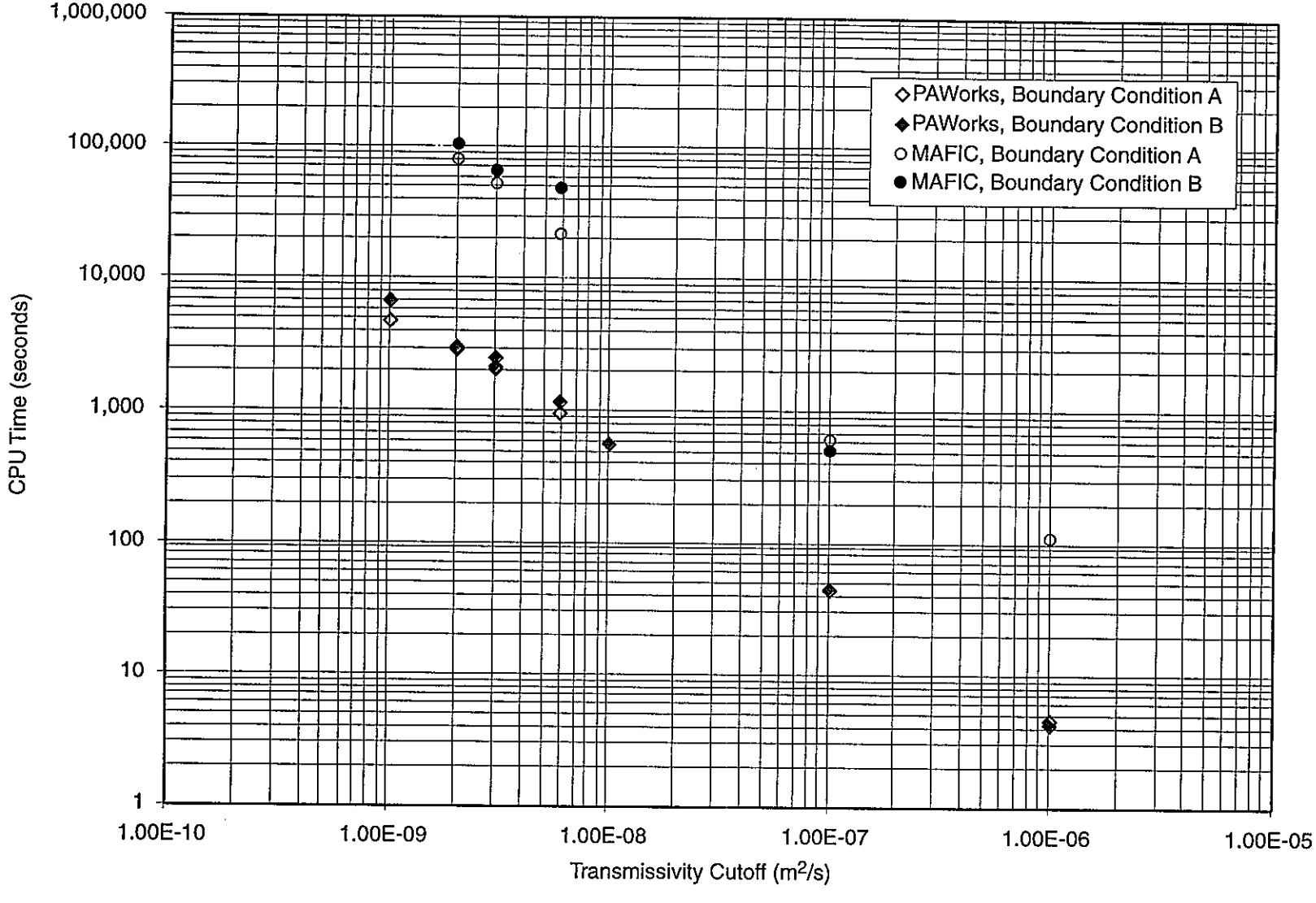

FIGURE **5-10**

REQUIRED CPU TIME VERSUS TRANSMISSIVITY CUTOFF, NO TRANSPORT

PNC/PAW-LTG/JAPAN

PROJECT NO. 923 1089.824 DRAWING NO. 72749 DATE 11/21/97 DRAWN BY CB

Golder Associates

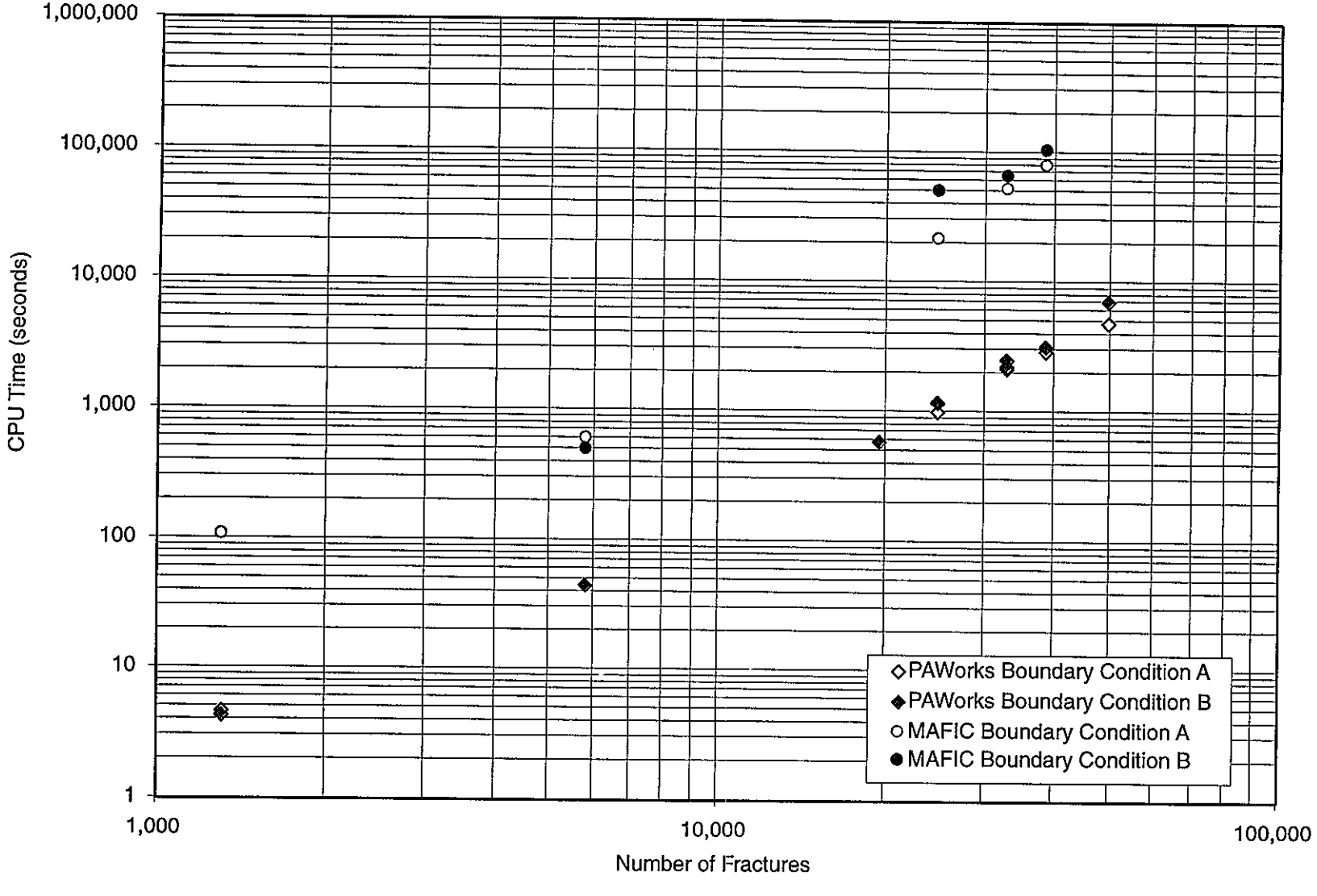

FIGURE **5-11**

REQUIRED CPU TIME VERSUS NUMBER OF FRACTURES, NO TRANSPORT

PNC/PAW-LTG/JAPAN

PROJECT NO. 923 1089.824 DRAWING NO. 72750 DATE 11/21/97 DRAWN BY CB

Golder Associates

For both PAWorks and MAFIC the required CPU time is power law proportional to the number of fractures, or the inverse of the transmissivity cutoff. The results indicate that the CPU time required to run the MAFIC fracture network is approximately two and a half orders of magnitude greater than that required for the PAWorks pipe network.

The memory requirement for MAFIC and PAWorks was tracked for the finite element solution of the flow equations, as these codes required the largest allocation. The required memory to run the MAFIC and PAWorks simulations are presented in Figures 5-12 and 5-13 against T_{cutoff} and number of fractures respectively. These figures show the memory required is power law proportional to the number of fractures and inversely proportional to the transmissivity cutoff. The figures also show that the MAFIC simulations require approximately 5 times as much memory as an equivalent PAWorks simulation.

5.7 Fracture Network Densities (PAWorks and MAFIC)

The analyses presented in Sections 3 and 4, and summarized in the preceding text, indicates that required transmissivity threshold to ensure that the addition of more lower transmissivity fractures will not affect the hydrogeological properties of the modelled network is variable. This threshold depends on the hydrogeological measure of interest (e.g. a different threshold is required for K_{eff} and head). The PAWorks fracture networks generally reached a non-varying solution at higher values of T_{cutoff} than the MAFIC counterpart. However, the simulations showed low transmissivity sensitivity on all the hydrogeological measures considered for minimum transmissivity values of 3×10^{-9} m^2/s or less. Therefore this threshold has been used for the PAWorks and MAFIC simulations presented in Sections 6 and 7.

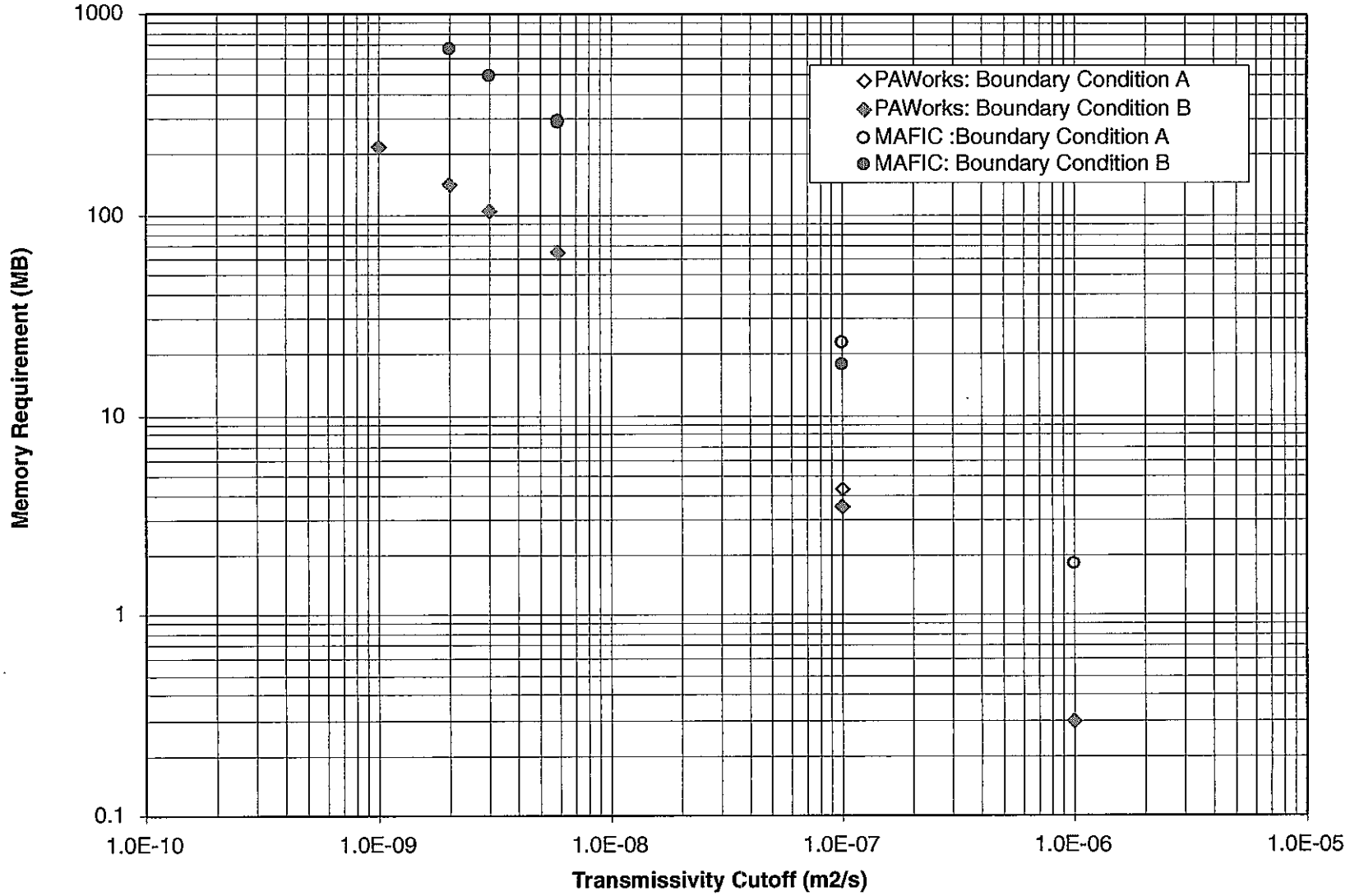

FIGURE **5-12**

MEMORY REQUIREMENT VERSUS TRANSMISSIVITY CUTOFF (NO TRANSPORT)

PNC/PAW-LTG/JAPAN

PROJECT NO. 923 1089.824 DRAWING NO. 74768 DATE 11/24/97 DRAWN BY TK

Golder Associates

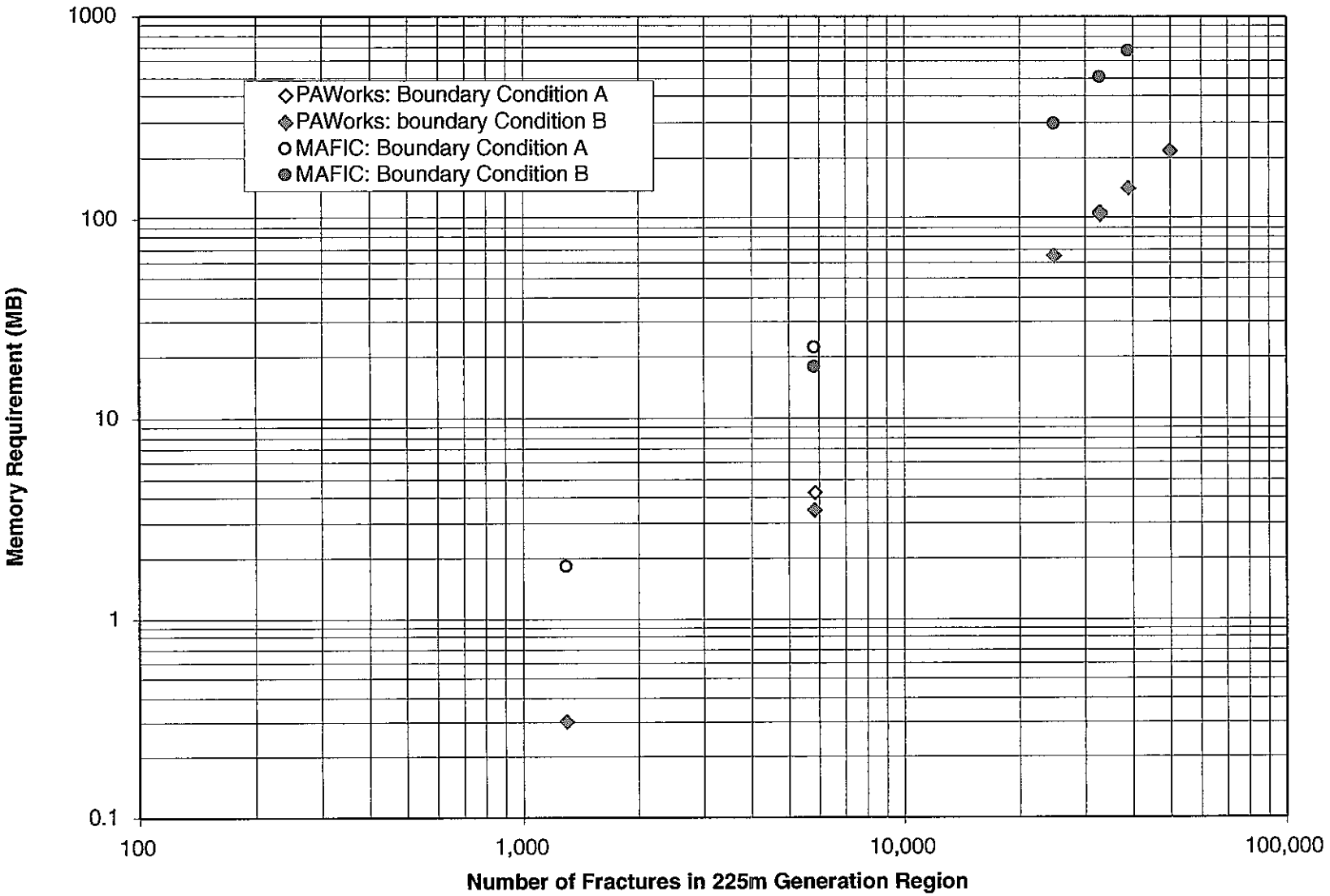

FIGURE **5-13**

MEMORY REQUIREMENT VERSUS NUMBER OF FRACTURES (NO TRANSPORT)

PNC/PAW-LTG/JAPAN

PROJECT NO. 923 1089.824 DRAWING NO. 74767 DATE 11/24/97 DRAWN BY TK

Golder Associates

6. EVALUATION OF PAWORKS BASED ON MAFIC SIMULATIONS

This section presents studies of the PAWorks assumptions which are necessary for the PAWorks 1-D approach to produce flow and transport results which are comparable to those obtained by MAFIC. The range of PAWorks assumptions to be studied includes:

I. Pipe Generation Options:

A. Pipes formed from the mid-point of all traces. The only restriction is that the newly formed pipe cannot cross an existing one

B. Same as (A) but with two additional restrictions: (i) Pipes cannot cross traces, (ii) each midpoint trace node has at least one pipe connected

C. Pipes added to (B) to ensure that all pipes on the same fracture are connected

D. Effective pipes added to (C) to reduce tortuous connections between nodes. An effective pipe is added when the distance from one node to another node on the same fracture is larger than the effective factor 'N' times the distance between the two nodes. This additional pipe must not cross the existing pipes.

The effective factor, N, is a factor greater than 1.0, and values in the range 1.2 to 3.0 are recommended.

The issues associated with pipe generation, and a pictorial explanation of the four pipe generation options are presented as Figures 6-1 and 2-4 respectively.

II. Pipe Width Options

A) $W = W_{min} * L_{min} + W_{max} * L_{max}$

B) $W = W_{area} * (W_{min} * L_{min} + W_{max} * L_{max})$

For option A

W = pipe width

L_{min} = length of the shorter trace

L_{max} = length of the longer trace

W_{min} = factor associated with the shorter trace (usually in the range 0-1)

W_{max} = factor associated with the longer trace (usually in the range 0-1)

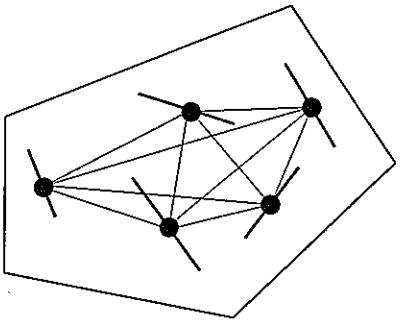

(a) Pipes crossing traces overconnect fracture

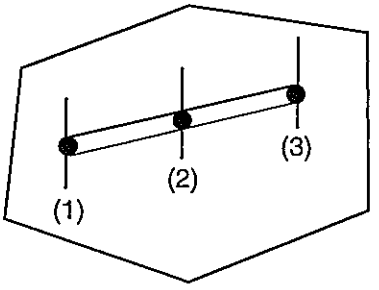

Pipe between (1) and (3) crosses trace (2), duplicates

(b) Double generation of pipes

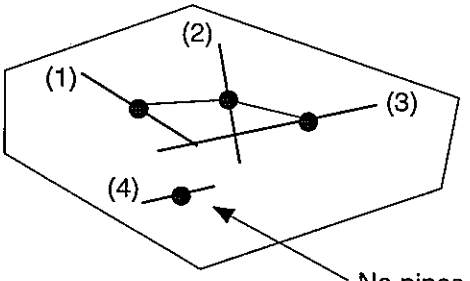

(c) Incomplete connectivity of fracture

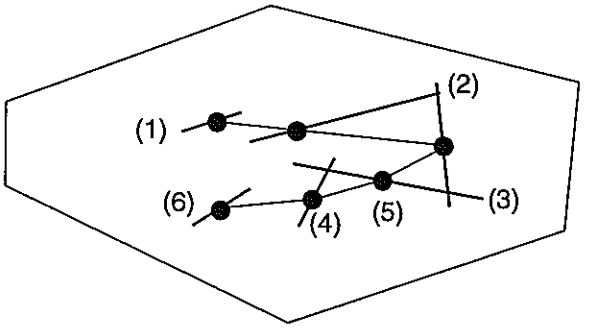

(d) Tortuous paths

FIGURE **6-1**
PIPE GENERATION ISSUES
PNC/PAW-LTG/JAPAN

PROJECT NO. 923 1089.824 DRAWING NO. 72754 DATE 11/24/97 DRAWN BY CB

Golder Associates

The user has the option to choose whether the trace length is the true trace length, or the length of the trace projected perpendicular to the orientation of the pipe.

Option B allows the pipe width of each pipe on the same fracture to be correlated to the fracture area. For the equation

$$W = W_{area} * (W_{min} * L_{min} + W_{max} * L_{max})$$

the terms are defined as;

W = pipe width
W_{area} = sum of $\{W_i * L_i\} / A_f$
W_i = width of pipe *i* on the fracture, $(X_{min}*L_{min} + X_{max}*L_{max})$
L_i = length of pipe *i* on the fracture
A_f = fracture area
L_{min} = length of the shorter trace
L_{max} = length of the longer trace
W_{min} = factor associated with the shorter trace (usually in the range 0-1)
W_{max} = factor associated with the longer trace (usually in the range 0-1)

Parameters which give a value of W_{area} of 1 assign the sum of the fracture and pipe areas to be equivalent.

6.1 Simulations Undertaken

A single MAFIC simulation was used as the reference case for evaluation of PAWorks options. Based on the sensitivity study presented in Section 5, the Kamaishi block with T_{cutoff} equal to 3×10^{-9} m^2/s (32,889 fractures in a 225m fracture generation region) was used with boundary condition "B" for the final simulations. The fracture geometry is as discussed in previous sections using the equation, aperture = $2.0\ T^{0.5}$.

The PAWorks simulations investigate a range of possible pipe generation and width options. The initial simulations concentrated on matching the flux between the MAFIC and PAWorks network simulations. With this achieved, the variation of travel times

using the differing methods of generating the pipes was investigated. The connectivity of the mesh obviously affects the flux and head distribution, therefore convergence to the optimum choice of pipe generation options for the Kamaishi bloch is an iterative process.

The PAWorks simulations used for the choice of pipe generation for the Kamaishi block are summarized in Table 6-1. Pipe width equation "A" combined with the projected trace length is used for all these simulations. Results are organized according to the comparative measures,

- Effective block hydraulic conductivity (K_{eff}),
- Head Distribution within the fracture network (H_{xyz})
- Minimum and Median transport time (t_0 and t_{50}),
- Effective network dispersion (t_{85} and t_{50}),

Table 6-1 PAWorks Simulations for Comparison to MAFIC

Simulation Name	Boundary Condition	Pipe Generation (A-D)	Eff. Pipe Path. Fac.	W_{min} (-)	W_{max} (-)
k1dss7a_d	B	D	2.0	0.5	0.5
k1dss7b_d	B	D	1.5	0.4	0.6
k1dss7c_d	B	D	1.5	0.5	0.7
k1dss7d_d	B	D	1.5	0.7	0.7
k1dss7e_d	B	D	1.5	0.75	0.75
k1dss7f_d	B	D	1.5	0.9	0.9

6.2 Effective Hydraulic Conductivity

The simulation effective hydraulic conductivities are presented on Figure 6-2. The results indicate that with an effective pipe factor of 1.5 and a width factor of 0.75 the block effective hydraulic conductivities of the MAFIC and PAWorks simulations are similar.

6.3 Travel Time and Effective Dispersion

The results of the comparison between the MAFIC travel time and that derived from the PAWorks simulations are shown in Table 6-2. The results show that the PAWorks transport times are almost exactly half the MAFIC results for the fastest, T_{50} and T_{85} travel times when the effective pipe factor is set equal to 1.5.

Table 6-2 Comparison of PAWorks and MAFIC Travel Times

Simulation Name	Eff. Pipe Path. Fac.	X_{min} (-)	X_{max} (-)	T_{min} (years)	T_{50} (years)	T_{85} (years)
K3dss7a (3-D case)	N/A	N/A	N/A	2.43	7.97	13.51
k1dss7a_d	2.0	0.5	0.5	6.62	13.53	17.48
k1dss7b_d	1.5	0.4	0.6	6.48	15.18	29.33
k1dss7c_d	1.5	0.5	0.7	6.48	15.18	29.33
k1dss7d_d	1.5	0.7	0.7	6.48	15.18	29.33
k1dss7e_d	1.5	0.75	0.75	6.48	15.18	29.33
k1dss7f_d	1.5	0.9	0.9	6.48	15.18	29.33

For the simulations undertaken in Section 7 the k1dsse_d pipe network was used. This results in slower travel times than the MAFIC simulations, but with a near constant scaling factor.

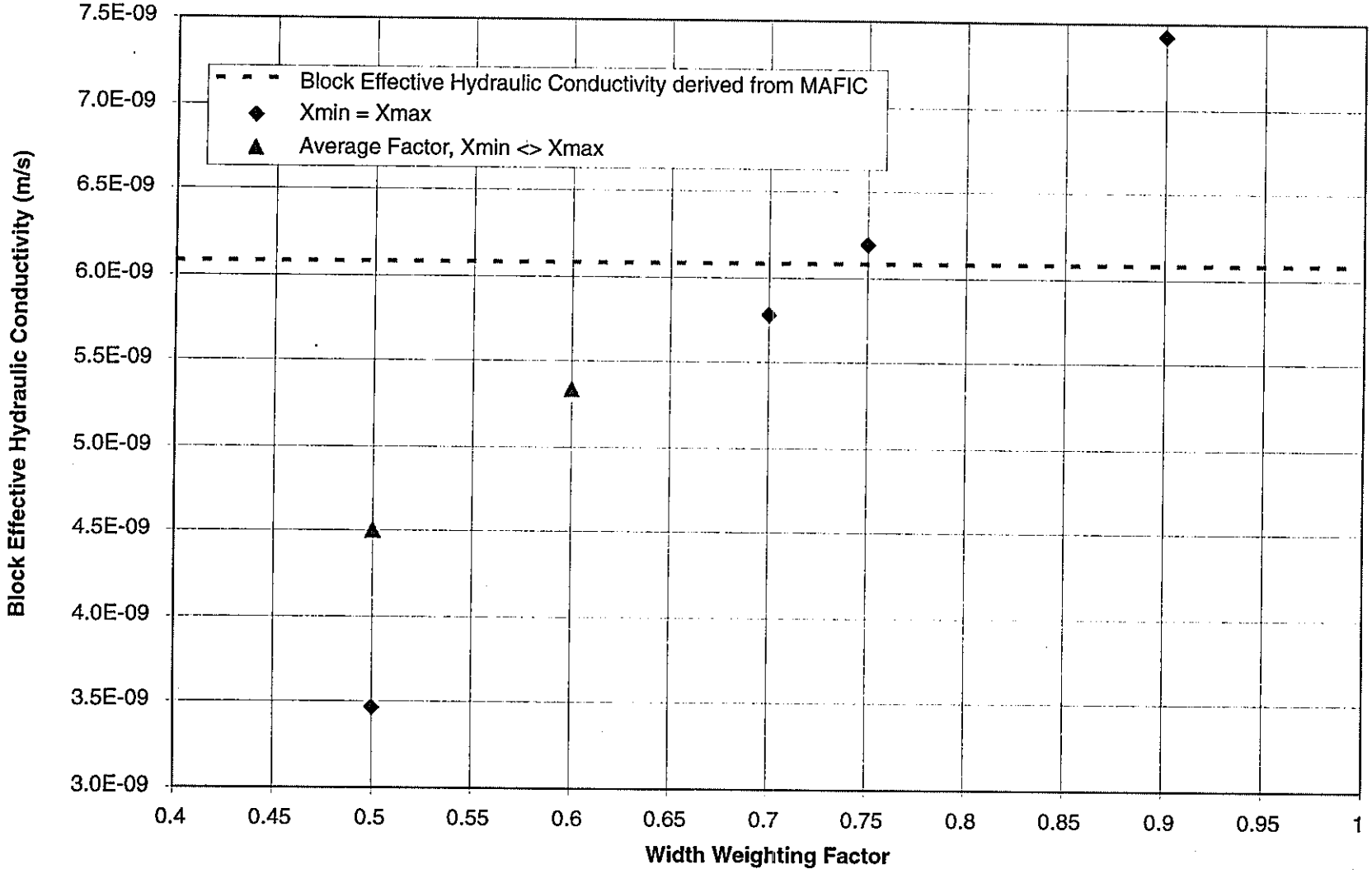

FIGURE **6-2**
EFFECTIVE HYDRAULIC CONDUCTIVITY VERSUS WIDTH WEIGHTING FACTOR
PNC/PAW-LTG/JAPAN

The MAFIC and PAWorks codes do not use the same algorithm for finding the travel times, and therefore some difference in transport times should be expected. MAFIC releases a number of particles at the upstream boundary, the number being assigned to each fracture being in proportion to the flow in that fracture. Each particle group is then individually monitored as it moves through the network, and at each fracture junction the number of particles moved to each connected fracture is proportional to the flow in the fracture. Hence, the particles are preferentially moved into higher flow pathways.

The PAWorks pathway search algorithm is structured differently. For each source a specified number of pathways will be created (if available pathways exist). Assuming the user specifies a flux search, all pipes downstream of the source will be assigned a weight in proportion to the flow in the pipe. The search algorithm moves through the network always moving through the next highest flow pipe which is connected to any pipe which has already been traversed. This means that the search algorithm typically moves through the network in a non-continuous manner. And while the first traversed pathway has the highest fluxes observed during the traversal, it does not necessarily have the highest weighted flux. In addition, for the second traversal, no pipes may be accessed from their upstream end (excluding the final pipe which is never marked as visited). Conceptually it is like adding branches to a tree; you may grow the branch, but not pass through an existing branch. This means that the penultimate pathway pipes are only ever used once, and that new pipes cannot leave the tree and then re-enter at a different location.

The travel times in the MAFIC and PAWorks higher flux pathways could be matched more closely by using a different traversal algorithm. This is outside the scope of the current report. However, it is important to note that the traversal algorithm only affects the PAWorks traversal and representative pathway properties. The pathway search algorithm has no effect on the PAWorks/LTG analyses. PAWorks/LTG uses the entire downstream pipe network, and flow is assigned in accordance with the full finite element flow solution.

6.4 CPU and Memory Requirements

The memory and CPU requirements of the MAFIC and PAWorks simulations are presented in Table 6-3.

The transport memory requirements are not given because the amount of memory required is a function of the number of particles tracked. However, as a guide the MAFIC simulation with 108 tracked particles required allocation of 780 MB of memory. The PAW pathways analysis required 160 MB for 100 pathways. For this dense fracture network the PAWorks transport analysis required approximately 6 hours of additional CPU time, while the MAFIC analysis required only an additional 2.1 hours.

Table 6-3 Comparison of PAWorks and MAFIC CPU & Memory Requirements

Simulation Name	Eff. Pipe Path. Fac.	X_{min} (-)	X_{max} (-)	CPU (hours)	Memory (MB)
K3dss7a (3-D case)	N/A	N/A	N/A	18.4	490.81
k1dss7a_d	2.0	0.5	0.5	0.75	124.84
k1dss7b_d	1.5	0.4	0.6	0.76	138.62
k1dss7c_d	1.5	0.5	0.7	0.77	138.62
k1dss7d_d	1.5	0.7	0.7	0.76	138.62
k1dss7e_d	1.5	0.75	0.75	0.76	138.62
k1dss7f_d	1.5	0.9	0.9	0.76	138.62

7. PERFORMANCE ASSESSMENT DEMONSTRATION CALCULATIONS

This chapter of the report presents a series of demonstration computations, which indicate how the PAWorks suite of codes may be used to undertake full performance assessment computations, or be used to generate input parameters for other PA codes such as Crystal.

7.1 PAWorks / RIP Cross Verification

This section describes a series of simulations which compare the results from the PAWorks/LTG code with those from the Repository Integration Program (RIP). The purpose of the comparison was to determine whether two codes which treat hydrogeological phenomenon in entirely differently numerically would produce similar results. Thereby increasing confidence in both conceptualizations.

This section presents one of two demonstration applications of the Laplace Transport Galerkin (LTG) component of PAWorks. The LTG component was added to PAWorks to simulate the advective-dispersive transport of multi-species decay chain through a network of interconnected one-dimensional pipes in three-dimensional space.

For generality, the LTG decay chain can be either straight or it can be comprised of a complex branching network where each daughter species can have multiple parent species. The model can also accommodate processes known to be important in the context of radionuclide transport in the subsurface such as 1) diffusion from the pipes containing mobile groundwater into the surrounding rock matrix containing immobile groundwater, 2) diffusion into the immobile porewater within the fracture "plane" attached to a pipe containing the flowing groundwater, 3) diffusion from the mobile groundwater in a pipe to attached "dead-end" pipes that contain immobile groundwater and 4) diffusion into fracture infilling or surface-coating material. Thus, in general, each pipe containing the flowing groundwater can be connected to multiple interacting immobile porosity zones. The model also allows for the sorption of the solutes onto the geologic materials within each immobile zone, including sorption onto the surfaces of the pipes in the network.

The RIP code is a performance assessment code used extensively for modeling radionuclide transport from nuclear repositories. A description of the RIP code is given in the Section 7.2, and a more complete description of this code may be found in the RIP Theory Manual and User's Guide (1997).

The comparison LTG and RIP simulations were all run on a 200m fracture pathway. The pathway had either constant properties along its length, or it was split into 50m sections each having a separate set of properties. Different aspects of the LTG model (e.g. surface sorption, matrix diffusion) were progressively added to the LTG and RIP models and the results of the simulation compared.

The RIP model comprised of 20 cells in series, each representing 10m of the pathway length. Associated with each of the pathway cells were 20 matrix diffusion cells, each containing a connection from the pathway to the diffusion cell. Figure 7-1 schematically represents the RIP model configuration. Every RIP cell has a volume, turnover rate (equivalent to flow rate which is set to zero to represent a matrix diffusion volume), and connections to adjacent cells. However, the RIP cell does not have any explicit geometry. The RIP model has an internal dispersion length of 5m which is a function of the spatial discretization.

The LTG model comprises 200 elements each of length 1.0m. To be consistent with the RIP simulations a dispersion length of 5.0m was used for all the realizations.

The upstream boundary condition for all the simulations was an assigned concentration which remained constant for the duration of the analysis. The results are presented as relative concentration, C/C_0.

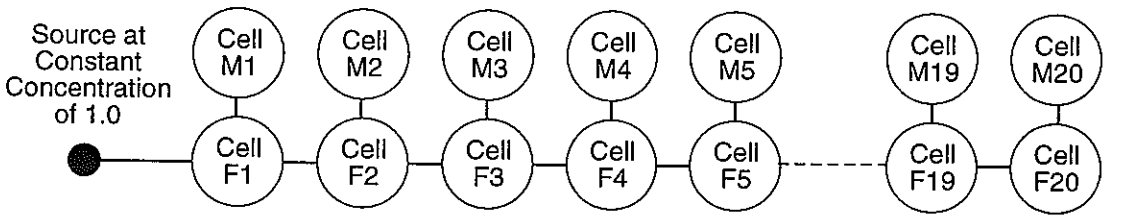

F = Fracture cell
M = Matrix diffuison cell

FIGURE **7-1**
CELL CONFIGURATION USED FOR THE RIP MODEL
PNC/PAW-LTG/JAPAN

PROJECT NO. 923 1089.824 DRAWING NO. 73171 DATE 5/13/97 DRAWN BY EA

Golder Associates

The input parameters are tabulated in Table 7-1. The problem material parameters were based on the range of values presented in "Research and Development on Geological Disposal of High-Level Radioactive Waste, First Progress Report, September, 1992", referenced in this section as PNC (1992). Parameters such as the path length were based on the initial PAWorks computations.

Table 7-1 Material Input Parameters for the PAWorks / RIP Cross Verification

Property	Value	Reference
Pathway length	200 m	Approx. tortuous length from initial PAWorks simulation
Pathway width	4.7 m	Approx. tortuous length from initial PAWorks simulation
Aperture	10^{-4} m	Assumed
Velocity[1]	8×10^{-6} m/s	Computed from travel time of initial PAWorks simulation
Matrix density	2700 kg/m^3	Assumed
Matrix porosity	0.01	p 4-128, PNC 1992
Infill thickness	5 mm	Assumed
Infill density	2650 kg/m^3	Assumed
K_d for Am-243	0.1 m^3/kg	From range Table 4.5-1 , PNC 1992
K_d for Pu-239	0.25 m^3/kg	From range Table 4.5-1 , PNC 1992
Diffusion thickness	0.1 m	Facsimile from Masahiro Uchida
Rock eff. diffusivity	10^{-11} m^2/s	Facsimile from Masahiro Uchida
Dispersion length	5 m	Based on RIP discretisation

[1] The velocity was reduced for simulations case_v1 and case_v2 to allow integer year step sizes within RIP

The comparison consists of eleven simulations which range from very simple cases where the exact solutions are known, to more complex simulations where the results are not amenable to simple analytical solution. A summary of the simulations undertaken is shown in Table 7-2, and the results of the simulations are discussed individually in the following paragraphs.

Table 7-2 Summary of PAWorks / RIP Comparison Simulations

Simulation	Verification	Summary
case_v1	velocity	advective velocity in single property pipeline
case_v2	velocity	advective velocity in multiple property pipeline
case_s1	sorption	surface sorption in single property pipeline
case_s2	sorption	surface sorption in multiple property pipeline
case_d1	diffusion	diffusion in single property pipeline ($D_0=10^{-9}$ m^2/s)
case_d2	diffusion	diffusion in multiple property pipeline ($D_0=10^{-9}$ m^2/s)
case_d3	diffusion	diffusion in single property pipeline ($D_0=10^{-11}$ m^2/s)
case_r1	retardation	matrix retardation and diffusion in single property pipeline ($D_0=10^{-9}$ m^2/s)
case_r2	retardation	matrix retardation and diffusion in multiple property pipeline ($D_0=10^{-9}$ m^2/s)
case_r3	decay	matrix retardation, diffusion and decay in single property pipeline ($D_0=10^{-9}$ m^2/s)
case_r4	retardation	matrix retardation and diffusion in single property pipeline ($D_0=10^{-11}$ m^2/s)

The first simulations undertaken were a comparison of the advective transport time in the fracture. For these two simulations, case_v1 and case_v2, a lower pathway velocity (1/100 of the PAWorks velocity) was used as RIP requires that the time output be an integer number. For the units of meters and years, reducing the velocity by 100 changes the advective travel time from 0.8 years to 80 years in the base case; allowing use of integer years for consideration of transient results. This simulation could have been run in units of seconds instead of years, but it was more convenient to alter the pathway velocity. Case_v1 therefore assumes a unretarded velocity of 2.5246 m/yr. The comparison of the PAWorks and RIP results for this simulation at an elapsed time of 40 years are shown in Figure 7-2. The figure shows excellent agreement between the results from both codes. The distance the solute would have traveled in 40 years is 101m, and it will be observed that the 50% concentration is located at this distance along the fracture.

The second velocity comparison, case_v2, assumes varying properties along the fracture, and is more representative of typical fracture networks where fracture properties vary spatially. The 200m fracture is split into four 50m sections, each with a separate set of properties. This set of four different property pipes is used for many of the following

simulations, assuming the same pipe geometry. These properties are tabulated in Table 7-3, and shown pictorially in Figure 7-3.

Table 7-3 Properties of the 50m Fracture Sections

Property	Pipe Type 1	Pipe Type 2	Pipe Type 3	Pipe Type 4
Length (m)	50	50	50	50
Width (m)	4.7	4.7	2.35	9.4
Perimeter (m)	9.4	9.4	4.7	18.8
Aperture (m)	1.00E-04	2.50E-05	2.00E-04	1.00E-04
Area (m^2)	4.70E-04	1.18E-04	4.70E-04	9.40E-04
Unretarded Velocity (m/s)[1]	8.00E-06	3.20E-05	8.00E-06	4.00E-06
Unretarded Velocity (m/yr)[1]	252.3	1009.2	252.3	126.1
Flux (conserved) (m^3/s)	3.76E-09	3.76E-09	3.76E-09	3.76E-09
Flux (conserved) (m^3/yr)	4.47744E-06	4.47744E-06	4.47744E-06	4.47744E-06
Individual pipe length (m)	1.0	1.0	1.0	1.0
Max. pipe length for numerical Pe=2 (m) [2]	10	10	10	10
Retardation due to Sorption, Am-243	26501	106001	13251	26501
Immobile zone depth (m)	0.1	0.1	0.1	0.1
Immobile zone porosity	0.01	0.01	0.01	0.01
Immobile zone Volume/length (m^3/m)	0.94	0.94	0.47	1.88
Diffusion coefficient (m^2/yr)	3.156E-02	3.156E-02	3.156E-02	3.156E-02
Diffusion length (m)	5	5	5	5
α (m/yr)	0.00473364	0.00473364	0.00473364	0.00473364

[1]The velocity and flux values shown in the table correspond to the typical simulation parameter values; in case_v2 these values were reduced by a factor of 100, as described in the text.

[2]The numerical Peclet number is given by $Pe = \frac{velocity \Delta x}{(D_0 + dispersion\,length velocity)}$ where D_0 is the free water diffusivity ($=10^{-9}$ m^5/s)

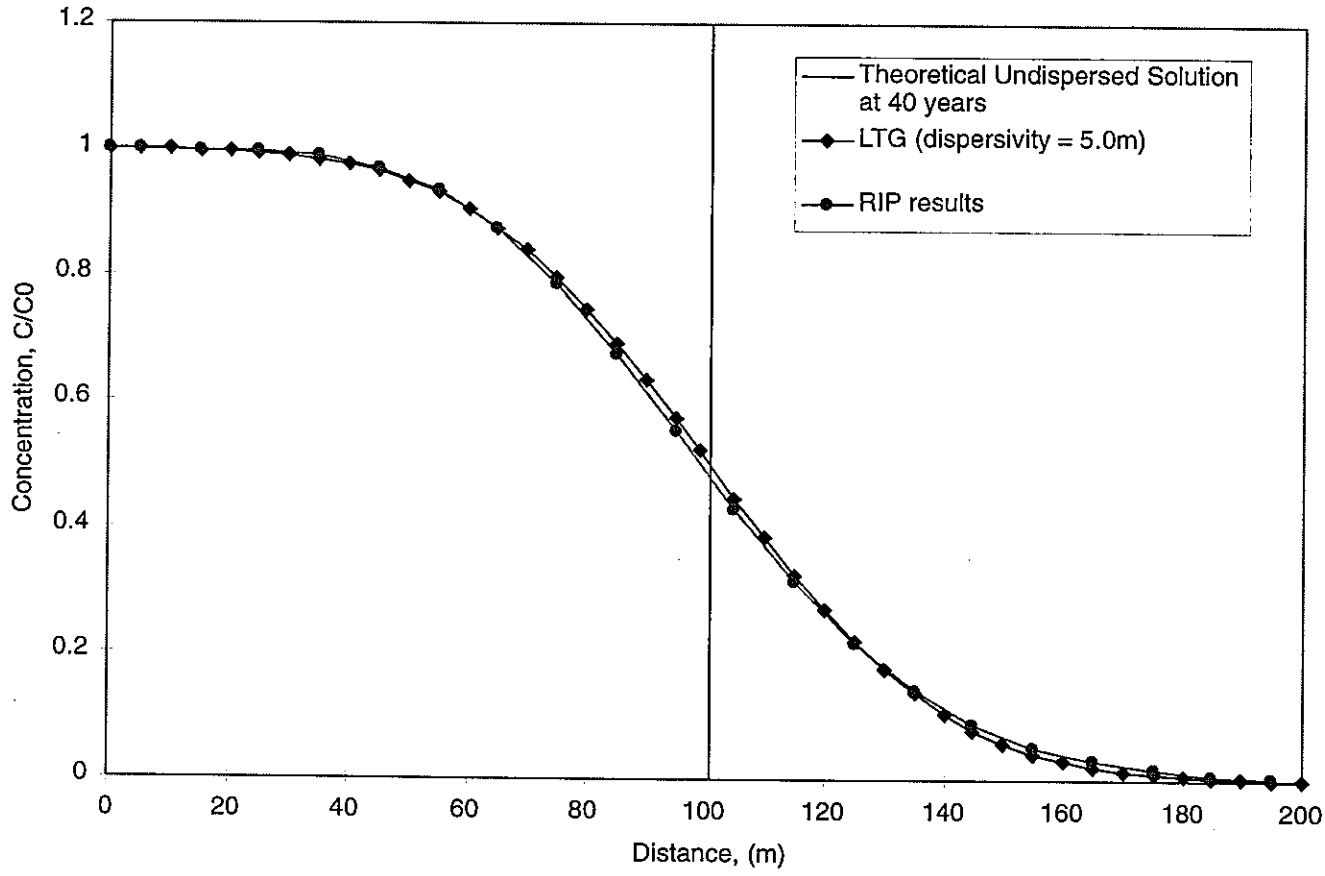

FIGURE **7-2**
CASE VI, CONSTANT VELOCITY OF 2.5246 M/YR: TIME = 40 YEARS
PNC/PAW-LTG/JAPAN

PROJECT NO. 923 1089.824 DRAWING NO. 73174 DATE 11/17/97 DRAWN BY EA

Golder Associates

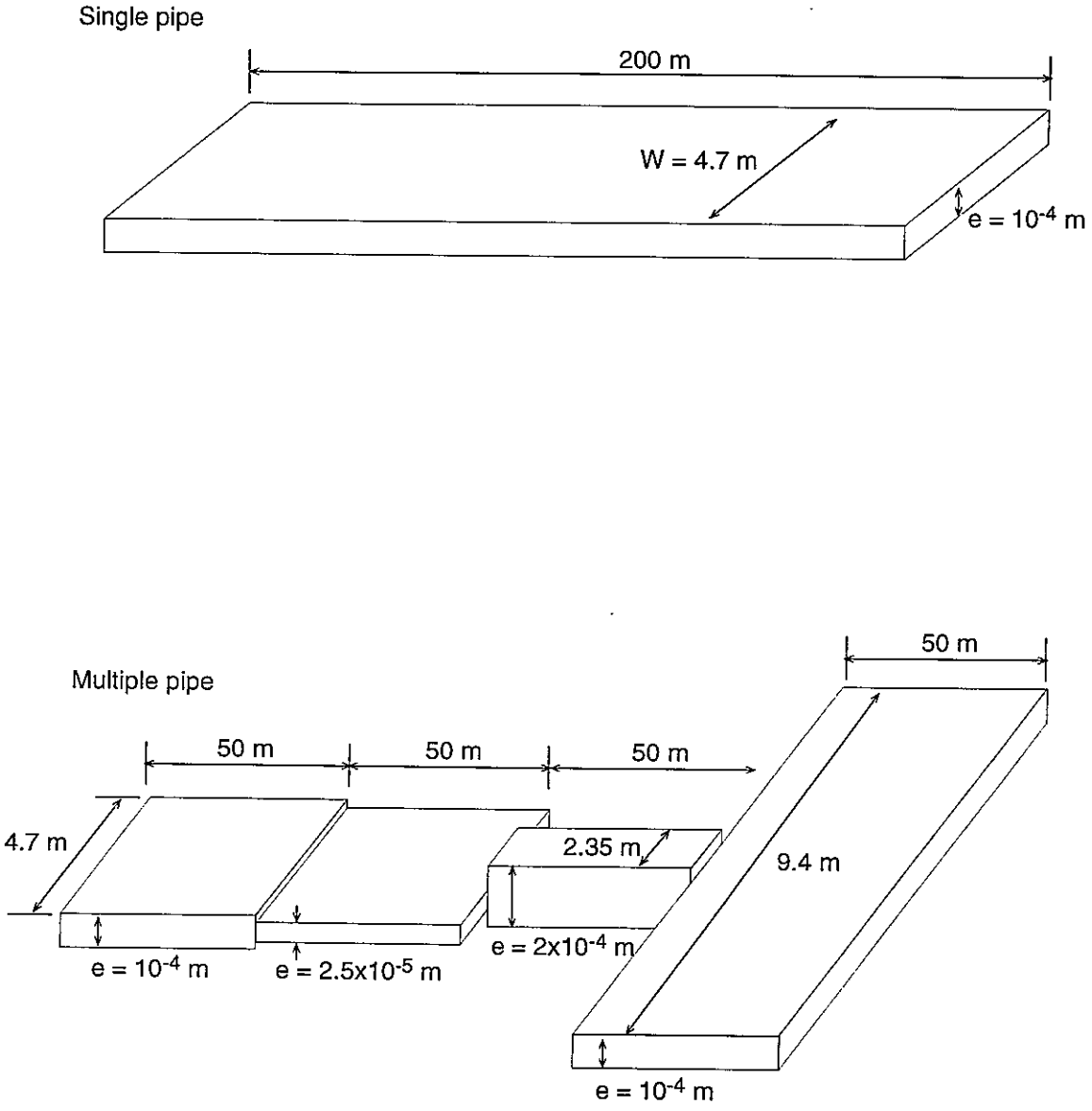

FIGURE **7-3**
SINGLE AND MULTIPLE PIPE MODEL
PNC/PAW-LTG/JAPAN

PROJECT NO. 923 1089.824 DRAWING NO. 73170 DATE 5/12/97 DRAWN BY EA

Golder Associates

The varying velocity of the case_v2 simulation, tests that both the PAWorks and RIP codes model varying property flow accurately. The results of the unretarded velocity comparison at 40 years is shown in Figure 7-4. The results show an excellent match between the two codes. For this set of properties the solute would have traveled 138.5m in forty years with no dispersion. The 50% concentration is at this value.

The case_s1 simulation includes surface sorption in the modeled transport computations. A value of distribution coefficient for surface sorption, K_a, was not explicitly noted in PNC (1992), therefore K_a was computed from the bulk distribution coefficient, K_d, using the equation;

$$K_a = K_d * \text{infill thickness} * \text{rock density}$$

where K_a has the units $(m^3/kg)(m)(kg/m^3)$ or m

The LTG component of the PAWorks code requires the surface sorption input in the form of an equivalent retardation, given by $R_s = 1 + 2/e.K_a$, where e is the aperture of the pipe. For the radionuclide Am-243, this resulted in an effective retardation of 26501.

RIP does not explicitly include surface sorption. However, sorption can be by adding a mass of sorptive material to the relevant pathway cell. In this example the sorptive material is conceptually a mass of infill on the fracture surfaces. The infill is assigned a K_d and this is used to compute the transport behavior of the fracture system.

The results of the single property fracture sorption simulation at 10,000 years elapsed time, case_s1, are presented in Figure 7-5. The figure shows excellent agreement between the PAWorks and RIP results. The fracture velocity is 252.3 m/yr. Based on a retardation of 26,501 the distance traveled in 10,000 years is 95.3m. The 50% concentration is very close to this value.

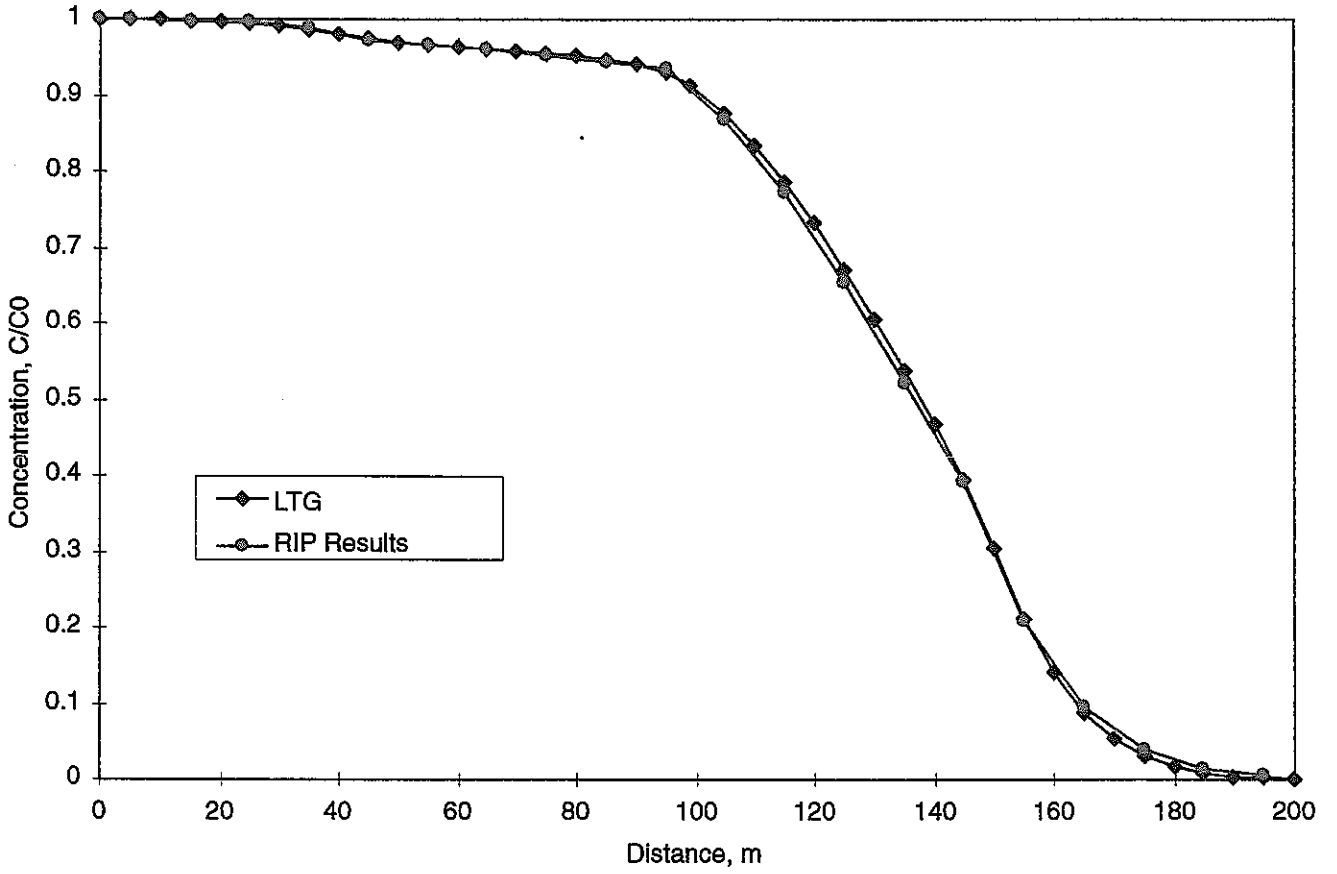

FIGURE **7-4**
CASE V2, VARIABLE VELOCITY AT TIME = 40 YEARS
PNC/PAW-LTG/JAPAN

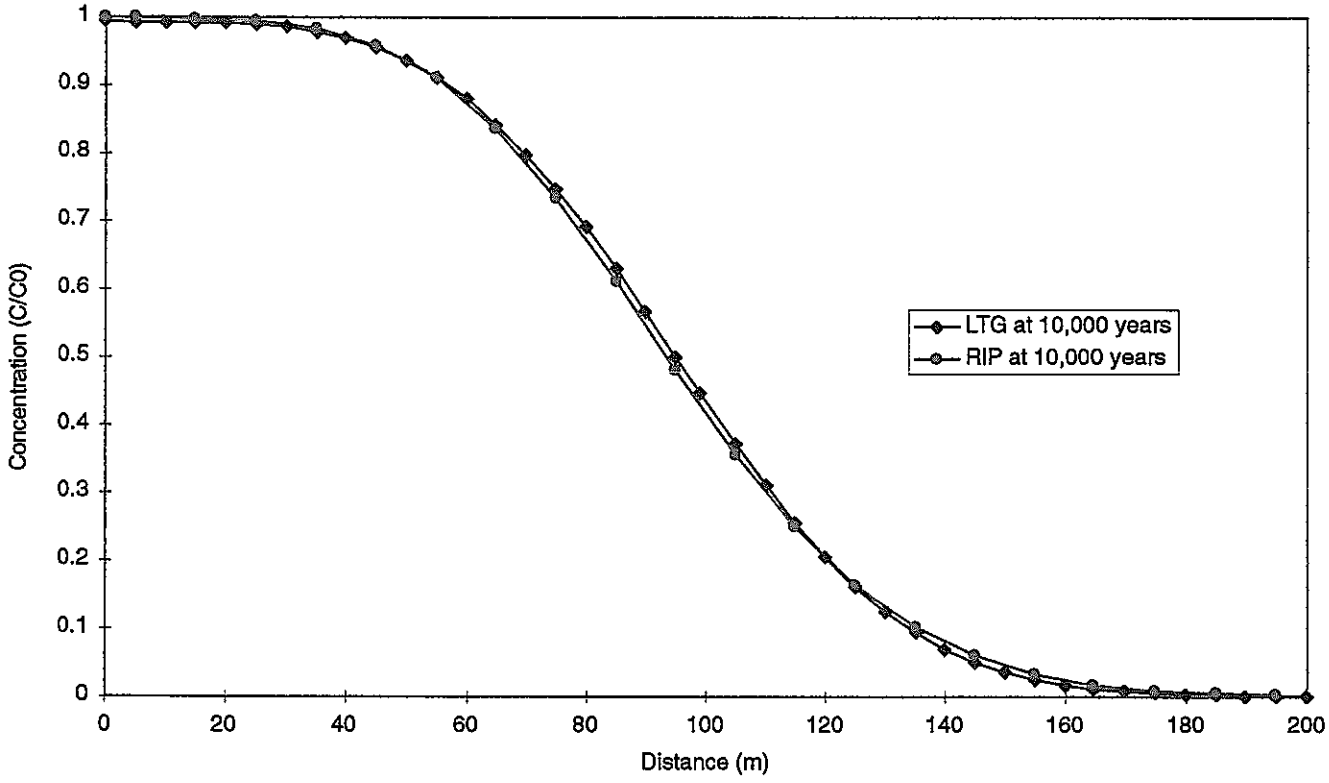

FIGURE **7-5**

CASE SI, SINGLE PROPERTY PIPE - RETARDATION DUE TO SURFACE SORPTION (Am) = 26501

PNC/PAW-LTG/JAPAN

PROJECT NO. 923 1089.824 DRAWING NO. 73176 DATE 5/12/97 DRAWN BY EA

Golder Associates

The results from the multiple property pipe version of the same simulation, case_s2, are presented in Figure 7-6. As the retardation due to surface sorption is related to the fracture aperture, which now varies along the pathway, each pipe type has a separate retardation velocity. This is shown on the concentration distribution in Figure 7-6, which indicates a change in the slope of the concentration curves at 150m, 100m, and to a lesser degree 50m. As in the previous examples the results from the RIP and LTG simulations are essentially the same. The distance traveled by a particulate undergoing no dispersion in 10,000 years would be 95.2m. The 50% concentration is again very close to this value.

In the next three simulations the surface sorption is set to zero, and diffusion occurs between the main fracture and the fluid in the rock matrix. Two values of diffusion were considered, to indicate the sensitivity of the solution to the assumed parameters.

Within PAWorks, diffusion is modeled in the LTG code by assigning a diffusion coefficient (the free water diffusion coefficient not accounting for porosity) for each radionuclide. For transport to each immobile zone (in this example the rock matrix porosity) a diffusion distance, porosity and tortuosity are assigned. In these examples the diffusion distance was 0.1m, the rock matrix porosity was 0.01, and tortuosity was assumed as unity.

RIP models the diffusion process as transport across the cell boundaries. In the RIP model used for these examples each of the fracture cells has a non-advective rock matrix cell associated with it. Solute may move from a fracture cell to a matrix cell by diffusion across the connection.

The first diffusion case considered is case_d1, which assumes a single property fracture for the 200m pathway, and a free water diffusion coefficient of 10^{-9} m^2/s. The resulting concentration distribution at an elapsed time of 4 years is shown in Figure 7-7. The match between the LTG and RIP simulations is excellent.

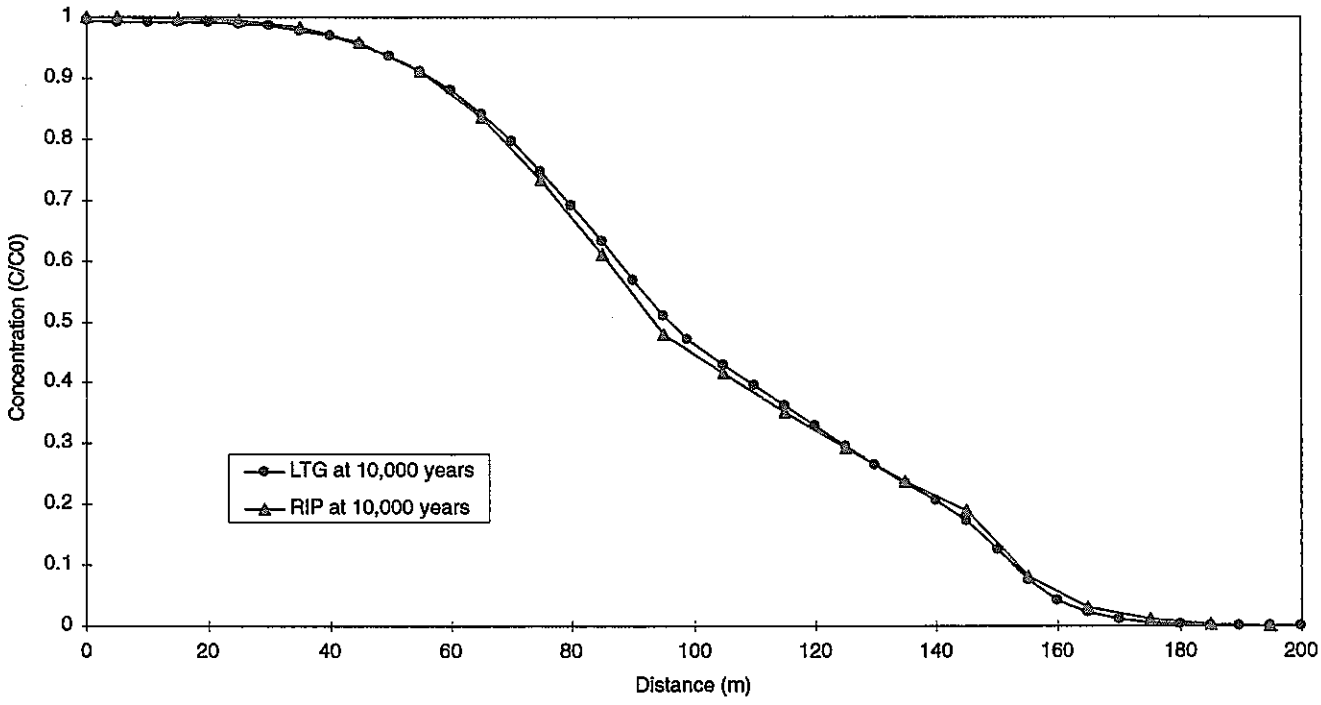

FIGURE **7-6**

CASE S2, MULTIPLE PROPERTY PIPE - RETARDATION DUE TO SURFACE SORPTION (Am)

PNC/PAW-LTG/JAPAN

PROJECT NO. 923 1089.8240 DRAWING NO. 73177 DATE 5/12/97 DRAWN BY EA

Golder Associates

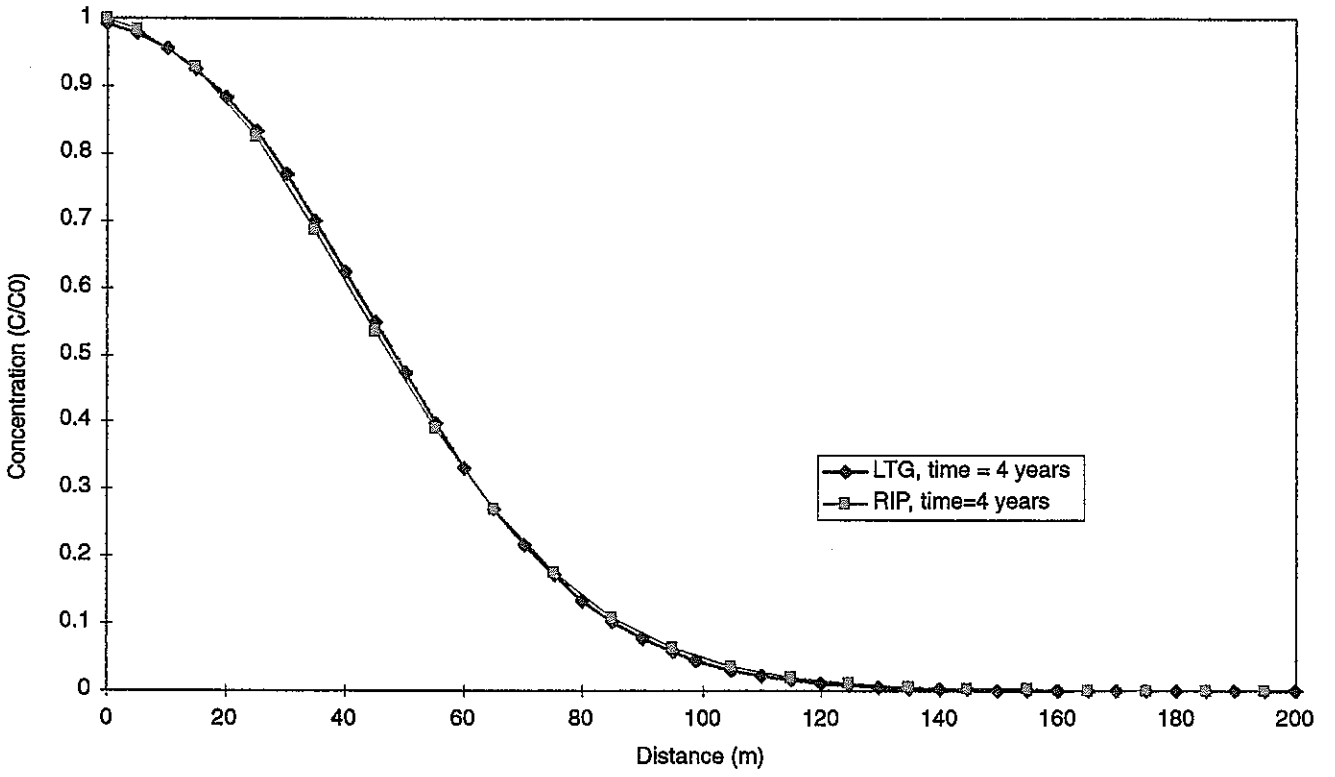

FIGURE **7-7**

CASE D1, SINGLE PROPERTY PIPE - DIFFUSION = 1.e-9 m2/S, NO DECAY

PNC/PAW-LTG/JAPAN

The second diffusion example is case_d2, which incorporates the four 50m pipes with differing properties for the 200m pathway, with the original free water diffusion coefficient of 10^{-9} m^2/s. The resulting concentration distribution at an elapsed time of 4 years is shown in Figure 7-8. Compared with the single pipe example, higher concentrations are observed further along the pipeline, due to the higher velocity in pipe type 2 than pipe type 1 (used for the constant property example). However, in this simulation the pipe intersections are obscured the concentration distribution. As in previous examples, there is a close match between the PAWorks and RIP simulations.

The third diffusion case, case_d3, assumes a single property fracture for the 200m pathway similar to case_v1, but in this simulation a free water diffusion coefficient of 10^{-11} m^2/s is used. The resulting concentration distribution at an elapsed time of 4 years is shown in Figure 7-9. The match between the PAWorks and RIP simulations is again excellent. However, the concentration distribution in Figures 7-7 and 7-9 show a completely different behavior. The lower diffusivity results in much lower movement of the solute into the rock matrix, resulting in release to the AE at earlier time.

The final four cases build on the previous simulations, and add retardation within the rock matrix to diffusion. Conceptually, the process comprises diffusion from the fracture into the rock matrix, and once inside the rock matrix the solute is then available to be sorbed onto the rock.

The PAWorks LTG code allows for retardation in the rock matrix by assigning a retardation value to the immobile zone. In these simulations the retardation of Am-243 was used, computed from $R_m = 1 + \rho/n.K_d$, where ρ is the rock matrix bulk density, n is the matrix porosity, and K_d is the partition coefficient for Am-243. For these examples, R_m= 27,001. The RIP code models the rock matrix sorption by associating a mass of rock and K_d value with the rock matrix cells.

The results for the case_r1, a single property fracture with a free water diffusion coefficient of 10^{-9} m^2/s, are presented in Figure 7-10. The results show excellent agreement between the RIP and PAWorks simulations.

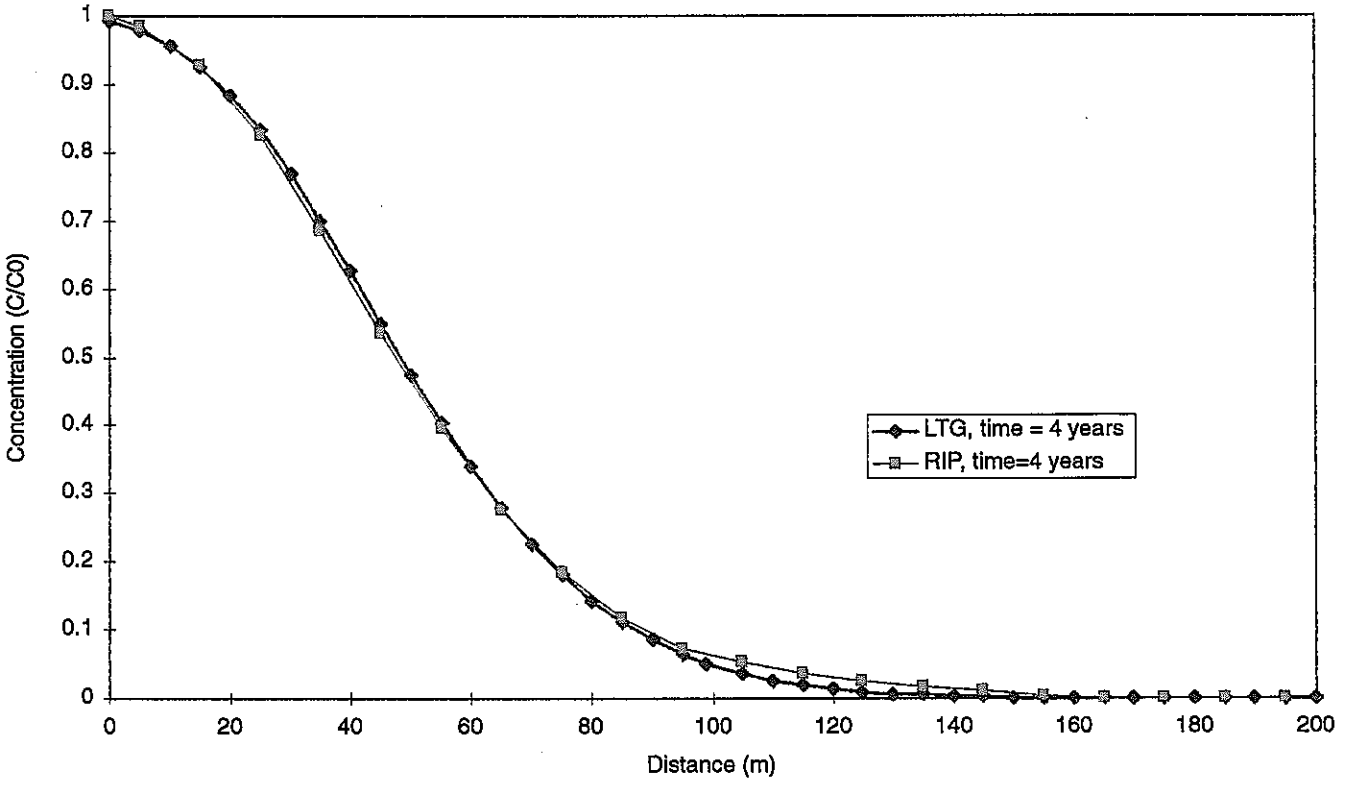

FIGURE **7-8**
CASE D2, MULTIPLE PROPERTY PIPE - DIFFUSION = 1.e-9 m2/S, NO DECAY
PNC/PAW-LTG/JAPAN

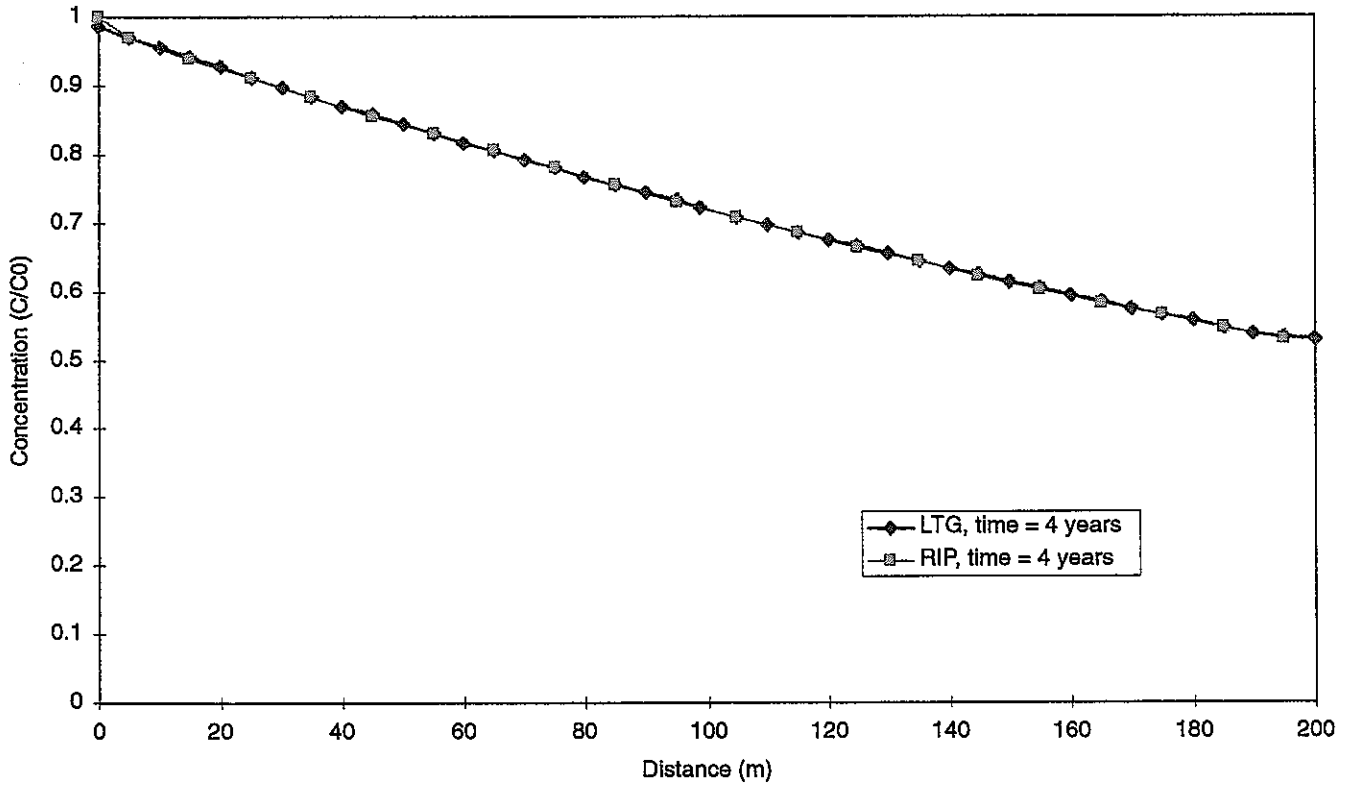

FIGURE **7-9**

CASE D3, SINGLE PROPERTY PIPE - DIFFUSION = 1.e-11 m2/S, NO DECAY

PNC/PAW-LTG/JAPAN

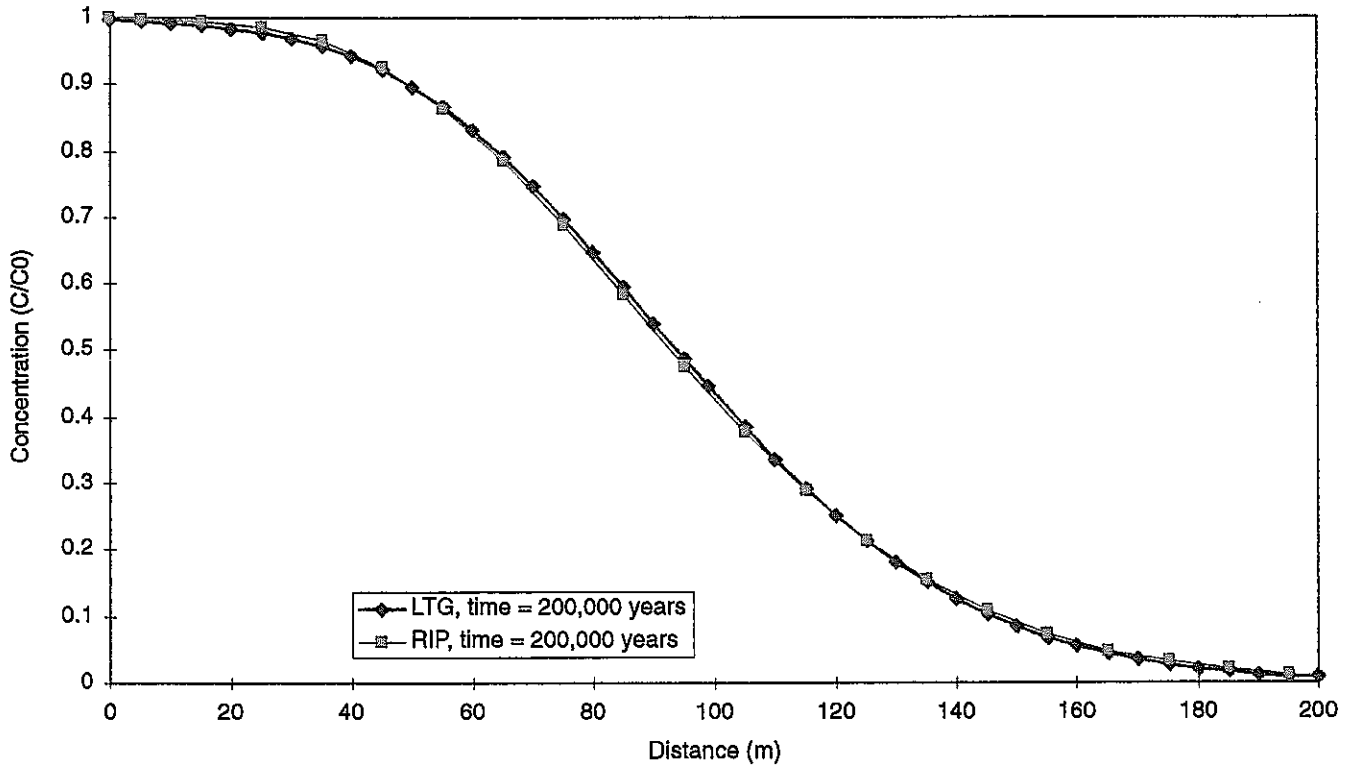

FIGURE **7-10**

CASE R1, SINGLE PROPERTY PIPE - RETARDATION & DIFFUSION0 (D0=1.e-9) WITHOUT DECAY

PNC/PAW-LTG/JAPAN

Figure 7-11 shows the results for a four pipe type fracture, again assuming a free water diffusion coefficient of 10^{-9} m^2/s. The retardation value is independent of the pipe type, however the amount of diffusion which can occur as the solute flows along the fracture is a function of the pipe velocity. Therefore the concentration distribution associated with case_r2 shows a distinct correlation with the pipe type boundaries at 50, 100, and 150m. The PAWorks and RIP results are in close agreement.

Case_r3 is identical to case_r1, a single property fracture with a free water diffusion coefficient of 10^{-9} m^2/s, except that radionuclide decay is now included in the simulation. A simple two radionclide chain was considered, from Am-243 to Pu-239. The decay rate used for Am-243 was 9.389×10^{-5} yr^{-1}, and the decay rate for Pu-239 was 2.879×10^{-5} yr^{-1}.

The results of the case_r3 simulation are presented in Figures 7-12 and 7-13 for Am-243 and Pu-239 respectively. The results show a good match between the PAWorks and RIP results.

The final example considered, case_r4, is a single fracture property simulation similar to case_r1 but using a lower value of free water diffusion of 10^{-11} m^2/s. The results of the simulation are presented in Figure 7-14. The RIP and PAWorks models produce essentially identical results. However, the lower diffusivity reduces the overall retardation in the fracture system.

This section of the report has presented a comparison between two codes, PAWorks LTG module and RIP, which model solute transport in using very different approaches. However, the results of the code comparison indicate that the results from both codes are nearly identical over a wide range of problems.

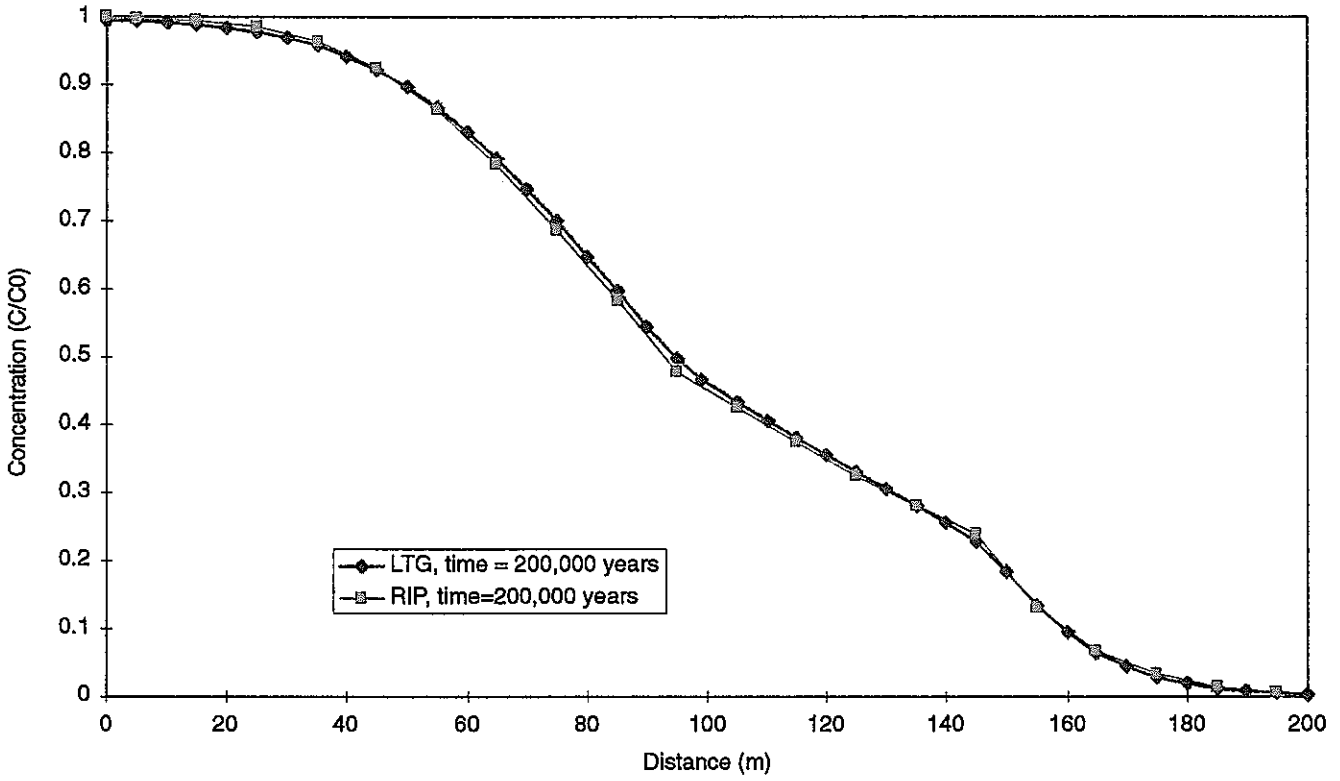

FIGURE **7-11**
CASE R2, MULTIPLE PROPERTY PIPE - RETARDATION & DIFFUSION (1.e-9) WITHOUT DECAY
PNC/PAW-LTG/JAPAN

PROJECT NO. 923 1089.824 DRAWING NO. 73182 DATE 5/12/97 DRAWN BY EA

Golder Associates

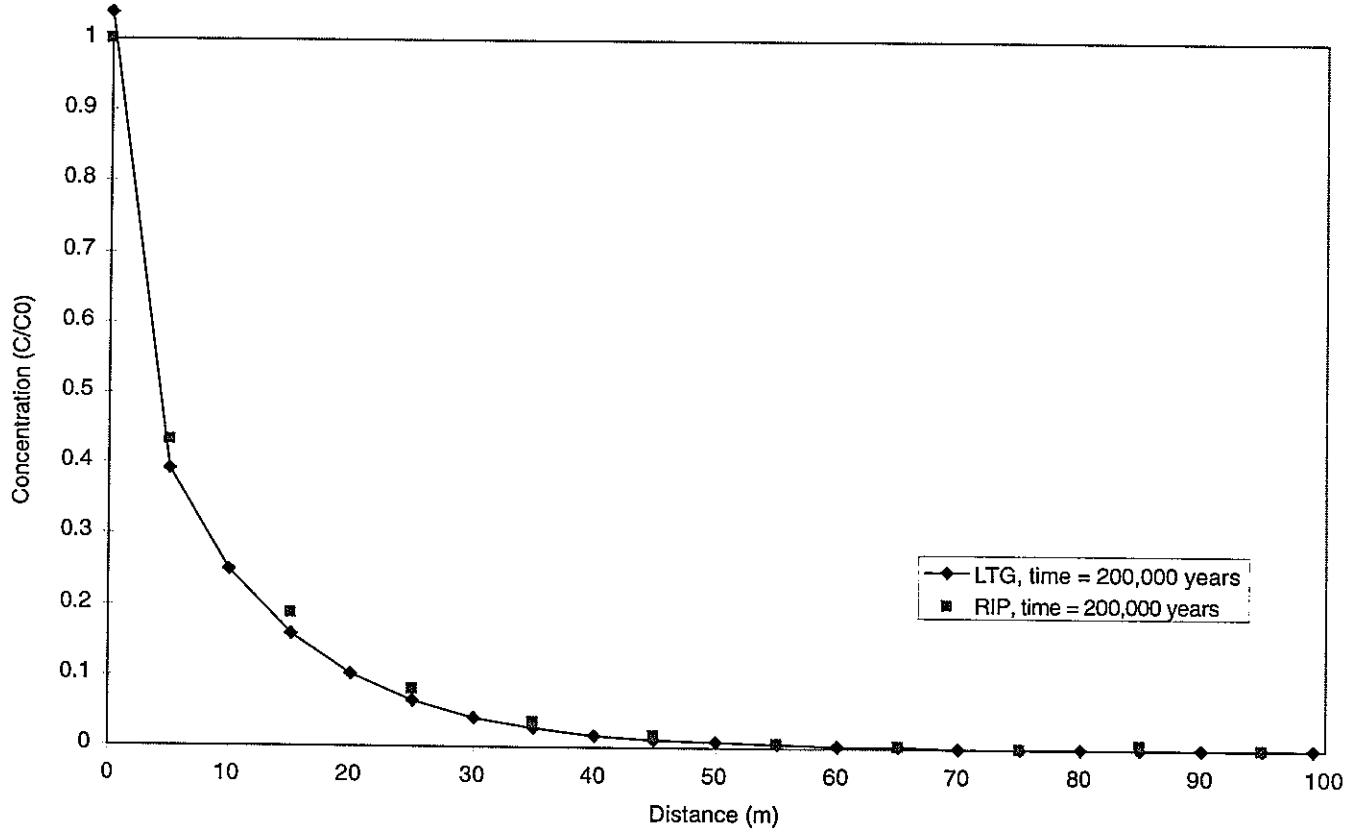

FIGURE **7-12**
CASE R3, SINGLE PROPERTY PIPE - AM243 - RETARDATION & DIFFUSION (D0=1.e-9) & DECAY
PNC/PAW-LTG/JAPAN

PROJECT NO. 923 1089.824 DRAWING NO. 73183 DATE 11/17/97 DRAWN BY EA

Golder Associates

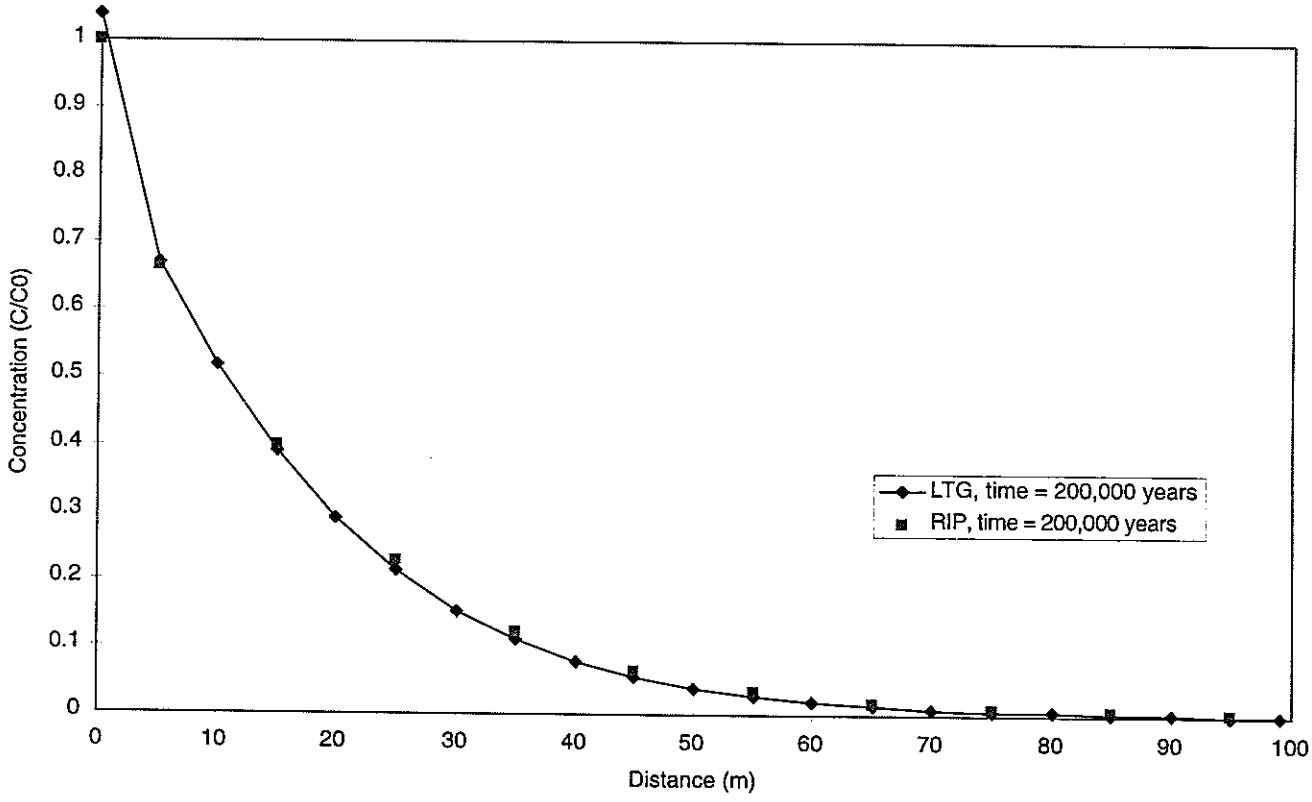

FIGURE **7-13**
CASE R3, SINGLE PROPERTY PIPE - PU239 - RETARDATION & DIFFUSION (D0=1.e-9) & DECAY
PNC/PAW-LTG/JAPAN

PROJECT NO. 923 1089.824 DRAWING NO. 73184 DATE 11/17/97 DRAWN BY EA

Golder Associates

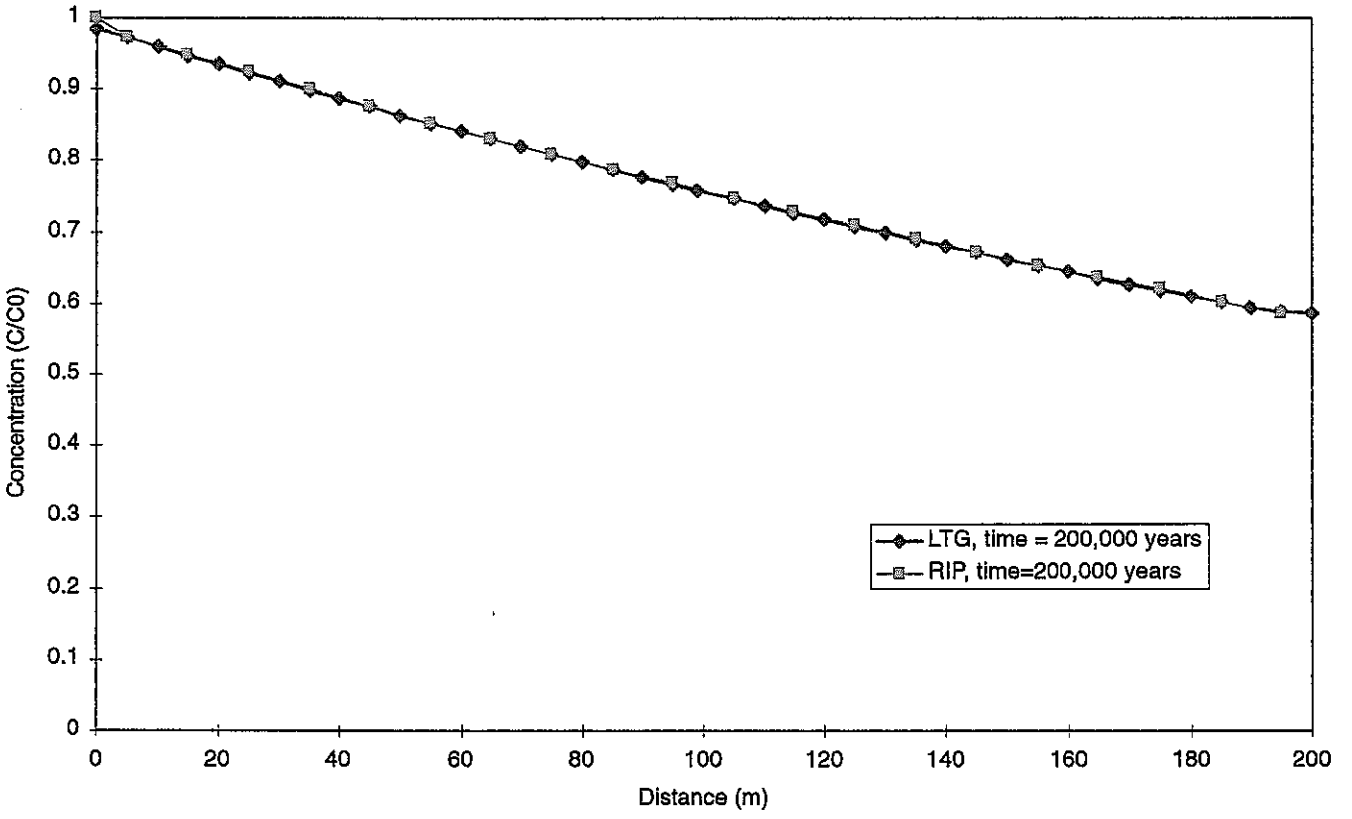

FIGURE **7-14**

CASE R4, SINGLE PROPERTY PIPE - MATRIX RETARDATION & DIFFUSION (D0=1.e-11) WITHOUT DECAY

PNC/PAW-LTG/JAPAN

PROJECT NO. 923 1089.824 DRAWING NO. 73185 DATE 5/12/97 DRAWN BY EA

Golder Associates

7.2 PAWorks / LTG Demonstration Application

A demonstration application for the Laplace Transport Galerkin (LTG) component of the PAWorks suite of codes is presented in this section. The LTG component was added to PAWorks to simulate the advective-dispersive transport of multi-species decay chain through a network of interconnected one-dimensional pipes in three-dimensional space. A general description of LTG is given in Section 7.1. A more detailed description may be found in Foxford et al., 1997.

In this demonstration simulation we used the same fracture generation as used elsewhere in this report, namely that of Doe et al. (1996). These fracture generation parameters are reproduced in Table 2-1. As described earlier in this report, the 200m rock block representation of the Kamaishi site was produced by generating the fractures in a 225m cube to prevent the edges of the cube affecting the fracture intensity. Based on the results of the MAFIC to PAWorks comparison discussed in Section 5.0, the fracture intensity was set by assigning a minimum fracture transmissivity of 3×10^{-9} m^2/s, which is equivalent to 32,889 fractures generated in the 225m cube region. This fracture intensity at the Kamaishi site is sufficient to minimize the effect of the neglecting the lower transmissivity fractures.

In this example we represent transport of solute from the repository to the effective outflow boundary 100m distant. A full repository was not modeled, instead a single fracture was used to represent the source location in the repository. This fracture was 50m in length (x direction), 10m in height (z direction), and oriented perpendicular to the flow gradient with its center located at (0.0, 0.0, 0.0) giving a minimum transport distance of 100m. The "repository fracture" was assigned a transmissivity lower than that of the surrounding fracture network so that its presence would not influence the flow field, or add additional connectivity to the fracture system.

The boundary conditions were identical to boundary condition "B" presented in Section 2. The geometry and boundary conditions used for this simulation are shown in Figure 7-15.

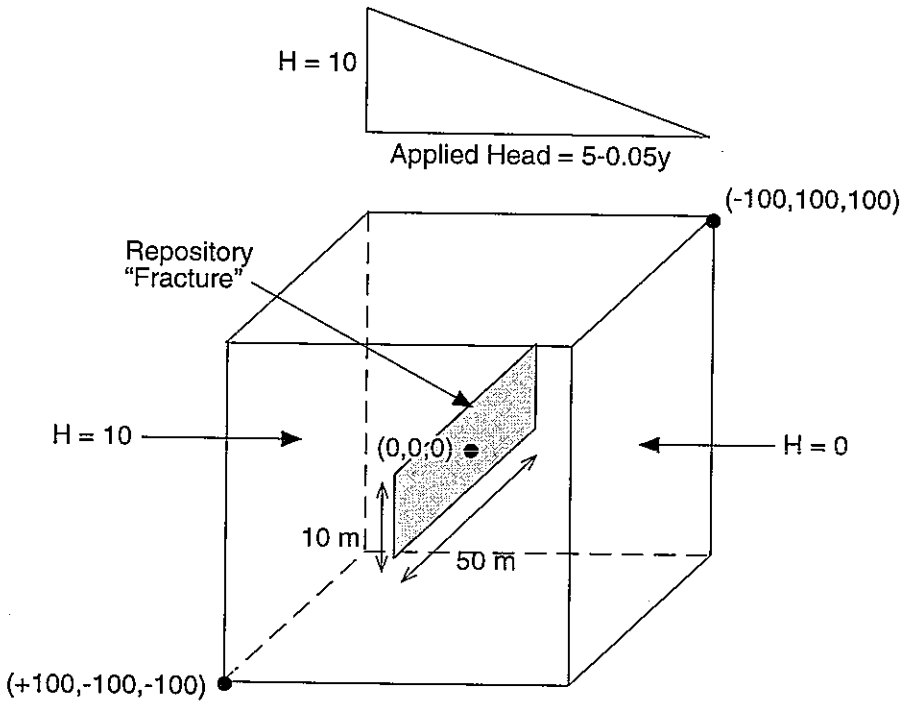

FIGURE **7-15**
MESH CONFIGURATION FOR THE PAWorks CRYSTAL INPUT
PNC/PAW-LTG/JAPAN

The full fracture network downstream of the repository fracture is included in the output to the PAWorks LTG module.

Transport of five species was simulated. Four of these species are released directly (Pa-231,Cs-135,Se-79,Sn-126). Their release rates versus time are shown in Figure 7-16. One species (AC-227) is introduced by the decay of Pa-231. LTG requires the decay and transport properties of the five species. These properties are presented in Table 7-4.

Table 7-4 Radionuclide Properties

Radionuclide	Distribution Coefficient (m^3/kg)	Decay (1/year)	Free Water Diffusion Coefficient (m^2/yr)
Se-79	10^{-4}	1.07×10^{-5}	3.1536×10^{-2}
Cs-135	10^{-4}	2.31×10^{-7}	3.1536×10^{-2}
Pa-231	0.01	2.12×10^{-5}	3.1536×10^{-2}
Ac-227	0.01	3.18×10^{-2}	3.1536×10^{-2}
Sn-126	0.1	6.93×10^{-6}	3.1536×10^{-2}

The conceptual model of the fractured rock mass consists of three elements: the flowing part of the fracture, the surrounding matrix and a non-flowing fracture area.

It is assumed that only a portion of the fracture plane has significant advective flow velocities. Both the flowing and the non-flowing portions of the fracture have a mineral infilling, which is assumed to be in sorptive equilibrium with the fracture water. The non-flowing portion of the fracture is connected via diffusion to the flowing portion. In addition, a thickness of the rock matrix adjacent to the flowing portion of the fracture is available for matrix diffusion. Table 7-5 shows the dimensions and the input parameter for the three zones.

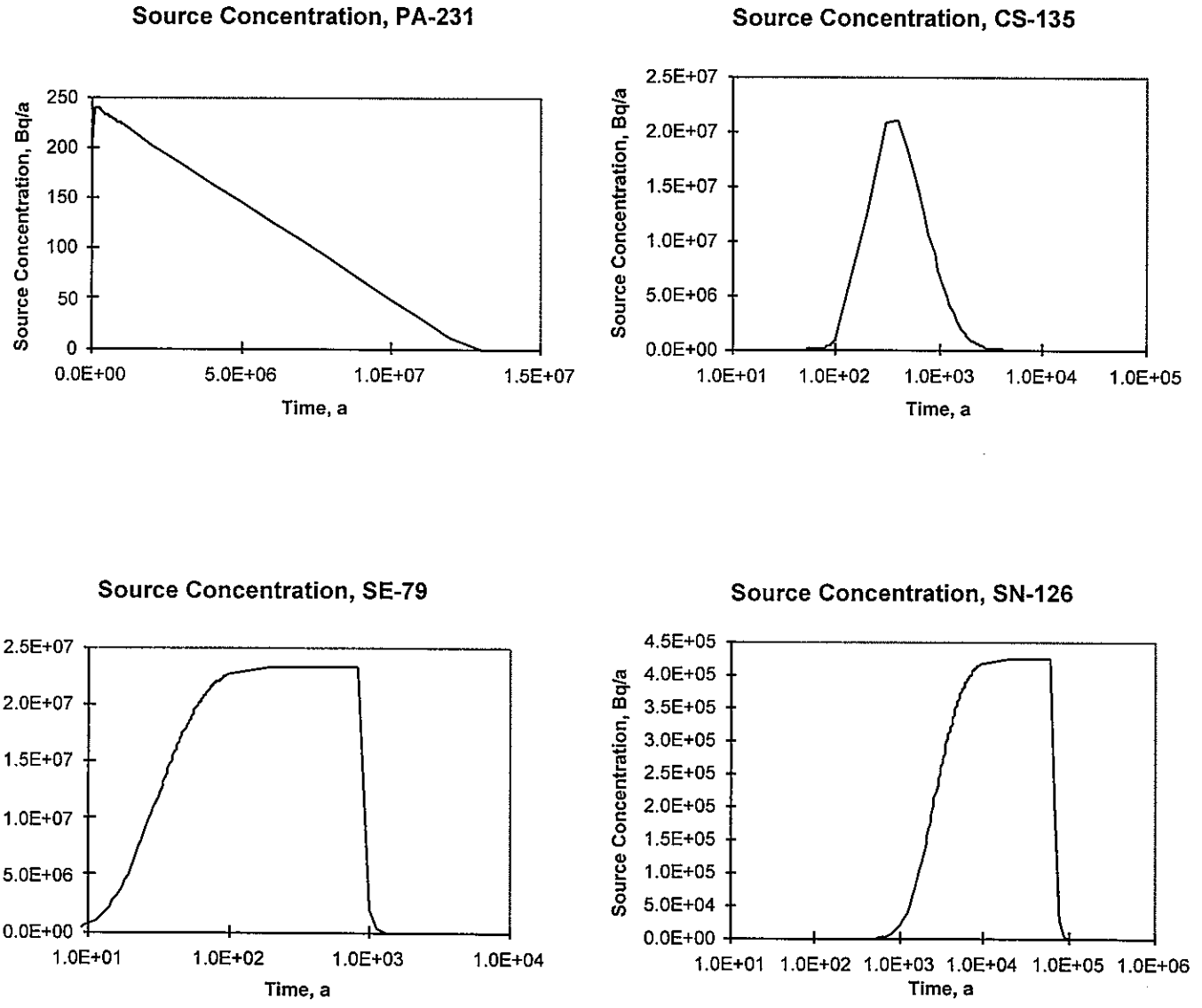

FIGURE **7-16**

SOURCE BOUNDARY CONDITION FOR PAWorks/LTG DEMONSTRATION APPLICATION

PNC/PAW-LTG/JAPAN

Table 7-5 Properties used for the PAWorks/LTG Input

Property	Fracture, flowing part	Fracture, non-flowing part	Matrix
Thickness	aperture and width as calculated by PAW	1 m	0.1 m
Porosity	N/A	100 %	10 %
Tortuosity	N/A	1	1
Dispersion Length	0.5 m	N/A	N/A
Infilling thickness	1e-03 m	1e-03 m	N/A
Infill density	2400 kg/m^3	2400 kg/m^3	N/A
Density	N/A	N/A	2500 kg/m^3

The results of the LTG simulation are presented as release from the downstream boundary (Bq/year) against elapsed time in Figures 7-17 to 7-20. To illustrate the residence time in the network, the source distribution of the radionuclides are also shown on the figures.

The Se-79 results show breakthrough occurring at 40 years followed by a rapid rise in release rate to a peak at approximately 1000 years. The peak release rate of just less than 2×10^7 Bq/year is only slightly lower than the peak release rate of the boundary condition. After peak release, the release rate falls quickly following the rapid reduction in input concentration at 800 years. However, some release of Se-79 is still occurring at 10^6 years, indicating the presence of lower velocity pathways within the system.

The behavior of Cs-135 is similar. The results show a small breakthrough occurring at 40 years, with significant breakthrough starting at 100 years. The preak release is approximately half of the maximum input release rate. Again the release follows the general shape of the input curve, but the presence of lower velocity pathways results in release occurring at over a million years.

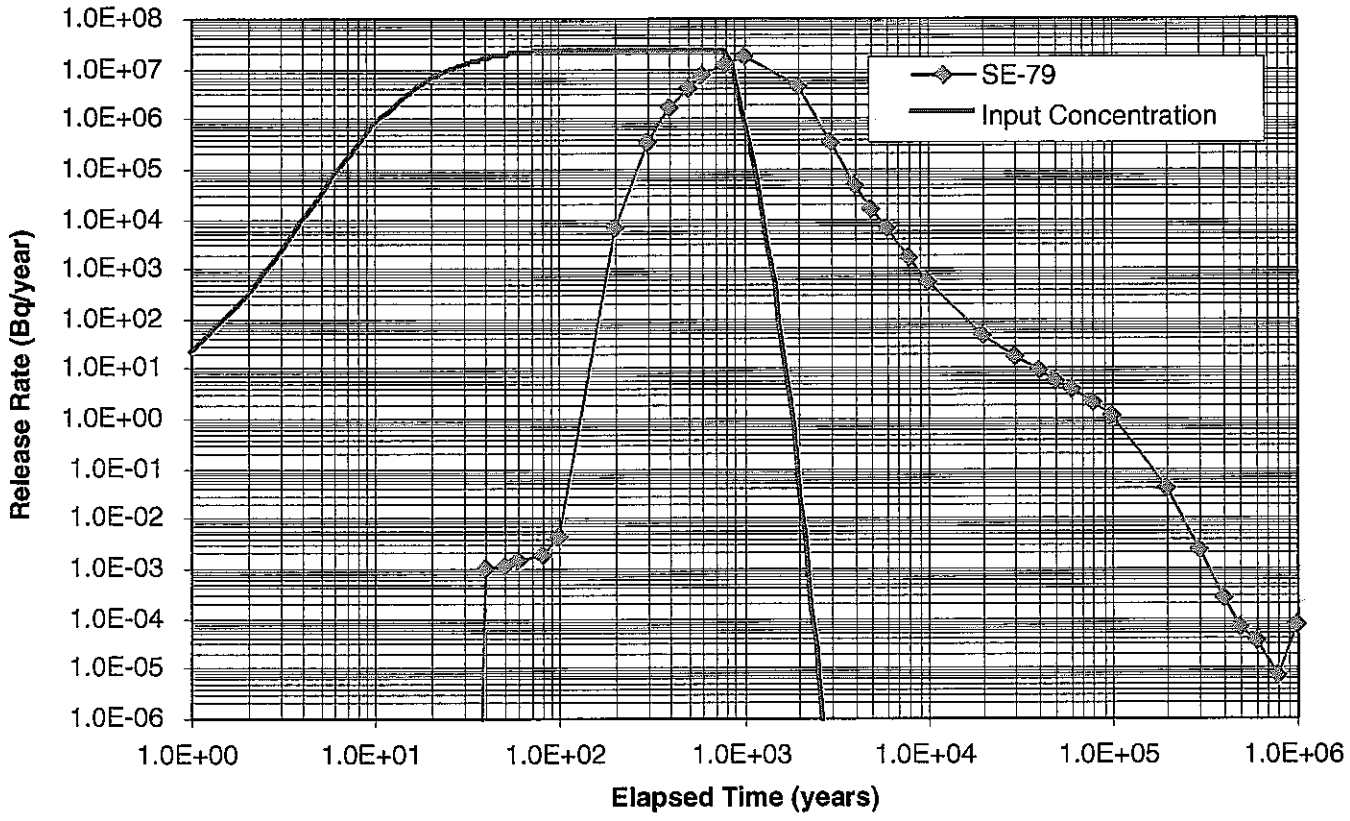

FIGURE **7-17**
RELEASE OF SE-79 FROM DOWNSTREAM BOUNDARY
PNC/PAW/LTG/JAPAN

PROJECT NO. 923 1089.824 DRAWING NO. 76067 DATE 11/24/97 DRAWN BY EA

Golder Associates

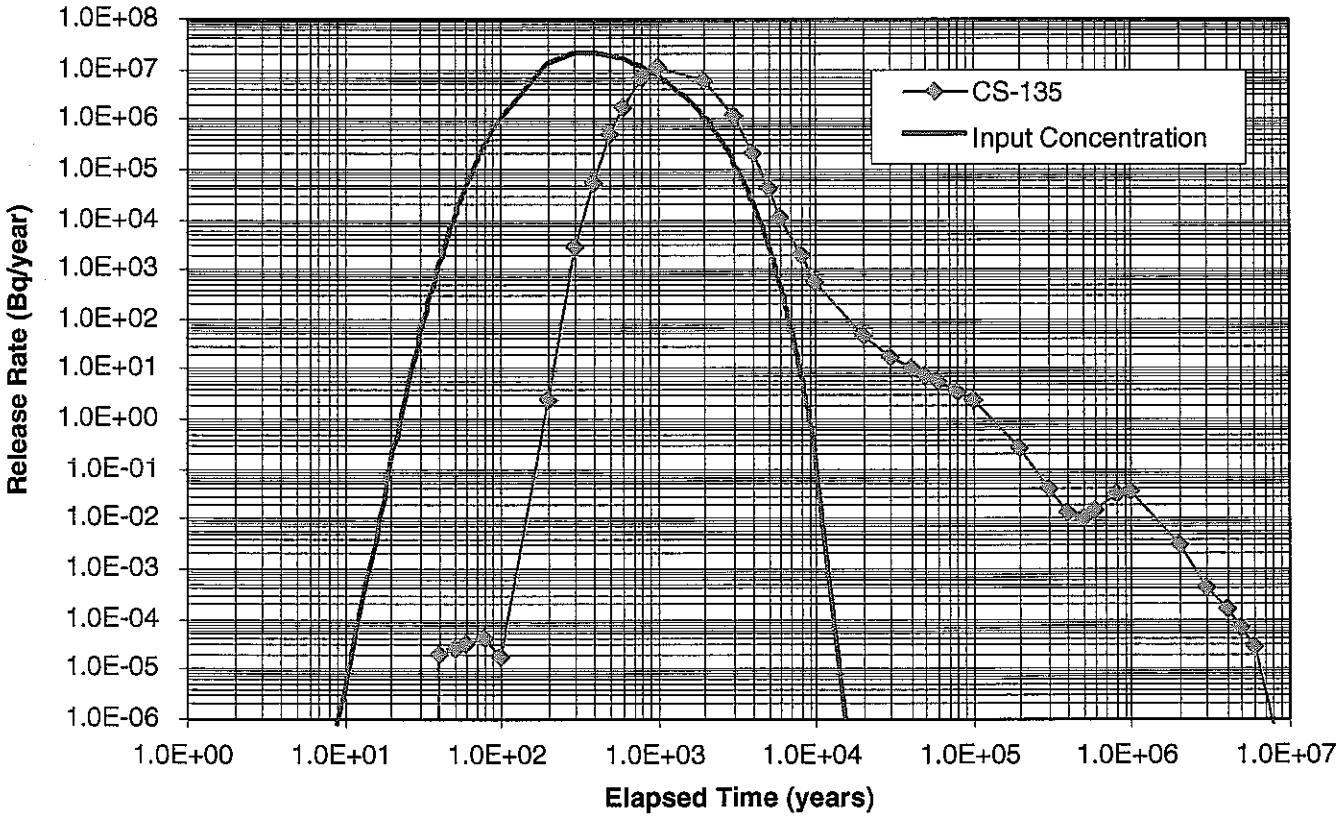

FIGURE **7-18**
RELEASE OF CS-135 FROM DOWNSTREAM BOUNDARY
PNC/PAW/LTG/JAPAN

PROJECT NO. 923 1089.824 DRAWING NO. 76068 DATE 11/24/97 DRAWN BY EA

Golder Associates

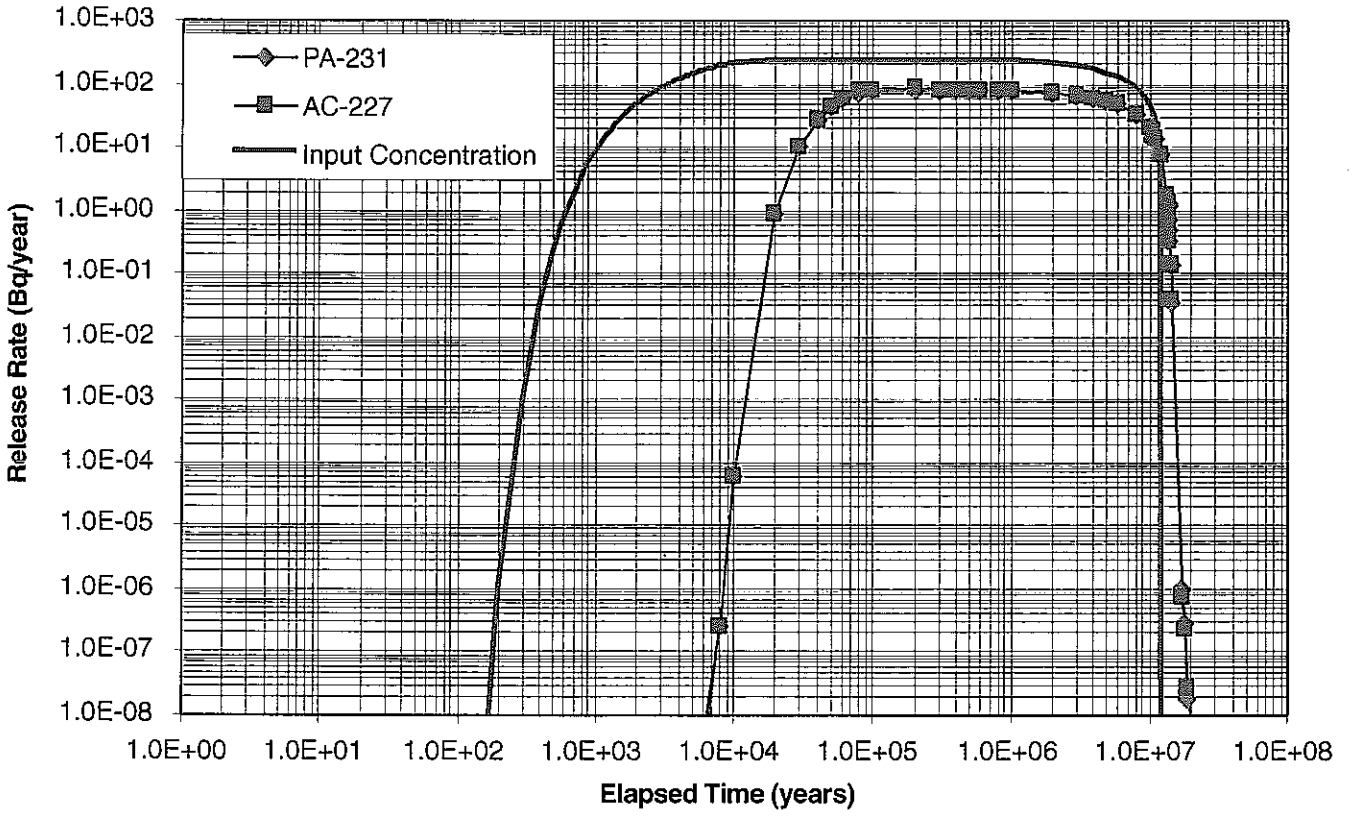

FIGURE **7-19**
RELEASE OF PA-231 AND AC-227 FROM DOWNSTREAM BOUNDARY
PNC/PAW/LTG/JAPAN

PROJECT NO. 923 1089.824 DRAWING NO. 76069 DATE 11/24/97 DRAWN BY EA

Golder Associates

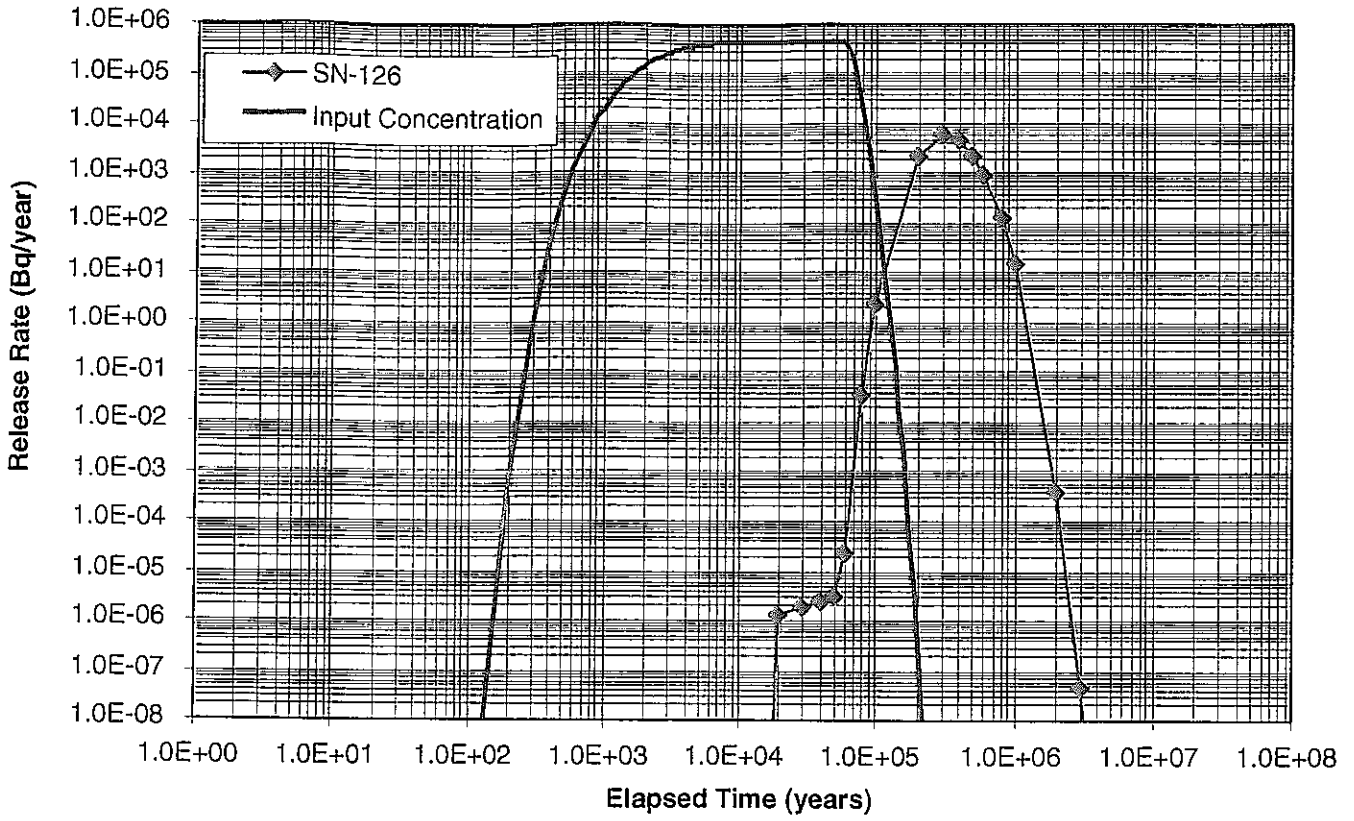

FIGURE **7-20**
RELEASE OF SN-126 FROM DOWNSTREAM BOUNDARY
PNC/PAW/LTG/JAPAN

PROJECT NO. 923 1089.824 DRAWING NO. 76070 DATE 11/24/97 DRAWN BY EA

Golder Associates

The release of Pa-231 and Ac-227 are essentially identical, due to the very fast decay rate of Ac-227. The peak release rate from the downstream boundary is only a factor of three lower than that input, again indicating that some fast low retardation pathways exist in the system. The reduction in release rate beyond 10^7 years appears rapid, but the log scale is deceptive. The reduction is occurring over 10^7 years.

The release of Sn-126 shows the large reduction in peak release rate; a factor of 67. This is due to the higher Kd of 0.1 m^3/kg, which is a factor of ten higher than the other radionuclides considered in this demonstration application.

Overall, the results indicate that PAWorks used in combination with LTG is able to produce a realistic representation of the fracture network, accounting for both the occurrence of fast pathways with faster breakthrough, and much slower pathways resulting in release over much longer periods of time.

7.3 Demonstration PAWorks / Crystal Calculation

This section describes a set of simulations of the Kamaishi block which were used to generate input parameters for use within the Crystal performance assessment code. The fracture model was the same as used for the PAWorks/LTG example application, but the details have been reproduced here for convenience.

The fracture generation model for the Kamaishi block was that used produced by Doe et al. (1996) and used throughout this report. This model is described in Section 7.2 of the report.

To produce input into the Crystal code, it was necessary to track particle movement from a location in the center of the 200m cube. A full repository was not modeled; instead a single fracture was used to represent the source location in the repository. This fracture was 50m in length (x direction), 10m in height (z direction), and oriented perpendicular to the flow gradient with its center located at (0.0, 0.0, 0.0). Therefore the minimum transport distance is 100m. The "repository fracture" was assigned a transmissivity lower than that of the surrounding fracture network so that its presence would not influence the flow field, or add additional connectivity to the fracture system.

Boundary condition "A" presented in Section 2 was used. The geometry and boundary conditions used for the Crystal simulations are shown in Figure 7-21.

Within the pathway output from PAWorks, pathway parameters are computed for true and representative pathways. A true pathway is a single traversal between the source and sink. A representative pathway is an amalgamated pathway representing the behavior of the pathways with a common source or sink node.

The Crystal performance assessment code models a single fracture, rather than the entire discrete fracture network. Therefore to provide input into the Crystal code the results from PAWorks simulations involving perhaps thousands of individual pipes must be compressed into a single, or series of, representative pathways. How PAWorks combines the individual pathways into representative pathways is discussed in detail in the PAWorks manual (Foxford et al., 1997). The methodology used for this set of Crystal input parameters is described later in this section.

A subset of the parameters required as input into the Crystal code are presented in Table 7-6. Not all of these parameters are generated by PAWorks in this format. Therefore, to clearly indicate the output from PAWorks, the PAWorks notation has been used in the following examples.

Table 7-6 Crystal Input Parameters

Model Parameter	Symbol	Units
Block area/Unit Volume	A	m^2/m^3
Path length	l	m
Distance to downstream boundary (generally infinite)	l	M
Average velocity in the fracture	q	m/yr
Slab thickness	d	m
Advective fracture porosity	θ	-

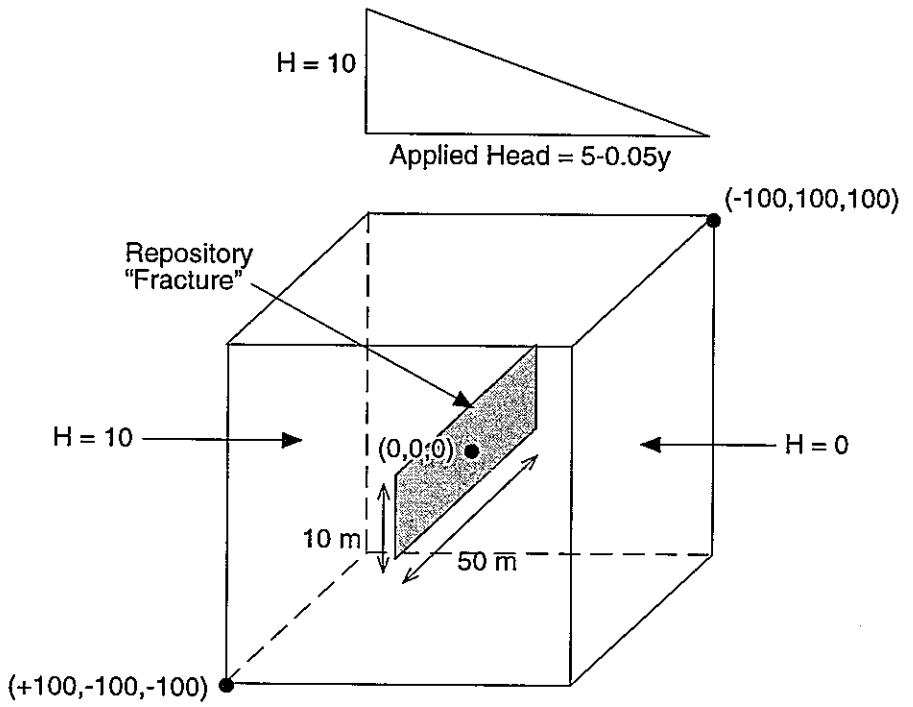

FIGURE **7-21**
BOUNDARY CONDITIONS FOR THE PAWorks CRYSTAL DEMONSTRATION
PNC/PAW-LTG/JAPAN

The range of PAWorks options investigated for the Crystal demonstration application are presented in Table 7-7. The results are ordered by the fracture pruning used for each representative pathway.

Table 7-7 Options considered for PAWorks Crystal Demonstration Application

Parameter	Options Calculated
Fracture pruning for representative path	Single least resistive pathway
	All advective pathways
	Pathways with 90% of outflow flux
Fracture area	Sum of true fracture areas (A_f)
	0.2 * Sum of true fracture areas (A_f)
Pathway length	Tortuous length
Aperture	Based on flux
Weighting for pathway	Flux
Pathway option	Common source
Number of representative pathways	Single pathway
	One for each cluster
Pathway spacing	From PAW pathway spacing

7.3.1 Single least resistive pathway

The first set of Crystal input parameters presented are for the single least resistive "true" pathway computed by the PAWorks code. A "true" pathway is simply a pathway between the source and the sink made up of PAW pipes.

To generate the pathways from the source nodes, the "maximum flux" search algorithm was selected. The PAWorks maximum flux search progresses through the mesh by incrementally moving along the connected pipe with the highest flux. This search algorithm is shown graphically in Figure 7-22. The traversals specified 10 source locations and therefore the highest 10 flux pipes connected to the source will comprise the source pipes.

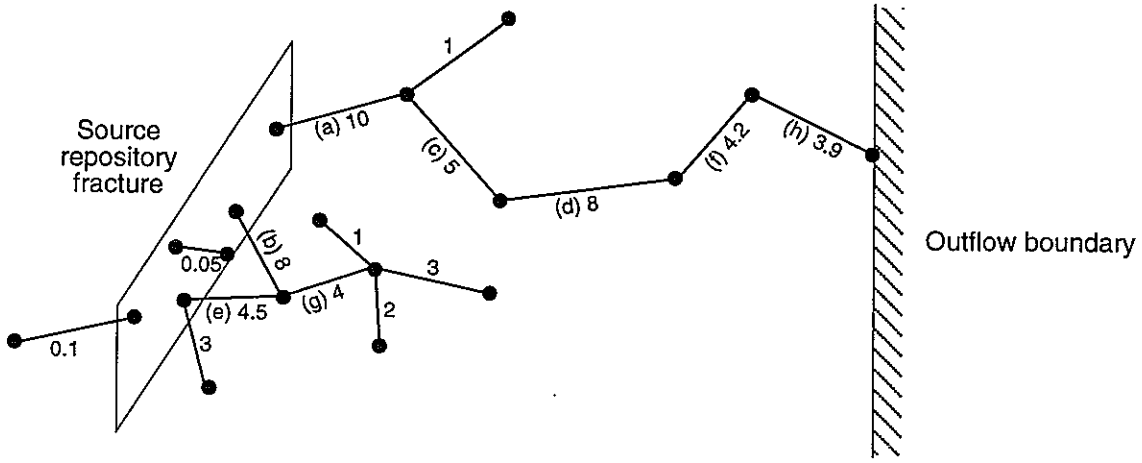

Numeric value on fracture is scaled weighted flux
Alphabetical index is order of progress through network

FIGURE **7-22**
PAWorks PATHWAY SEARCH BASED ON FLUX
PNC/PAW-LTG/JAPAN

PROJECT NO. 923 1089.824 DRAWING NO. 73172 DATE 11/21/97 DRAWN BY EA

Golder Associates

After the traversals are complete, PAWorks orders the pathways based on the same parameter as used for the search; in these examples, the pathway flux. The "single least resistive pathway" is the pathway with the highest pathway flux. However, the way in which the pathway flux is computed is user defined; it depends on how the pathway aperture is computed, which in turn controls the values of all other pathway properties.

In these demonstration simulations, two pathway aperture options have been used. The first was based on the flow (Q) using the equation $e_{flux} = \frac{Q}{KiW}$ where for a pathway computed based on flux weighting, Q is the flow weighted flow (equal to $\Sigma (Q_i * Q_i)/\Sigma Q_i$) along the pathway, K is the back-calculated hydraulic conductivity, i is the pathway head gradient, and W is the flux-weighted pathway width.

The second aperture computation is a "flux-weighted" weighting of the aperture, $e_w = \Sigma (e_i * Q_i)/\Sigma Q_i$.

The results of the "based on Q" aperture analysis are presented in Table 7-8. The true fracture area of 4347 m^2 shown in Table 7-8 is the total area of each fracture, as generated within FracWorks. For the generation of pipes to compute the flow field, this value of area is not used. Instead the flow areas are based on the area between the fracture traces (intersections).

The pathway length given in Table 7-8 is the total length traveled by a particle, including tortuosity within individual fractures, and in the path itself. The tortuous length of 146.7m is a approximately 50% greater than the minimum transport length.

The value of aperture computed using the "based on Q" aperture computation is unrealistically high at 1.09×10^{-3} m. This occurs due to the boundary conditions used for this Crystal example. The constant head boundaries allow the flow to shortcut across the corners of the cube. Therefore a single high transmissivity fracture may develop an unrealistically high flux. Using flux weighting, the pathway chooses the high flux pathway and biases the overall flux for the traversal, resulting in an erroneously high aperture.

The pathway parameters for the "flux weighting" method for computing the aperture are presented in Table 7-9. This method of computing the pathway aperture results in a more reasonable aperture value of 9.79e-5 m. The travel time for the traversal was 1.50 years. This value was computed based on the summation of the travel times of the individual pipes along the pathway. The longer travel time is associated with a longer traversal length of 188.9 m and greater fracture flow area of 6237 m^2.

Table 7-8 Results of PAWorks Crystal Input for Single Least Resistive Path based on Q

Parameter	Option Calculated	Value
Fracture pruning for representative path	N/A	N/A
Fracture area	Sum of true fracture areas (A_f)	4347 m^2
	0.2 * Sum of true fracture areas (A_f)	869 m^2
Pathway length	Tortuous length	146.7 m
Width	Flux weighted	7.32 m
Aperture	Based on flux	1.09e-3 m
Travel time	From flux weighted traversal	0.278 yr
Number of representative pathways	Single pathway	N/A
Pathway spacing	From PAW pathway spacing	N/A

Table 7-9 Results of PAWorks Crystal Input for Single Least Resistive Path based on weighting

Parameter	Option Calculated	Value
Fracture pruning for representative path	N/A	N/A
Fracture area	Sum of true fracture areas (A_f)	6237 m^2
	0.2 * Sum of true fracture areas (A_f)	1247 m^2
Pathway length	Tortuous length	188.9 m
Width	Flux weighted	13.31 m
Aperture	Flux weighted aperture	9.79e-5 m
Travel time	From flux weighted traversal	1.50 yr
Number of representative pathways	Single pathway	N/A
Pathway spacing	From PAW pathway spacing	N/A

7.3.2 Representative pathways based on 100% of flux

In all the Crystal simulations presented in this section the common source algorithm has been used to generate the representative pathways. This means that representative pathways are merged from the true pathways based on the set of pathways attached to a single source node. The representative pathways include all the pathways associated with a source; hence 100% of the flux is included.

For these simulations a maximum of 10 source nodes were generated. Associated with each source node were up to 10 exit locations.

During this simulation 10 source locations were generated, each associated with 10 individual pathways. The options used for the 100% flux simulation are presented in Table 7-10. The results for representative pathways "based on Q" for aperture for each of the 10 sources are presented in Tables 7-11 and 7-12. The corresponding results for representative pathways based on "weighting" are given in Tables 7-13 and 7-14.

Tables 7-11 to 7-14 contain pathway spacing, S. In these simulations the pathway spacing is taken to be equal to the penetration depth of the pathway fractures (i.e. only including the fractures on the 200 pathways generated within PAWorks). It should therefore be noted that the number of pathways in the search affects the computed pathway spacing.

The spacing for these pathway fractures is computed by projecting normal to the fracture along the pathway in both directions until another pathway fracture is intersected. The representative pathway penetration depth is the weighted average of the ten pathways starting at each source.

Table 7-10 PAWorks Crystal Options for 100% Flux Representative Pathways

Parameter	Option Calculated	Symbol
Fracture pruning for representative path	100%	N/A
Fracture area	Sum of true fracture areas	A_f
	0.2 * Sum of true fracture areas	0.2 A_f
Pathway length	Tortuous length	L
Width	Flux weighted	W
Aperture	Based on flux	e_{flux}
Aperture	Flux weighted aperture	e_w
Travel time	From flux weighted traversal	Tt
Number of representative pathways	One for each source	N/A
Pathway spacing	From PAWorks pathway spacing	S

Table 7-11 Results of Simulations 1-5, PAWorks Crystal 100% Flux Pathways based on Q

Property	Realization				
	1	2	3	4	5
A_f	6758	6385	4492	5457	4636
0.2 A_f	1352	1227	898	1019	927
L	198.4	191.9	164.5	156.6	169.7
W	7.53	7.53	11.74	11.69	11.68
e_{flux}	0.831	0.899	4.01e-3	1.81e-3	3.84e-3
Tt	1.27	1.33	1.61	0.70	1.59
S	59.01	64.33	29.86	30.17	29.25

Table 7-12 Results of Simulations 6-10, PAWorks Crystal 100% Flux Pathways based on Q

Property	Realization				
	6	7	8	9	10
A_f	6592	6419	7660	6439	7441
0.2 A_f	1318	1284	1532	1288	1488
L	196.4	190.5	211.8	184.9	207.3
W	7.53	7.53	7.53	7.53	7.53
e_{flux}	1.01	0.91	1.32	0.83	1.30
Tt	1.53	1.34	2.17	1.19	2.08
S	58.34	61.92	55.16	72.22	55.84

Table 7-13 Results of Simulations 1-5, PAWorks Crystal 100% Flux Pathways based on weighting

Property	Realization				
	1	2	3	4	5
A_f	6867	6494	4648	5457	4793
0.2 A_f	1373	1299	930	1091	959
L	179.2	181.9	155.2	157.9	160.1
W	8.42	8.98	10.21	11.81	10.11
e_w	3.26e-4	2.95e-4	1.13e-4	1.10e-4	1.13e-4
Tt	0.91	0.96	0.76	0.66	0.74
S	42.61	46.25	28.65	31.05	28.07

Table 7-14 Results of Simulations 6-10, PAWorks Crystal 100% Flux Pathways based on weighting

Property	Realization				
	6	7	8	9	10
A_f	6701	6527	7768	6547	7550
0.2 A_f	1340	1305	1554	1309	1510
L	178.2	175.8	197.1	180.1	176.5
W	9.18	9.15	9.70	9.08	8.64
e_w	2.91e-4	2.97e-4	3.08e-4	2.96e-4	3.15e-4
Tt	1.03	0.95	1.72	0.91	1.33
S	41.20	43.41	44.70	53.59	43.67

7.3.3 Representative pathways based on 90% of flux

The representative pathways for 90% flux vary from the 100% flux simulation in that not all of the true pathways are used to form the overall representative path associated with each source. For the 90% flux simulations only the highest (weighted) flux pathways containing the top 90% of the total flux are included in the simulation.

The options used for the 90% flux simulation are presented in Table 7-15. The 90% of flux representative pathways based on "Q" for aperture for each of the 10 sources are presented in Tables 7-16 and 7-17. The corresponding results for pathway aperture based on "weighted" are given in Tables 7-18 and 7-19.

Table 7-15 PAWorks Crystal Options for 90% Flux Representative Pathways

Parameter	Option Calculated	Symbol
Fracture pruning for representative path	90%	N/A
Fracture area	Sum of true fracture areas	A_f
	0.2 * Sum of true fracture areas	0.2 A_f
Pathway length	Tortuous length	L
Width	Flux weighted	W
Aperture	Based on flux	e_{flux}
Aperture	Flux weighted aperture	e_w
Travel time	From flux weighted traversal	tt
Number of representative pathways	One for each source	N/A
Pathway spacing	From PAW pathway spacing	S

Table 7-16 Results of Simulations 1-5, PAWorks Crystal 90% Flux Pathways based on Q

Property	Realization				
	1	2	3	4	5
A_f	6867	6494	5779	5233	5923
0.2 A_f	1373	1299	1156	1047	1185
L	199.15	192.67	167.57	155.04	172.78
W	7.42	7.42	12.27	11.34	12.21
e_{flux}	0.817	0.883	0.004	0.0019	0.0040
tt	1.28	1.33	1.76	0.71	1.75
S	60.23	65.68	29.56	29.89	28.97

Table 7-17 Results of Simulations 6-10, PAWorks Crystal 90% Flux Pathways based on Q

Property	Realization				
	6	7	8	9	10
A_f	6701	6527	7768	6547	7550
0.2 A_f	1340	1305	1554	1309	1510
L	197.06	191.24	212.44	185.76	207.86
W	7.42	7.42	7.42	7.42	7.42
e_{flux}	0.995	0.894	1.295	0.817	1.279
tt	1.53	1.34	2.17	1.19	2.08
S	59.56	63.19	56.41	73.70	57.06

Table 7-18 Results of Simulations 1-5, PAWorks Crystal 90% Flux Pathways based on weighting

Property	Realization				
	1	2	3	4	5
A_f	6758	6385	4492	5673	4636
0.2 A_f	1352	1277	898	1135	927
L	175.0	179.7	160.0	156.0	164.8
W	8.40	9.08	10.75	11.36	10.65
e_w	2.66e-4	2.38e-4	1.08e-4	1.10e-4	1.08e-4
tt	0.83	0.87	0.88	0.67	0.86
S	40.47	43.96	28.36	30.82	27.80

Table 7-19 Results of Simulations 6-10, PAWorks Crystal 90% Flux Pathways based on weighting

Property	Realization				
	6	7	8	9	10
A_f	6592	6419	7660	6439	7441
0.2 A_f	1318	1284	1532	1288	1488
L	174.5	172.6	193.2	179.0	170.5
W	9.30	9.28	10.00	9.20	8.66
e_w	2.35e-4	2.40e-4	2.47e-4	2.41e-4	2.56e-4
tt	0.92	0.86	1.60	0.84	1.17
S	39.05	40.94	43.57	51.31	42.49

7.4 PAWorks / RIP Demonstration Application

This section of the report describes a PAWorks/RIP demonstration analysis.

The Repository Integration Program (RIP) is a coupled radionuclide-source term and transport model, and consists of a series of inter-connected, fully-coupled component models. The component models consist, in general, of simple representations of the processes affecting radionuclide release and transport.

The application presented here is not stochastic, and illustrates a very simplified model of the system. Most RIP models make use of the simulation approach, utilizing the Monte Carlo method to sample probability distributions for the uncertain parameters that describe both processes and events. RIP can then simulate a large number of realizations to determine probability distributions of system performance (e.g. cumulative release, risk, or transport time). As shown in Figure 7-23, RIP can create a random time history of disruptive events and other system parameters for each system realization, simulate the behavior of the system under those conditions, and then combine the results of all of the realizations in an appropriate manner to determine probability distributions of site performance.

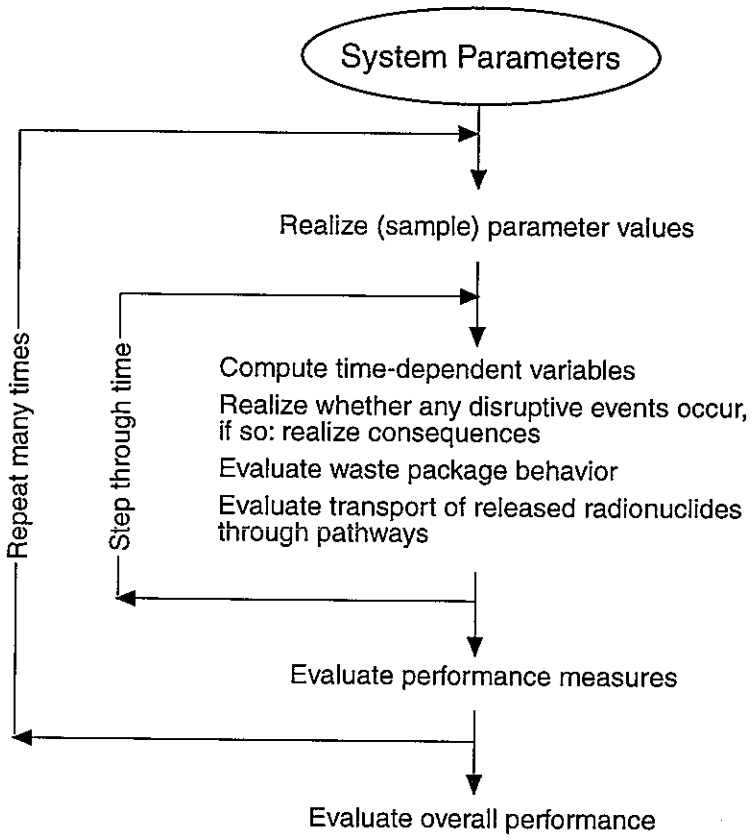

FIGURE **7-23**
RIP PERFORMANCE ASSESSMENT MODEL SIMULATION LOGIC
PNC/PAW-LTG/JAPAN

As stated above, in this example RIP is run using deterministic properties only. The conceptual model comprises three parts as shown in Figure 7-24. The source terms are released inside a source cell, conceptually representing the waste and overpack. On release, the radionuclides move through the bentonite buffer by diffusion. Two pathways are available; upward towards the disposal tunnel, and laterally directly into the fracture network. The radionuclides which diffuse towards the disposal tunnel are intersected by a higher transmissivity fracture within the fractured zones (EDZ) surrounding the repository. To represent the higher fracture area available for diffusion in the EDZ, the diffusion area between the bentonite buffer and the EDZ is represented by the bentonite diffusion area. At the edge of the enhanced transmissivity EDZ, the radionuclides move into the main fracture network.

The radionuclides diffusing laterally do not pass through the EDZ and are transported directly into the main fracture network. To represent the lower area connection between the background fracture network and the bentonite buffer, only the fracture flow area is available for diffusion between the bentonite buffer into the fracture network. Additionally, only a sub-section of the full fracture network is available in this model to the laterally diffusing mass (Pathway 4), to indicate the higher connectivity created by the EDZ zone.

The RIP model developed is shown schematically in Figure 7-25. The bentonite buffer comprises four cells to model the vertical diffusion (BEN1 to BEN4), and a single cell to represent the shorter lateral diffusion pathway (BEN5). The vertical bentonite pathway connects to the EDZ (an advective cell) and then into the four main fracture pathways (advective cells P1A-D through P4A-D). The radial bentonite buffer connects directly into pathway 4.

Each advective cell in the main fracture network is connected to a diffusive cell (D1A-D through D4A-D) which represents diffusion between the flowing fracture and the rock matrix.

The transport properties of the main fracture network are defined by PAWorks, assuming four separate flow pathways.

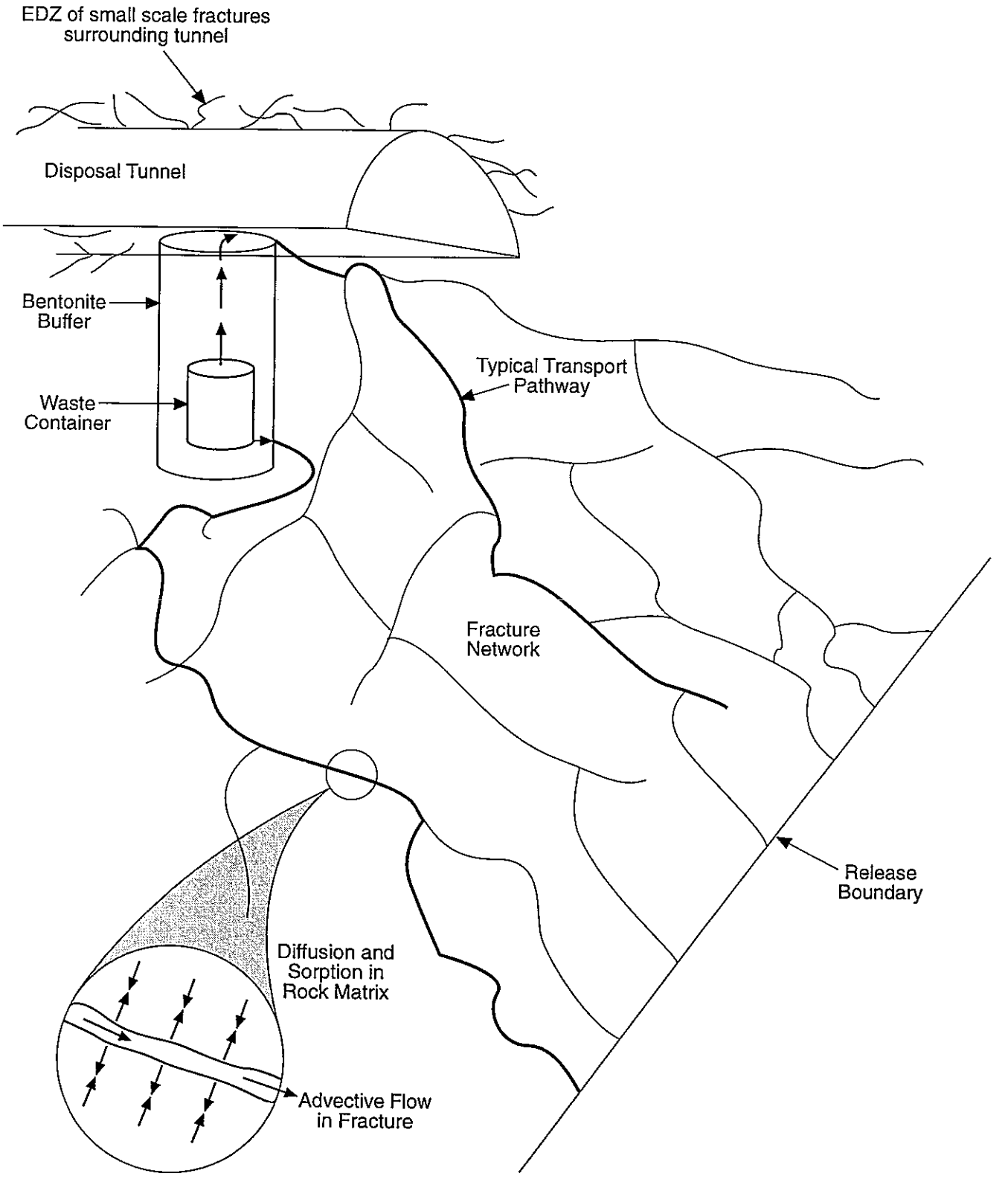

FIGURE **7-24**
CONCEPTUAL MODEL FOR PAWORKS/RIP DEMONSTRATION APPLICATION
PNC/PAW/LTG/JAPAN

PROJECT NO. 923 1089.824 DRAWING NO. 76066 DATE 11/24/97 DRAWN BY EA

Golder Associates

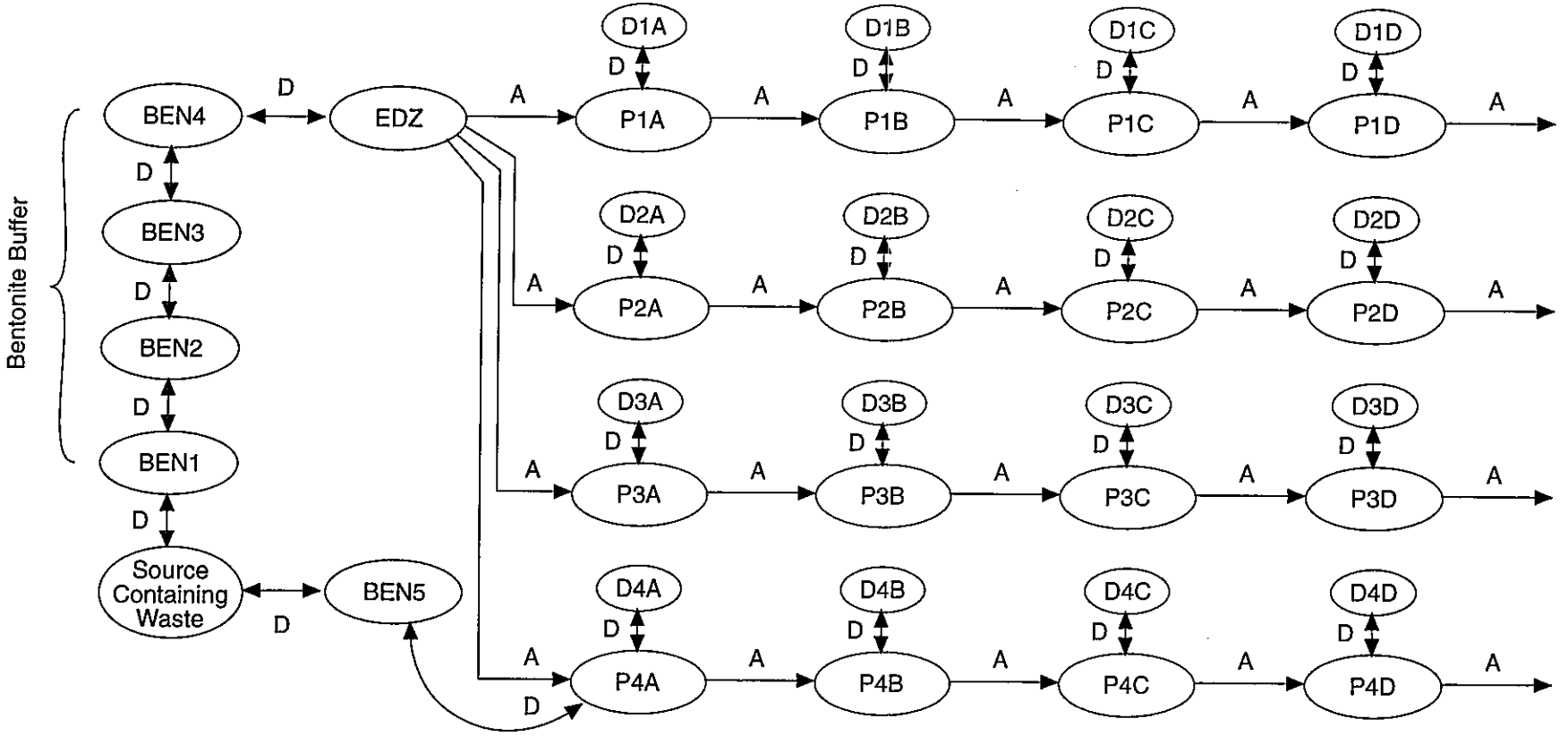

D = Diffusive Connection
A = Advective Connection

FIGURE **7-25**
RIP MODEL FOR PAWORKS/RIP DEMONSTRATION APPLICATION
PNC/PAW/LTG/JAPAN

PROJECT NO. 923 1089.824 DRAWING NO. 76065 DATE 11/24/97 DRAWN BY EA

Golder Associates

As in this analysis we use the output from PAWorks as input into RIP, we discuss the fracture network used to generate the representative pathway properties first. The fracture model and boundary conditions were the same as those used for the PAWorks/LTG example application, but the details have been reproduced here for clarity.

The fracture generation model for the Kamaishi block was that used produced by Doe et al. (1996) and used throughout this report. These input parameters to FracMan are reproduced as Table 2-1. The previously used 200m rock block representation of the Kamaishi site was produced by generating the fractures in a 225m cube to prevent the edges of the cube affecting the fracture intensity. Based on the results of the MAFIC to PAWorks comparison, the fracture intensity was set by assigning a minimum fracture transmissivity of 3×10^{-9} m^2/s, which is equivalent to 32,889 fractures generated in the 225m cube region. This fracture intensity at the Kamaishi site is sufficient to minimize the effect of the neglecting the lower transmissivity fractures.

To produce input into the RIP code, it was necessary to track particle movement from a location in the center of the 200m cube. A full repository was not modeled. Instead a single fracture was used to represent the source location in the repository. This fracture was 50m in length (x direction), 10m in height (z direction), and oriented perpendicular to the flow gradient with its center located at (0.0, 0.0, 0.0). Therefore the minimum transport distance is 100m. The repository fracture was assigned a transmissivity lower than that of the surrounding fracture network so that its presence would not influence the flow field, or add additional connectivity to the fracture system.

Boundary condition "B" presented in Section 2 was used. The geometry and boundary conditions used for the PAWorks/RIP simulations are shown in Figure 7-15.

To generate the four representative pathways used in the RIP analysis PAWorks generated pathways between the repository fracture and the outflow boundary, using flux weighting to traverse the fracture network. Flux weighting was chosen as in this simulation we wished to follow the major release routes from the repository. The

weighted method of computing the aperture was used, i.e. $e_w = \Sigma(e_i * Q_i)/\Sigma Q_i$. Pathways were merged based on combining pathways with the same source.

The representative pathway properties for the four highest weighted flux pathways are given in Table 7-20.

Table 7-20 Representative Pathway Properties

Property	Pathway 1	Pathway 2	Pathway 3	Pathway 4
Length	176	151	164	157
Width	8.27	7.53	8.65	7.13
Aperture	5.06e-3	4.15e-3	4.39e-3	4.27e-3
Travel Time	7.82	8.12	7.40	6.71

Using this pathway information the RIP model was built, with the majority of additional input parameters being based on the conceptual model given in the First Progress Report (PNC, 1992).

The source term was assumed to comprise six radionuclides; Se-79, Cs-135 and the chain Am-241, Np-237, U-233, Th-229. The inventory of one unit of vitrified waste was used and the waste container was assumed to fail at a time of 1000 years. For consistency with the PNC (1992) report, the RIP simulation began at 1000 years, and the decayed inventory at 1000 years after emplacement is used as the initial condition. The properties of these six species are given in Table 7-21.

The solubilities used in the RIP analysis are also reproduced in Table 7-21. They were based on the values given in Table 4.4-5 of the PNC First Progress Report, 1992. For example purposes the saline reducing low pH values were used.

Table 7-21 Properties of the Radionuclides used in the RIP Analysis

Species	Initial Inventory (Bq/unit waste)	Decay Rate (1/year)	Solubility (g/m^3)
Se	0.559	1.07×10^{-5}	5.45×10^{-5}
Cs	0.571	3.01×10^{-7}	9.18×10^{-5}
U	0.0238	4.37×10^{-6}	8.37
Np	0.59	3.24×10^{-7}	1.21×10^{-3}
Am	190.	1.60×10^{-3}	2.43×10^{-2}
Th	0.	9.44×10^{-5}	118

The properties of the bentonite buffer are given in Table 7-22, and the properties of the rock matrix in Table 7-23. For completeness the entire parameter set input into the RIP model is presented as Table 7-24.

Table 7-22 Properties of the Bentonite Buffer

Property	**Value**	**Reference**
Thickness in vertical direction (m)	2.0	PNC (1992) Figure 2
Thickness in lateral direction (m)	0.33	PNC (1992) Figure 2
Dry Density (kg/m^3)	1800	PNC (1992) 4-106
Porosity (-)	0.33	PNC (1992) 4-106
Tortuosity (-)	0.5	Assumed
Kd of Se (m^3/kg)	0.001	PNC (1992) 4-104
Kd of Cs (m^3/kg)	0.001	PNC (1992) 4-104
Kd of Am (m^3/kg)	10.	PNC (1992) 4-104
Kd of Np (m^3/kg)	0.1	PNC (1992) 4-104
Kd of U (m^3/kg)	0.1	PNC (1992) 4-104
Kd of Th (m^3/kg)	0.1	PNC (1992) 4-104

Table 7-23 Properties of the Rock Matrix

Property	Value	Reference
Dry Density (kg/m^3)	2400	Assumed
Porosity (-)	0.01	PNC (1992) 4-128
Tortuosity (-)	0.5	Assumed
Kd of Se (m^3/kg)	0.01	Range from PNC (1992) 4-130
Kd of Cs (m^3/kg)	0.05	Range from PNC (1992) 4-130
Kd of Am (m^3/kg)	0.1	Range from PNC (1992) 4-130
Kd of Np (m^3/kg)	0.1	Range from PNC (1992) 4-130
Kd of U (m^3/kg)	0.001	Range from PNC (1992) 4-130
Kd of Th (m^3/kg)	0.5	Range from PNC (1992) 4-130

Table 7-24 RIP Parameter Database

RIP Variable	Property	Value
BNAREA	Cross-sectional area of bentonite buffer (m^2)	PI * 1.7 * 1.7 / 4.
BNDENS	Density of bentonite buffer (kg/m^3)	1800.
BNDLEN	Diffusion distance within Bentonite Cell (m)	BNSLEN/2.
BNKDAM	Kd of Am in bentonite	10.
BNKDCS	Kd of Cs in bentonite	0.001
BNKDNP	Kd of Np in bentonite	0.1
BNKDSE	Kd of Se in bentonite	0.001
BNKDTH	Kd of Th in bentonite	0.1
BNKDU	Kd of U in bentonite	0.1
BNLENG	Total length of bentonite buffer (bentonite diffusion distance) (m)	2.0
BNMASS	Mass of bentonite in one cell (kg)	BNDENS * BNSVOL
BNPOR	Porosity of bentonite buffer (-)	0.33
BNRARE	Bentonite radial diffusion area (m^2)	1.95 * 1.04
BNRDDS	Bentonite average radial diffusion distance (m)	0.165
BNRMAS	Bentonite radial mass (kg)	BNRVOL * BNDENS
BNRVOL	Bentonite radial diffusion volume (m^3)	BNRARE * 0.33
BNRWVL	Bentonite radial water volume (m^3)	BNRVOL * BNPOR
BNSLEN	Length of Bentonite cell (m)	BNLENG/4.
BNSVOL	Diffusion distance in bentonite cell (m)	BNVOL / 4.
BNTORT	Tortuosity in bentonite buffer (-)	0.5
BNVOL	Total volume of bentonite buffer (m^3)	BNAREA * BNLENG
BNWVOL	Volume of water in a bentonite cell (m^3)	BNPOR * BNSVOL
D1AREA	Diffusive area between Pathway 1 & rock matrix (per cell) (m2)	(P1LENG / DIVISN) * P1WIDT

RIP Variable	Property	Value
D1RMAS	Mass of rock in diffusions cells on Pathway 1 (kg)	D1VOL * ROCKDN
D1VOL	Volume of diffusion cell on Pathway 1 (m^3)	(P1LENG / DIVISN) * P1WIDT * DIFLEN
D1WVOL	Volume of water in diffusion cell on Pathway 1 (m^3)	D1VOL * ROCKPR
D2AREA	Diffusive area between Pathway 2 & rock matrix (per cell) (m2)	P2WIDT * P2LENG / DIVISN
D2RMAS	Mass of rock in diffusions cells on Pathway 2 (kg)	D2VOL * ROCKDN
D2VOL	Volume of diffusion cell on Pathway 2 (m^3)	(P2LENG / DIVISN) * P2WIDT * DIFLEN
D2WVOL	Volume of water in diffusion cell on Pathway 2 (m^3)	D2VOL * ROCKPR
D3AREA	Diffusive area between Pathway 3 & rock matrix (per cell) (m2)	P3WIDT * P3LENG / DIVISN
D3RMAS	Mass of rock in diffusions cells on Pathway 3 (kg)	D3VOL * ROCKDN
D3VOL	Volume of diffusion cell on Pathway 3 (m^3)	(P3LENG / DIVISN) * P3WIDT * DIFLEN
D3WVOL	Volume of water in diffusion cell on Pathway 3 (m^3)	D3VOL * ROCKPR
D4AREA	Diffusive area between Pathway 4 & rock matrix (per cell) (m2)	P4WIDT * P4LENG / DIVISN
D4RMAS	Mass of rock in diffusions cells on Pathway 4 (kg)	D4VOL * ROCKDN
D4VOL	Volume of diffusion cell on Pathway 4 (m^3)	(P4LENG / DIVISN) * P4WIDT * DIFLEN
D4WVOL	Volume of water in diffusion cell on Pathway 4 (m^3)	D4VOL * ROCKPR
DIFDIS	Average diffusion distance (m)	DIFLEN / 2.
DIFLEN	Maximum diffusion distance (m)	0.1
DIVISN	Number of cells on main pathways	4
EDZAPR	Aperture of the EDZ fracture (m)	8.E-3
EDZLEN	Length of the EDZ (m)	2.
EDZVOL	Volume of the EDZ fracture (m^3)	EDZWID * EDZAPR * EDZLEN
P1APER	Aperture of Pathway 1	5.06e-3
P1AREA	Flow area of Pathway 1 (m^2)	P1APER * P1WIDT
P1DDS	Diffusion distance inside Pathway 1 (m)	P1APER/2
P1FLOW	Volumetric flow through Pathway 1 (m^3/year)	P1AREA * P1LENG/ P1TRAV
P1LENG	Length pathway 1 (m)	176
P1SLEN	Length of cell in Pathway 1 (m)	P1LENG / DIVISN
P1TRAV	Travel time in Pathway 1 (years)	7.82
P1VOL	Volume of Pathway 1 fracture (m^3)	P1AREA * P1LENG / DIVISN
P1WIDT	Width of Pathway 1	8.27
P2APER	Aperture of Pathway 2	4.15e-3
P2AREA	Flow area of Pathway 2 (m^2)	P2APER * P2WIDT

RIP Variable	Property	Value
P2DDS	Diffusion distance inside Pathway 2 (m)	P2APER/2
P2FLOW	Volumetric flow through Pathway 2 (m^3/year)	P2AREA * P2LENG/ P2TRAV
P2LENG	Length pathway 2	151
P2SLEN	Length of cell in Pathway 2 (m)	P2LENG / DIVISN
P2TRAV	Travel time in Pathway 2 (years)	8.12
P2VOL	Volume of Pathway 2 fracture (m^3)	P2AREA * P2LENG / DIVISN
P2WIDT	Width of Pathway 2	7.53
P3APER	Aperture of Pathway 3	4.39e-3
P3AREA	Flow area of Pathway 3 (m^2)	P3APER * P3WIDT
P3DDS	Diffusion distance inside Pathway 3 (m)	P3APER/2
P3FLOW	Volumetric flow through Pathway 3 (m^3/year)	P3AREA * P3LENG/ P3TRAV
P3LENG	Length pathway 3	164
P3SLEN	Length of cell in Pathway 3 (m)	P3LENG / DIVISN
P3TRAV	Travel time in Pathway 3 (years)	7.4
P3VOL	Volume of Pathway 3 fracture (m^3)	P3AREA * P3LENG / DIVISN
P3WIDT	Width of Pathway 3	8.65
P4APER	Aperture of Pathway 4	4.27e-3
P4AREA	Flow area of Pathway 4 (m^2)	P4APER * P4WIDT
P4DDS	Diffusion distance inside Pathway 4 (m)	P4APER/2
P4FLOW	Volumetric flow through Pathway 4 (m^3/year)	P4AREA * P4LENG/ P4TRAV
P4LENG	Length pathway 4	157
P4SLEN	Length of cell in Pathway 4 (m)	P4LENG / DIVISN
P4TRAV	Travel time in Pathway 4 (years)	6.71
P4VOL	Volume of Pathway 4 fracture (m^3)	P4AREA * P4LENG / DIVISN
P4WIDT	Width of Pathway 4	7.13
PI	π	3.142
RKKDAM	Kd of Am in rock (m^3/kg)	0.1
RKKDCS	Kd of Cs in rock (m^3/kg)	0.05
RKKDNP	Kd of Np in rock (m^3/kg)	0.1
RKKDSE	Kd of Se in rock (m^3/kg)	0.01
RKKDTH	Kd of Th in rock (m^3/kg)	0.5
RKKDU	Kd of U in rock (m^3/kg)	0.001
RKTORT	Tortuosity in rock matrix (-)	0.5
ROCKDN	Density of rock matrix (kg/m^3)	2400.
ROCKPR	Porosity of rock matrix (-)	0.01
SOLAM	Solubility of Am in water (Bq/m^3)	2.43×10^{-2}
SOLCS	Solubility of Cs in water (Bq/m^3)	9.18×10^{-5}
SOLNP	Solubility of Np in water (Bq/m^3)	1.21×10^{-3}
SOLSE	Solubility of Se in water (Bq/m^3)	5.45×10^{-5}
SOLTH	Solubility of Th in water (Bq/m^3)	118.
SOLU	Solubility of U in water (Bq/m^3)	8.37
SRCVOL	Volume of waste container (m^3)	(pi * 1.04 * 1.04 /4) * 1.95

The results of the RIP simulation are shown in Figures7-26 to 7-33.

Figures 7-26 and 7-27 show the release from the source into the vertically and radially located bentonite buffers respectively. Initially the release into the bentonite buffer vertically and radially is approximately equal, due the approximately equal diffusion areas. However, the area available for diffusion at the outer radial edge of the buffer is small and the bentonite reaches its solubility limit at about 100 years. After 100 years mass diffuses back from the radial bentonite buffer into the source and then diffuses along the radial pathway which has a larger diffusion area connecting it to the EDZ.

This behavior is mirrored in the releases from the bentonite buffer to the EDZ and Pathway 4 (see Figures 7-28 and 7-29 respectively). Initially the release rate from the radial bentonite cell into Pathway 4 is higher than that into the EDZ, due to the shorter diffusion distance radially from the canister. However, Figure 7-29 shows the diffusion reaching a maximum rate by 100 years due to a small diffusion area out of the bentonite buffer, while Figure 7-28 indicate the diffusion release rate continuing to increase over much longer time frames (1000 to 100,000 years). Similarly, the peak release rate is higher into the EDZ.

Release from the fracture network pathways (Figures 7-30 to 7-33) show only small difference between Pathways 1, 2 and 3; on the time frame considered in this analysis the differences between the pathways are small. However, Pathway 4 shows higher releases of all radionuclides at early time and reaches peak release rate earlier for Cs-135 and Se-79. The difference in release is particularly apparent for Am-241, as the short half life of this radionuclide means that it has negligible release from Pathways 1 to 3. But the shorter diffusion distance radially causes higher release to the accessible environment.

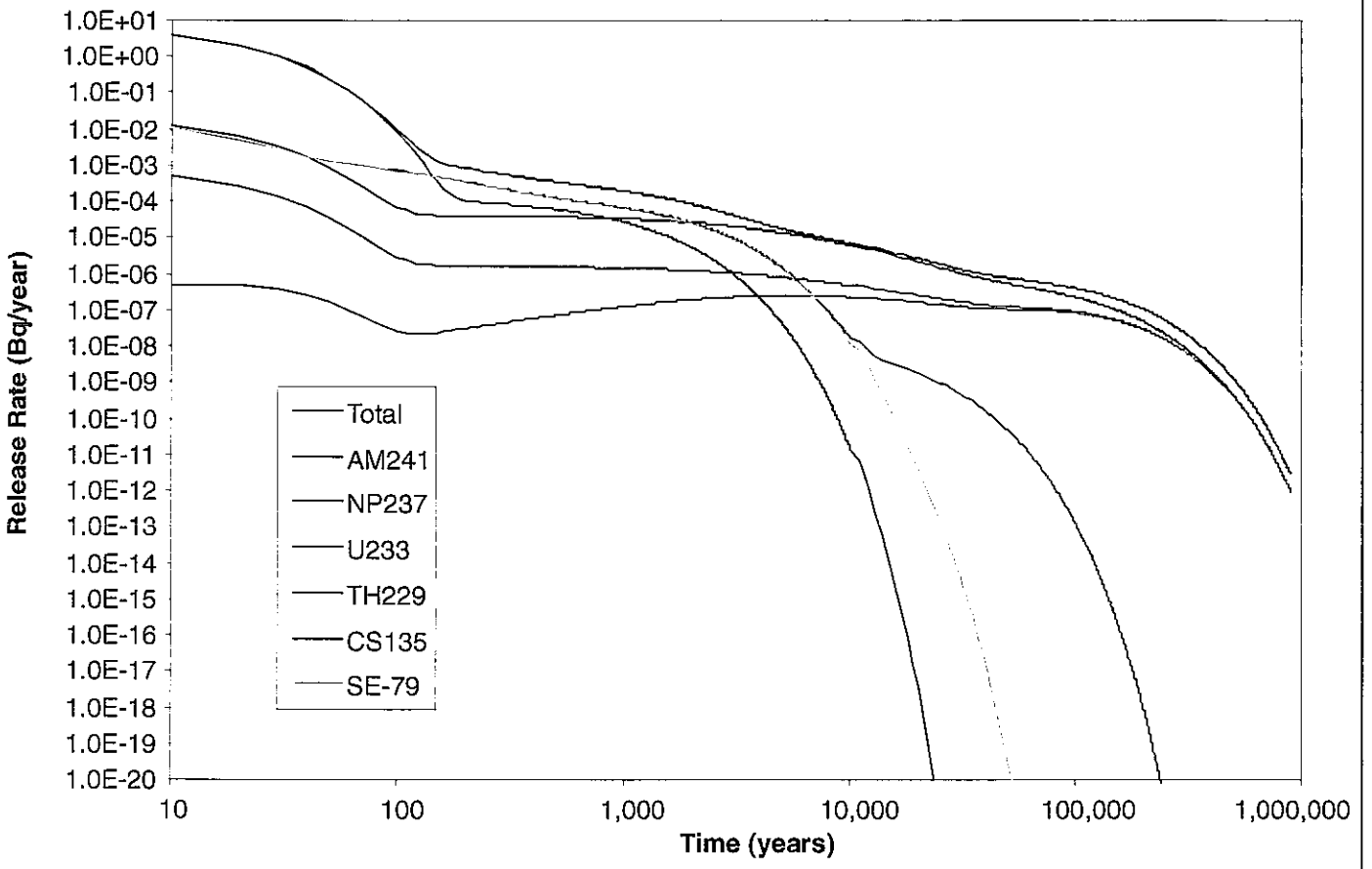

FIGURE **7-26**
RELEASE FROM SOURCE TO VERTICAL BENTONITE BUFFER
PNC/PAW/LTG/JAPAN

PROJECT NO. 923 1089.824 DRAWING NO. 76071 DATE 11/24/97 DRAWN BY EA

Golder Associates

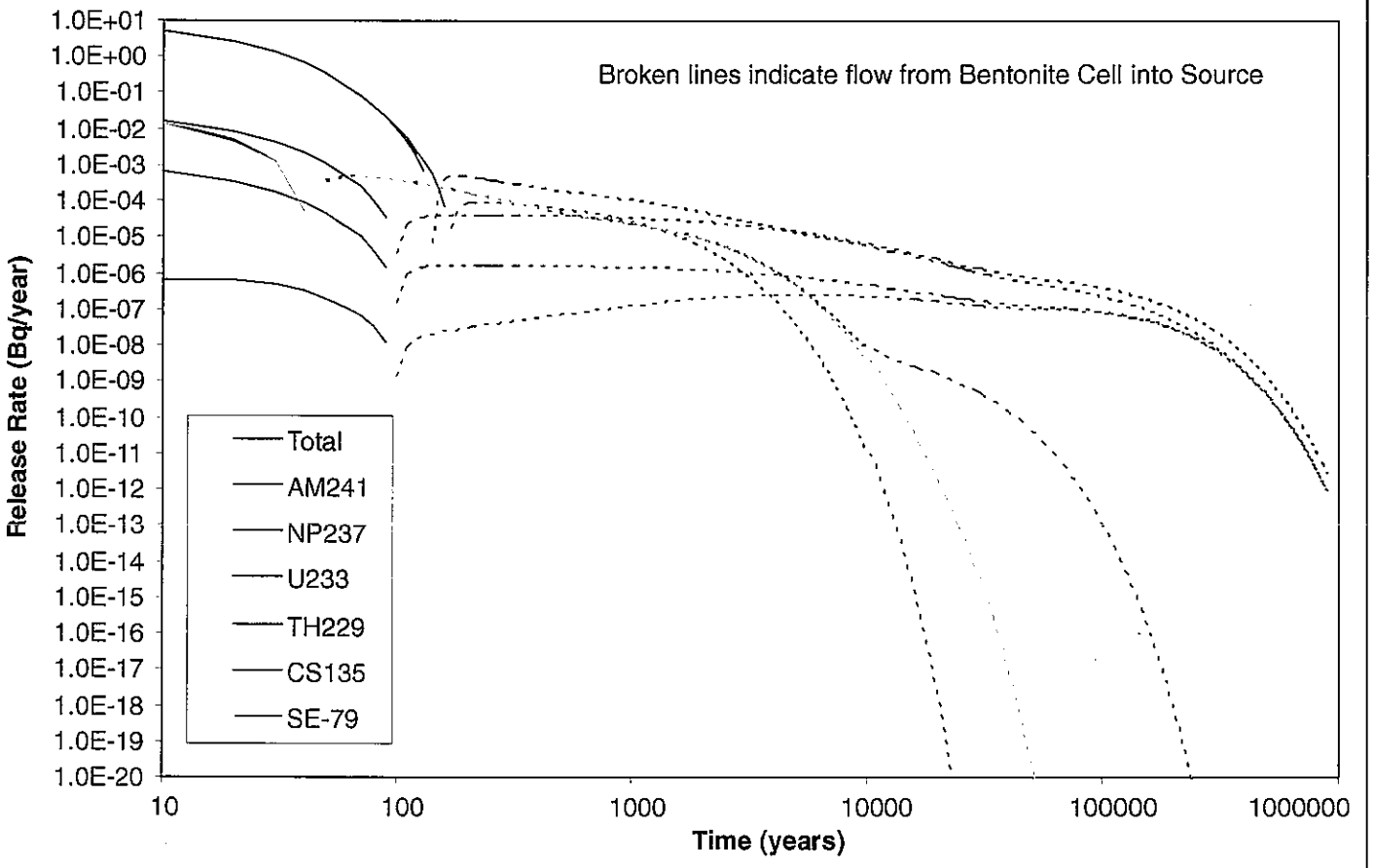

FIGURE **7-27**

RELEASE FROM SOURCE TO RADIAL BENTONITE BUFFER

PNC/PAW/LTG/JAPAN

PROJECT NO. 923 1089.824 DRAWING NO. 76072 DATE 11/24/97 DRAWN BY EA

Golder Associates

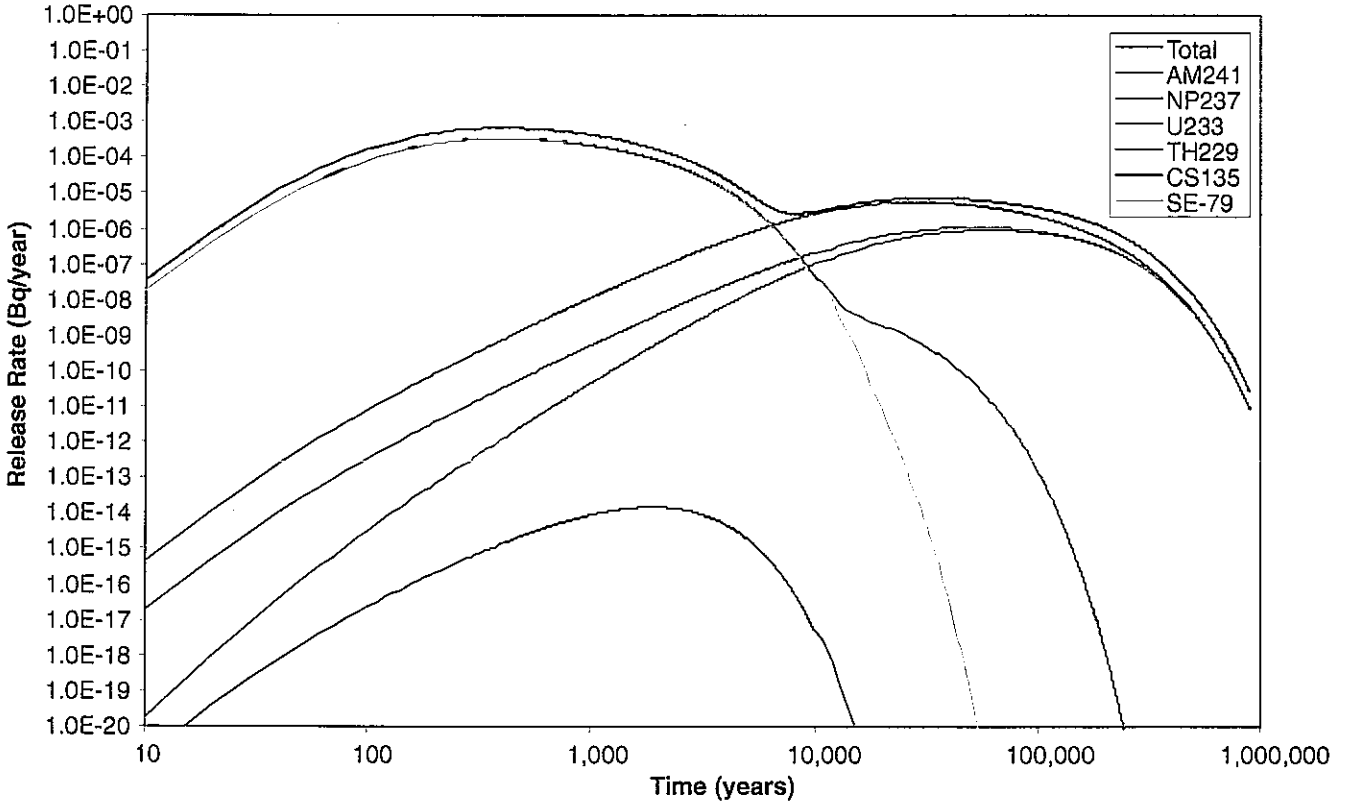

FIGURE **7-28**

RELEASE FROM BENTONITE BUFFER TO EDZ

PNC/PAW/LTG/JAPAN

PROJECT NO. 923 1089.824 DRAWING NO. 76073 DATE 11/24/97 DRAWN BY EA

Golder Associates

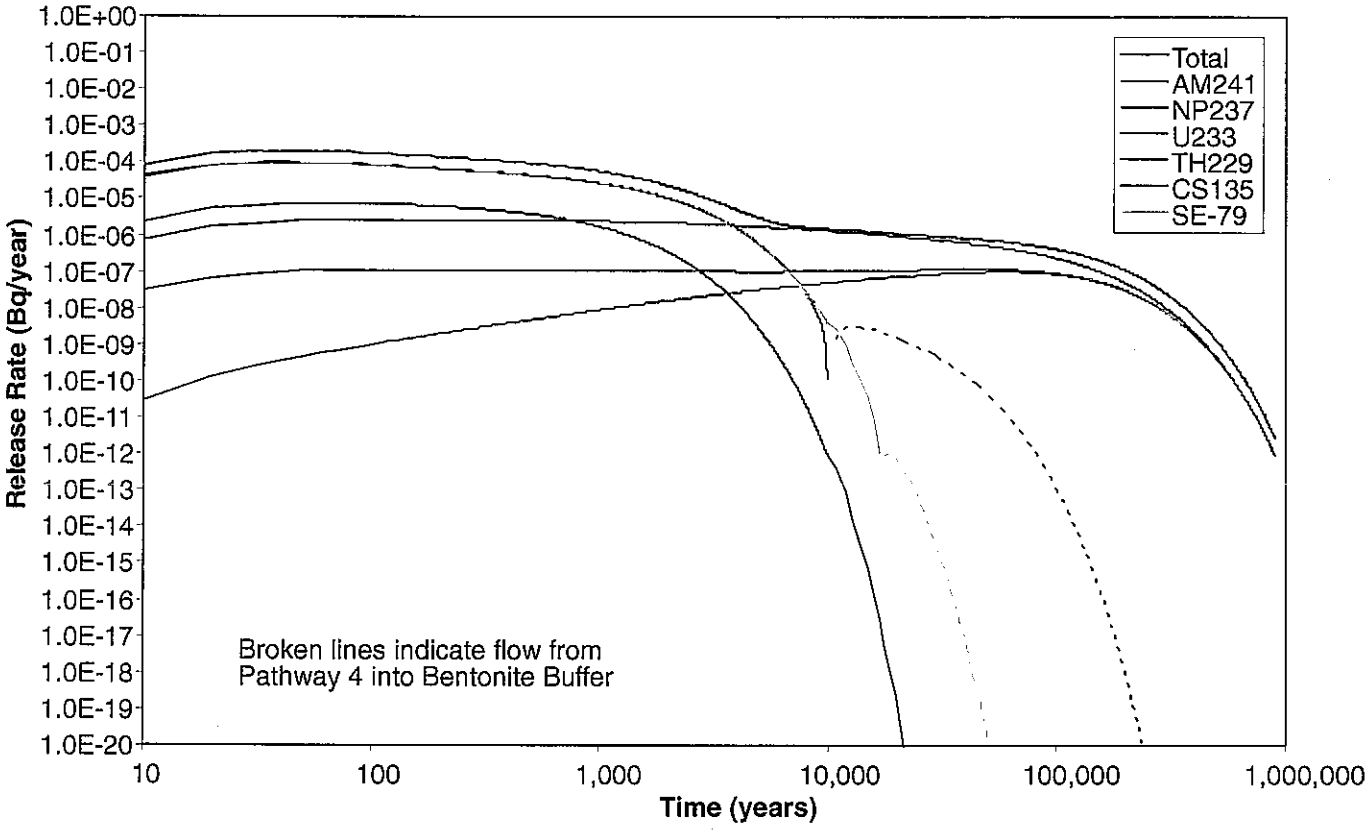

FIGURE **7-29**
RELEASE FROM BENTONITE BUFFER TO PATHWAY 4
PNC/PAW/LTG/JAPAN

PROJECT NO. 923 1089.824 DRAWING NO. 76074 DATE 11/24/97 DRAWN BY EA

Golder Associates

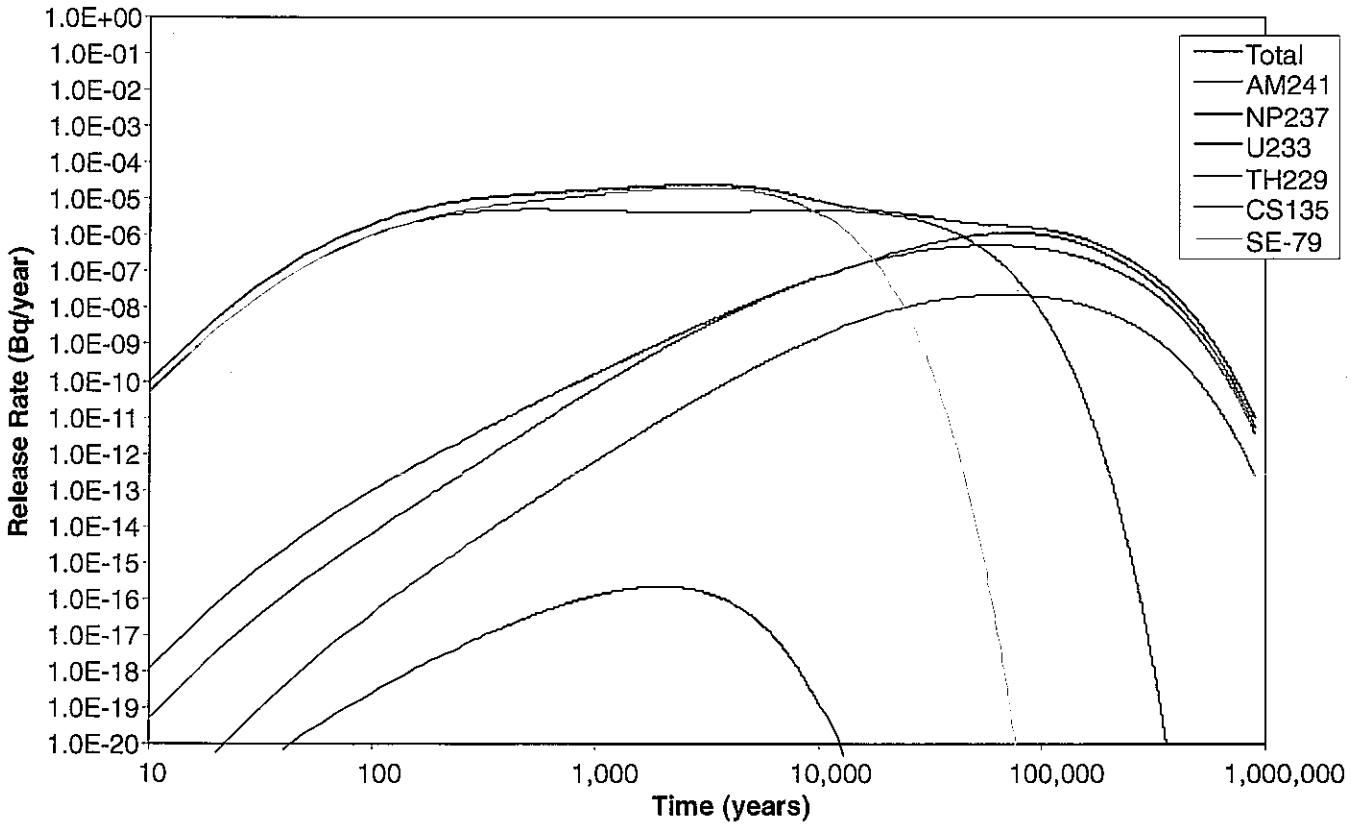

FIGURE **7-30**
RELEASE FROM PATHWAY 1
PNC/PAW/LTG/JAPAN

PROJECT NO. 923 1089.824 DRAWING NO. 76075 DATE 11/24/97 DRAWN BY EA

Golder Associates

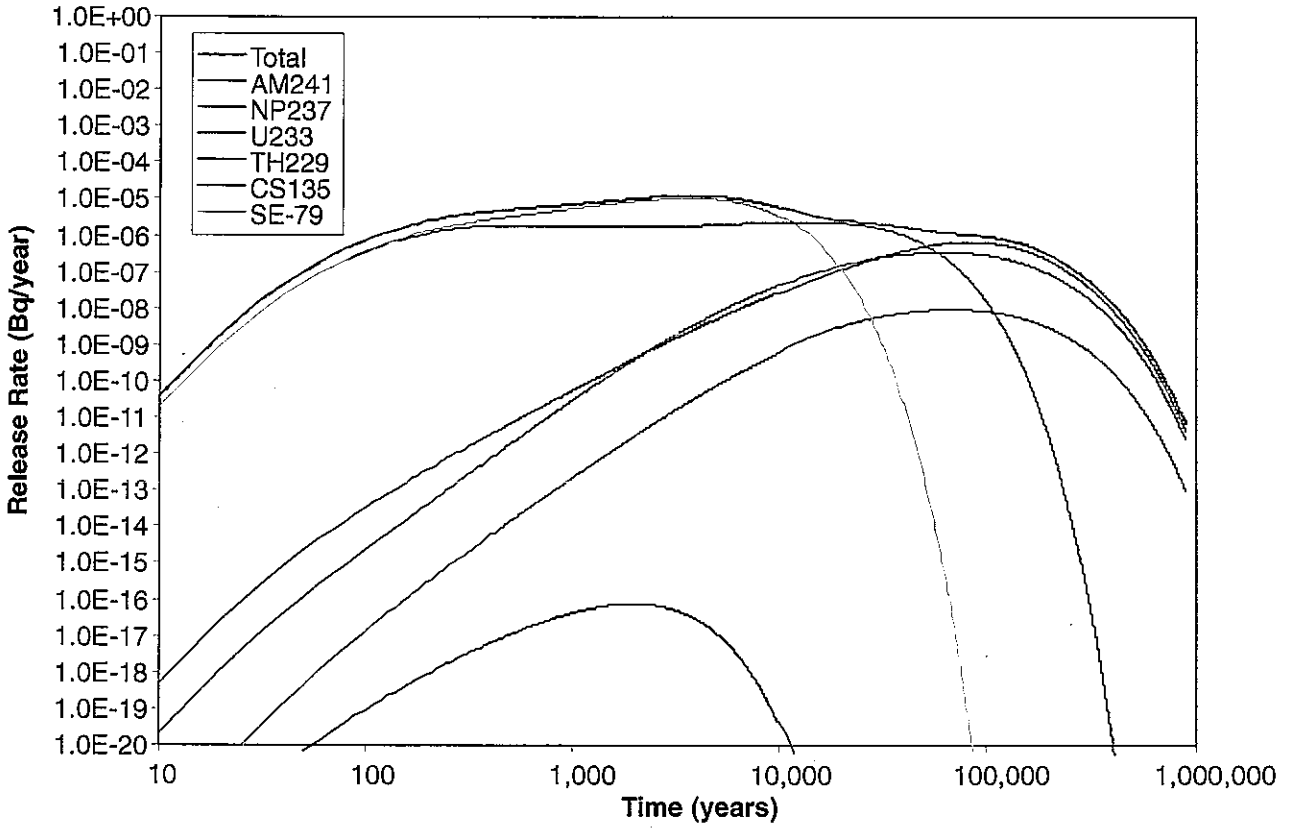

FIGURE **7-31**
RELEASE FROM PATHWAY 2
PNC/PAW/LTG/JAPAN

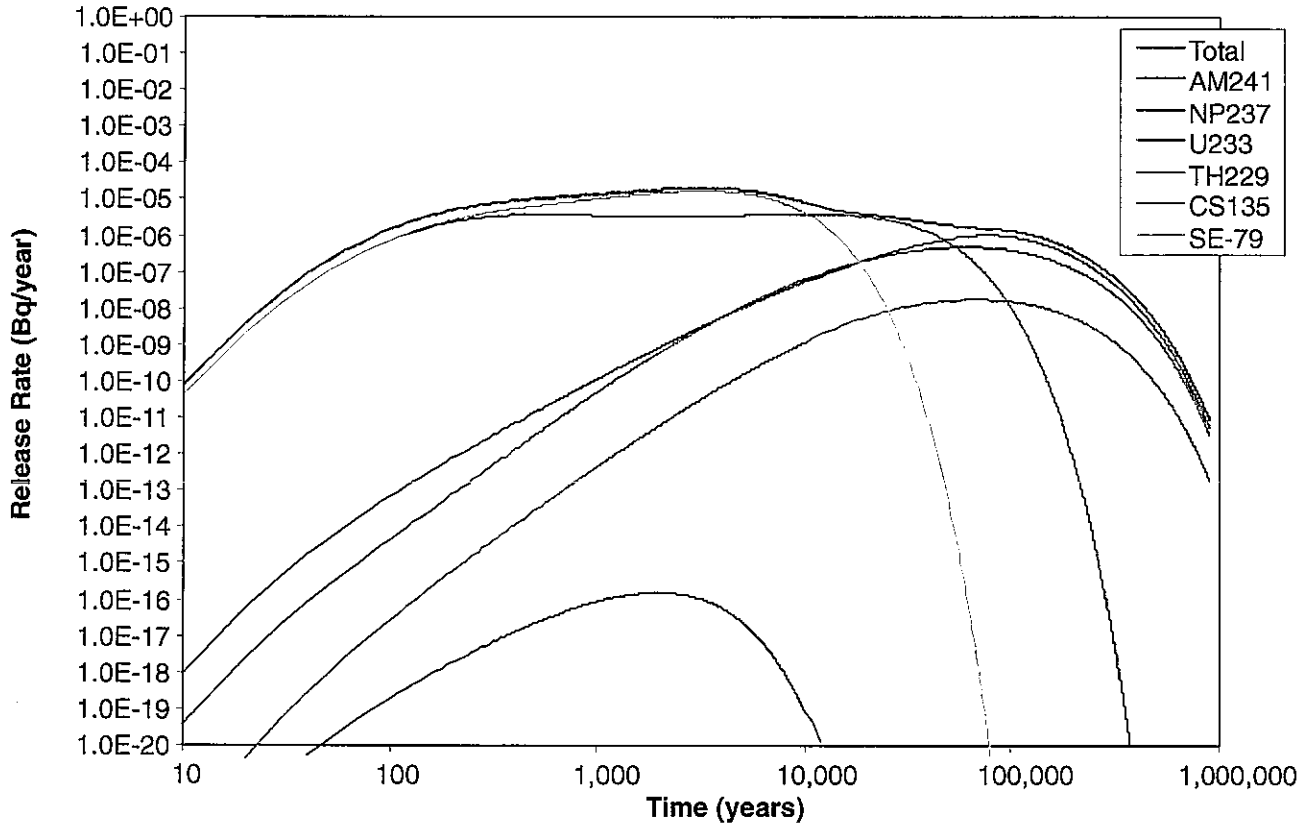

FIGURE **7-32**
RELEASE FROM PATHWAY 3
PNC/PAW/LTG/JAPAN

PROJECT NO. 923 1089.824 DRAWING NO. 76077 DATE 11/24/97 DRAWN BY EA

Golder Associates

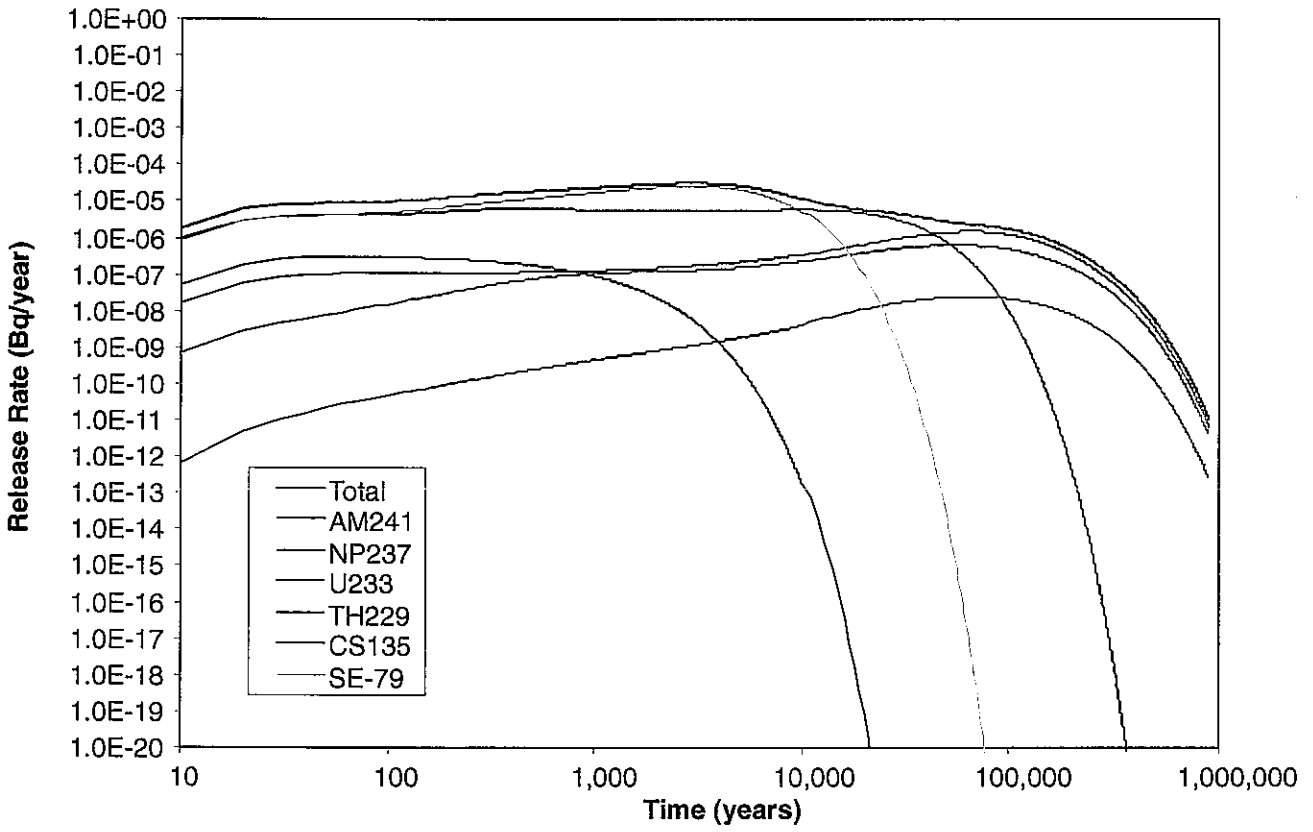

FIGURE **7-33**
RELEASE FROM PATHWAY 4
PNC/PAW/LTG/JAPAN

PROJECT NO. 923 1089.824 DRAWING NO. 76078 DATE 11/24/97 DRAWN BY EA

Golder Associates

In conclusion, even this fairly simple PAWorks/RIP model of the system is able to represent the variation in release due to conceptually different transportation pathways. This model could be expanded with minimal effort to include parameter variation (e.g. solubility ranges, non-instantaneous release of canisters). In addition, more representative PAWorks/RIP models could be developed to reflect a more complex conceptual model of the repository disposal system.

8. CONCLUSIONS

This report has investigated two separate issues in some depth. Chapters 3 to 6 looked at the correspondence between flow solutions undertaken using the plate element representation (MAFIC) and the pipe approximation (PAWorks) in terms of both the equivalence of the solution and the required computational power. Chapter 7 investigated the applicability of the PAWorks/LTG suite of codes to performance assessment type computations.

The MAFIC/PAWorks comparison indicated that PAWorks and MAFIC can give very similar solutions in terms of effective hydraulic conductivity and head variability provided care is taken to hone the PAWorks pipe generation properties. The effort appears worthwhile because PAWorks is able to handle much larger fracture networks for the same amount of CPU and memory. For example, Figures 5-10 and 5-11 indicate a CPU usage of about 20 times more for the equivalent MAFIC fracture network, while the MAFIC memory requirement (see Figures 5-12 and 5-13) is approximately 5 times higher.

However, PAWorks does have some limitations. The transport portion of PAWorks (called PAW) is only as efficient as the MAFIC counterpart, although it is able to handle larger networks. This disadvantage may be countered by improving the PAWorks pathways algorithm, or by using the LTG component of PAWorks directly. LTG can compute transport for the entire PAWorks pipe network, making computation of representative paths unnecessary, and the authors believe that if LTG is used as the solute transport code this is the preferred option.

The other limitation of PAWorks at this time is the lack of a good correlation between MAFIC and PAWorks travel times. The PAWorks and MAFIC pathways algorithms do not operate in the same manner, therefore the results presented in Section 5 and 6 are not conclusive. However there appears to be a slower transport time associated with the PAWorks pipe network. This may be related to the orientation of the generated pipes, and needs to be investigated further in future work.

Overall, the match between the MAFIC and PAWorks flow solutions was good, and

suggests that the larger fracture networks handled by PAWorks will make it a useful performance assessment tool for future analyses.

The final section of this report concentrated on the use of PAWorks in demonstration performance assessment computations. The purpose of these computations was to determine whether PAWorks/LTG could be a useful tool for performance assessment analysis. These four demonstration applications were distinct, and are therefore summarized independently.

The first demonstration application was a cross verification between the LTG component of PAWorks and RIP (an integrated probabilistic simulator used extensively by Golder for performance assessment of waste repositories). The purpose of these computations was to demonstrate that LTG and RIP provide the same solution for a series of fracture models, thereby generating confidence in LTG for solute transportation problems. The results were excellent, with LTG and RIP giving near identical solutions for all modeled problems.

The second demonstration application concentrated on showing how LTG can be used for solute transportation modeling of an entire fracture network. The model comprised release from a 50m by 10m source in the center of a 200m rock cube. The model included five radionuclides (including one daughter product), diffusion into the rock porosity and into the non-flowing fracture volume, and retardation on both the fracture surface and in the rock matrix. The results of this demonstration simulation were good, and provide confidence for future applications of this code to radionuclide transport.

PAWorks pathways analysis generate representative properties for fracture attributes such as width, length, aperture, flow wetted surface area, travel time, etc. which may be input into a solute transport code such as Crystal or RIP. The third demonstration application involved the generation of parameters for an example set of Crystal analyses. The parameters were based on the highest weighted flux pathway traversed, and representative pathways containing both 100% and 90% of the outflow flux from each source location. The results indicate that the parameter values generated by PAWorks are suitable as input for performance assessment codes.

The final demonstration application was an example performance assessment using PAWorks to generate the pathway properties, and RIP to carry out the solute transport analysis. The RIP analysis was deterministic. The conceptual model included solute transport through a bentonite buffer, advective flow through the EDZ, and advective and diffusion in the main fracture network. The demonstration indicated that PAWorks combined with RIP can model the advection and diffusion processes between canister failure and release to the accessible environment. In future analyses, RIP's stochastic capabilities could be combined with multiple PAWorks analyses and realistic ranges of the important material parameters, to more clearly define the important processes at the Kamaishi site.

REFERENCES

W. Dershowitz ,T. Doe, G. Lee, P. Wallman ,A. Thomas, T. Foxford, Reed Busse and P. LaPointe (1996), Appendix A of "Discrete fracture network code development", Heisei-7 Progress Report, PNC ZY 1579 96-001, March 1996.

T. Doe, W. Dershowitz, P. Wallman, G. Lee, P. LaPointe, S. Hitchcock and C. Chakrabarty (1993) "Discrete fracture network code development", Heisei-4 Progress Report, PNC PJ 1579 93-001, March 1993.

T. Foxford, E. Sudicky, W. Dershowitz, D .A. Shuttle and Th. Eiben (1997). PAWorks User Documentation, Version 1.4.

Golder Associates Inc. (1997) RIP Integrated Probalistic Simulator for Environmental Systems, Theory Manual and Users' Guide.

PNC (1992), Research and Development on Geological Disposal of High-Level Radioactive Waste, First Progress Report, September 1992.

Appendix B Äspö TRUE-1 -Radially Converging Experiment Report

SUMMARY OF SIMULATIONS FOR THE ÄSPÖ TRACER RETENTION UNDERSTANDING EXPERIMENT RADIALLY CONVERGING TRACER EXPERIMENT (TRUE-1/RC)

William S. Dershowitz

Reed Busse

Ian Kluckow

Peter C. Wallmann

Golder Associates, Inc.

Redmond, Washington USA

June 1996

Keywords: Fracture Flow, FracMan, Interference Testing, Structural Geology, Tracer Testing

TABLE OF CONTENTS

LIST OF FIGURES

LIST OF TABLES

EXECUTIVE SUMMARY

This report describes PNC/Golder analysis of the radially converging tracer experiment carried out by SKB as "Task 4c" of the Äspö Modeling Task Force (AMTF). PNC/Golder used three different analytical techniques, and a variety of boundary condition assumptions. The analyses carried out included analytical solutions, 2-D confined aquifer finite element analysis, and 3-D discrete fracture network simulation.

The conclusions from the analysis, as presented at the June, 1996 meeting of the AMTF were as follows:

- The head gradient assumption is critical to the analysis results.
- Tracer transport out of the plane of "Feature A" would be significant, based on the measured fracture intensity.
- In-plane heterogeneity probably causes poor recovery from boreholes KXTT2:P1/2 and KA3005A:P2, which have heads lower than that expected for the pumping borehole.
- The level of detail for the analysis should be appropriate for the experiment. In the current analysis, the assumption of boundary conditions and material properties, rather than the use of analytical, continuum, or fracture flow codes was the key consideration.

1. INTRODUCTION

The TRUE experiment is a series of flow and transport experiments at different scales and sites throughout the Äspö laboratory, designed to provide a better understanding of the nature of radionuclide transport in fractured granites. The TRUE-1 block is a well characterized rock block of approximately 50 m scale at the northern end of the Äspö Hard Rock Laboratory (HRL), near the 400 meter depth level (Figure 1-1).

The Äspö Modeling Task Force (AMTF) established modeling Task 4c, "Radially Converging Tracer Experiment RC-1", as the first predictive modeling exercise of the TRUE project. The RC-1 experiment was carried out on a single well defined fracture, "Feature A", within the "TRUE-1" experimental site (Figure 1-2).

The PNC/Golder team was directly involved in the data analysis for the TRUE-1 site as part of the TRUE project team during the Fall of 1995 and Winter of 1996. As a result, the PNC/Golder team recognized early on the importance of boundary condition assumptions for the experiment, and in particular the possibility that tracer would not be recovered to the pumping well unless high pumping rates were used. The PNC/Golder team recommended the use of relatively low pumping rates to avoid disguising the true in-situ conditions.

In order to clarify the modeling issues raised by the RC-1 experiment, the PNC/Golder team implemented three analytical techniques and four sets of boundary conditions, as summarized in Figure 1-3.

1.1 SCOPE

The scope of this report is to present the PNC/Golder team's participation in the TRUE-1, radially converging tracer test RC-1. This report is organized as follows. Section 1.1 below provide a brief description of the layout of the RC-1 experiment within the TRUE-1 block. . Section 2 describes the derivation of alternative boundary conditions. Section 3 describes the models implemented and simulation results as presented to the AMTF in advance of completion of simulations. Section 4 provides conclusions. Numerical model summaries as required by SKB are provided in Appendices A and B.

1.2 BACKGROUND

The prediction of the radially converging tracer test was based on information contained in Winberg, ed. (1996), Anderson et al. (1996), and

Dershowitz et al. (1996). These sources provided the following data, which provided the basis for the modeling.

a) fracture geometric and geological information from core logging, borehole television logging, and trace mapping on adjacent tunnel walls

b) fracture hydraulic properties derived from flow logs and packer tests

c) characterization of fracture connectivity by hydraulic interference testing

d) transport aperture and dispersivity from preliminary tracer testing in "Feature A"

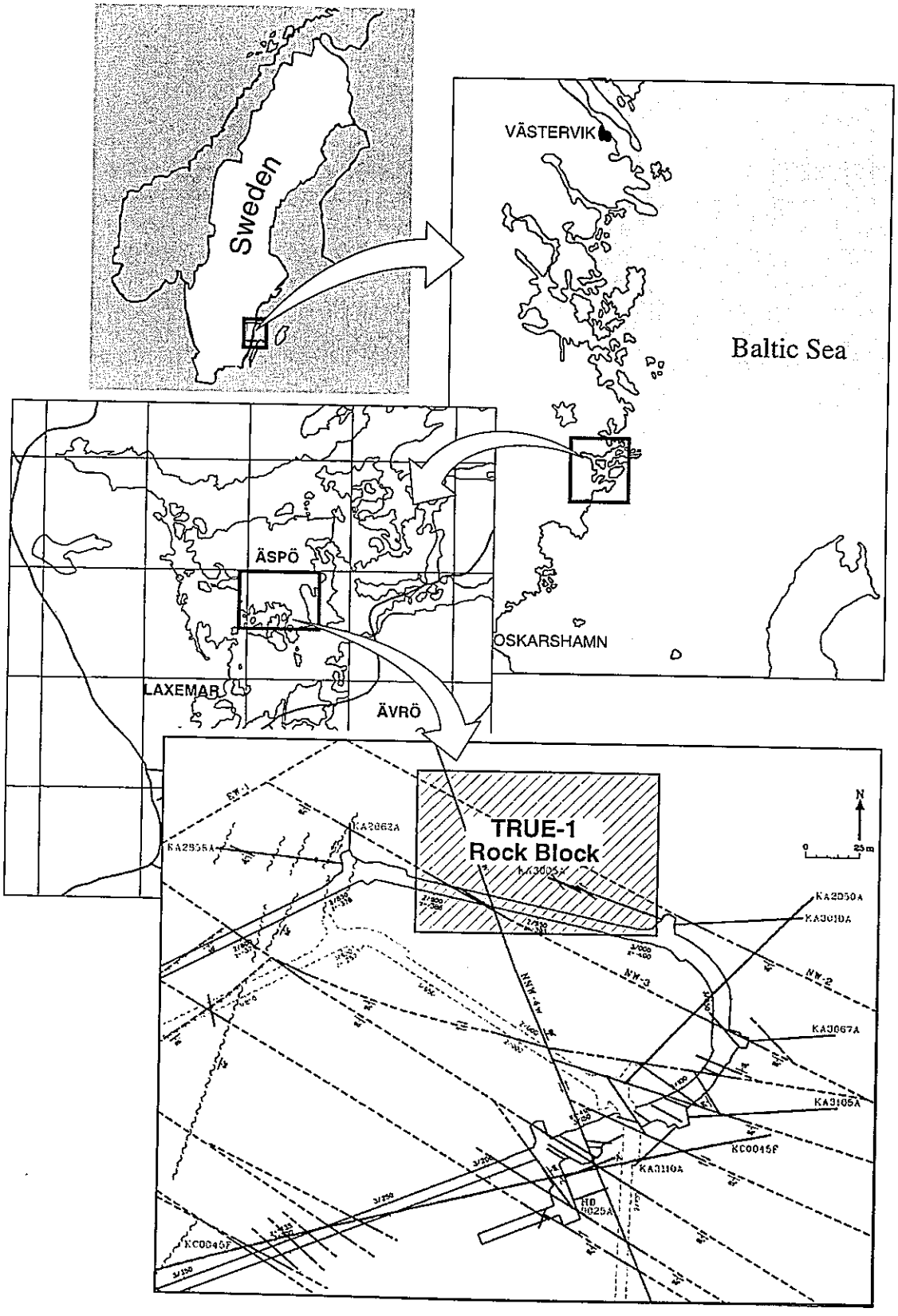

FIGURE **1-1**
TRUE-1 EXPERIMENT SITE
PNC/FRACTURE FLOW/JAPAN

PROJECT NO. 923 1089.831 DRAWING NO. 67562 DATE 9/19/96 DRAWN BY CB

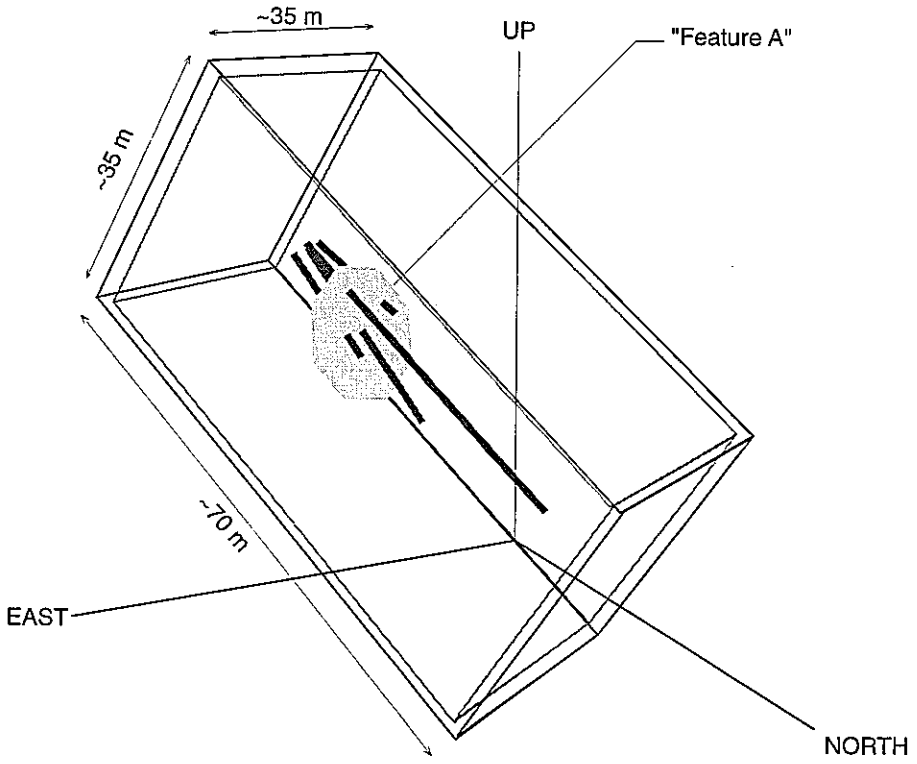

FIGURE **1-2**
TRUE-1 ROCK BLOCK
PNC/FRACTURE FLOW/JAPAN

PROJECT NO. 923 1089.831 DRAWING NO. 67583 DATE 3/11/97 DRAWN BY CB

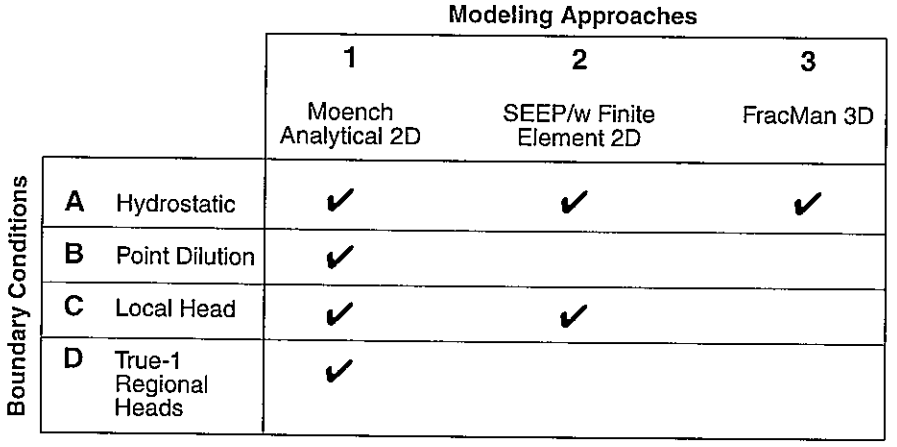

FIGURE **1-3**
PNC/GOLDER ANALYSES FOR TRUE-1/RC
PNC/FRACTURE FLOW/JAPAN

PROJECT NO. 923 1089.831 DRAWING NO. 67585 DATE 3/11/97 DRAWN BY CB

The layout of the preliminary tracer test and the radially converging tracer test RC-1 are illustrated in Figure 1-4. The test parameters of the two experiments are summarized in Table 1-1. These two experiments were carried out in the same fracture, and between two of the same boreholes, with only the pumping rate of the withdrawal well changed.. As a result, it is quite logical to predict that the results from this pair of boreholes will be similar. In the absence of other information, or assuming confined aquifer flow, it would also be logical to predict a priori that the other tracer injections would also be the same. However, as will be demonstrated in the next section, their is good reason to assume that the different tracer injection sections will behave quite differently.

Table 1-1 *True-1 Preliminary Tracer Experiment (after Anderson et al., 1996).*

Parameter	Feature A	Comment
Travel distance, x (m)	5.03	Geometrical distance
Delay in injection hole (min)	2	Calculated
Delay in sampling hole (min)	7	Calculated
Mean head difference, Δh (m)	24.3	Measured
Fracture conductivity, K_{fr} (m/s)	3.5×10^{-4}	Calculated
Equivalent fracture aperture, e (m)	1.4×10^{-3}	Calculated
Flow porosity, θ_k	1.8×10^{-4}	Calculated
Recovery, Injection period, R_{inj} (%)	92	Measured/Calculated

Table 1-1b *Tracer injection sequence during the TRUE radially converging tracer test (after Anderson et al, 1996).*

Borehole	Sec	Tracers	Inj. conc C_{oo} (mg/l)	Max conc C_{oo} (mg/l)	Vol. section (l)
KXTT1	P2	Uranine	5000	42	1.560
		Gd-DTPA	5000	42	
KXTT2	P2	Rhodamine WT	87502	73	1.548
		Eu-DTPA	3000	25	
KXTT4	P3	Amoino G Acid	9000	450	1.898
			1000	50	
KA3005A	P3	Eosin Y	13000	130	2.285
		Tb-DTPA	9000	90	

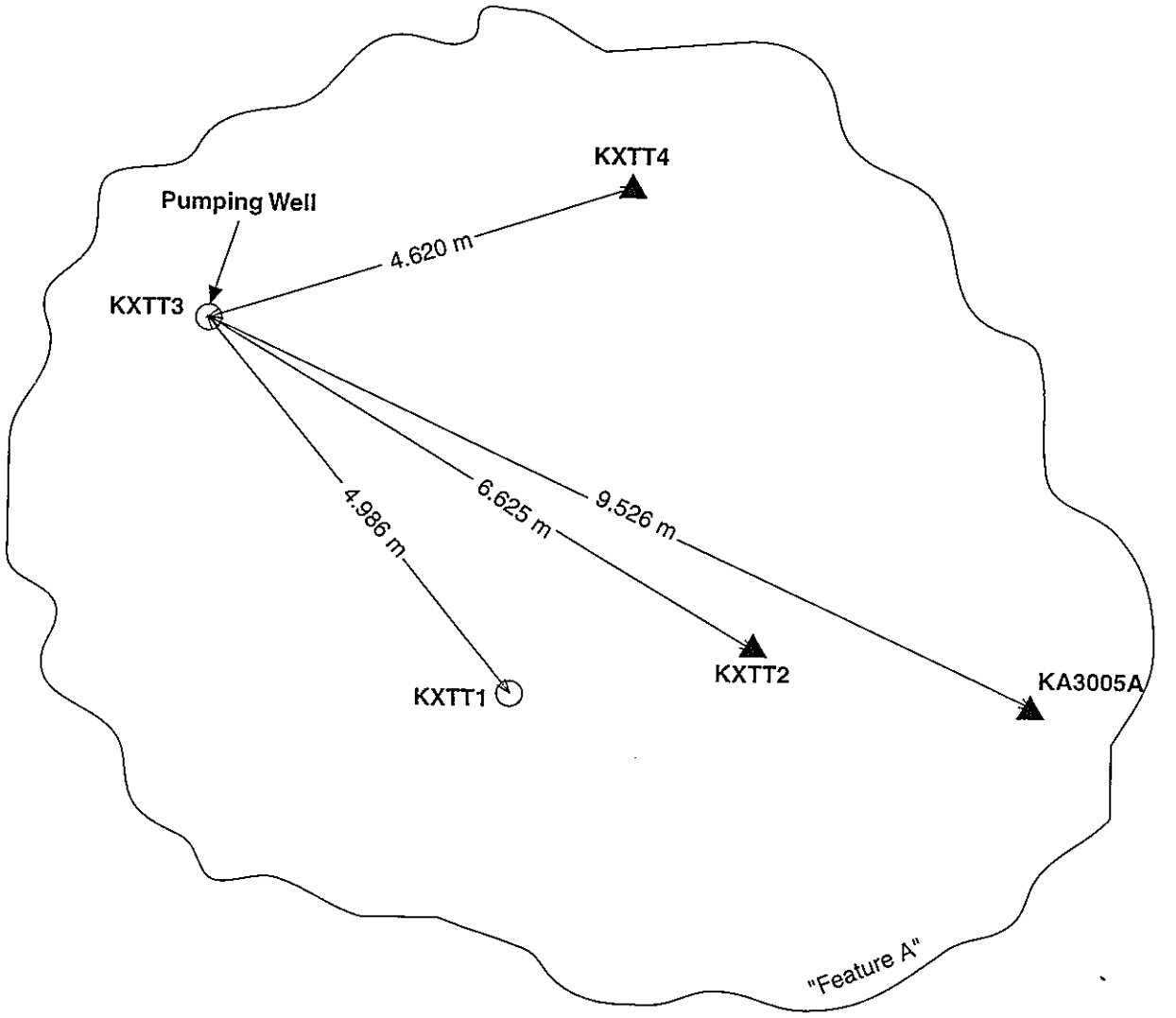

○ Used for both preliminary and RC-1 experiments

▲ RC-1 ONLY

Note: Preliminary test used extraction well KXTT3 pumping rate 0.87ℓ/min. RC-1 used extraction well KXTT3 with pumping rate 0.20ℓ/min. Distances shown above are slightly different from those reported by Winberg et al. (1996)

after Winberg et al. (1996)

FIGURE **1-4**
TRUE PRELIMINARY AND RC-1 EXPERIMENTS
PNC/FRACTURE FLOW/JAPAN

PROJECT NO. 923 1089.800 DRAWING NO. 72737 DATE 5/9/97 DRAWN BY CB

Golder Associates

Much of the AMTF modeling focused on defining appropriate stochastic continuum fields for "Feature A". Stochastic continuum fields were not used in the PNC/Golder modeling, because the preliminary tracer experiment indicated little longitudinal dispersion (Figure 1-5). If a stochastic continuum field were defined which resulted in pathways through several different areas with varying transmissivity, the result would be to over estimate the dispersion in the fracture plane. If a stochastic continuum field were defined which resulted in multiple pathways through channels of constant transmissivity, the result would not be differentiable from that of a homogeneous fracture, with sensitivity studies to reflect different transmissivities in different channels. In either case, a stochastic continuum approach would not be appropriate.

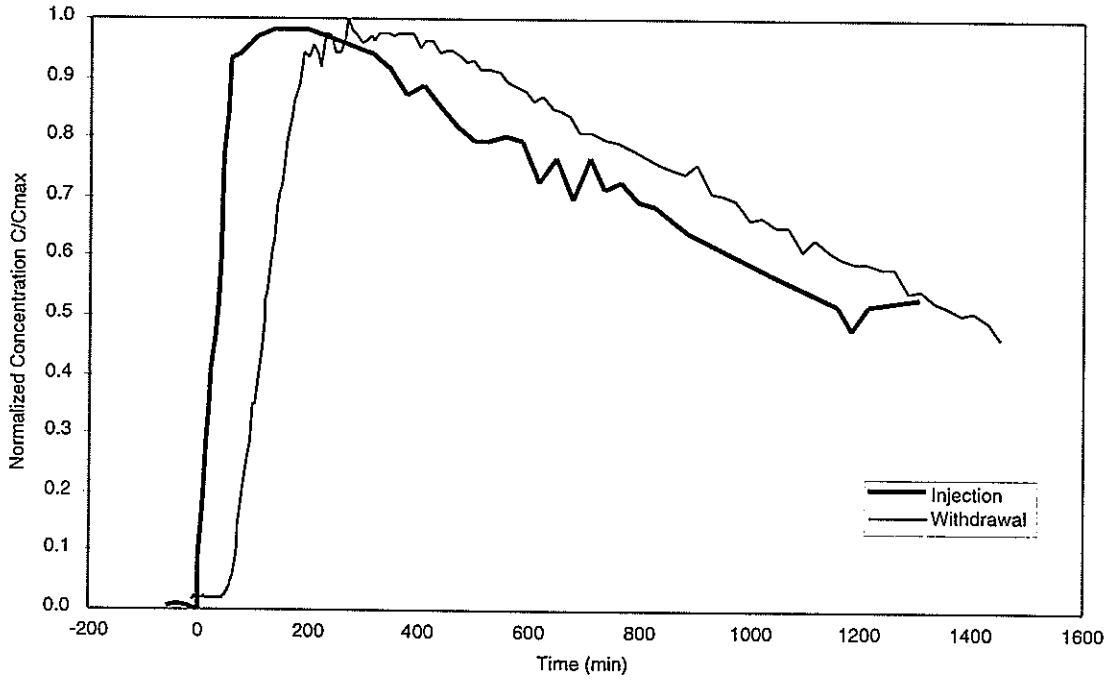

(a) Feature A Tracer Test

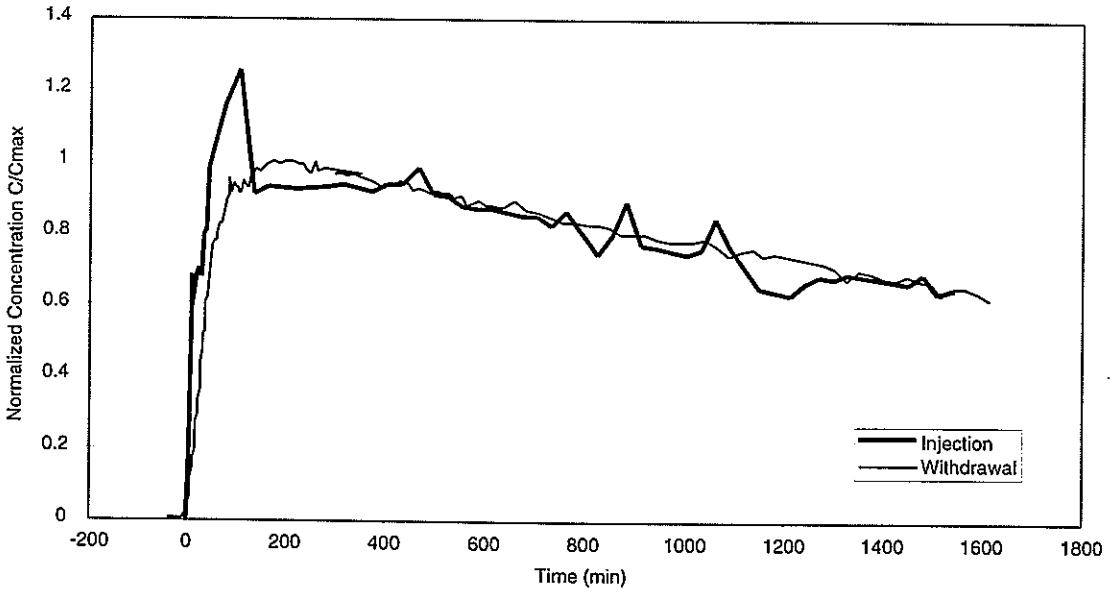

(b) Feature B Tracer Test

FIGURE **1-5**
INJECTIONAL WITHDRAWAL CURVES FOR PRELIMINARY TRACER TESTS
PNC/FRACTURE FLOW/JAPAN

after Dershowitz et al. (1996)

PROJECT NO. 923 1089.831 DRAWING NO. 67587 DATE 3/11/97 DRAWN BY CB

2. BOUNDARY CONDITIONS

This section describes the four sets of boundary conditions assumed in the simulations for the radially converging tracer test. As noted in the introduction, it is the opinion of the PNC/Golder team that a proper understanding of boundary conditions is the key to prediction of tracer tests, and without proper boundary conditions, no experimented prediction can be successful. The boundary conditions which were implemented are designated as follows:

A: **Hydrostatic:** Constant head on the boundaries of the model such that the only hydraulic sink is provided by the pumping well.

B: **Point Dilution**: Boundary conditions consistent with the a point dilution interpretation of the tracer time histories in the injection boreholes.

C: **Local Head**: Boundary conditions consistent with the heads measured in the injection and withdrawal boreholes of "Feature A" before initiation of the experiment.

D: **TRUE-1 Regional Heads**: Boundary conditions based on the heads measured in all of the boreholes of the TRUE-1 block.

All of these boundary conditions have a theoretical basis, and the selection of one for an "official prediction" is a matter of judgment. However, we have chosen the "point dilution" boundary condition as the primary basis for the prediction because it is directly related to the head field within Feature A at the time of the RC-1 experiment.

2.1 HYDROSTATIC BOUNDARY CONDITION "A"

If the withdrawal well KXTT3 were pumped at a high rate, it would result in a head field which would be simple, and radially converging from all of the boreholes to the pumping well. If this were the case, then the external applied headfield would be unimportant, and a simply hydrostatic unattached assumption would be adequate. This is not a particularly realistic boundary condition at the relatively low pumping rate (0.2 liters/minute) of the RC-1 experiment. However, the hydrostatic boundary condition does provides a good baseline for comparison of alternative boundary conditions.

The primary issue is applying a hydrostatic boundary condition to "Feature A" is the distance at which it is applied. If the boundary condition were

applied too near to the five experimental boreholes, then it could prevent the radially converging flow field from developing. However, if the boundary condition were applied at a great distance, this could significantly increase computation requirements.

For a rigorous analysis, the distance from the hydrostatic boundary condition to the RC-1 boreholes should be decided on the basis of numerical sensitivity studies. In the present case, however, the hydrostatic boundary condition was applied

(a) at infinity for the analytical solution

(b) at the edge the model, approximately 20 to 25 m from the pumping well for the numerical simulations (SEEP/W and FracMan).

As implemented, the hydrostatic boundary condition was defined as a head H of 360 m at all locations on the edges of "Feature A" for the SEEP/W model, and a head of 360 m on the edges of the 50 m scale model for the FracMan model. "Feature A" is only 10 m in the FracMan model, and is connected to the hydrostatic boundary conditions at the edge of the 50 m scale model by a complex fracture network. As a result, the initial heads on the boundaries of "Feature A" are not hydrostatic in the FracMan model as they are in the analytical and SEEP/W implementation.

Based on the hydrostatic boundary condition assumption, the initial head at the pumping well and the injection wells would all be at 360 m.

2.2 POINT DILUTION BOUNDARY CONDITION "B"

The radially converging tracer experiment uses a "decaying pulse" injection. That is, a fixed amount of tracer is introduced into the injection interval, and the concentration in the injection interval is allowed to decrease as a result of dilution as the experiment progresses. For a simple radially converging test, the decrease in concentration of all of the injection intervals would be similar. However, visual inspection of the concentration time histories for the injection boreholes demonstrates that this is clearly not the case (Figure 2-1). Clearly, there is a substantially greater flow through KXTT1 and KXTT4 than through KXTT2 and KA3005A. This can be due to either:

- Local heterogeneity of the transmissivity field which increases the flow through KXTT1 and KXTT4, or
- Differences in the local head field which result in higher gradients and greater flows.

Figure 2-1a Tracer Injection - KXTT1

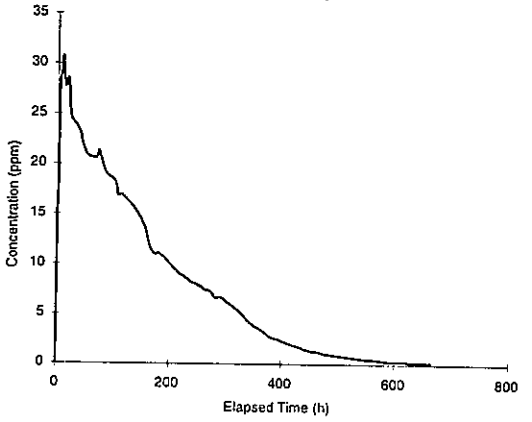

Figure 2-1b Tracer Injection - KXTT2

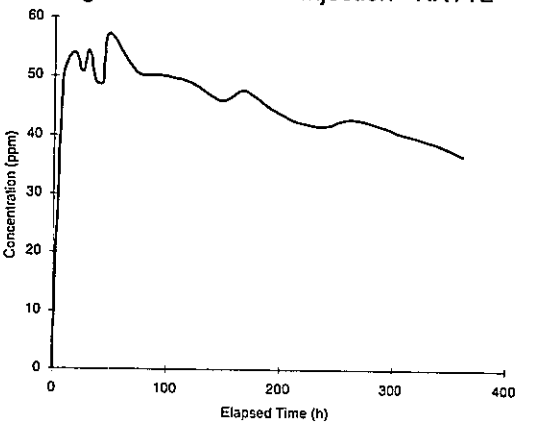

Figure 2-1c Tracer Injection - KXTT4

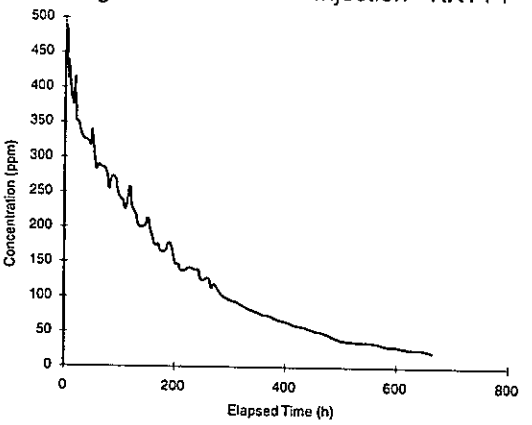

Figure 2-1d Tracer Injection - KA3005A

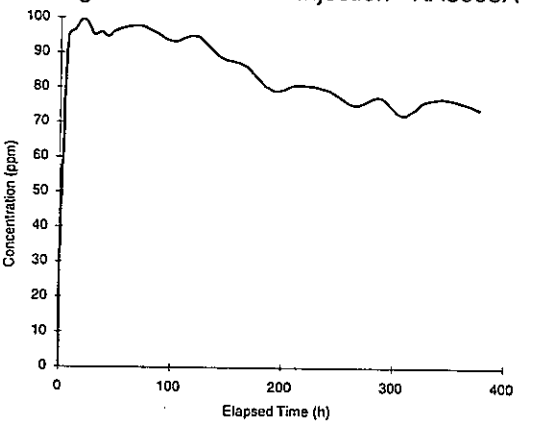

FIGURE **2-1**
TRACER INJECTION CURVES
PNC/FRACTURE FLOW/JAPAN

PROJECT NO. 923 1089.831 DRAWING NO. 67588 DATE 9/20/96 DRAWN BY CB

The lack of longitudinal dispersion in the preliminary tracer test indicates that variations in pressure rather than local heterogeneity may be dominating in this case.

Tracer concentrations in the injection wells were provided by Winberg et al. (1996) based on measurements over the duration of the tracer experiments (Figure 2-1). Because of borehole storage effects, the tracer was slowly being "bled" from the injection well. The first step of the analysis was to calculate the flux through the injection wells. This was done as follows.

A concentration can be described as a function of time by solving the first order differential equation:

$$\frac{dC}{dt} = -\frac{Q}{V}C \qquad 2\text{-}1$$

$$C = C_o e^{\frac{-Qt}{V}} \qquad 2\text{-}2$$

where Q is the volumetric flow through the well and V is the storage volume of the well ($V=\pi r^2 h$).

The fits of Equation 2-2 to the tracer injection concentration curves of is shown in Figure 2-1. The flux values from these fits are plotted against the radial distance from the extraction well in Figure 2-2. From Figure 2-2, it can be seen that flow is approximately proportional to e^{-r}_{1} (where r is the distance from the pumping well) rather than $^{1}/_{r}$ as would be expected for parallel plate flow with a point sink if no external gradient was present.

The assumption could then be made that the reason for the behavior seen in Figure 2-2 is the superposition of a pre-existing homogeneous steady state head field $H_e(x,y)$ on the induced head field due to the extraction well $H_p(x,y)$.

$$H(x,y) = H_e(x,y) + H_p(x,y) \qquad 2\text{-}3$$

The superposition of this steady state head field on the head field due to pumping would produce a different gradient at each injection well. This head field can be back calculated from the flux Q, since the flux Q is proportional to the local gradient, which is just the first derivative of the head field.

For the current analysis, we assumed that the external head field could be described by a linear function,

$$H_e(x,y) = ax + by + c_1 \qquad 2\text{-}4$$

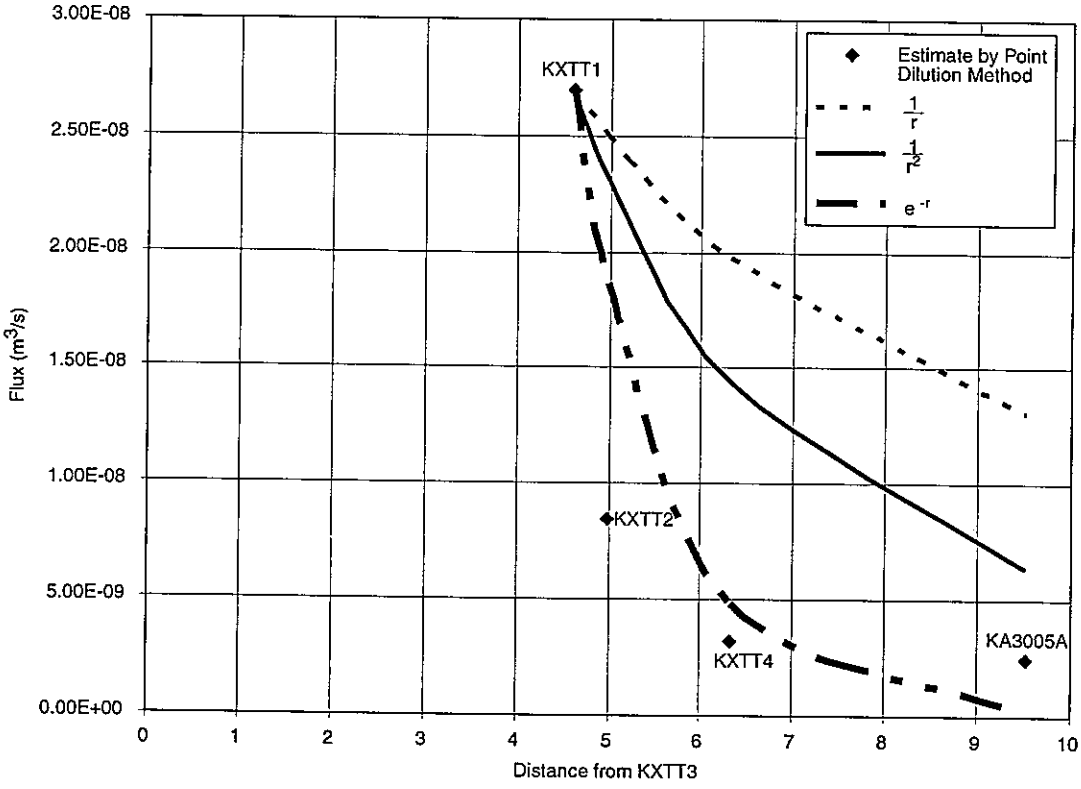

FIGURE **2-2**
DISTANCE VS WELL FLUX
PNC/FRACTURE FLOW/JAPAN

PROJECT NO. 923 1089.831 DRAWING NO. 67589 DATE 3/11/97 DRAWN BY CB

For the present derivation, (x,y) refer to a local coordinate system in Feature A centered on the extraction well.

Assuming Darcy flow, the head $H_p(x,y)$ caused by the pumping well flux Q_p can be found using the confined aquifer solution (Bear, 1972),

$$Q_p = K\,i\,A \qquad 2\text{-}5$$

where K is hydraulic conductivity, i is the local gradient dH/dr, and A is the flow area. In this case the flow area is calculated as

$$A = 2\pi re \qquad 2\text{-}6$$

where e is fracture aperture. Replacing hydraulic conductivity by transmissivity T,

$$i = dH_p/dr \qquad 2\text{-}7$$

$$T = K\,e \qquad 2\text{-}8$$

$$Q_p = T\,(dH_p/dr)\,(2\,\pi\,r) \qquad 2\text{-}9$$

Solving for the local gradient i,

$$\frac{dH}{dr} = i = \frac{Q_p}{2\pi rT} \qquad 2\text{-}10$$

The solution for this first order differential equation is,

$$H_p(x,y) = \frac{Q_p}{2\pi rT}\ln(r) + c_2 \qquad 2\text{-}11$$

Using superposition for the heads due to the external head field and the head due to pumping,

$$H(x,y) = H_e(x,y) + H_p(x,y) \qquad 2\text{-}12$$

$$H(x,y) = ax + by + \frac{Q_p}{2\pi eT}\ln\left(\sqrt{x^2+y^2}\right) + c \qquad 2\text{-}13$$

The local gradient i_w at each of the injection well w can be found by differentiation of Equation 2-13.

$$i_w = |\nabla H| = \sqrt{\left(\frac{\partial H}{\partial x}\right)^2 + \left(\frac{\partial H}{\partial y}\right)^2} \qquad 2\text{-}14$$

$$= \sqrt{\left(a + \frac{Q_p}{2\pi T}\frac{x}{x^2+y^2}\right)^2 + \left(b + \frac{Q_p}{2\pi T}\frac{y}{x^2+y^2}\right)^2}$$

The local gradient i_w is related to the flux at the injection wells Q_w as,

$$Q_w = T\, i_w\, (2\,\pi\, r) \qquad 2\text{-}15$$

Substituting Equation 2-16 into 2-15,

$$Q_w = T\,(2\,\pi\,\left(\sqrt{x^2+y^2}\right))\sqrt{\left(a + \frac{Q_p}{2\pi T}\frac{x}{x^2+y^2}\right)^2 + \left(b + \frac{Q_p}{2\pi T}\frac{y}{x^2+y^2}\right)^2} \qquad 2\text{-}16$$

Equation 2-16 represents four non-linear equations (on for each injection well) with two unknowns, a and b. Equation 2-16 could also be solved for three unknowns by also solving for fracture transmissivity T. These simultaneous equations were solved using the Microsoft Excel 5.0 solver to minimize the difference between the flows calculated from the head-gradient field and the flows calculated by fitting the injection well concentration curves.

The above "Point Dilution" Head field solution has a few limiting assumptions, including the use of superposition and the assumption of an external head field linear in x and y coordinates. However, the ability of the solution to provide consistency with the fluxes through the injection wells makes the solution clearly preferable to the hydrostatic assumption, and generally the best assumption available for this analysis. The point dilution head field solution provides the heads ***during the tracer experiment*** directly, such that the gradients can also be calculated directly.

Five scenarios were calculated for the point dilution method using the Excel Solver:

Scenario #1: External head field defined using regional gradients (see boundary condition "D" below).

Scenario #2: The direction and strength of the external gradient, as the aperture and conductivity of the fracture are allowed to vary as the solver minimizes the difference between the theoretical and curve-fit flow through injection wells.

Scenario #3: Aperture and conductivity are held constant to the values of Dershowitz et al. (1996) , but external flow field is allowed to vary using the Excel solver.

Scenario #4: Same as Scenario #3, but the solver converged on a different solution.

Scenario #5: Same as Scenario #1, but assuming hydrostatic regional gradients (see boundary condition "A" above).

The five scenarios calculated using the point dilution method are summarized in Table 2-1. In this table, the values in bold are fixed, and all other values are found by the Excel solver to match the measured fluxes.

Table 2-1 Point Dilution Head Analysis Scenarios

Parameter	Scenario 1	Scenario 2	Scenario 3	Scenario 4	Scenario 5
X Gradient a	**0.425**	0.0812	-0.07175	0.009828	**0.0000**
Y Gradient b	**-1.03**	-1.3512	-0.1052	-0.16358	**0.0000**
Aquifer Thickness e [m]	**0.0014**	4.87E-04	**0.0014**	**0.0014**	**0.0014**
Hydraulic Conductivity K [m/s]	**0.0003**	1.04E-04	**0.0003**	**0.0003**	**0.0003**
Flux at Pumping Well q_0 [m^2/s]	**3.33E-06**	**3.33E-06**	**3.33E-06**	**3.33E-06**	**3.33E-06**
Well Radius r [m]	**0.056**	**0.056**	**0.056**	**0.056**	**0.056**
Q/2peK	1.261871	10.42308	1.261871	1.261871	1.261871
Transmissivity T [m^2/s]	4.2E-07	5.1E-08	4.2E-07	4.2E-07	4.2E-07

Table 2-2 shown the heads at each of the wells based on the point dilution method for each the following scenario assumptions. Table 2-3 shows:

- the magnitudes of the gradient
- the direction of the local gradient, expressed as the angle of the gradient vector away from the direction of KXTT3
- with an assessment as to whether that flow direction will bring tracer to the pumping borehole

Weak gradients and gradients away from the pumping borehole could both result in poor recovery to KXTT3.

Table 2-2 Heads at Wells During TRUE-1/RC Experiment by Point Dilution Method

Borehole	Scenario 1	Scenario 2	Scenario 3	Scenario 4	Scenario 5
KXTT1	-0.79959	11.60836	1.393167	1.405384	2.027373
KXTT2	-3.30524	11.31247	1.579961	1.369571	2.386035
KXTT3					
KXTT4	-3.17493	10.34352	1.673334	1.252255	1.931139
KA3005A	-5.93386	11.0511	1.723728	1.337941	2.84423

Table 2-3 Local Gradient Solution Magnitude (Direction)

Borehole	Scenario 1	Scenario 2	Scenario 3	Scenario 4	Scenario 5
KXTT1	**1.01 (108°)**	1.38 (40°)	0.13 (3°)	0.17 (39°)	0.25 (0.0°)
KXTT2	**0.98 (133°)**	**0.57 (57°)**	0.08 (29°)	**0.07 (58°)**	0.19 (0.0°)
KXTT4	**0.88 (170°)**	1.20 (30°)	0.25 (28°)	0.15 (30°)	0.27 (0.0°)
KA3005A	**1.01 (142°)**	**0.41 (121°)**	**0.05 (74°)**	**0.05 (121°)**	0.13 (0.0°)

Gradients in bold are generally away from KXTT3, and would not be likely to be recovered (angles greater than 45°)

Since there are more equations than unknowns, multiple solutions are possible. Possible head field solutions based on the above "Point Dilution Method" derivation are illustrated in Figure 2-3. Figure 2-4 shows the corresponding gradient field, which demonstrates that the external gradient field is far from negligible in the tracer-test area. In general, these solutions indicate that, for the experimental pumping rate in KTTT3, the gradients for injections to KXTT2 and KA3005A may be away from the pumping well such that these tracers would not be recovered. The solutions above could be used to predict the pumping rates which would be necessary to achieve a gradient toward the extraction well from all four of the injection wells.

a) Scenario 1

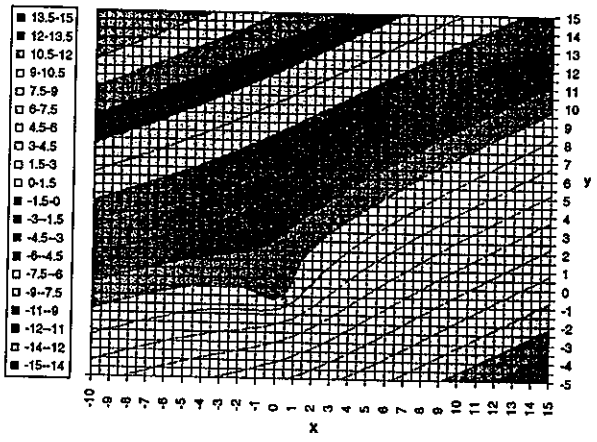

a) Scenario 2

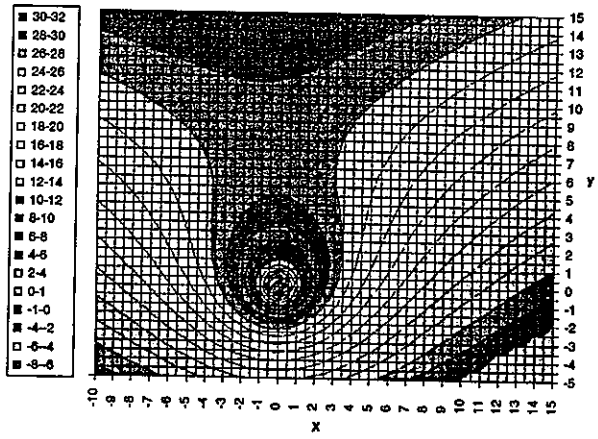

a) Scenario 3

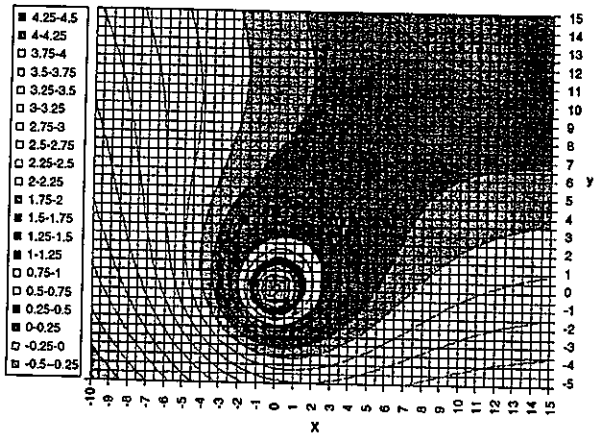

a) Scenario 4

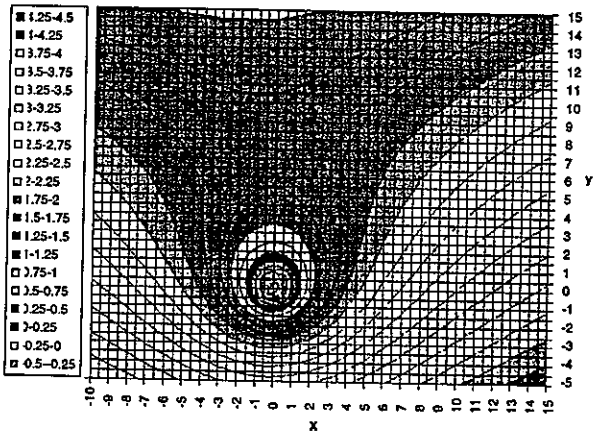

a) Scenario 5

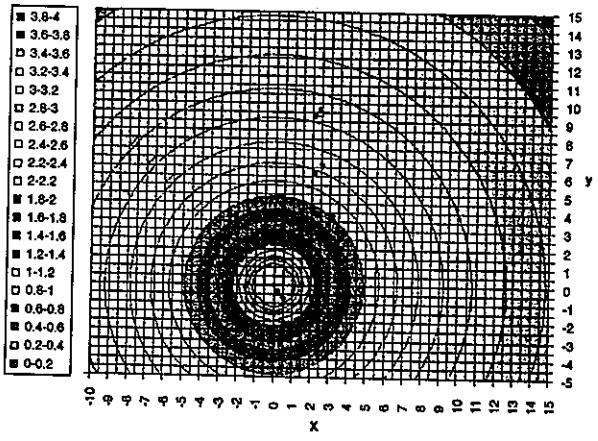

Note: See text for description of scenarios.

FIGURE **2-3**
HEAD FIELDS BY POINT DILUTION METHOD
PNC/FRACTURE FLOW/JAPAN

PROJECT NO. 923 1089.831 DRAWING NO. 67594 DATE 9/20/96 DRAWN BY CB

a) Scenario 1

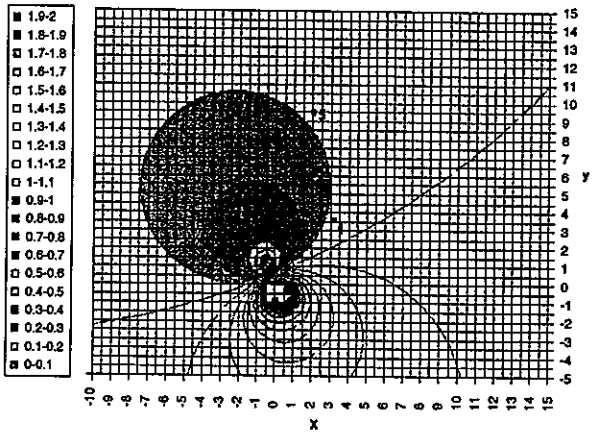

a) Scenario 2

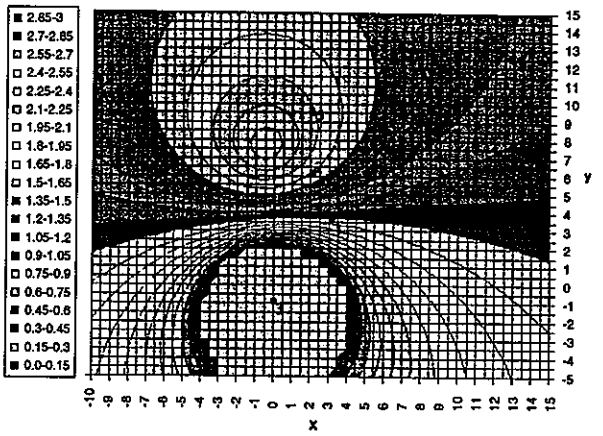

a) Scenario 3

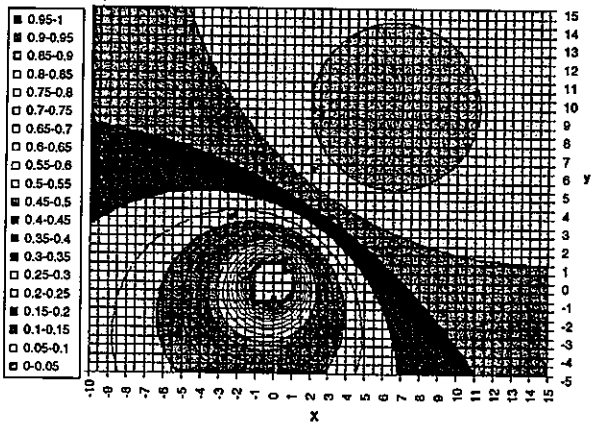

a) Scenario 4

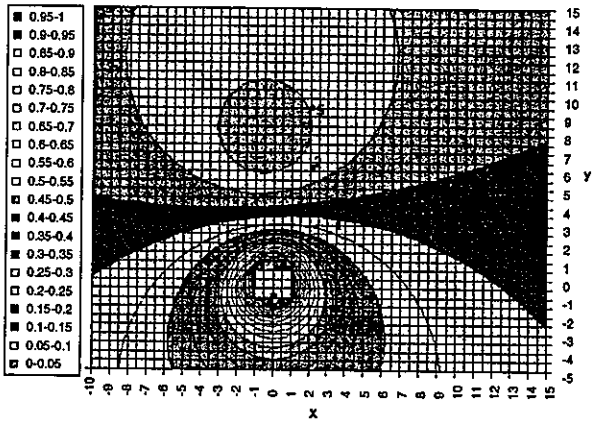

a) Scenario 5

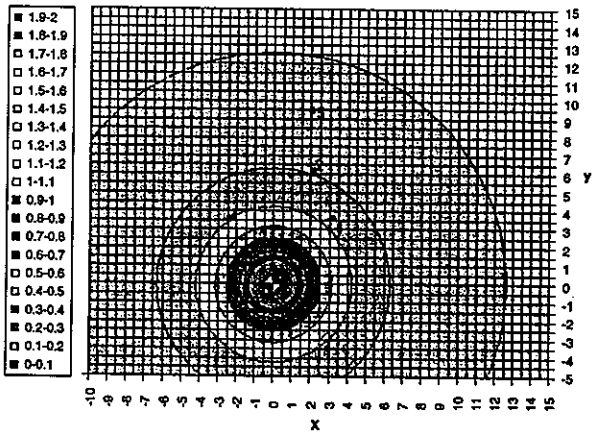

Note: See text for description of scenarios.

FIGURE **2-4**
GRADIENT BY POINT DILUTION METHOD
PNC/FRACTURE FLOW/JAPAN

PROJECT NO. 923 1089.831 DRAWING NO. 67595 DATE 9/20/96 DRAWN BY CB

2.3 LOCAL HEAD FIELD BOUNDARY CONDITION "C"

Steady state pressures were measured in each of the TRUE-1/RC experiment test intervals, and are reported by Winberg, et al. (1995) and Winberg, et al. (1996). These values are given in Table 2-4. The values used in the present analysis were based on Winberg, et al. (1995), except for KA3005A, which was estimated from adjacent measurements.

Figure 2-5, illustrates the local head field boundary condition, together with heads relative to the extraction well interval KXTT3:2. Similar to the result found from the point dilution boundary condition analysis, this analysis shows an in situ head field with a gradient away from KXTT3:2 for boreholes KXTT2 and KA3005A.

Table 2-4 Heads at TRUE-1/RC Boreholes

Borehole	Winberg (1996) Pressure (kPa)	Winberg (1996) Head (MasL)	Winberg (1995) Head (KXTT3:P2=360m)	Gradient
KXTT1:P2	3604	-41.8	361.2	Toward KXTT3
KXTT2:P2*	3600	-42.3	351.3	Away from KXTT3!
KXTT3:P2	3591	-43.2	360	---
KXTT4:P3	3605	-41.8	361.3	Toward KXTT3
KA3005A:P4	3611	-41.3	340(?)	Away from KXTT3?

The local head field boundary condition "C" was derived by visual estimation of heads on the edges of "Feature A" which would produce heads at the boreholes consistent with Figure 2-5. These visual approximations were made using SEEP/W (see Section 3.2 below).

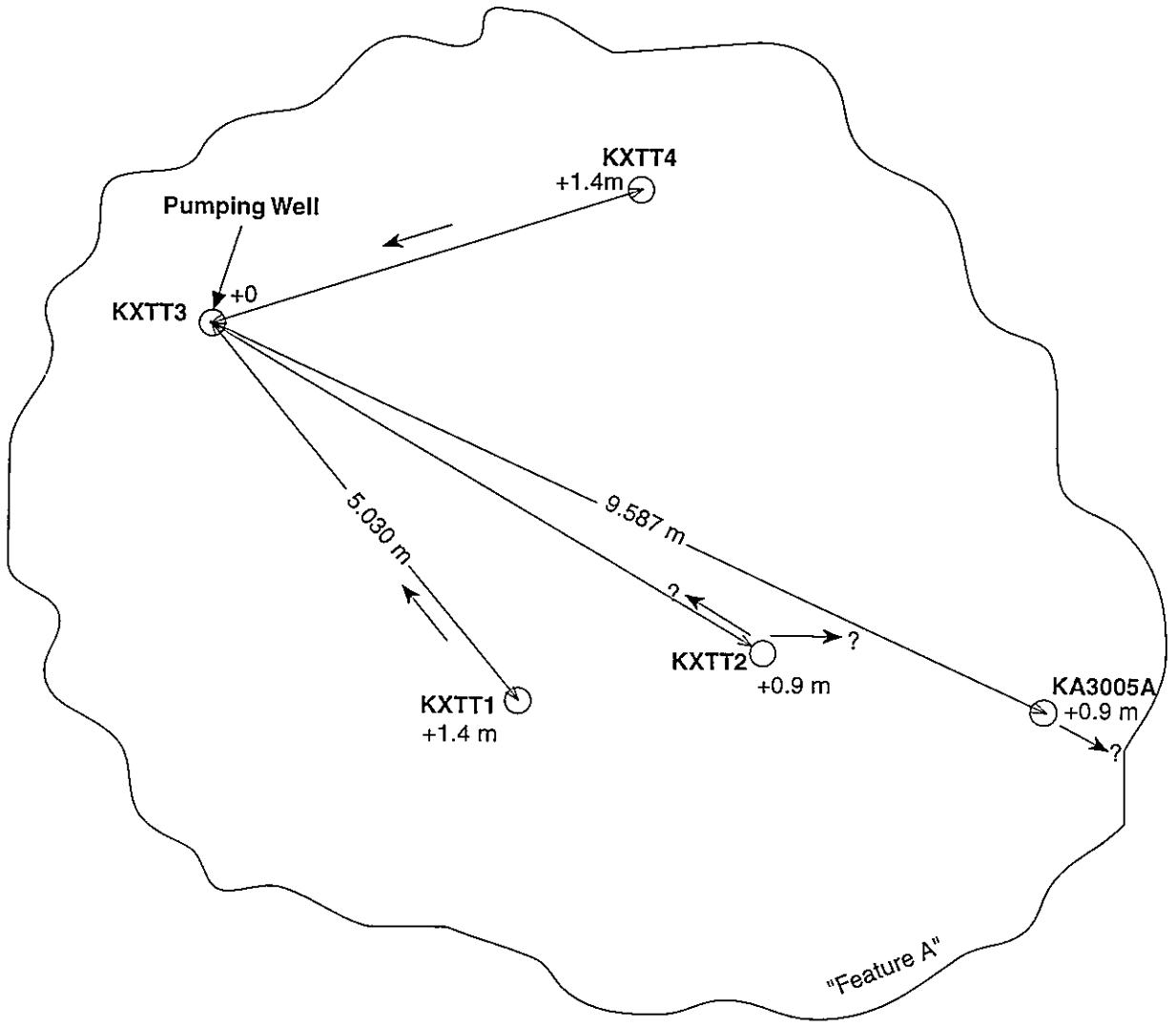

○ Used for both preliminary and RC-1 experiments

▲ RC-1 ONLY

after Winberg et al. (1996)

FIGURE **2-5**
STEADY STATE HEAD FIELDS RELATIVE TO KXTT3:P2 (masl)
PNC/FRACTURE FLOW/JAPAN

PROJECT NO. 923 1089.800 DRAWING NO. 72738 DATE 5/9/97 DRAWN BY CB

Golder Associates

2.4 TRUE-1 REGIONAL HEAD FIELD BOUNDARY CONDITION "D"

Dershowitz et al (1995) evaluated measured pressures in all of the boreholes of the TRUE-1 rock block, based on preliminary head values provided by the TRUE project (Winberg, et al., 1995). Based on measurements in all of the TRUE-1 rock block intervals, they developed the head field relationship,

$$P(x,y,z) = C_x x + C_y y + C_z z + P_0$$

The regression for this relationship is shown in Figure 2-6. The fitted parameters are:

$C_x = -1.09$
$C_y = 0.19$
$C_x = -0.16$
$P_0 = 346.74$ m

This pressure field would provide a strong gradient to the west, toward the TRUE-1 niche. Since Feature A is dipping at 76 to 79 degrees toward the north-east (60 to 75 degrees) this indicates that the regional gradient could draw tracer out of the plane of Feature A, particularly from the boreholes which are further from KXTT3, which are nearer to intersecting fracture zones, and therefore more susceptible to the regional gradients.

However, the regional gradient based on measurements in the rock block is not expected to be as directly applicable for predictions as the pressures derived from the boreholes in the block (Boundary Conditions B and C).

2.5 IMPLICATIONS OF BOUNDARY CONDITIONS FOR TRACER RECOVERY

2.5.1 Boundary Condition "A"

When applied to "Feature A" as a confined aquifer, the hydrostatic boundary condition implies 100% ultimate recovery from all four injection intervals. This includes the Moench and SEEP/W models described below. Lower recovery could occur for the FracMan model, due to the complexity of the head field in "Feature A" resulting from the interconnections of the fracture network.

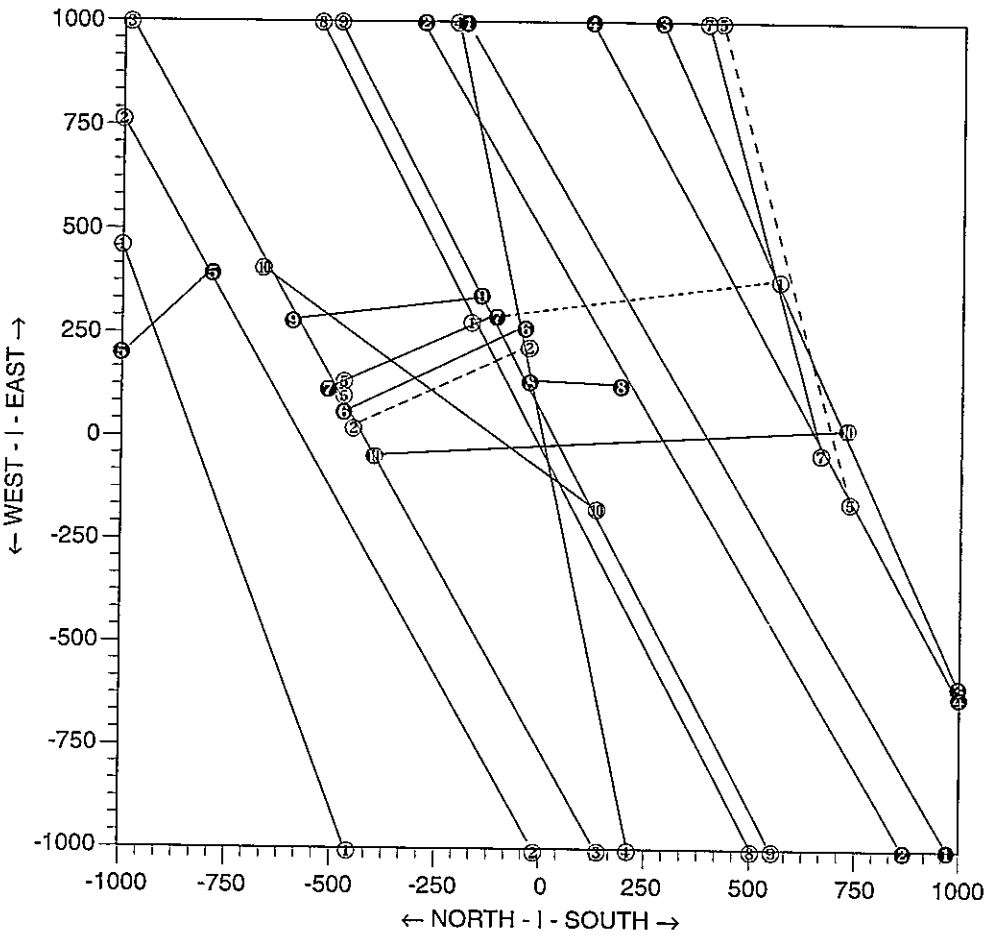

① EW-1wp	⑦ EW-7r 81 SE	⑬ NE-4r 71 SE	⑲ NNW-3wp 90
② EW-1r 88 SE	⑧ NE-1r 70 NW	⑭ NE-4r 78 SE	⑳ NNW-4wr 85 NE
③ EW-1r 78 SE	⑨ NE-1r 75 NW	⑮ NW-1p 30 NE	⑩ NNW-5wp 90
④ EW-3r 79 S	⑩ NE-2r 77 SE	⑯ NNW-1wp 90	① NNW-6wp 90
⑤ EW-5wp	⑪ NE-3r 80 NW	⑰ NNW-2wr 90	② NNW-7w 85 NE
⑥ EW-7wp	⑫ NE-3r 70 NW		

FIGURE **X**
TITLE
PNC/FRACTURE FLOW/JAPAN

PROJECT NO. 923 1089.831 DRAWING NO. 72528 DATE 3/11/97 DRAWN BY CB

2.5.2 Boundary Condition "B"

The point dilution method provides the head field during the tracer test, such that the recovery from each injection interval can be calculated based on the direction of the local gradients. This is described in Section 2.3.3 above. Based on this calculation, there is a significant probability that tracer will not be recovered from KXTT2 and KA3005A.

2.5.3 Boundary Condition "C"

For the local head boundary condition, the drawdowns at the pumping and injection wells can be calculated by superposing the regional gradients on the gradients due to pumping in KXTT3 using the Theis Solution, equation 2-11. This allows calculation of the gradient from the injection wells to the pumping well, and hence the probability that tracer will in fact be recovered from any given injection well.

Using equation 2-11 above, the drawdowns due to pumping in a homogeneous confined aquifer would be as given in Table 2-5.

Table 2-5 *Theis Drawdown*

Well	Distance	Theis Drawdown
KXTT1	5.030	2.59 m
KXTT2	6.62	2.25 m
KXTT3	0	8.22 m
KXTT4	4.684	2.68 m
KA3005A	9.587	1.79 m

Table 2-6 presents the preliminary head measurements (Winberg 1995) in the "Feature A" borehole intervals, with the superposed analytic solution for drawdowns. Negative gradients indicate intervals which will probably not be recovered to the pumping well. Lower gradients indicate intervals which may or may not be recovered to the pumping well.

Thus, even before the initiation of transport modeling, the data provided in data distributions to the Äspö task force was sufficient to indicate the probability that tracer recovery would not be very good from KXTT2 and KA3005A.

Table 2-6 Local Head Boundary Condition "B"

Well	Steady State Head (Boundary Condition "C")	Theis Drawdown	Head With Theis Drawdown	Gradient	Recovery
KXTT1	361.2	2.59 m	358.61	1.36	Very Rapid
KXTT2	351.3	2.25 m	349.05	-1.21	Probably Not
KXTT3	***360.0***	***8.22 m***	***351.78***	***NA***	***NA***
KXTT4	361.3	2.68 m	358.62	1.46	Very Rapid
KA3005A	340 (?)	1.79 m	338.31	-1.41	Probably Not

2.5.4 Boundary Condition "D"

The same analysis used in the previous section can be applied for the assumption that local pressures within "Feature A". However, the fundamental concept of boundary condition "D" is that it should be applied at a distance from "Feature A", such that the head distribution within "Feature A" would be a function of the fracture connections. It is therefore less appropriate to use the type of analysis developed for boundary condition "C" for this boundary condition.

No a priori statement can therefore be made concerning recovery based on the assumption of boundary condition "D".

3. MODELS IMPLEMENTED

This section describes the three conceptual and numerical models used in the simulations for the radially converging tracer test. The models implemented are designated as follows:

Model #1: **Moench:** An analytical solution for radially converging flow in a confined aquifer by Moench (1995). This solution requires simple boundary condition assumptions. The advantage of this model is in its simplicity.

Model #2: **SEEP/W**: A two dimensional finite element model, capable of modeling heterogeneity and more complex boundary conditions. This model is more powerful than the analytical solution, but more difficult to apply.

Model #3: **FracMan**: The discrete fracture model provides a more realistic model for the TRUE-1 rock block. However, definition of geometry and properties is significantly more difficult.

As stated previously, the PNC/Golder team believes that in the current exercise, the understanding of boundary conditions is more important than the details of the numerical implementation. As a result, more emphasis was placed on the Moench solution. However, the local boundary conditions on "Feature A" are related to fracture geometry. As a result, any attempt to understand the boundary conditions will require the use of a discrete feature model.

3.1 MOENCH MODEL "1"

3.1.1 Background

Moench (1995) developed an exact Laplace transform solution for confined aquifer transport in a radially converging flow field. This solution provides consideration for:

- Double-porosity (fracture/rock matrix)
- Borehole storage (well bore mixing)
- Borehole skin
- Fracture skin (preventing diffusion from the fracture to the rock matrix)
- Longitudinal dispersion
- Retardation (sorption)

The solution is based on an earlier publication by Moench (1989). Dr. Moench graciously provided us with the FORTRAN program which he implemented for the solution. The basic equation solved is (Bear, 1979)

$$\frac{1}{r}\frac{\partial}{\partial r}\left[rD_L\frac{\partial C}{\partial r}\right]-v\frac{\partial C}{\partial r}-q'=R\frac{\partial C}{\partial t} \qquad 3\text{-}1$$

where r is the radial coordinate with its origin at the center of the pumped well, t is the time from the start of the tracer test, and C is the tracer concentration in the fracture system. The coefficient of longitudinal hydrodynamic dispersion takes on the form $D_L=\alpha_L|v|$.

In Laplace Space, the equation for dimensionless concentration C'_D is (Moench, 1995),

$$C_D(S)=\psi\exp\left[\frac{Pe}{2}(1-r_{wD})\right]G(S) \qquad 3\text{-}2$$

where

$$\bar{G}(s)=\psi\exp\left[\frac{Pe}{2}(1-r_{wD})\right]\bar{G}(s)$$

$$F=\omega^{1/3}(A_1B_3-A_3B_1)+0.5(A_3B_2-A_2B_3)$$

$$+0.5((A_1-B_1)+0.25\omega^{-1/3}(B_3-A_2)$$

$$A_1=Ai'\left(\omega^{1/3}y_0\right)/Ai\left(\omega^{1/3}y_L\right)$$

$$A_2=Ai\left(\omega^{1/3}y_0\right)/Ai\left(\omega^{1/3}y_L\right)$$

$$A_3=Ai'\left(\omega^{1/3}y_L\right)/Ai\left(\omega^{1/3}y_L\right)$$

$$B_1=Bi'\left(\omega^{1/3}y_0\right)/Bi\left(\omega^{1/3}y_L\right)$$

$$B_2=Bi\left(\omega^{1/3}y_0\right)/Bi\left(\omega^{1/3}y_L\right)$$

$$B_3=Bi'\left(\omega^{1/3}y_L\right)/Bi\left(\omega^{1/3}y_L\right)$$

$$y_0=Pe\,r_{wD}+0.25\omega^{-1}$$

$$y_L=Pe+0.25\omega^{-1}$$

$$\omega=\frac{2R\left(s+\bar{q}_D\right)}{Pe^2\left(1-r_{wD}^2\right)}$$

$$\bar{q}_D = \frac{3\gamma'[m \coth(m) - 1]}{1 + S_k[m \coth(m) - 1]}$$

Ai and *Bi* are Airy functions. The value of ψ takes on different forms depending on the type of tracer input. For a Dirac input, ψ=1, and for a step input, ψ=1/s. For a rectangular input, ψ=[1-exp(-t_{Dp}s)]/s where t_{Dp} is the duration of the constant input divided by the time of travel by pure advection.

This equation was used earlier by Dershowitz (1995) to analyze the preliminary well tests. The Moench solution is used for predictive modeling in Feature A by applying the different gradients from the geometry, boundary condition ,and material properties assumptions appropriate for the TRUE-1/RC experiment.

3.1.2 Implementation

The Moench solution provides type curves of dimensionless time vs. dimensionless concentration given dimensionless input parameters. For the current analysis, parameters are specified as physical parameters such as well radius, well separation, pumping rate, etc. The conversion equations are taken from Moench(1991) and Moench(1995).

The Moench solution requires the following parameters:

Geologic Parameters:

- h: Height of aquifer
- ϕ_f: Fracture porosity
- R: Retardation coefficient
- α_L: Longitudinal dispersion
- bd: block diffusion (0=no, 1=yes)
- γ: block diffusion parameter
- σ: block storage parameter
- sk: block skin parameter

Well Test Parameters:

- r_L: well separation
- r_w: radius of sampling well
- r_i: radius of injection well
- h_w: height of sampling well
- h_i: height of injection well
- q_o: pumping rate
- it: injection type (0=constant, 1=dirac, 2=top hat)
- t_i: injection duration
- C_o: concentration of injection

Time Frame Parameters:

- t_o: begin time
- n_{LC}: number of log cycles
- n_p: number of points per cycle
- n_{TS}: number of time steps

The input parameters used by the analysis, expressed in dimensionless and dimensional values are provided in Table 3-1. Parameter names are those used in the FORTRAN program provided by Moench (1995). Parameters not provided in this table are do not require transformation to dimensionless values.

3.1.3 Simulations

The simulations carried out using the Moench analytical solution are summarized in Table 3-2. The geometric assumptions are based on the experimental setup as described by Anderson, et al. (1996). The hydrologic and transport parameter assumptions are based on back analysis of the preliminary transport experiments, as described in Dershowitz et al (1995).

The results for the fit to Tracer Test A are shown in Figure 3-1. The results for the simulations of TRUE-1/RC injections are shown in Figure 3-2. Table 3-5 provides a numerical summary of the results for the Moench analysis. Note that these breakthrough curves are based on the flux rate in KXTT3, assuming a simple radially converging flow field. They do not reflect the actual head field, which indicates a probable lack of recovery from KXTT2 and KA3005A.

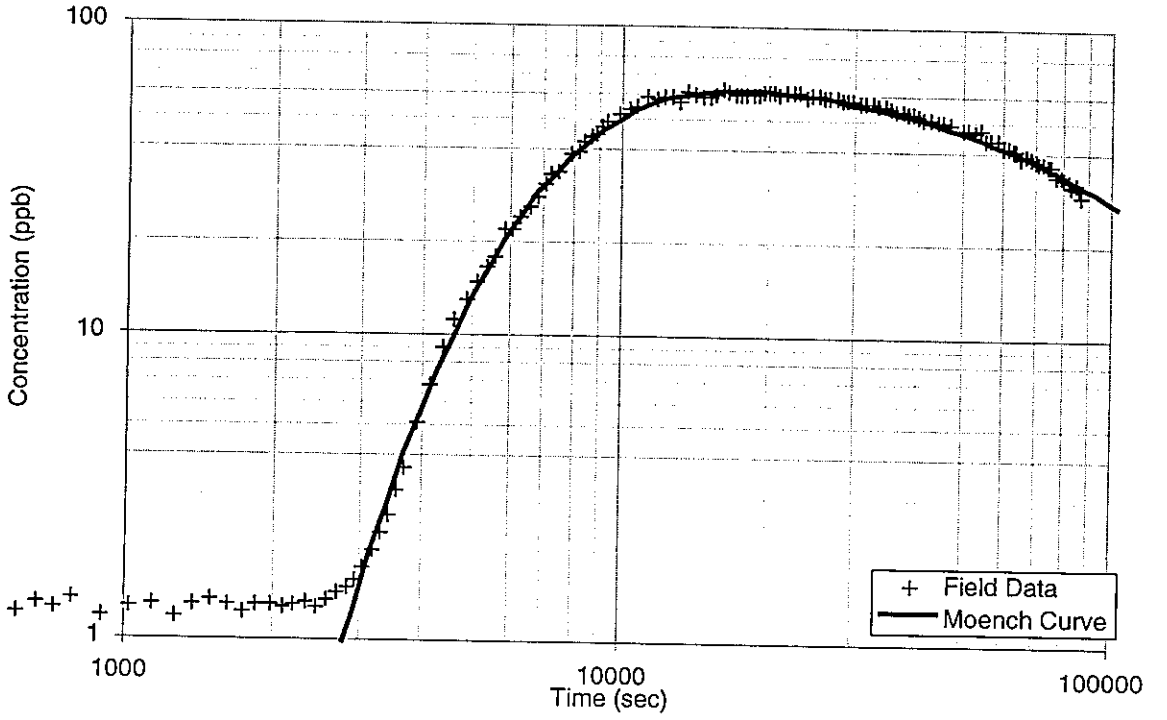

(a) Feature A

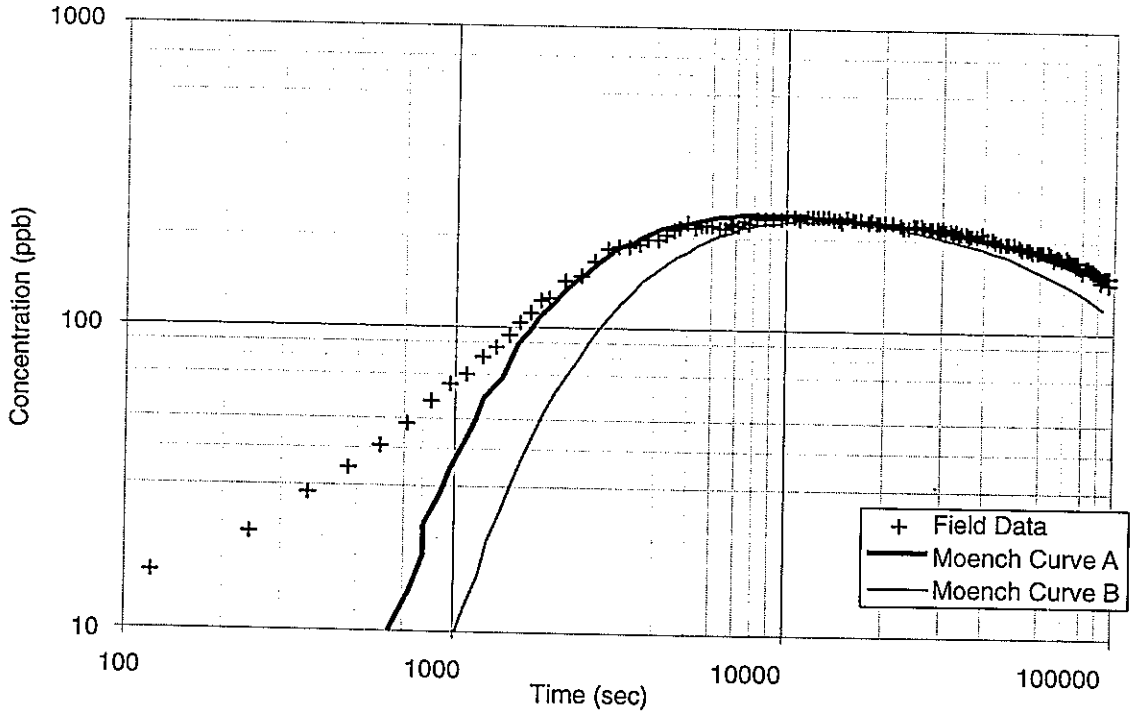

(b) Feature B

FIGURE **3-1**
MOENCH (1995) ANALYSIS OF PRELIMINARY TRACER TESTING "FEATURE A"
PNC/FRACTURE FLOW/JAPAN

PROJECT NO. 923 1089.631 DRAWING NO. 67592 DATE 9/20/96 DRAWN BY CB

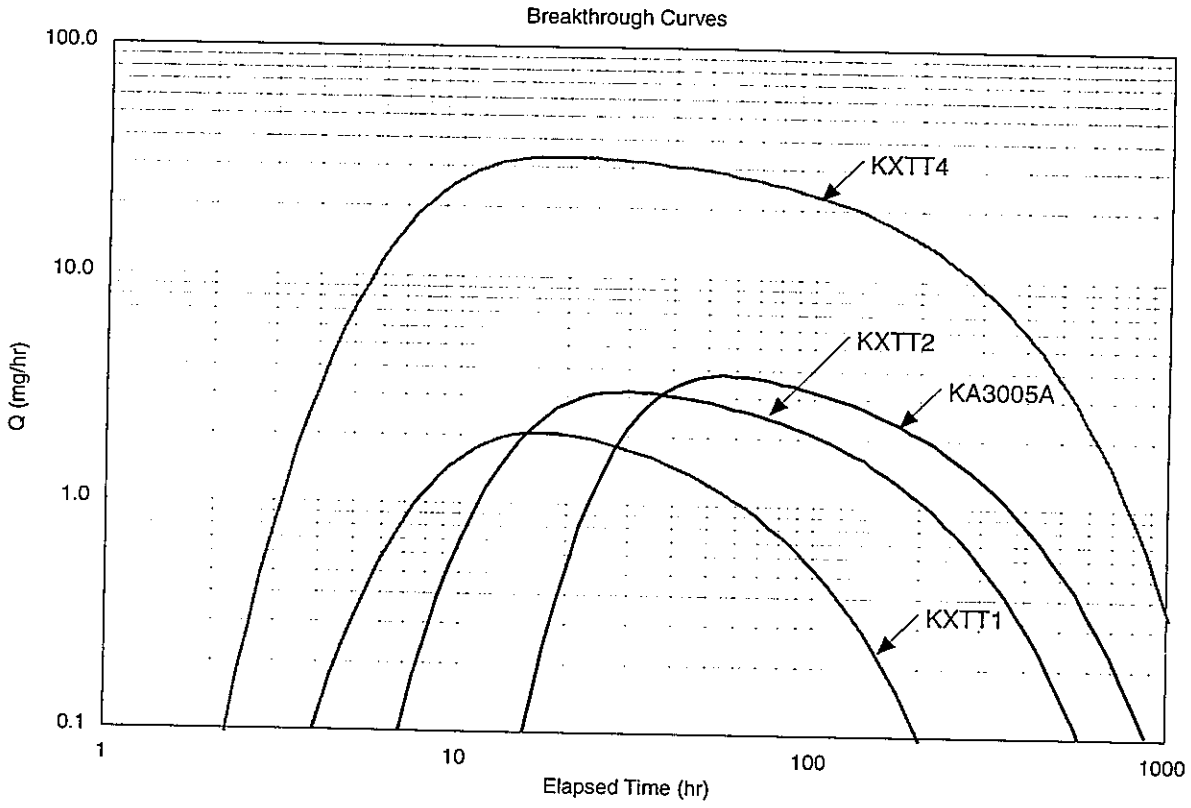

FIGURE **3-2**
MOENCH (1995) BREAKTHROUGH CURVES
PNC/FRACTURE FLOW/JAPAN

PROJECT NO. 923 1089.831 DRAWING NO. 67593 DATE 9/20/96 DRAWN BY CB

Table 3-1 Parameters of Moench Analysis

Parameter	Value Assumed
TDFIRST: First value of dimensionless time	$TDFIRST = t_o/t_a$ where $t_a = \frac{\pi h \varphi_f (r_\lambda^2 - r_w^2)}{q_o}$
TDP: Dimensionless time duration for top-hat pulse	$TDP = t_i/t_a$
XMUI: Dimensionless wellbore mixing factor (input well)	$XMUI = \frac{r_i h_i}{\varphi_f h (r_\lambda^2 - r_w^2)\varepsilon}$ where $\varepsilon = \frac{4r_i}{2\pi r_\lambda}$
XMUW: Dimensionless wellbore mixing factor (pumping well)	$XMUW = \frac{r_w h_w}{\varphi_f h (r_\lambda^2 - r_w^2)}$
PE: Peclet Number	$PE = \frac{r_\lambda}{\alpha_\lambda}$
RWD: Dimensionless radius of pumping well	$RWD = \frac{r_w}{r_\lambda}$
RTARD: Retardation coefficient	RTARD = R
XMULT: Multiplier for computing different type curves	XMULT = 0
BIGT: Maximum value of dimensionless time	$BIGT = TDFIRST \times 10^{NLC}$
METH: Method (1=epsilon algorithm, 2=ordinary quotient difference algorithm, 3=quotient difference algorithm with acceleration)	METH = 3
NN: Parameter for Hoog algorithm	NN = 30

Table 3-2 Geologic Parameters for Moench Simulations

Geologic Parameters:		Fit to Tracer Test A	KXTT1	KXTT2	KXTT4	KA3005A
h	Height of aquifer (m)	0.00135	0.0014	0.0014	0.0014	0.0014
ff	Fracture porosity	1	1	1	1	1
R	Retardation Coefficient	1	1	1	1	1
aL	Longitudinal Dispersivity	0.55	0.55	0.55	0.5	0.5
-	Block diffusion (0=no, 1=yes)	0	0	0	0	0
g	Block diffusion parameter	0.1	0.1	0.1	0.1	0.1
s	Block storage parameter	25	25	25	25	25
sk	Block skin parameter	0.006	0.006	0.006	0.006	0.006

Table 3-3 Well Test Parameters for Moench Simulations

	Well Test Parameters:	Fit to Tracer Test A	KXTT1	KXTT2	KXTT4	KA3005A
rL	Well Separation (m)	5.03	4.98	6.63	4.62	9.53
rw	Radius of sampling well (m)	0.056	0.056	0.056	0.056	0.056
ri	Radius of injection well (m)	0.056	0.056	0.056	0.056	0.056
hw	Length of sampling well section (m)	3.5	3.5	3.5	3.5	3.5
hi	Length of injection well section (m)	1	1.0	0.5	2.0	1.0
qo	Well Pumping Rate (m^3/min)	$1.5x10^{-5}$	$1.5x10^{-5}$	$1.5x10^{-5}$	$1.5x10^{-5}$	$1.5x10^{-5}$
-	Injection type (0=constant, 1=dirac, 2-tophat)	1	1	1	1	1
ti	Injection duration (tophat only) (sec)	1	1	1	1	1
Co	Concentration of injection (ppb)	10000	30	56	420	99.3

Table 3-4 Time-Frame Parameters for Moench Simulations

	Time Frame Parameters:	Fit to Tracer Test A	KXTT1	KXTT2	KXTT4	KA3005A
to	Begin time (sec)	2000	2000	2000	2000	2000
-	No. Log Cycles	2	2	2	2	2
-	No. Points per log cycle	30	30	30	30	30
-	No. Time steps	10	10	10	10	10

Table 3-5 Tracer Results

		KXTT1	KXTT2	KXTT4	KA3005A
Mass Injected	mg	148	552	7683	975
Mass Recovered	mg	148	546	6277	766
Mass Recovery During Experiment		100%	99%	82%	78%
Breakthrough Time t_5 (sec)	sec	41063	81960	69069	150621
Breakthrough Time t_{50} (sec)	sec	182896	443746	571408	673958
Breakthrough Time t_{95} (sec)	sec	683415	1734306	2344020	2490223

3.2 SEEP/W FINITE ELEMENT MODEL "2"

3.2.1 Background

If a strong external gradient exists, or in-plane heterogeneity plays an important role in defining transport, the analytic solution would be inadequate. SEEP/W is a commercial, Microsoft Windows 3.X finite element flow solution (Geo-Slope, 1995). SEEP/W was chosen for this exercise because of its combination of an easy to use graphical user interface for input, analysis, and display, and the tight coupling of its transport solver, CTRAN/W (Geo-Slope, 1995). CTRAN/W directly solves solute transport by the finite element method, using the same solver as SEEP/W.

3.2.2 Implementation

The mesh implemented for the SEEP/W model is illustrated in Figure 3-3. The properties assigned for the SEEP/W model are summarized in Table 3-6

Table 3-6 Parameters for SEEP/W Simulation

Parameter	Value
Size of Model	48 m x 48 m
Typical Grid Cell Size	2 m near boreholes refined
Flux Rate at KXTT3:	3.33×10^{-6} m^3/s
Boundary Conditions	"A" and "C"
Confined Aquifer Thickness	1.4×10^{-3} m
Confined Aquifer Porosity	50%
Confined Aquifer Transmissivity	4.9×10^{-7} m^3/s
Longitudinal Dispersion	0.55 m
Transverse Dispersion	0.05 m

3.2.3 Simulations

The finite element program SEEP/W was selected primarily for flexibility in assignments of heterogeneity within "Feature A". and in assignment of boundary conditions. However, time constraints prevented us from taking advantage of this flexibility. The SEEP/W simulations were carried out with only one set of homogeneous material properties, shown in Table 3-6 above.

Simulations were carried out for boundary conditions "A" and "C". The pressure fields for these two boundary conditions are illustrated in Figures 3-4 and 3-5. The heads and drawdowns for these boundary conditions are summarized in Table 3-7.

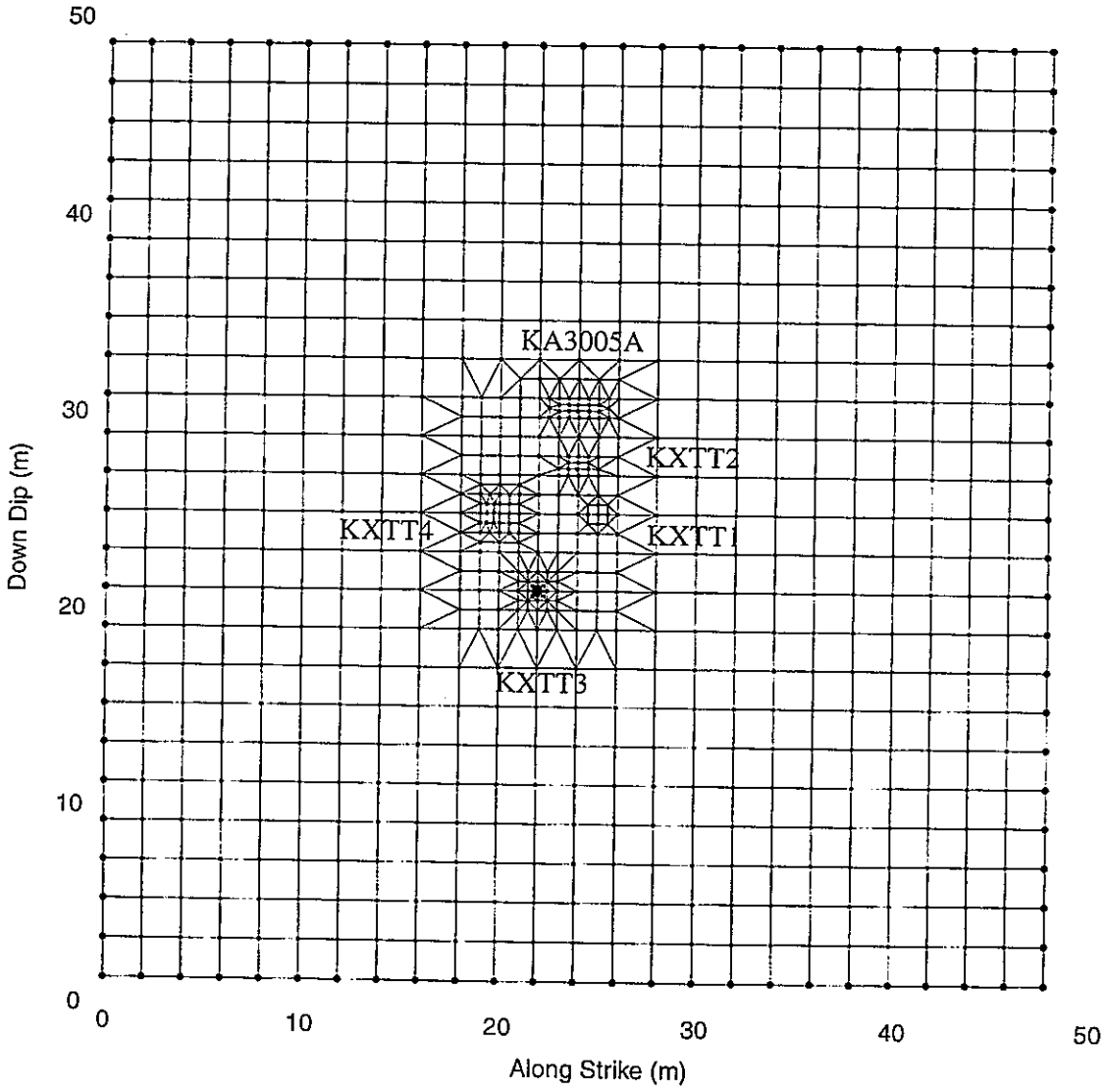

FIGURE **3-3**
SEEP/W MESH
PNC/FRACTURE FLOW/JAPAN

PROJECT NO. 923 1089.831 DRAWING NO. 67609 DATE 9/20/96 DRAWN BY CB

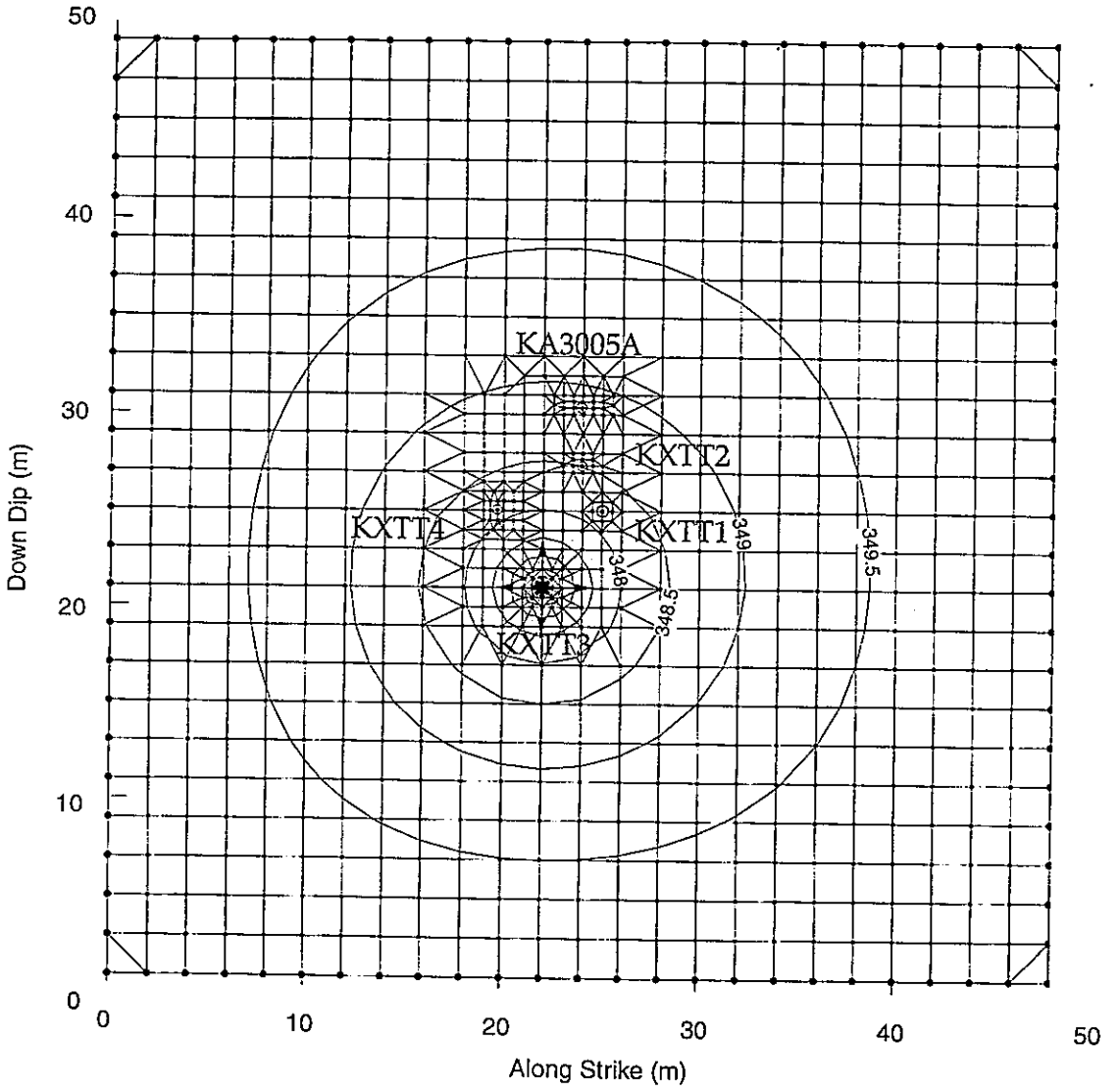

FIGURE **3-4**

SEEP/W HEAD FIELDS FOR BOUNDARY CONDITION "A"

PNC/FRACTURE FLOW/JAPAN

PROJECT NO. 923 1089.831 DRAWING NO. 67611 DATE 9/20/96 DRAWN BY CB

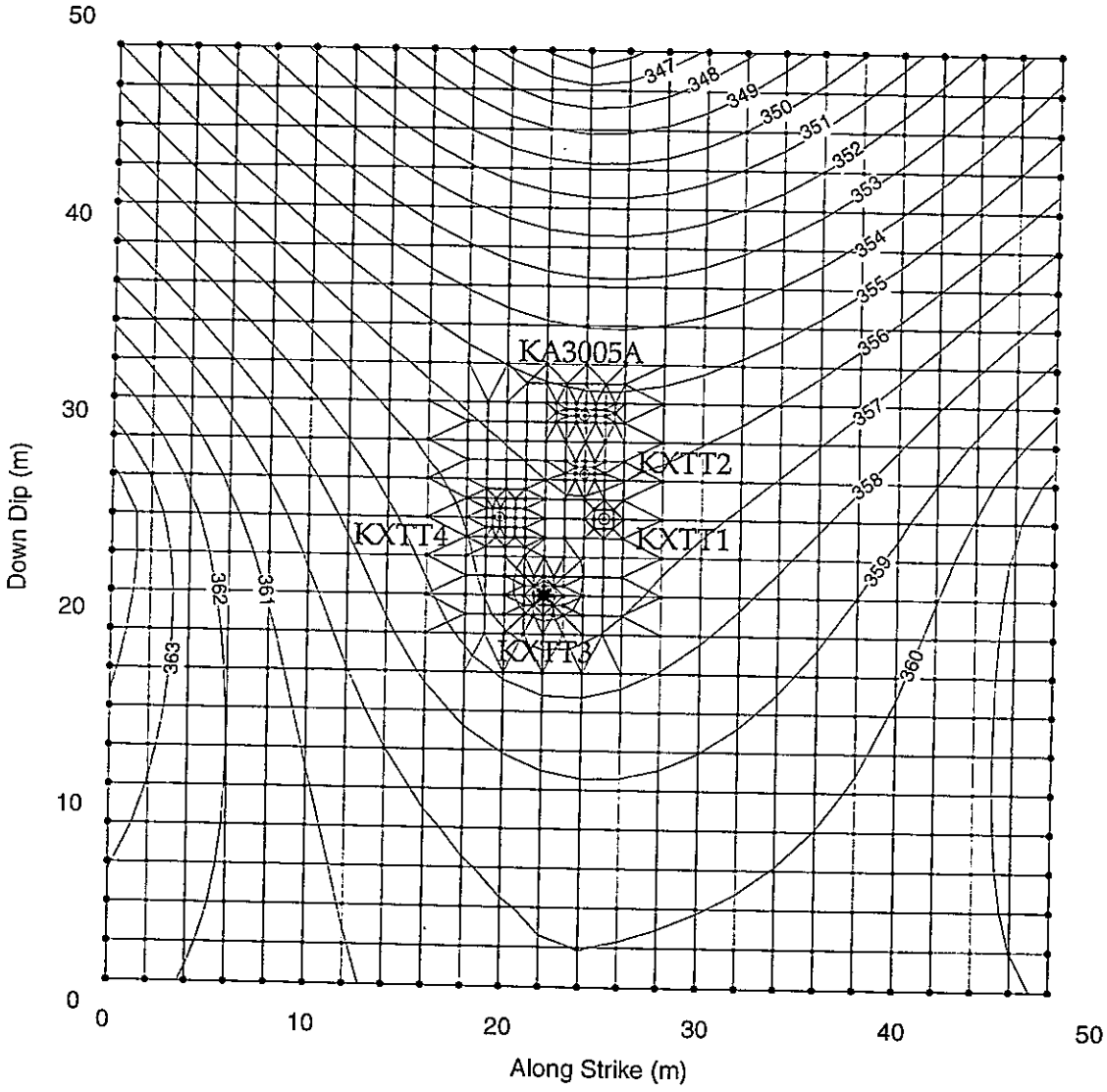

FIGURE **3-5**

SEEP/W HEAD FIELDS FOR BOUNDARY CONDITION "C"

PNC/FRACTURE FLOW/JAPAN

PROJECT NO. 923 1089.831 DRAWING NO. 67610 DATE 9/20/96 DRAWN BY CB

Table 3-7 Heads and Drawdowns for Hydrostatic Boundary Condition "A" and Local Head Condition "C"

Hydrostatic Boundary Condition "A"

Borehole	Initial Head	Head	Drawdown
KXTT1:R2	350	348.2	1.8
KXTT2:R2	350	348.5	1.5
KXTT3:R2	350	343.8	6.2
KXTT4:R3	350	348.1	1.9
KA3005A:R3	350	348.9	1.1

Local Head Condition "C"

Borehole	Initial Head	Head	Drawdown
KXTT1	357.9	356.2	1.7
KXTT2	357.4	355.9	1.5
KXTT3	358.9	352.9	6.0
KXTT4	359.3	356.5	1.8
KA3005A	356.4	355.3	1.1

Based on Table 3-7, it can be seen that the SEEP/W simulation would have 100% ultimate recovery for the hydrostatic boundary condition, and for the local head field boundary condition, recovery from KXTT2 and KA3005A would be questionable.

The breakthrough curves for hydrostatic and local head field boundary condition assumptions are given in Figures 3-6 and 3-7. The solute transport results are summarized in Table 3-8.

3.3 FRACMAN MODEL "3"

3.3.1 Background

FracMan modeling is used primarily to understand the behavior of networks of fractures. The TRUE-1/RC experiment is designed as an experiment in a single fracture with relatively well known boundary conditions. As a result, it is not necessary to understand the flow pattern in the intersecting fractures to understand the flow and transport in "Feature A". FracMan modeling was therefore seen primarily as a supplement to the analytical evaluation of the head field and the breakthrough curves for this task.

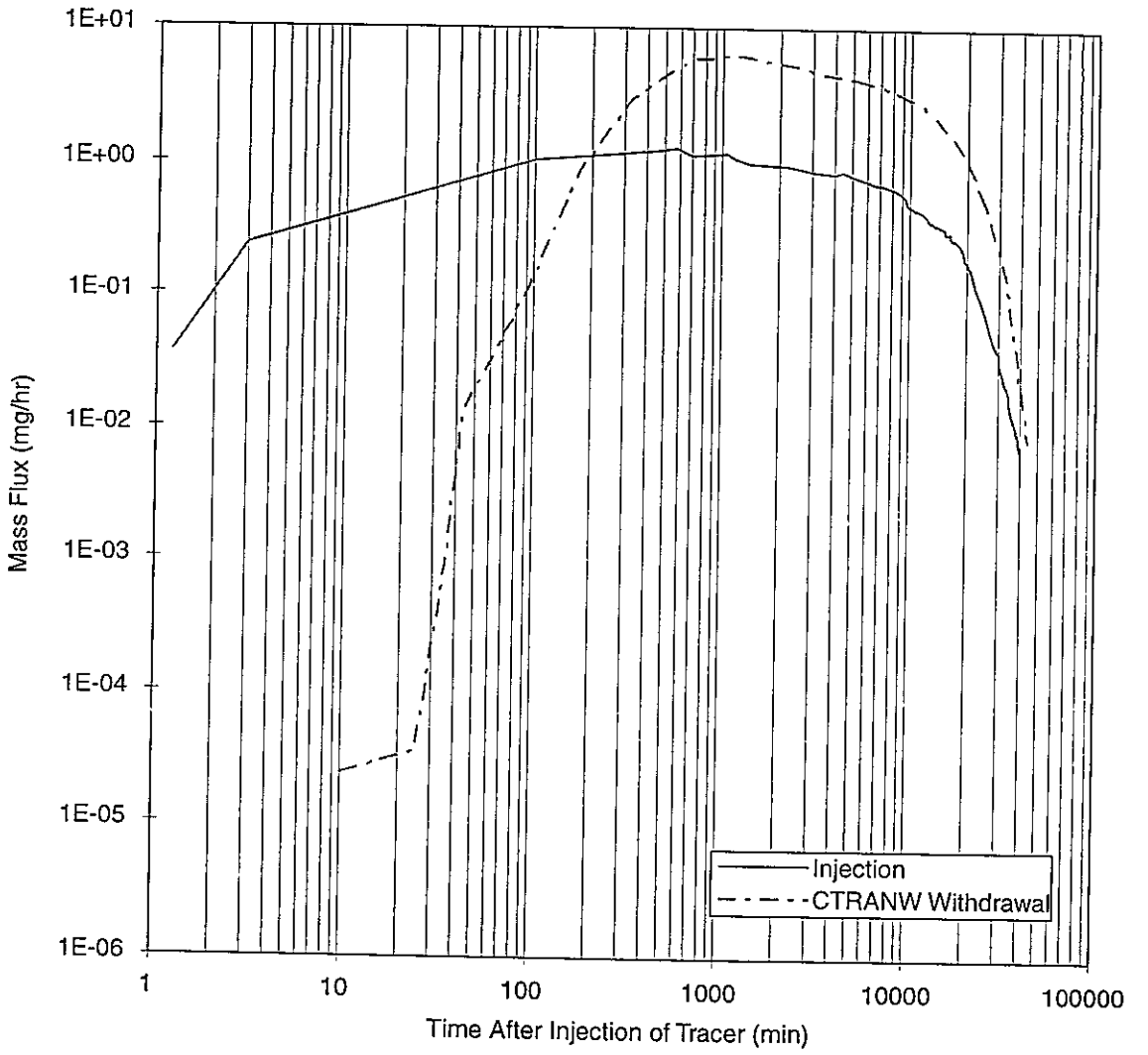

FIGURE **3-6a**
BREAKTHROUGH CURVE AT KXTT3 FOR TRACER FROM KXTT1 HYDROSTATIC CONDITIONS
PNC/FRACTURE FLOW/JAPAN

PROJECT NO. 923 1089.831 DRAWING NO. 67596 DATE 9/20/96 DRAWN BY CB

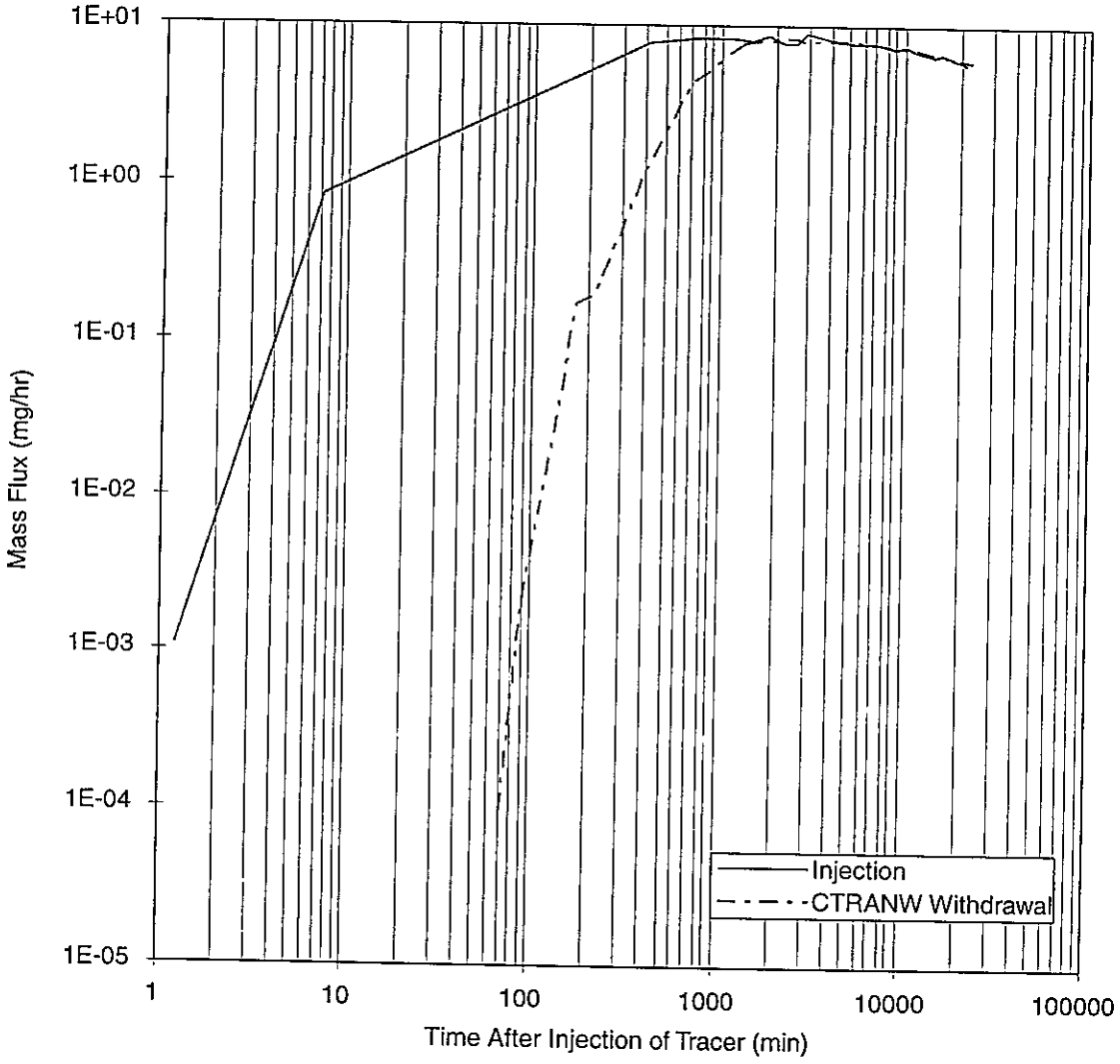

FIGURE **3-6b**
BREAKTHROUGH CURVE AT KXTT3 FOR TRACER FROM KXTT2 HYDROSTATIC CONDITIONS
PNC/FRACTURE FLOW/JAPAN

PROJECT NO. 923 1089.831 DRAWING NO. 67597 DATE 9/20/96 DRAWN BY CB

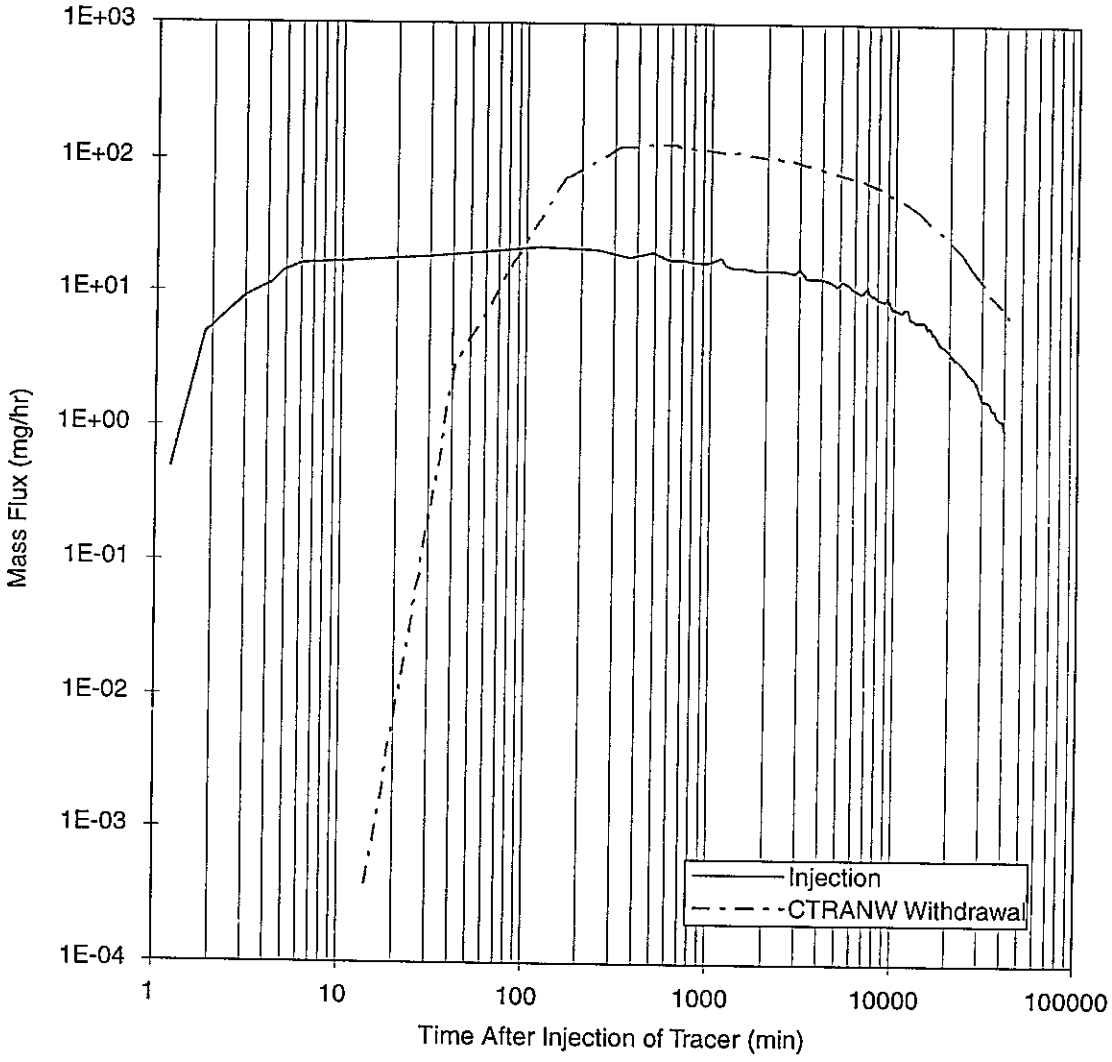

FIGURE **3-6c**
BREAKTHROUGH CURVE AT KXTT3 FOR TRACER FROM KXTT4 HYDROSTATIC CONDITIONS
PNC/FRACTURE FLOW/JAPAN

PROJECT NO. 923 1089.831 DRAWING NO. 67598 DATE 9/20/96 DRAWN BY CB

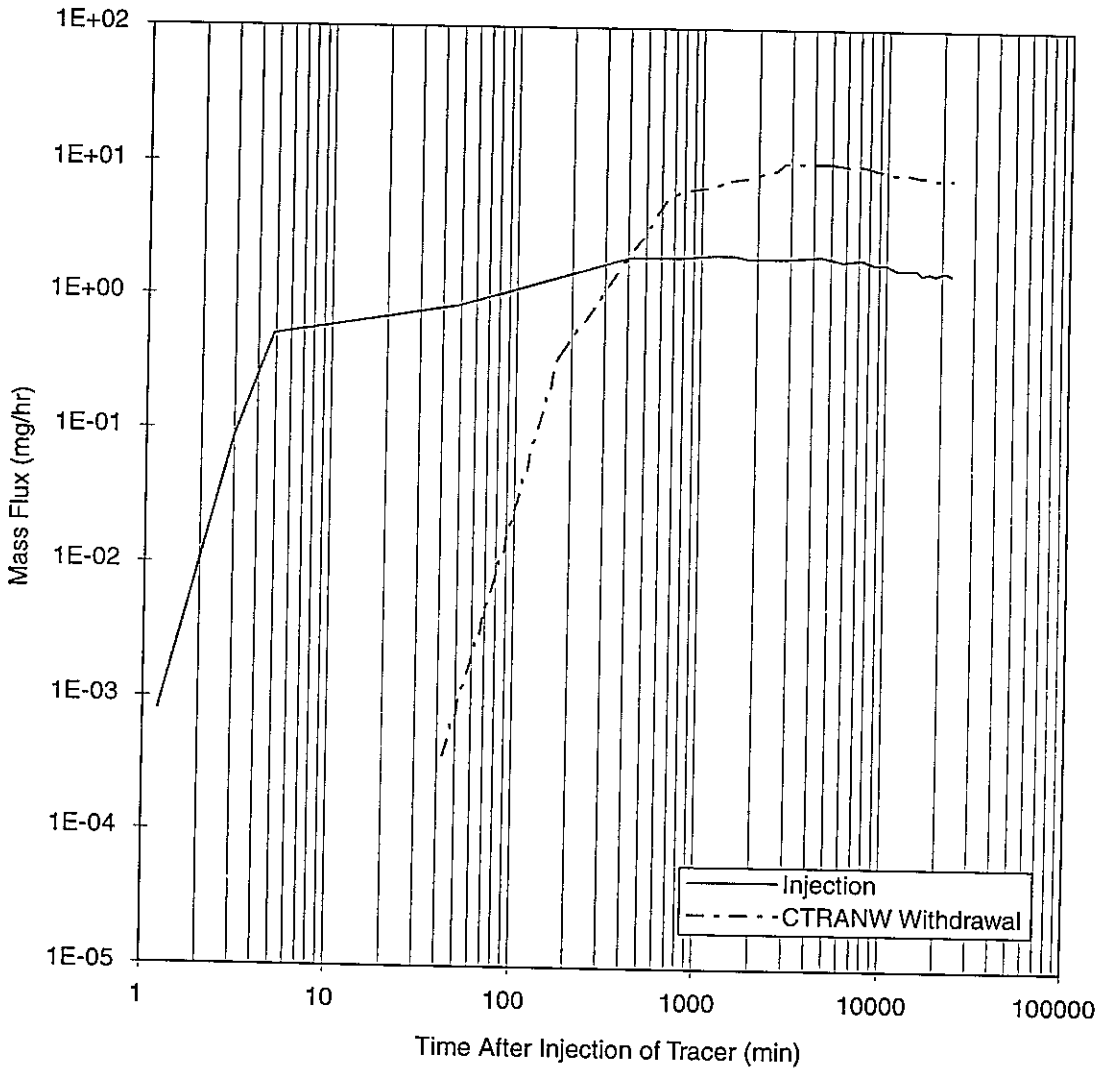

FIGURE **3-6d**

BREAKTHROUGH CURVE AT KXTT3 FOR TRACER FROM KA3005A HYDROSTATIC CONDITIONS

PNC/FRACTURE FLOW/JAPAN

PROJECT NO. 923 1089.831 DRAWING NO. 67599 DATE 9/20/96 DRAWN BY CB

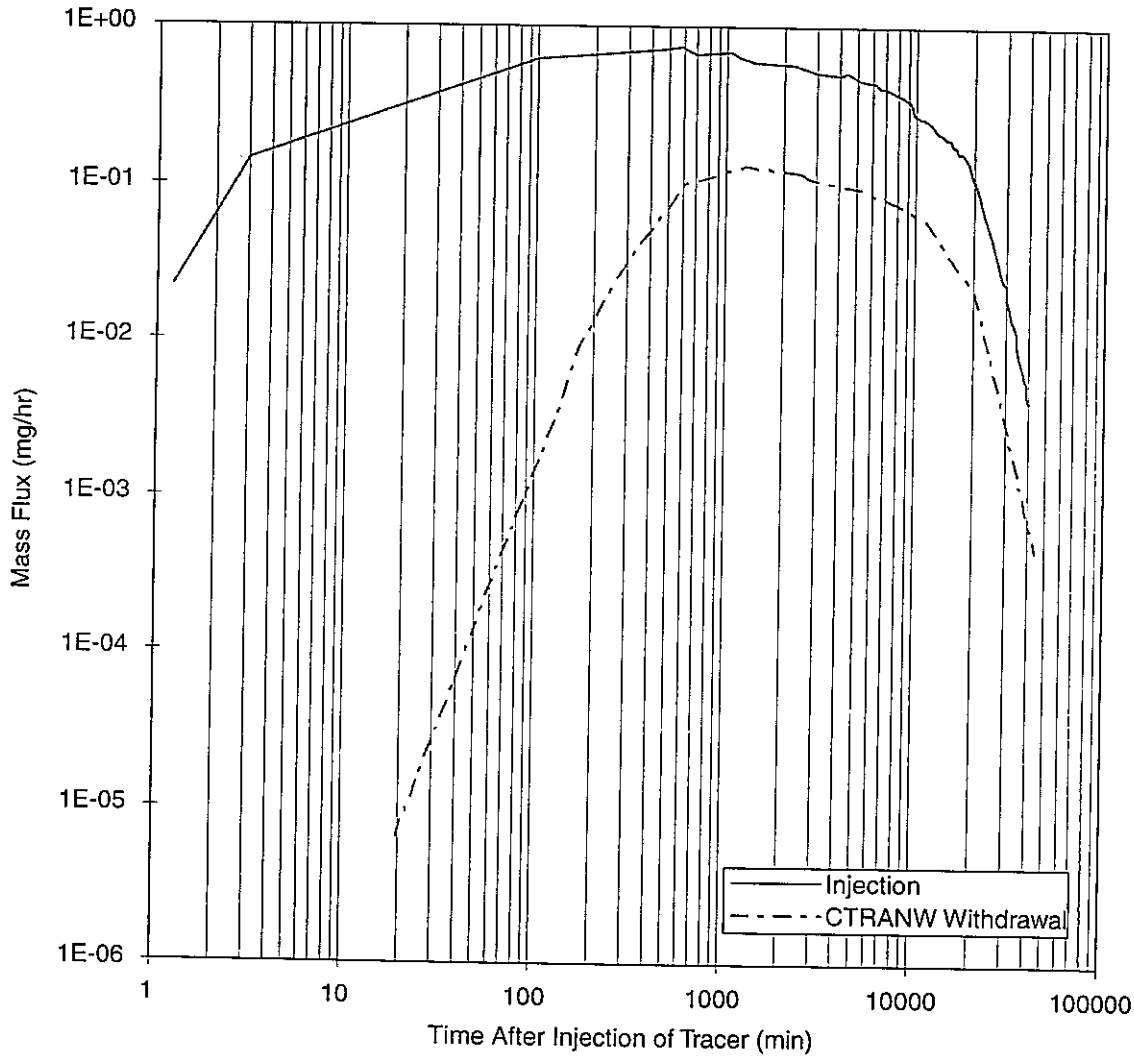

FIGURE **3-7a**
BREAKTHROUGH CURVE AT KXTT3 FOR TRACER FROM KXTT1 HYDROSTATIC CONDITIONS
PNC/FRACTURE FLOW/JAPAN

PROJECT NO. 923 1089.831 DRAWING NO. 67600 DATE 9/20/96 DRAWN BY CB

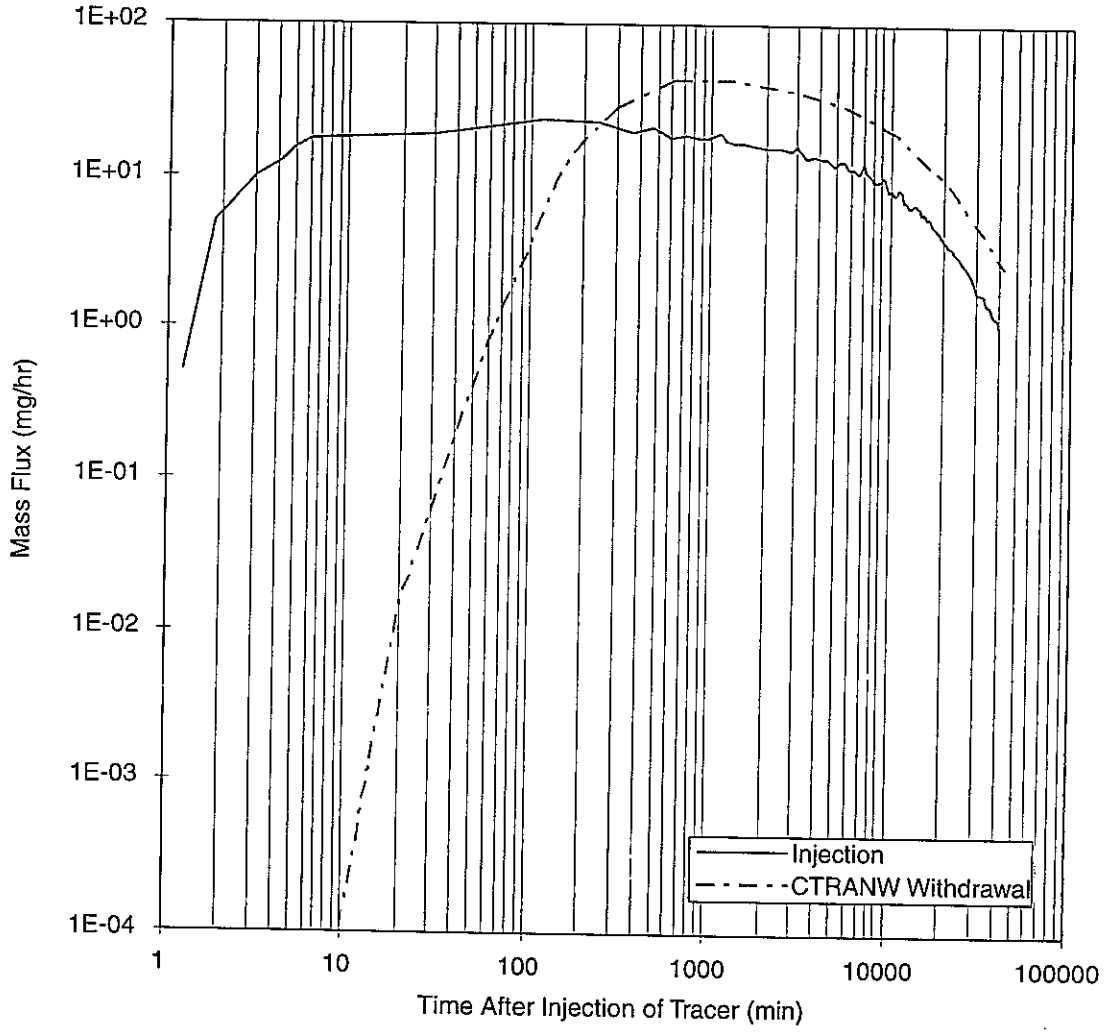

FIGURE **3-7b**
BREAKTHROUGH CURVE AT KXTT3 FOR TRACER FROM KXTT4 HYDROSTATIC CONDITIONS
PNC/FRACTURE FLOW/JAPAN

PROJECT NO. 923 1089.831 DRAWING NO. 67601 DATE 9/20/96 DRAWN BY CB

Table 3-8 *Tracer Results: SEEP/W Simulation: Hydrostatic Boundary Condition "A" and Local Head Field Boundary Condition "C"*

Hydrostatic Boundary Condition "A"

		KXTT1	KXTT2	KXTT4	KA3005A
Mass Recovery		100%	100%	100%	100%
Breakthrough Time t_5 (sec)	sec	15.5	28.8	12.8	29.6
Breakthrough Time t_{50} (sec)	sec	127.2	182	148.6	182.5
Breakthrough Time t_{95} (sec)	sec	405.1	364	568.1	362.4

Local Head Field Boundary Condition "C"

		KXTT1	KXTT2	KXTT4	KA3005A
Mass Recovery		6.5% (100% Ultimate)	0%	12.5% (100% Ultimate)	0%
Breakthrough Time t_5 (sec)	sec	18.5	No breakthrough	15.8	No breakthrough
Breakthrough Time t_{50} (sec)	sec	145	No breakthrough	155.9	No breakthrough
Breakthrough Time t_{95} (sec)	sec	592.2	No breakthrough	598.9	No breakthrough

We have already demonstrated the importance of appropriate definition of the boundary conditions on "Feature A" to predict tracer transport. Given the availability of local head measurements on "Feature A". it is not reasonable to expect FracMan modeling, which applies the head boundary conditions at distance, to provide a better representation of the local heads in "Feature A". As a result, the FracMan modeling described here is considered of secondary importance for predictive modeling.

Nevertheless, the FracMan modeling is significantly better at representing the head field within "Feature A" than a simple confined aquifer representation with a hydrostatic applied head field. In addition, future FracMan modeling to understand the head field within "Feature A", however, could be very useful.

3.3.2 Implementation

The parameters used for FracMan modeling are given in Table 3-9. These parameters are based on the values derived by Dershowitz et al. (1996), with the exception of fracture intensity and transmissivity, which were derived by additional analysis of flow logging in the TRUE-1 borehole array. This analysis was made using the OxFilet approach, as described in Dershowitz, et al. (1995).

OxFilet analysis was carried out by converting the flow logs for boreholes KXTT1-5 and KA3005A to equivalent 0.5 m results, and then determining the conductive fracture frequency corresponding to the observed results. This analysis is illustrated in Figure 3-8. The resulting fracture frequency λ of 1.79 m^{-1} corresponds to a fracture intensity P_{32C} of 4.35 m^{-1} (Dershowitz, et al., 1996). This intensity is very high but is consistent with the frequency of geologically identified conductive features in the core (Figure 3-9).

Our original intent was to run the FracMan model using the regional gradient boundary condition "D". However, due to time constraints, the FracMan model was run only with the hydrostatic boundary condition "A". Nevertheless, this result presented very interesting results, because even with a hydrostatic boundary condition on the model rock block, "Feature A" exists in a much more complex boundary condition, including flows out of the plane of "Feature A".

The FracMan model is illustrated in Figure 3-10. Figure 3-11 illustrates the conductive fracture which would be expected to intersect "Feature A" at this level of fracture intensity.

3.3.3 Simulations

Only one realization was made using the FracMan model, with the hydrostatic boundary condition. Additional simulations and additional boundary conditions may be reported at a later date.

Figure 3-12 presents the injection time histories used for the FracMan simulations, compared to the measurements for the injection boreholes. The breakthrough curves to KXTT3 are presented as normalized mass recovery C/C0 in Figure 3-13. These plots are as expected in that with the very low dispersion values, the breakthrough curves basically match the injection curves. Tracer transport results are summarized statistically in Table 3-10.

UTILS ISIS FRACSIZE OXFILET HETERFRAC FRACDIM EXIT

```
**** OXFIL SIMULATION RESULTS ****
  Input File : t1t5amd2.fil
  Fracture Network [Const]:        M=    1
  Min. Transimissivity:                1e-010
  Distribution option : LogNormal
Arith.(Mean,Dev): 3.98e-008 5.17e-007
Log10 (Mean,Dev):     -8.51       0.984
(# Frac/M, Length):    1.79         0.5
-----------------------------------------

                    Simulation  FIL Data
# of Intervals            264         264
Mean                2.45e-008   3.99e-008
Std Dev             8.33e-008   1.73e-007
Log10 Mean              -8.85       -8.84
Log10 Std Dev            1.16        1.17
Skewness                 7.51        7.93
Kurtosis                 70.1        76.4
% Nonconductive            42        40.9
-----------------------------------------

(Smirnov, % Signif):0.0455          94.8
(Chi-Sqr, % Signif):   22.3          38.2
   ===> Print File (Y/N) ?
```

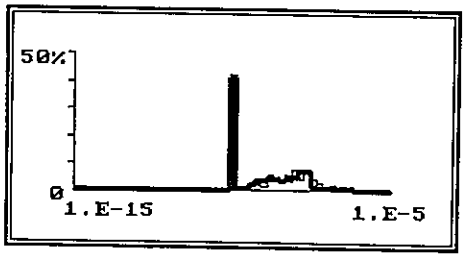

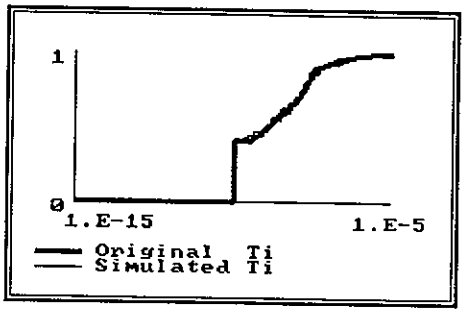


```
Version: Fracsys 2.511
   Date: 12:01 May 29 1996
   File: t1t5amd2.fil
```

Golder Associates

FIGURE **3-8**
OXFILET ANALYSIS FOR CONDUCTIVE FRACTURE FREQUENCY
PNC/FRACTURE FLOW/JAPAN

PROJECT NO. 923 1089.831 DRAWING NO. 67602 DATE 9/20/96 DRAWN BY CB

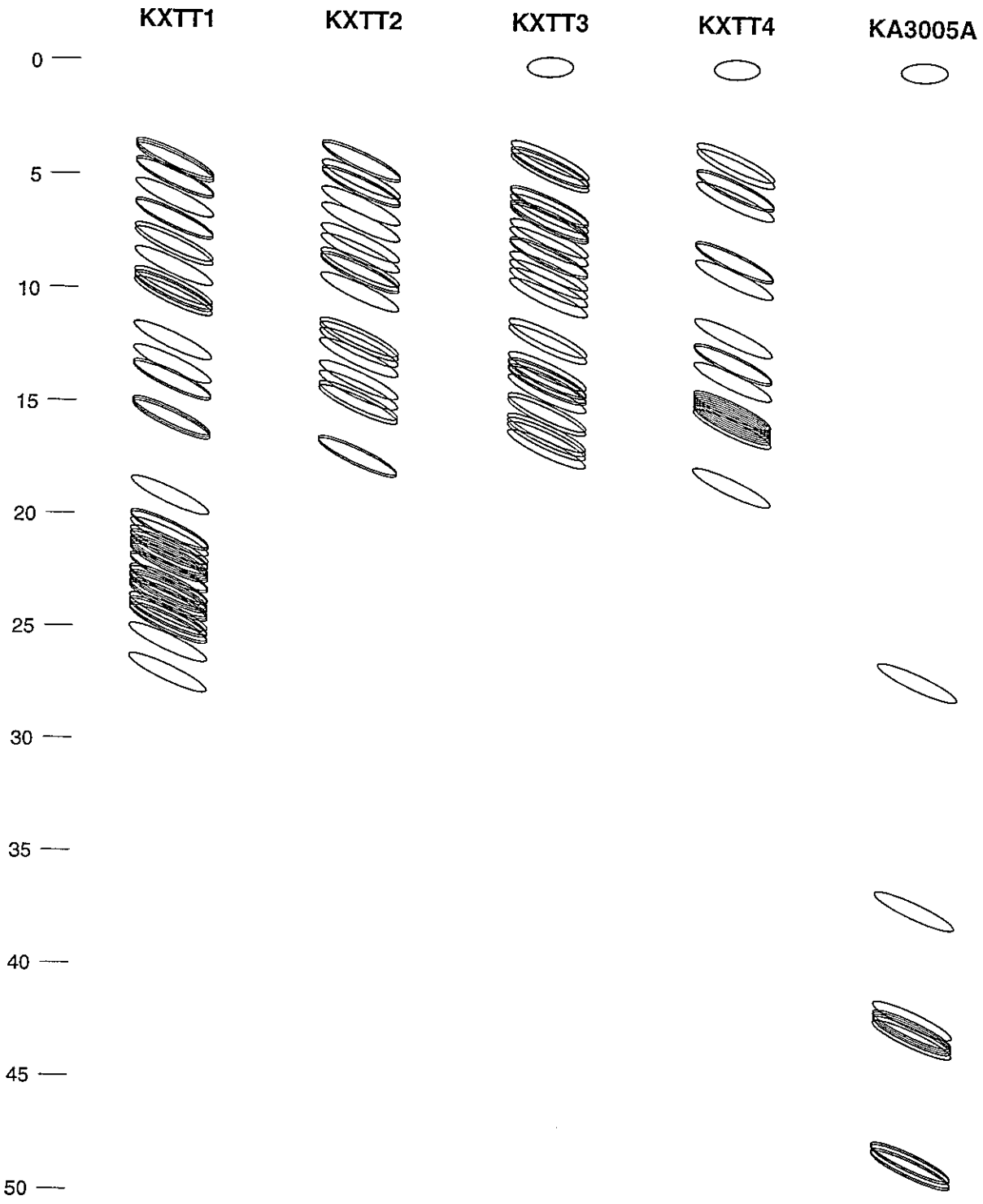

Note: Schematic for fracture location only. Size and orientation are held constant in this visualization.

FIGURE **3-9**
CONDUCTIVE FEATURES IDENTIFIED IN BHTV LOGS FOR KXTT1-4, KA3005A
PNC/FRACTURE FLOW/JAPAN

PROJECT NO. 923 1089.831 DRAWING NO. 67603 DATE 9/19/96 DRAWN BY CB

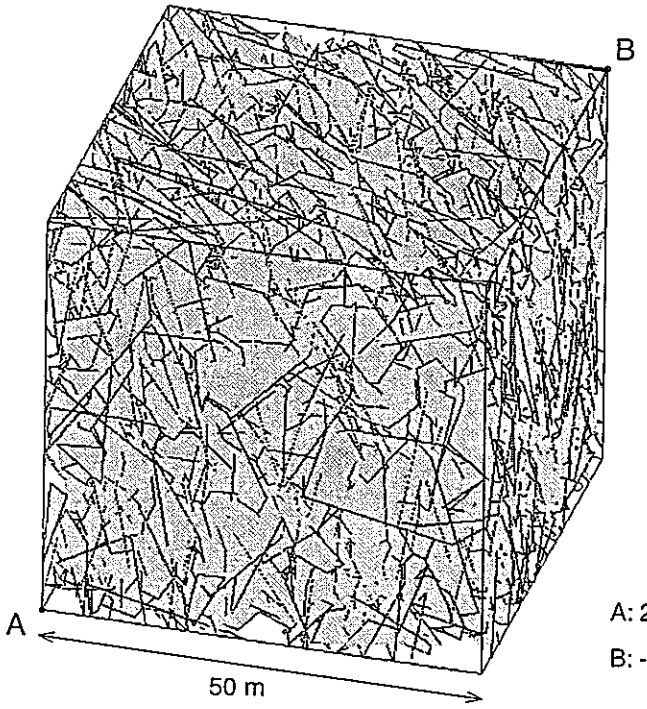

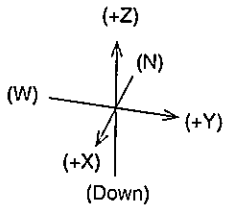

A: 25,0,-25

B: -25,50,25

FIGURE **3-10**
FRACMAN MODEL FOR TRUE-1/RC
PNC/FRACTURE FLOW/JAPAN

PROJECT NO. 923 1089.831 DRAWING NO. 67604 DATE 9/19/96 DRAWN BY CB

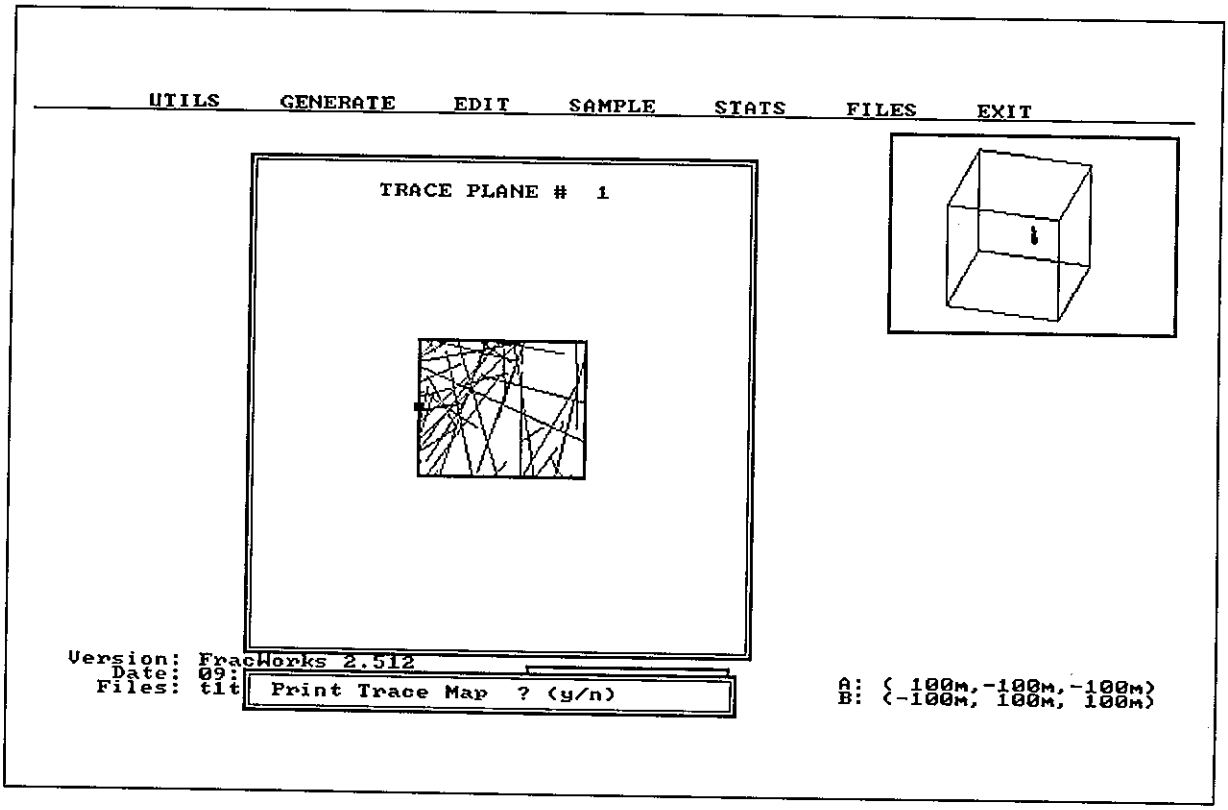

FIGURE **3-11**
INTERSECTION WITH "FEATURE A"
PNC/FRACTURE FLOW/JAPAN

PROJECT NO. 923 1089.831 DRAWING NO. 67605 DATE 9/19/96 DRAWN BY CB

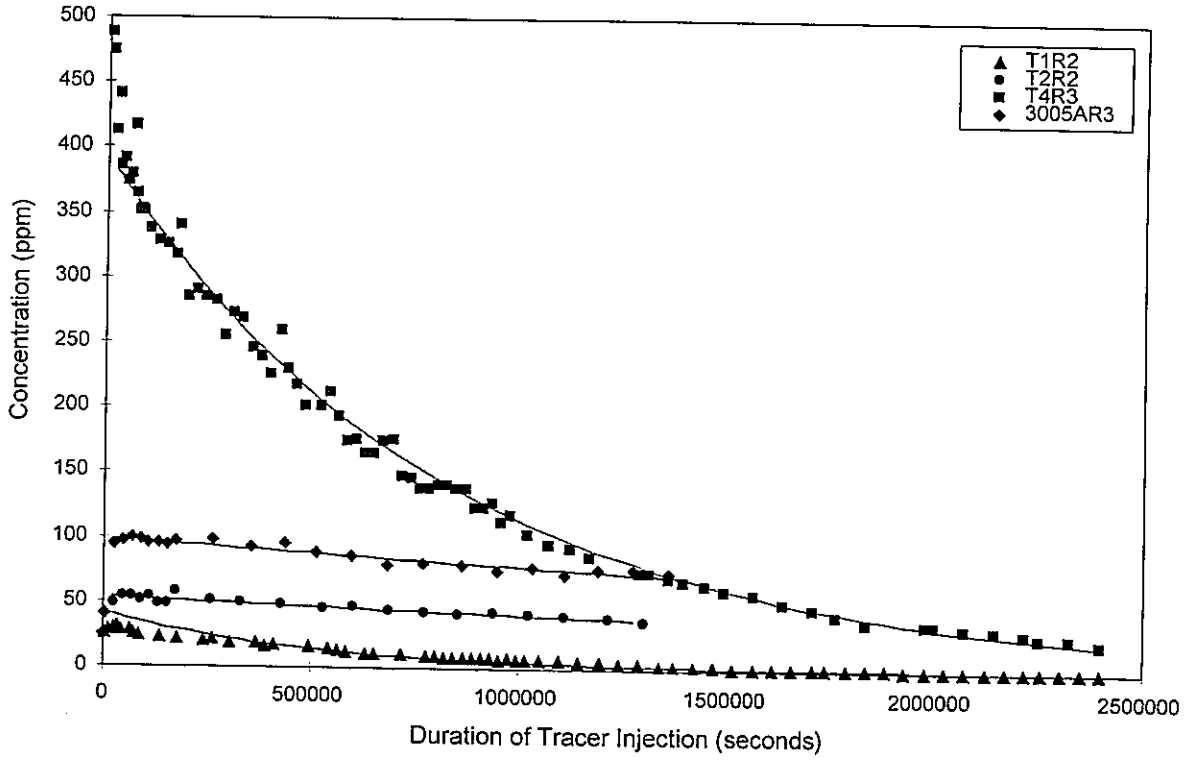

FIGURE **3-12**
INJECTION TIME HISTORIES FOR FRACMAN SIMULATION
PNC/FRACTURE FLOW/JAPAN

PROJECT NO. 923 1089.831 DRAWING NO. 67606 DATE 9/19/96 DRAWN BY CB

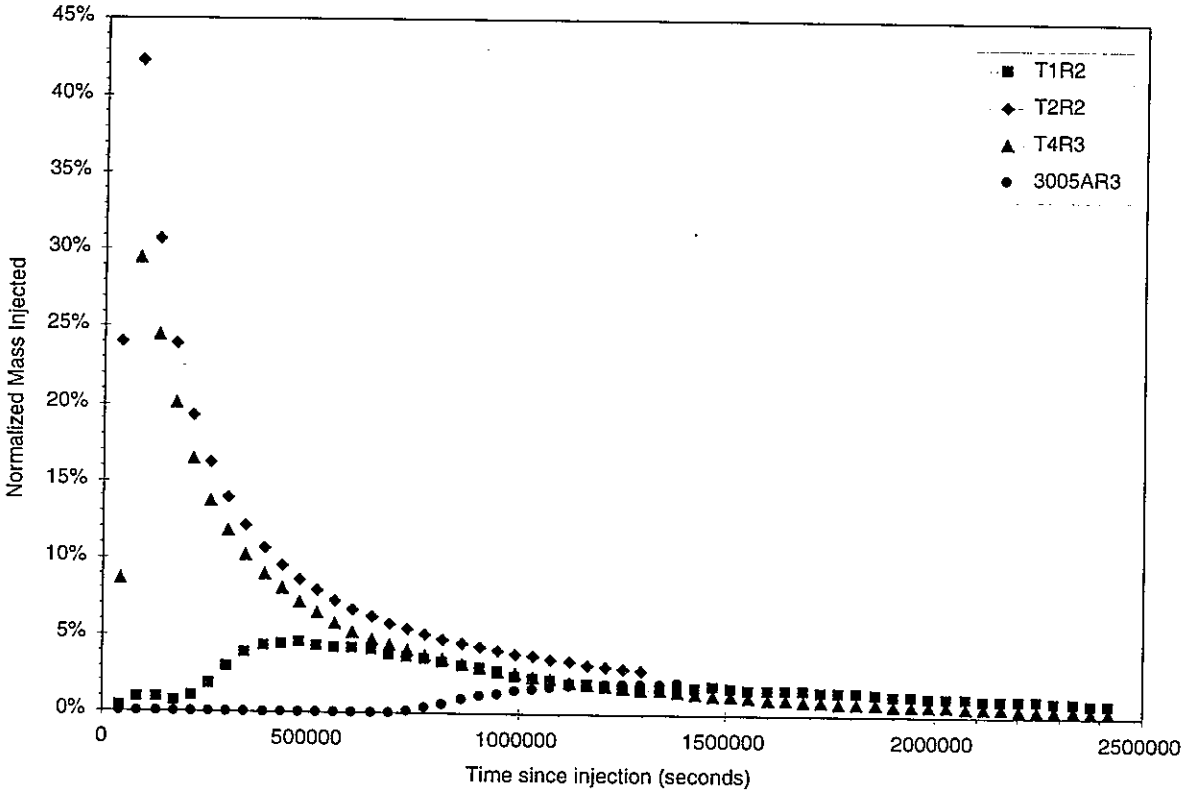

FIGURE **3-13**
FRACMAN ANALYSIS, NORMALIZED MASS RECOVERY
PNC/FRACTURE FLOW/JAPAN

PROJECT NO. 923 1089.831 DRAWING NO. 67607 DATE 9/19/96 DRAWN BY CB

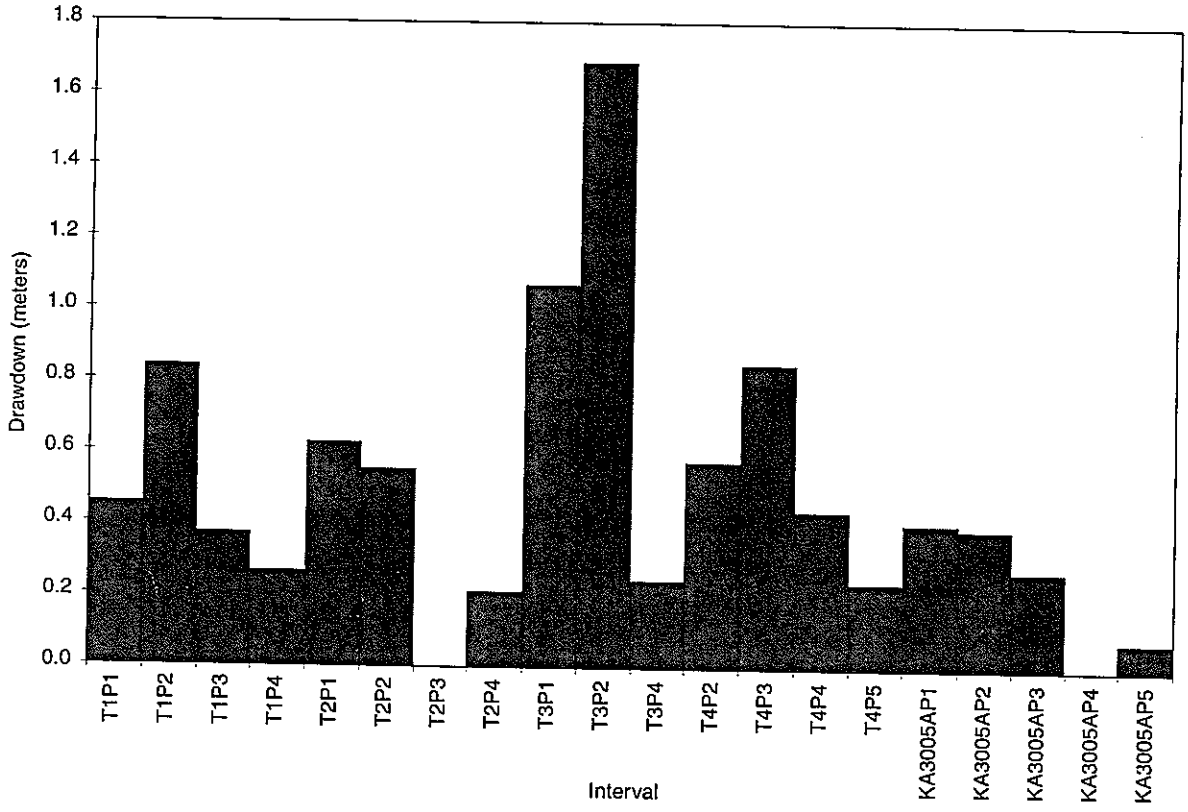

FIGURE **3-14**
DRAWDOWN IN TRUE-1 ROCK BLOCK
PNC/FRACTURE FLOW/JAPAN

PROJECT NO. 923 1089.831 DRAWING NO. 67608 DATE 9/19/96 DRAWN BY CB

Table 3-9 *FracMan Implementation of TRUE-1 Rock Block*

	Stochastic Features	Feature A
Generation Region	Center = (0,25,0) 50 m x 50 m x 50 m	
Boundary Condition	Hydrostatic H=360 m	
Location (FracMan Coordinates)	Baecher Model, Unconditioned	Deterministic X_C=-5.31 Y_C=23.17 Z_C=17.34
Orientation Distribution	Bootstrap from KXTT1-4 and KA3005A "Conductive Features" κ=500	3 point solution Pole Trend=254.71 Pole Plunge=14.34
Size Distribution	Lognormal, Mean= 6 m, Std Dev= 2 m	R = 5 m
Shape	Hexagon	Octagon
Conductive Feature Intensity	$P_{32c} = 4.35\ m^{-1}$ truncated by T_{min} to $P_{32c} = 1.309\ m^{-1}$	N/A
Transmissivity Distribution	Lognormal Mean=$5.17\ 10^{-7}\ m^2/s$ Std. Dev. = $1\ 10^{-8}\ m^2/s$ T_{min}= $5x10^{-9}\ m^2/s$	$T = 1.1 \times 10^{-7}\ m^2/s$
Storativity	$S = 0.001\ T^{1/2}$	$S = 0.001\ T^{1/2}$
Transport Aperture	$S = 0.5\ T^{1/2}$	$S = 0.5\ T^{1/2}$
Longitudinal Disp.	$\alpha_L = 0.6$ m	$\alpha_L = 0.6$ m
Transverse Disp.	$\alpha_T = 0.06$ m	$\alpha_T = 0.06$ m

Table 3-10 *FracMan Tracer Transport Results: Hydrostatic Boundary Condition*

		KXTT1	KXTT2	KXTT4	KA3005A
Mass Recovery		99%	100%	100%	45%
Breakthrough Time t_5 (sec)	sec	93	26	28	233
Breakthrough Time t_{50} (sec)	sec	274	172	178	322
Breakthrough Time t_{95} (sec)	sec	611.2	339	550.9	378

Figure 3-14 presents the more interesting result, for the drawdown. Because the FracMan model is implemented for a 50 meter scale rock block, it was able to predict drawdowns not only in "Feature A" but throughout the intervals monitored in the TRUE-1 rock block.

The FracMan model has substantially lower drawdowns than the SEEP/W and Analytical (Theis) solutions. This is because of the extent of intersecting fractures, which result in a leaky aquifer model for "Feature A", rather than the confined aquifer assumption implemented in the other models. The drawdowns within "Feature A" for the FracMan model are given in Table 3-11.

Table 3-11 *Drawdowns for FracMan Simulation Hydrostatic Boundary Condition "A"*

Borehole	Drawdown
KXTT1	0.5 m
KXTT2	0.6 m
KXTT3	1.7 m
KXTT4	0.9 m
KA3005A	0.4 m

4. CONCLUSIONS

Conclusions from preliminary modeling of the Äspö TRUE-1/RC radially converging tracer experiment include the following:

- The fractures intersecting "Feature A" result in a distinctly non-hydrostatic boundary condition on the experiment, such that the flow can not be considered to be radially converging.

- The most likely pressure field interpretation for conditions during the experiment is that obtained by interpretation of the point dilution process of the injection concentrations. This pressure fields indicates a high probability that tracer would be not recovered from KXTT2 and KA3005A for the experiment as run.

- The Moench analytical solution appears to be adequate for describing the shape of the breakthrough, which is in any event expected to match that for the injection time histories, since this was the response observed in the preliminary tracer testing.

- The FracMan modeling appears to have been useful primarily in terms of understanding the non-hydrostatic pressure field during the experiment. The low drawdowns from the FracMan model are consistent with a leaky aquifer interpretation, but are much lower than would be expected based on the response seen in the preliminary tracer test.

5. ACKNOWLEDGMENTS

The authors would like to thank Power Reactor and Nuclear Fuel Development Corporation (PNC), and in particular, Masahiro Uchida for support, guidance, and key technical contributions The authors would also like to acknowledge the SKB Äspö Modeling Task Force (AMTF), its chairman Gunnar Gustavsson, and secretary Anders Strom. We would also like to acknowledge our colleagues from Golder Associates, Paul La Pointe, Tom Doe, Sven Follin, and Jan Hermanson who provided important technical review comments. We would also like to thank Al. Moench of the USGS, Menlo Park for generously providing access to his analysis program for radially converging tracer tests.

6. REFERENCES

Anderson, P, A. Winberg, V. Cvetkovic, and J-O Selroos, 1996. *TRUE 1st Stage Tracer Test Program.* Contera AB, Gothenberg.

Bear, J., 1979, *Hydraulics of Groundwater,* 569 pp., McGraw-Hill, New York.

Dershowitz, W., G. Lee, J. Geier, T. Foxford, P. La Pointe and A. Thomas, 1995. *FracMan Interactive Discrete Feature Data Analysis, Geometric Modeling, and Exploration Simulation: User Documentation Version 2.5.* Golder Associates Inc., Redmond, Washington.

Dershowitz, W., J. Geier, M. Uchida, R. Busse, 1996. *A Stochastic Approach for Fracture Set Definition.* Proceedings, 2nd North American Rock Mechanics Symposium, Montreal, PQ.

Geo-Slope, Inc., 1995. *SEEP/W User Documentation.* Geo-Slope Inc., Calgary.

Geo-Slope, Inc., 1995 *CTRAN/W User Documentation.* Geo-Slope Inc., Calgary.

Moench, A., 1995. *Convergent Radial Dispersion in a Double-Porosity Aquifer with Fracture Skin: Analytical Solution and Application to a Field Experiment in Fractured Chalk.* Water Resources Research, Vol. 31, No. 8, Pages 1823-1835

Moench, A.F., 1991. Convergent radial dispersion: A note on evaluation of the Laplace transform solution, *Water Resour. Res.,* 27(12), 3261-3264.

Moench, A.F., 1989. Convergent radial dispersion: A Laplace transform solution for aquifer tracer testing, *Water Resour. Res.,* 25(3), 439-447.

Uchida, M, T. Doe, A. Sawada, W. Dershowitz, and P. Wallmann, 1995. *Simulation of the LPT-2 Flow and Transport Experiment.* International Cooperation Report ICR-95-09. SKB, Stockholm.

Uchida, M., T. Doe, W. Dershowitz, A. Thomas, P. Wallmann, A. Sawada, 1994. *Discrete-fracture Modeling of the Äspö LPT-2, large-scale Pumping and Tracer Test.* SKB International Cooperation Report ICR 94-09. SKB, Stockholm.

Winberg, A., ed., 1996. *First TRUE Stage Descriptive Structural Hydraulic Models on Block and Detailed Scales.* SKB International Cooperation Report ICR 94-09. SKB, Stockholm.

Winberg, A., et al., 1995. *Data Distribution for TRUE-1/RC Experiment*, SKB, Stockholm.

7. APPENDIX A: SEEP/W AND CTRAN/W MODEL AND CODE SPECIFICATION FOR ÄSPÖ TRUE-1 SIMULATIONS

7.1 NAME, VERSION, AND ORIGIN

Name: SEEP/W and CTRAN/W

Code Versions:

Origin: SEEP/W and CTRAN/W originated in the finite element dam seepage program SEEP originally developed for the US Army Corps of Engineers during the 1960's. Extensive further development has been carried out by Geo-Slope, Inc., including improvements to the solver and implementation of a Windows user interface.

7.2 GENERAL DESCRIPTION

SEEP/W and CTRAN/W are finite element programs which solve the conservation of mass equations for transient flow and tracer transport. The key feature of these codes are their Windows user interface for mesh generation, finite element simulation, and graphical post-processing.

Conceptual and Mathematical Model

The conceptual model used in SEEP/W and CTRAN/W is a 2-D heterogeneous aquifer. For section models, the aquifer can be modeled as unconfined using a coupling between hydraulic conductivity and (negative) pore pressures. Plan models such as those implemented in this project, must be defined as confined aquifers.

Numerical Method

Flow and transport solutions in SEEP/W and CTRAN/W uses a Galerkin finite element solution. Elements can be three to nine noded. Linear and quadratic basis functions are supported. An iterative method is used to solve for phreatic surfaces based on a user defined hydraulic conductivity-tension pressure function/

Limitations

SEEP/W and CTRAN/W are limited to flow in two dimensions. Coupled processes such as decay and density driven flow are not simulated.

Parameters Required

- **Geometric**: Parameters are required for the mesh and boundary condition geometry
- **Hydraulic and Transport Properties**: Hydraulic conductivity, and porosity, and storatitivity and be defined as constants, or as functions of pressure. For transport simulations, , longitudinal and transverse dispersivity must be defined.
- **Boundary Conditions**: Boundary conditions for steady state or transient head. flux, and concentration.

Type of Results

Output from SEEP/W and CTRAN/W are generally provided graphically from the built in post processor. Numerical values can be obtained by analysis of the (un-documented) finite element output files.

Computer Requirements

SEEP/W and CTRAN/W runs on Intel x86 based MS-DOS compatible computers running Windows 3.X, Windows 95, or Windows NT. . A minimum configuration recommended is an i486DX with 8 Meg RAM, and 500 Meg hard drive.

User Interface

SEEP/W and CTRAN/W share a common and reasonably decent MS-Windows based graphical user interface.

Code Availability

SEEP/W and CTRAN/W are distributed by:

Geo-Slope International, Inc.
830 Ford Tower
6733 6th Ave SW
Calgary, T2P 245 CANADA
+1 403 269 2002
+1 403 266 4851 fax

7.3 REFERENCES

User instructions and verification information are both contained in the User Manuals.

Geo-Slope, Inc., 1995. *SEEP/W User Documentation.* Geo-Slope Inc., Calgary.

Geo-Slope, Inc., 1995 *CTRAN/W User Documentation.* Geo-Slope Inc., Calgary.

8. APPENDIX A: FracMan MODEL AND CODE SPECIFICATION FOR ÄSPÖ TRUE-1 SIMULATIONS

8.1 NAME, VERSION, AND ORIGIN

Name: FracMan Discrete Feature Modeling Package

Code Versions:

Code	Application	Version
FracMan/FracSys	Data Analysis	2.511
FracMan/FracWorks	Fracture Generation	2.511
MeshMaker	Mesh Generation	1.42
EdMesh	Stochastic Continuum	1.33
MAFIC	Flow and Transport	1.53

Origin: The FracMan package was originally developed by William Dershowitz with Prof. G. Baecher and Prof. H. Einstein at MIT in Cambridge, MA, USA beginning in 1977. Research funding for initial versions was provided by the US Bureau of Mines and the US Army Research Office. The first version widely distributed, "**J**oints **I**n Networ**X** (*JINX*)" was designed for modeling flow in fractured rock for surface mining applications, and was released in 1984.

Development of FracMan for radioactive waste repositories was carried out by Golder Associates Inc., Seattle, WA, USA with the support of the US Department of Energy between 1985 and 1990. Primary support for development of FracMan codes since 1991 has been from the Power Reactor and Nuclear Fuel Development Corporation (PNC, Japan).

Additional development has been carried out in connection with radioactive waste repository projects carried out for NIREX (UK), Nagra (Switzerland), USDOE (US), SKB and SKI (Sweden). Features have also been added with support from a number of oil companies, and for the National Institute for Petroleum Energy Research (NIPER).

In addition, Golder Associates Corporation has supported development of a number of significant FracMan features.

8.2 GENERAL DESCRIPTION

The FracMan Package was designed to make discrete feature modeling approaches broadly accessible to hydrogeologists and engineers. To achieve this, FracMan provides an integrated suite of tools for all aspects of discrete fracture flow and transport modeling. FracMan combines data analysis (FracSys), geometric simulation and analysis (FracWorks), and stochastic continuum field generation (EdMesh) with flow and transport modeling (MAFIC). FracMan is currently being implemented within the MS-Windows graphical user interface.

Conceptual and Mathematical Model

The conceptual model used in FracMan assumes that discrete features provide the primary hydraulic flow paths and connections, and that accurate representation of flow path geometry is a key to successful hydrogeologic analysis. Discrete features may be fractures, faults, karsts, or paleochannels, depending on the scale and geology. Discrete features may be either one, two, or three dimensional features, but are generally modeled as polygons. Discrete features are generated in realistic three dimensional networks based on structural geology and statistical information, and can be conditioned to local measurements. Interaction between discrete features and the rock matrix is generally ignored, although the model has the capability for fully discretized matrix blocks, approximate matrix interaction, and matrix diffusion. Algorithms used by specific modules are summarized below.

Numerical Method

Flow solution in MAFIC uses a Galerkin finite element solution based on triangular finite elements. Linear and quadratic basis functions are supported. The solver is implemented using the preconditioned conjugate gradient approach. MAFIC uses a variable bandwidth array storage scheme which is optimized for fracture network connectivities.

Solute transport is solved using a particle tracking algorithm. Particles are tracked based on advective transport defined by the flow field from the finite element solution. Normally distributed longitudinal and transverse dispersivity terms are added to every timestep motion. Particles are tracked from element to element edge. Complete mixing is assumed at fracture intersections, such that transport occurs in proportion to the relative fluxes. Particles are marked to allow differentiation of retardation factors and decay for different tracers. Retardation is modeled as a change in the ratio of advective transport velocity to groundwater flux velocity in each element. Matrix diffusion is modeled using a random walk process between the fracture elements and the matrix blocks, based on the flow wetted surface area. Radionuclide decay is implemented using unlimited chains of single daughter products.

Limitations

FracWorks is limited to planar features, although non-planar features can be modeled using the non-planar fracture zone conceptual model. FracWorks has not yet been used for over 2 million fractures.

The accuracy of MAFIC flow solutions is limited by the fineness of the grid discretization - coarse grids are generally used. The accuracy of MAFIC particle tracking simulations depends on the number of particles tracked. Although theory indicates that millions of particles are necessary for an accurate solutions, computational constraints generally limit use to on the order of thousands of particles.

Although MAFIC includes both volumetric (continuum or matrix) and planar discrete fracture elements, no practical applications have yet been made using the volumetric elements. The approximate rock block solution based on the Warren and Root solution is limited to cases where no matrix to matrix flow occurs.

Parameters Required

- **Geometric**: Parameters are required for distributions or values of location, size, intensity, orientation, shape, and connectivity
- **Hydraulic and Transport Properties**: Transmissivity, storativity, and transport aperture distributions must be defined for all fracture surfaces. These may be constant on fracture planes, or may vary on fracture surfaces according to geostatistical or fractal field assumptions. For transport simulations, matrix diffusion parameters (flow wetted surface area), longitudinal and transverse dispersivity must be defined. Any correlation between properties, and any spatial structure of these properties must also be defined (i.e., using correlation lengths and correlation coefficients).
- **Boundary Conditions**: Boundary conditions for steady state or transient head, flux, and group flux must be defined for all internal and external boundaries. Injection concentrations must be defined for tracer simulations.

Type of Results

Output from FracMan/FracSys consists of statistical analyses of fracture data, and recommended parameters for fracture orientations, size, transmissivity, and spatial distribution.

Output from FracMan/FracWorks consists of (a) visualizations of fracture network patterns, (b) results of simulated exploration, and (c) statistics describing pathways within the fracture networks, and rock blocks defined by the fracture networks.

Results from MAFIC include time-histories of pressure or flux at locations within the fracture network, and at defined boundaries. For transport

simulations, they also include particle location histories and particle breakthrough curves.

Computer Requirements

FracMan runs on Intel x86 based MS-DOS compatible computers. A minimum configuration recommended is an i486DX with 8 Meg RAM, and 500 Meg hard drive. MAFIC, EdMesh, and MeshMaster run on Intel x86 based computers with a minimum of 2 Meg RAM. Larger simulations are generally carried out on Unix workstations. Versions are available for IBM RS/6000, DEC Alpha, HP/Apollo, and Silicon Graphics. A minimum of 64 Meg RAM is recommended. Larger problems (over 10,000 fractures) generally require 256 Meg RAM.

User Interface

The structure of the FracMan package is described in Figure A-1. FracSys, FracWorks, and MeshMaker use an interactive graphical user interface. MeshMaster, EdMesh, and MAFIC are generally run and post-processed using Unix and AWK scripts. AVS and Tecplot software are generally used for visualization.

Code Availability

FracMan is distributed by:

FracMan Technology Group	+1 206 883 0777
Golder Associates Inc.	+1 206 882 5498 fax
4104 148th Avenue NE	+1 206 885 7648 x2019(24 hour voice mail)
Seattle, WA 98052	email: fracman@golder.com
	internet web site: http://fracman.golder.com

Wide distribution of the FracMan codes is encouraged through flexible licensing agreements and frequent training workshops.

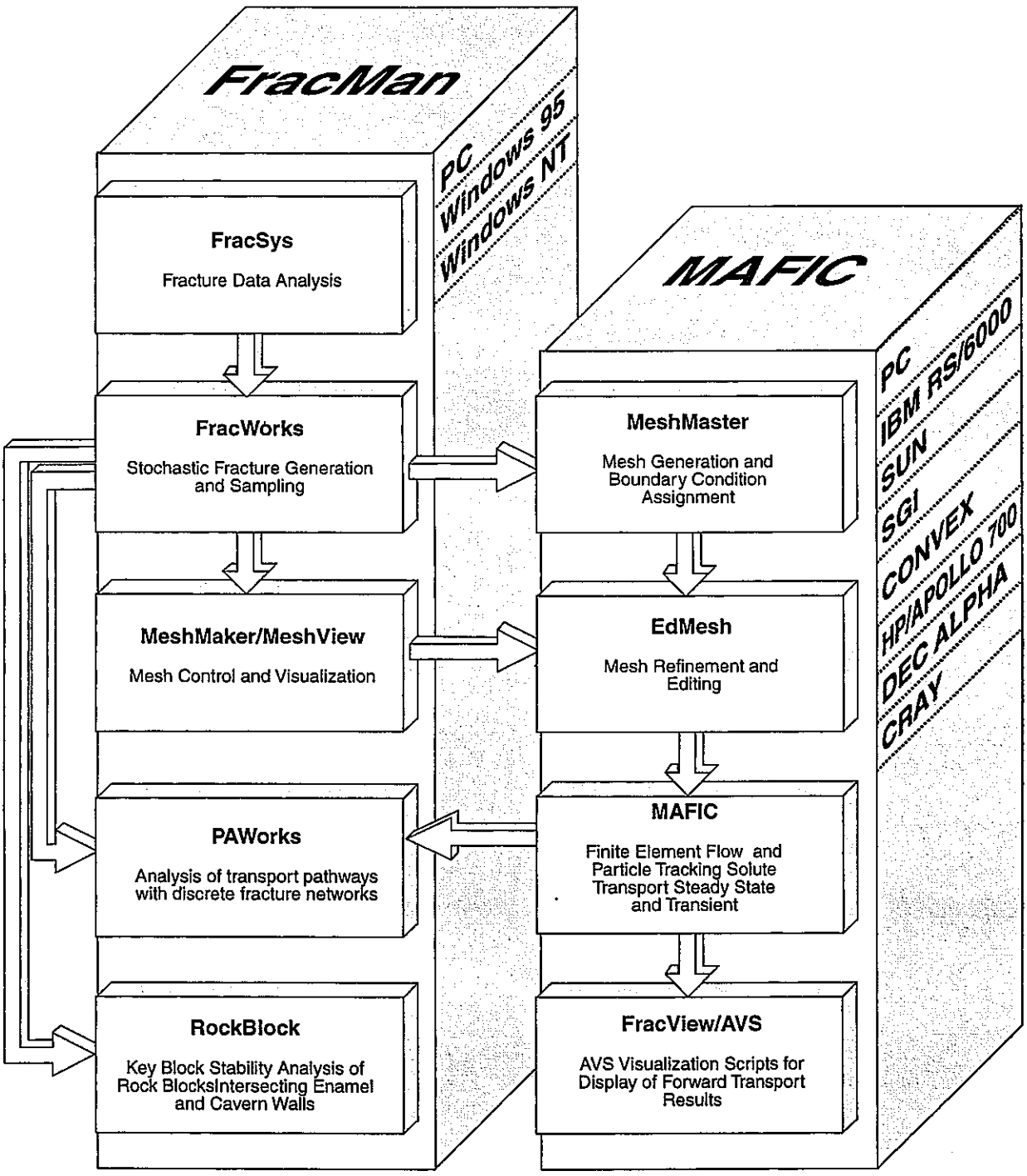

FIGURE **A-1**
FracMan/MAFIC MODELLING SUITE
PNC/HY-7/JAPAN

PROJECT NO. 923-1089.700 DRAWING NO. 64621 DATE 4/4/96 DRAWN BY TK

Golder Associates

Table A-1 FracMan/MAFIC Module Descriptions

Code	Algorithm
FracMan/FracSys	***ISIS:*** Fracture sets are identified by an iterative pattern recognition algorithm, which takes into account user specified fracture characteristics in addition to orientation. ***OxFilet***: Packer tests are simulated within simulated fracture networks, and fracture properties are adjusted by simulated annealing search until a match is found between simulated and measured distributions of packer interval transmissivity. ***FracSize***: Surface trace maps are simulated within simulated fracture networks, and fracture size distribution parameters are adjusted by simulated annealing search until a match is found between simulated and measured distributions of trace length. ***FlowDim:*** Type curve matching is used to derive apparent flow dimension, transmissivity, and storativity from transient well test responses. ***HeterFrac***: Geostatistical, statistical, and fractal methods are used to derive geometric parameters for the nine fracture geometric models available in FracWorks.
FracMan/FracWorks	Discrete Fractures are generated stochastically by Monte Carlo simulation and deterministically using user-specified parameters. Nine geological/geometric models are available. Models are validated for internal consistency by simulated exploration allowing comparison between simulated and field measurements.
MeshMaker	Polygonal discrete fractures generated by FracMan/FracWorks are converted to triangular finite elements by Delanauy Tessellation. These elements are then combined with user specified boundary conditions to produce a MAFIC format input file.
EdMesh	Provides control for fracture properties, boundary conditions, and MAFIC control parameters by automatic editing of MAFIC input files. Fracture properties can be assigned using a range of correlation functions and stochastic generators, including fractal and geostatistical field generators based on the Turning Bands algorithm.
MAFIC	Transient and steady state flow solution for networks of discrete 1-D and 2-D conductive features, and 3-D quadrahedral matrix blocks. Flow is assumed to follow Darcy's law for the water flow version, and is assumed to be laminar for the non-ideal gas flow version.

8.3 REFERENCES

8.3.1 Verification

FracMan and MAFIC have undergone ISO-9001 verification within the context of Golder Associates Inc. ABS certified ISO-9000 Quality Management Plan. ISO-9000 Verification of EdMesh and MeshMaster are currently ongoing. Verification are documented in:

Busse, R., 1995. *FracMan Version 2.511, FracSys Module, Verification Report.* Golder Associates, Inc., Redmond, WA.

Busse, R., 1995. *FracMan Version 2.511, FracWorks Module, Verification Report* Golder Associates, Inc., Redmond, WA.

Busse, R., 1995. *MAFIC Version 1.5: Matrix/Fracture Hydraulic Interaction Code with Solute Transport, Software Verification Report* Golder Associates, Inc., Redmond, WA.

Dershowitz, W. and G. Lee, 1995. *EdMesh Verification Plan* Golder Associates, Inc., Redmond, WA.

Dershowitz, W. and P. La Pointe, 1995. *FracMan Version 2.511, FracWorks Module, Verification Plan* Golder Associates, Inc., Redmond, WA.

Dershowitz, W and G. Lee, 1995. *MeshMaster Verification Plan* Golder Associates, Inc., Redmond, WA.

La Pointe, P., 1995. *FracMan Version 2.511, FracSys Module, Verification Plan.* Golder Associates, Inc., Redmond, WA.

Lee, G., 1995. *MAFIC Version 1.5: Matrix/Fracture Hydraulic Interaction Code with Solute Transport, Software Verification Plan* Golder Associates, Inc., Redmond, WA.

Code cross-verification and validation under the auspices of the OECD/NEA Stripa Project, and UK NIREX. Cross-Verification is documented in:

Dershowitz, W., A. Herbert, and J. Long., 1989. Fracture Flow Code Cross-Verification Plan. SKB Stripa Technical Report TR 89-02. SKB, Stockholm.

Jenkins, K., A. Hock and L. Wei, 1995. Cross-Code Verification between FracMan and NAMMU for the Transient Solver. NIREX Report 94524312-22. UK NIREX, Harwell, UK.

Schwartz, F. and G. Lee, 1991. Cross-Verification Testing of Fracture Flow and Mass Transport Codes. SKB Stripa Technical Report TR-91-29. SKB, Stockholm.

Validation status is documented in:

Dershowitz, W. and P. Wallmann, 1992. Discrete Fracture Modeling for the Stripa Tracer Validation Experiment Predictions. SKB Stripa Project Technical Report TR 92-15, SKB, Stockholm.

Dershowitz, W., P. Wallmann, and S. Kindred, 1991. Discrete Fracture Modeling for the Stripa Site Characterization and Validation Drift Inflow Predictions. SKB Stripa Project Technical Report TR 91-16, SKB, Stockholm.

Gnirk, P., 1993. OECD/NEA International Stripa Project, Overview Volume II, Natural Barriers. SKB, Stockholm. P 229.

Hodgkinson, D., 1992. A Compilation of Minutes for the Stripa Task Force on Fracture Flow Modeling. SKB, Stockholm.

O. Olsson, 1992. Site Characterization and Validation - Final Report. SKB Stripa Technical Report TR-92-22. SKB, Stockholm.

8.3.2 Technical Description

Dershowitz, W., G. Lee, J. Geier, T. Foxford, P. La Pointe, and A. Thomas, 1995. FracMan Interactive Discreet Feature Data Analysis, Geometric Modeling, and Exploration Simulation: User Documentation Version 2.5. Golder Associates Inc., Seattle.

Dershowitz, W., G. Lee, and J. Geier, 1995. MeshMaster Discrete Fracture Mesh Generation Utility for Use with FracMan. User Documentation, Version 1.4. Golder Associates Inc., Seattle.

Lee, G., W. Dershowitz, and J. Geier, 1995. EdMesh Discrete Fracture Mesh Editor. User Documentation, Version 1.3. Golder Associates Inc., Seattle.

Miller, I, G. Lee, W. Dershowitz, and G. Sharp, 1995. MAFIC Matrix/Fracture Interaction Code with Solute Transport. User Documentation, Version 1.5. Golder Associates Inc., Seattle.

8.3.3 Application

Dershowitz, W., P. Wallmann, T. Doe, and J. Geier, 1993. Discrete Feature Modeling at the Stripa Mine in Sweden: Significance for Hydrologic Modeling of Fractured Rock Masses. Proceedings, Fourth Annual International Conference on High Level Radioactive Waste Management, Las Vegas. American Society of Civil Engineers, NY.

Uchida, M., T. Doe, W. Dershowitz, and P. Wallmann, 1993. Simulation of Fracture Flow at the Kamaishi Validation Drift. Proceedings, Fourth Annual International Conference on High Level Radioactive Waste Management, Las Vegas. American Society of Civil Engineers, NY.

Dershowitz, W., 1992. Interpretation and Synthesis of Discrete Fracture Orientation, Size, Shape, Spatial Structure and Hydrologic Data by Forward Modeling. Proceedings, International Society for Rock Mechanics Symposium on Rock Joints, Tahoe.

Dershowitz, W., T. Doe, and P. Wallmann, 1992. Discrete Feature Dual Porosity Analysis of Fractured Rock Masses: Applications to Fractured Reservoirs and Hazardous Waste. Proceedings of the 33rd U.S. Symposium on Rock Mechanics, Santa Fe, NM. p. 543.

Appendix C Äspö TRUE-1 Dipole Experiment Report

Discrete Fracture Network Model
Äspö TRUE Experiment

Dipole Tracer Test Test Prediction

PNC/Golder Team

W. Dershowitz/Golder
M. Uchida/PNC
Th. Eiben/Golder
C. Chakrybarty/Golder

Table of Contents

1. Introduction

For the Task 4D prediction, the PNC/Golder team have used two strategies for predicting dipole tracer tests breakthrough in "Feature A":

- small scale DFN modelling conditioned to the TRUE-RC-1 experimental results, and
- analytical solutions for radially converging and dipole tracer experiments, calibrated to the TRUE-RC-1 experimental results.

The use of the TRUE-RC as the basis for calibration and conditioning was made somewhat problematic by lack of recovery from KXTT2 and KA3005A, particularly considering the large drawdown response seen in KXTT2. This is particularly problematic for the analytical solutions, which uses parameters derived solely by calibration from the TRUE-RC tracer breakthroughs, without considering the TRUE-RC head responses. KXTT2 will be used in three of the dipole experiments, but does not have any tracer transport information. However, the drawdown response indicates the KXTT2 is well connected to KXTT3 and less connected to KXTT1 and KXTT4, which are closer.

This document provides a brief summary of the modeling and predictions for Task 4. Sections 2 through 5 describe the FracMan DFN modeling. Section 6 presents tracer breakthrough predictions using analytical solutions.

2. FracMan DFN Model for Task4d

2.1 Modeling Approach

The DFN modeling for Task 4d evolved from the DFN modeling carried out for the TRUE-RC1 experiment (Dershowitz et al, 1996), in a series of stages. These stages will be described more fully in following versions of this document. Fundamentally, modeling proceeding from models of only Feature A with two intersecting fractures, to models including heterogeneous properties for feature A, to models including stochastically generated background fracturing, and finally to models including Feature A, NW-2', stochastic background fracturing, and an additional feature A* representing out-of plane connections between KXTT2 and KXTT3.

The basic approach taken for DFN modeling of Task 4d is summarized as follows. All predictions made are stochastic. Both probabilistic and stochastic versions of the SKB prediction formats are provided.

1. Define "Feature A" and "NW-2*" deterministically within a 30m scale discrete fracture model, using material properties postulated by Winberg et al (ICR-96-xx).
2. Generate 50 to 100 realizations of a population of stochastically generated background fractures based on the analysis of Dershowitz et al (ICR-96-xx), using only fractures with a transmissivity greater than 10^{-8} m^2/s.

3. Apply boundary conditions to the edges of the model to match the heads measured before TRUE-RC-1. Adjust these boundary conditions to obtain a head field which matches that before TRUE-RC-1 for a significant proportion of the realizations.
4. Simulate TRUE-RC-1 pumping from KXTT3, and calculate the drawdown in each of the five wells.
5. Implement a highly transmissive zone connecting KXTT2 and KXTT3 in order to reproduce the large observed drawdown response. Adjust transmissivities of "Feature A" and the channel between KXTT2 and KXTT3 to obtain a good match to the drawdown response for a significant portion of the realizations.
6. For realizations which reasonably match the drawdown responses of TRUE-RC-1, calculate tracer breakthrough for each of the four injection sections. Compare the simulated breakthrough curves to the measured breakthrough curves from TRUE-RC-1. Accept those realizations which have a reasonable match for breakthrough times t5, t50, t95, and the mass recovery percentage from KXTT1->KXTT3 and KXTT4->KXTT3.
7. For realizations with a reasonable match to both drawdown response and tracer breakthrough, carry out simulations of the four TRUE-Dipole experiments. This requires modification of the external head boundary condition to account for the change in ambient pressure between TRUE-RC-1 and TRUE-Dipole.
8. Use the TRUE-Dipole simulations, conditioned to the TRUE-Radially converging experiment results to calculate probabilistic predictions for drawdown, breakthrough (t5, t50, t95), and breakthrough.

The sections below provide additional detail on the DFN analyses.

2.2 Conceptual Model

The discrete fracture network model (DFN) used for the Task4d prediction is illustrated in Figures 2-1 and 2-2. This model is based on the DFN model of Dershowitz et al. (ICR 95-xx), with the addition of a fracture representing Feature NW-2* as described by Winberg et al (ICR-96-xx) and a Feature A* representing the highly conductive pathway between boreholes KXTT2 and KXTT3.

The coordinate system for the model was chosen so that the center of the experimental region on Feature A defines the origin. The coordinates of the new origin are (-5.31, 23.17, -3.4) in the old Golder/PNC system and (7435.23, 2323.15,-403.42) in the Äspö system.

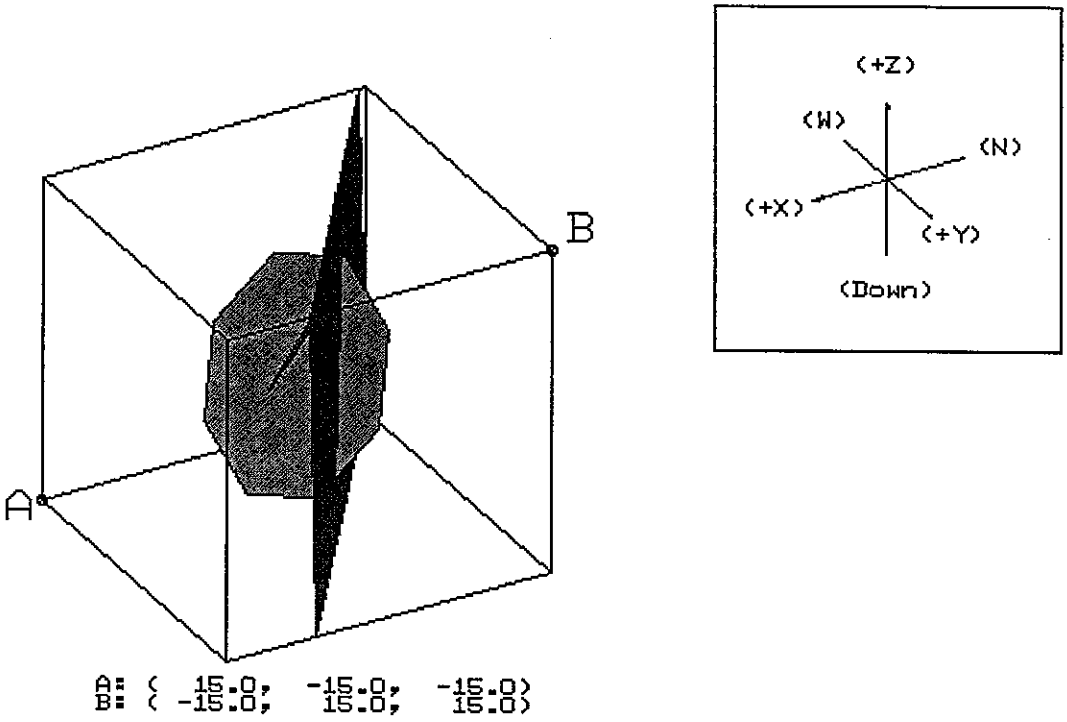

Figure 2-1 3D View of Deterministic "Feature A", "Feature A*" and "NW-2*" in Discrete Fracture Network Model (30 m rock block)

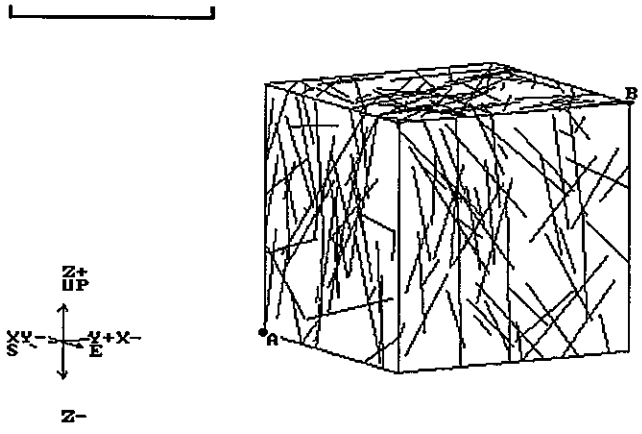

Figure 2-2 3D Trace View of Stochastic Background Fractures (30 m rock block)

The parameters used for "Feature A", "Feature A*", NW-2', and the background fracture population are summarized in Table 2-1.

The location and orientation data for Feature A were taken from Dershowitz et al (1996) International Cooperation Report ICR-96-05, page 61. The size of Feature A is limited by

two constraints. First all boreholes and the intersection with zone NW2' have to be included. Second, the size of Feature A does not extend to the nearby tunnel.

Transmissivity data for Feature A are available from all five boreholes. They vary from values as low as 1.1e-08 m^2/s in KXTT1 to values as high as 3.6e-07 m^2/s in KXTT3. The average value from all five boreholes is 9.6e-08 m^2/s. The model uses a homogeneous transmissivity of 1.25e-07 m^2/s. Storativity and fracture thickness were calculated as shown in ICR 96-05 on page 61.

Feature A* is located in the middle between KXTT2 and KXTT3 and parallel to Feature A. Because it needs to intercept only with boreholes KXTT2 and KXTT3 but not with the other boreholes in the model its areal extent parallel to Feature A is limited. This was modeled using a high aspect ratio for this fracture to give it a long and narrow shape. The transmissivity for Feature A* was derived by simulating the drawdown during the RC-1-Test. Storativity and fracture thickness were calculated as shown in ICR 96-05 on page 61.

Table 2-1 Input Parameter for Discrete Fracture Model

	Feature A	Feature A*	NW2*	Background Fractures
Generation Region				50m x 50m x 50m Center (0,0,0)
Location (x,y,z), m	0,0,0	-0.12,-0.46,2.18	-1.69,3.08,-3.60	Enhanced Baecher
Pole (tr,pl)	254.71,14.34	254.71,14.34	216.0,1.0	Bootstrap from TRUE Borehole data, Dispersion κ = 500
Size, m	10.1	2	30	Lognormal, m=6 St. Dev. = 2
Shape	Octagon	Octagon	Octagon	Hexagon
Aspect Ratio	1	10	1	1
Dir of Elongation (tr, pl)	N/A	155.66,30.67	N/A	N/A
Intensity	N/A	N/A	N/A	P_{32} = 4.35 m^{-1} truncated by Tmin to P_{32} = 1.309 m^{-1}
Transmissivity, m^2/s	1.25e-07	3.16e-05	1.0e-06	Truncated Lognormal, Mean = 3.98e-08 St. Dev. = 5.17e-07 Tmin = 1.0e-08
Storativity	2.9e-07	2.9e-07	1.0e-06	6.3e-08
Thickness, m	1.78e-04	2.82e-03	5.0e-04	3.2e-05

The geometry of zone NW2' is described in Winberg et al (1996) ICR-96-04, page 24. The strike and dip are given by (306,89), resulting in a pole vector trend and plunge of

(216,1). The location is the interception with borehole KXTT1. Because NW2' penetrates the whole model area, it was not necessary to know the exact position of the fracture center. Transmissivity for zone NW2' is given in the same report on page 37. The calculation of storativity and fracture thickness is the same as described for Feature A.

Orientation, size and transmissivity data for the background fractures were taken from Dershowitz et al (1997) "Summary of Simulations for the Äspö TRUE1 RC Experiment", page 22 (ICR in preparation).

2.3 Highly Conductive Pathway

From analysis of the observed head responses during the RC-1-Test it can be seen that it is not possible to model these observations with a homogeneous transmissivity field. The high drawdown in KXTT2 indicates the existence of a highly conductive connection between this borehole and the pumping borehole KXTT3. The following conceptual models were developed and investigated to model this connection:

a) a homogeneous transmissivity on Feature A, with the background fracture network providing the extraordinary hydraulic connection between KXTT2 and KXTT3,

b) a homogeneous transmissivity on Feature A, with a highly transmissive channel between KXTT2 and KXTT3,

c) a homogeneous transmissivity on Feature A, with a highly transmissive channel between KXTT2 and KXTT3, isolated from boreholes KXTT1 and KXTT4 by a low permeability zone surrounding the channel, and

d) a homogeneous transmissivity on Feature A plus a highly conductive fracture parallel to Feature A (Feature A*) providing the pathway between KXTT2 and KXTT3.

For concept a) multiple realizations of the background fracture network were created and used to simulate the RC-1-Test. However, while the results for most wells were satisfying, out of 100 realizations none was able to reproduce the high drawdown observed in KXTT2. Therefore concept b) was used in order to model the highly conductive pathway. Various models with different channel properties such as transmissivity, width and length of the channel on Feature A were developed. However, none of the models was able to reproduce the high drawdown in KXTT2 without effecting other boreholes (i.e. KXTT1), which were located close to the channel. Concept c) solved this problem, but at the expense of the introduction of a level of artificiality into the spatial structure of Feature A which was considered unsupportable.

Concept d) allowed us avoid the need to incorporate channel and low permeability zones into Feature A, while ensuring that the model could represent the hydraulic connection between KXTT2 and KXTT3. This model produced good results for drawdown in KXTT1, KXTT4, and KA3005A, as in the homogeneous model a) and also provided a good match for the drawdown in KXTT2 by introducing a separate pathway between the pumping well and KXTT2 (Feature A*). Results for this concept d) still did not provide as good a match for drawdowns in KXTT1, KXTT4, and KA3005A as the homogeneous model a). We believe that this may be due to the background fractures, which provide a good connectivity between Feature A and Feature A*. Therefore the effects were not

always better than the results observed with concept b). In many realizations of the background fracturing, t was possible to model the high drawdown in KXTT2, but this was always effecting drawdown in the other boreholes as well. This effect was minimized by making Feature A* long and skinny (i.e., a high aspect ratio) such that it was intersected by fewer background fractures to provide extraneous connections to Feature A.

3. Finite Element Mesh

MeshMaster was used to create a finite element mesh of the fracture system. There are a total of 11 boundary groups (BG). BG 1 to 6 represent the external boundaries, a cube with the dimension of 10m x 10m x 10m located at (0,0,0). BG 7 to 11 represent the packer intervals for the 5 boreholes. No real boundary conditions were set in the header file. This was done later with EdMesh. Here, all boundaries were set to no flow boundaries.

No refinement near boundaries was used but the elements were predivided. The maximum element area for predivision was set to 1 m^2 for Feature A and for the background fractures. For zone NW2' a maximum area of 4 m^2 was accepted. The input parameters for MeshMaster can be found in BACKGR.INP.

EdMesh was run once to remove any nasty elements. EdMesh was also used to change the boundary conditions. For the boreholes a group flux of 0.0 was defined in order to calculate the initial head field prior to the test. The other boundaries were changed during the matching process. The file which contains the EdMesh input is called BACKGR.SET.

4. Model Calibration

4.1 Boundary Conditions

Prior to running multiple realizations of the background fracture network, a single realization was used to calibrate the model.

The boundary conditions have to be chosen in a way that the model is able to at least represent the head distribution observed in the five boreholes intercepting with Feature A prior to the start of the dipole test. The model should also be able to reproduce the head distribution observed prior to the radially converging (RC) test and the main characteristics of the RC test. These are given in "Test design for TRUE-1 stage dipole tests 1-4", (Anderson, 1996).

Table 4-1 Measured and Calculated Heads prior to Dipole Test

Well	Boundary Group	Measured Head prior to RC test, m	Measured Head prior to dipole test, m
KXTT1	8	-46.50	-49.09
KXTT2	9	-46.85	-49.36

KXTT3	10	-46.50	-48.97
KXTT4	11	-46.40	-49.04
KA3005A	7	-46.95	-49.90

The head distribution prior to the RC test shows mainly a NW-SE striking head gradient with a head difference of approximately 0.5 m between KXTT3 and KA3005A and an average of -46.64 m. Prior to the dipole test the head difference has increased to approximately 1 m. The average head has fallen to -49.27 m. Obviously the global head field in the vicinity of the TRUE1 block is still changing. Therefore it is not necessary to use the same boundary conditions for both tests, however the other parameters of the model should be left unchanged.

4.2 Steady State Flow Field prior to and during RC-1

The steady state head field prior to RC-1 was matched with the boundary conditions shown in Table 4-2. The table indicates the resulting head values at the corners of the model and the resulting settings used for the boundary groups (BG).

Table 4-2 Heads used for calibration of model prior to RC-1 Test

Corners			H_o	H_x	H_y
NE: -45.5	NW: -45.5	BG1	-48.5	0	0.25
SE: -47.5	SW: -49.5	BG2	-45.5	0	0
		BG3	-46.5	0.1	0
		BG5	-47.5	0.2	0

The calibration was done using a single realization. After that, multiple realizations of the background fracture network were created with the derived boundary conditions. Approximately 50 % of the realizations were able to reproduce the observed head field within the chosen limits. Only those realizations with a head difference of less than 0.3m for all boreholes except KXTT4 and less than 0.5m for KXTT4 were accepted for further use. Table 4-3 shows the results for the accepted realizations for the 5 observation boreholes intercepting Feature A.

In addition to reproducing the undisturbed head field without pumping from any well, the model must also be able to simulate the observed drawdowns caused by the extraction in KXTT3. In order to match the observed drawdown, the transmissivity was changed for the elements representing Feature A and also for the elements representing Feature A*. The transmissivity of Feature A* is mainly responsible for the amount of drawdown in KXTT3 and KXTT2. The best match was obtained with a transmissivity of 3.16E-05 m^2/s ($=10^{4.5}$ m^2/s).

The parameter mainly effecting the other three boreholes, which are not intersected by A* is of course the transmissivity of Feature A. This parameter was set to 1.25E-07 ($=10^{6.9}$) during the matching process. However, because of the network of background fractures connecting Feature A to Feature A*, the effect of changing transmissivity is not limited to just one of those fractures.

Only those realizations which were able to reproduce the steady state head field prior to RC-1 were used for the drawdown calculations. The calculated drawdown results were then compared with the measured drawdowns during RC-1. Only those realizations showing a difference between measured and calculated values of less than 1m were accepted for further calculations. Of the realizations 16.7% met the chosen criteria. Table 4-3 shows the resulting drawdown results for the RC-Test for those remaining realizations.

Table 4-3 Measured and Calculated Heads and Drawdown

	Heads prior to RC-1*			Drawdown during RC-1**		
	measured, m	calculated mean, m	difference, m	measured, m	calculated mean, m	difference, m
KA3005A	-46.95	-46.985	-0.035	0.28	0.88	-0.60
KXTT1	-46.5	-46.63	-0.130	0.62	1.28	-0.66
KXTT2	-46.85	-46.662	0.188	2.23	2.19	0.04
KXTT3	-46.5	-46.625	-0.125	3.12	2.47	0.65
KXTT4	-46.4	-46.774	-0.374	0.32	1.05	-0.73

* based on 36 realizations
** based on 6 realizations

The results show that for the head field prior to RC-1 a good match was obtained for all wells except maybe KXTT4. The match for KXTT4, however, is still acceptable.

For the drawdown it was not possible to get a match of comparable quality. The effect of the high conductive pathway between KXTT3 and KXTT2 it not limited to these two wells. It was not possible to model the high drawdown in KXTT2 without also having larger drawdowns in the other boreholes. Because KXTT2 is used in three of the four dipole tests, however, the main effort was placed on simulating drawdown in KXTT2 correctly.

4.3 Recovery for RC-1

The results of the RC-1 test were used to calibrate the transport related parameters of the model. Surprisingly the values taken from the existing database as shown in Table 4-4 were giving satisfactory results.

Table 4-4 Transport related input parameters

Longitudinal Dispersion	0.6 m
Transverse Dispersion	0.06 m

The results from RC-1 show that tracer is recovered only in KXTT1 and KXTT4. A comparison of measured and calculated recovery and breakthrough for these boreholes is shown in Table 4-5.

Table 4-5 Ultimate recovery for RC-1 test

	measured, m	calculated mean, m	difference, m	Minimum, m	Maximum, m
KXTT1	91 %	63.02%	-27.98%	21.96%	99.58%
KXTT4	97 %	95.83%	-1.17%	84.13%	99.51%

It can be seen that recovery from KXTT4 is much better reproduced by the model than recovery from KXTT1. In fact the variety of results for recovery from KXTT1 is very large. However, none of the realizations showed bad results for both boreholes. Therefore, all 6 realization were used for further investigations.

The last step in model calibration compared the results for tracer breakthrough times. The model shows a good agreement between measured and calculated values (Table 4-6). Again results for recovery from KXTT4 are better than results for KXTT1.

Table 4-6 Breakthrough results for RC-1 test

T5	meas., h	calc. mean, h	diff., h	min, h	max, h
KXTT1	26	19.84	-6.16	17.58	26.06
KXTT4	21	21.75	0.75	17.99	24.51
T50	**meas., h**	**calc. mean, h**	**diff., h**	**min, h**	**max, h**
KXTT1	154	133.93	-20.07	129.16	141.88
KXTT4	156	164.27	8.27	157.11	183.69
T95	**meas., h**	**calc. mean, h**	**diff., h**	**min, h**	**max, h**
KXTT1	488	406.03	-81.97	401.52	416.51
KXTT4	560	592.44	32.44	587.42	606.51

5. Dipole Tests Predictions

5.1 Calibration to new head field

The six realizations of the background fracture network which were identified during the calibration process described above were used to predict the results of the four dipole tests. Before the model could be used to actually predict any results from the dipole tests, it had to be adjusted to the changed head field prior to the tests. It is assumed that the head field in the vicinity of the nearby tunnel still has not reached steady state conditions. Table 5-1 shows the boundary conditions which were derived.

Table 5-1 Heads used for calibration of model prior to Dipole Tests

Corners			H_o	H_x	H_y
NE: -48.0	NW: -48.0	BG1	-51.5	0	0.375
SE: -50.0	SW: -53.0	BG2	-48.0	0	0
		BG3	-49.0	0.1	0
		BG5	-50.5	0.25	0

No other changes were made to the model. The resulting head values for the six realizations used for the dipole tests predictions are shown in Table 5-2.

Table 5-2 Measured and calculated heads prior to Dipole Tests for 6 final realizations

	measured, m	calculated mean, m	difference to mean, m	minimum, m	maximum, m
KA3005A	-49.90	-49.58	0.32	-49.80	-49.425
KXTT1	-49.09	-49.25	-0.16	-49.32	-49.138
KXTT2	-49.36	-49.27	0.09	-49.35	-49.142
KXTT3	-48.97	-49.24	-0.27	-49.31	-49.124
KXTT4	-49.04	-49.37	-0.33	-49.49	-49.28

It is recognized that the calibration to the head field prior to the dipole tests is not extremely good. This is especially true when looking at the overall head gradient across Feature A (KXTT3 towards KA3005A). However KA3005A is not involved in any of the dipole tests and with expected drawdowns in the range of 1 to 2 m the differences between the other wells are acceptable.

The following sections contain the predictions for the dipole test in the presentation format required be SKB. Note, however, that due to the small number of realizations it was not possible to compute 5th and 95th percentiles directly. Instead normal

distributions based on the mean and standard deviation calculated from the six realizations were used.

5.2 Prediction Format required by SKB

5.2.1 Dipole Test 1

5.2.1.1 Predicted Drawdown

Table 5-3 Predicted Drawdown during Dipole Test 1

Borehole	$s_{(5\%)}{}^{c}$	$s_{(50\%)}{}^{c}$	$s_{(95\%)}{}^{c}$
KA3005A	0.321	0.436	0.551
KXTT1	0.214	0.309	0.405
KXTT2	0.676	1.016	1.356
KXTT3	0.809	1.129	1.448
KXTT4	0.394	0.482	0.570

5.2.1.2 Predicted Breakthrough Curve

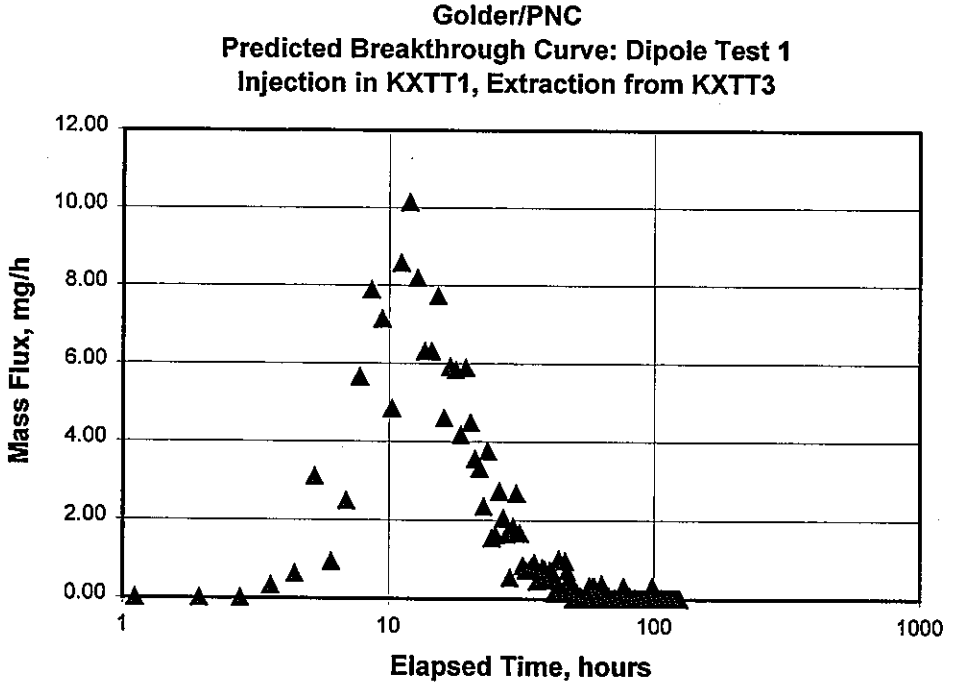

Figure 5-1 Predicted Mass Recovery for Dipole Test 1 (Realization 17)

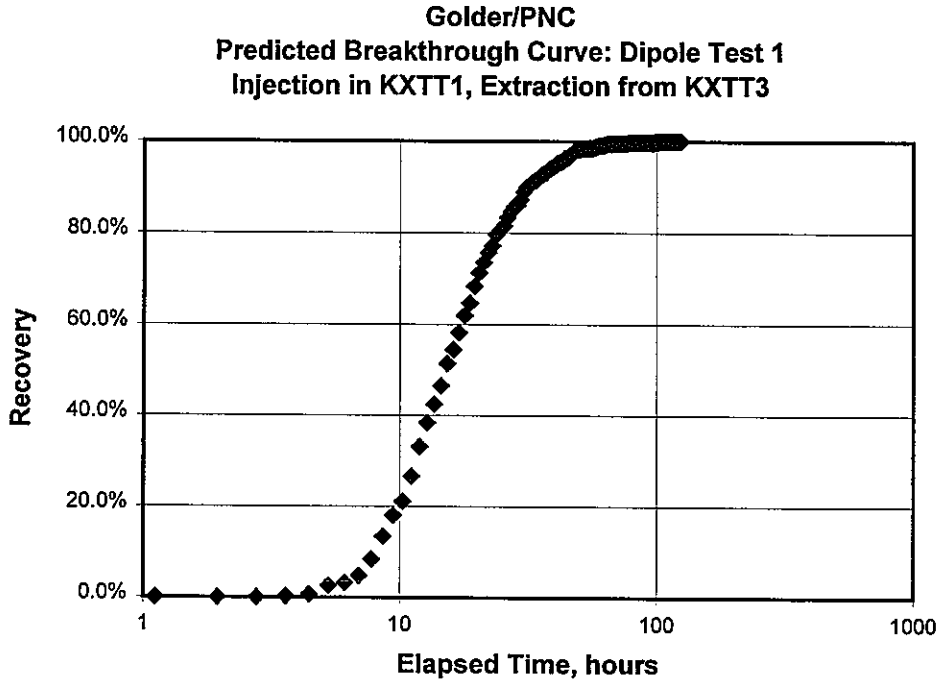

Figure 5-2 Predicted Cumulative Mass Flux for Dipole Test 1 (Realization 17)

Table 5-4 Predicted Breakthrough Times for Dipole Test 1

Pump hole	Injection hole	$t_{5(5\%)}$	$t_{5(50\%)}$	$t_{5(95\%)}$	$t_{50(5\%)}$	$t_{50(50\%)}$	$t_{50(95\%)}$	$t_{95(5\%)}$	$t_{95(50\%)}$	$t_{95(95\%)}$
KXTT3	KXTT1	4.34	6.44	8.54	10.03	15.69	21.36	15.83	53.95	92.07

5.2.1.3 Predicted Mass Recovery

Table 5-5 Predicted Mass Recovery for Dipole Test 1

Borehole	$F_{(5\%)}{}^{c}$	$F_{(50\%)}{}^{c}$	$F_{(95\%)}{}^{c}$
KXTT3	22.76	63.31	100.0

5.2.2 Dipole Test 2

5.2.2.1 Predicted Drawdown

Table 5-6 Predicted Drawdown during Dipole Test 2

Borehole	$s_{(5\%)}{}^{c}$	$s_{(50\%)}{}^{c}$	$s_{(95\%)}{}^{c}$
KA3005A	0.055	0.082	0.109
KXTT1	0.460	1.179	1.899
KXTT2	0.093	0.123	0.153
KXTT3	0.095	0.125	0.154
KXTT4	0.079	0.097	0.115

5.2.2.2 Predicted Breakthrough Curve

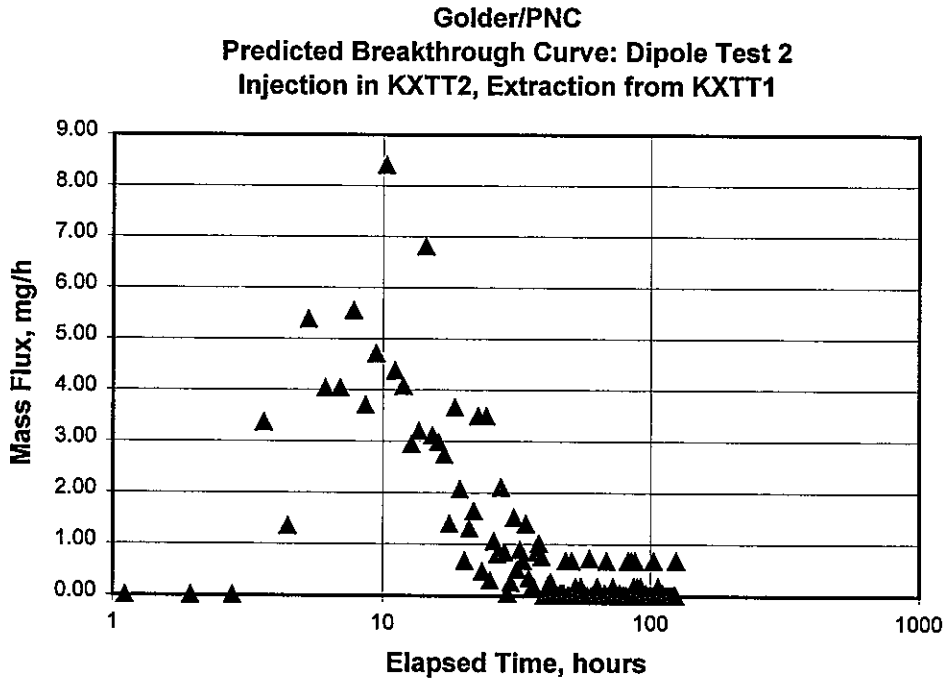

Figure 5-3 Predicted Mass Recovery for Dipole Test 2 (Realization 14)

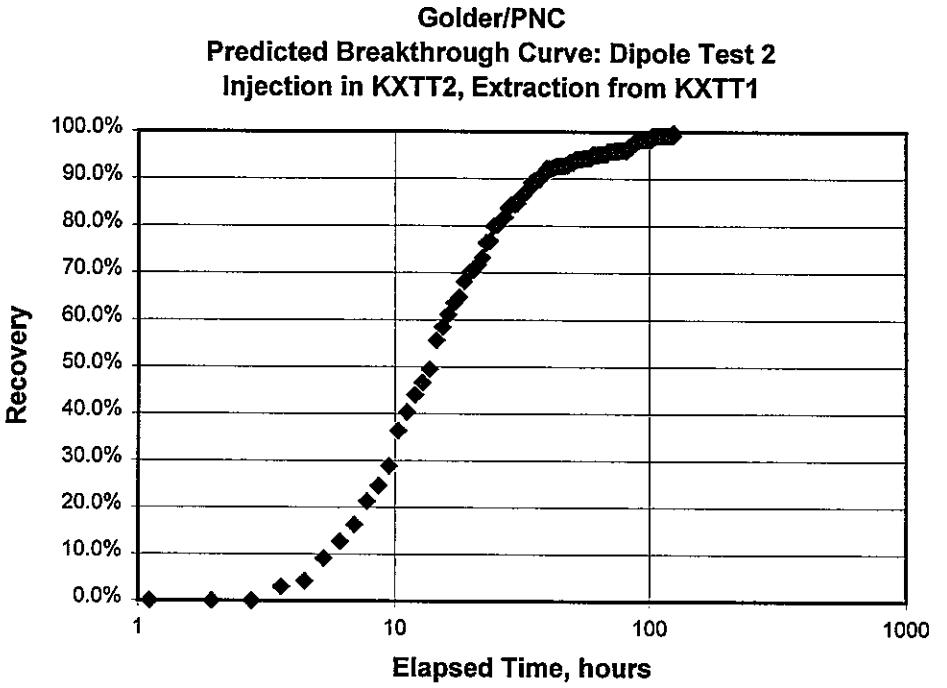

Figure 5-4 **Predicted Cumulative Mass Flux for Dipole Test 2 (Realization 14)**

Table 5-7 **Predicted Breakthrough Times for Dipole Test 2**

Pump hole	Injection hole	$t_{5(5\%)}$	$t_{5(50\%)}$	$t_{5(95\%)}$	$t_{50(5\%)}$	$t_{50(50\%)}$	$t_{50(95\%)}$	$t_{95(5\%)}$	$t_{95(50\%)}$	$t_{95(95\%)}$
KXTT1	KXTT2	0.81	3.14	5.48	1.56	9.96	18.36	< 0.5	50.55	102.03

5.2.2.3 Predicted Mass Recovery

Table 5-8 **Predicted Mass Recovery for Dipole Test 2**

Borehole	$F_{(5\%)}{}^{c}$	$F_{(50\%)}{}^{c}$	$F_{(95\%)}{}^{c}$
KXTT1	12.86	49.51	86.15

5.2.3 Dipole Test 3

5.2.3.1 Predicted Drawdown

Table 5-9 Predicted drawdown during Dipole Test 3

Borehole	$s_{(5\%)}{}^{c}$	$s_{(50\%)}{}^{c}$	$s_{(95\%)}{}^{c}$
KA3005A	0.086	0.115	0.145
KXTT1	0.493	1.223	1.953
KXTT2	0.151	0.201	0.251
KXTT3	0.146	0.193	0.241
KXTT4	0.107	0.130	0.153

5.2.3.2 Predicted Breakthrough Curve

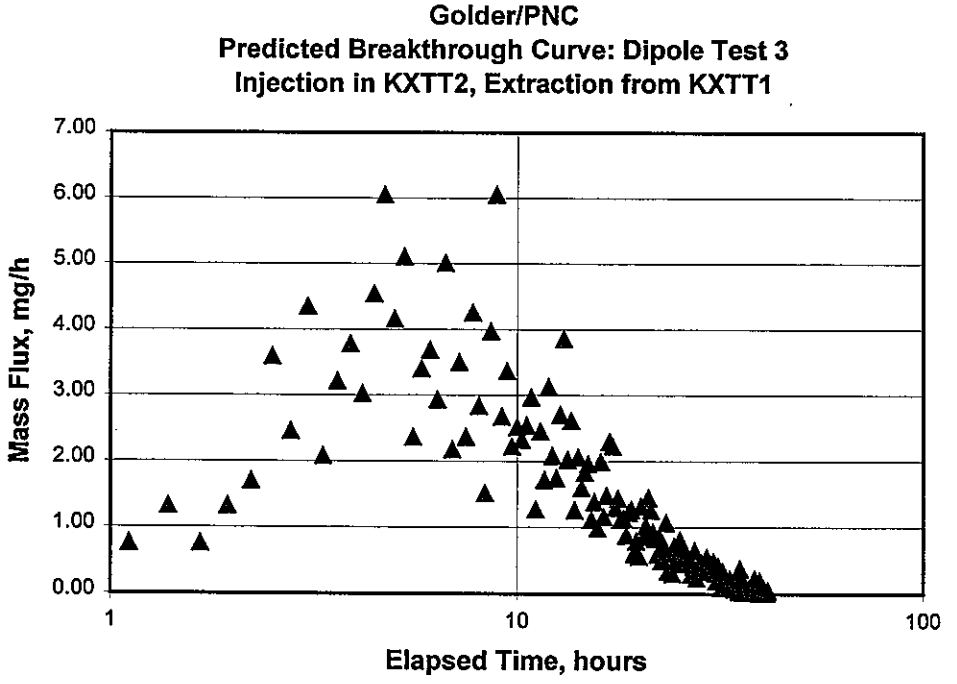

Figure 5-5 Predicted Mass Recovery for Dipole Test 3 (Realization 54)

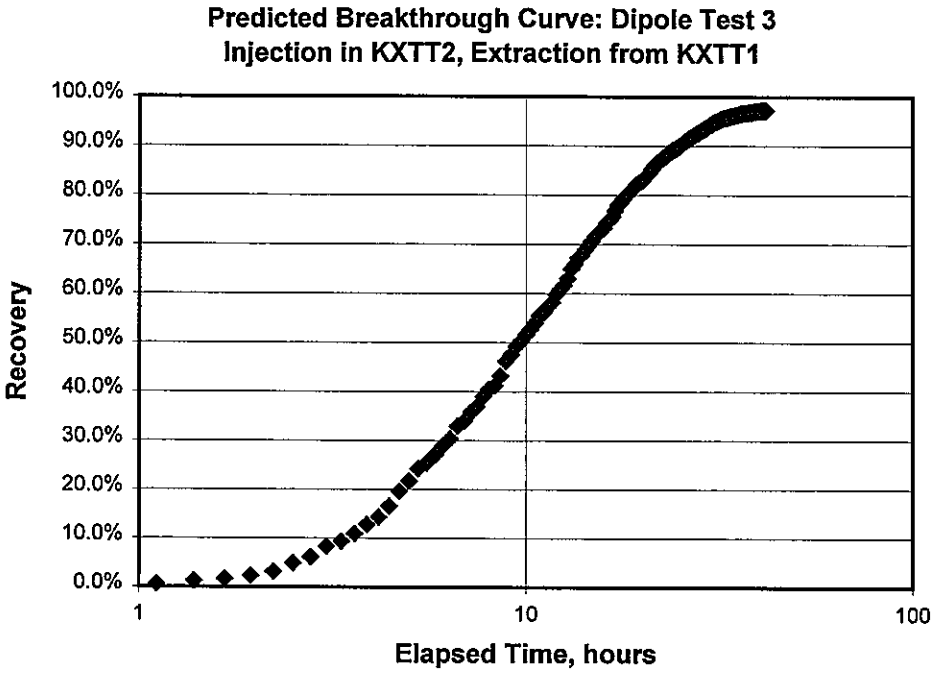

Figure 5-6 **Predicted Cumulative Mass Flux for Dipole Test 3(Realization 54)**

Table 5-10 **Predicted Breakthrough Times for Dipole Test 3**

Pump hole	Injection hole	$t_{5(5\%)}$	$t_{5(50\%)}$	$t_{5(95\%)}$	$t_{50(5\%)}$	$t_{50(50\%)}$	$t_{50(95\%)}$	$t_{95(5\%)}$	$t_{95(50\%)}$	$t_{95(95\%)}$
KXTT1	KXTT2	1.51	3.20	4.90	7.08	11.60	16.12	20.52	37.21	53.91

5.2.3.3 Predicted Mass Recovery

Table 5-11 **Predicted Mass Recovery for Dipole Test 3**

Borehole	$F_{(5\%)}{}^{c}$	$F_{(50\%)}{}^{c}$	$F_{(95\%)}{}^{c}$
KXTT1	7.02	50.91	94.80

5.2.4 Dipole Test 4

5.2.4.1 Predicted Drawdown

Table 5-12 Predicted drawdown during Dipole Test 4

Borehole	$s_{(5\%)}{}^{c}$	$s_{(50\%)}{}^{c}$	$s_{(95\%)}{}^{c}$
KA3005A	0.088	0.116	0.144
KXTT1	0.123	0.146	0.169
KXTT2	0.112	0.146	0.180
KXTT3	0.127	0.160	0.193
KXTT4	0.631	1.383	2.135

5.2.4.2 Predicted Breakthrough Curve

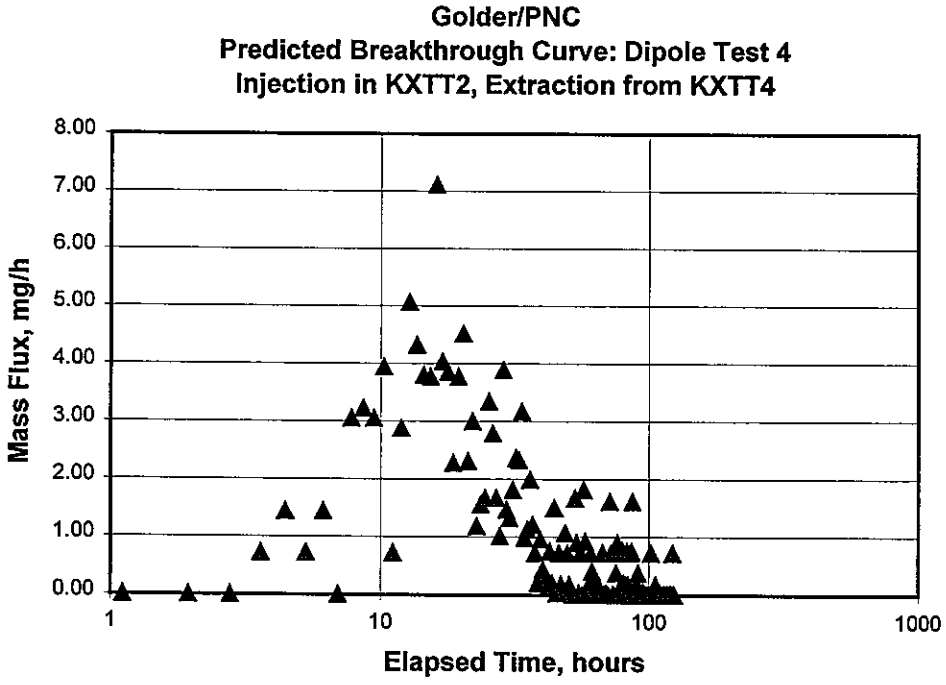

Figure 5-7 Predicted Mass Recovery for Dipole Test 4 (Realization 14)

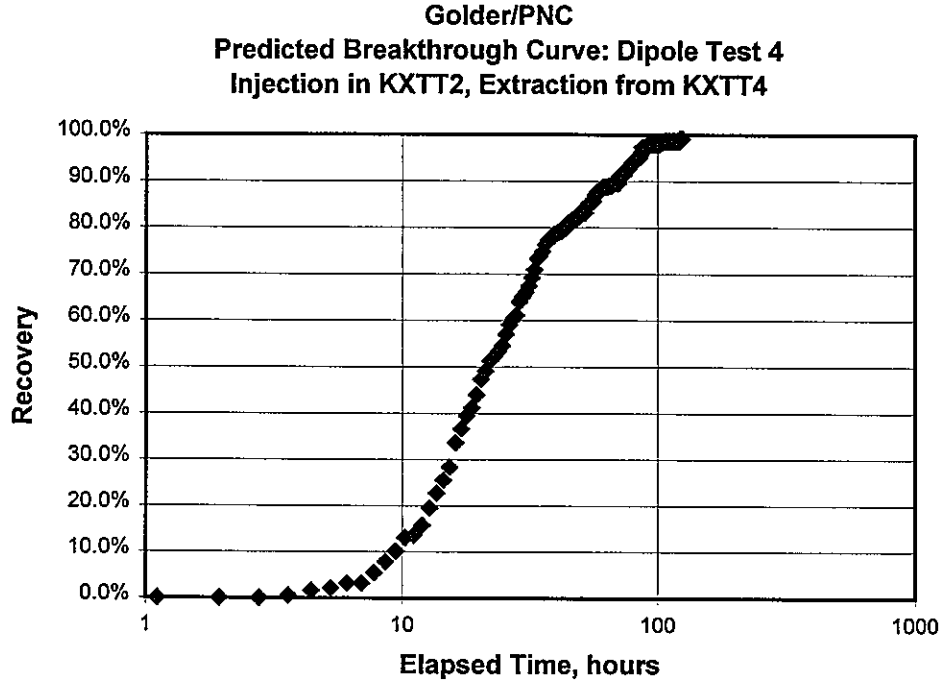

Figure 5-8 **Predicted Cumulative Mass Flux for Dipole Test 4(Realization 14)**

Table 5-13 **Predicted Breakthrough Times for Dipole Test 4**

Pump hole	Injection hole	$t_{5(5\%)}$	$t_{5(50\%)}$	$t_{5(95\%)}$	$t_{50(5\%)}$	$t_{50(50\%)}$	$t_{50(95\%)}$	$t_{95(5\%)}$	$t_{95(50\%)}$	$t_{95(95\%)}$
KXTT4	KXTT2	3.10	7.18	11.25	6.52	24.09	41.66	31.75	87.12	142.49

5.2.4.3 Predicted Mass Recovery

Table 5-14 **Predicted Mass Recovery for Dipole Test 4**

Borehole	$F_{(5\%)}{}^{c}$	$F_{(50\%)}{}^{c}$	$F_{(95\%)}{}^{c}$
KXTT4	2.11	53.54	100.0

5.3 Additional Prediction Results

This section contains some more detailed results of dipole test predictions which were not required by SKB. However, they still provide valuable information for the interpretation of the dipole test simulation.

5.3.1 Dipole Test 1

5.3.1.1 Predicted Drawdown

Table 5-15 Predicted drawdown during Dipole Test 1

Borehole	drawdown (mean), m	minimum m	maximum m	st. dev. m
KA3005A	0.44	0.364	0.559	0.070
KXTT1	0.309	0.220	0.379	0.058
KXTT2	1.02	0.821	1.320	0.207
KXTT3	1.129	0.943	1.409	0.194
KXTT4	0.48	0.406	0.555	0.054

5.3.1.2 Predicted Breakthrough Curves

Table 5-16 Predicted Breakthrough Times for Dipole Test 1

	mean, m	minimum m	maximum m	st. dev. m
T5, h	6.44	4.91	8.63	1.28
T50, h	15.69	13.03	21.99	3.44
T95, h	53.95	30.09	90.46	23.18

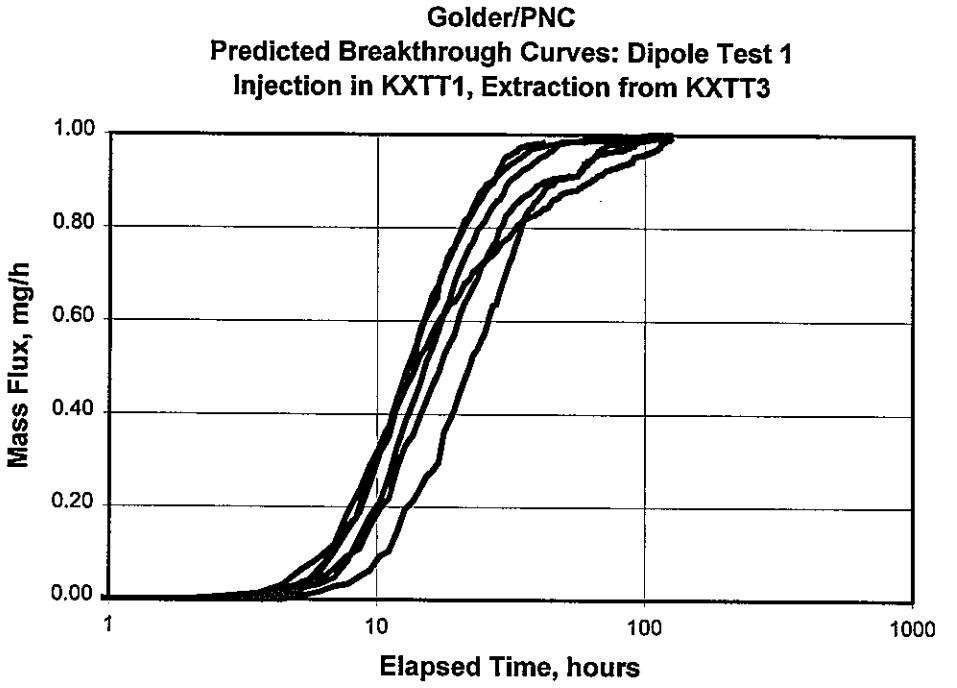

Figure 5-9 **Predicted Cumulative Mass Flux for Dipole Test 1 (6 Realizations)**

5.3.1.3 Predicted Mass Recovery

Table 5-17 **Predicted Mass Recovery for Dipole Test 1**

	mean, m	minimum, m	maximum, m	st. dev. m
Recovery	63.31%	29.24%	98.89%	24.65%

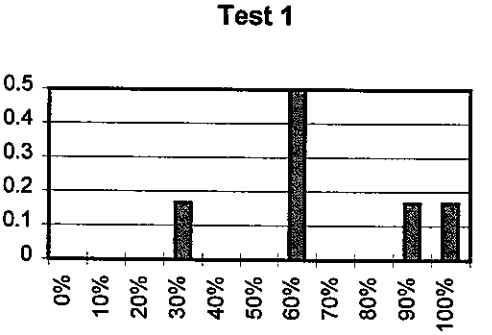

Figure 5-10 **Predicted Mass Recovery Histogram for Dipole Test 1**

5.3.2 Dipole Test 2

5.3.2.1 Predicted Drawdown

Table 5-18 Predicted drawdown during Dipole Test 2

Borehole	drawdown (mean), m	minimum m	maximum m	st. dev. m
KA3005A	0.08	0.068	0.112	0.016
KXTT1	1.179	0.662	1.719	0.437
KXTT2	0.12	0.096	0.150	0.018
KXTT3	0.125	0.096	0.150	0.018
KXTT4	0.10	0.081	0.110	0.011

5.3.2.2 Predicted Breakthrough Curves

Table 5-19 Predicted Breakthrough Times for Dipole Test 2

	mean, m	minimum m	maximum m	st. dev. m
T5, h	3.14	1.97	5.24	1.42
T50, h	9.96	5.99	18.59	5.11
T95, h	50.55	16.95	98.96	31.30

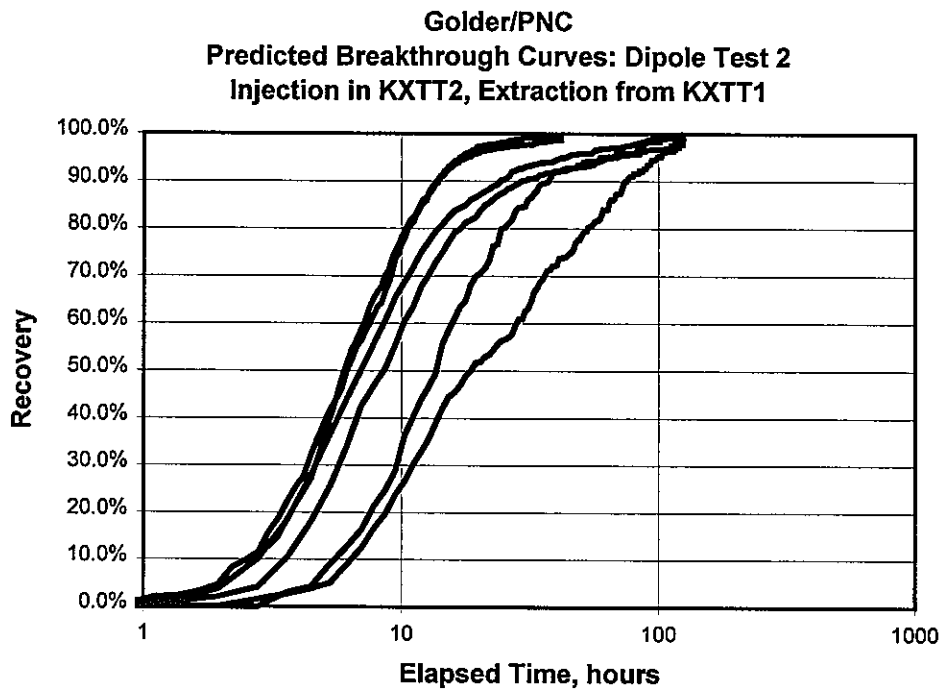

Figure 5-11 Predicted Cumulative Mass Flux for Dipole Test 2 (6 Realizations)

5.3.2.3 Predicted Mass Recovery

Table 5-20 Predicted Mass Recovery for Dipole Test 2

	mean, m	minimum, m	maximum, m	st. dev. m
Recovery	49.51%	19.60%	70.73%	22.28%

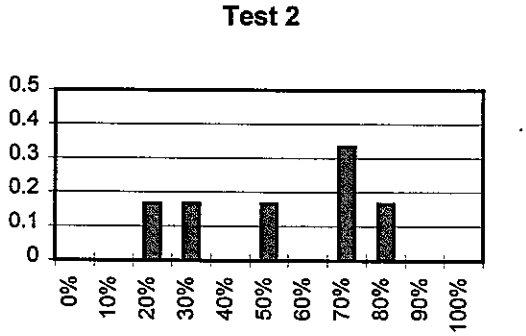

Figure 5-12 Predicted Mass Recovery Histogram for Dipole Test 2

5.3.3 Dipole Test 3

5.3.3.1 Predicted Drawdown

Table 5-21 Predicted drawdown during Dipole Test 3

Borehole	drawdown (mean), m	minimum m	maximum m	st. dev. m
KA3005A	0.12	0.096	0.143	0.018
KXTT1	1.223	0.700	1.774	0.444
KXTT2	0.20	0.164	0.250	0.030
KXTT3	0.193	0.156	0.239	0.029
KXTT4	0.13	0.111	0.146	0.014

5.3.3.2 Predicted Breakthrough Curves

Table 5-22 Predicted Breakthrough Times for Dipole Test 3

	mean, m	minimum m	maximum m	st. dev. m
T5, h	3.20	2.30	4.82	1.03
T50, h	11.60	8.97	15.09	2.75
T95, h	37.21	26.67	49.20	10.15

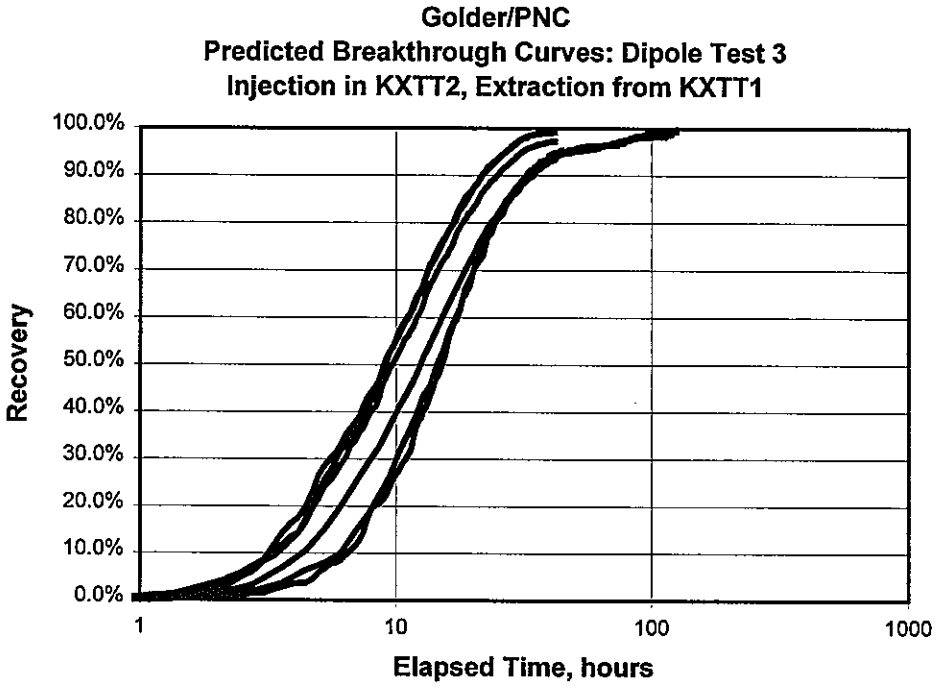

Figure 5-13 Predicted Cumulative Mass Flux for Dipole Test 3 (6 Realizations)

5.3.3.3 Predicted Mass Recovery

Table 5-23 Predicted Mass Recovery for Dipole Test 3

	mean, m	minimum, m	maximum, m	st. dev. m
Recovery	50.91%	17.14%	78.60%	26.68%

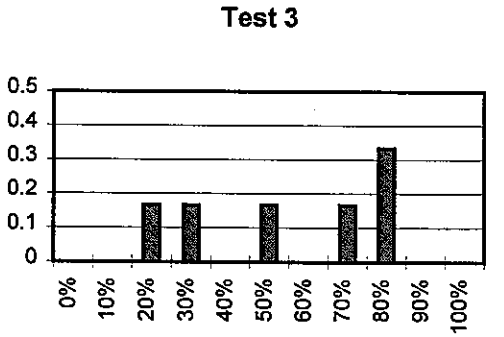

Figure 5-14 Predicted Mass Recovery Histogram for Dipole Test 3

5.3.4 Dipole Test 4

5.3.4.1 Predicted Drawdown

Table 5-24 Predicted drawdown during Dipole Test 4

Borehole	drawdown (mean), m	minimum m	maximum m	st. dev. m
KA3005A	0.12	0.095	0.135	0.017
KXTT1	0.146	0.126	0.160	0.014
KXTT2	0.15	0.119	0.170	0.020
KXTT3	0.160	0.133	0.184	0.020
KXTT4	1.38	1.096	2.297	0.457

5.3.4.2 Predicted Breakthrough Curves

Table 5-25 Predicted Breakthrough Times for Dipole Test 4

	mean, m	minimum m	maximum m	st. dev. m
T5, h	7.18	2.48	4.47	11.05
T50, h	24.09	10.68	10.66	37.62
T95, h	87.12	33.66	22.65	116.15

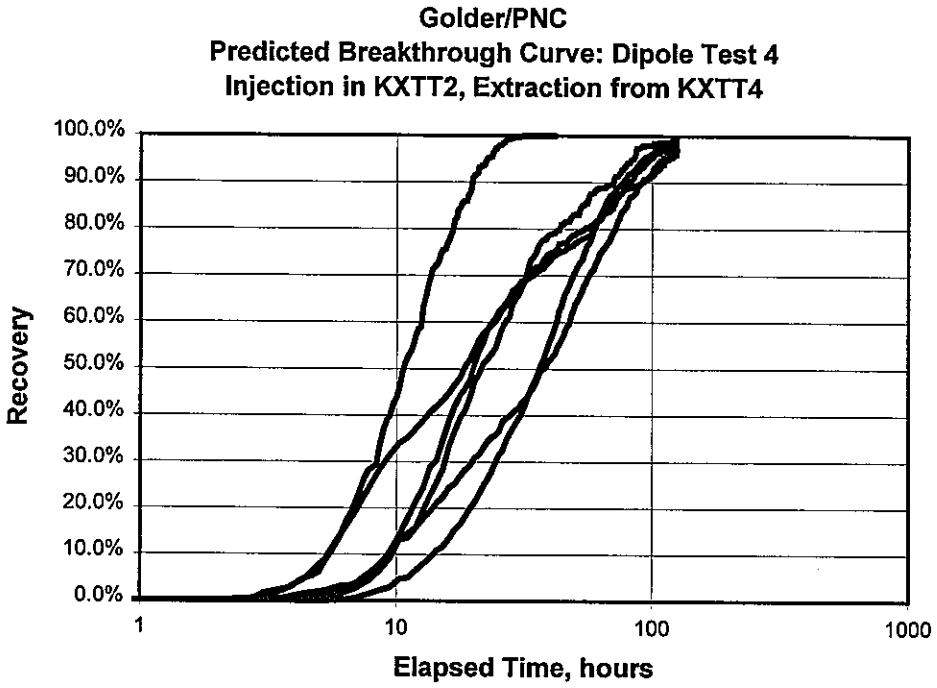

Figure 5-15 Predicted Cumulative Mass Flux for Dipole Test 4 (6 Realizations)

5.3.4.3 Predicted Mass Recovery

Table 5-26 Predicted Mass Recovery for Dipole Test 4

	mean, m	minimum, m	maximum, m	st. dev. m
Recovery	53.54%	23.32%	96.31%	31.27%

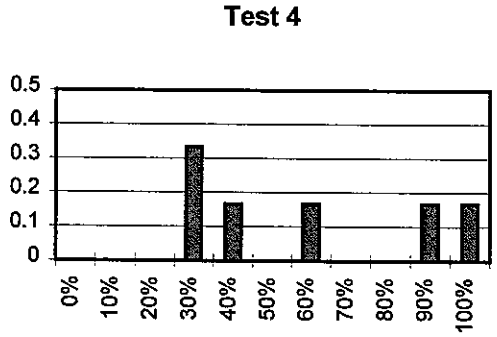

Figure 5-16 Predicted Mass Recovery Histogram for Dipole Test 4

6. Transport Modeling Using Analytical Solution

6.1 Background

Moench (1995) developed an exact LaPlace transform solution for confined aquifer transport in a radially converging flow field, based on an earlier work of Moench (1989). This solution was used for predictions of the radially converging tracer test TRUE-RC1 (Dershowitz et al, 1996).

For the dipole experiment, the Moench (1995) solution was used to derive calibrated parameters from the results of the TRUE-RC1 experiment, by directly applying the FORTRAN program provided by Dr. Moench. These parameters were then used to predict the TRUE Dipole experiments DP1 through DP4, using an analytical solution by Guvanasen and Guvanasen, 1987. The Guvanasen and Guvanasen solution converts the radially converging solution to a dipole solution by adding terms for the effect of injection volumes and tracer volumes on the flow field, and adding a background flow field term.

Both solutions solve the basic transport equation (Bear, 1979) using LaPlace methods,

$$\frac{1}{r}\frac{\partial}{\partial r}\left[rD_L\frac{\partial C}{\partial r}\right]-v\frac{\partial C}{\partial r}-q'=R\frac{\partial C}{\partial t} \qquad 3\text{-}1$$

where r is the radial coordinate with its origin at the center of the pumped well, t is the time from the start of the tracer test, and C is the tracer concentration in the fracture system. The coefficient of longitudinal hydrodynamic dispersion takes on the form $D_L=\alpha_L|v|$.

In LaPlace Space, the equation for dimensionless concentration C'_D is (Moench, 1995),

$$C_D(S)=\psi\exp\left[\frac{Pe}{2}(1-r_{wD})\right]G(S) \qquad 3\text{-}2$$

where

$$\bar{G}(s)=\psi\exp\left[\frac{Pe}{2}(1-r_{wD})\right]\bar{G}(s)$$

$$F=\omega^{1/3}(A_1B_3-A_3B_1)+0.5(A_3B_2-A_2B_3)$$

$$+0.5((A_1-B_1)+0.25\omega^{-1/3}(B_3-A_2)$$

$$A_1 = Ai'\left(\omega^{1/3} y_0\right) / Ai\left(\omega^{1/3} y_L\right)$$

$$A_2 = Ai\left(\omega^{1/3} y_0\right) / Ai\left(\omega^{1/3} y_L\right)$$

$$A_3 = Ai'\left(\omega^{1/3} y_L\right) / Ai\left(\omega^{1/3} y_L\right)$$

$$B_1 = Bi'\left(\omega^{1/3} y_0\right) / Bi\left(\omega^{1/3} y_L\right)$$

$$B_2 = Bi\left(\omega^{1/3} y_0\right) / Bi\left(\omega^{1/3} y_L\right)$$

$$B_3 = Bi'\left(\omega^{1/3} y_L\right) / Bi\left(\omega^{1/3} y_L\right)$$

$$y_0 = Pe\, r_{wD} + 0.25\omega^{-1}$$

$$y_L = Pe + 0.25\omega^{-1}$$

$$\omega = \frac{2R\left(s + \bar{q}_D\right)}{Pe^2\left(1 - r_{wD}^2\right)}$$

$$\bar{q}_D = \frac{3\gamma'\left[m \coth(m) - 1\right]}{1 + S_k\left[m \coth(m) - 1\right]}$$

Ai and *Bi* are Airy functions. The value of ψ takes on different forms depending on the type of tracer input. For a Dirac input, ψ=1, and for a step input, ψ=1/s. For a rectangular input, ψ=[1-exp(-t_{Dp}s)]/s where t_{Dp} is the duration of the constant input divided by the time of travel by pure advection.

6.1.1 Implementation

The Moench solution provides type curves of dimensionless time vs. dimensionless concentration given dimensionless input parameters. For the current analysis, parameters are specified as physical parameters such as well radius, well separation, pumping rate, etc. The conversion equations are taken from Moench(1991) and Moench(1995).

The Moench solution requires the following parameters:

Geologic Parameters:

- h: Height of aquifer
- ϕ_f: Fracture porosity
- R: Retardation coefficient
- α_L: Longitudinal dispersion

- bd: block diffusion (0=no, 1=yes)
- γ: block diffusion parameter (not used here)
- σ: block storage parameter (not used here)
- sk: block skin parameter (not used here)

Well Test Parameters:

- r_L: well separation
- r_w: radius of sampling well
- r_i: radius of injection well
- h_w: height of sampling well
- h_i: height of injection well
- q_o: pumping rate
- it: injection type (0=constant, 1=dirac, 2=top hat)
- t_i: injection duration
- C_o: concentration of injection

Time Frame Parameters:

- t_o: begin time
- n_{LC}: number of log cycles
- n_P: number of points per cycle
- n_{TS}: number of time steps

The parameters derived by calibration to the breakthrough curves for the TRUE-RC1 experiment are provided in Table 6-1. The calibrated breakthrough curves are provided in Figures 6-1 and 6-2. Table 6-2 provides a tabular comparison between the calibrated and measured breakthrough curves.

Table 6-1 Parameters Calibration for Matches to TRUE-RC1 breakthrough curves

	KXTT1	KXTT4	Injection in
Geologic Parameters:			
h	0.2	0.2	Height of aquifer (m)
ϕ_f	0.03	0.02	Fracture porosity
R	1	1	Retardation Coefficient
α_L	0.3	0.6	Longitudinal Dispersivity
-	0	0	Block diffusion (0=no, 1=yes)
γ	0.1	0.1	Block diffusion parameter
σ	25	25	Block storage parameter
sk	0.006	0.006	Block skin parameter
Well Test Parameters:			
r_L	5.03	4.68	Well Separation (m)
r_w	0.056	0.056	Radius of sampling well (m)
r_i	0.056	0.056	Radius of injection well (m)
h_w	2	2	Length of sampling well section (m)
h_i	1	2	Length of injection well section (m)
q_o	0.0002845	2.80E-04	Well Pumping Rate (m^3/min)
-	1	1	Injection type (0=constant, 1=dirac, 2-tophat)
t_i	1	1	Injection duration (tophat only) (sec)
C_o	46062	487800	Concentration of injection (ppb)
Time Frame Parameters:			
t_o	300	150	Begin time (sec)
-	3	3	No. Log Cycles
-	30	30	No. Points per log cycle
-	25	25	No. Time steps

Table 6-2: Comparison of Measured and Calibrated Moench Solutions for TRUE-RC-1

a) Injection from KXTT1

	meas. h	calc. h	diff. h
T5	26	27.50	+1.50
T50	154	85.55	-68.45
T95	488	292.17	-195.83

b) Injection from KXTT4

	meas. h	calc. h	diff. h
T5	21	21.33	+0.33
T50	156	125.33	-30.67
T95	560	498.33	-61.67

Figure 6-1 Moench Calibration to TRUE-RC1 results, Injection in KXTT1

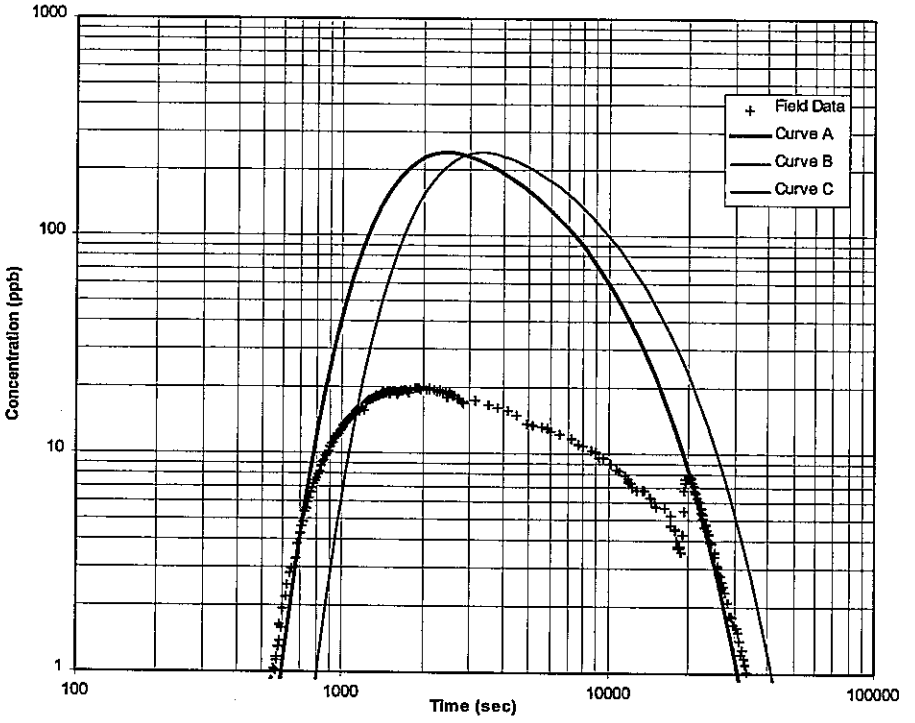

Figure 6-1 Moench Calibration to TRUE-RC1 results, Injection in KXTT4

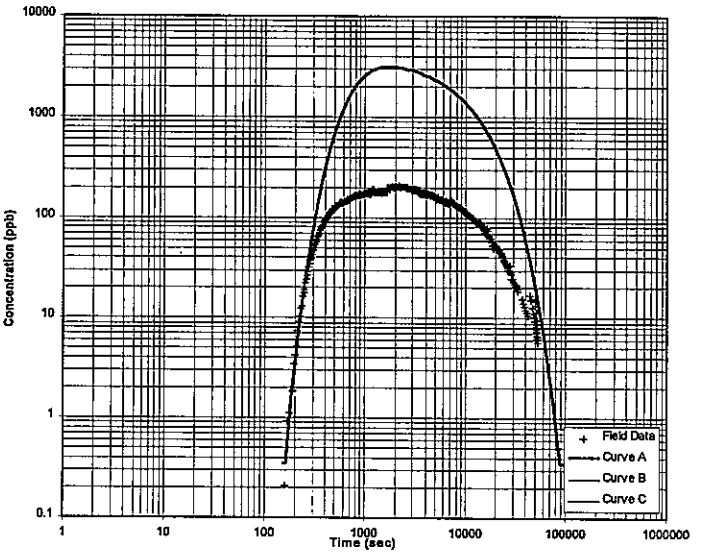

6.2 Results

The calibrated parameters from the Moench(1995) solution were used to produce predictions for breakthrough using the Guvanasen and Guvanasen (1987) dipole solution. The parameters calibrated from the RC-1 KXTT1 injection were used for Dipole tests with injection in KXTT1 or KXTT2, and the parameters calibrated from the RC-1 KXTT3 injection were used for the dipole with injection in KXTT4.

No predictions were made for drawdown, since this is not provided by the Guvanasen and Guvanasen (1987), and there was not sufficient time to derive the drawdown by alternative analytical solutions, as was done by Dershowitz et al.(1996) for the TRUE-RC1 prediction.

6.2.1 Dipole Test 1

6.2.1.1 Predicted Drawdown

Table 6-27 Predicted Drawdown during Dipole Test 1

Not predicted

6.2.1.2 Predicted Breakthrough Curve

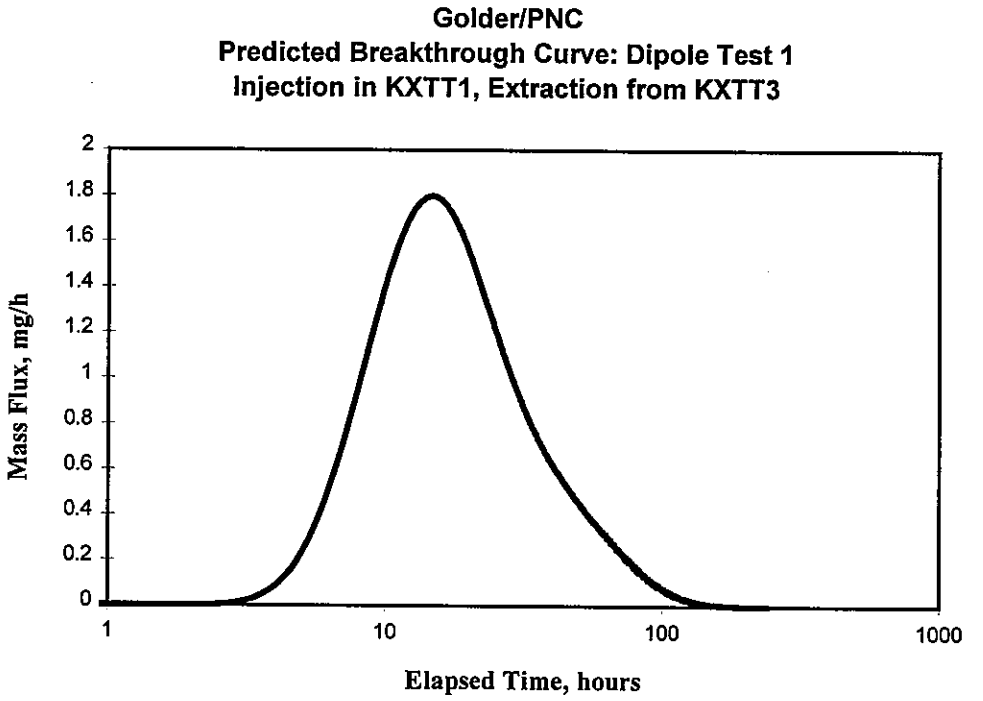

Figure 6-1 Predicted Mass Recovery for Dipole Test 1

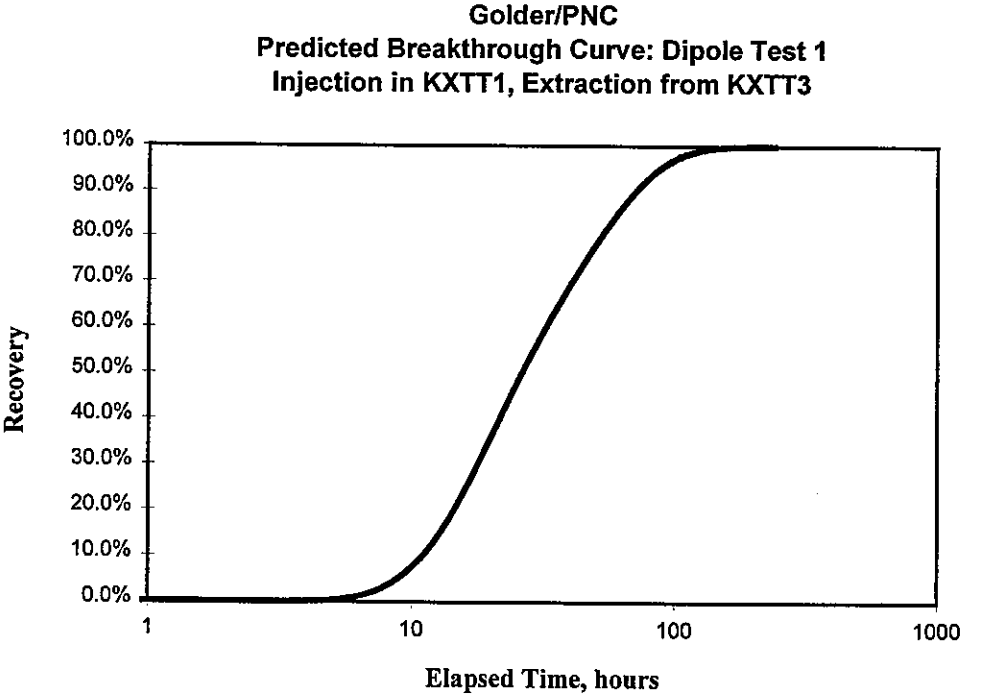

Figure 6-2 Predicted Cumulative Mass Flux for Dipole Test 1

Table 6-28 Predicted Breakthrough Times for Dipole Test 1

Pump hole	Injection hole	T5, h	T50, h	T95, h
KXTT3	KXTT1	8.9	26.4	87.84

6.2.1.3 Predicted Mass Recovery

Table 6-29 Predicted Mass Recovery for Dipole Test 1

Borehole	calculated mean, %
KXTT3	76.91%

6.2.2 Dipole Test 2

6.2.2.1 Predicted Drawdown

Table 6-30 Predicted Drawdown during Dipole Test 2

Not predicted.

6.2.2.2 Predicted Breakthrough Curves

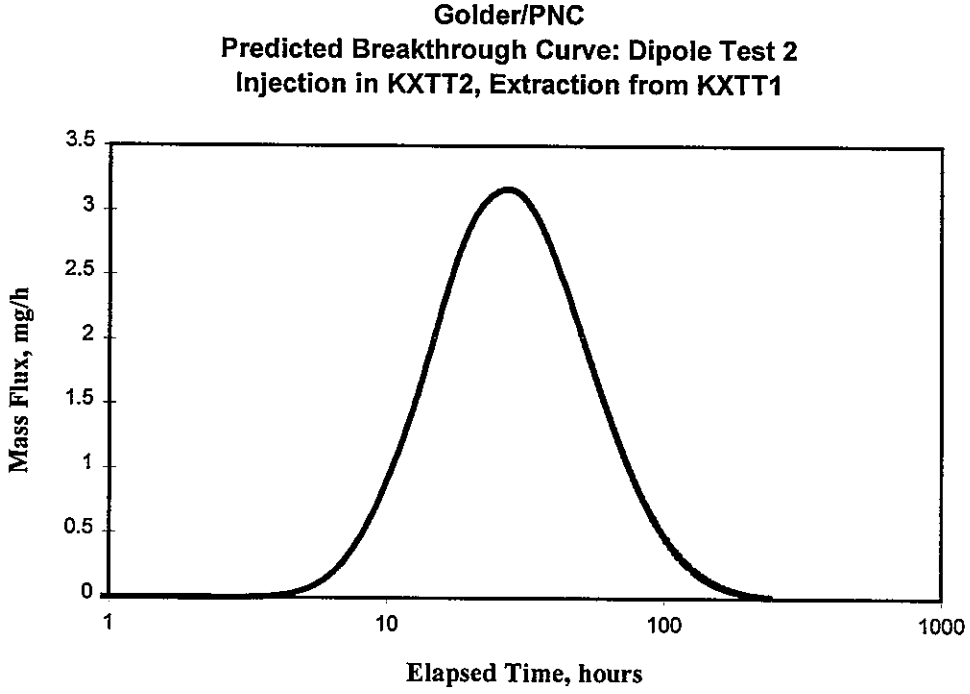

Figure 6-1 Predicted Mass Recovery for Dipole Test 2

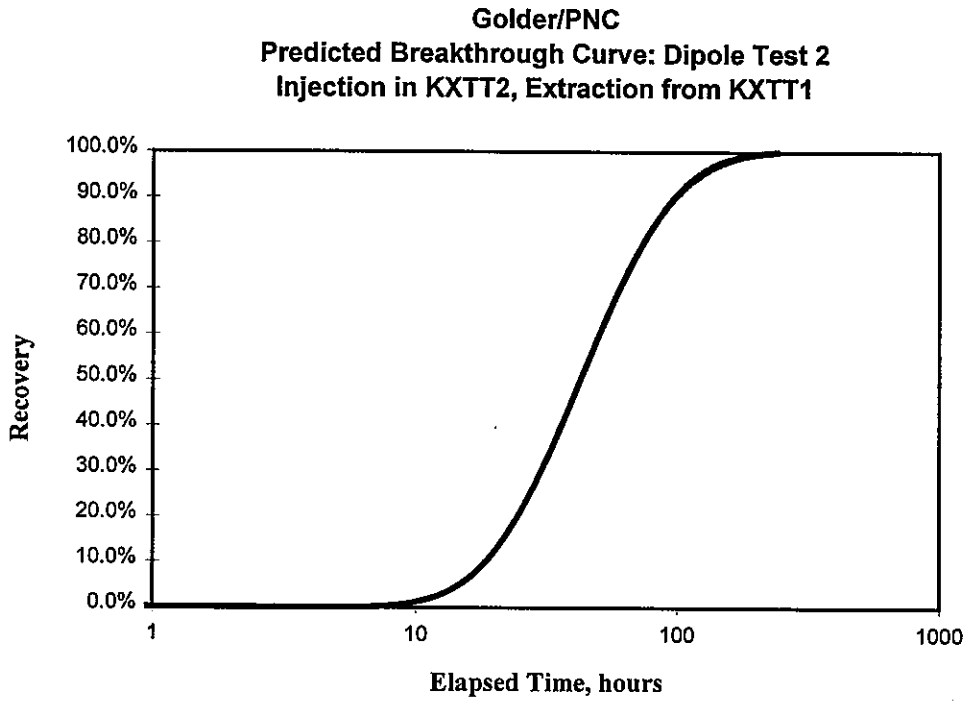

Figure 6-2 **Predicted Cumulative Mass Flux for Dipole Test 2**

Table 6-31 **Predicted Breakthrough Times for Dipole Test 2**

Pump hole	Injection hole	T5, h	T50, h	T95, h
KXTT1	KXTT2	14.7	42.4	122.3

6.2.2.3 Predicted Mass Recovery

Table 6-32 **Predicted Mass Recovery for Dipole Test 2**

Borehole	calculated mean, %
KXTT3	

6.2.3 Dipole Test 3

6.2.3.1 Predicted Drawdown

Table 6-33 Predicted drawdown during Dipole Test 3

Not predicted.

6.2.3.2 Predicted Breakthrough Curves

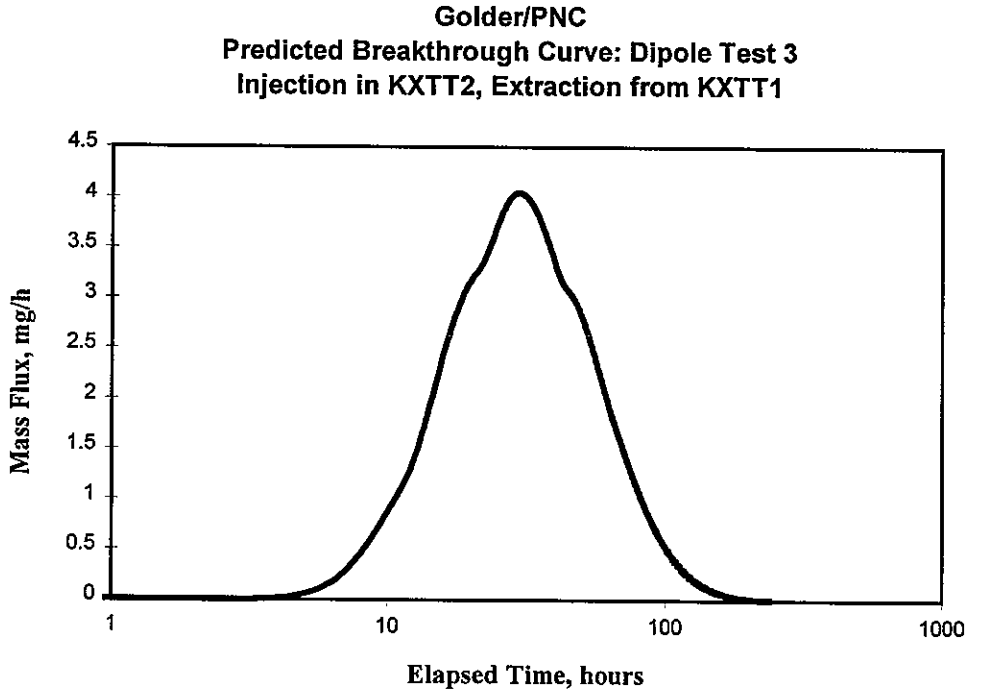

Figure 6-1 Predicted Mass Recovery for Dipole Test 3

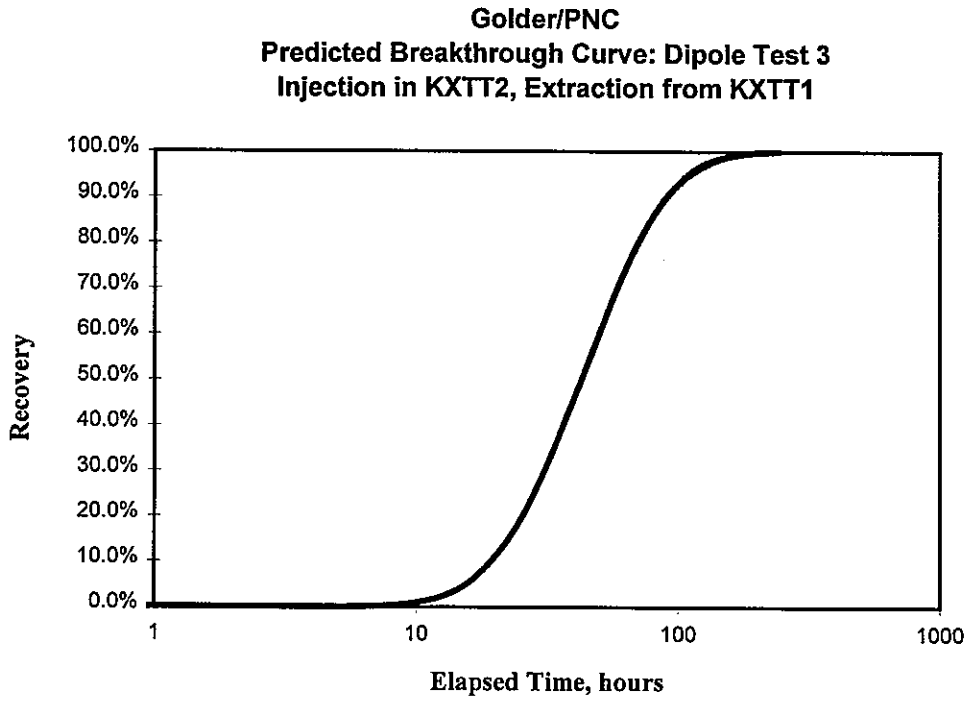

Figure 6-2 **Predicted Cumulative Mass Flux for Dipole Test 3**

Table 6-34 **Predicted Breakthrough Times for Dipole Test 3**

Pump hole	Injection hole	T5, h	T50, h	T95, h
KXTT1	KXTT2	15.6	43.0	109.5

6.2.3.3 Predicted Mass Recovery

Table 6-35 **Predicted Mass Recovery for Dipole Test 3**

Borehole	calculated mean, %
KXTT3	

6.2.4 Dipole Test 4

6.2.4.1 Predicted Drawdown

Table 6-36 Predicted drawdown during Dipole Test 4

Not predicted

6.2.4.2 Predicted Breakthrough Curves

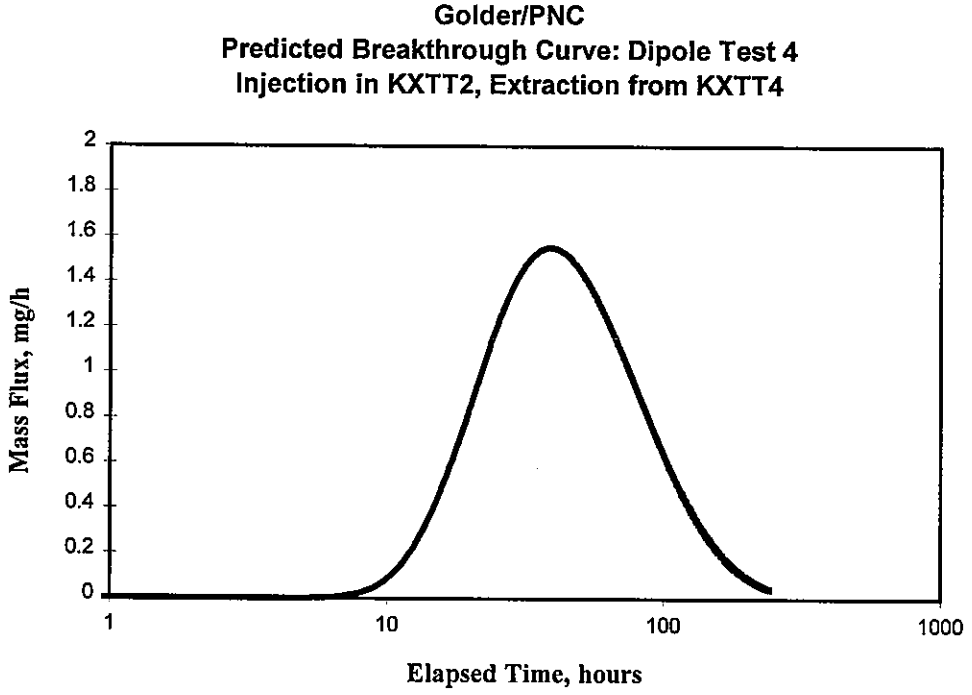

Figure 6-1 Predicted Mass Recovery for Dipole Test 4

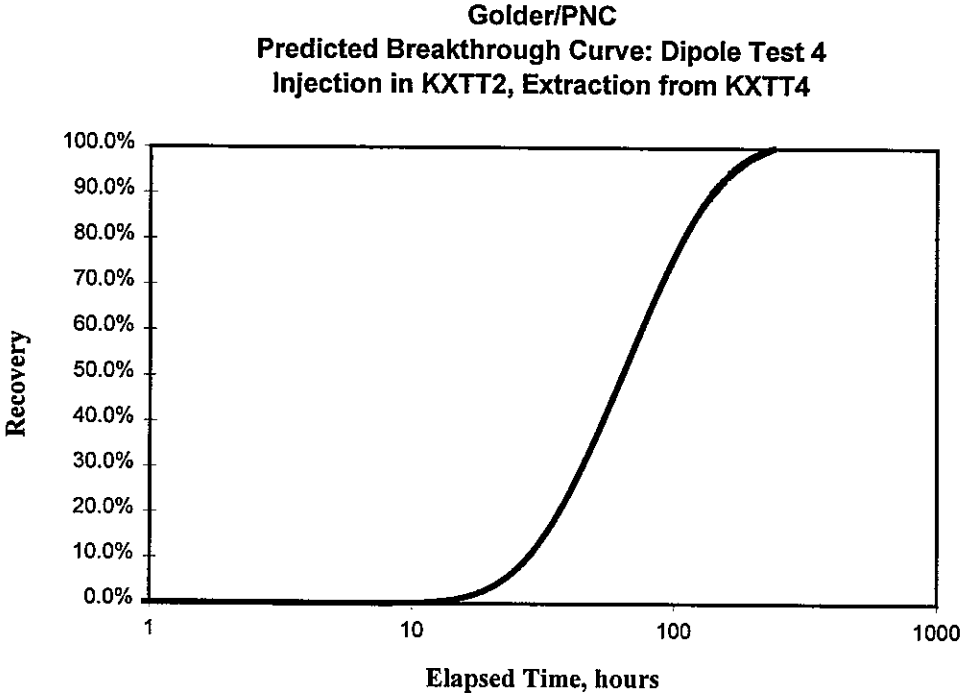

Figure 6-2 **Predicted Cumulative Mass Flux for Dipole Test 4**

Table 6-37 **Predicted Breakthrough Times for Dipole Test 4**

Pump hole	Injection hole	T5, h	T50, h	T95, h
KXTT4	KXTT2	22	63.28	169.36

6.2.4.3 Predicted Mass Recovery

Table 6-38 **Predicted Mass Recovery for Dipole Test 4**

Borehole	calculated mean, %
KXTT3	80.62%

7. Conclusions

- Much but not all of TRUE-RC behavior can be explained by intersecting fractures. Alternatively, a strange isolated channel between KXTT2 and KXTT3 would be required if this were to be explained by heterogeneity within Feature A.
- Anomalous behavior of KXTT2:R3 Injection (good hydraulic connection, no tracer recovery in TRUE RC1) is only partially explained by models incorporating "Feature A*" or heterogeneity within "Feature A".
- Use of heterogeneity within "Feature A" did not help calibration much
- Varying flow rates in TRUE-RC1 makes calibration somewhat problematic
- DFN Approach recognizing the importance of intersecting fractures significantly improved calibration for drawdown response to TRUE-RC1
- Possible lack of tracer recovery seen in True RC-1 can be explained to some extent by intersecting fractures, as well as the effect of the local head field. This head field and intersecting fractures will also effect recovery in the TRUE dipole experiments.

8. References

Anderson, P, A. Winberg, V. Cvetkovic, and J-O Selroos, 1996. *TRUE 1st Stage Tracer Test Program.* Contera AB, Gothenberg.

Anderson, P, et al., 1996. *Data Distribution for TRUE-1/Dipole Experiment*, SKB, Stockholm.

Bear, J., 1979, *Hydraulics of Groundwater,* 569 pp., McGraw-Hill, New York.

Dershowitz, W., G. Lee, J. Geier, T. Foxford, P. La Pointe and A. Thomas, 1995. *FracMan Interactive Discrete Feature Data Analysis, Geometric Modeling, and Exploration Simulation: User Documentation Version 2.5.* Golder Associates Inc., Redmond, Washington.

Dershowitz, W., R. Busse, I. Kluckow, and P. Wallmann, 1996. *Summary of Simulations for the Äspö Tracer Retention Understanding Experiment Radially Converging Tracer Experiment (TRUE-1/RC).* Draft Report to SKB, June.

Dershowitz, W., A. Thomas, and R. Busse, 1996. *Discrete Fracture Analysis in Support of the Äspö Tracer Retention Understanding Experiment (TRUE-1).* SKB International Cooperation Report ICR-96-05. SKB, Stockholm

Guvanasen, V. and V. Guvanasen, 1987. *An Approximate Semianalytical Solution for Tracer Injection Tests in a Confined Aquifer with a Radially Converging Flow Field and*

Finite Volume of Tracer and Chase Fluid. Water Resources Research, Vol 23, No 8, pp 1607-1619, August.

Moench, A., 1995. *Convergent Radial Dispersion in a Double-Porosity Aquifer with Fracture Skin: Analytical Solution and Application to a Field Experiment in Fractured Chalk.* Water Resources Research, Vol. 31, No. 8, Pages 1823-1835

Moench, A.F., 1991. *Convergent Radial Dispersion: A Note on Evaluation of the LaPlace Transform Solution,* Water Resources Research, Vol 27, No. 12, 3261-3264.

Moench, A.F., 1989. *Convergent Radial Dispersion: A LaPlace Transform Solution for Aquifer Tracer Testing,* Water Resources. Research., Vol 25, No 3, 439-447.

Winberg, A., ed., 1996. *First TRUE Stage Descriptive Structural Hydraulic Models on Block and Detailed Scales.* SKB International Cooperation Report ICR 94-09. SKB, Stockholm.

Winberg, A., et al., 1995. *Data Distribution for TRUE-1/RC Experiment,* SKB, Stockholm.

Appendix D Fractal User Manual

Fractal for Windows 1.0

User's Guide: Task Index

Major Screen Elements

Basic Layout

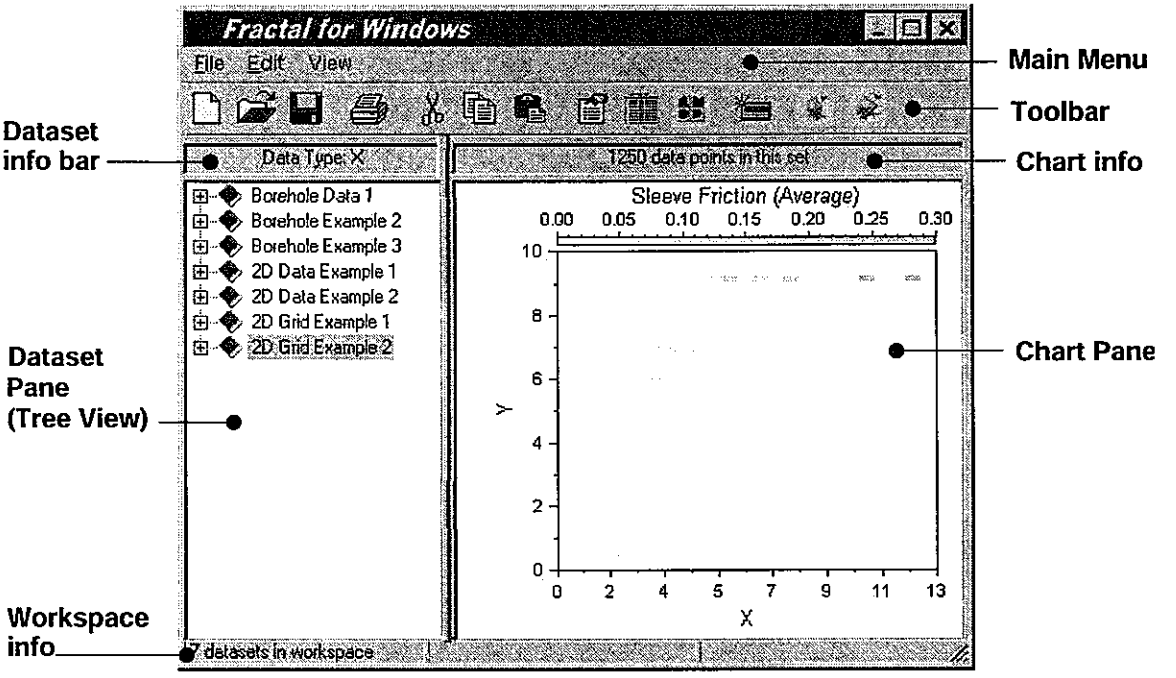

Major Screen Elements

Tree View and Chart Hierarchy

1. FRACTAL FOR WINDOWS recognizes three types of data: borehole (one dimensional) data, two-dimensional data that do not follow a regular, gridded structure, and two-dimensional gridded data. A borehole data consists of two items: the measurement and the location (depth) of the measurement. A two-dimensional data consists of three items: the measurement and the location (specified by two numbers) of the measurement. The two terms 'data' and 'measurement' will be used interchangeably.

2. For each set of data, FRACTAL FOR WINDOWS generates a set of charts that form a hierarchy represented by the tree view. Each item in the tree view corresponds to a chart in the hierarchy. Click an item in the tree view, and FRACTAL FOR WINDOWS will display the corresponding chart in the chart pane.

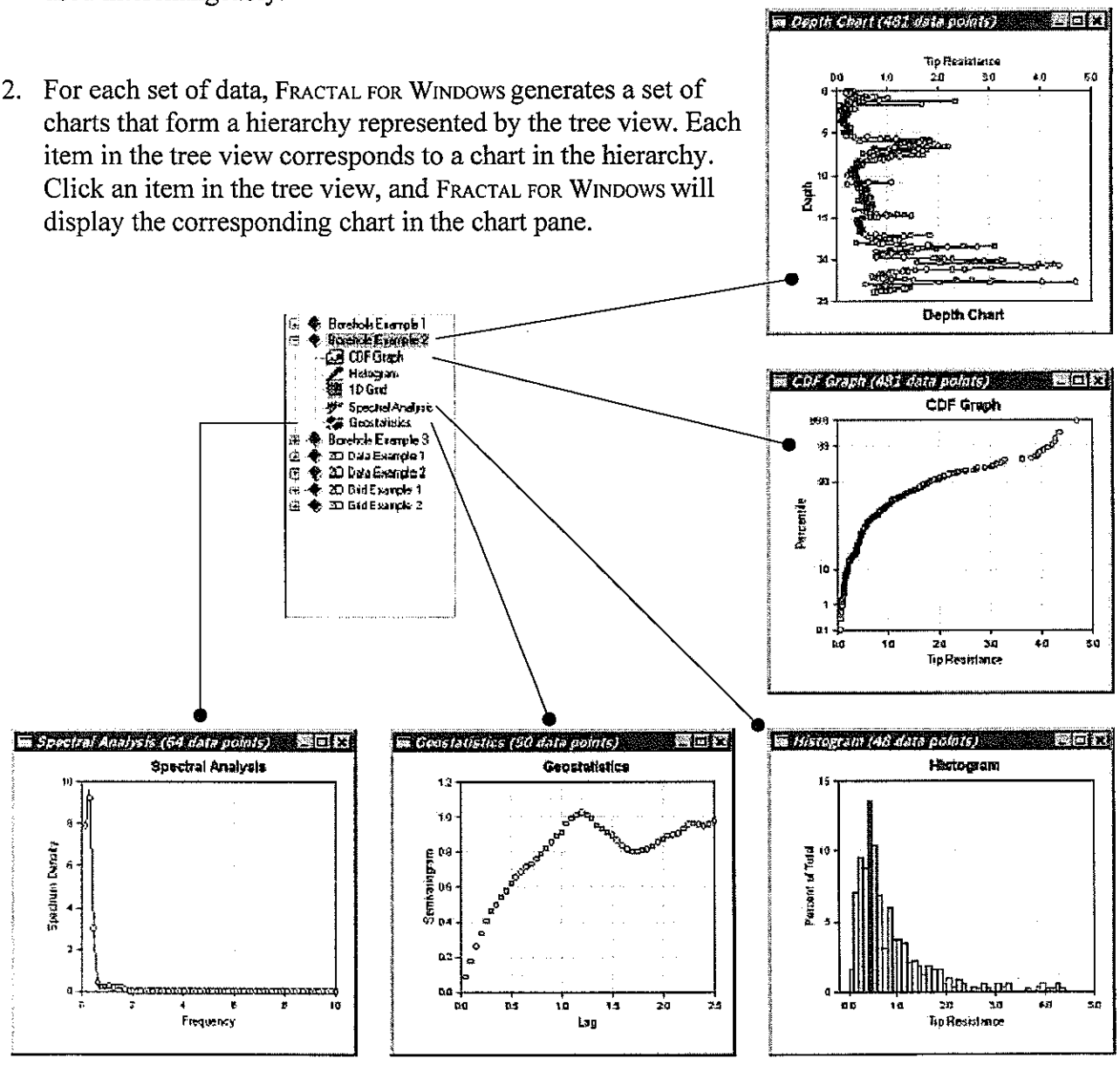

Tree View and Chart Hierarchy (Continued)

3. At the top of the hierarchy is the chart that plots the data against its location, this is always followed by the quantile plot (CDF graph) and the histogram of the data.

4. For equally-spaced borehole data, FRACTAL FOR WINDOWS will also produce a grid chart, the power spectrum of the gridded data, and the semivariogram of the gridded data. For borehole measurements that do not follow a regular interval, FRACTAL FOR WINDOWS will produce the spacing distribution of the data.

5. Similar hierarchy of charts also exists in general two-dimensional data and two-dimensional gridded data. For two-dimensional data, FRACTAL FOR WINDOWS produces a data plot, a quantile plot, and a histogram. In the data plot, the value is represented by the color.

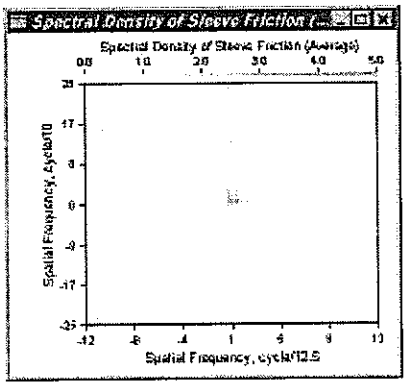

6. For two-dimensional gridded data, FRACTAL FOR WINDOWS will produce the power spectrum and the semivariogram of the data in addition to the three basic charts.

Major Screen Elements

Main Menu

File Menu:

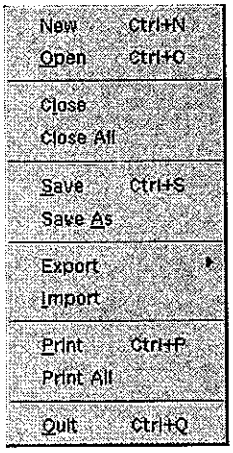

Edit Menu:

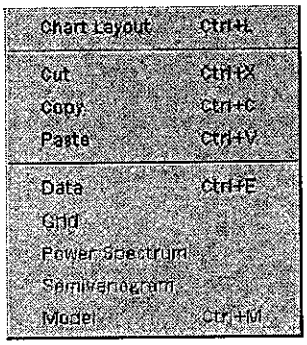

View Menu:

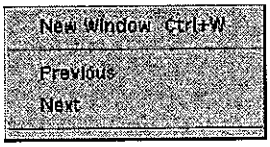

Toolbar

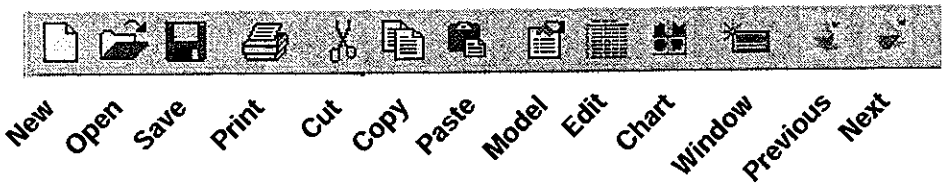

Popup Menu

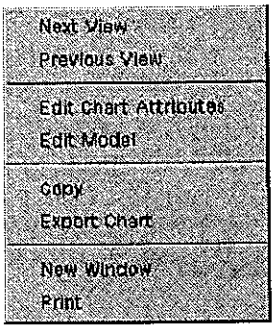

Create a New Dataset

Borehole Data

1. Open the New Data dialog box, select borehole data:
   Main Menu: File ⇒ New or File ⇒ Import
   Keyboard Shortcut: Ctrl+N
   Toolbar: 
   Popup Menu: None

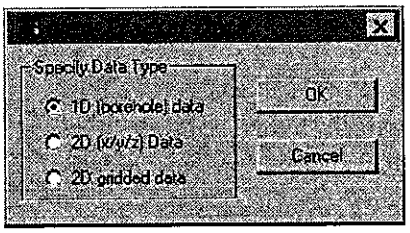

2. Provide a description for the dataset. This description will appear in the title of the tree item representing the dataset. A common choice is the identification of the borehole. Also provide a description for the data type. This will appear in the title of the x axis of the chart. A common choice is the type of measurement such as conductivity.

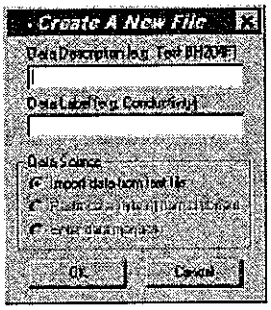

3. Select a file containing the data. This must be an ASCII text file with one line for each data item. Each data item consists of two or more numbers (for borehole data) separated by space, comma, or tabs. Press the Open button to open the file.

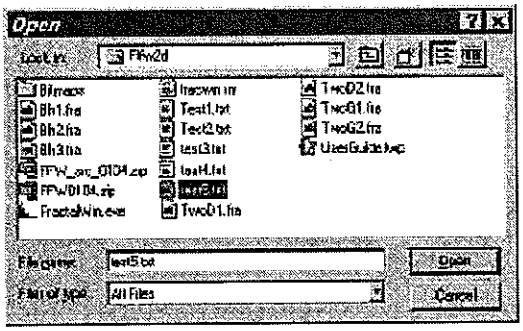

4. FRACTAL FOR WINDOWS will parse the file and skip lines starting with letters. FRACTAL FOR WINDOWS will also separate the numbers in each line into columns. By default, FRACTAL FOR WINDOWS assumes the first column corresponds to the depth of the measurement and the second column contains the data. If this is not the case, use the drop-down lists and the Set button to show FRACTAL FOR WINDOWS which columns contain depth and data. After making the assignment, press the Update Datablock View to confirm the selection. Finally, press the Extract Data button to generate the dataset.

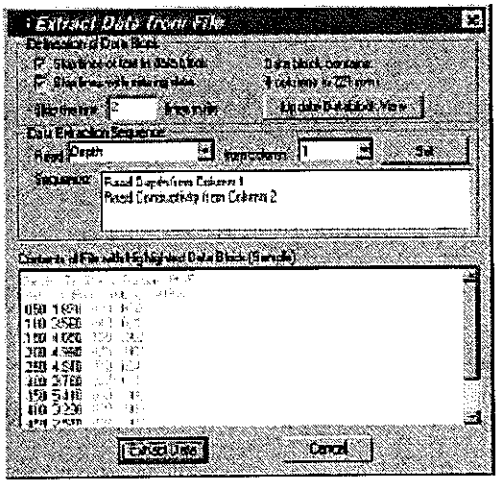

Create a New Dataset

Two-Dimensional Data

1. Open the New Data dialog box and select 2d data:
   Main Menu: File ⇒ New or File ⇒ Import
   Keyboard Shortcut: Ctrl+N
   Toolbar: 
   Popup Menu: None

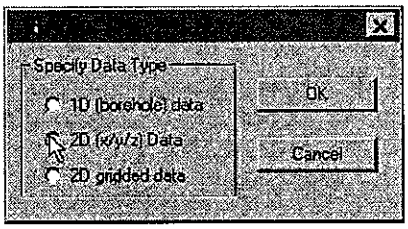

2. Provide a description for the dataset. This description will appear in the title of the tree item representing the dataset. A common choice is the location or other types of information that distinguishes this dataset from others. Also provide a description for the data type. This will appear in the title area of the chart. A common choice is the type of measurement such as the aperture.

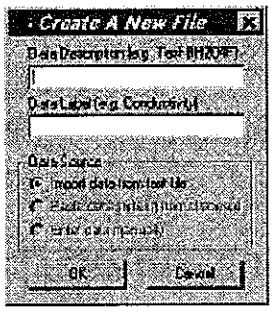

3. Select a file containing the data. This must be an ASCII text file with one line for each data item. Each data item consists of three or more numbers separated by space, comma, or tabs.

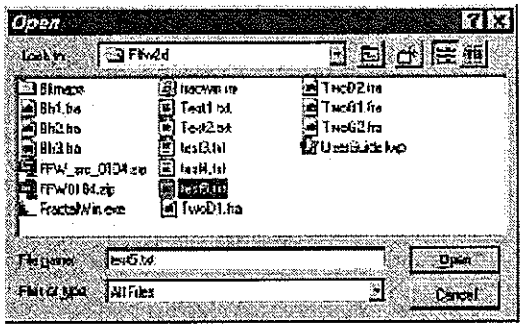

4. FRACTAL FOR WINDOWS will skip lines starting with letters. FRACTAL FOR WINDOWS will also separate the numbers in each line into columns. By default, FRACTAL FOR WINDOWS assumes the first two columns correspond to the x and y coordinates of the measurement and the third column contains the data. If this is not the case, use the drop-down lists and the Set button to show FRACTAL FOR WINDOWS which columns contain depth and data. After making the assignment, press the Update Datablock View to confirm the selection. Finally, press the Extract Data button to generate the dataset.

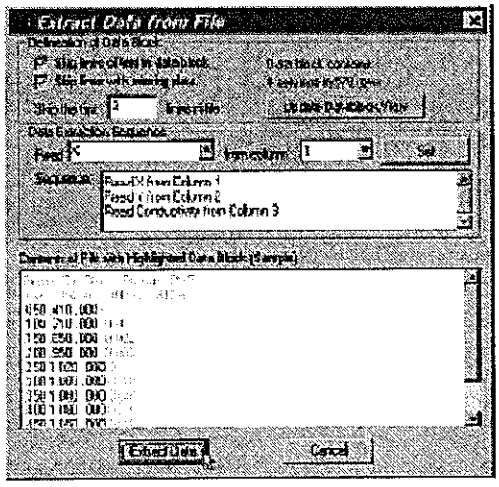

Create a New Dataset

Two-Dimensional Gridded Data

1. Open the New Data dialog box, select 2D gridded data:
   Main Menu: File ⇒ New or File ⇒ Import
   Keyboard Shortcut: Ctrl+N
   Toolbar: 
   Popup Menu: None

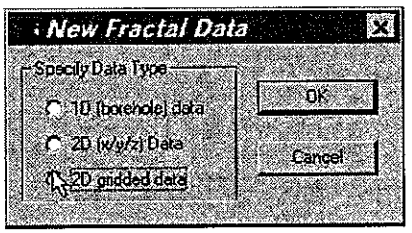

2. Provide a description for the dataset. This description will appear in the title of the tree item representing the dataset. A common choice is the location or other information that distinguishes this dataset from the others. Also provide a description for the data type. This will appear in the title area of the chart. A common choice is the type of measurement such as conductivity. Additionally, provide the number of rows and columns in the dataset. As an option, provide the grid size (width and height) and the origin (x and y coordinates of the grid in the first column and row) of the grid.

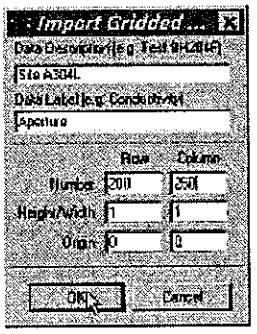

3. Select a file containing the data. This must be an ASCII text file with one line for each data item. Each data item consists of one or more numbers separated by space, comma, or tabs. The items must be organized in row-major order: if there are *m* rows and *n* columns, the first *n* lines correspond to the data in the first row, the next *n* lines correspond to the data in the second row, and so forth.

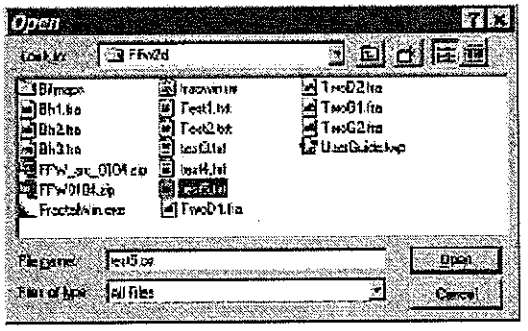

4. FRACTAL FOR WINDOWS will skip lines starting with letters. FRACTAL FOR WINDOWS will also separate the numbers in each line into columns. By default, FRACTAL FOR WINDOWS assumes the first column corresponds to the data. If this is not the case, show FRACTAL FOR WINDOWS which column contains the data. Press the Extract Data button to generate the dataset.

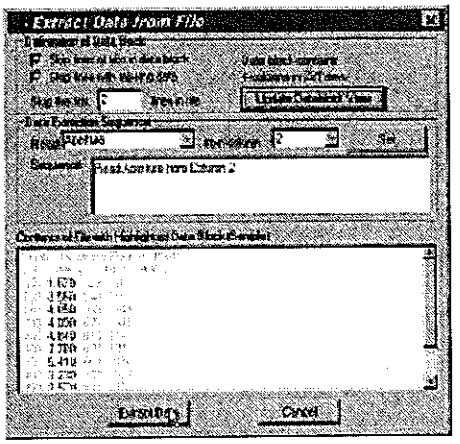

Modify and Examine Data

Examine Data

1. Open the Edit Data dialog box:
   Main Menu: Edit ⇒ Data or View ⇒ Data
   Keyboard Shortcut: Ctrl+E or double-click chart
   Toolbar: 
   Popup Menu: Edit Data

2. (Borehole or two-dimensional data) The Edit Data dialog box is organized in two halves. The left half presents the data in a spreadsheet-like list view, the right half shows the chart. The data in the spreadsheet is organized by the drawing order. The first column corresponds to the x coordinate of the chart, the second column to the y coordinate. There is a one way spreadsheet-to-chart hot link: Click a row in the spreadsheet, and the chart will highlight the corresponding data point.

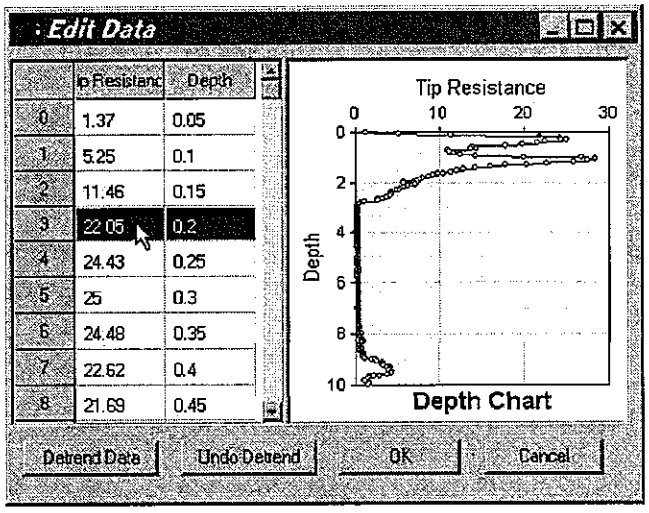

3. (Two-dimensional grid) The Edit Data dialog box also shows the chart but does not have the spreadsheet and thus only one data point can be examined at a time. There is a two-way hot link between the data and the chart: Change the row and column number, the grid value will be displayed and the corresponding grid highlighted in the chart. Also, click anywhere within the chart and the row and column number and grid value of the grid beneath the pointer will be displayed.

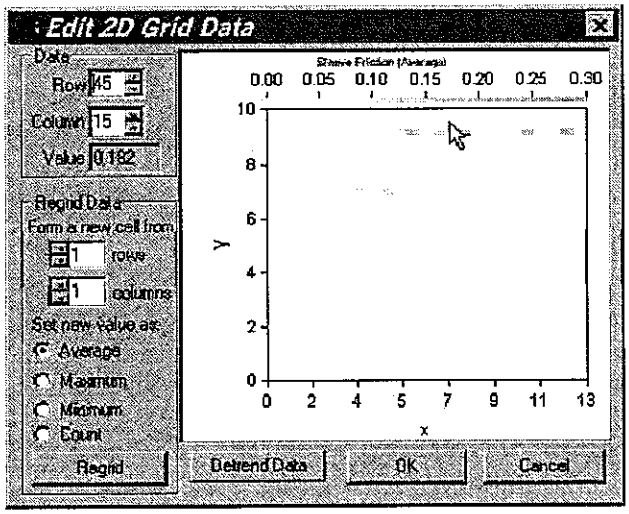

Modify and Examine Data

Cut, Copy, and Paste

Main Menu: Edit ⇒ Cut, Edit ⇒ Copy, or Edit ⇒ Paste
Keyboard Shortcut: Ctrl+X (cut), Ctrl+C (copy), or Ctrl+V (paste)
Toolbar:

Popup Menu: Copy

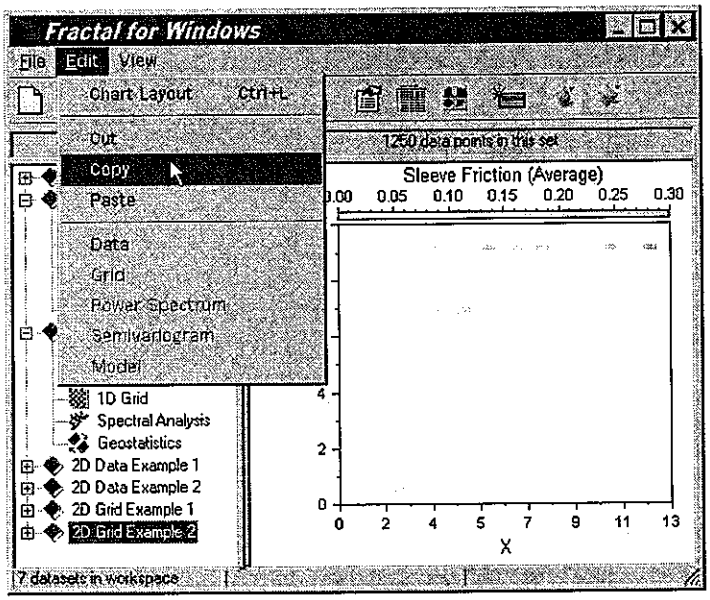

Begin Copy

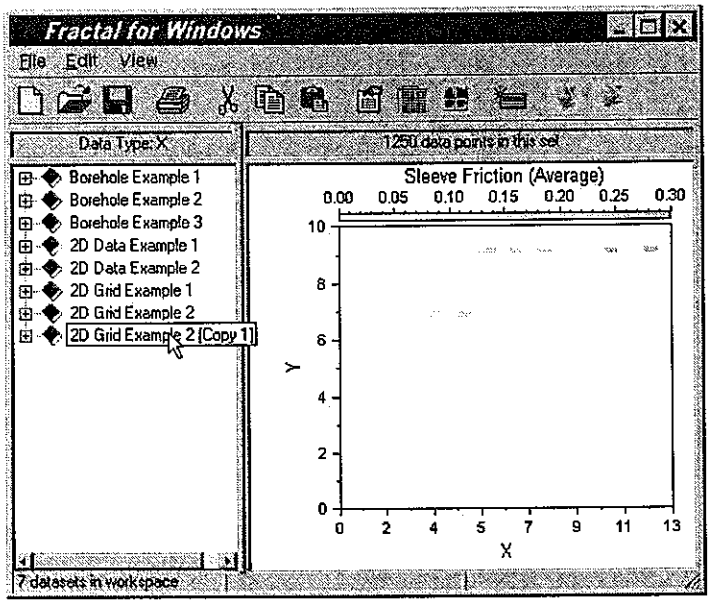

After Paste

Modify and Examine Data

Compare Charts

Use the New Window command to place each chart to be compared in a new window, resize and reposition the windows as necessary to aid comparison:

Main Menu: View ⇒ New Window
Keyboard Shortcut: Ctrl+W
Toolbar: 
Popup Menu: New Window

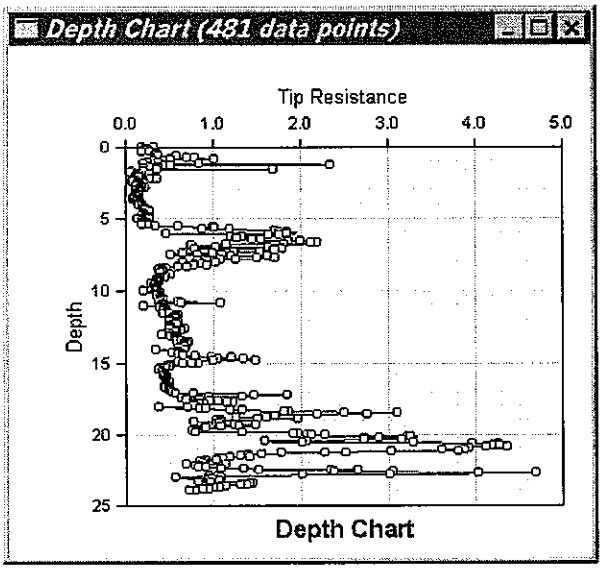

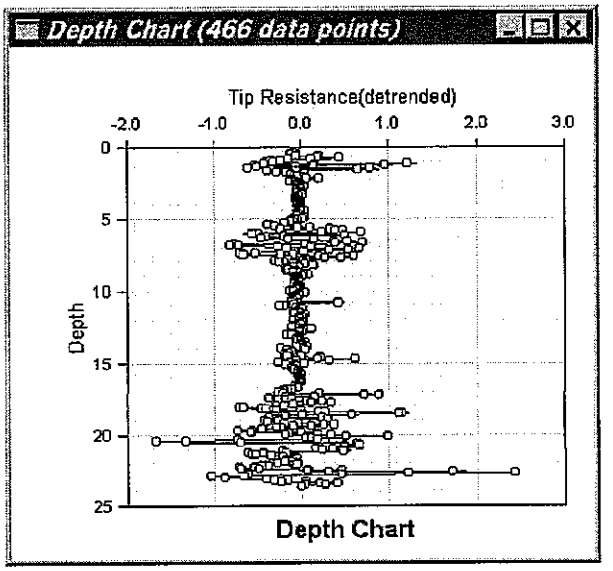

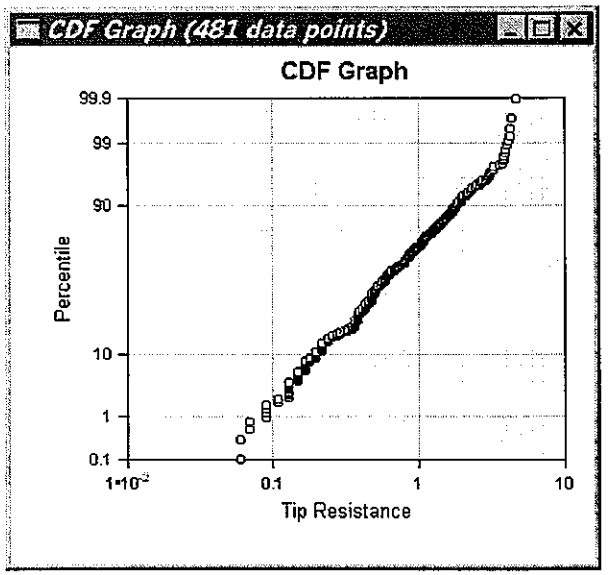

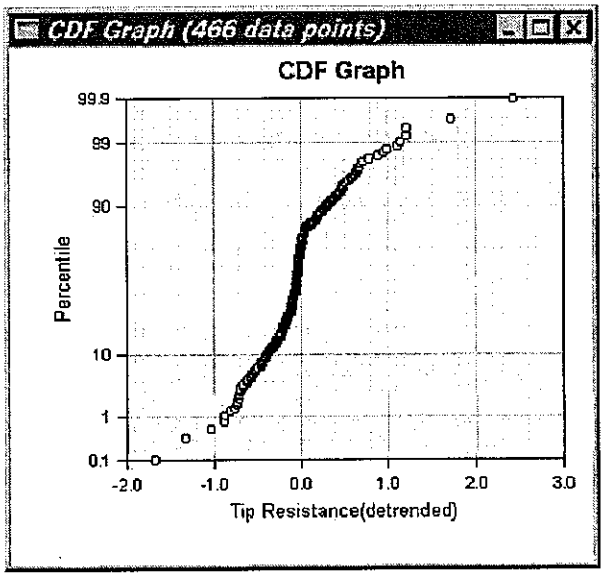

Modify and Examine Data

Remove Trends in Data

1. Open the Edit Data dialog box, click Detrend Data:
   Main Menu: Edit ⇒ Data or View ⇒ Data
   Keyboard Shortcut: Ctrl+E or double-click chart
   Toolbar: 
   Popup Menu: Edit

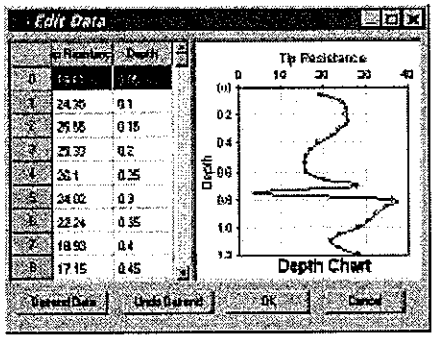

2. (Borehole data) Provide the transition zone and the corresponding gain (attenuation factor). The attenuation factor is the amount by which the spectral power of any spatial features longer than the specified cutoff distance will be attenuated. Because of the nature of digital filters, some experimentation using different combinations of parameters (change the numbers and click Update) may be needed to develop a satisfactory filter.

3. (Borehole data) Click Detrend to proceed. After the trend has been removed, FRACTAL FOR WINDOWS will offer a choice of replacing the existing data with the new detrended data, or placing the new detrended data as a new dataset.

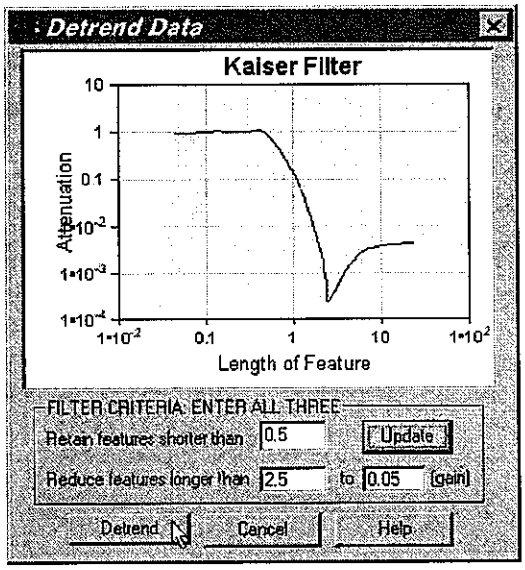

4. (Two-dimensional grid) Provide the cutoff distance and the rolloff factor for the Butterworth filter. The cutoff distance is the distance at which the spectral power will be reduced by half (i.e. an attenuation factor of 0.5). The rolloff factor must be an integer; larger factors will produce steeper attenuation around the cutoff distance.

5. (Two-dimensional grid) Click OK to proceed. The detrended data will be placed in a new dataset. To change the title of this new dataset, single-click the corresponding tree item to edit the title. Press enter or click other parts of the tree view when completed.

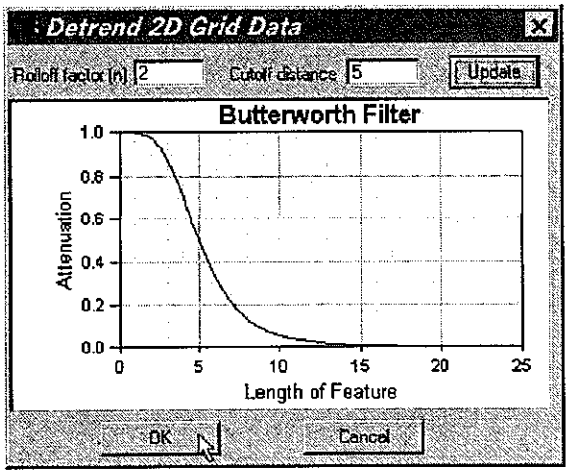

Modify and Examine Data

Change Lag Classes in Geostatistics Analysis

1. Select the semivariogram chart to be edited and open the Edit Semivariogram Dialog box:
   Main Menu: Edit ⇒ Semivariogram
   Keyboard Shortcut: none
   Toolbar: none
   Popup Menu: none

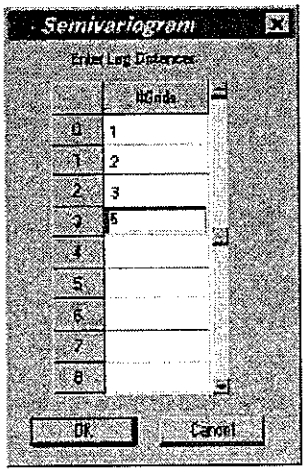

2. (Borehole data) Key in the desired lag classes. Press the OK button when done, FRACTAL FOR WINDOWS will replace the existing semivariogram with the one calculated from the new set of lag classes.

3. (Two-dimensional grid) Define the search region by specifying the range (number of rows and columns) and direction (between two angles). Pairs of data grids that fall within the range and the direction bounds are used in the calculation.

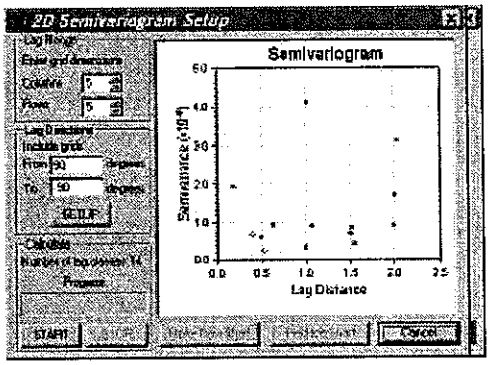

4. (Two-dimensional grid) Press the Setup button to set the direction of the search region interactively.

5. (Two-dimensional grid) After defining the search region, press the Start button to calculate the corresponding semivariogram. In a long calculation, FRACTAL FOR WINDOWS will run the calculation in a separate thread and display the partial results as these become available. During such a long calculation, press the Stop button to suspend the calculation and the Resume button to continue after the calculation is suspended. When the calculation is completed, press the Save As New Chart button to produce a new chart or the Replace Existing Chart button to replace the data in the existing chart.

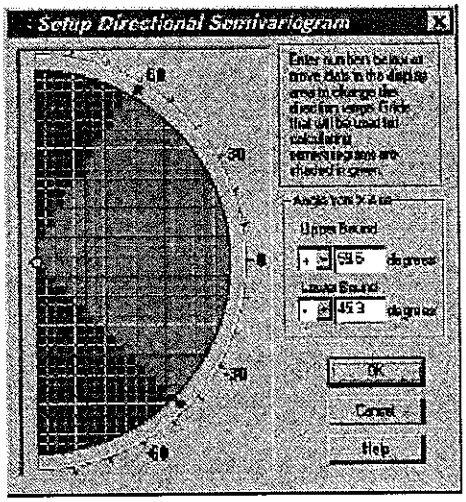

Modify and Examine Data

Fit Geostatistics Models

1. Selected the semivariogram chart to be fitted and open the Select Semivariogram Model dialog box:
   Main Menu: Edit ⇒ Model
   Keyboard Shortcut: Ctrl+M
   Toolbar: 
   Popup Menu: Edit Model

2. Click one of the option buttons to switch to a different model. If the model has not been fitted, FRACTAL FOR WINDOWS will calculate the set of model parameters that minimize the square of the error. Editing the model parameters after a model has been fitted will cause FRACTAL FOR WINDOWS to display the corresponding least square error and the new curve.

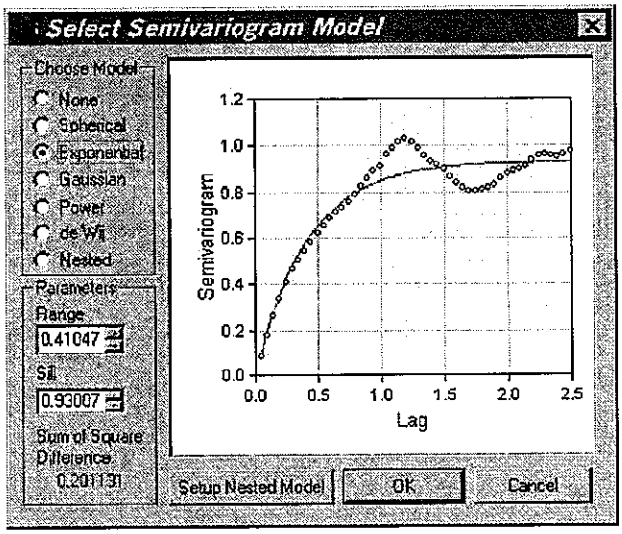

3. Press the Setup Nested Model button to open the Nested Model dialog box. Select each component model to be included in the nested model and specify the weight to be applied to that component. After specifying the independent components, press the Fit Model button to fit the nested model to the data using the least square error criteria. Press the OK button when done.

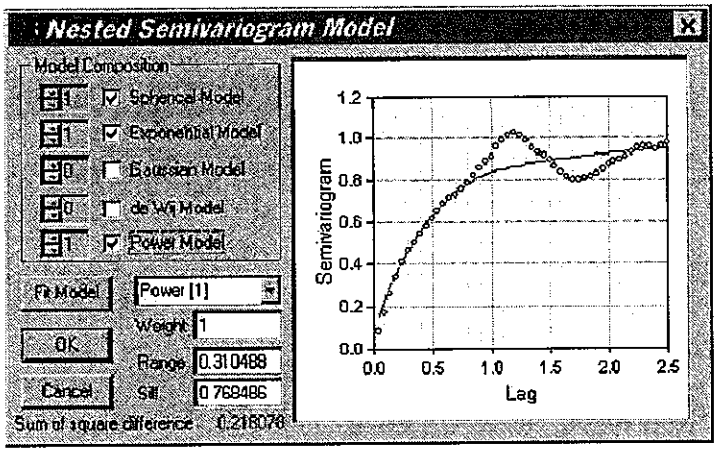

Modify and Examine Data

Add Harmonics in Power Spectrum Analysis

(Borehole data only)

1. Select the power spectrum chart to be modified and open the Spectral Analysis dialog box:
   Main Menu: Edit ⇒ Model
   Keyboard Shortcut: Ctrl+M
   Toolbar: 
   Popup Menu: Edit Model

   This dialog box will not open if the chart already includes the spectral density of all harmonics that can be calculated from the dataset.

2. Set the total number of harmonics to be calculated. Press the OK button when done, FRACTAL FOR WINDOWS will calculate the power spectrum up to the specified number of harmonics and update the chart.

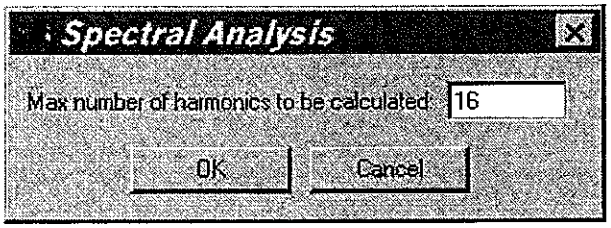

Modify and Examine Data

Change Histogram Intervals

1. Open the Edit Histogram dialog box:
   Main Menu: Edit ⇒ Histogram
   Keyboard Shortcut: Ctrl+M
   Toolbar: 
   Popup Menu: Edit Model

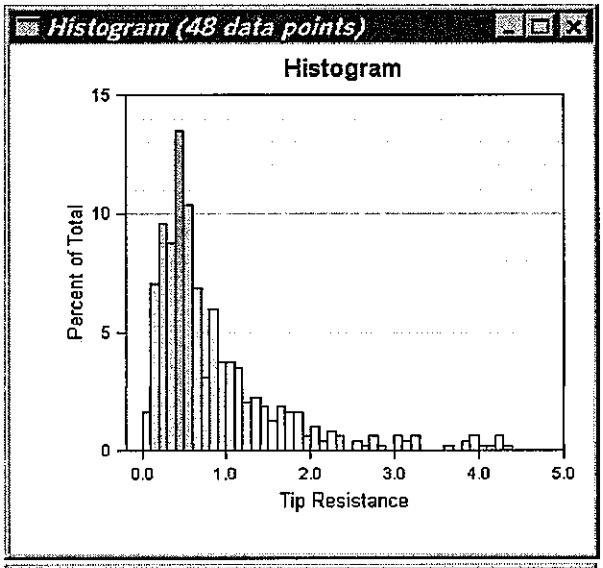

2. Specify the range of the histogram; any data outside of this range will be excluded from the histogram. Also specify the size of the increment. FRACTAL FOR WINDOWS will calculate the number of intervals and update the histogram.

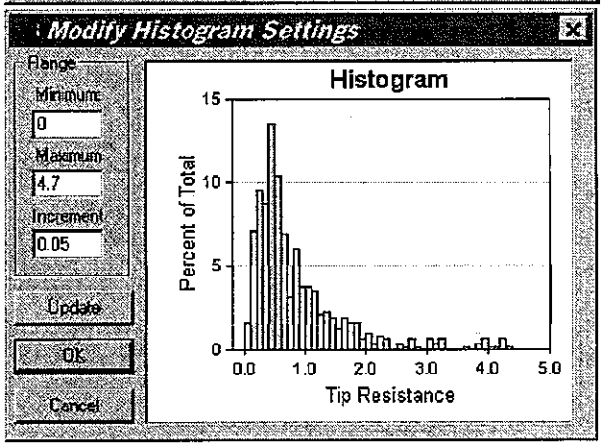

3. Press the Update button to replace the existing histogram with the new one.

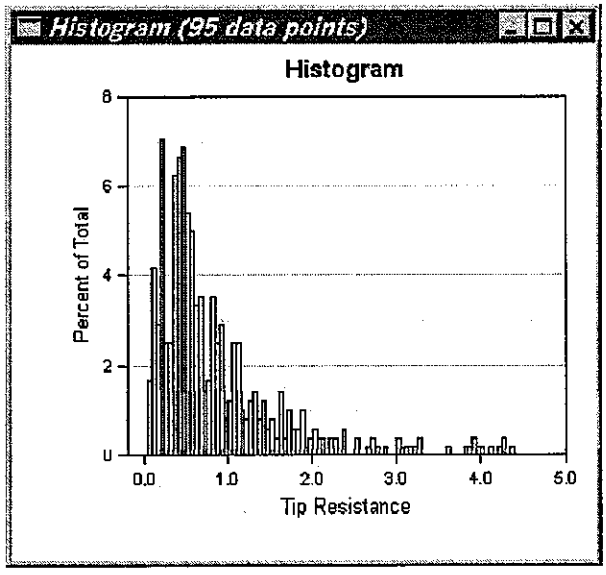

Modify and Examine Data

Use a Larger or Smaller Grid

Borehole Data:

1. Select the grid chart to be modified and open the Edit Grid dialog box:
   Main Menu: Edit ⇒ Grid
   Keyboard Shortcut: Ctrl+M
   Toolbar: 
   Popup Menu: Edit Model

2. Specify the starting location and the size of the grid. Press the OK button when done, FRACTAL FOR WINDOWS will regrid the data and calculate the power spectrum and the semivariogram from the regridded data.

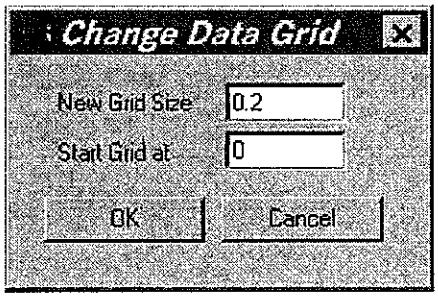

Two-dimensional Grid:

1. Select the grid chart to be modified and open the Edit Data dialog box:
   Main Menu: Edit ⇒ Data
   Keyboard Shortcut: Ctrl+E or double-click chart
   Toolbar: 
   Popup Menu: none

2. In the Regrid Data group box, specify how many rows and columns are to be combined into a new grid. Also specify whether the new grid should contain the average, maximum, or minimum value of the grids being combined, or just the count of the number of grids that contain non-zero value.

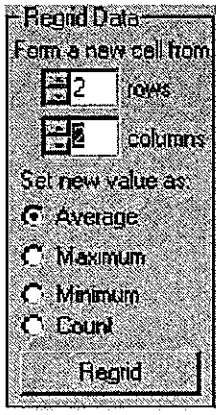

3. Press the Regrid button when done, FRACTAL FOR WINDOWS will regroup the grids and create a new dataset containing the newly regrouped grids.

Modify and Examine Data

Spacing Distribution of Data

(Borehole data only)

1. Switch between histogram and quantile plot:
   Main Menu: View ⇒ Spacing ⇒ Histogram or CDF
   Keyboard Shortcut: none
   Toolbar: none
   Popup Menu: none

2. Inspect data:
   Main Menu: Edit ⇒ Data
   Keyboard Shortcut: Ctrl+E or double-click chart
   Toolbar: 
   Popup Menu: Edit Data

Customize Charts

Default and Alternate Views

Each chart may be displayed in more than one way by changing the type of x and y axis between normal (linear) and logarithmic scale. In a quantile plot (CDF graph), the y axis can also be displayed in probability scale. When a dataset is first created, each chart is displayed in default view. This view can be switched to one of the alternative views to reveal the hidden trend, if any, in the data.

1. To switch to a different view:
   Main Menu: View ⇒ Previous or View ⇒ Next
   Keyboard Shortcut: none
   Toolbar: 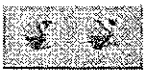
   Popup Menu: Next View or Previous View

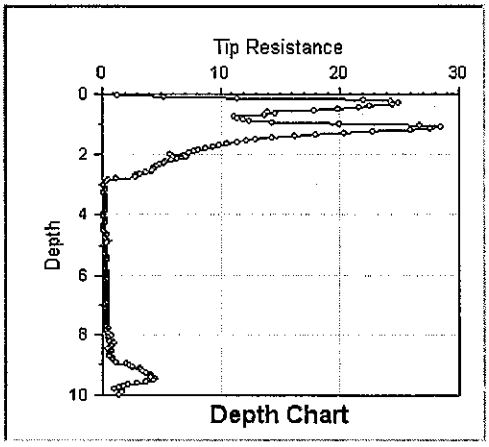

Default View

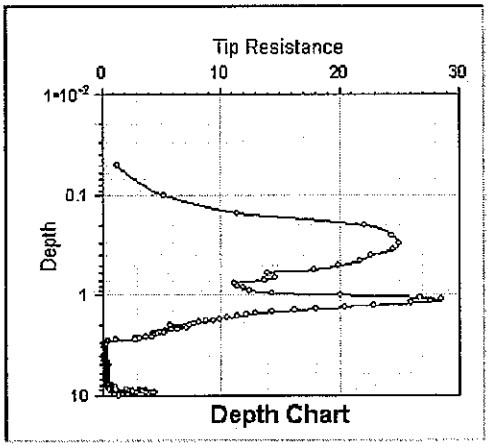

View 1 (linear - log)

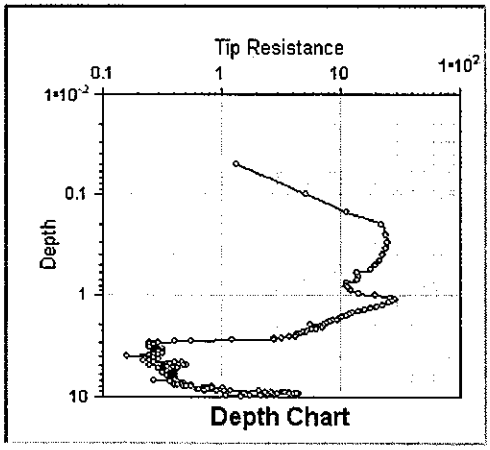

View 2 (log - log)

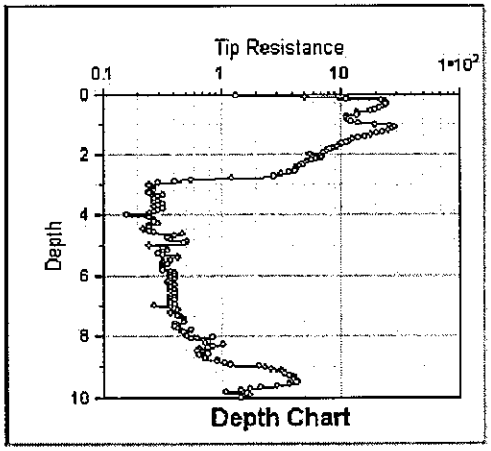

View 3 (log - linear)

Customize Charts

Use Logarithmic or Probability Axis

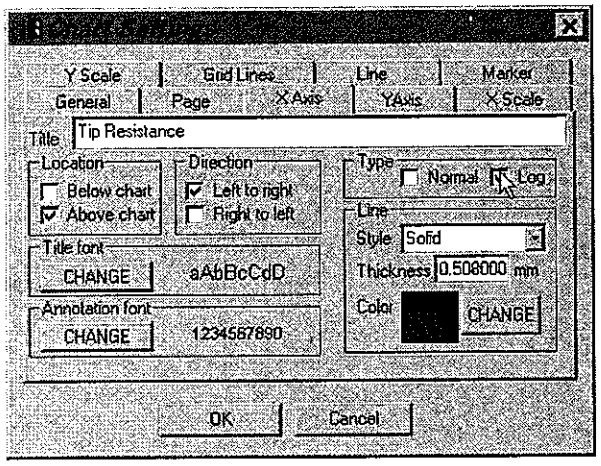

1. Open the Chart Settings dialog box:
   Main Menu: Edit ⇒ Chart Layout
   Keyboard Shortcut: Ctrl+L
   Toolbar:

   Popup Menu: Edit Chart Attributes

2. Click the X Axis or the Y Axis tab.

3. Find the Type group box and select one of the choices.

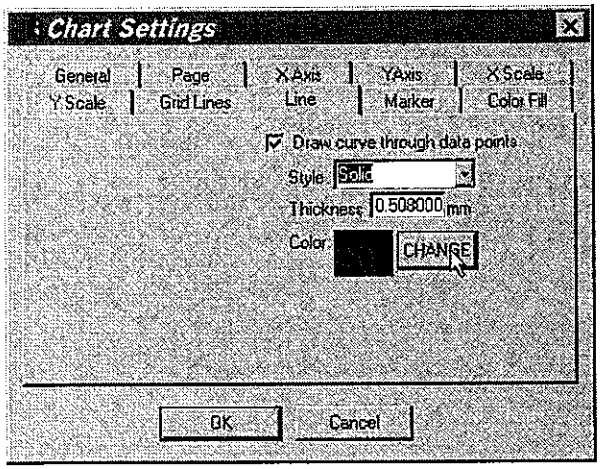

Lines

1. Click the Line tab.

2. Modify line style, thickness, or color as needed.

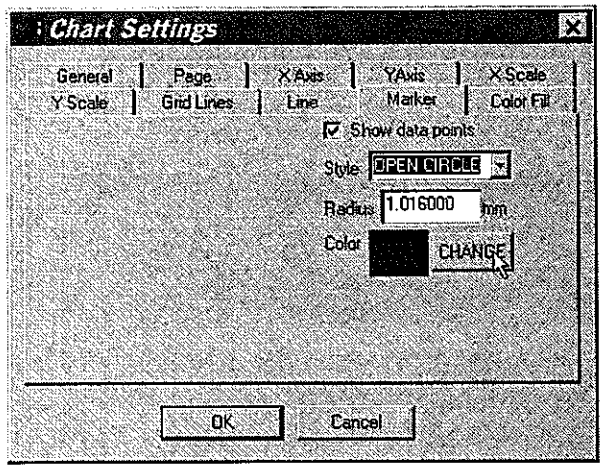

Markers

1. Click the Marker tab.

2. Modify marker type, size, or color as needed.

Customize Charts

Change Titles

1. Open the Chart Settings dialog box:
   Main Menu: Edit ⇒ Chart Layout
   Keyboard Shortcut: Ctrl+L
   Toolbar: 
   Popup Menu: Edit Chart Attributes

2. (To change title in X or Y axis or to add units of measurement) Click the X Axis or the Y Axis tab. Make change in the title edit box. Change the font by clicking the corresponding Change button in the font group box.

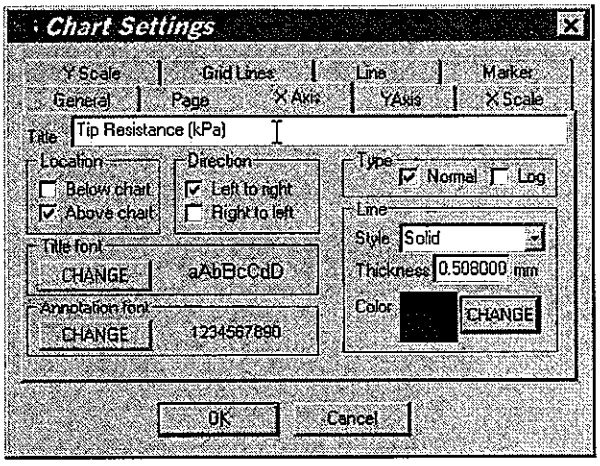

3. (To change chart title) Click the General tab and make change in the chart title edit box. Change the font by clicking the corresponding Change button in the font group box.

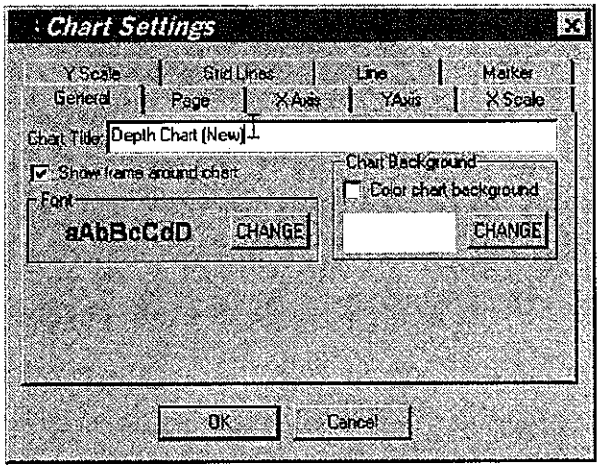

Customize Charts

Change Location and Direction of Axis

1. Open the Chart Settings dialog box:
   Main Menu: Edit ⇒ Chart Layout
   Keyboard Shortcut: Ctrl+L
   Toolbar: 
   Popup Menu: Edit Chart Attributes

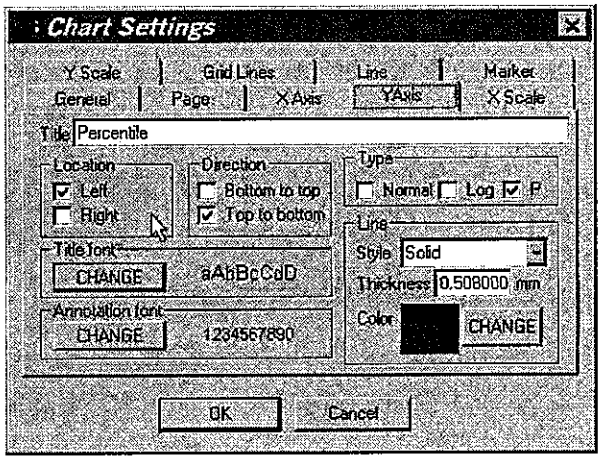

2. Click the X Axis or the Y Axis tab.

3. Switch the location of the axis by selecting one of the two choices in the Location group box.

4. Switch the direction of the axis by selecting one of the two choices in the Direction group box.

Tick Marks and Grid Lines

1. To change the tick mark, click X Scale or Y Scale tab. Find the tick group box and choose whether to display the tick marks as well as the type of marks to be displayed. To change the spacing between adjacent marks, change the corresponding entries in the Range and Division group box.

2. To turn the grid lines on and off, click the Grid Lines tab and check or uncheck the corresponding checkboxes. The thickness, style, and color of the grid lines can also be changed.

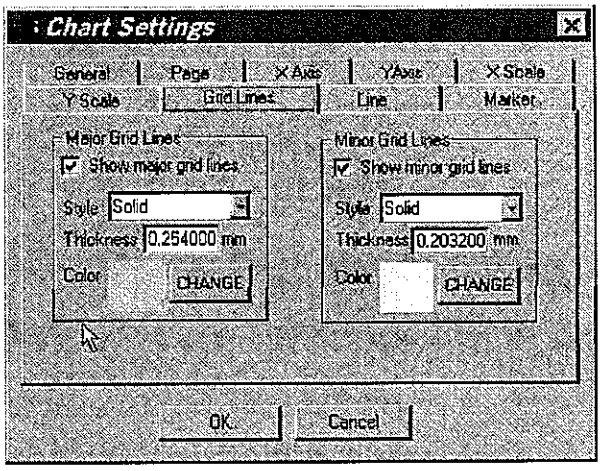

Customize Charts

Add Color to Chart Background

1. Open the Chart Settings dialog box:
   Main Menu: Edit ⇒ Chart Layout
   Keyboard Shortcut: Ctrl+L
   Toolbar: 
   Popup Menu: Edit Chart Attributes

2. Click the General tab, check the color chart background checkbox and press the Change button to change the color.

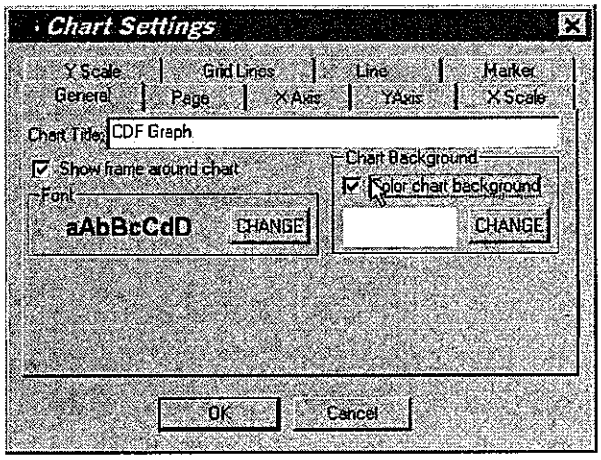

Customize Charts

Color Fills

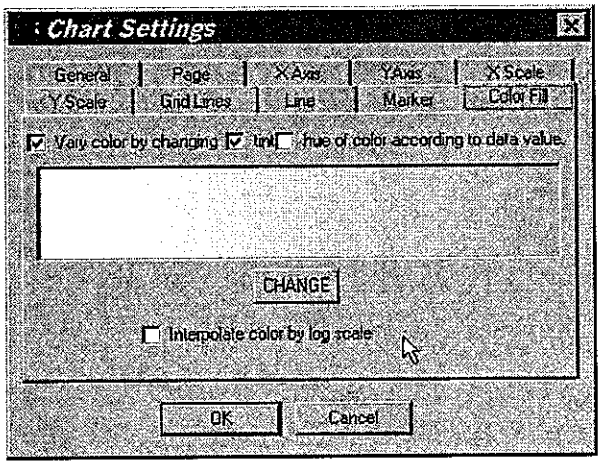

1. Open the Chart Settings dialog box:
   Main Menu: Edit ⇒ Chart Layout
   Keyboard Shortcut: Ctrl+L
   Toolbar:
   Popup Menu: Edit Chart Attributes

2. Click the Color Fill tab. Check or uncheck the Vary color checkbox to turn the color fill on or off.

3. To switch to the tint mode where the intensity (tint) of the color changes with the data value, check the tint checkbox. Press the Change button to vary the hue.

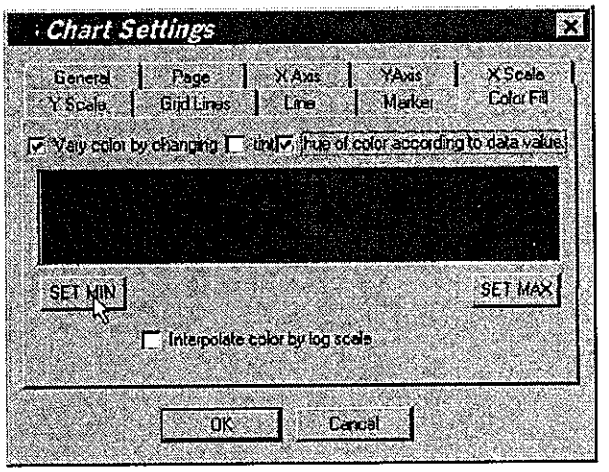

4. To switch to the hue mode where the data value is reflected by the hue of the color, check the hue checkbox. Change the color on either end of the spectrum by pressing the Set Min or Set Max button.

Interpolate Color by Logarithmic Scale (Two-dimensional grid only)

1. Click the Color Fill tab. Check the checkbox labeled 'Interpolate color by log scale.' If none of the grids contains zero or negative value, then the color of each grid will be chosen using the logarithmic scale to enhance the contrast of the display.

Customize Charts

Use Metric Units

1. Open the Chart Settings dialog box:
   Main Menu: Edit ⇒ Chart Layout
   Keyboard Shortcut: Ctrl+L
   Toolbar: 
   Popup Menu: Edit Chart Attributes

2. Click the Page tab and check the ckeckbox labeled mm or inch.

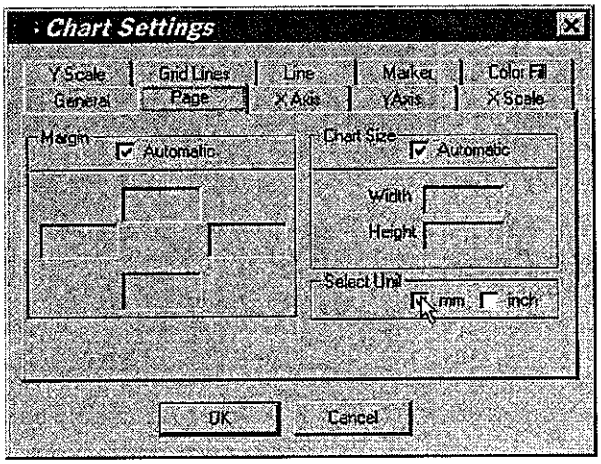

Print Charts

Basic

1. To print the chart currently displayed:
   Main Menu: File ⇒ Print
   Keyboard Shortcut: Ctrl+P
   Toolbar: 
   Popup Menu: Print

2. To print all the charts in the current dataset:
   Main Menu: File ⇒ Print All
   Keyboard Shortcut: none
   Toolbar: none
   Popup Menu: none

Page Setup

1. Open the Chart Settings dialog box:
   Main Menu: Edit ⇒ Chart Layout
   Keyboard Shortcut: Ctrl+L
   Toolbar: 
   Popup Menu: Edit Chart Attributes

2. Click the Page tab. In the group box entitled Margin, uncheck the checkbox labeled Automatic and set the margins around the page.

3. In the group box entitled Chart Size, uncheck the checkbox labeled Automatic to set the width and the height of the chart. In the default, automatic mode, FRACTAL FOR WINDOWS select the size of the chart such that the spacing between two major grids on either axes is a whole number of the unit used.

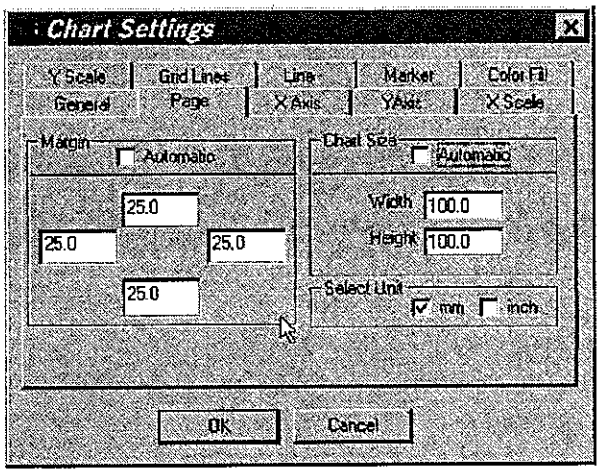

Managing Dataset

Save Dataset to File

Main Menu: File ⇒ Save
Keyboard Shortcut: Crtl+S
Toolbar: 
Popup Menu: none

Load Dataset from File

Main Menu: File ⇒ Open
Keyboard Shortcut: Ctrl+O
Toolbar: 
Popup Menu: none

Workspace

A workspace is a collection of datasets. The organization of the workspace is saved at the end of each session and restored when FRACTAL FOR WINDOWS next starts.

1. To remove a dataset from the current workspace:
   Main Menu: File ⇒ Close
   Keyboard Shortcut: none
   Toolbar: none
   Popup Menu: none

2. To remove all datasets in the current workspace:
   Main Menu: File ⇒ Close All
   Keyboard Shortcut: none
   Toolbar: none
   Popup Menu: none

3. To add a dataset to the current workspace:
   Main Menu: File ⇒ Open, File ⇒ New, or File ⇒ Import
   Keyboard Shortcut: Crtl+O (open), Ctrl+N (new)
   Toolbar: 
   Popup Menu: none

Managing Dataset

Export Data

The data in each chart can be exported to an external disk file which may then be imported into a document or spreadsheet. Alternatively, the data can be copied to the clipboard using the Cut or the Copy command and then pasted into another document or spreadsheet.

Main Menu: File ⇒ Export ⇒ Data
Keyboard Shortcut: none
Toolbar: none
Popup Menu: none

Export Chart

The chart can be exported to an external disk file as an enhanced Windows metafile which can be imported into a document or drawing by any application that recognizes the enhanced Window metafile. The current version does not support copying the chart to the clipboard for directly pasting into another application.

Main Menu: File ⇒ Export ⇒ Chart
Keyboard Shortcut: none
Toolbar: none
Popup Menu: none

Appendix: Specifications of Data Objects

1. Data tables

```
#----
#       Data tables
#
#       A data table is characterized by its structure and entity.
#       The table structure must be defined within the definition block,
#       the data entity can appear in a separate ASCII file.
#
#----
BEGIN   data_table
        name =  "Example data table"
        location_col =  1,3                 # column containing data
                                            # location (x,y,z)
        data_col =      4,6-8               # column containing data
        data_label =    4,"porosity"        # label for column# 4
        data_label =    6,"aperture"
                                            # any unnamed label will default
                                            # to data_n
        missing_value_char =    "*"         # "*" is default, include this
                                            # only if other characters such
                                            # as "-" is used.
        BEGIN   data_entity
                #       x       y       z       Data_1  Data_2  . . .
                0       0       0       1       1.1     1.2     ...
        END
        # Alternatively, specify file where data can be read.
        # If a data_table block contains more than one data_entity
        # block, then the data from the blocks will be joined.
        BEGIN   data_entity
                data_file =     "filename.dat"
        END
END
```

Appendix: Specifications of Data Objects (continued)

2. Borehole data

```
#----
#
#   borehole data
#
#   borehole measurements contains both borehole and data measured
#
#   IMPORTANT NOTES ON CONFLICT RESOLUTION:
#   1.  If the same object (such as a borehole_simple) is specified more
#       than once either within the same block, in the same file, or in
#       the same group of files within the same project, the MORE RECENT
#       definitions will overwrite the earlier definitions. As each
#       object is identified by name, make sure the names are unique.
#   2.  If more than one data table definition exists within the same
#       block, the data will be joined unless the data structure in the
#       different blocks has changed. In that case, the MORE RECENT
#       definition will overwrite the earlier ones.
#
#----
BEGIN   borehole_data
    name =  "unique_borehole_id"
    #
    # borehole info
    #
    # either include the info in the block
    BEGIN   borehole_simple
        # use existing borehole_simple object
    END
    # or point to a file where the borehole object can be found
    borehole_name = "BH_1"          # must provide name in case the file
    data_file =     "borehole.dat"  # contains more than one borehole
                                    # object
    #
    # data type, point measurement of interval measurement
    # the location of point measurement is specified in one column
    # the location of interval measurement must be specified in two
    # columns (x1,x2)
    #
    point_measurement = 1           # 0 if interval measurement
    #
    # data block
    #
    # again, either include the data_table object in the block
    BEGIN   data_table
            # ........
    END
    # or point to a file where the data table can be found
    data_table_name =   "Example data table"    # must provide name to
                                                # aid search
    data_file =         "filename.dat"          # note that both
                                                # "borehole.dat" and
                                                # "filename.dat" will
                                                # both on the search
                                                # path and will be
                                                # searched in order of
                                                # their presence in the
                                                # block. In this
```

```
                                    # example,"borehole.dat"
                                    # will be searched
                                    # first.
END
```

Appendix: Specifications of Data Objects (continued)

3. Surface data

```
#----
#   surface data
#
#   surface measurement contains both surface description and data
#
#   SEE NOTES ON CONFLICT RESOLUTION UNDER BOREHOLE DATA
#
#----
BEGIN   surface_data
    name =  "unique_surface"
    #
    #   surface info
    #
    # either include the info in the block
    BEGIN   traceplane
        # use existing traceplane object
    END
    # or point to a file where the object can be found
    traceplane_name = "TP_1"          # must provide name in case the
                                      # file contains more
    data_file =     "traceplane.dat"  # than one traceplane object
    #
    # data type, point measurement or interval measurement
    # the end points of an interval measurement are ends of fracture
    # trace and the data may contain orientation, aperture, and other
    # measurements or the data may be absent in the case of a simple
    # fracture trace plane.
    # the location of point measurement is specified in two columns
    # (x,y) the location of interval measurement must be specified in
    # four columns as (x1,y1,x2,y2), the order must be strictly observed
    #
    point_measurement = 1           # 0 if interval measurement
    #
    # data block
    #
    # again, either include the data_table object in the block
    BEGIN   data_table
            # ........
    END
    # or point to a file where the data table can be found
    data_table_name =   "Example data table"    # must provide name to
                                                # aid search
    data_file =         "filename.dat"          # note that both
                                                # "traceplane.dat" and
                                                # "filename.dat" will
                                                # both on the search
                                                # path and will be
                                                # searched in order of
                                                # their presence in the
                                                #block. In this
                                                # example,
                                                # "traceplane.dat" will
                                                # be searched
                                                # first.
END
```

Appendix: Specifications of Data Objects (continued)

4. Statistics

```
#----
#
#   Data bins
#
#   Type:       containee
#   Container:  statistics
#----
BEGIN   bin_data
    num_bins    =   10
    bin_low     =   0
    bin_high    =   10
    item_in_bin =   1,2,1,..,0  # number of item in each bin, comma
                                # separated
END


#----
#
#   Statistics of data
#
#   Type:       containee
#   Container:  surface_data, borehole_data, trace_map, grid
#
#----
BEGIN   statistics
    num_points  =   100
    mean        =   0
    std_dev     =   1
    BEGIN   bin_data
        #   frequency
    END
END
```

Appendix: Specifications of Data Objects (continued)

5. Power spectrum

```
#----
#
#   Power spectrum
#
#   Type:       containee
#   Container:  grid
#
#----
BEGIN   power_spectrum
    BEGIN   data_table
        # data goes here
    END
END
#----
#
#   Simple semivariogram models
#
#   Type:       containee
#   Containers: semivariogram, semivariogram_model_compounded
#
#----
BEGIN   semivariogram_model_simple
    model_type  =   "spherical"     # valid entries: spherical,
                                    # exponential
                                    # fractal, and null
    alpha       =   10
    C           =   3
    chi_sq      =   4.11
    sig_level   =   86
END

#----
#
#   Compounded semivariogram models
#   Type:       container and containee
#   Container:  semivariogram
#   Containee:  semivariogram_model_simple
#
#----
BEGIN   semivariogram_model_compounded
    num_models  =   3
    weights     =   0.3,0.4,0.3
    chi_sq      =   4.11
    sig_level   =   86
    BEGIN   model       # model 1
        # model parameters
    END # model 1
    BEGIN   model       # model 2
        # model parameters
    END # model 2
    BEGIN   model       # model 3
        # model parameters
    END # model 3
END

#----
```

```
#
#   Semivariogram object, contains data and (optionally) fitted models
#
#   Type:       container and containee
#   Container:  grid
#   Containee:  data_table, (optional)
semivariogram_model_simple/compounded
#
#----
BEGIN   semivariogram
    name =  "Omni directional"
    dir  =  0,0,0
    lag_low =   0
    lag_high =  10
    lag_classes = 10
    lag_unit =  "m"
    BEGIN   data_table
        # h, v pairs, see data_table specifications
    END
    #
    #   Place fitted models (simple or compounded) in BEGIN/END blocks
    #
END
```

Appendix: Specifications of Data Objects (continued)

6. Data grids

```
#----
#
#   Grid object:
#
#   Type:        container and containee
#   Container:   surface_data, borehole_data, trace_map
#   Containee:   color_map, semivariogram, power_spectrum
#
#----
BEGIN   grid
    name         =   "simple grid"        # more descriptive names if
                                          # needed
    dim          =   3                    # 1, 2, or 3
    grid_origin  =   0,0,0
    grid_size    =   1,1,1                # grid size in each dimension
    grid_dim     =   10,10,10             # number of grids in each
                                          # dimension
    data_file    =   "Traceplane1.grd"    # data stored in external binary
                                          # file to save space
    #
    #   Place derived object in BEGIN/END blocks
    #
                                    END
```

Appendix: Specifications of Data Objects (continued)

7. Color map

```
#----
#
#   Color map object, maps a scalar value into a color
#
#   Type:       containee
#   Container:  surface_data, borehole_data, grid
#
#----
BEGIN   color_map
    use_rgb =   0           # 0: HSV model, 1: RGB model
    hue =   100             # hue value ignored if RGB model chosen
    rgb_low =   0,0,0       # rgb values ignored if HSV model chosen
    rgb_high =  255,255,255
    color_steps =   100     # number of color steps
                            END
```

Appendix: Specifications of Data Objects (continued)

8. Contours

```
#----
#
#   Contour object
#
#   Type:       containee
#   Container:  surface_data
#
#----
BEGIN   contour
    num_contour =   20
    contour_level = 0,10,1
    BEGIN   contour_data
        0                   # contour level
        x0,y0               # series of data points
        x1,y1
    END
    #   more contour data
END #   contour
```

Appendix: Specifications of Data Objects (continued)

9. Project folder

```
#----
#
#       Project folder
#
#       A project folder contains several objects, each object contains
#       its own subsets.
#
#       Type:       container (highest level)
#       Containee:  surface_data, borehole_data, trace_map
#
#----
BEGIN   project_folder
        #
        #   Header
        #
        name =  "Active"
        creation_date = "3/25/97"
        last_modified_date = "3/25/97"
        last_access_date =  "3/25/97"
        #
        #   Object 1
        #
        BEGIN   surface_data
            #
            #   Object name, file name, and file location
            #
            name =  "unique_surface"
            file_path = "c:\trace"
            data_file = "traceplane1.zzz"
            #
            #   Derived object 1 - contours
            #
            BEGIN   contour
                #   contour data
            END #   contour
            #
            #   Derived object 2 - color map
            #
            BEGIN   color_map
                # color map data
            END
            #
            #   Derived object 3 - grid
            #
            #   More than one grid can be developed from the same
            #   surface data; these grids may have different dimensions
            #   or occupy different areas
            #
            BEGIN   grid
                #   grid data
                #   Place objects derived from grid in BEGIN/END blocks
                #   For example, a color map and a semivariogram
                BEGIN   color_map
                    # color map data
                END
                BEGIN   semivariogram
```

```
                    # semivariogram data
                    BEGIN   semivariogram_model_simple
                        # model data
                    END
                    #   more models
                    BEGIN   semivariogram_model_compounded
                        # data for compounded model
                    END
                END # semivariogram
                #
                #   More semivariograms (in different
                #   directions, perhaps
                #
                BEGIN   semivariogram
                    #   semivariogram data
                END
            END # grid
        END # surface_data "unique_surface
END project_folder "Active"
#
#   More folders
#
```

Appendix E PAWorks User Manual

PAWorks

Pathways Analysis and Solute Transport

User Documentation

Version 1.4

T. Foxford
E. Sudicky
W. Dershowitz
Th. Eiben
D.A.Shuttle

Golder Associates Inc.
Redmond, Washington

March 31, 1997

923-1089.800
paworks2.doc

LICENSING

ABSTRACT

This manual provides user documentation for PAWorks, a Microsoft Windows 95 and Unix software package developed by Golder Associates Inc. to identify and characterize flow and transport pathways through fractured rock. Pathways are calculated using the methods of graph theory. This manual describes the use of PAWorks and provides theoretical background regarding the algorithms used.

Table of Contents

List of Figures

List of Tables

1. INTRODUCTION

Geometry is the key to understanding flow and transport in a wide range of practical flow and transport problems. Examples include connections between radioactive waste repositories and the biosphere, connections between contaminated zones and monitoring systems, and connections between wells for wellhead protection projects.

PAWorks was designed to provide an easy to use, approximate method for evaluating the properties of geometric connections in fractured rock masses. These geometric connections are referred to as "pathways." Pathways are defined by searching through the fracture system between user defined boundary conditions to determine the most significant connections, according to user-defined selection criteria.

PAWorks is part of the FracMan discrete feature modeling package, and works directly with discrete feature conceptual models generated using FracMan/FracWorks. PAWorks provides a tool to analyze the hydrogeological behavior of discrete feature networks.

FracMan/PAWorks requires input consisting of (a) Fracture network geometries generated by FracMan/FracWorks as .FAB format files, and (b) Boundaries, boundary conditions, and analysis control as .SAB format files. Once these files have been loaded, the user must select the source for which the analysis is to be carried out. FracMan/PAWorks then identifies potential transport pathways by graph theory analysis, and calculates approximate flow and transport solutions.

The role of FracMan/PAWorks within the FracMan modeling package is illustrated in Figure 1-1. The overall FracMan modeling package provides:

- **FracMan/FracSys** for data analysis to transformation field data into fracture modeling geometric, geological, and hydrogeological parameters,
- **FracMan/FracWorks** for stochastic simulation of three dimensional fracture patterns, with validation by simulated exploration,
- **FracMan/RockBlock** for keyblock stability analysis of rock blocks intersecting tunnel and cavern walls,
- **FracMan/PAWorks** for analysis of transport pathways within discrete fracture networks,
- **FracMan/FraCluster** for analysis of hydraulic compartmentalization, tributary drainage volume, and rock block size within discrete fracture networks,
- **MeshMaster** to generate finite element meshes from FracMan/FracWorks discrete fracture realizations and FracMan/MeshMaster boundary conditions,

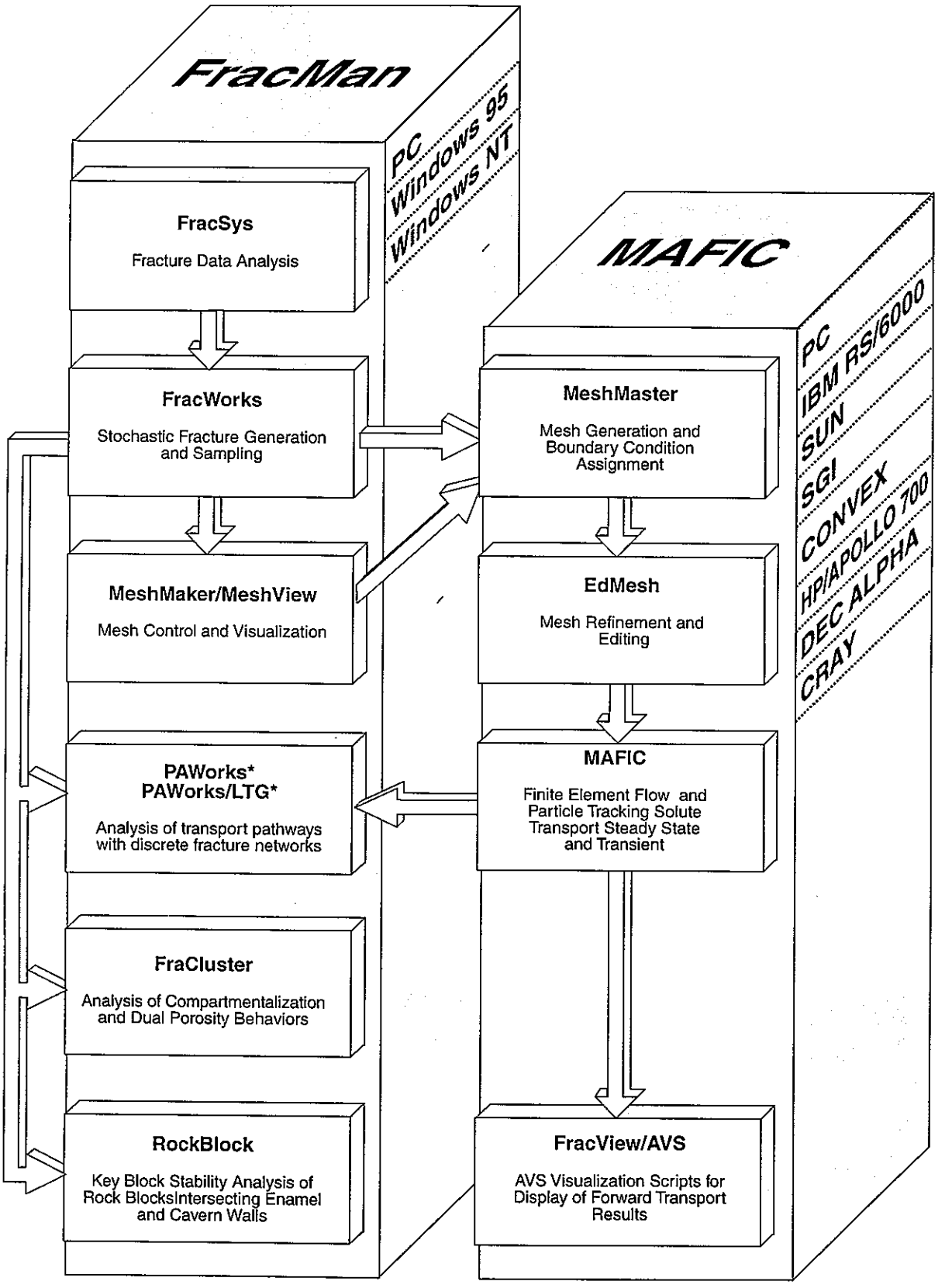

FIGURE **1-1**
FracMan/MAFIC MODELLING SUITE
PNC/PAWORKS

* Also available for Dec Alpha

- **EdMesh** to refine finite elements, modify solution specifications and boundary conditions, and adjust material properties, including specification of stochastic continuum properties on fracture surfaces

- **MAFIC** for solution of flow and pressure by conjugate gradient finite element methods, and to solve solute transport by particle tracking.

In its most basic form, PAWorks is concerned only with geometric connections, and therefore does not require any information concerning heads, gradients, or fluxes. The effective properties of pathways can be calculated by assuming simple series flow through the fracture network (Figure 1-2). However, for many applications, it is desirable to use more sophisticated approximations for the head field. For these purposes, PAWorks includes options to calculate approximate head field solutions based on pipe flow assumptions, and also an option to read head field values directly from the MAFIC three dimensional flow and transport simulator (Figure 1-3). Once approximate head solutions have been obtained, pathway searches can be carried out based on flux and travel time as well as pipe network properties. PAWorks/LTG provides a multiple porosity advection-sorption-diffusion-decay solute transport solution based on PAWorks pipe networks. The conceptual model for transport used in PAWorks/LTG is shown in Figure 1-4.

This manual is organized as follows: Sections 2 and 3 describe installation and operation of PAWorks; Section 4 provides theoretical background; and Section 5 presents verification cases. Appendix A provides a walkthrough demonstration PAWorks/LTG application.

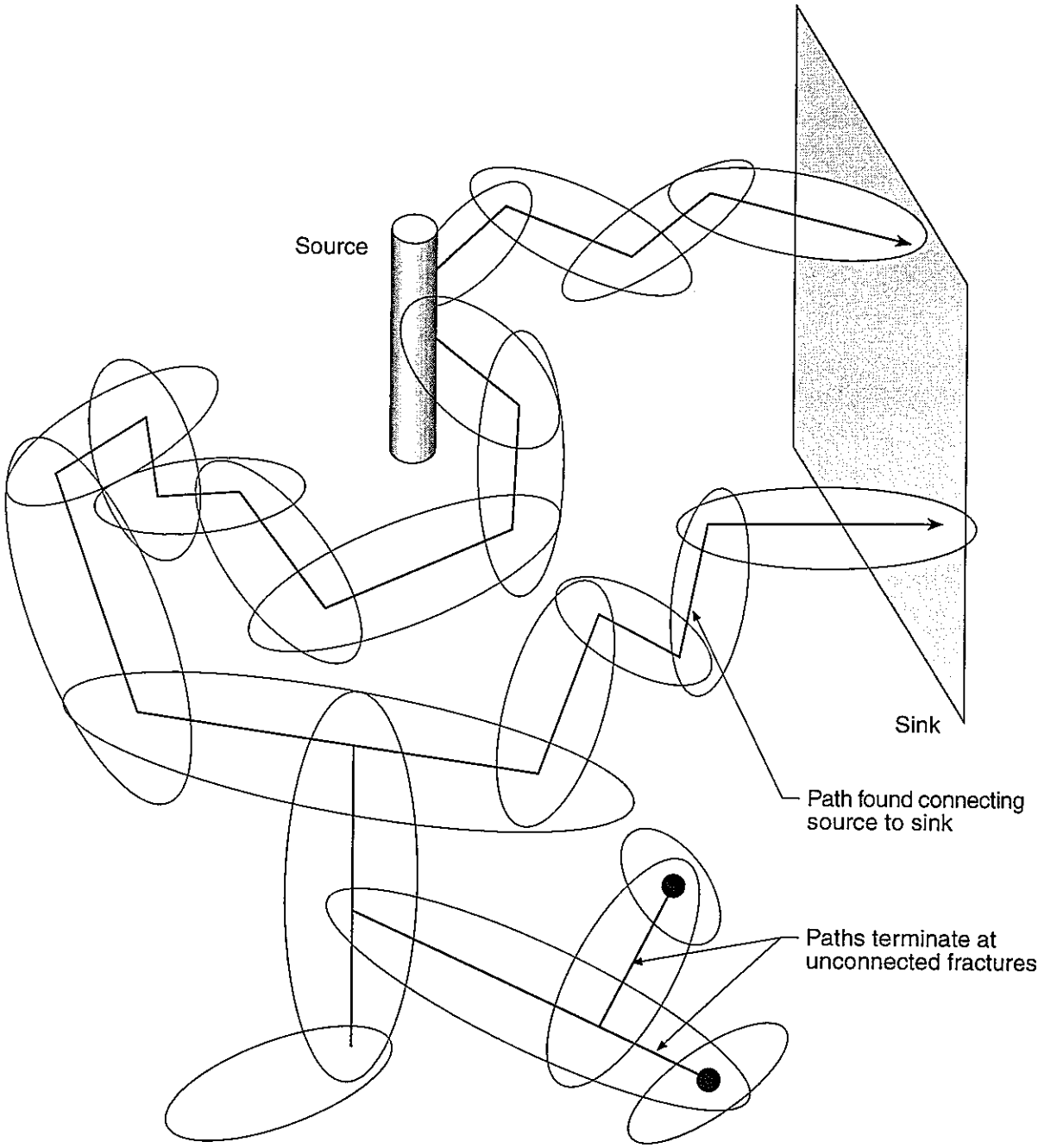

FIGURE **1-2**
SIMPLE SERIES FLOW
PNC/PAWORKS

PROJECT NO. 923 1089.811 DRAWING NO. 72315 DATE 5/12/97 DRAWN BY TK

Golder Associates

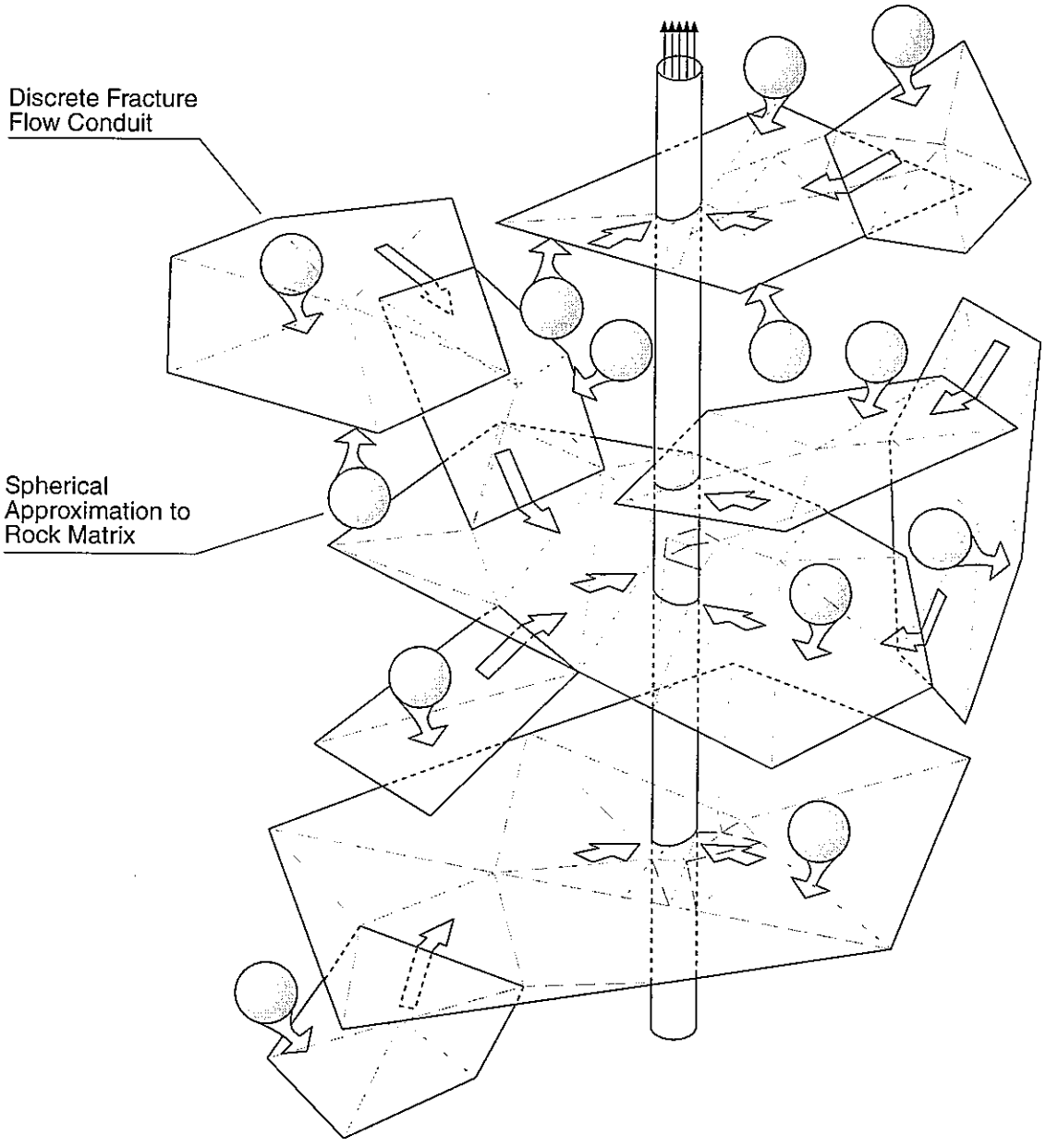

FIGURE **1-3**
MAFIC 3-D FLOW AND TRANSPORT SIMULATOR
PNC/PAWORKS

PROJECT NO. 923 1089.811 DWG. NO. 72316 DATE 5/12/97 DRAWN CB

Golder Associates

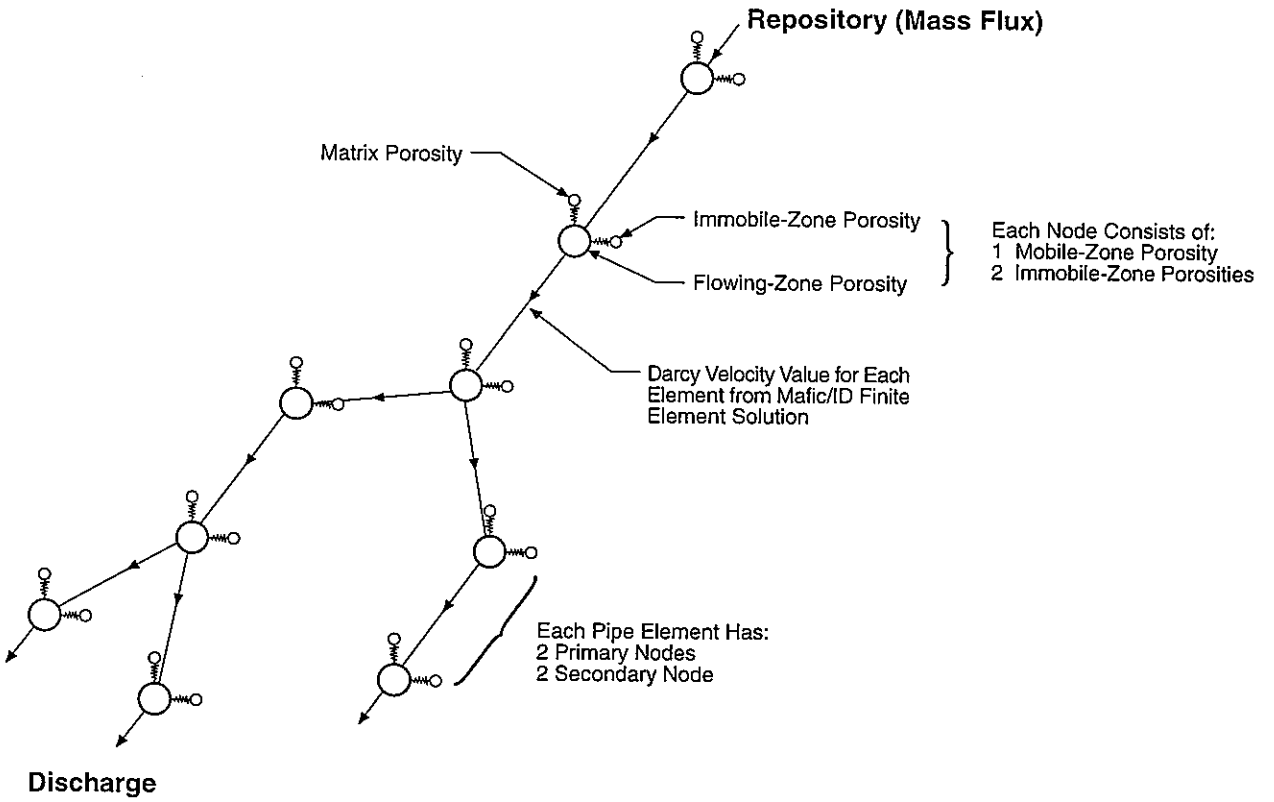

FIGURE **1-4**

PAWORKS/LTG SOLUTE TRANSPORT

PNC/PAWORKS

2. INSTALLATION OF PAWORKS

2.1 Hardware and Software Requirements

PAWorks is implemented as both 32-bit Microsoft Windows and Unix applications. As a result, it can be run on any computer which supports Microsoft Windows 95 or Windows NT Version 3 or higher, and most Unix-based workstations. PAWorks is currently used primarily on Intel Pentium based PC's, with 16 Megabytes of RAM.

2.2 Distribution Files

The PAWorks installation for Windows comprises three disks containing all the source files.

2.3 Installation Procedures

To install PAWorks on your personal computer, insert the PAWorks diskette into your floppy drive. From within Microsoft Windows NT, choose File|Run, and specify the file name A:\SETUP. For within Microsoft Windows 95 or Windows NT 4.x, choose Run from the Start button, and specify the file name A:\SETUP. PAWorks will then be installed automatically with its own program group.

To install PAWorks on a Unix workstation, copy the files to a working directory, unzip them, and copy the executable files to your /bin directory.

3. USER INSTRUCTIONS FOR PC VERSION

To execute FracMan/PAWorks, select the FracMan/PAWorks icon, and double click with the mouse. Once the program is launched you will see the FracMan/PAWorks shell (Figure 3-1).

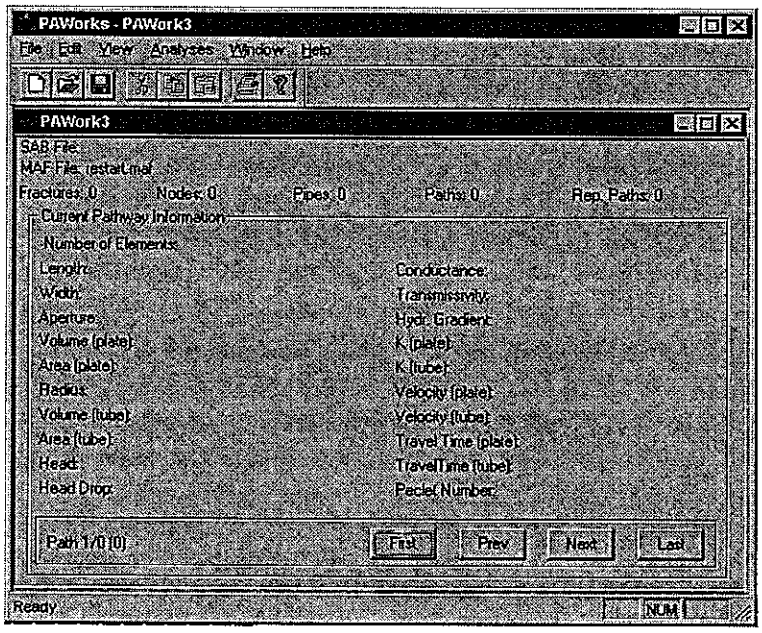

Figure 3-1 FracMan/PAWorks Shell

The shell contains the main window, containing all the menu items, and one or more current project windows. The project windows show the names of the files belonging to that project as well as basic statistics (i.e. number of fractures, node, pipes, paths and representative paths) and after an analysis is completed, the results (currently empty). The general sequence of a PAWorks session is:

1. Begin a new analysis and load source/sink and analysis parameter files.
   File|New
   File|Open
2. Define Analysis Parameters. This section includes specification of fracture files, pathway parameters, and information required to create LTG input files.
   Edit|Analysis Parameters
3. Perform PAWorks analyses to determine fracture intersections, pipe networks, head drops, and flow patterns.
   Analysis|Genpipes (Pipe Generation)
   Analysis|Mafic (Calculate Heads)
   Analysis|Path Search (Pathways Analysis)
   Analysis|Representative Path Generation
   Analysis|Penetration Depth

4. View and save the results.
   Window|3D View
   File|Save
   File|Save As
   File|Save All

This section describes how to navigate the menu system and use the mouse to take full advantage of PAWorks. Section 3.1 describes PAWorks input, Section 3.2 describes the various PAWorks analyses, and Section 3.3 describes the PAWorks graphical and textual output. Section 3.4 describes each menu command individually.

3.1 Input Files

In order to carry out a PAWorks analysis first a project has to be created. This is done by selecting the (**FILE|NEW**) menu option. Alternatively an existing PAWorks project can be loaded using the (**FILE|OPEN**) option.

FracMan/PAWorks generates head and flow information based on three things: the fracture network, specific boundary conditions and the analysis parameter settings.

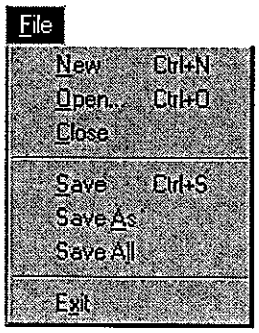

The boundary conditions are specified within FracMan/MeshMaker. FracMan creates a header file (.HDR) which needs to be converted to the .SAB file format using the utility HDRTOFAB.EXE. Once in .SAB format, the file may be read into PAWorks using the (**FILE|OPEN ...**) menu item. Once the .SAB file is loaded into the project it may be saved as part of a PAWorks project.

The .SAB file contains also contains all the analysis parameters (specified in the **EDIT|ANALYSIS PARAMETERS** menu). This information is may also be created and/or edited within the PAWorks environment and saved as part of the PAWorks project.

The fracture network is generated by FracMan/FracWorks and saved as a .FAB file. The fracture file(s) are specified in the **EDIT|ANALYSIS PARAMETERS|PIPE GENERATION** menu.

3.2 Analysis Parameters

PAWorks includes a wide variety of options for control of the analysis. After selecting **EDIT|ANALYSIS PARAMETER**, these can be changed using a tab user interface (Figures 3-2 to 3-9). The available options are summarized in Table 3-3.

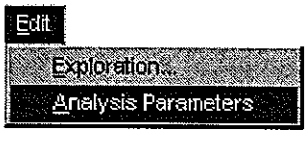

Table 3-1 Analysis Parameters

Head Calculation Parameters	section where options for calculating the heads are defined	
	LinearInterpolation	linear interpolation
	Mafic	finite element solution
	Mafic Restart File	using MAFIC restart file
Aperture Calculation Parameters	section where options for effective pathway aperture calculation are defined	
	Weighted	using weighting parameter same as graph traversal
	Use effective transmissivity	using effective transmissivity
	Use effective flux	using effective flux
	Use output flux	using the last flux value on the pathway
Pipe Generation Parameters	section where fracture files, pipe generation options and file locations are defined	
	SAB File	header file name
	MAFIC Transfer File	name to be used for the transfer file
	MAFIC Output File	results of MAFIC simulation
	Fracture Files	file(s) containing fracture network (.FAB)
(genpipes)	*Minimum Transmissivity*	truncation transmissivity used to prune fractures used in pipe network
	Merge Factor	minimum distance between two nodes
Search Parameters	section where path search options are defined	
	Primary Options	
	Compute Paths	compute PAW pathways
	Compute Clusters (LTG)	compute LTG downstream cluster output files
	Weight Generation Options	
	None	
	Transmissivity	
	Flux	
	Resistance	
	Travel Time	
	Pathway Options	
	Maximum Paths to Find	
	Maximum Branch/Source	
	Maximum Search Time	
	Fracture Area Factor	Used to scale the PAW and/or LTG pathway area

Table 3-3 (continued)

	Penetration Depth Options	
	Compute Penetration Depths	Select to do penetration depth computations
	Use Fractures	Compute penetration depths perpendicular to fractures
	One-dimensional Sampling	Use vertical boreholes to compute penetration depths
	Number of Samples	Number of samples to be used for one-dimensional sampling
	Fractures to be used in Penetration Depth Calculation	
	All Fractures	
	Pathway fractures only	Uses only the PAW pathway fractures
	Damkohler Fractures	Uses fractures with a Damkholer number less than the specified threshold
	Damkohler Threshold	Used only with Damkohler fracture option
Representative Pathway Generation Options	section where pathway generation options are defined for the representative pathway	
	Generate Representative Pathway based on:	
	Travel Time	
	Source Location	
	Sink Location	
	Max. Number of Src/Sinks	
	Max. Number of Branches	
	Weight Fraction	Include only pathways in the top weight fraction of weighted parameter in the representative pathways

Table 3-3 (continued)

Output Options	section where output options and file names are selected	
	Statistics File	PAWorks Results
	RIP Files	RIP Input File Results
	GeomView File	GeomView Input Files
	Diagnostics File	
	Dump runtime parameters	Additional detailed information on
	Dump Nodes	Pathways
	Dump Pipes	"
	Dump Adjacency Lists	"
	Dump Path Information	"
	Dump Representative Path Information	"
	LTG Output	Create LTG output files
Boundary Specification	section where boundaries are specified	
	Sources	
	Fractures	
	Fracture Sets	
	Boundary Groups	
	Sinks	
	Fractures	
	Fracture Sets	
	Boundary Groups	
LTG Parameters	section where options for LTG input files (if selected in search options)	
	Output Files	These names may not be changed by the user
	Additional Information	
	Title	Title to be used in LTG Output
	logprt	Select for detailed echo output
	Cauchy Boundary Type	Select for Cauchy boundary condition, unselected gives Dirichlet boundary condition
	Peclet Threshold	Used for pipe sub-division
	Dispersion Length	
	Infill Density	
	Infill Thickness	
	Output spacing	Select 0 for nodes on outflow boundary
	Output Times	
	Immobile zones	
	Nuclides	Number of radionuclides
	deltol	Numerical convergence

Table 3-3 (continued)

Level	Numerical Solution Parameter
nitmax	Maximum number of iterations
Order	Numerical Solution Parameter
Reduce	Numerical Solution Parameter
nterm	Numerical Solution Parameter
relerr	Numerical Convergence

The different options are described in detail in the following sections. Figures 3-2 to 3-9 show the graphical use interface to edit the analysis parameters.

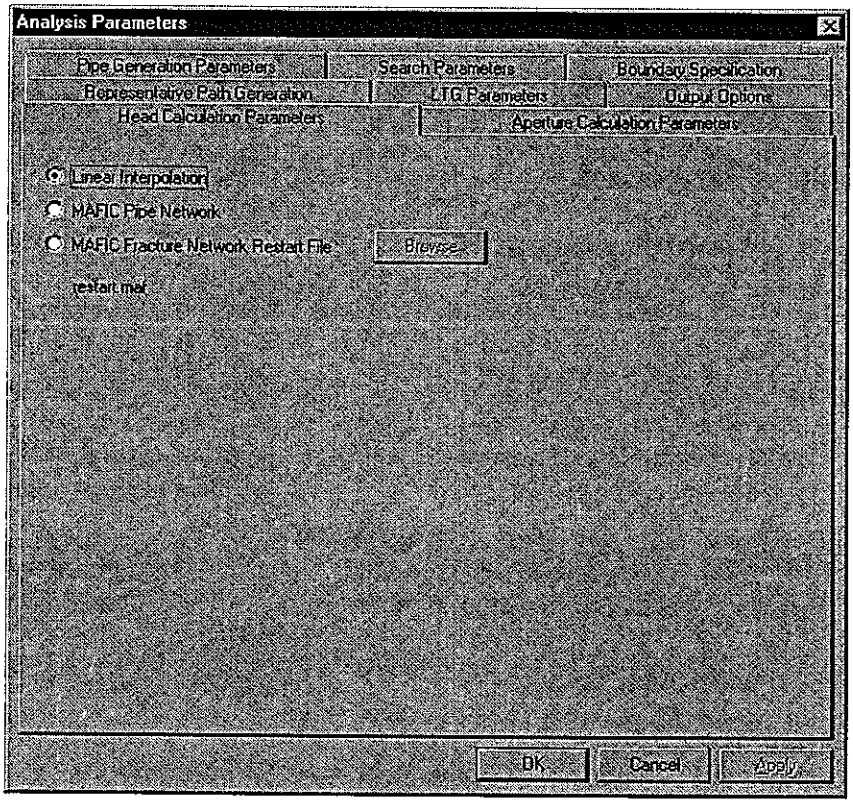

Figure 3-2 Analysis Parameters Head Calculation Menu

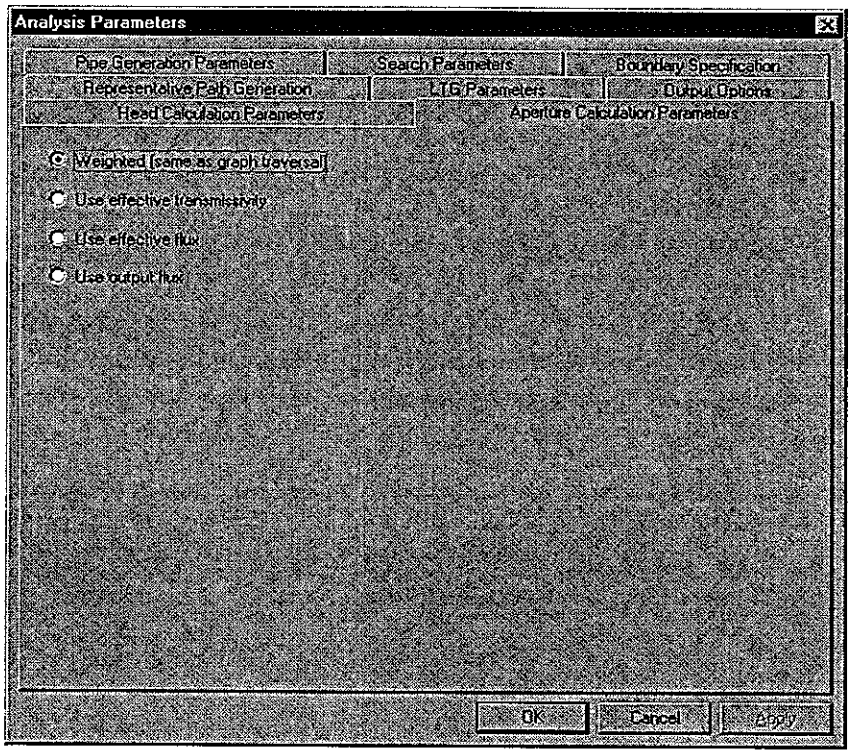

Figure 3-3 Analysis Parameters Aperture Calculation Menu

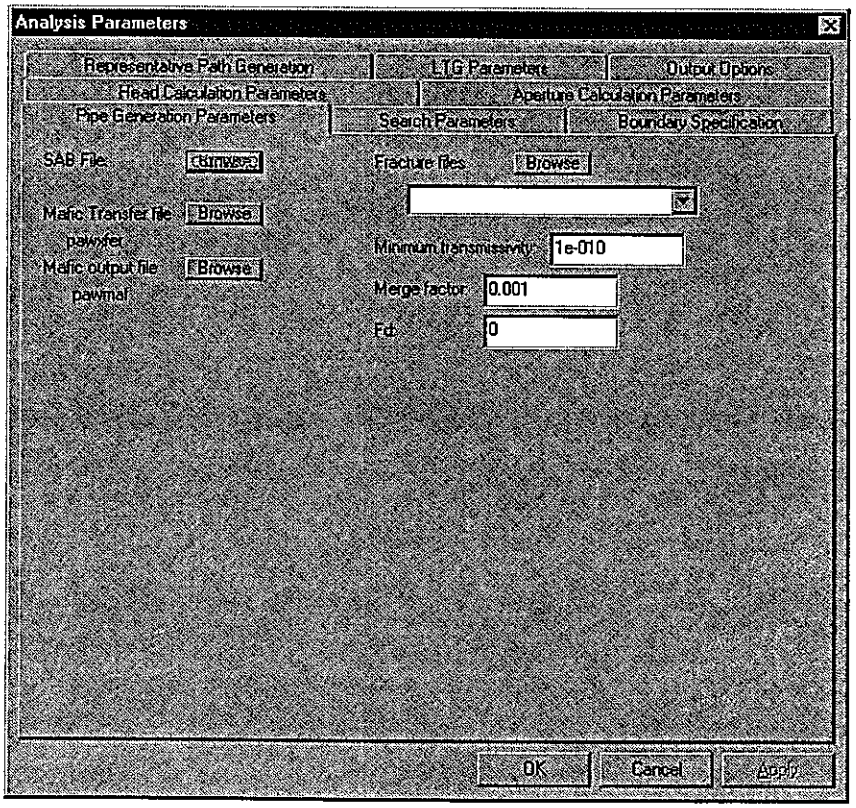

Figure 3-4 Analysis Parameters Pipe Generation Menu

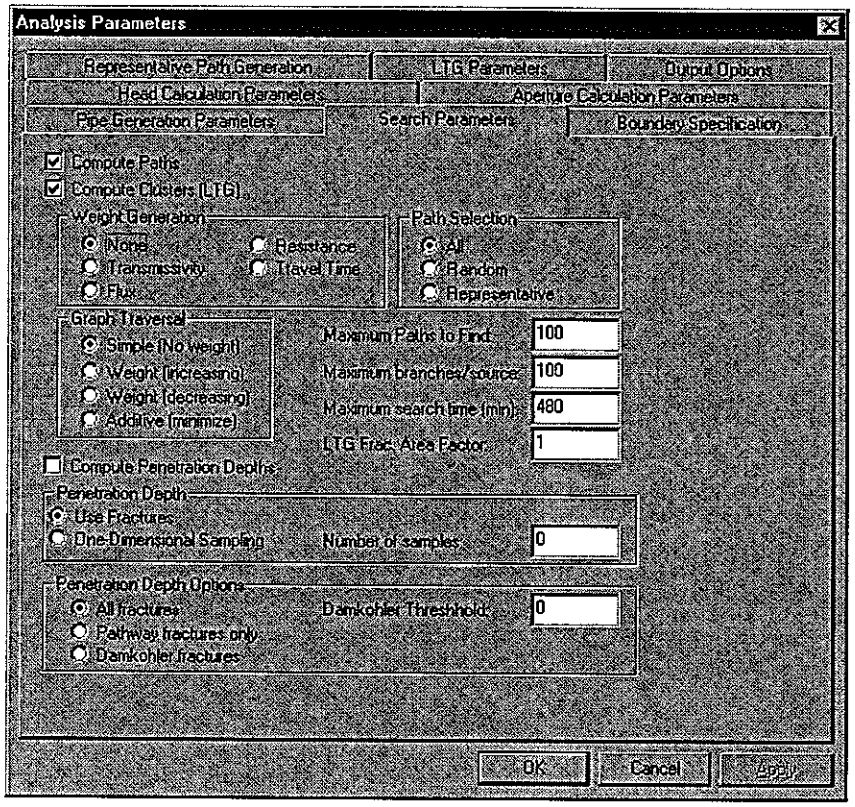

Figure 3-5 Analysis Parameters Search Parameters Menu

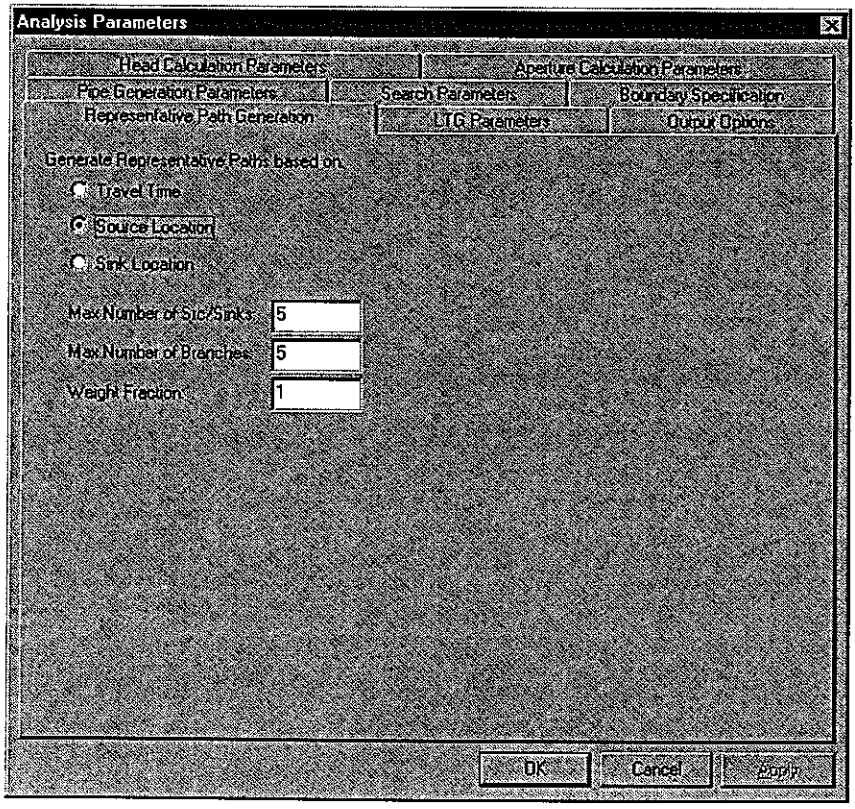

Figure 3-6 Analysis Parameters Representative Pathways Menu

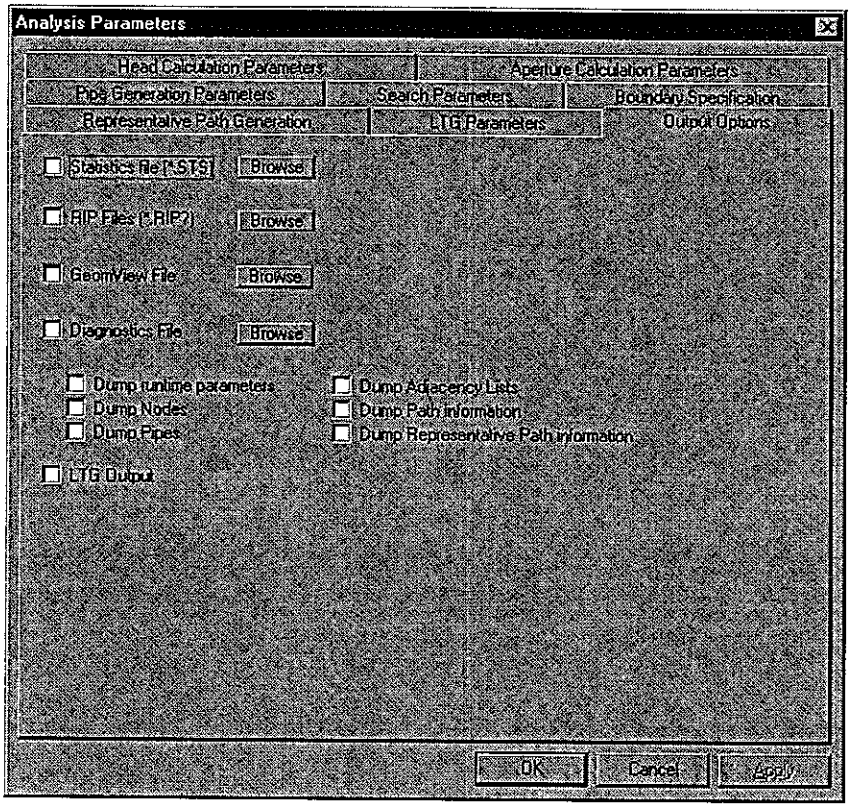

Figure 3-7 Analysis Parameters Output Options Menu

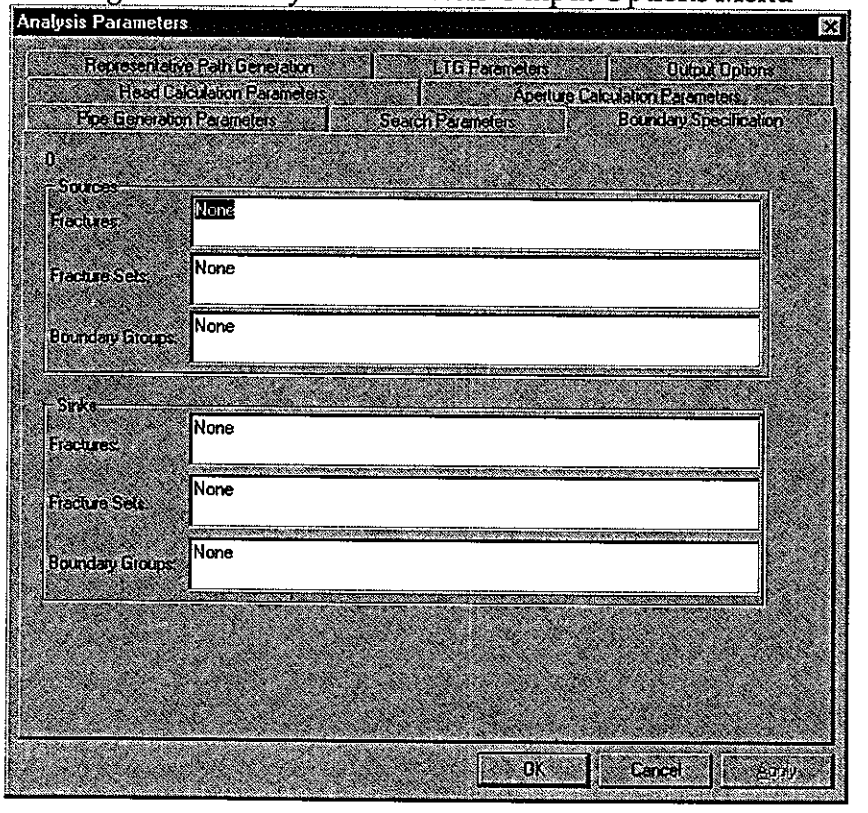

Figure 3-8 Analysis Parameters Boundary Specification Menu

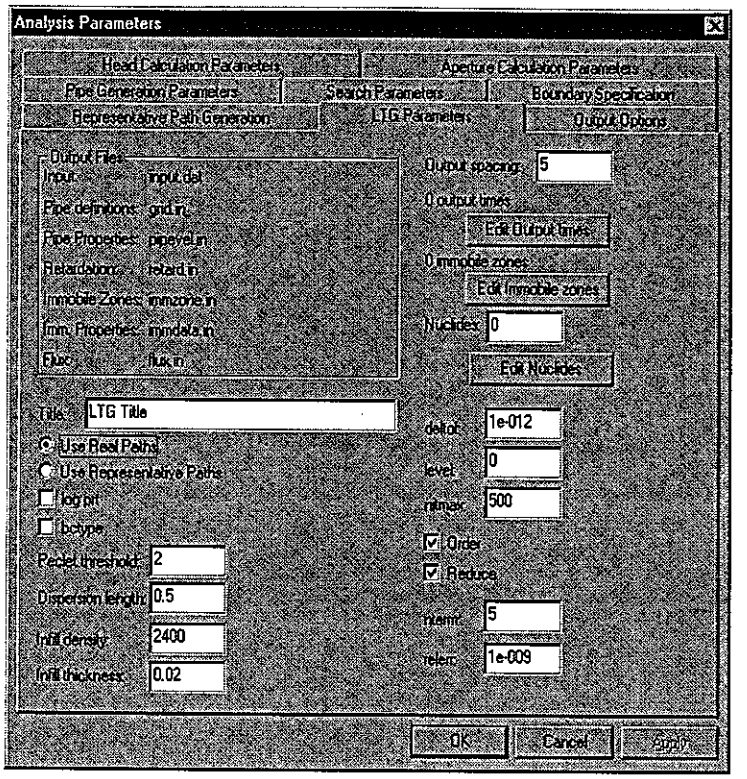

Figure 3-9 Analysis Parameters LTG Menu

3.3 PAWorks Analyses

The PAWorks analyses are the heart of PAWorks. The analyses are initiated by selecting from the Analyses menu, and are generally completed in sequence.

1. **Pipe Generation**
   Selecting **ANALYSES | PIPE GENERATION** initiates three things. First intersections between the planar fractures in the model are computed. Second, the intersections are reduced to zero-dimensional nodes and one-dimensional pipes are defined between the nodes. Finally, the pipes are assembled into an interconnecting network. To minimize computation time, only as many fractures as necessary should be included in the .FAB file.

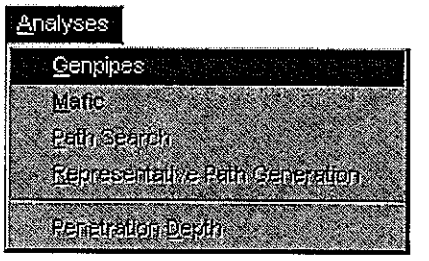

   During pipe generation an additional DOS window pops up, which shows the progress of the generation calculations. The window is closed automatically when the **generation** is finished.

2. **Head Field**

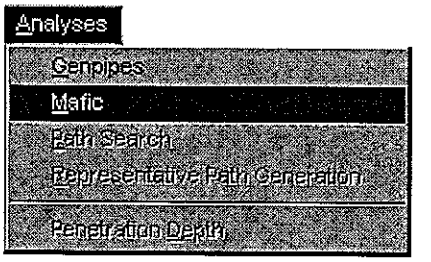

Upon selecting ANALYSES|HEAD GENERATION, PAWorks assigns heads using the head assignment option specified under analysis parameters. If the MAFIC option is calculated an additional DOS window is launched and MAFIC is started to provide the head calculation. The progress of the calculation can be monitored in the DOS window. The window closes automatically on completion of the calculation.

3. **Pathways Search**

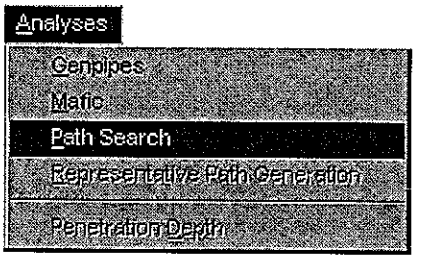

After the fracture network has been transformed to an **equivalent** pipe network, and heads have been assigned to each node, the pathways search may be initiated. Note that the ANALYSES|PATHWAYS SEARCH option has to be shown in black font, indicating that the menu option is active. The pathway search will end when one of three things happens:
1. The **search** parameters are exceeded, 2. all pathways have been found, 3. the user presses **[Stop]** on the button bar.

4. **Representative Pathway**

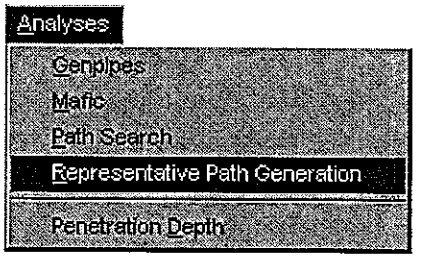

A **representative** pathway is calculated based on the parameters defined in the respective EDIT|ANALYSIS PARAMETER section. The representative pathway can be based on travel time or on source or sink location. Again, please note that this menu option only becomes available after the pathway search has been successfully completed (indicated by the black font).

5. **LTG Transport Analysis**

Input **files** for a solute transport analysis using the LaPlace Transform Gallerkin method can becreated for the full pipe network. The option for solute species, sorption, diffusion, and multiple parasites are provided as Analysis Parameters option.

6. **Penetration Depth**

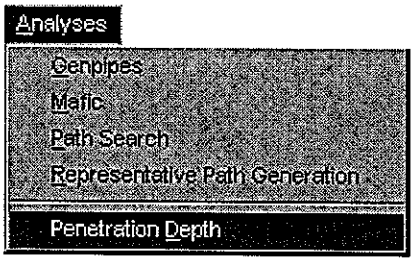

For each fracture in each pathway, the volume of rock associated with that fracture is calculated as illustrated in Figure 3-10. A perpendicular is drawn to the fracture at a point half way between the nodes. The intersections with this perpendicular are then identified. The penetration depth for each fracture on a pathway is then calculated as 25% of the distance between the fractures on either side of the fractures, measured along this perpendicular. Until **ANALYSIS/PENETRATION DEPTH** is selected, PAWorks displays all pathways information except for the rock block parameters.

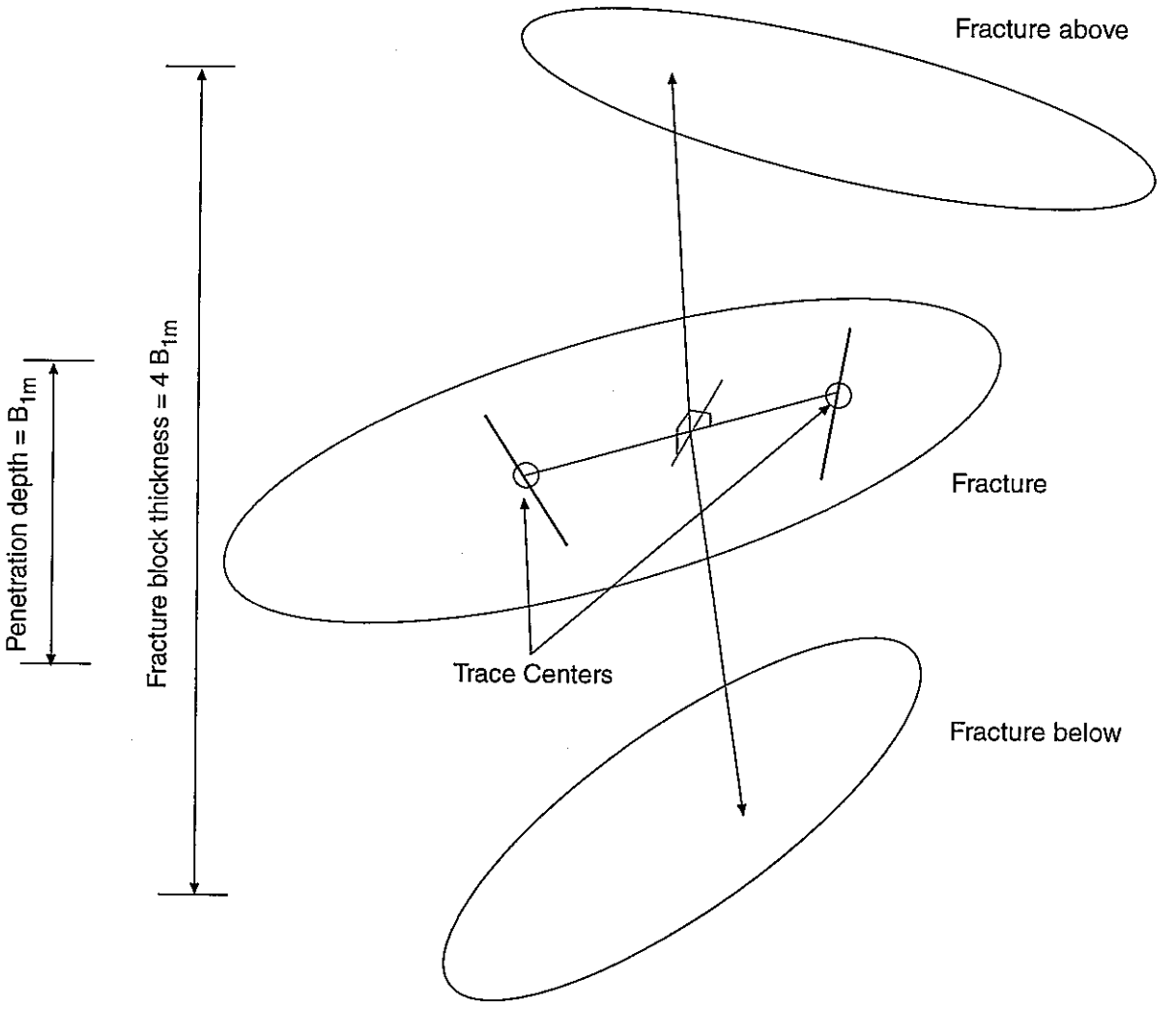

FIGURE **3-10**
PENETRATION DEPTH
PNC/PAWORKS

PROJECT NO. 923 1089.811 DRAWING NO. 72319 DATE 6/16/98 DRAWN BY TK

Golder Associates

3.3.1 Saving Analyses

At any time during the analysis, the user may choose to save the progress. Selecting **FILE|SAVE** will save all information so far loaded and derived by PAWorks including fractures, boundary conditions, intersections, pipe networks and pathways. During a later session, the analysis may be reloaded using **FILE|OPEN**.

3.4 Graphical and Text PAWorks Output

After the analyses are complete, the PAWorks user interface lists properties of each pathway one by one (Figure 3-11). Buttons labeled [FIRST], [PREV], [NEXT], and [LAST] allow the user to navigate through the found pathways. In addition to this summary information, the user may view the information graphically and output it to numerous text files which summarize the analysis results in a variety of ways.

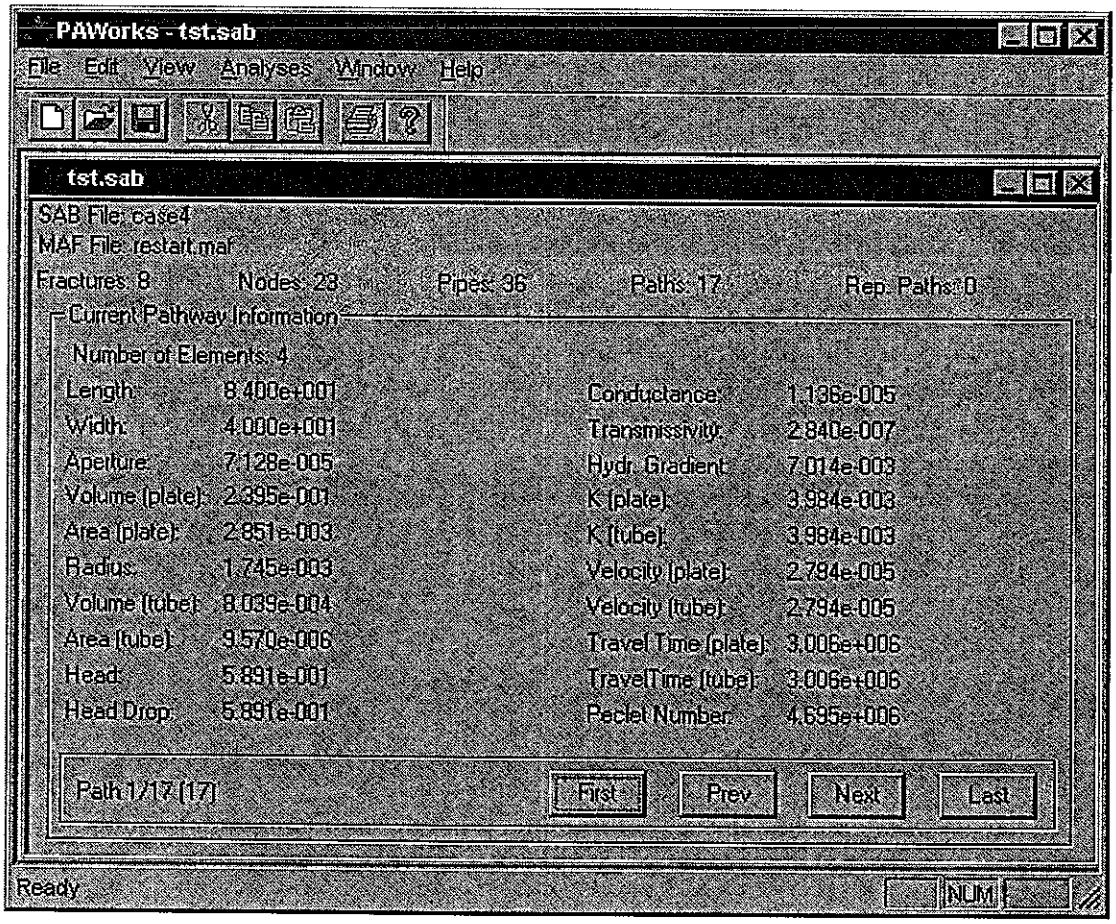

Figure 3-11 Pathway Search Results

3.4.1 Graphical Output

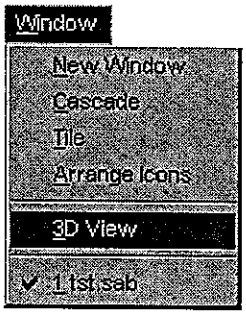

To view a three-dimensional representation of the fracture system, boundaries, pathways and head values, select **WINDOW|3D VIEW**. A new window opens as illustrated in Figure 3-12.
Note that the bottom of the **WINDOW** menu will now show a second entry for the project. Click on entry 1 or 2.to toggle between the pathway statistics and the 3D view windows. Each window may be resized manually, and by selecting **WINDOW|CASCADE** or **WINDOW|TILE** both windows may be displayed simultaneously. It may be advantageous to view both the three dimensional representation and the statistics of the pathways at the same time.

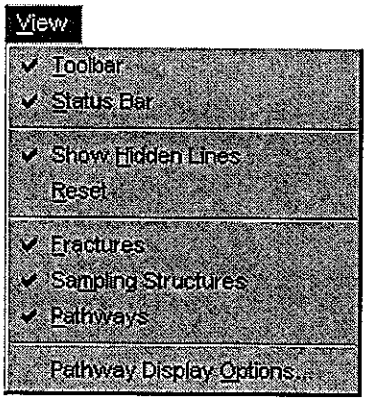

Once the 3D view window is open, there are a number of ways to manipulate it, to allow the user to view precisely what is wanted. The options are selected using the **VIEW** menu:
Fractures, boundaries (a.k.a. sampling structures), and pathways may be viewed individually or together by toggling their display using **VIEW|FRACTURES**, **VIEW|SAMPLING STRUCTURES** and **VIEW|PATHWAYS**. The user may also choose to show or hide hidden lines (making the fractures either transparent or opaque) by toggling **VIEW|SHOW HIDDEN LINES**. Finally, the user may display only certain pathways by selecting **VIEW|PATHWAY DISPLAY OPTIONS**. The pathway display options menu allows the user to select the number of pathways to display, and the method to select which pathways are displayed: representative paths, random paths or all paths.

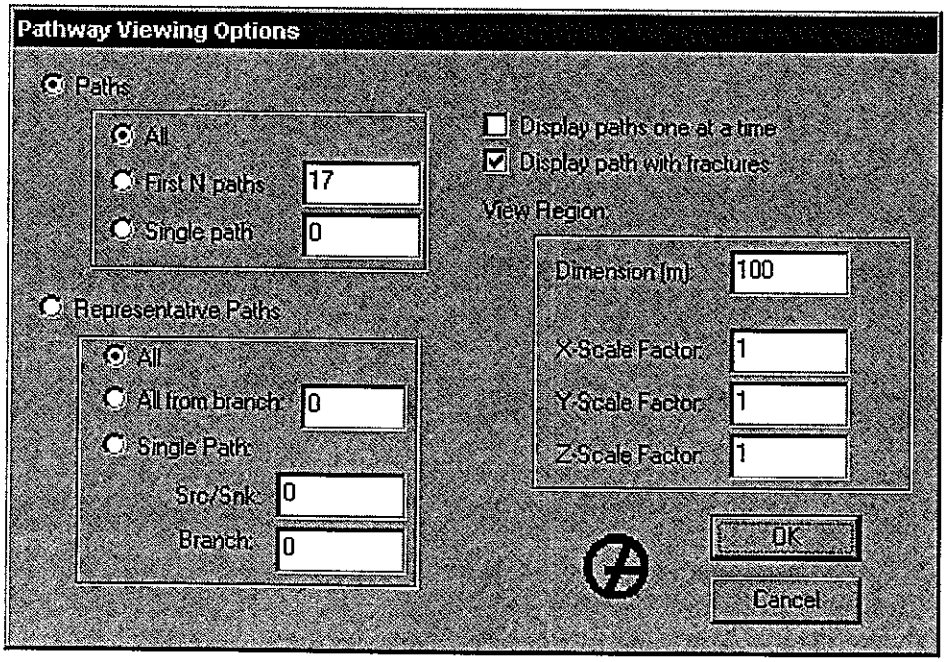

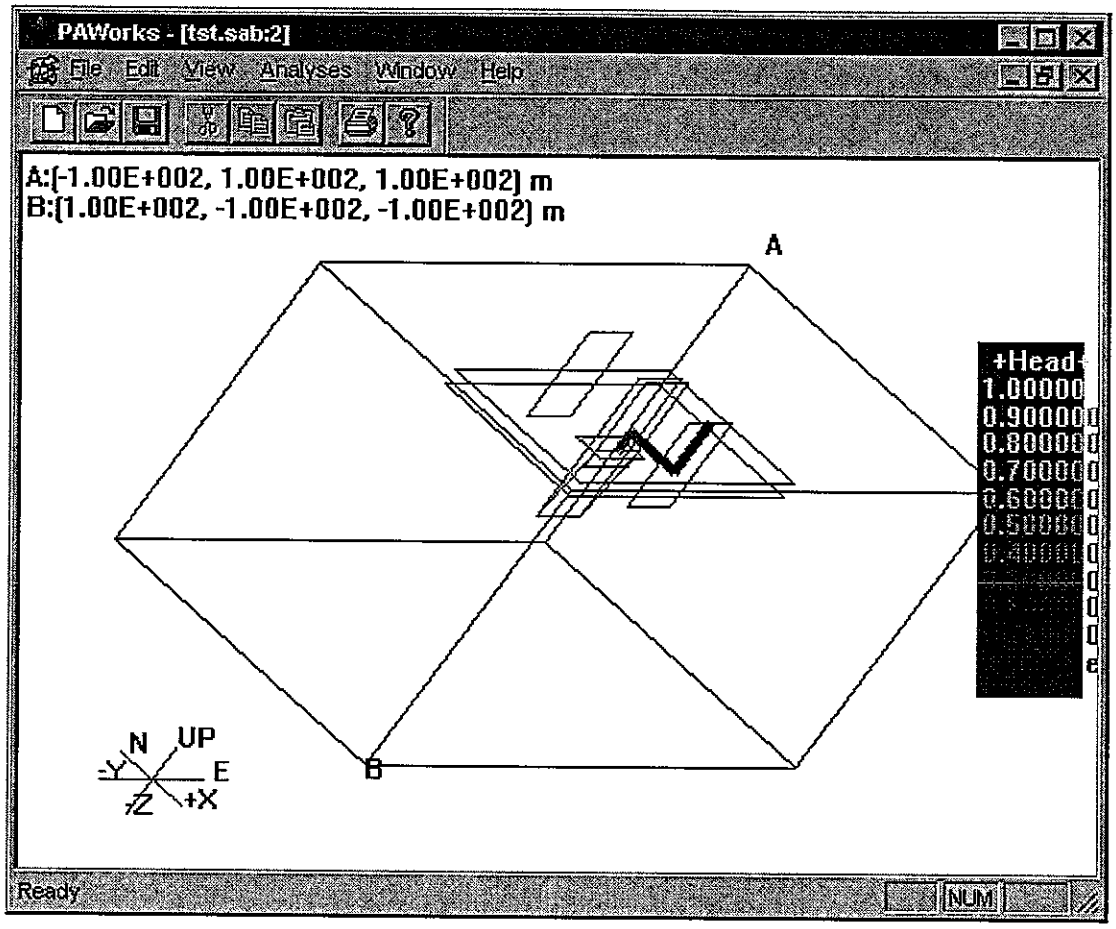

Figure 3-12 3D View Window

Using the mouse and certain buttons, the image of the model may by zoomed or rotated:

- **Rotate:** Press and hold the *right mouse button* while dragging the mouse up, down, right or left.
- **Zoom:** Press and hold *shift and the right mouse button* while dragging the mouse up to zoom out or down to zoom in.

3.4.2 Text Output Files

Pipe network and pathway information may be saved to a text file by using FILE|SAVE AS then choosing the .STS file type. Five files are saved using PNC specified formats (described in Table 3-4) with the filenames, PA1_##.STS, PA2_##.STS, PA3_##.STS, PA4_##.STS, and PA5_##.STS. The "##" denotes a serial number which PAWorks assigns -- the first time save is used, the number 00 is assigned, the second time 01 is assigned and so on. Note: this numbering sequence returns to 00 when each time PAWorks is loaded, take care to avoid overwriting a previous sessions output!

Table 3-2 PAWorks Statistical Output Files

File	Description
PA1_##.STS:	equivalent pipe or plate flow and transport properties of the fractures which make up each pathway,
PA2_##.STS:	equivalent pipe or plate flow and transport properties of pathways,
PA3_##.STS:	coordinates of fracture intersections along each pathway,
PA4_##.STS:	coordinates of "representative" pathway
PA5_##.STS:	"representative" pathway values formatted for CRYSTAL input file.

4. PAWORKS ON UNIX

4.1 General

The general sequence of a PAWorks analysis on a UNIX workstation is the same as on a PC. It consists of the following steps:

1. Generation of a discrete fracture network (DFN) model using FracMan/FracWorks
2. Conversion of the DFN into a pipe network (genpipes)
3. Calculation of the flow solution for the pipe network (MAFIC)
4. Pathway search (PAW)
5. Simulation of solute transport (LTG)

Unlike for the PC however, there is no graphical user interface combining the various modules for the UNIX operating system. The analysis is controlled by the user using ASCII input data files and UNIX commands. The following section describes all necessary steps and data formats in detail. Using the information provided an inexperienced UNIX user should be able to run PAWorks on UNIX and benefit from the significantly larger computational power of a UNIX workstation.

4.2 GenPipes

The GenPipes code generates a pipe network from a fracture network file (.FAB) and a file containing the boundary conditions (header file with .SAB extension). GenPipes works very much like MeshMaster. It is a mesh generator and it discretizes the fracture network into finite elements. The finite elements are one dimensional and specifically tailored to work with MAFIC. They are referred to as pipes in the remainder of this document.

4.2.1 Starting GenPipes

GenPipes is started by typing `genpipe` at the prompt. If this is not working, make sure that your path is set to the location of the GenPipes program. When starting GenPipes you should see:

```
*******************************************
**    GenPipes Version 1.22                **
**    Copyright Golder Associates Inc.      **
*******************************************

Enter name of header file >
```

GenPipes prompts you to provide the name of the header file containing the boundary condition information. Only provide the file name root, without extension. GenPipes already uses the improved .SAB file type which will be standard in all Windows versions of FracMan. If you are using a DOS-version of FracMan for creating your header file you have to convert the old .HDR file format into the new .SAB-format. You can use the

included utility program HdrToSab.exe to do this. The PC version of PAWorks also allows the user to create a new .SAB format header file interactively.

The next line prompts you to provide the output file name:

```
Enter name of output file >
```

Again, only input the file name root, because the file name extension is automatically set by GenPipes. The output from GenPipes is a .MAF file in the format for MAFIC. The file contains header information, the x, y, z coordinates of all nodes and a section describing the one dimensional finite elements (pipes). An example of the file format can be found in Appendix B.

Next you need to specify the type of input file for your fracture network data:

```
Input file type (1) fracture (.fab) (2) intersection >
```

There are two different options

1. fracture FracMan output file format (.FAB)
2. intersection GenPipes restart file

Only files compatible to FracWorks Version 2.60 (.FAB) can be used. The old .DCM or .BAB file formats are no longer supported in GenPipes. The included utility programs DcmToFab.exe and BabToFab.exe can be used to convert old FracMan files. See the FracMan manual for more information on FracMan file formats. The restart option can be used to re-run GenPipes using the files generated by a previous Genpipes simulation. The intersection option saves a significant amount of computation time because it uses previously generated files and does not need to regenerate the fracture intersection locations.

The next input parameterspecifies the number of fracture network files to use:

```
Number of fracture files >
```

Because the fracture network files are normally generated on the PC you may encounter some limitations regarding the maximum number of fractures that can be handled. GenPipes allows you to combine multiple fracture files, thus allowing the user for example to generate fracture sets separately on the PC and later blend them together on the more powerful workstation. Note that the code will ask you for the number of fracture files even if you choose the intersection option.

The user is then prompted for the fracture network input file name root for each fracture file:

```
Enter file name >
```

Again Genpipes will ask you for this information even if you have selected the intersection option. However, the intersection option will not use the files in the

computation; instead it uses the interxs.xyz, transfm.mtx and farea.bin files created by a previous Genpipes simulation.

If GenPipes can find the specified file name(s) the user has four different options to generate the pipe network:

```
Generation of pipe network on each fracture :

   (1) All possible pipes
   (2) Pipes do not cross traces
   (3) Pipes in (2) plus new pipes that make the pipe network
       connect all nodes on the fracture
   (4) Pipes in (2) plus more pipes with effective distance
       between two nodes

Enter (1, 2, 3 or 4) >
```

The options mean the following:

1. All pipes that can be formed from the midpoints of the traces. The only restriction is that a new pipe cannot cross an existing one.
2. Pipe generation identical to (1) apart from the additional restriction that pipes are not allowed to cross traces, and that each node (located at the mid-point of each trace) has at least one pipe connected.
3. Pipes from (2) plus additional pipes to ensure that all pipes on the same fracture are connected to each other.
4. Pipes from (3) plus effective pipes. An effective pipe will be formed when the pipe pathway distance between two nodes is greater than an effective pipe factor times the cartesian distance between the nodes.

Regardless of the option chosen the user is currently asked for the effective pipe path factor. Note however, that this factor is not used for options (1) to (3).

```
Factor of effective pipe path ( > 1.0 ) >
```

The recommended range for the factor is between 1.2 to 3.0.

The next parameter that has to be provided by the user affects when nodes are merged. The user is asked to input a minimum distance between two nodes. Any nodes closer to each other than this minimum distance will be merged and treated as a single node.

```
Merge distance between two nodes in [m] >
```

Next the user is prompted for the minimum transmissivity to be used in the pipe generation process:

```
Minimum transmissivity   >
```

Fractures whose transmissivity is smaller than the minimum transmissivity assigned by the user will be effectively deleted, and not used to generate the finite element mesh.

The aperture which is assigned to a pipe can be defined in two different ways:

```
Assign transport aperture (A):
    (1) from .FAD file (2) from transmissivity, T

 Enter 1 or 2 >
```

Option (1) reads the aperture values directly from the FracMan output file, i.e. the aperture has been calculated by FracMan using the distribution(s) defined there. The user however, has the possibility to scale the aperture using a constant:

```
A= a1*Aperture,    a1= >
```

When selecting option (2) the aperture is calculated from the transmissivity of the fracture using the following equation:

$$A = a_1 * T^{a_2} \qquad \text{(Equation 4-1)}$$

The form of the equation allows a large variety of functions (e.g. the power law) to be considered when describing the relationship between fracture transmissivity and aperture, thus giving the user a high amount of flexibility. The user is asked to provide the parameters a1 and a2:

```
A= a1*T**a2,    a1,a2= >
```

Next the user specifies how GenPipes should compute the fracture width to be assigned to a pipe:

```
Assign pipe width (W):
    (1) W=a*L_min + b*L_max
    (2) W=(a*L_min + b*L_max) * C, where
        C=sum of {Wi*Li} / A_f

 Enter 1 or 2 >
```

The first option allows the user to define the weighting of the lengths of the two traces making up the pipe. Using a=b=0.5 will produces the arithmetic mean. Option two allows you to scale the width by the area of the fracture the pipe is representing. A value of C close to 1 is recommended. See the theoretical background section for more details.

After choosing an option the user can select how the trace lengths L_{min} and L_{max} are calculated:

```
Trace length (L_min, L_max) calculated from
    (1) length  (2) projected length >

 Enter 1 or 2 >
```

Either the original trace length or the projected length perpendicular to the pipe direction can be used.

Finally the values for a and b (pipe width option 1), or a, b and C (pipe width option 2) have to be provided:

```
Enter a, b >
```

or

```
Enter a, b, C >
```

GenPipes should now start the calculations.

4.2.2 GenPipes Output

The output from GenPipes is a .MAF file. The file contains header information, the x, y, z coordinates of all nodes and a section describing the finite elements.

4.2.3 Running GenPipes in Batch Mode

GenPipe can be run in batch mode using standard UNIX piping commands:

```
genpipes < filename
```

where `filename` is the name of the GenPipes input file. The input file contains the same information which would normally be provided when running GenPipes interactively. Each input is stored on a separate line within a standard ASCII text file.

4.3 EdPipe

EdPipe is an interactive pipe editing program which can be used to improve finite element meshes (pipe networks) created by GenPipes. An improved mesh is less likely to produce numerical problems during the flow simulation and can result in faster computation times.

4.3.1 Starting EdPipe

EdPipe is started by typing `edpipe` at the prompt. If this is not working, make sure that your path is set to the location of the EdPipe program. When starting EdPipe you should see:

```
EdPipe Version 1.200

-- Assign Pipe Properties --

-- Reset Boundary Conditions --

MAFIC Pipe Editing Utility

Copyright Golder Associates Inc., 1997


Name of file to change >
```

EdPipes prompts you to provide the name of the input file. This is the GenPipes output file (.MAF), which contains the finite element mesh (pipe network) for MAFIC.

Next the user can define a problem title to describe the changes made by EdPipe.

```
Problem Title     >
```

Following this the main menu is displayed:

```
**** MAIN MENU ****

  (0) Quit without saving changes!
  (1) Merge or remove pipes
  (2) Assign properties (T, S or A)
  (3) Reset conditions for a specific boundary
  (4) Save EdPipe file
  (5) Run  EdPipe

Selections >
```

The main menu contains six options:

0. Quit EdPipe.
1. Set parameters to merge or remove pipes.
2. Assign fracture properties (Transmissivity, Storativity, or Aperture).
3. Reset conditions for a specific boundary.
4. Save the parameter settings to an EdPipe runfile and leave EdPipe.
5. Run EdPipe using the current settings.

On selecting option (1) ("merge or remove pipes") the user is presented with three options for improving mesh quality:

```
  0- Keep unconnected pipes;
  1- Remove pipes which are not connected to head boundary;
  2- Remove pipes which are not connected to any kinds of
     boundaries;
Enter index for removal of pipes [0, 1, 2] >2
```

The first option only optimizes the finite element mesh. It does not remove any pipes. Options (1) and (2) will optimize the mesh **and** remove the pipes that are not connected to the specified boundaries.

The first action in optimizing the mesh is to remove extremely small pipes:

```
Minimum pipe length    >
```

The second action is to remove pipes whose transmissivity is below a user defined threshold value:

```
Minimum Transmissivity >
```

EdPipe then returns to the main menu.

You can now choose further Edpipe options (2) or (3), run EdPipe by selecting option (5) from the main menu, or you can save the settings by selecting option(4) and run EdPipe in batch mode. EdPipe will save the parameter setting to the file `edpipe.set`. Note, that EdPipe will automatically quit after saving.

To change pipe properties within EdPipe choose option (2), assign fracture properties. On selecting this option you will see the following options;

```
**** ELEMENT PROPERTIES ***
 (0 ) Quit, return to main menu
 (1 ) Assign Transmissivity
 (2 ) Assign Storativity
 (3 ) Assign Aperture

Selection >
```

The first option returns the user back to the main menu.

The second option allows the user to reassign fracture transmissivities. On selecting this option the user is presented with the following screen;

```
(0) Quit, return to previous menu
(1) Exponential correlation to A
(2) Linear correlation to A
(3) Uncorrelated to original T

    Enter 1, 2 or 3 >
```

The "Exponential correlation to A" option assigns the fracture transmissivities as an exponential function of the original pipe aperture, A (e.g. the Cubic law). For this option the following menu is displayed.

```
Formula:  T = Xo + A^[ bX + N(0,eX)]
Enter parameters (Xo, bX, eX) >
```

If the linear correlation option is chosen the following menu is displayed;

```
Formula:  T = Xo + A*[ bX + N(0,eX)]
Enter parameters (Xo, bX, eX) >
```

The final option, uncorrelated to original transmissivity, allows the user to remove any correlation between aperture and transmissivity. For this option the following menu is displayed;

```
Formula:  T = Xo + 10^[ bX + N(0,eX)]
Enter parameters (Xo, bX, eX) >
```

The parameters Xo, bX and eX assign an exponential relationship.

You can now run EdPipe by selecting option (5) from the main menu, or you can save the settings by selecting option(4) and run EdPipe in batch mode as described earlier. For both these options the following screen is shown;

```
Seed value for random numbers >
```

This screen is displayed if any of the assign transmissivity options is selected, however the seed value is only used if the transmissivity is uncorrelated to the aperture.

Returning to the element properties menu, the second selection is "Assign Storativity". The user options for assigning fracture storativity are;

```
(0) Quit, return to previous menu
(1) Exponential correlation to T
(2) Linear correlation to T
(3) Uncorrelated to original S

    Enter 1, 2 or 3 >
```

This menu is essentially the same as that used for the transmissivity assignment, except now the reference parameter to assign storativity is transmissivity, T (not aperture). The three menus associated with the three options are;

Exponential correlation to T -

```
Formula:  S = Xo + T^[ bX + N(0,eX)]
Enter parameters (Xo, bX, eX) >
```

Linear correlation to T -

```
Formula:  S = Xo + T*[ bX + N(0,eX)]
Enter parameters (Xo, bX, eX) >
```

Uncorrelated to original S -

```
Formula:  S = Xo + T^[ bX + N(0,eX)]
Enter parameters (Xo, bX, eX) >
```

Again on saving the Edpipe file by selecting option (4) , or running EdPipe interactively by selecting option (5) the user is prompted for a seed for the random number;

```
Seed value for random numbers >
```

This screen is displayed if any of the assign storativity options is selected, however the seed value is only used if the storativity is uncorrelated to the transmissivity.

The last fracture property that the user may change from within edpipe is aperture. The user options for assigning fracture aperture are;

```
(0) Quit, return to previous menu
```

```
(1) Exponential correlation to T
(2) Linear correlation to T
(3) Uncorrelated to original A

    Enter 1, 2 or 3 >
```

This menu is essentially identical to that used for the storativity assignment, with the reference parameter to assign aperture being transmissivity, T. The three menus associated with the three options are;

Exponential correlation to T -

```
Formula:  A = Xo + T^[ bX + N(0,eX)]
Enter parameters (Xo, bX, eX) >
```

Linear correlation to T -

```
Formula:  A = Xo + T*[ bX + N(0,eX)]
Enter parameters (Xo, bX, eX) >
```

Uncorrelated to original A -

```
Formula:  A = Xo + T^[ bX + N(0,eX)]
Enter parameters (Xo, bX, eX) >
```

Again on saving the Edpipe file by selecting option (4) , or running EdPipe interactively by selecting option (5) the user is prompted for a seed for the random number;

```
Seed value for random numbers >
```

This screen is displayed if any of the assign aperture options is selected, however the seed value is only used if the aperture is uncorrelated to the transmissivity.

Note only one seed value is required, irrespective of whether transmissivity, storativity and aperture are changed.

Returning to the main menu, repeated again below, the user has the option of reassigning the boundary condiditons for a specific boundary.

```
**** MAIN MENU ****

      (0) Quit without saving changes!
      (1) Merge or remove pipes
      (2) Assign properties (T, S or A)
      (3) Reset conditions for a specific boundary
      (4) Save EdPipe file
      (5) Run  EdPipe
```

The screen display on choosing option (3) is

```
Boundary to reset >
```

The user should type in the number of the boundary to be edited. On hitting <return> the following menu is displayed.

```
(1) Constant H: H(x,y,z) = F(Hx,Hy,Hz,Ho)
(2) Constant H: H(x,y,z) = Conditioned field data
(3) Constant Q: Q(x,y,z) = F(Qx,Qy,Qz,Qo)
(4) Constant Q: Q(x,y,z) = Conditioned field data
(5) Variable H
(6) Variable Q
(7) Group Flux

Select boundary type  >
```

Option (1) assigns the boundary as a constant head boundary of the type

$$H = Hx.x + Hy.y + Hz.z + Ho$$

The screen prompt is

```
Enter 4 data: [Hx,Hy,Hz,Ho]    >
```

Option (2) reassigns the boundary using the head information stored in a .SAB file

The screen prompt is

```
runit = -20
Enter .sab file name    >


**** Conditioned Field ****
Conditioned field object name    >

# of the nearest points to be considered (0<N<10), N=

Weighting function W_i = 1/(D_i**p); where D_i is
the distance between element centroid and and field.

Enter exponent of the weighting (p > 0), p =
```

Option (3) assigns the boundary as a constant flux boundary of the type

$$Q = Qx.x + Qy.y + Qz.z + Qo$$

The screen prompt is

```
Enter four data: [Qx,Qy,Qz,Qo]    >
```

Option (4) reassigns the boundary using the flux information stored in a .SAB file

The screen prompt is

```
runit = 20
AF runit       20***.sab
```

```
**** Conditioned Field ****
Conditioned field object name    >

# of the nearest points to be considered (0<N<10), N=

Weighting function W_i = 1/(D_i**p); where D_i is
the distance between element centroid and and field.

Enter exponent of the weighting (p > 0), p =
```

Option (5) assigns the boundary as a variable head boundary. The screen prompt is

```
  Number of field data pairs >

  Enter data pairs:

  Time    Grpflx
1>
2>
```

Option (6) assigns the boundary as a variable flux boundary. The screen prompt is

```
  Number of data pairs >

  Enter data pairs:

  Time    Grpflx
1>
2>
```

Option (7) assigns the boundary as a group flux boundary. The screen prompt is

```
  Number of data pairs >

  Enter data pairs:

  Time    Grpflx
1>
2>
```

4.3.2 EdPipe Output

EdPipe produces a .MFT file which has the same format as the .MAF file. The EdPipe output file can be read as input directly into MAFIC.

4.3.3 Running EdPipe in Batch Mode

EdPipe can be run in batch mode using standard UNIX piping commands:

```
edpipe <filename
```

where `filename` is the name of the EdPipe input file (e.g. edpipe.set). The EdPipe input file contains exactly the same information as the user would type when running EdPipe interactively. Each input is stored on a separate line within a standard ASCII file.

If you use EdPipe to generate the input file it is necessary however to make two changes to the edpipe.set file before it can be used:

1. add a line at the beginning of the file (line 1) and add the file name root for the input file (.MAF). This is currently not saved automatically by EdPipe.
2. change the last line from

```
2      [ Save EdPipe file ]
```

to

```
3      [ Run EdPipe ]
```

To change to runfile from saving the settings to running EdPipe.

4.4 MAFIC

MAFIC is the finite element solver used to calculate the flow solution for the pipe or three dimensional plate fracture network.

The only differences between the 1-D MAFIC input files and those used for 3-D networks are:

1. the parameter I2D in the 3rd line of the input file is set to 1 for the 1-D pipe network .
2. there are only two nodes for each pipe finite element instead of three for the 3-D fractures.
3. the properties 3, 4 and 5 are automatically set to the pipe properties width, trace length 1 and trace length 2

Please see the MAFIC manual for more details on MAFIC file formats. It is not recommended to change MAFIC input files other than the header information.

4.4.1 Starting MAFIC

MAFIC is started by typing `mafic` at the prompt. If this is not working, make sure that your path is set to the location of the MAFIC program. When starting MAFIC you should see:

```
ENTER DATA FILE NAME:
```

MAFIC prompts you to provide the name of the input file. This is the EdPipe output file (.MFT), which contains the finite element mesh (pipe network) for MAFIC. Because

MAFIC would also accept .MAF files you need to specify the complete file name this time (i.e. including the file extension).

Next you are asked for the output file name:

```
ENTER OUTPUT FILE NAME:
```

Again, specify the full file name including extension.

4.4.2 MAFIC Output

MAFIC produces up to two output files. The first is the results file which has the name you specified as output file name. The second is a restart file which is used by PAW. This file automatically gets the name `restart.maf`. If you do not get a restart file make sure that the parameter `iStart` in the first line of the MFT file is set to 1 (or set `istart` to 1 in the header file prior to mesh generation). It is prudent to rename the restart file once it has been created to avoid overwritting it the next time you run MAFIC.

4.5 PAW

PAW is the Unix version of the core of the PAWorks program on the PC. Like PAWorks it uses a graph-theory search algorithm to find pathways within a pipe network between a source and a sink specified by the user.

4.5.1 Starting PAW

PAW only runs in batch mode. You start PAW by typing:

```
paw filename
```

at the prompt. `filename` is the complete filename of the PAW input file including the .SAB extension.

4.5.2 PAW Input File

The PAW input file is a standard ASCII file which can be created or edited using any standard ASCII text editor (e.g. vi). The input to paw is object oriented using a keyword system. Each section begins with the keyword BEGIN and ends with the keyword END. Within each section certain keywords followed by the respective input parameters are used to retrieve the input data. Nesting of sections is allowed.

The input file for PAW has a mandatory main part and an optional second part. The first contains the PAW pathway search parameters. The optional second part contains the information required to generate input files for the solute transport code LTG. Table 4-1 contains an example of the mandatory part of the input file for PAW. The meanings of the options are summarized after Table 4-1, and a more detailed description of most options may be found in Section 5 of this report.

Table 4-1 Example of PAW Input File

```
#
#  Example of .SAB file for PAW
#

BEGIN paworks_runtime
   dopath = 1
   docluster = 0
   BEGIN frac_files
      watari7a
   END


   BEGIN head_calc
      head_calc_type = file
      maf_file = restart.maf
   END

   BEGIN aperture_calc
      apert_calc_type = weighted
   END

   BEGIN path_search_options
      path_weights = flux
      path_search  = weight_larger
      max_num_paths = 200
      max_branches = 10
      compute_penetration = TRUE
                     depth_option = fracs
                     depth_fracs = path_fracs
                     depth_samples = 50
                     damk_thresh = 100.
      Fa = 1.
   END

   BEGIN rep_path_generation
      path_option  = source
      max_roots    = 10
      max_branches = 10
      weight_fraction = 1.
   END

   BEGIN source_def
      BEGIN bdry_groups
      END
      BEGIN frac_sets
         3-6
      END
      BEGIN frac_ids
      END
   END

   BEGIN sink_def
      BEGIN bdry_groups
         4
      END
      BEGIN frac_sets
      END
      BEGIN frac_ids
      END
   END

   BEGIN pa_output
      rip_file = watari01
      sts_root = watari01
      view_transfer = paw.list
   END
END
```

The parameters of the input file are:

#	the '#' symbol is used to add comments		
dopath	option to select PAWorks pathways analysis		
docluster	option to select LTG fracture network files		
frac_files	section containing the file name root for the fracture file (.FAB)		
head_calc	section defining the head calculation method		
	head_calc_type	options to calculate heads	
		linear	linear interpolation
		mafic	finite element solution
		file	using MAFIC restart file (maf_file)
aperture_calc	section defining the effective pathway aperture calculation method		
	apert_calc_type	options to calculate effective pathway aperture	
		weighted	same as for the main traversal process
		use_T	using weighted transmissivity
		use_Q	using weighted flux
		use_Qout	using the last flux value on the pathway
path_search_options	section defining the path search options		
	path_weigths	weighting property options	
		none	
		transmissivity	
		flux	
		resistance	
		travel_time	
	path_search	weighting search options	
		simple	no weighting
		weight_larger	use larger weight to find next pipe
		weight_smaller	use smaller weight to find next pipe
		minimize_weight	minimizes weight for all pipes
	max_num_paths	maximum number of pathways to be traversed by PAW	
	max_branches	number of branches (maximum) to be generated from each source for PAW traversals	

	compute_penetration	switch to compute fracture spacing
	depth_option	options to compute fracture spacing
		fracs — from fractures
		one_dim — 1D search
	depth_fracs	fractures to be used in computing the fracture spacing
		all_fracs — all fractures
		path_fracs — only fractures on the pathways
		damk_fracs — only fractures with a Damkohler number smaller than dmk_thres
		one_dim — 1D search
	depth_samples	number of fracture spacing samples
	damk_thres	Damkohler type I number threshold (upper bound)
	Fa	Area fraction used for LTG and PAW fracture areas
rep_path_generation	section defining the representative pathway generation options	
	path_option	basis for combining true paths into representative pathways
		travel_time — travel time
		source — source location
		exit — sink location
	max_roots	maximum number of roots used to compute representative pathways
	max_branches	maximum number of branches used to compute representative pathways
	weight_fraction	fraction (<=1) used to prune pathways
source_def	section defining the source locations*	
	bdry_groups	boundary group(s)
	frac_sets	fracture set(s)
	frac_ids	single fracture(s)
sink_def	section defining the sink locations *	
	bdry_groups	boundary group(s)
	frac_sets	fracture set(s)
	frac_ids	single fracture(s)
pa_output	rip_file	filename root for RIP files (performance assessment)
	sts_root	filename root for text output
	view_transfer	filename for GeomView file (graphical output)

* Specify numeric ranges as comma delimited numbers with ranges specified using hyphens, e.g. 1,2,3,5,7-12,15,18

4.5.3 Preparing LTG Input

In addition to searching the pipe network for pathways PAW can also be used to prepare input for the solute transport code (LTG). In preparing input data for LTG three tasks are fulfilled by PAW:

- select the pipes to be analysed in LTG
- option to discretize the selected pipes into smaller elements
- prepare the input files for LTG

The final optional part of the PAW input file holds the information required to generate the LTG input files. The data in the PAW input file are either passed unedited into the correct location in the LTG files, or the inputs are processed by PAW to form parameters in the form required by LTG.

In the following pages the PAW/LTG parameters are described, with the reference number relating to the line numbers used in the right hand column of Table 4-2.

Notes:

1. the current version of LTG requires specific file names for the input files; these are given in the following text.

2. inside the PAW input file, LTG parameters should be given in units of kg, metres, and years. PAW internally converts all MAFIC output to these units.

3. the damk_threshold option in the path_search_options section of PAW input may be used to prune the fractures considered in the LTG mesh based on the pipe Damkohler number.

Two LTG related input parameters are placed before the LTG_options section. The parameter, `docluster`, defines whether the LTG fracture network files are created.

1	`docluster`	toggle for generating the LTG files, comprising the entire fracture network downstream of the source (1=on, 0=off)
2	`dopath`	toggle for generating PAW pathways (1=on, 0=off)

The associated file for pathway analysis is dopath. The user has the option of generating both PAWorks and LTG output together by setting docluster and dopath to 1.

The second LTG related parameter which is specified outside the LTG section is Fa, the fracture area scaling factor, which scales the available diffusion area available inside LTG.

The input parameters in the LTG section of PAW are:

3	`BEGIN LTG_options`	start of LTG section
4	`RunOut`	main LTG input file name

		(=ltg.dat)
5	PipeOut	filename for file containing pipe network (finite element mesh) (=grid.in)
6	PipePropOut	filename for file containing pipe properties (velocity, area, dispersivity) (=pipevel.in)
7	RetardOut	filename for file containing surface sorption retardation factors (=retard.in)
8	ImmZoneOut	filename for file containing immobile zones connected to each pipe (=pipeimm.in)
9	ImmPropOut	filename for file containing the immobile zone properties (=immdata.in)
	FluxOut	filename for file containing external fluxes (only used for verification purposes)
10	out_root	root filename to be used for the LTG output files
11	title	title for current problem (in form = "title.....")
12	logprt	flag for full (.TRUE.) or condensed (.FALSE.) output to log file
13	multifile	flag for echoed input data echoed to multiple output files (.TRUE.) or information sent to main output file (.FALSE.)
14	Cauchy	flag for Cauchy (.TRUE.) or Direchlet (.FALSE.) release boundary conditions
15	multiflux	flag for information generated every timestep sent to multiple time files (.TRUE.) or information sent to main output file (.FALSE.)
16	peclet_threshold	this is a mesh refinement parameter used to improve numerical convergence. Pipes with a numerical Peclet number smaller than the threshold are subdivided into smaller pipes. Note that this procedure may also be carried out inside LTG (recommended as this produces smaller input files and saves hard drive space). To opt for no mesh refinement by LTG set Peclet_threshold to a large number
17	dispersion_length	dispersion length for transport calculations
18	infill_density	density of the infill in the flowing part of the fracture
19	infill_thickness	thickness of the infill in the flowing part of the fracture
20	immobile_zones	section holding general immobile zone parameters
21	nzones	number of immobile zones attached to each pipe

The input properties required vary depending on whether the immobile zone is matrix porosity (matrix) or non-flowing pore space (noflow)

22	zone_data	parameters for each ***matrix*** immobile zone (separated by blanks)

		zone_type tortuosity porosity density diffusion_distance
23	zone_data	parameters for each *noflow* immobile zone (separated by blanks) zone_type tortuosity infill_thickness infill_density diffusion_distance
24	END	end of immobile zone data
25	BEGIN radio_nuclides	section containing description of radionuclides
26	number_of_species	number of radionuclide species
27&41	BEGIN nuclide	section which holds all information for one species

The section nuclide holds the information about properties, release rates and release times for a species. A separate section is required for each nuclide species present in the model. The species will be assigned an ID which be equal to the ordering of the species in the input file. The parameters within the section are:

28&42	Kd	distribution coefficient (m^3/kg)
29&43	diffusivity	free water diffusivity (m^2/yr)
30&44	lambda	decay rate (1/yr)
31&45	nparent	number of parent species (integer value)
	if nparent > 0	
46	kparent	parent species ID
47	aparent	fraction of parent species which decays to this daughter
32&48	n_czero_nodes	number of source nodes for this species
	if n_czero_nodes > 0	
33	BEGIN c_zero_data	section which contains release data
34	c_zero_node	node ID
35	c_zero_times	number of data entries (c_zero_data)
36-38	c_zero_data	times and concentrations (separated by blank) time concentration
39	END	end of c_zero_data block
40&49	END	end of nuclide block
50	END	end of radio_nuclides block

The remainder of the file contains the output and numerical control parameters required by LTG.

51	BEGIN output	section containing output settings
52	ouput_spacing	must be set to zero. This gets output nodes as all nodes on the user-specified outflow boundary.
53	n_output_times	number of output times (output_time)
54&55	output_time	output time
56	END	end of section containing output settings

57	deltol	solver update tolerance
58	level	level of fill for ILU preconditioner
59	nitmax	maximum solver iterations
60	order	logical switch; set to .true. for rcm ordering
61	reduce	logical switch; set to .TRUE. for red-black reduction
62	nterm	number of Laplace p-space solutions
63	relerr	relative Laplace inversion error
64	END	end of the LTG input block

Table 4-2 Example PAW Input file, LTG parameters

```
docluster = 1                                                                    1
dopath = 0                                                                       2
BEGIN LTG_options                                                                3
        # input files
        RunOut =       ltg.dat                                                   4
       PipeOut =      grid.in                                                   5
       PipePropOut = pipevel.in                                                 6
       RetardOut =    retard.in                                                 7
       ImmZoneOut = pipeimm.in                                                  8
       ImmPropOut = immdata.in                                                  9
       FluxOut =      qdata.in
       out_root = "acpazz"                                                       10
       title = "PAWorks-LTG Watari 01 "                                          11
       logprt = .TRUE.                                                           12
       multifile = .FALSE.                                                       13
       Cauchy = .TRUE.                                                           14
       multiflux = .FALSE.                                                       15
       peclet_threshold = 100.0                                                  16
       dispersion_length = 10.0                                                  17
       infill_density = 2.7E3                                                    18
       infill_thickness = 1.E-3                                                  19

       BEGIN immobile_zones                                                      20
       n_zones = 2                                                               21
       #              zone_type   tortuosity   porosity,   density,   diffusion distance
       zone_data =    matrix        0.1          0.01         2.7E3      0.1      22
       #              zone_type   tortuosity   porosity,   density,   diffusion distance
       zone_data =    noflow        1            0.001        2.7E3      1.0      23
       END     # end of immobile zone data                                       24

       BEGIN radio_nuclides                                                      25
              number_of_species = 2                                              26
              BEGIN nuclide  # species 1 AM243                                   27
                     Kd =            0.1        #kd                              28
                     diffusivity =   1.e-9      #free water diffusivity          29
                     lambda =        2.98E-12   #decay for species              30
                     nparent =       0          #nparents for species            31
                     n_czero_nodes = 1  #no.of nodes at spec.conc. or flux rate  32
                     BEGIN c_zero_data                                           33
                            c_zero_node =         1                              34
                            c_zero_times =        3                              35
                            # species 1
                            #              czero_times,   czero
                            c_zero_data =  0.0             1.0                   36
                            c_zero_data =  100000.0        1.0                   37
                            c_zero_data =  100001.0        1.0                   38
                     END     #end c_zero_data                                   39
              END     #end radionuclide                                          40
              BEGIN nuclide  #species 2  PU239                                   41
                     Kd =            0.25          #kd                          42
                     diffusivity =   1.0E-9        #free water diffusivity      43
                     lambda =        9.130E-13     #decay for species           44
                     nparent =       1             #nparents for species        45
                     kparent =       1             #species number of parent    46
                     aparent =       1.   #all of species 1 decays to species 2  47
                     n_czero_nodes = 0    #no of nodes with assigned conc.      48
              END     #end radionuclide                                          49
       END     #end radio_nuclides section                                       50
```

Table 4-2 (continued)

```
BEGIN output                                                    51
        output_spacing = 0                                      52
        n_output_times = 2                                      53
        output_time = 10000    #years                           54
        output_time = 20000                                     55
END     # end of output sus-section                             56
deltol = 1.E-12                                                 57
level = 0                                                       58
nitmax = 500                                                    59
order = .TRUE.                                                  60
reduce = .TRUE.                                                 61
nterm = 5                                                       62
relerr = 1.E-09                                                 63
END                                                             64
```

4.5.4 PAW Output

The output produced by PAW depends on the settings specified by the user. There are three main groups of output files:

- PAW statistics (.STS) and pathway visualization (.LIST)
- RIP (performance assessment) input files (.RP1, .RP2)
- LTG (Laplace Transform Gallerkin solute transport) input files (.IN and .DAT)

4.6 LTG

LTG (Laplace Transform Galerkin) was developed to model transport phenomena such as surface sorption, retardation and matrix diffusion within a pipe network. LTG uses a finite element mesh representing the pipe network which is prepared using genpipes and PAW. The solute transport calculations are based on flow velocities which are derived by MAFIC and PAW.

4.6.1 Input files for LTG (created from PAW)

As discussed in the previous section, the LTG input files may be created using PAW. The files contain:

- information about the pipe elements (e.g. location)
- information about the flow in the each pipe
- information about retardation within the pipe
- information about which immobile zones are attached to each pipe
- information about retardation and diffusion for the immobile zones

The input files must be assigned the following names:

`ltg.dat`	main LTG input file
`grid.in`	file containing pipe network (finite element mesh)
`pipevel.in`	file containing pipe properties (velocity, area, dispersivity)
`retard.in`	file containing surface sorption retardation factors
`pipeimm.in`	file containing immobile zones connected to each pipe
`immdata.in`	file containing the immobile zone properties

The user is unlikely to need to edit any of the PAW generated input files apart from `ltg.dat`. An example input file for LTG is provided as Table 4-3. The options inside `ltg.dat` which the user may wish to change are;

Peclet threshold number	to enable additional mesh refinement inside LTG
results to separate files (i.e. echo data and time output)	.true. or .false.
boundary condition information	number of boundary condition nodes boundary node number
output node information	number of output nodes output node number

For the `dopipe` option, the output node numbers are generated automatically by PAW using the user assigned spacing along the pathway. For the `docluster` option, PAW automatically assigns all the nodes of the source as inflow nodes, and all the nodes on the sink as output nodes. However, the user may edit the input and output nodes after PAW is completed. A complete list of the nodes on the input and output boundaries may also be found in the PAW output file idx.in.

A more detailed description of the LTG input file (LTG.DAT) parameters may be found in the following section of this report.

Table 4-3 Example LTG Input File using PAW Output

```
!
acpa_a                                    !6 character file root
!specification of array sizes
!mxnn  maxne  maxspecies  maxpipes  maxzonespp
!maxbcs  maxipnodes  maxbctimes mxopnodes  mxoptimes  mxterm  mxlev
333965 396856 2 92339 2      1 2 8 10 4 5 5

PAWorks-LTG 2x8 Panels PA-231 & AC-227

.FALSE.                                   !logprt
.TRUE.                                    !multi-files for echo data
.TRUE.                                    !Cauchy
.FALSE.                                   !time output to multiple files
2.                                        !Peclet threshold number

2                                         !nspecies
0, 3.153600e-02, 2.120000e-05             !npa, diffusion, lamda (1)  !Pa-231
1, 3.153600e-02, 3.180000e-02             !npa, diffusion, lamda (2)  !Ac-227
1                    !kparen
1.000000e+00,        !aparen
92339                !number of pipe types
.TRUE.               !immob_zone_from_file
.TRUE.               !pipe_vel_from_file
.TRUE.               !retard_from_file
184678               !number of immobile zone types
.TRUE.               !immob_zone_from_file
.TRUE.               !grid_from_file
1                    ! number of bc nodes for species i
2                    ! number of nodes
138889  144234       ! node number(s)
8                    ! number of Bq/year points
0.000000e+00, 0.000000e+00       ! time, Bq/year
1.000000e+03, 8.430000e+00
2.000000e+03, 4.640000e+01
3.000000e+03, 8.320000e+01
4.000000e+03, 1.140000e+02
6.000000e+03, 1.590000e+02
8.000000e+03, 1.880000e+02
1.000000e+04, 0.000000e+00
0                                 ! number of bc nodes for species 2
10                                ! n_output_nodes
5     149    529    675    719
846   1126   1305   1346   1394   ! output nodes
4                                 !n_output_times
2.000000e+04                      ! output times
4.000000e+04
6.000000e+04
8.000000e+04
1.000000e-08                       !deltol
5                                  !level
200                                !nitmax
.TRUE.                             !order
.TRUE.                             !reduce
5                                  !nterm
1.000000e-05                       !relerr
```

4.6.2 Input files for LTG ("stand-alone" version)

LTG may also be run independently of the PAWorks module, with the input files being created by hand. Generally the "stand alone" version of the code is used to model simple fracture geometry. For convenience, LTG allows the user to generate a number of fractures all connected in series using internal mesh generation options. For this simplified fracture system only a single input file is required, LTG.DAT.

This section describes the input file for an example problem, as shown in Table 4-4. The input format allows the user to add comments throughout the file by the addition of ! in column 1 of the data file.

The first line of the input file contains the root for the filenames 'chains' in this example. As described in the previous section, many of the output files will have names based on this root.

The following four lines contain comments, the last of which describe the maximum array sizes to be input on line 6. In the order input, the maximum values refer to the maximum.....

- number of nodes,
- number of elements,
- number of species,
- number of pipe types,
- number of immobile zones per pipe,
- number of boundary conditions,
- number of input boundary condition nodes,
- number of boundary condition times,
- number of output nodes,
- number of output times,
- value of mxterm,
- value of level

It is important to remember the difference between pipes and elements. A pipe is defined in this context as a series of elements with the same cross-sectional geometry, and same sorptive properties. Therefore a single pipe may be made up of many elements.

The next input line is the title of the simulation, `Comparison with Parallel Fracture Chain-decay Analytic Solution`, which is echoed into the main output files. `logprt` is used to toggle between detailed (`.true.`) and summary (`.false.`) output. The peclet number defined the numerical Peclet number to be used to subdivide the elements.

Table 4-4 Example "Stand-Alone" LTG Input file

```
chains
! root for output file IDs
! following record contains limits for different components
! mxnn    maxne       maxspecies  maxpipes    maxzonespp
! maxbcs  maxipnodes  maxbctimes  maxopnodes  maxoptimes  mxterm  mxlev
51  50  2  1  2        1  1  2  51  1  10  5

Comparison with Parallel Fracture Chain-decay Analytic Solution
.true.                          ! logprt; set to true for detailed output
.true.                          ! output echo data to multiple files
.false.                         ! Cauchy; true if flux-type bc; false if dirichlet bc
.false.                         ! send output to separate files
2.                              ! Peclet

2                               ! nspecies
0  3.1536d-1 2.83d-6            ! number of parents(i),diffusion(i),decay(i)
1  3.1536d-1 9.00d-6            ! number of parents(i),diffusion(i),decay(i)
1                               ! kparen(1) (species # of parent of species 2)
1.0                             ! aparen(1) (all of species 1 decays to species 2)

1                               ! number of pipe-types
.false.                         ! pipe immobile zone information from file "pipeimm.im"
1  1                            ! 1 immobile zone, it is #1
.false.                         ! pipe_vel_from_file
1.d+2 1.d-4 10.0                ! constant_velocity, constant_area, pipe dispersivity
.false.                         ! retard_from_file
1.0  1.0                        ! pipe retardations for species 1-2
1                               ! number of immobile-zone types
.false.                         ! material immobile zones from file "immdata.in"
0.01  2.0  0.05  0.4            ! porosity, perim, dmax, tortuosity
1.43e4                          ! retard_im  - species 1
5.00e4                          ! retard_im  - species 2

.false.                         ! grid_from_file
500.0  10.0                     ! xl, deltax
1  50  1                        ! ielem1,ielem2,ipipe_prop

1                               ! n_BCs (for species 1)
1  1                            ! 1 BC node: 1
2                               ! n_BC_times
0.0      1.0                    ! BC_times, BVal; (species 1)
100000.0 1.0                    ! BC_times, BVal; (species 1)

1                               ! n_BCs; (for species 2)
1  1                            ! 1 BC node: 1
2                               ! n_BC_times (for species 2)
0.0      0.0                    ! BC_times, BVal; (for species 2)
100000.0 0.0                    ! BC_times, BVal; (for species 2)

51                              ! n_output_nodes
     1      3      5      7      9    11    13    15    17    19
    21    23    25    27    29    31   33    35    37    39
    41    43    45    47    49    51
1                               ! n_output_times
100000.0                        ! output_times

1.d-8                           ! deltol
5                               ! level
500                             ! nitmax
.true.                          ! order
.true.                          ! reduce
5                               ! nterm
1.d-5                           ! relerr
```

The next portion of the input file reads in the decay chain information.

```
number of species  (nspecies)
loop number of species
     number of parents(i),diffusion(i) in m²/yr, decay(i)in yr⁻¹
end loop

loop from 2 to number of species
     kparen(1) (species # of parent of species 2)
     aparen(1) (all of species 1 decays to species 2)
end loop
```

Following the species information are the material properties relating to the pipe types and immobile zones. Although units of m, years, kg are shown here, in the stand alone version of LTG any consistent input set may be used.

```
number of pipe-types
pipe immobile zone information from file "pipeimm.im"
                                        (false to read from LTG.DAT)
number of immobile zones, immobile zone number


pipe velocity data from file            (false to read from LTG.DAT)
loop number of pipe types
     constant_velocity(m/yr), constant_area (m²),
     pipe dispersivity (m)
end loop

retard_from_file                        (false to read from LTG.DAT)
loop number of pipe types
     loop pipe retardations for species 1 to number of species (-)
end loop

number of immobile-zone types
material immobile zones from file "immdata.in"
                                        (false to read from LTG.DAT)
loop number of immobile zone types
     porosity (-), perimeter (m), max. diffusion distance (m),
     tortuosity (-)

     loop number of species
          retard_im  - species i
     end species loop
end immobile zones loop

read finite element grid_from_file    (false to read from LTG.DAT)
total pipe network length (xl), element size(deltax)
loop number of pipe types
     starting element, final element, pipe type
end pipe type loop
```

The next section of the data file relates to assigning the boundary conditions.

```
loop number of species
     number of boundary conditions (n_BCs) for species i
     loop number of boundary conditions
          number of BC node, (numbers of the BC nodes - up to 10)
          number of boundary condition times (n_BC_times)
          loop number of boundary condition times
               time (BC_times), release value (BVal)
          end boundary condition times loop
     end boundary condition loop
end species loop
```

The output information is provided in the next few lines of output.

```
number of output nodes (n_output_nodes)
loop to number of output nodes
     output node (10 per line maximum)
end loop
number of output times (n_output_times)
loop to number of output times
     output times (output_times)
end loop
```

The final section of the input file relates to numerical convergence. It is recommended that these values are not altered without first reading the more detailed solver information available in the WatSolv manual.

```
1.d-8                          ! deltol
5                              ! level
500                            ! nitmax
.true.                         ! order
.true.                         ! reduce
5                              ! nterm
1.d-5                          ! relerr
```

4.6.3 Starting LTG

LTG only runs in batch mode. You start LTG by typing:

```
ltg
```

at the prompt. LTG will automatically use the input files generated by PAW. If you have problems running LTG make sure all the LTG.DAT file is in your current directory. Also check that the path to LTG is set correctly.

4.6.4 LTG Output

The output produced by LTG can be divided into three parts:

- a number of files echoing your input data

- a file summarizing the progress of the simulation
- files holding the transport calculation results for each timestep

The file name root for all files will be the same as for the respective input file. The file name extension, however is set by LTG. It is recomended that the user set the logprt flag to .true. to enable full echoing of the input data when using a new set of PAW files. Checking the echo files is important as this is the data all your calculations will be based on.

The echo file names are;

root.out	main output file containing the simulation progress information
root.pvl	pipe velocities
root.rtd	pipe surface sorption retardation factors
root.imz	immobile zone information
root.grd	finite element frid information
root.flw	additional information on the source nodes (e.g. location, flux)
root.obs	additional information on the output observation nodes (e.g. location, flux)

For each time step the concentrations at all output nodes specified by the user is written to file, together with the total flux rate (eg. Bq/yr) across all the outflow nodes (specified or unspecified), and the cumulative release from the output nodes (specified or unspecified) so far. This information is either included in the .OUT file with the general simulation information, or separate files for each time with the extension .TIM are created.

The total outflow flux rate and the cumulative release are computed by LTG assuming that flux is conserved within the mesh as a whole. Therefore any node where the flux is not balanced is by this definition an inflow or outflow node. For the PAW generated pathways flux will not be conserved along an individual pathway, therefore this information is not relevant unless the docluster=1 option is selected in the PAW input file. The total outflow flux rate and the cumulative release are summarized in a file with the extension .SUM . Note that the cumulative release is the total release from the system, not just the specified outflow nodes. If the release from a specific location is required, the user may sum the release from the relevant nodes.

All files are in standard ASCII format so they can be easily processed by other programs.

5. THEORETICAL BASIS FOR PAWORKS

PAWorks provides:

- A full pipe network solution for flow and transport;
- Approximate pathways analysis by graph theory;
- Input to conventional 1-D repository PA transport codes such as CRYSTAL and RIP; and
- Input into LTG, a transport code incorporating diffusion, decay, and surface and matrix retardation.

PAWorks provides approximate calculation of hydraulic heads within fracture networks, and approximate identification of transport pathways through fractured rock masses. As a result, it provides a useful tool for a wide range of applications, including site characterization and repository performance assessment.

5.1 Approach

Performance assessment codes such as RIP (Miller et al, 1995) and CRYSTAL (Intera, 1984) assume that groundwater transport can be simplified to a series of simple, linear, pipe pathways between the repository and the environmental "compliance boundary". These boundaries, at which doses to humans are calculated, may be the surface, specific geological features, or arbitrary surfaces, depending on environmental regulations.

In general, these simple pipe transport pathways are derived from continuum streamlines. However, this approach is not appropriate for fractured rocks such as those which are expected at many repository sites. Therefore, a more sophisticated method for deriving transport path geometries and properties is required.

Continuum codes assume that solute transport can be described by a smooth, continuous field of streamlines, representing flow pathways. The number of pathways can be defined arbitrarily, dependent only on the contouring interval used for the pressure iso-contours perpendicular to the streamlines (Figure 5-1a). In fractured rock, the situation is quite different. The geometry of transport pathways is controlled by the geometry of discrete fractures, and cannot be defined based on pressure iso-contours (Figure 5-1b). PNC/FracMan generates realistic, three dimensional fracture geometries, and is therefore an ideal method for deriving the pathways to be used in performance assessment calculations.

The approach used for the derivation of performance assessment pathways with PAWorks is illustrated in Figure 5-2. First, FracMan/FracWorks is used to generate realistic fracture geometries. These geometries are stored as .FAB fracture files. The geometry of the pathways to be considered then need to be defined in terms of sources and sinks. The sources and sinks are defined as standard FracMan .SAB files of boreholes or traceplanes (Figure 5-3). The heads within the fracture network must then be assigned

using one of three alternative approximations. If the user does not wish to analyse the entire fracture network, the pathways are may be searched using a graph-theory search algorithm to identify the pathways of concern. These pathways are then provided to a pipe-network performance assessment code such as RIP or CRYSTAL, or the PAW defined transport pathways can be assessed directly using PAWorks/LTG (Section 4.6). Alternatively PAWorks may be used to generate the entire fracture network downstream of the source location into input files for PAWorks/LTG.

5.2 Pipe Approximation for Fracture Network Topology

Flow and transport through fracture networks is constrained to occur through three dimensional networks of interconnected two dimensional fractures. However, pipe transport PA codes use one dimensional "stream tubes" to represent transport. This requires a significant simplification of the topology of the fracture network.

The approximation made here assumes that fractures can be represented topologically as a system of pipes interconnecting the fracture intersections on that fracture (Figure 5-1b). The errors which result from this approximation are illustrated in Figure 5-4 include:

- double counting of conductance of portions of the fracture network where pipes intersect,
- ignoring portions of the fracture surface area which are not directly between fracture intersections,
- double counting of flow area for overlapping pipes
- channeling and spreading in each pipe is controlled by trace sizes, not by pressure streamlines within the fracture planes.

These errors are assessed through comparison of plate flow MAFIC simulations to the pipe flow approximations.

The effect of overlapping pipes is reduced somewhat in the current algorithm for defining pipes. Pipes can be excluded when they pass through any fracture intersections between the pairs of fractures defining the pipes (Figure 5-5). The effect of channeling and spreading compared with the 3-D MAFIC solution can be reduced by using an alternative algorithm for calculating flow widths as a user defined function of the trace lengths, and of the total area of the fracture.

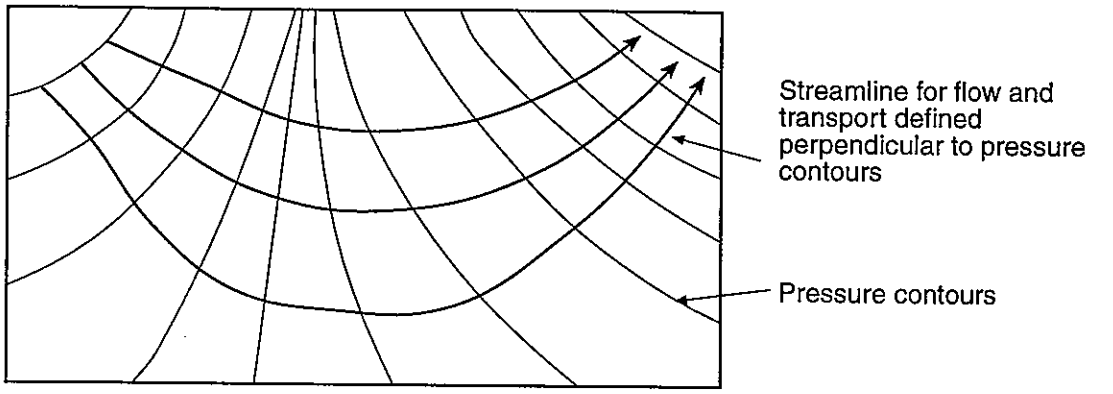

(a) Continuum Model

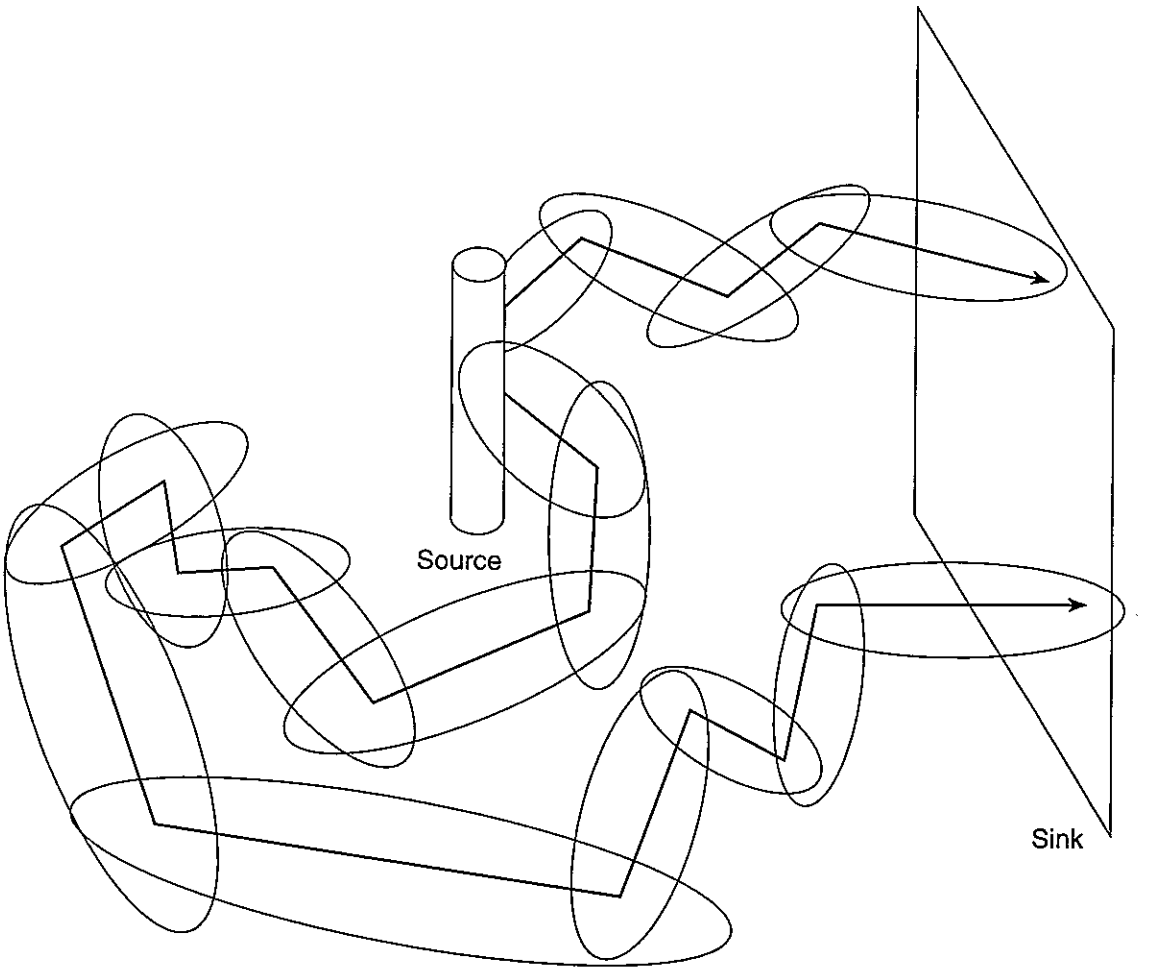

(b) Pathways Controlled by Fracture Geometry

FIGURE **5-1**
CONTINUUM STREAMLINES AND FRACTURE PATHWAYS
PNC/PAWORKS

PROJECT NO. 923 1089.811 DRAWING NO. 72338 DATE 6/16/98 DRAWN BY TK

Golder Associates

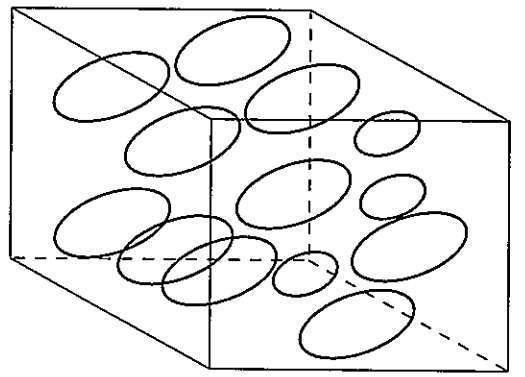

(1) Realistic fracture pattern

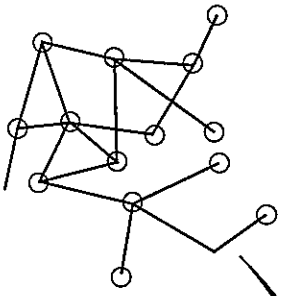

(2) 3D pipe connectivity topology

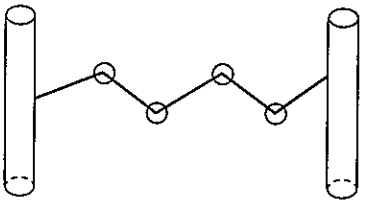

(3) Graph theory identification of non-reentrant path between sources and sinks

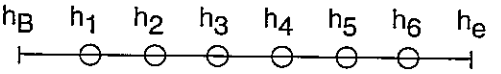

(4) Approximate calculation of conductor properties and head fields among conductors

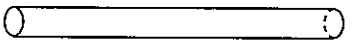

(5) Pathway effective flow and transport properties

FIGURE **5-2**
PAWORKS APPROACH
PNC/PAWORKS

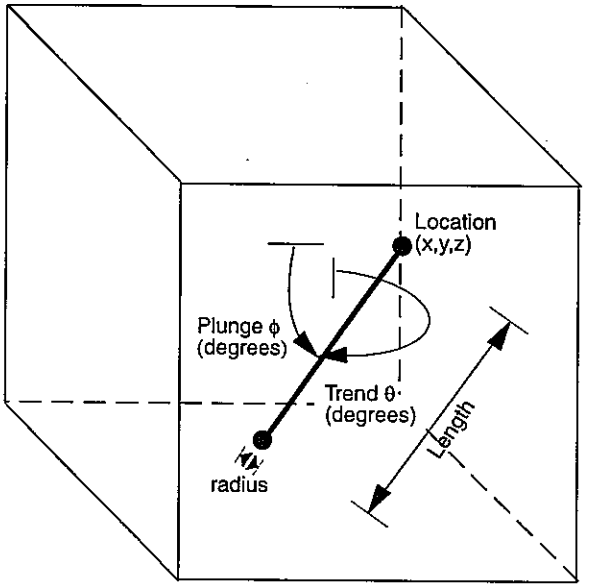

a) Borehole

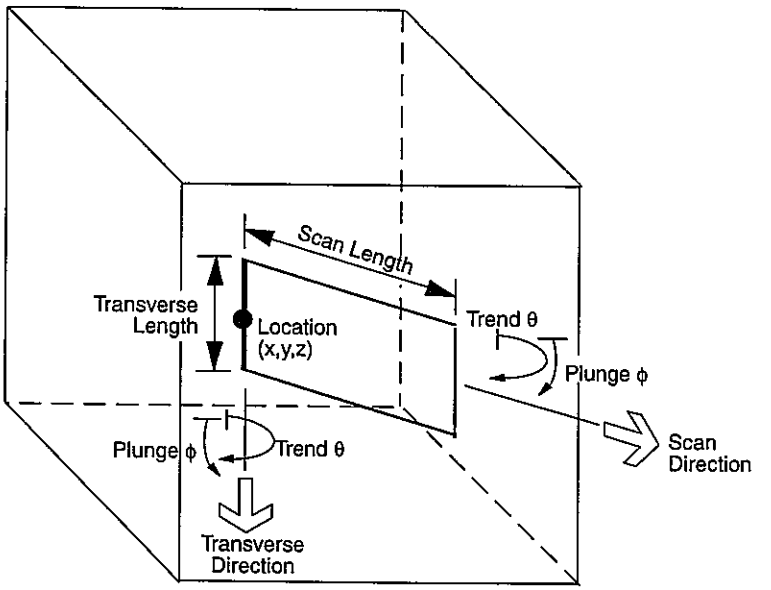

b) Traceplane

FIGURE **5-3**
GEOMETRY FOR BOREHOLE AND TRACEPLANE DEFINITION
PNC/PAWORKS

PROJECT NO. 923 1089.811 DRAWING NO. 72322 DATE 6/16/98 DRAWN BY TK

Golder Associates

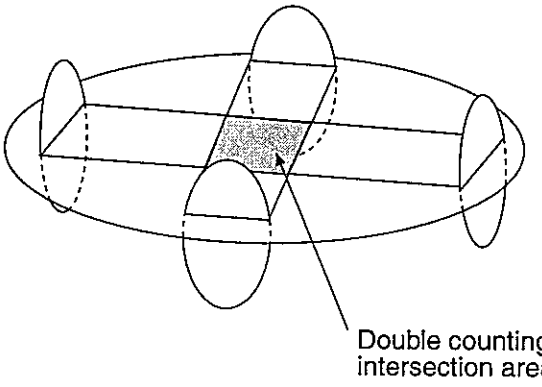

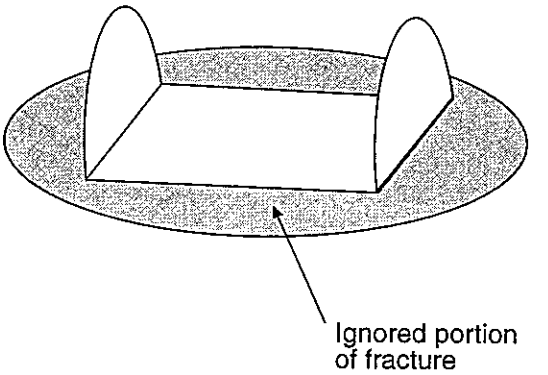

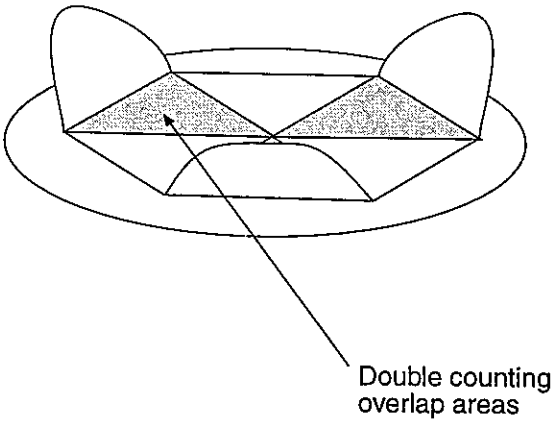

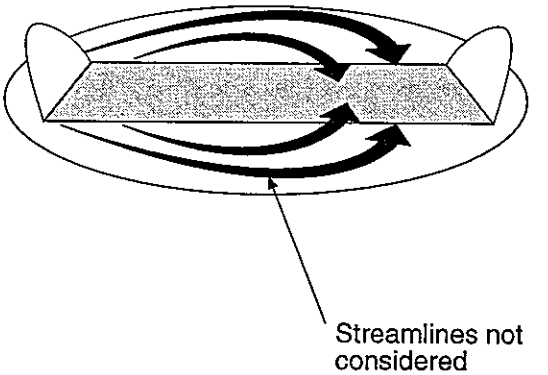

FIGURE **5-4**
APPROXIMATION ERRORS
PNC/PAWORKS

PROJECT NO. 923 1089.811 DRAWING NO. 72323 DATE 6/16/98 DRAWN BY TK

Golder Associates

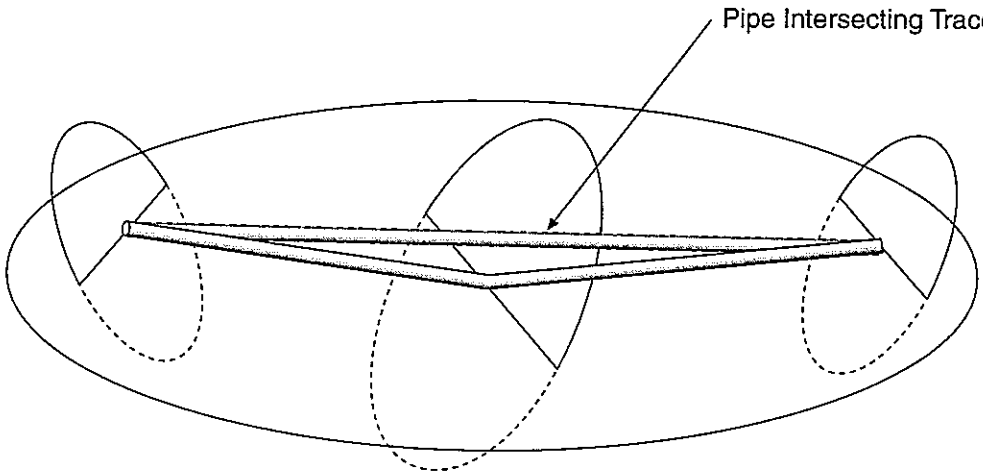

FIGURE **5-5**
DISCARDING OF REDUNDANT PATHWAYS
PNC/PAWORKS

PROJECT NO. 923 1089.811 DRAWING NO. 72324 DATE 6/16/98 DRAWN BY TK

Golder Associates

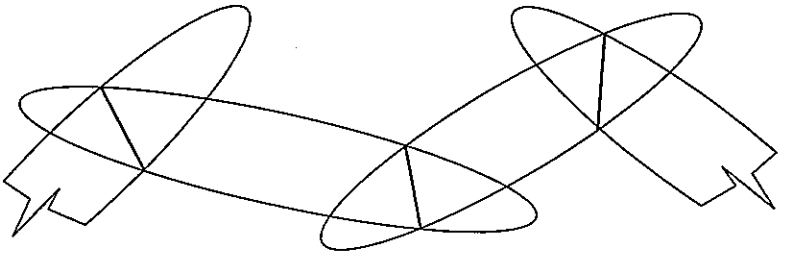

Step 1: Calculate Intersections

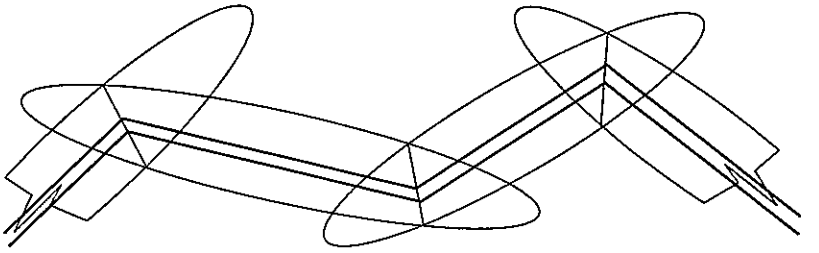

Step 2: Define Pipes

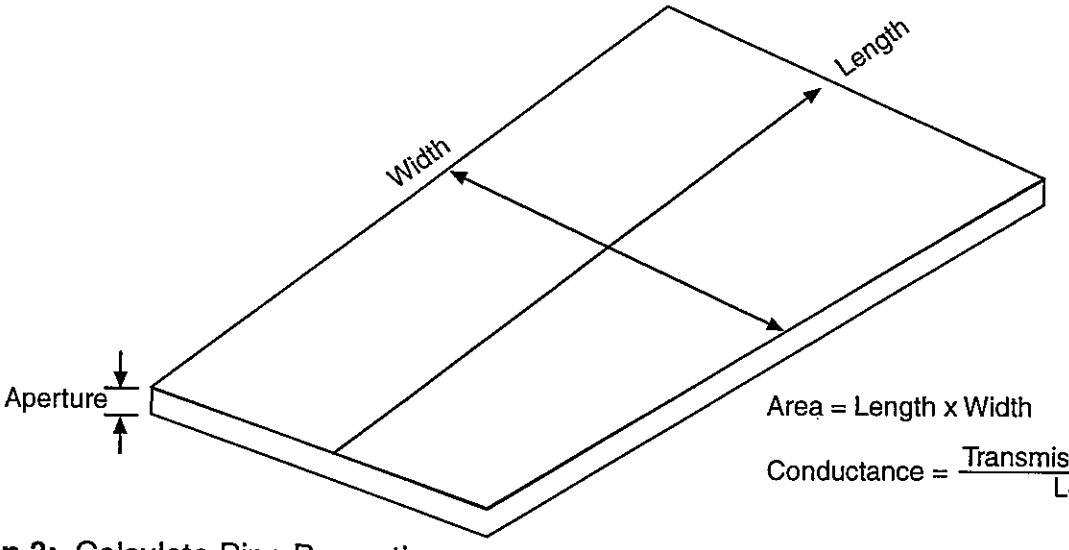

Step 3: Calculate Pipe Properties

FIGURE **5-6**
ALGORITHM FOR GENERATING PIPE NETWORK
PNC/PAWORKS

5.3 Pipe generation

The algorithm for generating networks of pipes from the plate fracture network is as follows (Figure 5-6).

1. Calculate intersections between every fracture in the user specified .FAB files to develop a linked list of fracture connections. This reduces the topology of the three dimensional fracture pattern to a series of nodes and links, where node represent the intersections between fractures, and links represent the fractures between each pair of nodes. Nodes are defined at the midpoint of each fracture intersection fiber, and also at any point where pipes intersect. The amount of time required for this calculation is proportional to N_f^2, where N_f is the number of fractures in the .FAB file.
2. Within each fracture, define pipes between every pair of nodes.
3. Eliminate pipes if option is chosen by the user
4. Create additional pipes if option is chosen by the user
5. Calculate the following properties for each pipe:

   Pipe length L_m: the distance between the centers of the traces formed by the intersections of fractures F_{m-1} and F_{m+1} with fracture F_m

   Pipe flow width W_m: see below for a description of the current options

   Pipe transport aperture a_m: see below for a description of the current options

   Pipe flow surface area A_m: the surface area available for flow ($W_m \times L_m$)

   Pipe flow conductance C_m: the conductance for the pipe ($W_m \times T_m$)

Four different pipe generation options are currently available (Figure 5-7):

1) All pipes that can be formed from the midpoints of the traces. The only restriction is that a new pipe cannot cross an existing one.
2) Pipe generation identical to (1) apart from the additional restriction that pipes are not allowed to cross traces, and that each node (located at the mid-point of each trace) has at least one pipe connected.
3) Pipes from (2) plus additional pipes to ensure that all pipes on the same fracture are connected to each other.
4) Pipes from (3) plus effective pipes. An effective pipe will be formed when the pipe pathway distance between two nodes is greater than an effective pipe factor, N, times the cartesian distance between the nodes. The effective factor, N, is requested and input by the user for all options, but is only used for Option 4. The recommended range for N is between 1.2 to 3.0. This new pipe must not cross any existing pipes.

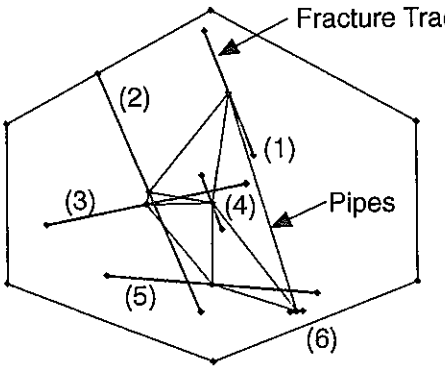

(a) Option 1 - All pipes not crossing each other

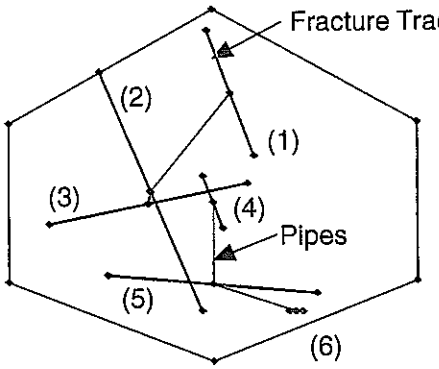

Note: (4), (5) and (6) have no connection to (1), (2), and (3)

(b) Option 2 - Remove pipes which cross traces

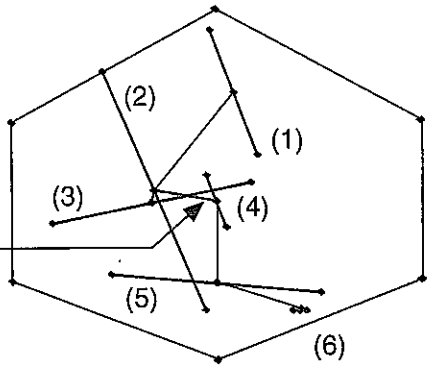

(c) Option 3 - Additional pipes to connect all nodes on fracture

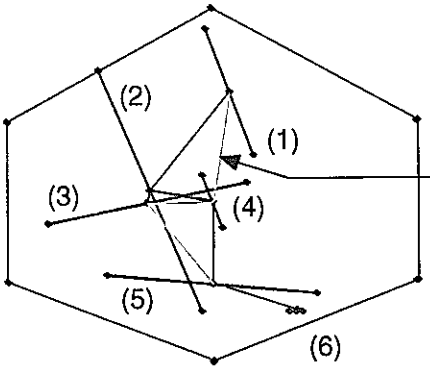

(Effective Factor 1.4)

Pipe added to ensure no tortuous paths greater than 140% of the cartesian distance

(d) Option 4 - Additional pipes to prevent excessively tortuous path

FIGURE **5-7**
PIPE GENERATION OPTIONS
PNC/PAWORKS

Two distinct options are available for defining the pipe width;

1) $W = X_{min} * L_{min} + X_{max} * L_{max}$

2) $W = W_{area} * (X_{min} * L_{min} + X_{max} * L_{max})$

For option 1)

W = pipe width
L_{min} = length of the shorter trace
L_{max} = length of the longer trace
X_{min} = factor associated with the shorter trace (usually in the range 0-1)
X_{max} = factor associated with the longer trace (usually in the range 0-1)

The user has the option to choose whether the trace length is the true trace length, or the length of the trace projected perpendicular to the orientation of the pipe.

Option 2) allows the pipe width of each pipe on the same fracture to be correlated to the fracture area. For the equation

$$W = W_{area} * (X_{min} * L_{min} + X_{max} * L_{max})$$

the terms are defined as;

W = pipe width
W_{area} = sum of $\{W_i * L_i\} / A_f$
W_i = width of pipe *i* on the fracture, $(X_{min}*L_{min} + X_{max}*L_{max})$
L_i = length of pipe *i* on the fracture
A_f = fracture area
L_{min} = length of the shorter trace
L_{max} = length of the longer trace
X_{min} = factor associated with the shorter trace (usually in the range 0-1)
X_{max} = factor associated with the longer trace (usually in the range 0-1)

A value of W_{area} close to 1 is recommended.

Three options are available within Genpipes for defining the fracture aperture;

1) use the aperture read from the .FAB file, as generated within FracMan

2) a = a1 * Aperture from .FAB file

3) a = a1 * Transmissivity^{a2}

The parameters a1 and a2 are constants read into GenPipes.

Note that PAWorks allows the reassignment of aperture as an option within Edpipe (see Section 5.3 for details).

5.4 Approximate Head Solutions

Three alternative solutions are provided for estimation of the heads in the pipe network:

- series flow approximation,
- finite element solution, and
- MAFIC output interpolations

5.4.1 Series Flow Approximation

The series flow approximation calculates the heads at each node along each pathway by assuming linear, series flow between the sources and sinks at each end of the pathway.

For the series flow solution, the effective conductance C_k for a pathway k from a source to a sink is,

$$C_k = \frac{L_k}{\sum_m \left(\frac{L_m}{C_m} \right)} \qquad \text{(Equation 5-1)}$$

Where the pathway length L_k is calculates as the sum of the lengths of the pipes making up the path,

$$L_k = \Sigma L_m \qquad \text{(Equation 5-2)}$$

Flow through the pathway is therefore,

$$Q_k = C_k (h_{source} - h_{sink})/L_k \qquad \text{(Equation 5-3)}$$

Since the flux through each part of a linear pathway must be constant and equal to the flow through the pathway, the head drop Δh_m across each pipe m can be calculated from,

$$Q_m = C_m \Delta h_m / L_m \qquad \text{(Equation 5-4)}$$

$$\Delta h_m = Q_m L_m / C_m \qquad \text{(Equation 5-5)}$$

Once the head drop across each pipe is known, the heads h_m at each node m can be found from the heads at the up-gradient node h_{m+1} as,

$$h_m = h_{m-1} + dh_{m-1} \qquad \text{(Equation 5-6)}$$

Note that this approach does not ensure that the head at each node will be the same for flow through the node on different pathways or in different directions (Figure 5-8). As a result, this method for calculating heads must be considered as a very approximate approach.

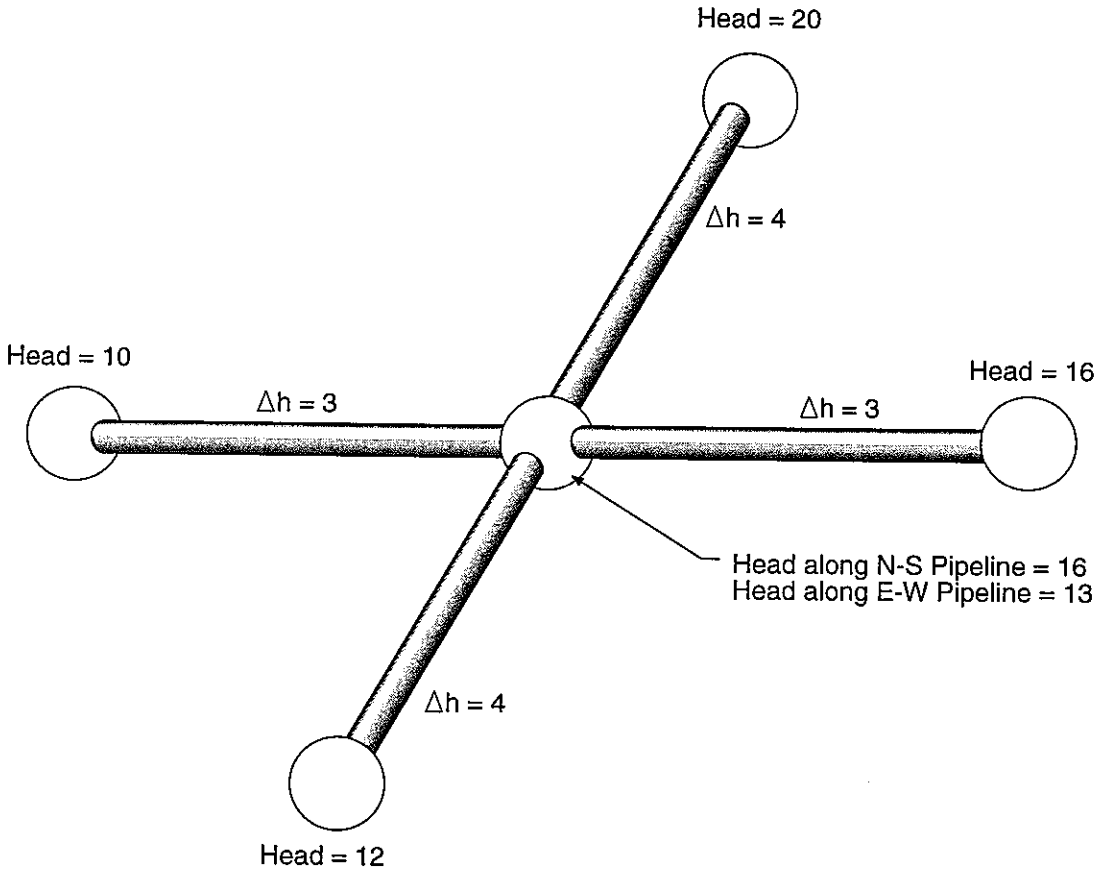

FIGURE **5-8**
SERIES FLOW APPROXIMATION
PNC/PAWORKS

PROJECT NO. 923 1089.811 DRAWING NO. 72326 DATE 6/16/98 DRAWN BY TK

Golder Associates

5.4.2 Finite Element Solution

The finite element solution for the pressures in a network of interconnected pipes is significantly more accurate than the solution based on linear flow. Heads are calculated to ensure compatibility of all flow paths simultaneously. As a result, every node has the same pressure on each of the pathways which pass through it (Figure 5-9).

This finite element solution is still approximate, because it computes flow through the network of pipes rather than through the actual network of plate fractures. However, the increase in computational efficiency relative to the full 3D MAFIC solution is sufficient to make the approach attractive.

The finite element solution was implemented inside the standard MAFIC code, using the same basic algorithms used in the full (3D) MAFIC simulation.

The finite element head solution as implemented in PAWorks includes the following features:

1. Support for both constant and time-dependent Dirichlet (prescribed head) and Neumann (prescribed flux) flow boundary conditions.

2. Choice of linear or quadratic basis functions to describe the variation of pressure within pipe elements.

3. An efficient incomplete Choleskii conjugate gradient equation solver, which significantly reduces memory and computation time requirements.

A description of the finite element solution follows:

5.4.2.1 Pipe Element

The approximate head solution, $\hat{h}^e$, of a pipe element, e, can be expressed in a simple linear form:

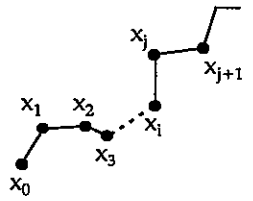

$$\hat{h}^e = a + bx \qquad \text{(Equation 5-7)}$$

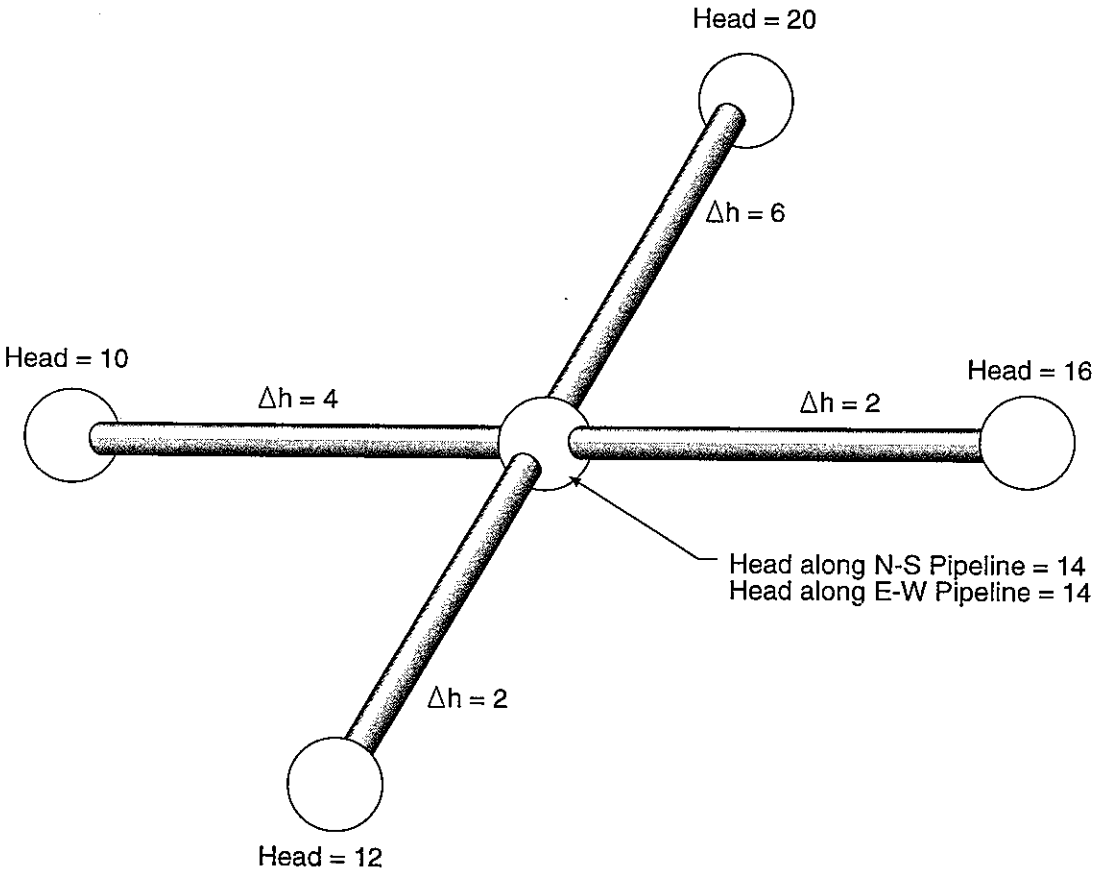

FIGURE **5-9**
FINITE ELEMENT SOLUTION REDUCES APPROXIMATION ERROR
PNC/PAWORKS

PROJECT NO. 923 1089.811 DRAWING NO. 72327 DATE 6/16/98 DRAWN BY TK

Golder Associates

The coefficients a and b are determined from two nodal heads, h_i and h_j of the element, e, that has two ends at $x=x_i$ and $x=x_j$.

$$\begin{cases} h_i = a + bx_i \\ h_j = a + bx_j \end{cases} \qquad \text{(Equation 5-8)}$$

$$\Rightarrow \begin{cases} a = \dfrac{x_j}{x_j - x_i} h_i - \dfrac{x_i}{x_j - x_i} h_j \\ b = \dfrac{-1}{x_j - x_i} h_i + \dfrac{1}{x_j - x_i} h_j \end{cases} \qquad \text{(Equation 5-9)}$$

Equation 5-7 can be rewritten as:

$$\hat{h}^e = \xi_i h_i + \xi_j h_j \qquad \text{(Equation 5-10)}$$

$$\text{with} \quad \xi_i(x) = \frac{x_j - x}{x_j - x_i} \quad \text{and} \quad \xi_j(x) = \frac{-x_i + x}{x_j - x_i} \qquad \text{(Equation 5-11)}$$

The function $\xi_i(x)$ is a linear basis function of the node i.

A quadratic basis function usually provides a better solution than a linear function. Starting from a quadratic polynomial of $\hat{h}^e$, the similar derivations from Equation 5-7 to Equation 5-10 will lead to the following solution:

$$\hat{h}^e = \xi_i h_i + \xi_m h_m + \xi_j h_j \qquad \text{(Equation 5-12)}$$

with

$$\xi_i = 2\frac{x - x_m}{x_j - x_i}\frac{x - x_j}{x_j - x_i}$$

$$\xi_m = -4\frac{x - x_i}{x_j - x_i}\frac{x - x_j}{x_j - x_i} \qquad \text{(Equation 5-13)}$$

$$\xi_j = 2\frac{x - x_m}{x_j - x_i}\frac{x - x_j}{x_j - x_i}$$

where:

x_m=the midpoint of the pipe = $\frac{1}{2}(x_i+x_j)$
h_m=Nodal head at $x=x_m$
ξ_m=basis function at $x=x_m$

In general, we can express the approximate solution as

$$\hat{h}^e = \sum_{k=0}^{M} \xi_k h_k \qquad \text{(Equation 5-14)}$$

The summation index M represents the degree of polynomial used in the basis functions.

5.4.2.2 Derivation of Equations using Galerkin Finite Element Method

Using the same notions in MAFIC User's Manual, Section 2.2, the approximate solution, Equation 2-3, will be derived for 1-D pipe flow.

Starting from the governing equation for the transient pipe flow:

$$S\frac{\partial h}{\partial t} - T\frac{\partial^2 h}{\partial x^2} = q \qquad \text{(Equation 5-15)}$$

apply the Galerkin method to the governing equation (Equation 5-15):

$$\int_L \left(S\frac{\partial \hat{h}}{\partial t} - T\frac{\partial^2 \hat{h}}{\partial x^2} - q \right) \xi_n dx = 0 \quad , \quad n = 1, 2, \ldots N. \qquad \text{(Equation 5-16)}$$

where,

$\hat{h}$ = the approximate solution of head,
N = total number of nodes,
L = length of the domain.

In the Galerkin method, the residues of the governing equation, i.e., the term $\left(S\frac{\partial \hat{h}}{\partial t} - T\frac{\partial^2 \hat{h}}{\partial x^2} - q \right)$ in Equation 5-16, weighted by each basis function, ξ_n, n=1, 2,...N, must be zero when integrated over the entire domain, L.

The second derivative term in Equation 5-16 can be reduced to a first derivative by applying integration by parts.

$$\int_L -T\frac{\partial^2 \hat{h}}{\partial x^2}\xi_n dx = \int_L T\frac{\partial \hat{h}}{\partial x}\frac{d\xi_n}{dx} dx - \int_\Gamma T\left(\frac{\partial \hat{h}}{\partial x} u_x \right) \xi_n d\sigma \qquad \text{(Equation 5-17)}$$

where,

Γ = the boundary of the problem domain,
u_x = the component of a unit vector normal to the boundary,
σ = an integration variable representing distance along the boundary.

Insert Equation 5-17 to Equation 5-16, the equation becomes,

$$\int_L \left(S\frac{\partial \hat{h}}{\partial t}\xi_n + T\frac{\partial \hat{h}}{\partial x}\frac{d\xi_n}{dx} \right) dx = \int_L q\xi_n dx + \int_\Gamma T\left(\frac{\partial \hat{h}}{\partial x} u_x \right) \xi_n d\sigma = Q_n \qquad \text{(Equation 5-18)}$$

n=1,2,...N

The terms on the right-hand side of Equation 5-18 represent the flow source term, q, weighted by ξ_n over the domain and the normal flux term, $T\left(\frac{\partial \hat{h}}{\partial x}u_x\right)$, weighted by ξ_n over the boundary. The total flux weighted by ξ_n is denoted by Q_n on the right-hand side of Equation 5-18.

The integration over the entire domain L can be done element by element, i.e., the summation of integrals over individual element in the domain.

$$\sum_e \left[\int \left(S_e \frac{\partial \hat{h}^e}{\partial t} \xi_n + T_e \frac{\partial \hat{h}^e}{\partial x} \frac{d\xi_n}{dx} \right) dx \right] = Q_n \quad n = 1, 2, \ldots N \qquad \text{(Equation 5-19)}$$

where:

S_e = Storativity of the element e,
T_e = Transmissivity of the element e.

Introduce the approximate solution $\hat{h}^e$, derived in Equation 5-11 to Equation 5-19, the equation becomes

$$\sum_{e=1}^{E} \int_{\ell^e} \left\{ S_e \left[\sum_{k=0}^{M} \xi_k \frac{dh_k}{dt} \right] \xi_n + T_e \left[\sum_{k=0}^{M} \frac{d\xi_k}{dx} h_k \right] \frac{d\xi_n}{dx} \right\} dx = Q_n \quad n = 1, 2, \ldots N. \qquad \text{(Equation 5-20)}$$

where:

ℓ^e = the subdomain of the element e,
E = total number of pipe elements.

In terms of the matrix notation Equation 5-20 can be transformed to

$$\sum_{e=1}^{E} D^e_{k,n} \frac{dh_k}{dt} + A^e_{k,n} h_k = Q_n \qquad \text{(Equation 5-21)}$$

Where D^e is the element storage matrix and A^e the element conductance matrix,

$$D^e_{k,n} = \int_{\ell^e} S_e \xi_k \xi_n dx$$

$$A^e_{k,n} = \int_{\ell^e} T_e \frac{d\xi_k}{dx} \frac{d\xi_n}{dx} dx \qquad \text{(Equation 5-22)}$$

The individual terms of $D^e_{k,n}$ and $A^e_{k,n}$ are found by evaluating the integration over element e in Equation 5-22. The global matrices D and A are simply assembled from the sum of each individual element matrix, D^e and A^e. Equation 5-21 in terms of the global matrices is

$$\sum_{m=1}^{N}\left[D_{nm}\frac{dh_m}{dt}+A_{nm}h_m\right]=Q_n \quad n=1,2,\ldots N \qquad \text{(Equation 5-23)}$$

This is same as the Equation 2-3 in the MAFIC manual.

5.4.2.3 Computer Algorithm for Galerkin Solution

The algorithm used by PAWorks to calculate the Galeikin solution is a follows:

1. Load nodal coordinates, initial and boundary conditions.
2. Construct element conductance matrix $A^e_{k,n}$ and storage matrix $D^e_{k,n}$
3. Assemble global conductance matrix A_{nm} and storage matrix D_{nm}
4. Compute the R.H.S. boundary column matrix, Q_n
5. Solve a system of equations for nodal heads, h_n, n=1, 2,...N, by using Cholesky algorithm.
6. For the transient flow solution repeat 4 and 5 for each time step.

5.4.2.4 Example of constructing element and global matrices [A^e] and [A]:

For the linear basis functions, Equation 5-21, the first derivatives are constant.

$$\frac{d\xi i(x)}{dx}=\frac{-1}{x_j-x_i}=\frac{-1}{\ell^e} \quad \text{and} \quad \frac{d\xi_j}{dx}=\frac{1}{x_j-x_i}=\frac{1}{\ell^e} \qquad \text{(Equation 5-24)}$$

The conductance term of the element e defined in $x=[x_i, x_j]$ is: (see Equation 5-20)

$$A^e_{i,n}=\int_{\ell^e}T_e\frac{d\xi_i}{dx}\frac{d\xi_n}{dx}dx=\int_{\ell^e}T_e\frac{-1}{\ell^e}\frac{d\xi_n}{dx}dx \qquad \text{(Equation 5-25)}$$

$$A^e_{i,n}=\int_{\ell^e}T_e\frac{d\xi_j}{dx}\frac{d\xi_n}{dx}dx=\int_{\ell^e}T_e\frac{1}{\ell^e}\frac{d\xi_n}{dx}dx$$

The nodal basis function ξ_n is non-zero only if ξ_n is defined within the element. Therefore, only when n=i and n=j are the terms non-zero. There are four terms in the element matrix [A^e]:

$$A^e_{i,i}=\int_{\ell^e}T_e\frac{d\xi_i}{dx}\frac{d\xi_i}{dx}dx=T_e\left(\frac{-1}{\ell^e}\right)\left(\frac{-1}{\ell^e}\right)\ell^e=\frac{+T_e}{\ell^e}$$

$$A^e_{i,j}=A_{ji}=\int_{\ell^e}T_e\frac{d\xi_i}{dx}\frac{d\xi_j}{dx}dx=\frac{-T_e}{\ell^e} \qquad \text{(Equation 5-26)}$$

$$A^e_{j,j}=\int_{\ell^e}T_e\frac{d\xi_j}{dx}\frac{d\xi_j}{dx}dx=T_e\left(\frac{1}{\ell^e}\right)\left(\frac{1}{\ell^e}\right)\ell^e=\frac{T_e}{\ell^e}$$

In PAWorks, the conductance and storage terms for each pipe element are evaluated in the subroutine FELEM ( ).

The element conductance matrix [A^e] represents element's contribution to two rows and two columns of the global matrix [A]. The global [A] use in Equation 5-22 is the sum of all elements:

$$[A] = \sum_{e} [A^e] \qquad \text{(Equation 5-27)}$$

In PAWorks, the global term is assembled in the subroutine MFORM ( ).

An example below shows how the global conductance matrix [A] is formed for a simple pipe network illustrated in Figure5-10. Presumed that the ends of the pipe network, Nodes 1, 4, 5 and 6, are the boundary nodes. They are prescribed with boundary values, $q_{i,b}$, i=1, 4, 5, and 6. The circles numbers represent pipe numbers.

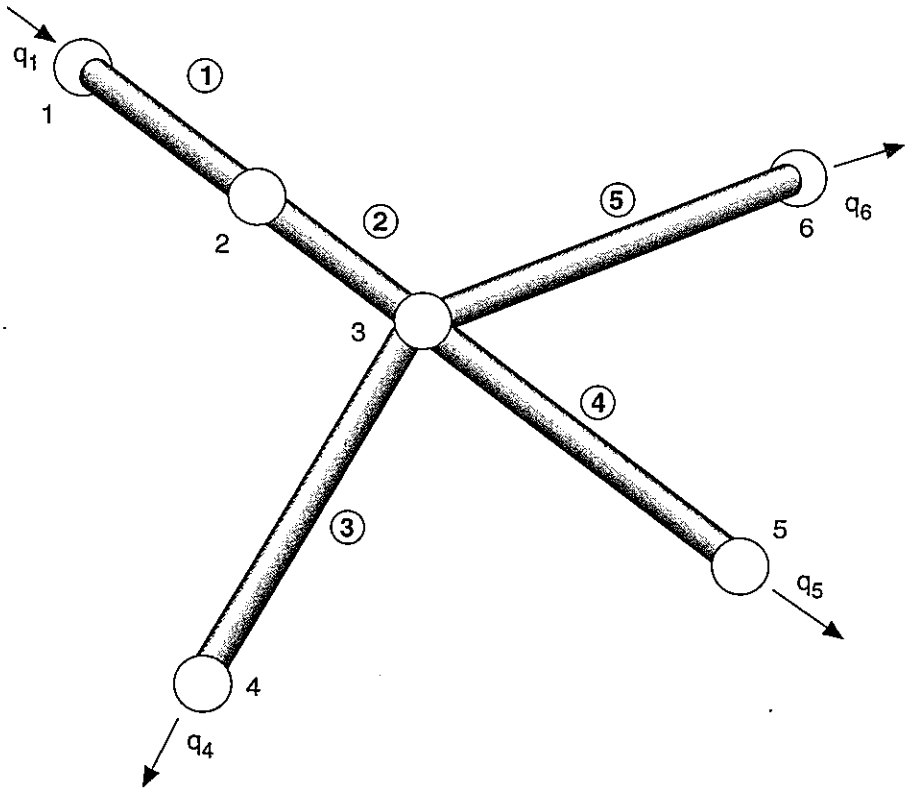

FIGURE **5-10**
SIMPLE PIPE NETWORK
PNC/PAWORKS

PROJECT NO. 923 1089.811 DRAWING NO. 76919 DATE 6/16/98 DRAWN BY EA

Golder Associates

For a steady state solution, Equation 5-23 is reduced to the conductance matrix [A] and the boundary vector $\tilde{Q}$:

$$[A]\tilde{h} = \tilde{Q} \qquad \text{(Equation 5-28)}$$

Where $h = (h_1, h_2, \ldots, h_6)$

$Q = (Q_1, Q_2, \ldots, Q_6)$, and

$$A = \begin{bmatrix} \frac{T_1}{\ell_1} & \frac{-T_1}{\ell_1} & 0 & 0 & 0 & 0 \\ \frac{-T_1}{\ell_1} & \frac{T_1}{\ell_1}+\frac{T_2}{\ell_2} & \frac{-T_2}{\ell_2} & 0 & 0 & 0 \\ 0 & \frac{-T_2}{\ell_2} & \frac{T_2}{\ell_2}+\frac{T_3}{\ell_3} \quad \frac{T_4}{\ell_4}+\frac{T_5}{\ell_5} & \frac{-T_3}{\ell_3} & \frac{-T_5}{\ell_5} & \frac{-T_4}{\ell_4} \\ 0 & 0 & \frac{-T_3}{\ell_3} & \frac{T_3}{\ell_3} & 0 & 0 \\ 0 & 0 & \frac{-T_5}{\ell_5} & 0 & \frac{T_5}{\ell_5} & 0 \\ 0 & 0 & \frac{-T_4}{\ell_4} & 0 & 0 & \frac{T_4}{\ell_4} \end{bmatrix}$$

5.4.2.5 Finite Differences Method for Transient Flow

The governing equation is:

$$\frac{\partial^2 h}{\partial x^2} = \frac{S}{T}\frac{\partial h}{\partial t} - \frac{q}{T} \qquad \text{(Equation 5-29)}$$

Suppose a grid of nodal points $\{x_i\}_{i=1,N}$ have been setup along the pipe network. The nodal interval Δx_i varies slightly pipe by pipe.

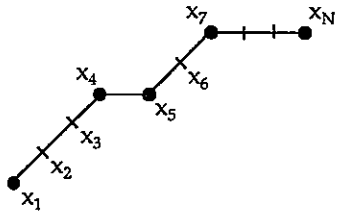

5.4.2.6 Explicit Finite Difference

The finite difference approximations are:

$$\frac{\partial h_i^k}{\partial t} \cong \frac{h_i^{k+1} - h_i^k}{\Delta t}$$

$$\frac{\partial^2 h_i}{\partial x^2} \cong \frac{\dfrac{h_{i+1} - h_i}{\Delta x_i} - \dfrac{h_i - h_{i-1}}{\Delta x_{i-1}}}{\dfrac{\Delta x_i + \Delta x_{i-1}}{2}} = \frac{2}{\Delta x_i + \Delta x_{i-1}}\left[\frac{1}{\Delta x_i}h_{i+1} - \left(\frac{1}{\Delta x_i} + \frac{1}{\Delta x_{i-1}}\right)h_i + \frac{h_{i-1}}{\Delta x_{i-1}}\right]$$

(Equation 5-30)

where k is the index of time step and i the spatial index.

When use the forward difference approximation the finite difference form of Equation 5-29 is.

$$\frac{2}{\Delta x_i + \Delta x_{i-1}}\left[\frac{1}{\Delta x_i}h_{i+1}^k - \left(\frac{1}{\Delta x_i} + \frac{1}{\Delta x_{i-1}}\right)h_i^k + \frac{1}{\Delta x_{i-1}}h_{i-1}^k\right] = \frac{S}{T}\frac{1}{\Delta t}\left(h_i^{k+1} - h_i^k\right) - \frac{q_i^k}{T}$$

(Equation 5-31)

Note that the space derivatives have been evaluated at the known time step k. The only unknown item inEquation 5-31 is h_i^{k+1}.

$$h_i^{k+1} = \left\{1 - \frac{2T\Delta t}{S(\Delta x_i + \Delta x_{i-1})}\left(\frac{1}{\Delta x_i} + \frac{1}{\Delta x_{i-1}}\right)\right\} + \frac{2T\Delta t}{S(\Delta x_i + \Delta x_{i-1})}\left(\frac{1}{\Delta x_i}h_{i+1}^k + \frac{1}{\Delta x_{i-1}}h_{i-1}^k\right) + \frac{\Delta t}{S}q_i^k$$

(Equation 5-32)

We can proceed in a recursive manner of computing heads over the spatial domain for future time steps after the initial head values are given.

5.4.2.7 Validity of the Explicit Solution

The ratio, $\frac{T\Delta t}{S(\Delta x_i + \Delta x_{i-1})}\left\{\max\left(\frac{1}{\Delta x_i}, \frac{1}{\Delta x_{i-1}}\right)\right\}$ must be no greater than 0.25 (Remson, et al. 1971) for the solution to be stable. If the ratio is not sufficiently small, errors will be amplified as the solution progresses.

5.4.2.8 Implicit Finite Difference Approximation

The solution from Equation 5-32 can be improved by using the implicit finite difference method where the spatial derivatives are evaluated between $t = k\Delta t$ and $t = (k+1)\Delta t$.

$$\frac{\partial^2 h}{\partial x^2} \cong \alpha \frac{\partial^2 h^{k+1}}{\partial x^2} + (1-\alpha)\frac{\partial^2 h^k}{\partial x^2} \qquad \text{(Equation 5-33)}$$

where, α is a relaxation parameter, $0 \le \alpha < 1$.

After inserting Equation 5-29 to Equation 5-33 the implicit finite difference equation becomes:

$$\alpha\delta_1 h_{i+1}^{k+1} - \left(\alpha\delta_2 + \frac{S}{T\Delta t}\right)h_i^{k+1} - \alpha\delta_3 h_{i-1}^{k+1} =$$
$$-(1-\alpha)\delta_1 h_{i+1}^{k} + \left[(1-\alpha)\delta_2 - \frac{S}{T\Delta t}\right]h_i^{k} - (1-\alpha)\delta_3 h_{i-1}^{k} - \frac{q_i^k}{T} \qquad \text{(Equation 5-34)}$$

where:

$$\delta_1 = \frac{2}{\Delta x_i + \Delta x_{i-1}}\frac{1}{\Delta x_i}$$
$$\delta_2 = \frac{2}{\Delta x_i + \Delta x_{i-1}}\left(\frac{1}{\Delta x_i} + \frac{1}{\Delta x_{i-1}}\right) \qquad \text{(Equation 5-35)}$$
$$\delta_3 = \frac{2}{\Delta x_i + \Delta x_{i-1}}\frac{1}{\Delta x_{i-1}}$$

Equation 5-34 contains two unknown heads around h_i at the advanced time step (k+1) in addition to the head at the point i. This is called implicit approximation because h_i^{k+1} is not expressed explicitly in terms of known quantities. The system of linear equations in Equation 5-34 must be solved simultaneously to obtain the nodal heads in each advanced time step.

5.4.2.9 Example of Pipe Networks

The following simple network of pipes is used to illustrate the forward explicit finite difference solution. The coefficients of Equation 5-32 are replaced by the variable δ_m defined as

$$\delta_m = \frac{2T_m \Delta t}{S_m(\Delta x_i + \Delta x_{i-1})}$$

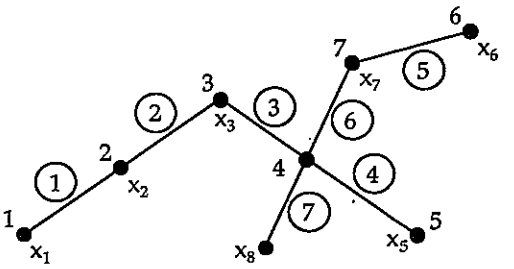

Pipe No.	Interval No	Nodes i	Nodes j	Properties
1	1	1	2	T_1, S_1
	2	2	3	
2	3	3	4	T_2, S_2
	4	4	5	
3	5	6	7	T_3, S_3
	6	4	7	
	7	4	8	

where:

m = pipe index
i = interval number

Equation 5-32 becomes:

$$h_i^{k+1} = \frac{\delta_m}{\Delta x_{i-1}} h_{i-1}^k + \left\{1 - \delta_m\left(\frac{1}{\Delta x_i} + \frac{1}{\Delta x_{i-1}}\right)\right\} h_i^k + \frac{\delta_m}{\Delta x_i} h_{i+1}^k + \frac{\Delta t}{S} q_i^k \qquad \text{(Equation 5-36)}$$

Presumed that the node numbers 1, 5, 6 and 8 are boundary nodes with constant head values prescribed as h_{1b}, h_{6b}, h_{6b}, and h_{8b} respectively. The system of eight linear equations based on Equation 5-36 are explicitly written below:

$$\begin{bmatrix} h_1 \\ h_2 \\ h_3 \\ h_4 \\ h_5 \\ h_6 \\ h_7 \\ h_8 \end{bmatrix}^{k+1} = \begin{bmatrix} 1 & 0 & 0 & 0 & 0 & 0 & 0 & 0 \\ \frac{\delta_1}{\Delta x_{21}} & \left[1-\delta_1\left(\frac{1}{\Delta x_{32}}+\frac{1}{\Delta x_{21}}\right)\right] & \frac{\delta_1}{\Delta x_{32}} & 0 & 0 & 0 & 0 & 0 \\ 0 & \frac{\delta_1}{\Delta x_{32}} & \left[1-\delta_1\left(\frac{1}{\Delta x_{43}}+\frac{1}{\Delta x_{32}}\right)\right] & \frac{\delta_2}{\Delta x_{43}} & 0 & 0 & 0 & 0 \\ 0 & 0 & \frac{\delta_2}{\Delta x_{43}} & [*] & \frac{\delta_2}{\Delta x_{54}} & 0 & \frac{\delta_3}{\Delta x_{74}} & \frac{\delta_3}{\Delta x_{48}} \\ 0 & 0 & 0 & 0 & 1 & 0 & 0 & 0 \\ 0 & 0 & 0 & 0 & 0 & 1 & 0 & 0 \\ 0 & 0 & 0 & \frac{\delta_3}{\Delta x_{74}} & 0 & \frac{\delta 3}{\Delta x_{67}} & \left[1-\delta_3\left(\frac{1}{\Delta x_{67}}+\frac{1}{\Delta x_{74}}\right)\right] & 0 \\ 0 & 0 & 0 & 0 & 0 & 0 & 0 & 1 \end{bmatrix} \begin{bmatrix} h_{1,b} \\ h_2 \\ h_3 \\ h_4 \\ h_{5,b} \\ h_{6,b} \\ h_7 \\ h_{8,b} \end{bmatrix}^k + \begin{bmatrix} 0 \\ \frac{\Delta t}{S_1} q_2 \\ \frac{\Delta t}{S_{1,2}} q_3 \\ \frac{\Delta t}{S_{2,3}} q_4 \\ 0 \\ 0 \\ \frac{\Delta t}{S_3} q_7 \\ 0 \end{bmatrix}^k$$

(Equation 5-37)

where, the term [*] is

$$[*]=\left\{1-\delta_2\left(\frac{1}{\Delta x_{54}}+\frac{1}{\Delta x_{43}}\right)\right\}+\left\{1-\delta_3\left(\frac{1}{\Delta x_{74}}+\frac{1}{\Delta x_{48}}\right)\right\} \quad \text{(Equation 5-38)}$$

The notations Δx_{ij} and $\overline{S}_{i,j}$ used in the matrix are

$$\Delta x_{ij} = x_i - x_j$$
$$\overline{S}_{i,j} = \frac{S_i + S_j}{2} \quad \text{(Equation 5-39)}$$

5.4.3 MAFIC Output Interpolation

The finite element program MAFIC (Miller et al, 1995) models fracture flow through a network of interconnecting triangular finite elements discretized from the two dimensional fractures. In order to obtain heads for the pipe flow network, a transformation needed to be made between the topology of the (2D) triangular elements to the (1D) pipes.

The algorithm implemented for this in PAWorks begins with a network of pipes and nodes derived as described above, and with a MAFIC output file for the same fracture network. For every node in the pipe network, the code then identifies the MAFIC nodes on the same fracture intersection (Figure 5-11). These nodes are sorted to identify the nodes which bracket the node in the pipe network. The head at the node in the pipe network is then calculated as the average of the pressures in the two bracketing nodes.

This approach produces heads which are more consistent with flow in the fracture network than that produced by the series flow approximation or pipe finite element solution. However, the heads are not necessarily consistent with the flow which would occur through the pipe network modeled.

5.5 Aperture Calculation

The aperture calculation options allows the user to define how the aperture is computed for the PAW effective pathways (whose properties are output to the RIP output files). Four options are available;

1. weighted
2. using transmissivity
3. using flow (referred to as flux)
4. using flow in sink element

The "weighted" option computes the effective pathway aperture using the same weighting that is used for the main traversal process. Thus, if you choose to traverse the fracture network using flux weighting, the aperture will be computed from

$$a = \Sigma(e_i * Q_i)/\Sigma Q_i. \quad \text{(Equation 5-40)}$$

The "transmissivity" option computes the effective pathway aperture using the weighted transmissivity for the pathway and the cubic law.

$$a = \left(\frac{12\mu T}{\rho g}\right)^{1/3} \quad \text{(Equation 5-411)}$$

The "flux" option computes the effective pathway aperture from the weighted value of flux, using the equation

$$a = \frac{Q}{K.i.W} \quad \text{(Equation 5-42)}$$

where W is the weighted fracture width, K is the hydraulic conductivity for the pathway, and i is the hydraulic gradient.

The "flux out" option computes the effective pathway aperture from the last value of flux on the pathway, using the equation

$$a = \frac{Q_{out}}{K.i.W} \quad \text{(Equation 5-43)}$$

where W is the weighted fracture width, K is the hydraulic conductivity for the pathway, and i is the hydraulic gradient.

5.6 Pathway Search Algorithms

Two distinct pathway search algorithms are available in PAWorks; weighted searches, and breadth or depth-first searches. Both pathway search algorithms are designed to identify the preferential pathways between user specified sources and sinks, where the sources and sinks may be any combination of traceplanes and boreholes.

For the linear interpolation head calculation approach, the pathways are based on purely geometric considerations, since the heads are calculated after identification of pathways. For this head calculation approach, the pathways may be weighted but are not directed. Weighted graphs have values assigned to each portion of the graph to determine its relative attractiveness for inclusion in the current pathway.

For the head calculation options based on a finite element solution, the pathways are controlled both by the geometry of the pipe network, and the nodal heads, since flow does not occur up-gradient. As a result, every pipe may have a weighting based upon a

user assigned criteria, and a direction defined by the direction of the gradients. These pathways are identified using a weighted, directed graph algorithm.

If the pathway search weighting is set to "none" the depth-first and breadth first search algorithms are used. In this approach the pipe network is traversed following specific rules describing the order in which pipes should be traversed. The properties of the pipe do not affect the traversal. The depth and breadth first searches are described in the following two sections. Depth and breadth first searches are not implemented in H-8.

To search for preferential pathways using PAWorks, the weighted search option should be specified. This pathways search algorithm uses a weighted "priority" first search approach. The priority first search uses the weights on each pipe to determine the pathway which optimizes the pathway criteria, and then continues searching for the remaining pathways by following the same criteria.

For weighted traversals the pipe weights take priority over any concept of breadth or depth first, although breadth and depth may be used to differentiate between pipes of equal weight. Weighted searches are described in Section 5.6.3.

The maximum number of pathways to be found by PAWorks set is by the user. The user also sets the maximum number of branches (equal to the number of pathways per source location). For example, for a maximum number of pathways of 500 and a maximum number of branches of 25, the maximum number of source locations used would be 20. PAWorks does not add additional source locations if the maximum number of branches is not reached.

Once all of the pathways have been identified, the pathway properties are calculated using the equations given in Section 5.10.

5.6.1 Depth-First Search

This search is illustrated in Figure 5-12, and is based on Segdewick (1988). The search algorithm identifies a set of non-reentrant paths, traversing from the user specified source to the user specified sink. The algorithm does not identify all combinations of possible paths. Depth first searches are not implemented in H-8.

In the PAW depth first traversals the pipe priority at a pipe intersection is based on the pipe number read from the MAFIC output file "restart.maf". The pipe with the highest pipe number is given priority at any intersection.

The depth-first, priority order search is as follows:

- all nodes connected to the source are identified, and the node representing the fracture pipe with the highest priority is selected as the source node
- from the source node, all connected pipes are identified and placed onto the stack, with the highest priority pipe towards the top

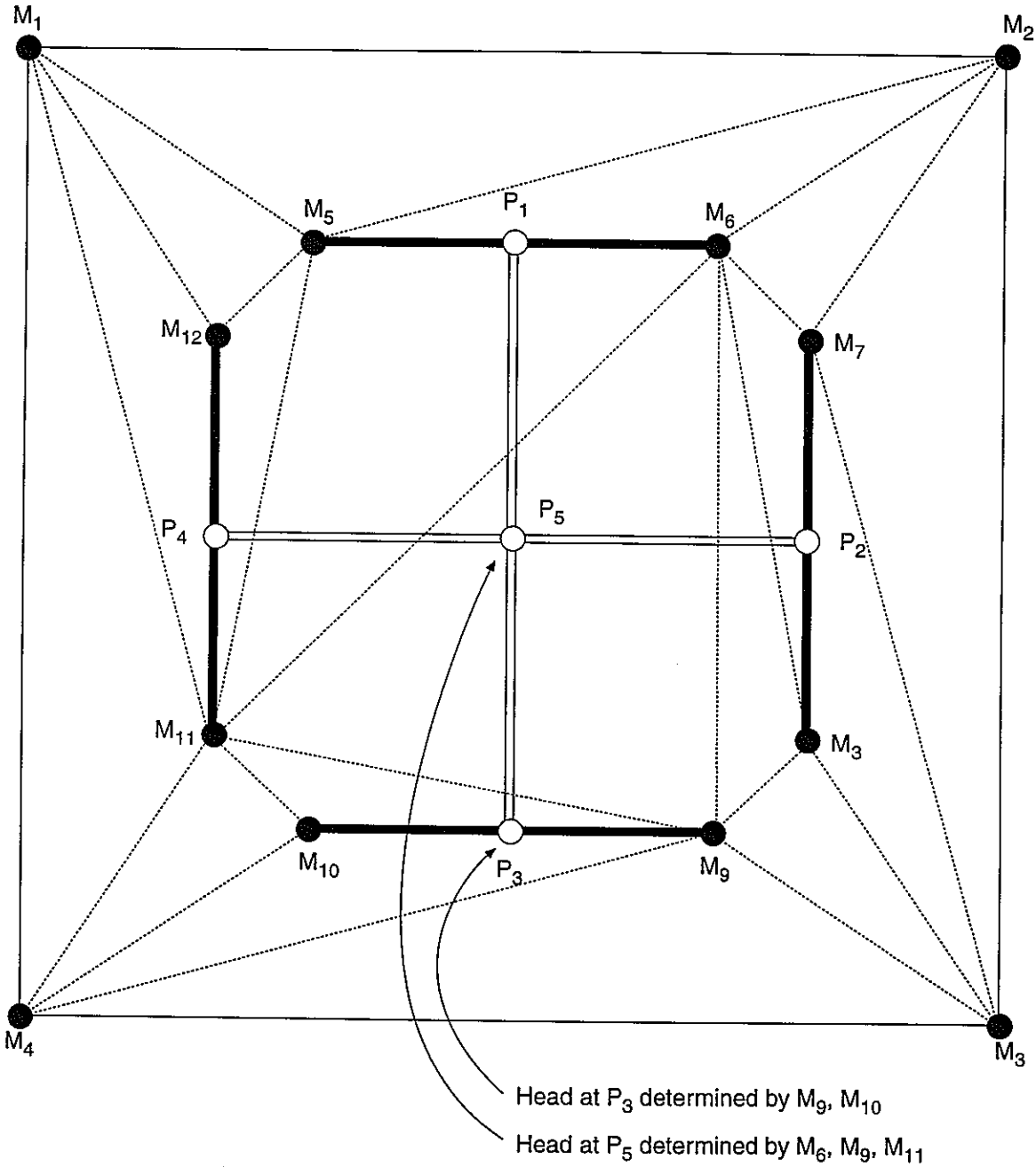

FIGURE **5-11**
PA WORKS NODES AND MAFIC NODES
PNC/PAWORKS

PROJECT NO. 923 1089.811 DRAWING NO. 72328 DATE 6/16/98 DRAWN BY TK

Golder Associates

- the top pipe is removed from the stack, all unmarked pipes directly downstream of this pipe are identified, marked, assigned the current pipe as their predecessor, and placed onto the top of the stack, highest numbered pipe towards the top

- the process is repeated until either a dead end or the sink is reached. When the sink is reached, the link between the source and the sink may be determined by tracing backward through the predecessor list

- As each pathway is identified, the pathway properties may be calculated using the equations below.

- A branch search is then formed by continuing through the traversal until the sink is reached or the branch dies.

- The process is repeated, with the depth-first search tending to find move backward from the sink as the search progresses.

5.6.2 Breadth-First Search

While the depth first search preferentially produces a "tree" structure starting with a straight trunk, and then adding the upper branches first, the breadth-first search preferentially spreads across the network; the trunk produces branches at every stage before the trunk grows higher. Breadth first searches are not implemented in H-8.

In the breadth first search, all searches begin at nodes intersecting the source (Sedgewick, 1988). For the PAW unweighted traversals the pipe priority at a pipe intersection is based on the pipe number read from the MAFIC output file "restart.maf". For breadth-first searched the pipe with the lowest pipe number is given priority at any intersection. The algorithm does not identify all combinations of possible paths.

The breadth first, priority search algorithm is as follows:

- from the source node, all connected pipes are identified, and placed onto the stack with the highest priority pipe towards the top

- the top pipe is removed from the stack, all of the unmarked pipes connected to this pipe are identified, marked, and assigned the current pipe as their predecessor, and then placed onto the bottom of the stack, highest priority pipe uppermost.

- the preceding step is repeated until either a dead end or the sink is reached. When the sink is reached, the pathway may be determined by moving backwards through the predecessor list

- As each pathway is identified, the pathway properties are calculated using the equations below.

5.6.3 Weighting Procedures

The weighting determines what the PAWorks search option will use as the reference property while traversing the fracture network. Five options are available;

1. none
2. transmissivity
3. flux
4. resistance
5. travel time

If the transmissivity, flux, travel time or resistance (defined as 1/conductance) option is selected, this property of each individual pipe is used to compute a weight for every pipe within the network. PAWorks will then traverse the fracture network using the assigned weights to determine the route. If the "none" option is specified the code will traverse the fracture network "breadth" or "depth first" based on the fracture numbering assigned internally within PAWorks.

Associated with these weights are the "path search" options, which describe how the weighting parameters listed above are used to traverse the network. Four options are available;

1. simple
2. weight larger
3. weight smaller
4. minimize weight

The simple option should only be used without weighting. If it is used with the other path weights the weight of the selected parameter will be computed, but not used to control the traversal (i.e. it will default to a depth or breadth first traversal).

The "weight larger" option may only be used with the properties flux and transmissivity. It is not logical to traverse the fracture network searching for the longest travel time or resistance. PAWorks traverses the fracture on an incremental basis, after each step looking at the weights of all the pipes connected to the previously selected pipes and progressing along the connected pipe with the highest weight.

The "weight smaller" option may only sensibly be used with the properties travel time and resistance. For this option PAWorks traverses the fracture network progressing along the connected pipe with the smallest weight.

The last option available is "minimize weight", which like to the "weight smaller" option may only be used with the properties travel time and resistance. This option is similar to the "weight smaller" option. The difference is that choosing the next pipe the algorithm

minimizes the weight for all the pipes up to and including the next pipe, rather than only considering the weight of the next pipe in the sequence.

5.7 Representative Pathway

There are three different options currently available for the user to define how the representative (or effective) pathways are computed within PAWorks:

1. based on the source location
2. based on the sink location
3. based on travel time

The user also has to specify the maximum number of roots and branches for the selected option. The values depend on the selected option.

If the "source location" option is selected, PAWorks generates the effective pathways combining all generated pathways from the same source. For this option the maximum number of roots is equal to the maximum number of starting locations. The maximum number of branches is equal to the maximum number of pathways to be generated from each of these starting locations. For example, for a maximum number of roots of 20 and a maximum number of branches of 25, the maximum number of generated pathways across the network would be 500. The user is also able to specify the maximum number of pathways written to the PA output files. PAWorks will still generate the pathways according to the specified number of roots and branches, however if the maximum number of pathways is less than the pathways generated only the "top" pathways will be written to file.

If the user selects the "sink location" option, the effective pathways are generated combining all pathways from the same sink. For this option the maximum number of roots is equal to the maximum number of sink locations. The maximum number of branches is equal to the maximum number of pathways to be generated from each of the sink locations. Again the user is also able to specify the maximum number of pathways written to the PA output files.

If the "travel time" option is selected PAWorks first generates the required number of pathways and then computes the average travel time for these pathways. For this option the maximum number of roots is ignored. The maximum number of branches is treated as equal to the maximum number of pathways to be generated across the network. These pathways are then sorted based on the closeness to the average travel time, and the pathway nearest to this average travel time is assigned as the representative pathway.

5.8 Penetration Depth Options

These options allow the user to compute the fracture spacing within the fracture network, for differing subsets of fractures, and using different spacing measures. The computed fracture spacing approximates the rock volume available for matrix diffusion, and is therefore part of the input to the LTG portion of the FracMan suite of codes.

The "depth" option allows the user to determine how PAWorks computes the fracture spacing for the selected fractures in the network. It has two options;

1. individual fractures
2. one dimensional

The "individual fractures" option means that the code will compute the fracture spacing from the actual fractures present in the system. For each fracture the code does a search perpendicular to the center of that fracture, looking for the closest fracture on the perpendicular path.

The "one dimensional" option specifies a one dimensional search through the entire mesh. In effect giving the same fracture spacing as would be observed by drilling boreholes through the fracture network. The algorithm generates a number of evenly spaced boreholes (defined by the user) divided equally between the x, y and z planes respectively.

The "fractures" option determines which of the fractures in the fracture network are used to compute the fracture spacing. Three options are available;

1. all fractures
2. path fractures
3. Damkohler fractures

If all fractures is selected, as the name suggests, all fractures in the fracture network are used to compute the fracture spacing.

The "path fractures" option uses the fractures which lie on the PAWorks representative pathways to determine the fracture spacing. This option allows the user to compute the effective fracture spacing based only on the fractures used for the transport computations.

The "Damkohler fractures option uses the Damkohler Type I Number, DaI_{im} for the immobile zone associated with diffusion into the rock matrix to remove less conductive fractures from consideration. The user defines a threshold number and all fractures with smaller Damkohler number are removed from the fracture spacing computation. Note that this option only considers the fractures on representative pathways and only affects the fracture spacing computation.

For Damkohler numbers less than 0.01 the mass transport in a fracture is dominated by advection. For Damkohler numbers greater than about 100 diffusion controls the transport process. For Damkohler numbers in the range $0.01 < DaI_{im} < 100$, the transportation processes are typically double porosity.

5.9 LTG Parameter

5.9.1 Introduction

This section provides a mathematical description of a numerical model, LTG, designed to simulate the advective-dispersive transport of multi-species decay chain through a network of interconnected one-dimensional pipes in three-dimensional space produced by PAWorks. For generality, the decay chain can be either straight or it can be comprised of a complex branching network where each daughter species can have multiple parent species. The model can also accommodate processes known to be important in the context of radionuclide transport in the subsurface such as 1) diffusion from the pipes containing mobile groundwater into the surrounding rock matrix containing immobile groundwater, 2) diffusion into the immobile porewater within the fracture "plane" attached to a pipe containing the flowing groundwater, 3) diffusion from the mobile groundwater in a pipe to attached "dead-end" pipes that contain immobile groundwater and 4) diffusion into fracture infilling or surface-coating material. Thus, in general, each pipe containing the flowing groundwater can be connected to multiple interacting immobile porosity zones. The model also allows for the sorption of the solutes onto the geologic materials within each immobile zone, including sorption onto the surfaces of the pipes in the network. Sorption is described by a linear Freundlich isotherm such that a retardation factor can be defined for each solute for each pipe and each immobile porewater zone.

In order to achieve a high degree of computational efficiency, especially for cases involving very large pipe networks and long simulation time frames, the governing transport equations are solved using the Laplace Transform Galerkin (LTG) finite element method (Sudicky, 1989; Sudicky, 1990, Sudicky and McLaren 1992). The primary advantages of the LTG method are that it avoids time stepping and it is more resistant to numerical dispersion artifacts that conventional time-marching numerical schemes. It is, however, restricted to linear problems and the flow must be steady state. Further computational efficiency is achieved through the use of an advanced iterative sparse matrix equation solver, WatSolv (VanderKwaak et al., 1997), which only stores and operates on the non-zero terms appearing in the finite element coefficient matrix. The LTG code employs ILU factorization with a user-defined level of infill and several re-ordering options including Red/Black system reduction, and it uses CGSTAB (van der Vorst, 1992) acceleration to solve the complex-arithmetic system that arises from the LTG discretization.

5.9.2 Governing Equations

In this section, the governing transport equations are presented based on the pipe network conceptualization to describe solute migration through a fractured rock mass. First, the equations as they exist in the time domain are given, followed by their corresponding forms in Laplace transform space which are the forms that are solved numerically according to the LTG method.

5.9.2.1 Time-domain Transport Equations

5.9.2.1.1 Pipe Transport

Assuming steady-state flow and a first-order approach to describe the diffusive mass transfer of a solute between the groundwater in a pipe and the multiple immobile porosity zones attached to it (see, e.g., Sudicky, 1990), the advective-dispersive transport of solute species k in a pipe network is given by:

$$A(\ell)\left[R_k(\ell)\frac{\partial C_k}{\partial t}+q(\ell)\frac{\partial C_k}{\partial \ell}-\frac{\partial}{\partial \ell}D_{\ell_k}(\ell)\frac{\partial C_k}{\partial \ell}+R_k(\ell)\lambda_k C_k-\sum_{j=1}^{m_k,k>1}\eta_{kj}R_j(\ell)\lambda_j C_j\right]$$

$$\pm\sum_{\ell'}\dot{M}\,\delta(\ell-\ell')+\sum_{\ell^*}Q(C_k-C_k^*)\delta(\ell-\ell^*)+\sum_{im=1}^{IM}P(im,\ell)\alpha_k(im,\ell)(C_k-C_k')=0$$

(Equation 5-44)

where:

$A(\ell)$	=	Pipe cross-sectional area [L^2]
$R_k(\ell)$	=	Retardation factor [-]
$q(\ell)$	=	Specific discharge (≡ Pipe velocity v) [L/T]
$D_{\ell_k}(\ell)$	=	Dispersion coefficient = $\alpha v + D_k^o$ [L^2/T]
α	=	Pipe longitudinal dispersivity [L],
D_k^o	=	Free-solution diffusion coefficient [L^2/T]
λ_k	=	Decay constant [1/T]
m_k	=	Number of parents for species k (=1 for straight chain)
η_{kj}	=	Stoichiometric constant indicating fraction of parent species j that decays to daughter species k = 1.0 for straight decay chain; ($0.0 < \eta_{kj} < 1.0$ for branching chain) Note that to use units of Ci, this factor also needs to account for specific activity.
$\dot{M}(t)$	=	Internal solute mass source/sink [M/T]
Q	=	External fluid source/sink [L^3/T]
$\delta(\ell-\ell'),\delta(\ell-\ell^*)$	=	Dirac delta [1/L]
$P(im, \ell)$	=	Immobile zone wetted perimeter for immobile zone "*im*" attached to pipe "ℓ" [L]
$\alpha_k(im, \ell)$	=	Pipe/immobile zone transfer coefficient for immobile zone "*im*" attached to pipe "ℓ" [L/T]
C_k	=	Pipe concentration [M/L^3]
C_k'	=	Immobile zone concentration [M/L^3]
C_k^*	=	Concentration of injectate in external fluid source [M/L^3]
ℓ	=	Distance along interconnected pipe network [L]
ℓ'	=	Location of solute mass source/sink [L]

ℓ^*	=	Location of external fluid source/sink
im	=	Immobile zone class number (note: if desired im can equal 0) [-]
$IM(\ell)$	=	Total number of immobile zones attached to pipe ℓ [-]
k	=	Species number [-]
m_k	=	Number of parent species decaying to species k [-]
t	=	time [T]

It should be noted that if there is no flow along a particular pipe within the network (i.e. $q\ (\ell) = 0$), then the model allows for diffusive transport along the length of this pipe. It should also be pointed out that if fluid is withdrawn at a resident concentration $C_k^* = C_k$, then the term involving Q in (1) vanishes. If the injectate concentration $C_k^* = 0.0$, then this term accounts for the dilution effect of the injection of solute-free water.

The initial concentrations of all species within the domain are assumed to be zero in the current version of LTG. For boundary conditions, they can be either of the Dirichlet-type where the input concentration history of each species is a specified function of time, or of the Cauchy-type where the advective input mass flux can be prescribed as a function of time at the origin of a pipe on the boundary of the domain. Mathematically, these boundary conditions are described by:

Dirichlet: $C_k = C_k^o(t)$ on Γ (Equation 5-45)

Cauchy: $A(\ell)q(\ell)C_k^o(t) = A(\ell)\left[q(\ell)C_k(\ell,t) - D_{\ell_k}(\ell)\frac{\partial C_k}{\partial \ell}\right]$ on Γ (Equation 5-46)

where $C_k^o(t)$ is the specified concentration for species k. LTG also allows the concentration of flux rate (e.g. Bq/yr) to be specified at an interior point.

5.9.2.1.2 Immobile Zone

In order to represent the diffusive exchange of solute mass between the pipes and any on the im immobile zones attached to them, LTG uses a first-order approach was has been commonly used in the past (see e.g. Sudicky, 1990, among others.) Accordingly, the governing equation for the im^{th} immobile zone, allowing for chain decay and sorption according to a linear equilibrium Freundlich isotherm is described by:

$$\theta_{im}(im,\ell)V_{im}(im,\ell)\left[R_k'(im,\ell)\frac{\partial C_k'}{\partial t} + R_k'(im,\ell)\lambda_k C_k' - \sum_{j=1}^{m_k,k>1}\eta_{kj}\lambda_j R_j'(im,\ell)C_j'\right] =$$

$$P(im,\ell)\alpha_k(im,\ell)[C_k - C_k'] \qquad \text{(Equation 5-47)}$$

where:

$\theta_{im}(im, \ell)$ = Immobile zone porosity for immobile zone "*im*" attached to pipe "ℓ" [-]

$V_{im}(im, \ell)$ = Immobile zone volume/unit pipe length for immobile zone "*im*" attached to pipe "ℓ" [L^2]

$R_k'(im, \ell)$ = Immobile zone retardation factor for immobile zone "*im*" attached to pipe "ℓ" [-]

Note that LTG assumes the initial condition $C_k'(\ell,0) = 0$. With the formulation given by Equations 5-44 and 5-47, the mass transfer coefficient α_k is interpreted to be:

$$\alpha_k = \frac{\theta_{im} D_k^o \tau}{d}; \qquad \text{(Equation 5-48)}$$

where:

τ = Tortuosity [-]

d = Effective diffusion distance [L]

For the assumption of "slab" fracture spacing geometry used in the current version LTG/PAWorks the effective diffusion distance, d, is equal to one third of the maximum diffusion distance. Note that LTG reads the maximum diffusion distance and computes the effective diffusion distance internally.

If a particular immobile zone is fluid-filled, such as within an immobile water zone attached to a pipe within a fracture plane, then the immobile zone porosity, θ_{im}, would equal 1.0.

Note that the definition of α_k given above differs from that used by Sudicky (1990) in that he uses d^{*2} in the denominator of Equation 5-48, where d^* is the maximum diffusion distance.

5.9.2.2 Laplace-transform Domain Transport Equations

The LTG method (Sudicky, 1989; Sudicky, 1990; Sudicky and McLaren, 1992) is a numerical solution procedure where the Laplace transform is first applied to the governing equation, and the transformed equation is then solved numerically using the Galerkin finite element procedure (or alternatively any other discretization method such as finite differences). Finally, upon a solution for the nodal Laplace-space solution, the time-domain solution is recovered by a numerical inversion of the Laplace transformed nodal solution.

Let the Laplace transform of a function *f(t)* be defined according to:

$$\bar{f}(p) = \int_0^\infty f(t) e^{-pt} dt \qquad \text{(Equation 5-49)}$$

where p is the Laplace-transform parameter and first apply it to (3) for the im^{th} immobile zone. Upon it's application and following algebraic manipulations, one obtains:

$$\overline{C}'_k = \frac{P\alpha_k \overline{C}_k + \theta_{im} V_{im} \sum_{j=1}^{m_k, k>1} \eta_{kj} \lambda_j R'_j \overline{C}'_j}{\theta_{im} V_{im} R'_k \mathcal{P}_k + P\alpha_k} \qquad \text{(Equation 5-50)}$$

where $\mathcal{P}_k = p + \lambda_k$ is the shifted Laplace parameter.

The next step involves application of the Laplace transform to the pipe transport equation 5-44, followed by substitution of Equation 5-50 for the transformed immobile-zone concentration into the term involving the mobile-immobile zone solute transfer process appearing in Equation 5-44. After algebraic manipulations, one obtains the following for the Laplace transform of the pipe transport equation:

$$A(\ell)\left[\{R_k(\ell)\mathcal{P}_k + \frac{1}{A(\ell)}\overline{g}\}\overline{C}_k + q(\ell)\frac{\partial \overline{C}_k}{\partial \ell} - \frac{\partial}{\partial \ell} D_{\ell_k}(\ell)\frac{\partial \overline{C}_k}{\partial \ell}\right] \pm \sum_{\ell'} \dot{\overline{M}}\delta(\ell-\ell') + \sum_{\ell^*} Q(\overline{C}_k - \overline{C}_k^*)\delta(\ell-\ell^*)$$

$$= A(\ell) \sum_{j=1}^{m_k, k>1} \eta_{kj} R_j(\ell) \lambda_j \overline{C}_j + \sum_{im=1}^{IM} \frac{P\alpha_k \theta_{im} V_{im} \sum_{j=1}^{m_k, k>1} \eta_{kj} \lambda_j \overline{R}'_j \overline{C}'_j}{\theta_{im} V_{im} \overline{R}'_k \mathcal{P}_k + P\alpha_k}$$

(Equation 5-51)

It can be seen that the application of the Laplace transformation to the governing equations describing transport in the pipe network and each of the multiple immobile zones, followed by algebraic manipulations, has acted as a form of preconditioning in that the primary variable in Equation 5-51 is now restricted to that of the Laplace transform of the pipe network concentrations. This implies further savings in computational efficiency in that only one unknown, the Laplace transform of the nodal pipe concentrations, need be solved for implicitly. Once the transform of the nodal pipe concentrations is solved for, Equation 5-50 can be used to compute the immobile-zone concentrations as a flash calculation.

$$\overline{g} = \sum_{im=1}^{IM} \frac{\theta_{im} V_{im} R'_k \mathcal{P}_k P\alpha_k}{\theta_{im} V_{im} R'_k \mathcal{P}_k + P\alpha_k} \qquad \text{(Equation 5-52)}$$

5.9.3 Numerical Solution Procedure

The numerical solution of the primary governing equation 5-51 is obtained using a standard Galerkin finite element procedure with linear interpolation functions used for each one-dimensional pipe finite element, and a consistent mass matrix formulation applied to the accumulation terms arising from the Laplace transform of the temporal derivative and decay terms. Details concerning the application of the Galerkin finite element method in the context of the LTG algorithm can be found elsewhere (e.g. Sudicky, 1989; Sudicky, 1990; Sudicky and McLaren, 1992) and will not be repeated here.

Inversion of the nodal Laplace-transformed concentrations is achieved using the discrete Fourier series methodology provided by de Hoog et al. (1982) which employs an efficient quotient-difference algorithm to enhance convergence of the inversion process, thus yielding a high degree of accuracy with relatively few discrete $p = p_n$ Laplace p-space vectors. Details concerning the implementation and performance of the de Hoog et al. scheme when applied to the inversion of nodal Laplace-transformed concentrations that arise from an application of the LTG method to solve for transport in fractured geologic media can be found in Sudicky and McLaren (1992).

The matrix equations arising from the LTG algorithm when used in conjunction with the de Hoog et al. (1982) Laplace inversion scheme are complex-valued, and the coefficient matrix is sparsely populated for an arbitrary network of interconnected pipes. Thus, the WatSolv iterative sparse-matrix solver library (VanderKwaak et al., 1997) was adapted to handle the complex system of matrix equations. The WatSolv library is based on an ILU factorization of the non-symmetric coefficient matrix with user-defined levels of infill and several alternative re-ordering methods, including Red/Black system reduction, and employs CGSTAB (van der Vorst, 1992) acceleration to solve the preconditioned system of matrix equations. It also uses a compact ia-ja data storage structure such that only the non-zero terms in the matrix equations are stored and operated on. Further details on the capabilities of WatSolv can be found in VanderKwaak et al. (1997). The WatSolv library is designed to solve systems of equations arising from finite element, finite difference or finite volume discretizations using either single- or double-precision real, or single- or double-precision complex arithmetic.

5.10 Pathway Properties

One goal of PAWorks is to estimate the conductance, transmissivity, conductivity, and geometric properties of a representative pipe connecting source to sink. PAWorks calculates these properties using two models:

1. The individual and representative pathways are fractures (idealized to be between two parallel surfaces) of specific length, width, and aperture, or

2. The individual and representative pathways are cylindrical tubes of specific length and radius.

These models represent extremes of possible fracture flow behavior; it is likely that flow will neither be perfectly even as between two parallel plates nor completely channelized into a single cylindrical tube.

For the plate fracture, the fracture geometry assigned within MAFIC is also used inside PAW. Therefore, the relationship between conductance, transmissivity and width is as follows:

$$C = T.W \qquad \text{(Equation 5-53)}$$

In tube flow, the geometry of the fracture is not assigned from MAFIC, and the conductance of the pipe element is used to link the tube fracture to the parameters read in from the MAFIC restart file. The relationship between conductance and radius is based on a perfect cylindrical tube, giving:

$$C = r^4 \frac{\rho . g}{8 . \mu} \qquad \text{(Equation 5-54)}$$

Once the conductance and geometry of the individual finite elements is known, all other properties (such as travel time and hydraulic conductivity) may be found by substitution.

Having determined the individual properties of each finite element either directly from the restart file (plate fractures), or from conductance (tube flow), PAW completes the traversals across the fracture network. PAW then assigns a single set of properties to each true and representative pathway, which represents the overall behaviour of the pathway. How PAW assigns these material properties is controlled by the user, based on the type of traversal chosen and on the aperture calculation option.

The pathway properties are calculated and reported as follows:

Prelude: Given Parameters

After the intersections and pipes are generated and the head values calculated, we have the following parameters:

L_i	Length of each component fracture
W_i	Width of each component fracture
T_i	Transmissivity of each component fracture
ΔH_i	Head drop over each component fracture
ΔH_{path}	Head drop over entire pathway
t_i	Travel time of each component fracture

The path length is sum of the lengths of each component pipe.

$$L_{path} = \sum L_i \qquad \text{(Equation 5-55)}$$

The path travel time is sum of the travel times of each component pipe.

$$t_{path} = \sum t_i \qquad \text{(Equation 5-56)}$$

Travel time values will be different for parallel plate or tube models.

Step #1: Calculate Pipe Hydraulic Gradients

The hydraulic gradient in each pipe as well as the entire pathway is the head drop per length:

$$i_i = \frac{\Delta H_i}{L_i} \qquad \text{(Equation 5-57)}$$

$$i_{path} = \frac{\Delta H_{path}}{L_{path}} \qquad \text{(Equation 5-58)}$$

Step #2: Calculate path conductivity

Knowing pathway advection time, the pathway conductivity can be calculated:

$$K_{path} = \frac{L_{path}}{t_{path} i_{path}} \qquad \text{(Equation 5-59)}$$

Conductivity values will be different for parallel plate or tube models.

Step #3: Calculate aperture, transmissivity and flux

This calculation is critical to the pathway property generation process. The three properties aperture, transmissivity and flux are inter-related, and which is computed first affects the overall pathway properties.

The user defines which property in the triangle should be calculated first, depending on the choice of aperture computation selected in the PAW input file.

The aperture may be computed in four ways;

- weighted
- use transmissivity
- use pathway flow
- use flow at exit element

Weighted
The weighted option computes the pathway aperture first. It uses the property on which the traversal was based to weight the individual pipe aperture values. For example, if we traverse the fracture network based on flux, the pathway aperture would be computed as;

$$a_{path} = \Sigma(a_i * Q_i)/\Sigma Q_i \quad \text{(Equation 5-59)}$$

Having computed the aperture, the transmissivity and flux are computed as follows;

$$T_{path} = K_{path} * a_{path} \quad \text{(Equation 5-60)}$$

$$Q_{path} = K_{path} * i_{path} * W_{path} * a_{path} \quad \text{(Equation 5-61)}$$

Transmissivity

The "transmissivity" option computes the pathway transmissivity first by weighting the transmissivity by the traversal property.

$$T_{path} = \Sigma(T_i * \text{weighting\_property}_i)/\Sigma\text{weighting\_property}_i \quad \text{(Equation 5-62)}$$

Again, one of the triad of properties is defined the others follow from substitution;

$$a_{path} = T_{path} / K_{path} \quad \text{(Equation 5-63)}$$

$$Q_{path} = K_{path} * i_{path} * W_{path} * a_{path} \quad \text{(Equation 5-64)}$$

Flux

The "flux" option computes the pathway flow first by weighting the flow by the traversal property.

$$Q_{path} = \Sigma(Q_i * \text{weighting\_property}_i)/\Sigma\text{weighting\_property}_i \quad \text{(Equation 5-65)}$$

The aperture is then computed using the equation;

$$a_{path} = \frac{Q_{path}}{K_{path} . i_{path} . W_{path}} \quad \text{(Equation 5-60)}$$

where W is the weighted fracture width, K is the hydraulic conductivity for the pathway, and i is the hydraulic gradient.

The "flux out" option computes the effective pathway aperture from the last value of flux on the pathway, using the equation

$$a_{path} = \frac{Q_{out}}{K.i.W} \qquad \text{(Equation 5-61)}$$

where W is the weighted fracture width, K is the hydraulic conductivity for the pathway, and i is the hydraulic gradient.

Step #4: Calculate Surface Area (plate model)

For each individual pipe PAW records two separate measures of an individual pipe area. The surface area of the fracture from which the pipe was derived, A_f, and the multiple of the individual pipe widths W_i and lengths L_i. Therefore PAW allows the user to see the surface area of the pipe pathway in three separate forms;

The first is as the sum of all the individual fracture areas along the pathway

$$SApath = \Sigma Afi \qquad \text{(Equation 5-62)}$$

The second is as the sum of pipe areas

$$SA_{path} = \Sigma(W_i * L_i)$$

The third form of the fracture area is as

$$SA_{path} = \Sigma\,(W_i * \text{weighting parameter}_i)/\Sigma\text{weighting parameter}_i * L_i$$

$$SA_{path} = W_{path} * L_{path}$$

Step #5: Rock Block Volume

Rock block volume is calculated by proportioning the total rock volume of the modeled region among fractures in proportion to their surface area SA_i and penetration depth distance B_{1i},

$$B_{3i} = V_{block}\frac{SA_iB_{1i}}{\sum SA_iB_{1i}} \qquad \text{(Equation 5-63)}$$

The penetration depth B_{1i}, the distance for matrix diffusion (or the average distance from the fracture to the center of a rock block containing the fracture) , calculated as one quarter of the length of a line segment between the fractures above and below fracture i, measured along the segment perpendicular to the fracture at the midpoint of a line between the middles of the source and sink end intersection traces. Figure 3-10 illustrates how the distance between fractures above and below is four times the average distance to the midpoint of the rock blocks bounding the fracture.

The penetration depth for the pathway, B_{1path}, is calculated as the area weighted average of fracture penetration depths B_{1i},

$$B_{1path} = \frac{\sum B_{1i} SA_i}{SA_{path}} \qquad \text{(Equation 5-64)}$$

The pathway rock block volume B_{3path} is calculated as the sum of the fracture block volumes B_{3i} for all fractures along the pathway:

$$B_{3path} = \sum B_{3i} \qquad \text{(Equation 5-65)}$$

6. PAWORKS VERIFICATION

This section of the report documents a series of verification tests which compare the results of PAWorks/LTG simulations with independent solutions.

6.1 PAWorks Verification

PAWorks requires a series of calculations to describe the geometry and properties of the fracture network and calculate pathways. Each of these algorithms is verified separately in the eight verification cases defined below.

- Case 1: Verification of the algorithm for calculating fracture intersections,
- Case 2: Verification of the algorithm for defining pipes based on fracture intersections,
- Case 3: Verification of the algorithm for calculating heads based on linear interpolation
- Case 4: Verification of the algorithm for calculating heads based on the finite element method
- Case 5: Verification of the algorithm for calculating heads based on MAFIC output files
- Case 6: Verification of the depth-first algorithm for identifying pathways, and
- Case 7: Verification of the breadth-first algorithm for identifying pathways, and
- Case 8: Verification of the algorithms for defining the properties of the pathways.

6.2 Case 1: Verification of the algorithm for calculating fracture intersections,

Two synthetic fracture networks (for Case 1a and Case 1b) were generated to verify the ability of PAWorks to calculate fracture intersections. The first network (Figure 6-1) consisted of three orthogonal fracture sets, each consisting of 10 fractures which span the entire model. This network should produce 300 fracture intersections. The second network (Figure 6-2) consisted of 10 circular fractures located and oriented such that each fracture has exactly two intersections.

Verification criteria for Case 1 were as follows:

- Case 1a: Fracture intersections calculated by PAWorks must match the known fracture intersections exactly (to within the precision of the output)
- Case 1b: Fracture intersections calculated by PAWorks must match within 0.5% of the model scale. (Tolerance is allowed to accommodate polygonal approximations of circular fractures.)

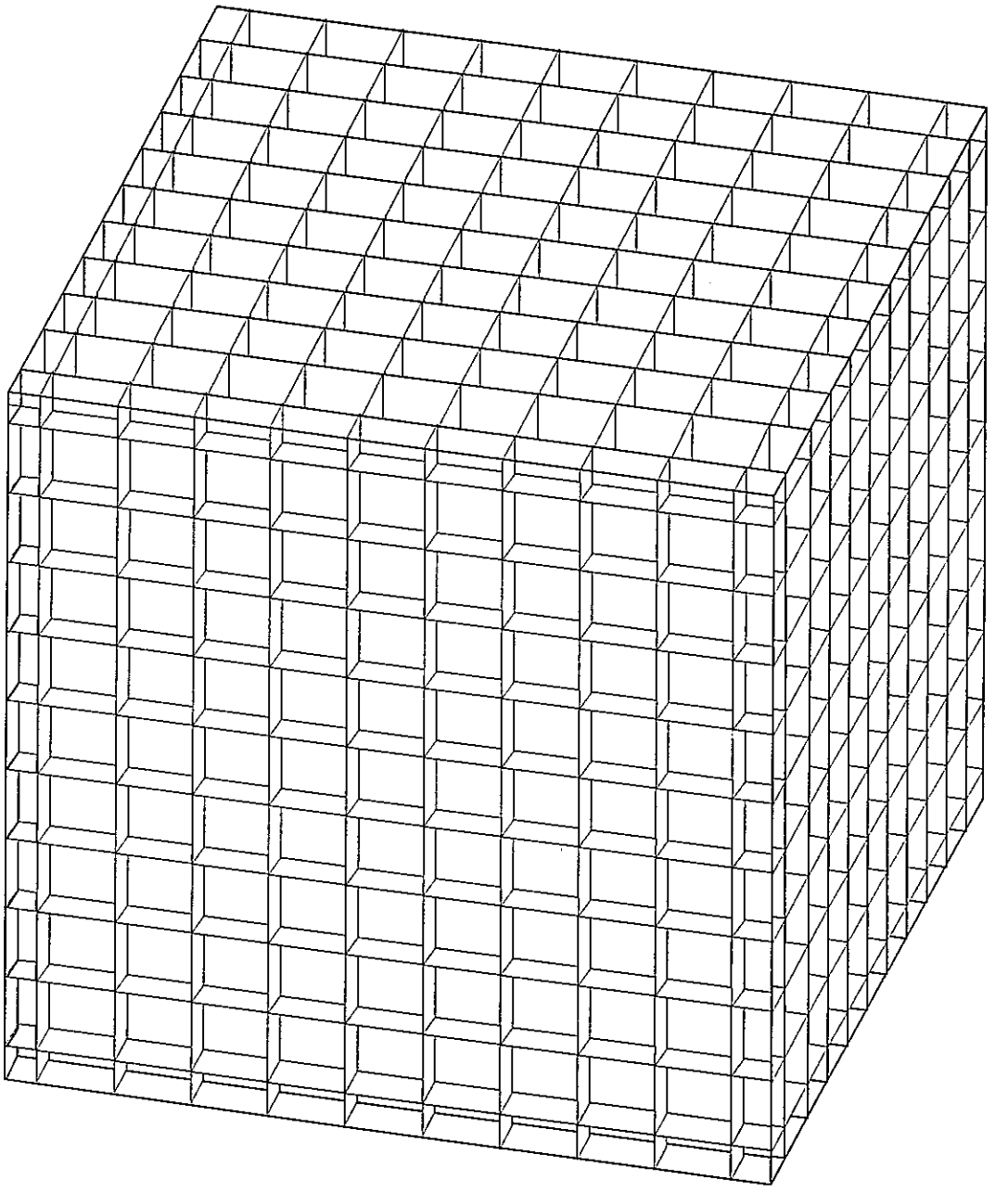

FIGURE **6-1**
FRACTURE NETWORK FOR CASE 1A
PNC/PAWORKS

PROJECT NO. 923 1089.811 DWG. NO. 72330 DATE 6/16/98 DRAWN CB

Golder Associates

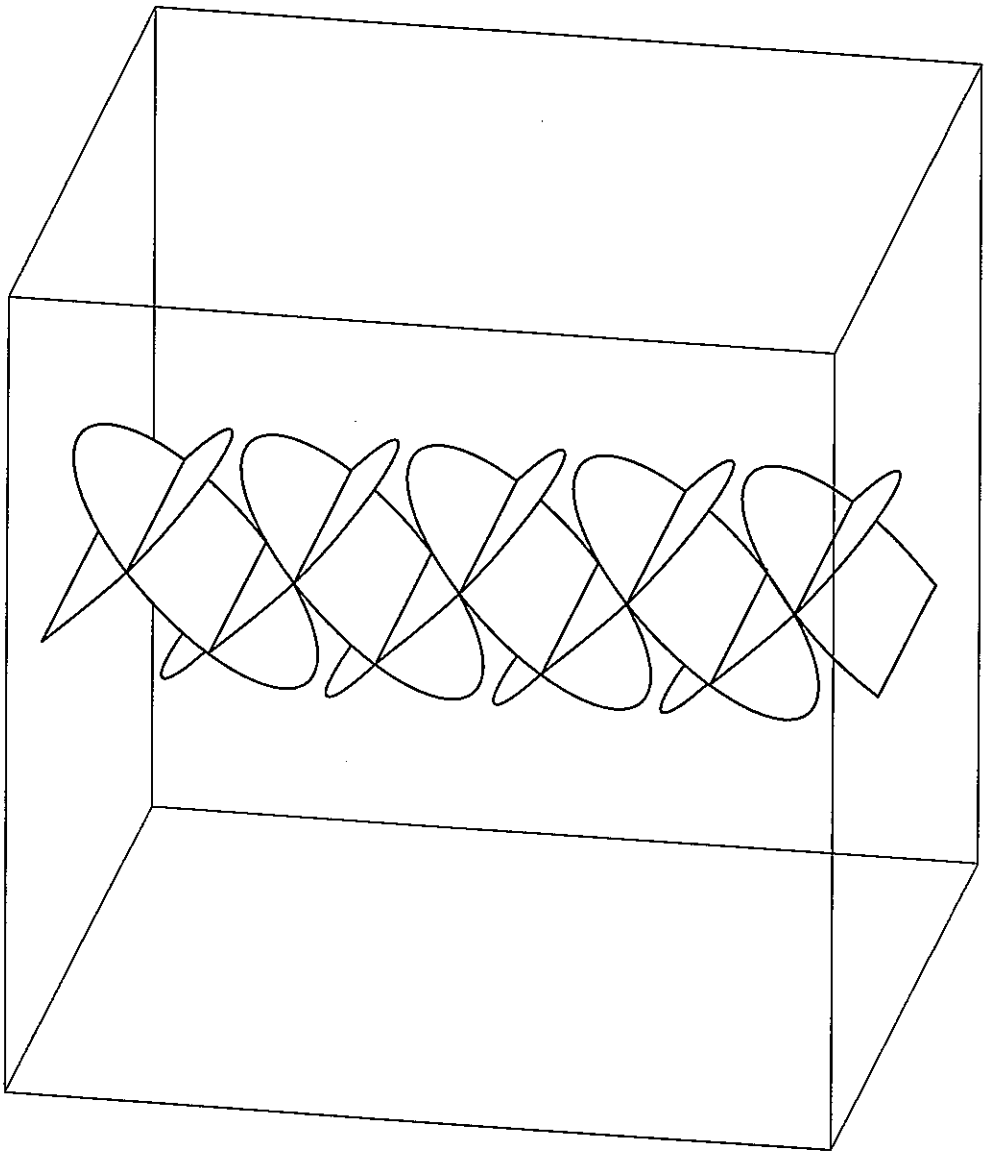

FIGURE **6-2**
FRACTURE NETWORK FOR CASE 1B
PNC/PAWORKS

PROJECT NO. 923 1089.811 DWG. NO. 72331 DATE 6/16/98 DRAWN CB

Golder Associates

The designed solutions for intersections are shown in Table 6-1. Because of the number of intersections, the PAWorks solution is not presented in a table, but examination of the spreadsheet PAWorks.xls demonstrates that the verification criteria have been met. The files Case1a.txt and Case1b.txt contain the raw output from PAWorks which were incorporated into the spreadsheet.

Table 6-1 Designed Intersections, Case 1

Intersections	x	y	z	where
Case 1a				
100 N-S Horizontal	[-100, 100]	(2i-11)×10	(2j-11)×10	i=1..10, j=1..10
100 E-W Horizontal	(2i-11)×10	[-100, 100]	(2j-11)×10	i=1..10, j=1..10
100 Vertical	(2i-11)×10	(2j-11)×10	[-100, 100]	i=1..10, j=1..10
Case 1b				
Upper 5	[-17.5, 17.5]	(i-3)×40	14.14	i=1..5
Lower 4	[-17.5, 17.5]	(2i-5)×20	-14.14	i=1..4

6.3 Case 2: Verification of the algorithm for defining pipes based on fracture intersections

The fracture network defined for Case 2 is shown in Figure 6-3a was designed to produce a set of pipes as shown in Figure 6-3b.

The verification criterion for Case 2 is as follows:

- Pipes defined by PAWorks match those shown in Figure 6-3b exactly.

Examination of the spreadsheet PAWorks.xls demonstrates that the pipes defined by PAWorks match those designed to within the precision of the machine. The file Case2.txt contains the raw output from PAWorks which was incorporated into the spreadsheet.

6.4 Case 3: Verification of the algorithm for calculating heads based on linear interpolation

Heads based on linear interpolation are calculated by (a) determining the effective conductance of each pipe along the pathway and the entire pathway using a series circuit assumption, (b) calculating the flux through the pathway, and (c) calculating the gradient through each section of the pathway to ensure constant flux through each portion of the series circuit. The fracture network shown in Figure 6-4 consists of 5 fractures in series. The series flow circuit solution for this network is summarized in Table 6-2.

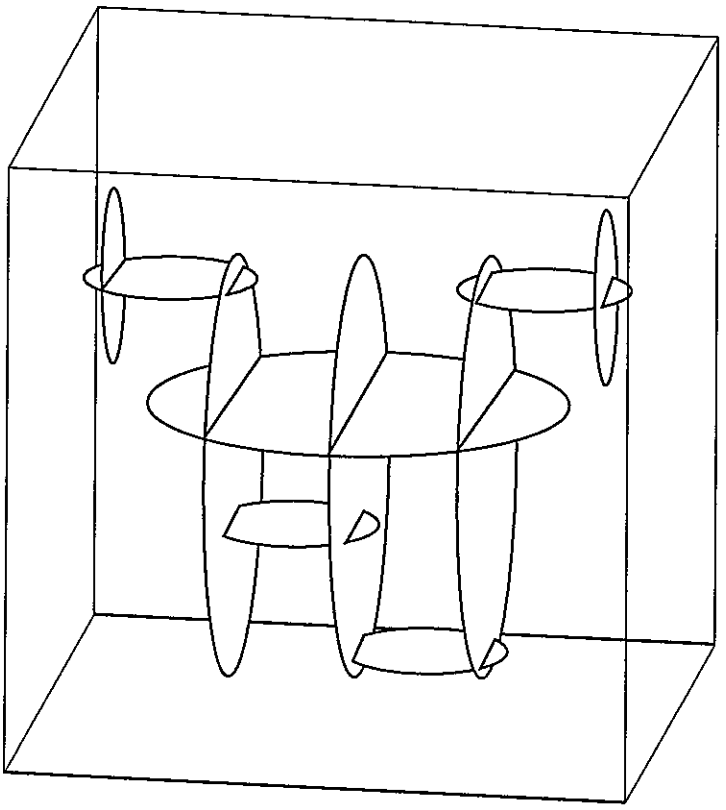

(a) Fracture Network

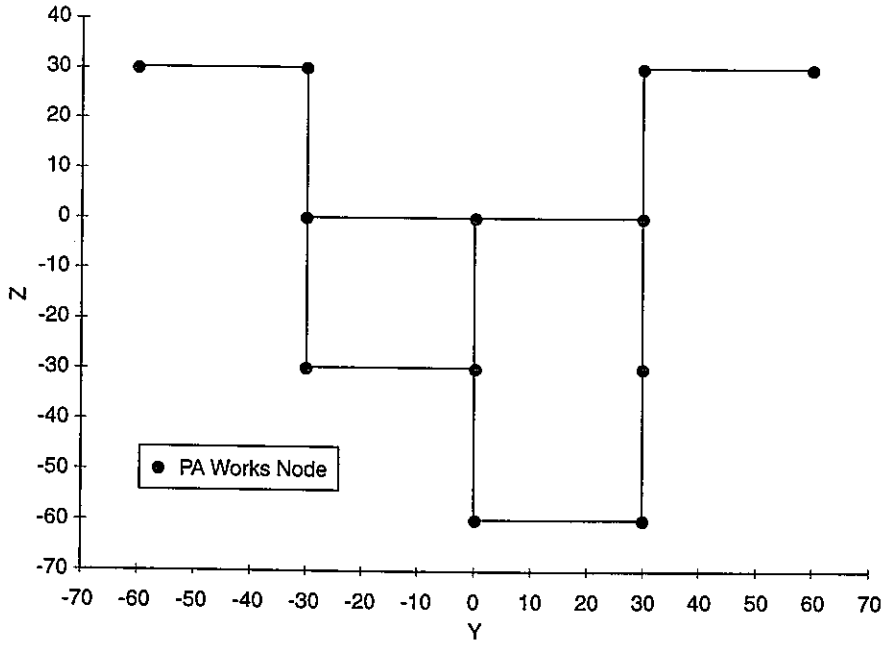

(b) Pipe Network

FIGURE **6-3**
FRACTURE AND PIPE NETWORK FOR CASE 2
PNC/PAWORKS

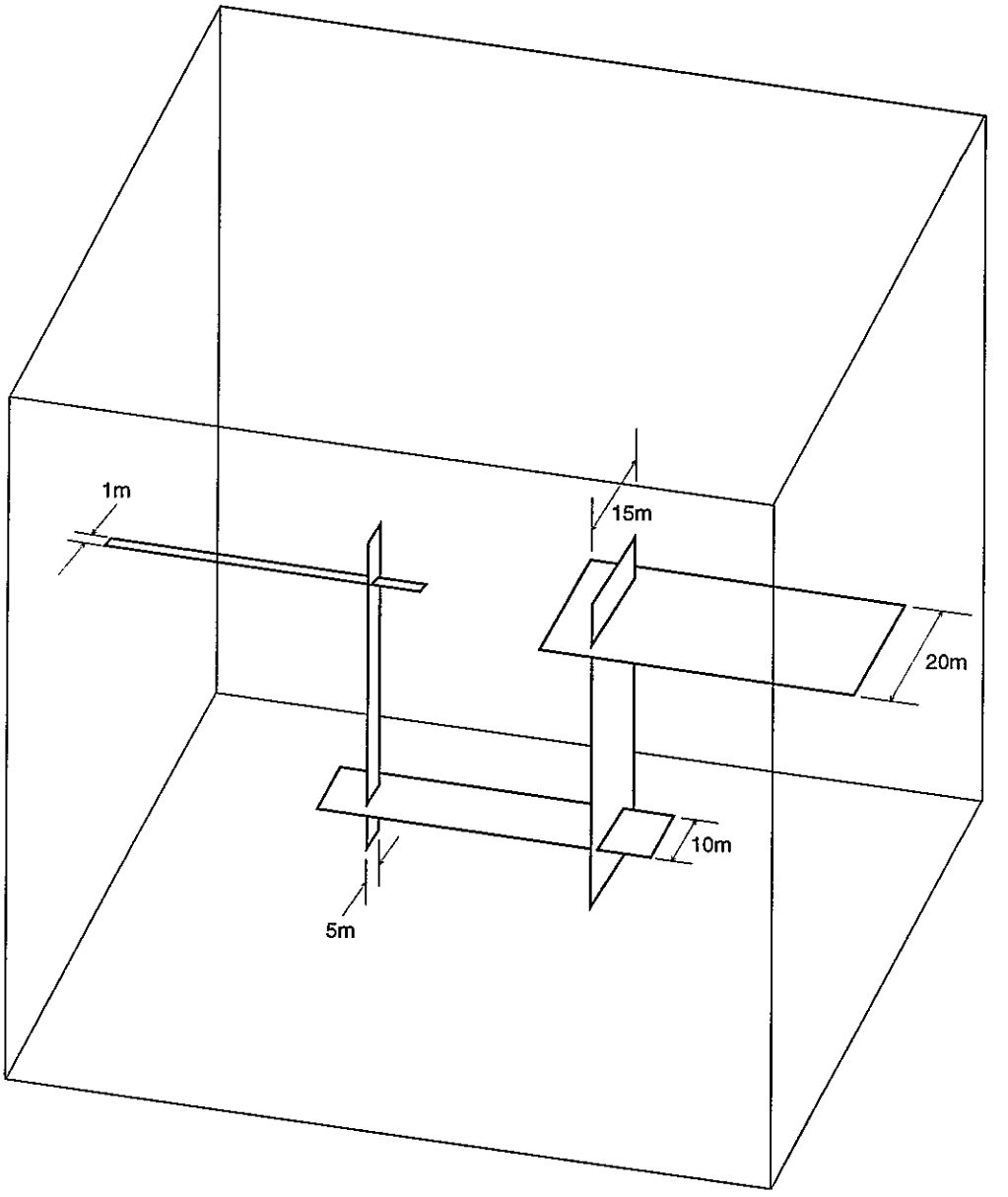

FIGURE **6-4**
FRACTURE NETWORK FOR CASE 3
PNC/PAWORKS

PROJECT NO. 923 1089.811 DWG. NO. 72333 DATE 6/16/98 DRAWN CB

Golder Associates

The verification criterion for Case 3 was as follows:

- Values for head drop reported by PAWorks must match those given in Table 6-2 to within 0.01m.

Theoretical solutions are calculated in the spreadsheet PAWorks.xls and summarized in Table 6-2 below. PAWorks statistical output file PA1_00.sts was renamed Case3.sts and the head values extracted for Table 6-2. Examination of the table demonstrates that the verification criterion has been met.

Table 6-2 Heads on PAWorks Pipes, Case 3

	Given			*Calculated with Excel*				*PAWorks*
Fracture	T	W_0, W_1	L	W_e	C	Φ	Δh	Δh
1	5.e-7	1m, 1m	10 m	1 m	5.00 e-7	2.97 e-6	59.48	59.48
2	1.e-6	1m, 5m	20 m	3 m	3.00 e-6	2.97 e-6	19.23	19.23
3	4.e-6	5m, 10m	30 m	7.5 m	3.00 e-5	2.97 e-6	2.97	2.97
4	3.e-7	10m, 15m	20 m	12.5 m	3.75 e-6	2.97 e-6	15.86	15.86
5	2.e-6	15m, 1m	10 m	8 m	1.60 e-5	2.97 e-6	1.86	1.86

6.5 Case 4: Verification of the algorithm for calculating heads based on the finite element method

The finite element algorithm for calculating heads in PAWorks was verified by comparison to an analytical solution for an equivalent electrical circuit. Figure 6-5 shows the pipe network -- there are a total of eight fractures, two constant head boundaries and two constant flow boundaries. Given the "resistance" of each pipe (resistance is a function of transmissivity, width and length of the fracture) the heads can be calculated at each node by solving a system of simultaneous linear equations. (These calculations are performed in the spreadsheet PAWORKS.XLS, sheets *Case4a*, *Case4b*, and *Case4c*.)

In three subcases, the transmissivities of the fractures were varied. In Case 4a, transmissivities for all fractures was equal. In Case 4b, the outer four fractures had transmissivities two orders of magnitude less than the inner four fractures. In Case 5c, transmissivities were randomly assigned to each of the eight fractures.

Table 6-3 demonstrates that PAWorks calculated the correct head values on all 20 nodes within 0.001m.

Table 6-3 PAWorks vs. Analytical Head Values

Node	Location		Head, Case 4a		Head, Case 4b		Head, Case 4c	
	x	y	PAWorks	Analytic	PAWorks	Analytic	PAWorks	Analytic
1	-5	4	201.929	201.929	350.981	350.981	208.604	208.604
2	-4	0	300.000	300.000	300.000	300.000	300.000	300.000
3	-4	1	248.148	248.148	233.766	233.766	258.280	258.280
4	-4	2	222.365	222.365	200.659	200.659	236.347	236.347
5	-4	3	207.836	207.836	200.987	200.987	217.985	217.985
6	-4	4	200.929	200.929	250.981	250.981	208.493	208.492
7	-3	1	222.079	222.079	200.640	200.640	236.673	236.673
8	-3	2	211.111	211.111	200.325	200.325	223.302	223.302
9	-3	3	200.214	200.214	200.490	200.490	209.115	209.115
10	-3	4	193.021	193.021	200.974	200.974	198.361	198.361
11	-2	1	206.979	206.979	199.026	199.026	223.672	223.672
12	-2	2	199.786	199.786	199.510	199.510	212.013	212.013
13	-2	3	188.889	188.889	199.675	199.675	198.223	198.222
14	-2	4	177.921	177.921	199.360	199.360	181.539	181.539
15	-1	1	199.071	199.071	149.019	149.019	214.693	214.693
16	-1	2	192.164	192.164	199.013	199.013	203.181	203.181
17	-1	3	177.635	177.635	199.341	199.341	188.243	188.243
18	-1	4	151.852	151.852	166.234	166.234	159.155	159.155
19	-1	5	100.000	100.000	100.000	100.000	100.000	100.000
20	0	1	198.071	198.071	49.019	49.019	214.578	214.578

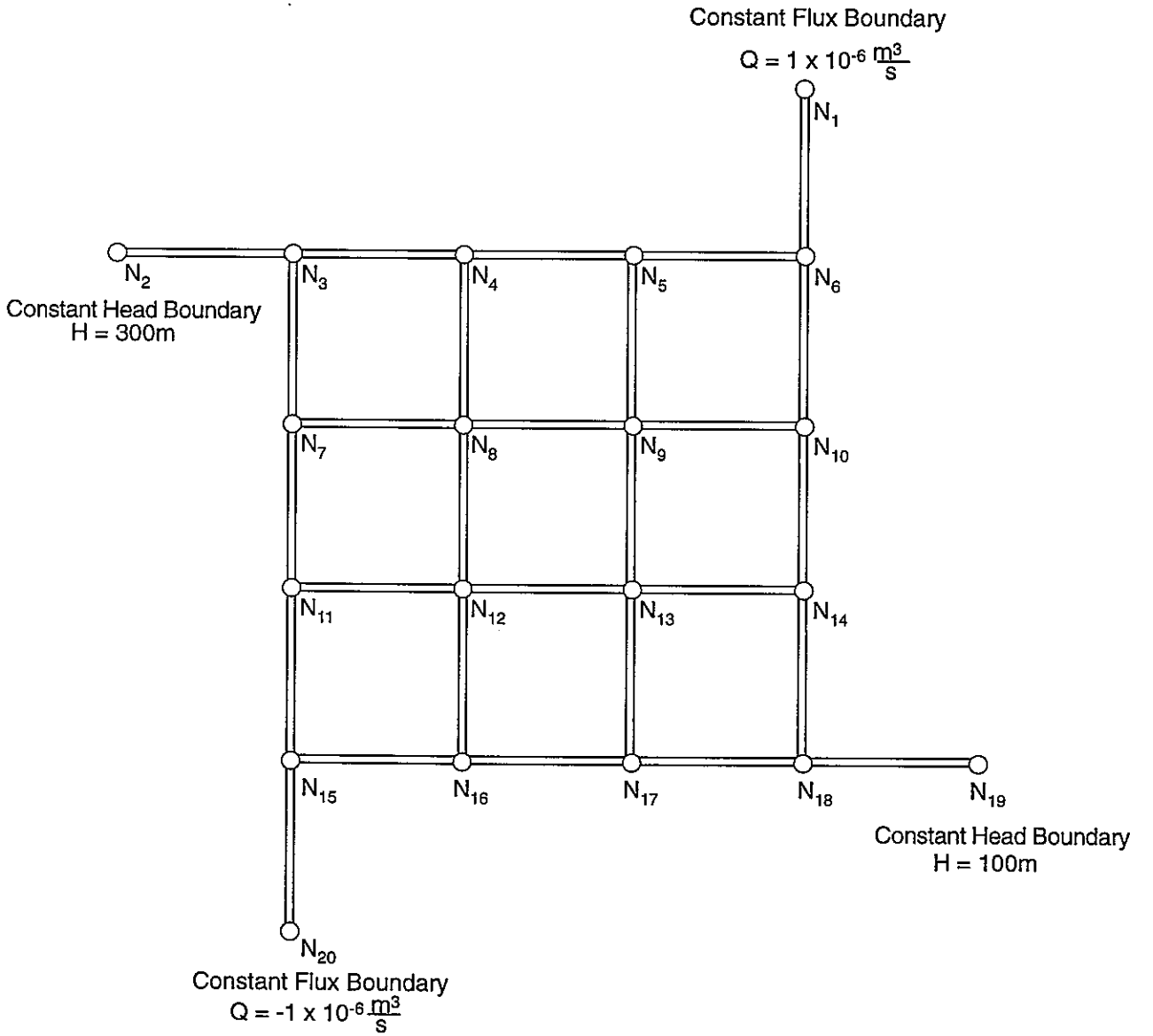

FIGURE **6-5**
PIPE NETWORK FOR CASE 4
PNC/PAWORKS

6.6 Case 5: Verification of the algorithm for calculating heads based on MAFIC output files

The algorithm for calculating heads based on MAFIC output files scans a user provided MAFIC output file for head values on the same element boundary with PAWorks nodes are located. Verification for this algorithm requires comparison of the heads calculated by PAWorks to head values calculated by hand from the MAFIC output file.

The fracture network used for this case is identical to that used in Case 2 (Figure 6-3a). The nodes and the expected head values based on the output file for this case are shown in Table 6-4.

The verification criterion for Case 5 was as follows:

Nodal heads produced by PAWorks must match the theoretical head values to within 1/2% of the maximum head value (0.05m).

Table 6-4 demonstrates that the verification criterion has been met. The PAWorks head values were taken from the raw output file Case5.txt.

Table 6-4 Head Values for Case 5

Node	Location			Head	
	x	y	z	Theoretical	PAWorks
1	0	-60	30	10.000	10.000
2	0	-30	30	7.280	7.280
3	0	-30	0	5.803	5.803
4	0	-30	-30	5.576	5.576
5	0	0	-30	5.049	5.049
6	0	0	0	4.937	4.937
7	0	0	-60	4.815	4.815
8	0	30	-60	4.430	4.430
9	0	30	0	4.087	4.087
10	0	30	30	2.777	2.721
11	0	60	30	0.000	0.000

6.7 Case 6: Verification of pathway identification

To verify the pathway identification algorithm, the model geometry was defined by a 200 meter scale cube, with a 30 meter long, vertical source borehole in the center of the model, and a 30 meter long vertical sink borehole at a distance of 60 meters north from the center of the model (Figure 6-6). A stochastic discrete fracture model was then generated consisting of 1000 fractures using the statistics given in Table 6-5. In addition to the stochastic fractures, ten deterministic fractures were defined, which form two distinct

pathways between the source and the sink boreholes. The geometry of these fractures is shown in Figure 6-7.

PAWorks was then used to identify pathways within the two discrete fracture systems. Case 6a included only the deterministic fractures. Case 6b included both deterministic and stochastic fractures. Verification was to be established if PAWorks could identify the deterministically defined pathway in addition to pathways formed by the stochastically generated fractures. The deterministic and stochastic pathways were identified between source and sink, thus fulfilling the verification requirement.

Table 6-5 PAWorks Verification Case 6

	Set #1	Set #2
Generation Region	200m x 200m x 200m	200m x 200m x 200m
Location Model	Deterministic	Baecher Centers
Orientation	Varied	Fisher, K=10
Size	R=10 to 15m	Lognormal, R_μ=10, R_σ=3
Intensity	10 Fractures	1000 Fractures
Transmissivity	10^{-4}	Constant T =10^{-6}
Storativity	10^{-4}	Constant S=10^{-6}
Aperture	10^{-4}	Constant A=10^{-6}
Flow-Wetted Surface	1	1

6.8 Case 7: Verification of the algorithms for defining the properties of the pathways

The pathway properties to be verified for PAWorks calculations include:

- geometric characteristics: pipe and network length, nodal coordinates, flow widths, penetration depths
- effective flow parameters: conductance, pipe flow radius, plate flow aperture
- effective transport parameters: flow wetted surface area, travel time, pipe transport radius, plate transport aperture.

For Case 7, the pathway properties for the pathways of Case 3 were calculated using the equation given in section 5 above. The calculations were performed using Excel; the results are shown in Table 6-6 comparing the theoretical values to PAWorks values. Pathway properties produced by PAWorks match theoretical values within 0.5%, thus verifying the PAWorks pathway properties algorithms.

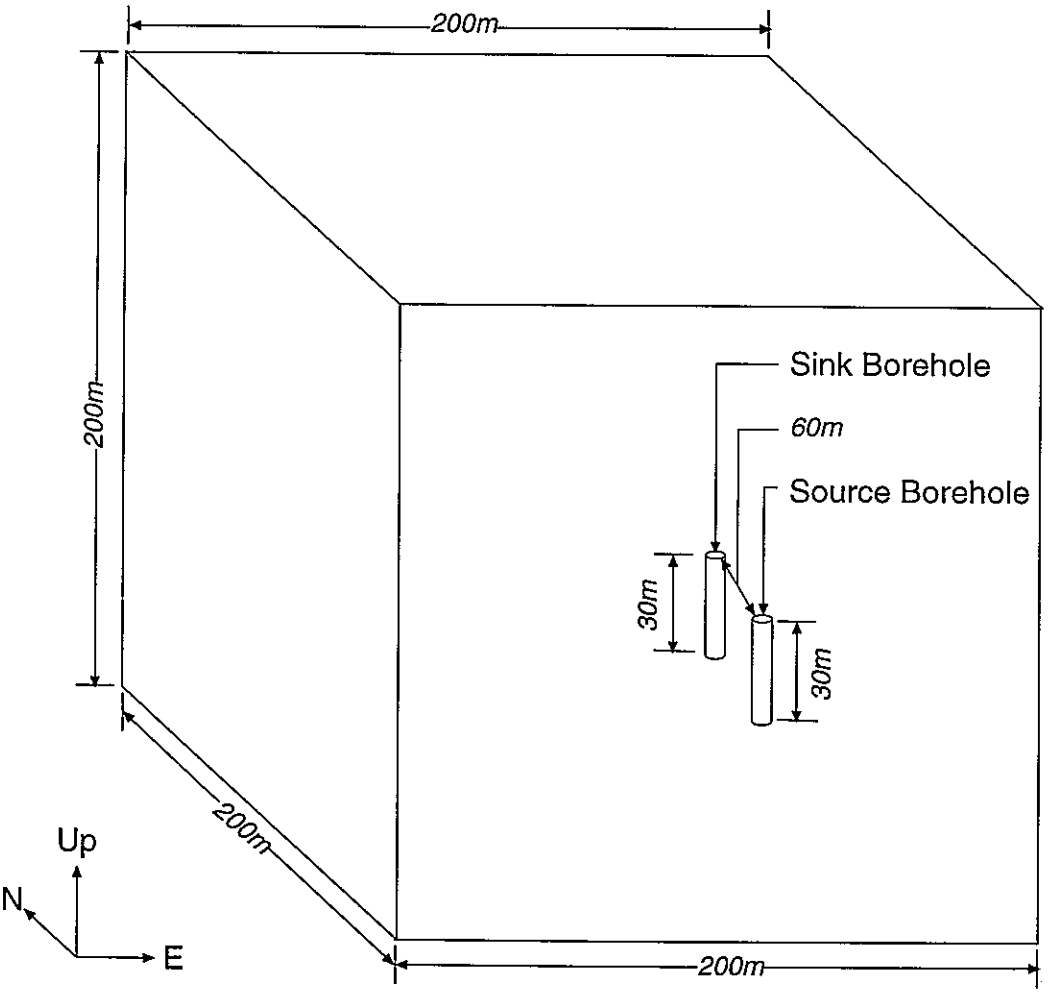

FIGURE **6-6**
MODEL GEOMETRY FOR CASE 6
PNC/PAWORKS

PROJECT NO. 923 1089.811 DRAWING NO. 72337 DATE 6/16/98 DRAWN BY TK

Golder Associates

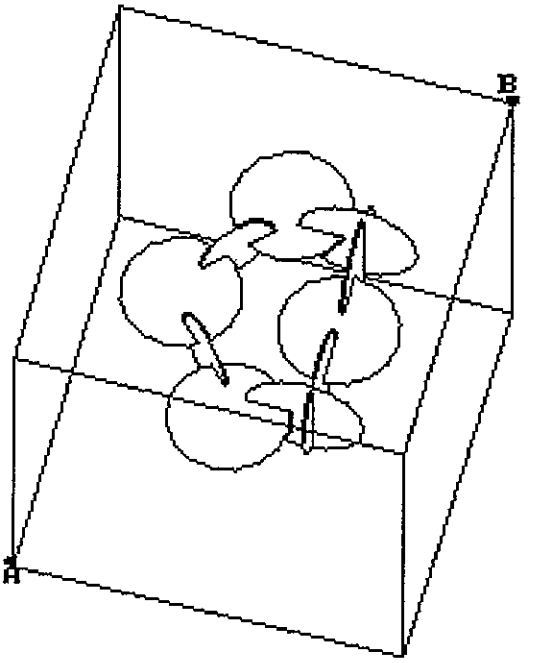

(a) Deterministic Fractures

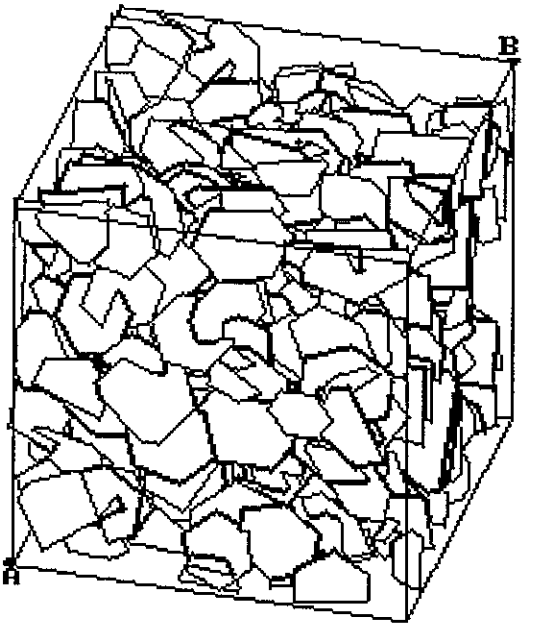

(b) All Fractures

FIGURE **6-7**
FRACTURE NETWORK FOR CASE 6
PNC/PAWORKS

Table 6-6: Expected Pathways from Excel Calculation

Parameters		PAWorks Values						Theoretical Values					
		Pipe 1	Pipe 2	Pipe 3	Pipe 4	Pipe 5	Pathway	Pipe 1	Pipe 2	Pipe 3	Pipe 4	Pipe 5	Pathway
Geometric Properties													
L	Length	10	20	30	20	10	90	10	20	30	20	10	90
W	Width	1.00	3.00	7.50	12.50	8.00	13.08	1.00	3.00	7.50	12.50	8.00	13.07
SA	Surface Area	n.r.	n.r.	n.r.	n.r.	n.r.	625	10	60	225	250	80	625
General Transport Properties													
T	Trans.	5.00E-7	1.00E-6	4.00E-6	3.00E-7	2.00E-6	2.05E-7	5.00E-7	1.00E-6	4.00E-6	3.00E-7	2.00E-6	2.05E-7
ΔH	delta Head	5.95E+1	1.98E+1	2.97E+0	1.59E+1	1.86E+0	n.r.	5.95E+1	1.98E+1	2.97E+0	1.59E+1	1.86E+0	1.00E+2
i	hydr. grad	5.95E+0	9.91E-1	9.91E-2	7.93E-1	1.86E-1	n.r.	5.95E+0	9.91E-1	9.91E-2	7.93E-1	1.86E-1	1.11E+0
C	Conductance	n.r.	n.r.	n.r.	n.r.	n.r.	2.68E-6	5.00E-7	3.00E-6	3.00E-5	3.75E-6	1.60E-5	2.68E-6
Plate Transport Properties													
e_p	Hydr. Aperture	0.00009	0.00011	0.00017	0.00007	0.00013	6.31E-5	8.49E-5	1.07E-4	1.70E-4	7.16E-5	1.35E-4	6.31E-5
A_p	X-Section Area	8.50E-5	3.21E-4	1.28E-3	8.96E-4	1.08E-3	8.25E-4	8.49E-5	3.21E-4	1.27E-3	8.95E-4	1.08E-3	8.24E-4
V_p	Volume	8.50E-4	6.43E-3	3.83E-2	1.79E-2	1.08E-2	n.r.	8.49E-4	6.42E-3	3.82E-2	1.79E-2	1.08E-2	7.42E-2
K_p	Plate Conductivity	5.88E-3	9.34E-3	2.35E-2	4.18E-3	1.48E-2	3.24E-3	5.89E-3	9.34E-3	2.35E-2	4.19E-3	1.48E-2	3.25E-3
t_p	Plate Travel Time	2.86E+2	2.16E+3	1.29E+4	6.03E+3	3.63E+3	2.50E+4	2.86E+2	2.16E+3	1.29E+4	6.02E+3	3.63E+3	2.49E+4
v_p	Plate Velocity	3.50E-2	9.26E-3	2.33E-3	3.32E-3	2.76E-3	3.61E-3	3.50E-2	9.26E-3	2.33E-3	3.32E-3	2.76E-3	3.61E-3
Tube Transport Properties													
r_t	Hydr. Radius	8.00E-4	1.25E-3	2.23E-3	1.32E-3	1.90E-3	1.22E-3	7.99E-4	1.25E-3	2.23E-3	1.32E-3	1.90E-3	1.22E-3
A_t	tube x-sect area	2.01E-6	4.92E-6	1.56E-5	5.50E-6	1.14E-5	4.65E-6	2.01E-6	4.92E-6	1.56E-5	5.50E-6	1.14E-5	4.65E-6
V_t	tube vol	2.01E-5	9.84E-5	4.67E-4	1.10E-4	1.14E-4	4.18E-4	2.01E-5	9.84E-5	4.67E-4	1.10E-4	1.14E-4	4.18E-4
K_t	Tube Conductivity	2.49E-1	6.10E-1	1.93E+0	6.82E-1	1.41E+0	2.98E-1	2.49E-1	6.10E-1	1.93E+0	6.82E-1	1.41E+0	2.98E-1
t_t	Tube Travel Time	6.75E+0	3.31E+1	1.57E+2	3.70E+1	3.82E+1	2.72E+2	6.75E+0	3.31E+1	1.57E+2	3.70E+1	3.82E+1	2.72E+2
v_t	Tube Velocity	1.48E+0	6.05E-1	1.91E-1	5.41E-1	2.62E-1	3.31E-1	1.48E+0	6.05E-1	1.91E-1	5.41E-1	2.62E-1	3.31E-1

6.9 LTG Verification Cases

The examples presented here are intended to serve as verification problems to ensure that LTG correctly solves the governing equations. Thus, the test problems all involve transport along a one-dimensional flow path for which exact analytic solutions exist. The results from these analytic solutions will therefore be compared to the output obtained from LTG. The test problems were designed to test a hierarchy of transport processes represented in LTG, and range in complexity from strictly one-dimensional advective-dispersive transport of a single, nonreactive solute, to the migration of a three-member decay chain comprised of sorbing radionuclides in a system of parallel fractures.

6.10 Single-porosity Test Problems 8 & 9: Transport of a Nonreactive Solute

This problem consists of the transport a single nonreactive solute (retardation $R = 1.0$, decay constant $\lambda = 0.0$) by advection and dispersion in a single-porosity domain. The input Darcy flux, q, is 1.0 m/day, the pipe area, A, equals 1.0 m^2 and the longitudinal dispersivity, α, is 1.0 m. Diffusion along the flow direction is neglected for simplicity. The domain is 100m in length and the spatial discretization is 2.0 m. This grid spacing, combined with an input dispersivity equal to 1.0 m, yields a grid Peclet number, Pe, equal to 2.0. A Dirichlet boundary condition was specified at the inflow end of the physical system in which the concentration was set to 1.0 Ci/m^3.

The LTG results are shown in Figure 6-8 for transport times equal to 25, 50, and 75 days and they are compared to those obtained with the well-known Ogata-Banks analytic solution. It can be seen that for $Pe = 2.0$, the LTG results are essentially identical to the analytical solution. The test problem was also repeated using a coarser grid spacing equal to 10.0 m ($Pe = 10.0$). The LTG results obtained with the coarse grid also compare very well with those calculated using the analytic solution. This demonstrates the effectiveness of the LTG scheme to resist unwanted numerical dispersion.

In order to test the effect of the injection of a solute-free (i.e., $C^* = 0.0$) groundwater, the problem described above was repeated ($Pe = 2.0$ case) using a flow system of length 200m and with groundwater injected at the rate of $Q = 10$ m^3/day at a point 100m from the inlet boundary. Thus, the Darcy flux, q, is 1.0 m/day at the inlet and abruptly increases to 11.0 m^3/day at distance of 100 m. Figure 6-9 shows the LTG results at a time equal to 150 days. The reduction in the concentration at the injection point agrees closely with that calculated analytically based on mass balance considerations.

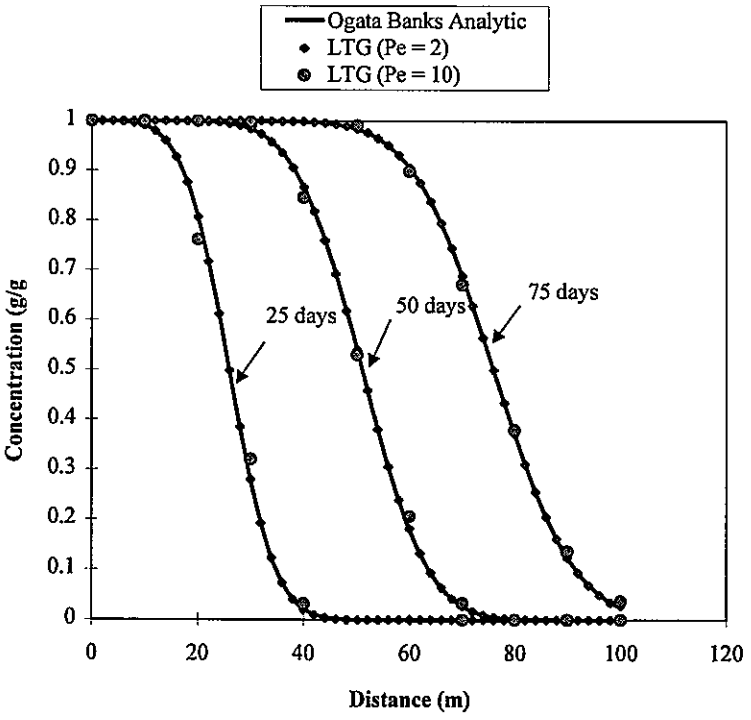

Figure 6-8 Test Problem 8:Comparison of LTG results to those from Ogata-Banks analytic solution for the case of one-dimensional advective-dispersive transport of a nonreactive solute.

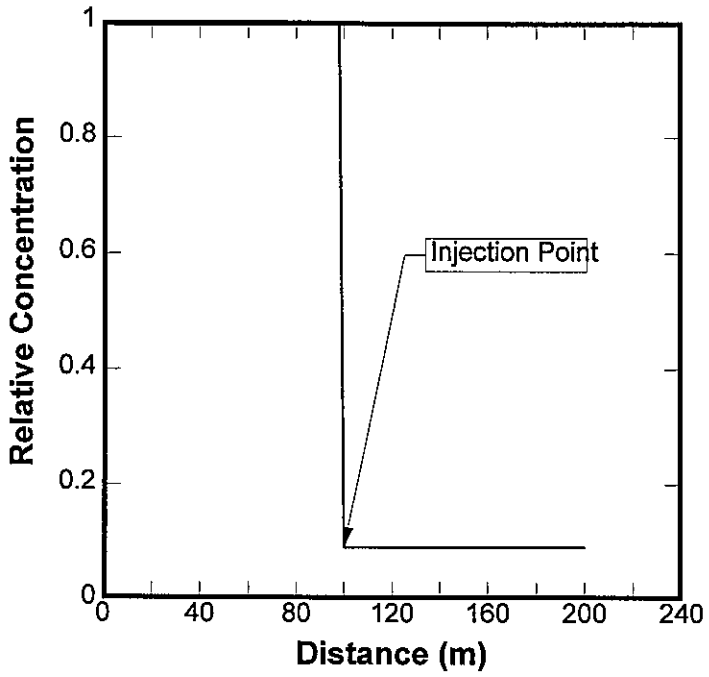

Figure 6-9 Test problem 9: LTG results for injection of solute-free groundwater at x = 100m.

6.11 Test Problem 10: Transport of Tritium in a System of Parallel Fractures

This problem is concerned with the transport of a decaying, non-sorbing (i.e., $R = 1.0$) solute in a double-porosity system comprised of parallel fractures embedded in low-permeability, low-porosity rock matrix. The solute is tritium which has a half-life of 12.35 years ($\lambda = 1.54 \times 10^{-4}$ days^{-1}). The flow system is 300 m in length and the aperture of the parallel fractures, spaced at 0.1 m, is 100 μm. With this setting, the pipe area, A, is equal to 10^{-4} m^2. The Darcy flux, q, is 0.1 m/day in the fractures and the longitudinal dispersivity of the fractures, α, is 0.1 m. The free-solution diffusion coefficient for tritium, D^o, equals 1.38×10^{-4} m^2/day. The matrix porosity, θ_{im}, and tortuosity, τ, are 0.01 and 0.1, respectively. A value of maximum diffusion distance, d^*, equal to the half-spacing of the fractures (0.05 m) was used.

In order to facilitate a comparison with the exact analytic solution of Sudicky and Frind (1982), it is necessary to account for the different definition of mobile/immobile zone mass transfer coefficient, α, used in Equation 5-48. The value of α used in of Sudicky and Frind (1982) uses $d^{*2}/3$ instead of d in Equation 5-48.

The mesh spacing used is 10.0 m which yields a grid *Pe* number equal to about 100. The concentration was fixed at 1.0 at the inlet boundary.

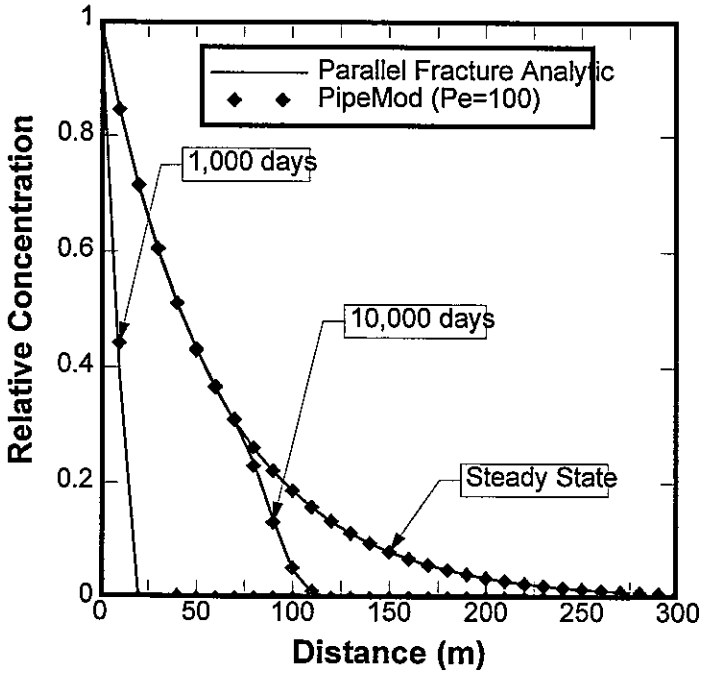

Figure 6-10 Test Problem 10: Transport of tritium in a system of parallel fractures.

Figure 6-10 compares the LTG results with those obtained with the analytic solution of Sudicky and Frind (1982) at times equal to 1,000, 10,000 days and at steady-state. It can be seen that LTG yields highly-accurate results even though a coarse grid is used. Indeed, at 1,000 days, only the first node within the domain has a non-zero concentration and the concentration at this node agrees with the analytic solution.

6.12 Test Problem 11: Decay Chain Transport in a System of Parallel Fractures

The final test problem involves the transport of the decay chain Uranium 234 → Thorium 230 → Radium 226 in a system of parallel fractures and is designed to verify many of the processes represented in LTG. The fracture aperture, fracture spacing and matrix porosity values are identical to those used for test problem 3 described above; however, for this example the Darcy flux, q, in the fractures is 100 m/year and the longitudinal dispersivity of the fractures, α, is 10.0 m. The flow system is 500 m in length and a grid spacing of 10 m was used. The matrix (i.e., immobile zone) retardation factors for U^{234}, Th^{230} and Ra^{226} were assigned values equal to 1.43×10^4, 5.00×10^4 and 5.00×10^2, respectively, and the decay constants equal 2.83×10^{-6}, 9.00×10^{-6} and 4.33×10^{-6} year^{-1}, respectively. For simplicity, retardation on the surfaces of the fractures (i.e., pipes) was neglected. Tortuosity in the matrix was set to 0.1 and the diffusion coefficients for each of the species, D^o, were assigned identical values equal to 3.154×10^{-2} m^2/year. Once again, to facilitate comparison to the analytic solution of Hodgkinson and Maul (1985) for chain-decay transport in a system of parallel fractures, account needs to be taken of the differing definition of the mobile/immobile zone mass transfer coefficient. A prescribed concentration of 1.0 was assigned for U^{234} at the fracture inlet, but 0.0 was used as the inlet concentration for Th^{230} and Ra^{226}.

Figure 6-11 compares the LTG results to those obtained with the analytic solution of Hodgkinson and Maul (1985) at a time equal to 100,000 years. It can be seen from the results that LTG is capable of accurately representing the transport of a reactive decay chain in a double porosity-medium. While all of the examples involved a flow system that is essentially one-dimensional, it should be kept in mind that the code is structured to handle an arbitrary network of interconnected pipes in three-dimensional space; however, exact analytic solutions for such a setting are unavailable for comparison to LTG. It should also be mentioned that LTG has been coded to achieve a high degree of efficiency. For example, the 100,000 year simulation involving test problem 4 required only 0.22 seconds of CPU time on a 200 *mhz* Pentium PC.

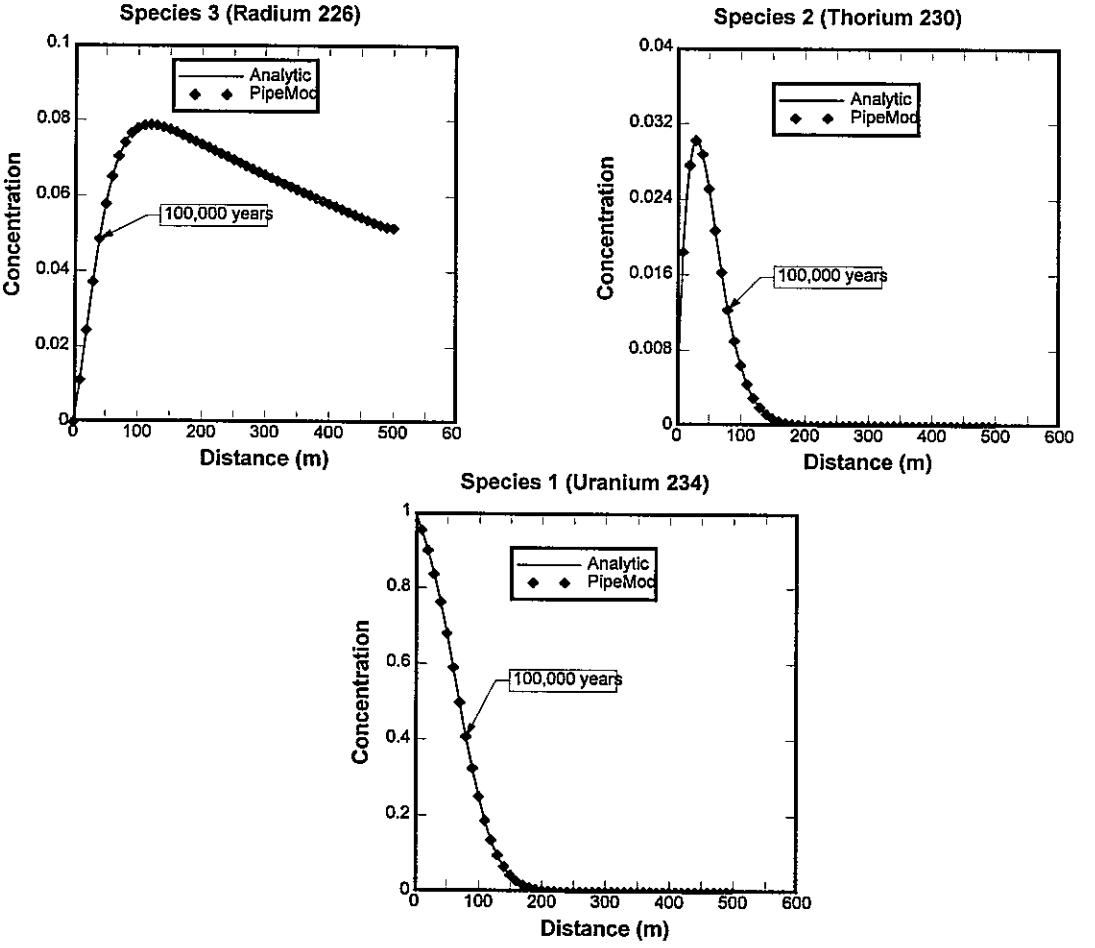

Figure 6-11 Test Problem 11: Decay Chain Transport in a System of Parallel Fractures.

7. REFERENCES

de Hoog, F.R., Knight, J.H. and Stokes, A.N., 1982. An improved method for numerical inversion of Laplace transforms, SIAM J. Sci. Stat. Comput., 3(3), 357-366.

Dershowitz, W., G. Lee, J. Geier, T. Foxford, P. LaPointe, and A. Thomas, 1995. FracMan Interactive Discrete Fracture Data Analysis, Geometric Modeling, and Exploration Simulation. User Documentation. Version 2.5. Golder Associates Inc. Report 923-1089. Golder Associates Inc, Seattle.

Hodgkinson, D.P. and Maul, P.R., 1985. Harwell Laboratory of the United Kingdom Atomic Energy Authority report "One-dimensional modelling of radionuclide migration through permeable and fractured rock for arbitrary length decay chains using numerical inversion of Laplace transforms", September, 1985.

Lee, G., W. Dershowitz, and J. Geier, 1994. EdMesh Discrete Fracture Mesh Editor. User Documentation. Version 1.3. Golder Associates Report 923-1089. Golder Associates Inc, Seattle.

Miller, I, G. Lee, W. Dershowitz, and G. Sharp, 1994. MAFIC Matrix/Fracture Interaction Code with Solute Transport. User Documentation, Version 1.5. Golder Associates Inc. Report 923-1089. Golder Associates Inc, Seattle.

Sudicky, E.A. and McLaren, R.G., 1992. The Laplace transform Galerkin technique for large-scale simulation of mass transport in discretely fractured porous formations, Water Resour. Res., 28(2), 499-514.

Sudicky, E.A., 1990. The Laplace transform Galerkin technique for efficient time-continuous solution of solute transport in double-porosity media, Geoderma, 46, 209-232.

Sudicky, E.A., 1989. The Laplace transform Galerkin technique: A time-continuous finite element theory and application to mass transport in groundwater. Water Resour. Res., 25(8) ,1833-1846.

Sudicky, E.A. and Frind, E.O., 1982. Contaminant transport in fractured porous media: Analytical solutions for a system of parallel fractures. Water Resour. Res., 18(3), 1634-1642.

van der Vorst, H., 1992. Bi-CGSTAB: A fast and smoothly converging variant of Bi-CG for the solution of nonsymmetric linear systems, SIAM J. Sci. Stat. Comput., 13, 631-644.

VanderKwaak, J.E., Forsyth, P.A., MacQuarrie, K.T.B. and Sudicky, E.A., 1997. WatSolv: Sparse Matrix Iterative Solver, User's Guide for Version 2.16, Groundwater Simulations Group, Waterloo, Ontario, Canada.

8. APPENDICES

Table A-1: Example PAWorks SAB File

```
#######################################################################
#######
#test.sab
#-- test file for paworks command line interface
#######################################################################
#######

BEGIN paworks_runtime
      dopath = 1
      docluster = 1

     ###
     # List fracture files (.FAB only) to process here
     # One file per line please.
     ###
     BEGIN frac_files
           sf
      END

      ###
      # The sab file that GenPipes will use
      # Usually this will be the same file PAWorks will use
      # but it doesn't necessarily have to be.
      ###
      BEGIN sab_file
           test
      END

      ###
      # These are the runtime parameters GenPipes requires.
      #     sab_transfer: the transfer file (.sab) that GenPipes
will generate
      #     mafic_output: the output file mafic will generate
      #     frac_area_file: the file for fracture areas
      #     min_T: minimum transmissivity cuttoff for fractures
      #     merge_factor: factor used in merging 2 nodes
      ###
      BEGIN gen_pipes_parameters
           sab_transfer = pawxfer
           mafic_output = pawmfc
           frac_area_file = farea.bin
           min_T = 1e-010
           merge_factor = 0
      END

      ###
      #Head calculation options:
      #     head_calc_type = linear
      #     head_calc_type = mafic
      #     head_calc_type = file
```

```
#     maf_file = restart.maf
###
BEGIN head_calc
      head_calc_type = mafic
END

###
#Aperture caluclation options:
#     apert_calc_type = weighted
#     apert_calc_type = use_T
#     apert_calc_type = use_Q
#     apert_calc_type = use_Qout
###
BEGIN aperture_calc
      apert_calc_type = weighted
END

###
#Graph traversal options:
#     path_weights = none
#     path_weights = transmissivity
#     path_weights = flux
#     path_weights = resistance
#     path_weights = travel_time
#     path_search = simple
#     path_search = weight_larger
#     path_search = weight_smaller
#     path_search = minimize_weight
###
BEGIN path_search_options
      path_weights = none
      path_search = weight_larger
      max_num_paths = 100000
      max_branches = 2
      compute_penetration = FALSE
      depth_option = fracs
      depth_fracs = all_fracs
      depth_samples = 50
      damk_thresh = 1e+020
      Fa = 1
END

###
#Representative path generation options:
#     path_option = travel_time
#     path_option = source
#     path_option = exit
###
BEGIN rep_path_generation
      path_option = source
      max_roots = 5
      max_branches = 5
      weight_fraction = 1
END
```

```
   ###
   # Boundary definition
   #     define sources and sinks for PAWorks graph traversals.
   #     you can define boundary pipes as coming from either a
   #           - boundary group
   #           - owner fracture fracture set
   #           - owner fracture index
   #
   # Specify numeric ranges as comma delimited numbers with
   # ranges specified using hyphens, eg. 1,2,3,5,7-12,15,18
   # Multilines are ok just remember the comma.
   #
   # It's also okay to remove the empty BEGIN/END blocks.
   ###
   BEGIN source_def
         BEGIN bdry_groups
               None
         END
         BEGIN frac_sets
               None
         END
         BEGIN frac_ids
               3
         END
   END
   BEGIN sink_def
         BEGIN bdry_groups
               None
         END
         BEGIN frac_sets
               None
         END
         BEGIN frac_ids
               2
         END
   END

###
#Output options
#  If an output option is missing you won't get it.
###
   BEGIN pa_output
         ###
         # root name for rip files (*.RIP, *.RIP2)
         ###
         rip_file = test

         ###
         # root name for stats files (root_01.sts, etc.)
         ###
         sts_root = test

         ###
```

```
            # view dec alpha output (GeomView)
            ###
            view_transfer = test

            ###
            # controls for diagnostic output
            ###
            diag_file = test.dig
            dump_runtime = TRUE
            dump_nodes = TRUE
            dump_pipes = TRUE
            dump_adjacency = TRUE
            dump_paths = TRUE
            dump_reppaths = TRUE
      END

      ###
      # LTG Options
      ###
      BEGIN LTG_options
            RunOut = ltg.dat
            PipeOut = grid.in
            PipePropOut = pipevel.in
            RetardOut = retard.in
            ImmZoneOut = immzone.in
            ImmPropOut = immdata.in
            FluxOut = flux.in
            out_root = ltgroot

            ###
            # path_selection = real
            # path_selection = representative
            ###
            path_selection = real

            title = LTG Title
            logprt = .FALSE.
            Cauchy = .TRUE.
            multifile = .FALSE.
            peclet_threshold = 2
            dispersion_length = 0.5
            infill_density = 2400
            infill_thickness = 0.02

            ###
            # immobile zone definition
            ###
            BEGIN immobile_zones
                  n_zones = 0
                  # matrix, toruousity, porosity, density, diffusion
distance
                  # noflow, toruousity, infill_thickness,
infill_density, distance
            END
```

```
            ###
            #output nodes
            ##
            BEGIN output
                  output_spacing = 5
                  n_output_times = 0
            END

            deltol = 1e-012
            level = 5
            nitmax = 500
            order = .TRUE.
            reduce = .TRUE.
            nterm = 5
            relerr = 1e-009
      END
END

# This is the end of the PAWorks runtime parameters          #
#####################################################################
###



#####################################################################
###
# Genpipes parameters
#
# From this point on is the sab file that GenPipes would expect
# to see. Defines boundaries, boundary conditions and header for
# mafic run.
#
# Mafic reads the output from GenPipes.
#####################################################################
###
BEGIN mesh_header
   mafic_header   = "MAF_Head.maf"
   outer_boundary = "out_bnd"
   #inner_boundary = "inner_1"
   initial_head = "init_H"
   initial_flux = "init_Q"
END

BEGIN boundary_condition
   name ="init_H"
   boundary_condition_type = constant_head
   BEGIN boundary_values
      Hx =   0.000E+00
      Hy =   0.000E+00
      Hz =   0.000E+00
      Ho =   0.000E+00
   END
END
```

```
BEGIN boundary_condition
    name ="init_Q"
    boundary_condition_type = constant_flux
    BEGIN boundary_values
       Qx =   0.000E+00
       Qy =   0.000E+00
       Qz =   0.000E+00
       Qo =   0.000E+00
    END
END


BEGIN flow_boundary
    name = "out_bnd"
    region_type = prism
    region_name = "out_bnd"

    BEGIN boundary_groups
       up =      1
       down =    2
       wall_1 =  3
       wall_2 =  5
       wall_3 =  4
       wall_4 =  6
    END
END


BEGIN prism_region
    name ="out_bnd"
    origin =   0.000E+00    100.       0.000E+00
    axis_trend  =      270.00
    axis_plunge =        0.00
    axis_length =      200.00
    cross_polygon = "out_bnd"
END

BEGIN polygon_2D
    name ="out_bnd"

    BEGIN 2d_data
          #    x           y
          # ----    --------
       -100.0000    100.0000
       -100.0000   -100.0000
        100.0000   -100.0000
        100.0000    100.0000
    END
END
```

```
BEGIN MAF_Head.maf
Benchmark Test Case Header # 1
 $MAFIC  $END
 Proj    iOut   iPlot  iEtype   iStart  iMtype  iTrans  I2D
 .900       0       0       1        1       1       0    1
 Tolerance   MaxIter
  1.000E-08   1000
  Time Steps       Output Flag   nSteps
      1.0000          1             1
      .00000          0             0
 NODAL GROUPS
     6
 Data Pairs for Nodal Group   1         BND-TYPE=  1
   0       0.000E+00  0.000E+00  0.000E+00  0.000E+00
[Hx,Hy,Hz,Ho]
 Data Pairs for Nodal Group   2         BND-TYPE=  1
   0       0.000E+00  0.000E+00  0.000E+00  0.000E+00
[Hx,Hy,Hz,Ho]
 Data Pairs for Nodal Group   3         BND-TYPE=  1
   0       0.000E+00  0.000E+00  0.000E+00  0.000E+00
[Hx,Hy,Hz,Ho]
 Data Pairs for Nodal Group   4         BND-TYPE=  1
   0       0.000E+00  0.000E+00  0.000E+00  0.000E+00
[Hx,Hy,Hz,Ho]
 Data Pairs for Nodal Group   5         BND-TYPE=  1
   0       0.000E+00  0.000E+00  0.000E+00  1.000E+01
[Hx,Hy,Hz,Ho]
 Data Pairs for Nodal Group   6         BND-TYPE=  1
   0       0.000E+00  0.000E+00  0.000E+00  0.000E+00
[Hx,Hy,Hz,Ho]
 Solute Transport Mode
    0
*** HEADER
END
```

Appendix F NETBLOCK Literature Review

Golder Associates Inc.

4104-148th Avenue, NE
Redmond, WA 98052
Telephone (206) 883-0777
Fax (206) 882-5498

Golder Associates

REVIEW OF RECENT NORTH AMERICAN AND EUROPEAN LABORATORY STUDIES OF FLOW IN FRACTURED MEDIA

Prepared for:

Power Reactor and Nuclear Fuel
Development Corporation
Tokai, Japan

Submitted by:

Charles Wilson
William S. Dershowitz

Golder Associates Inc.
Redmond, Washington

April 1, 1996

923-1089
0403WSD1.DOC

TABLE OF CONTENTS Page No.

1. INTRODUCTION

1.1 Background

A fracture network rock block experiment called NETBLOCK is being planned by the Power Reactor and Nuclear Fuel Development Corporation (PNC) of Japan to further the state of knowledge of fluid flow and transport in fractured geologic media. The review of North American and European recent laboratory experiments in fractured media presented in this report will support design of the NETBLOCK experiment by providing summaries of work being done by others, identifying key unresolved issues in fracture flow theory, and providing recommended experimental and numerical approaches to resolving the issues. PNC is already familiar with the state of the art of laboratory rock block experiments in Japan, and therefore these experiments were not included in the current survey.

The objective of the NETBLOCK experiment is to provide a better understanding of the hydraulic and transport properties of networks of natural fractures, with the ultimate goal of predicting the ability of a low permeability, fractured rock mass to safely isolate radioactive waste materials. NETBLOCK will allow detailed testing of a rock block up to one meter in size with the ability to isolate fluid injection and discharge occurring over small areas on the surfaces of the block. The NETBLOCK experiments will include flow and transport in single fractures, two intersecting fractures, and multiple fracture networks. The information presented in this report will be used to help develop the detailed objectives, design, implementing procedures, and analysis tools for the experiment.

1.2 Scope

The scope of this study is to review and summarize the current state-of-the-art in laboratory experiments in fractured media, and in the modeling and other analytical tools used to analyze and interpret the experimental results. Emphasis in this review is placed upon experiments conducted within the past ten years. A good review of fracture flow and transport studies through 1990 is provided by Joseph Wang (1991). The theoretical issues addressed in these experiments are reviewed and key unresolved issues in fracture flow theory are identified. Recommended experimental approaches to resolving the issues are presented, with emphasis on those issues that can be addressed by NETBLOCK. Recommended modeling tools are also presented for analyzing and interpreting the experimental results, and an overview of recommended testing methods is presented.

1.3 Report Organization

The results of this study are presented in seven sections. Following this introduction, a summary of the objectives, approach, and results of recent laboratory experiments is presented in Section 2. When available, references to published descriptions of the experiments are provided for more detailed information. A summary of the numerical

models that have been used for analyzing experimental results is provided in Section 3, with references again provided for more detailed information. Key unresolved issues in fracture flow theory are presented in Section 4, as identified from the review of experimental results. Recommendations are provided beginning in Section 5 for experimental approaches to resolving the theoretical issues, in Sections 6 and 7 for modeling tools to analyze experimental results, and in Section 8 for testing procedures, equipment design, and sample preparation.

2. SUMMARY OF RECENT LABORATORY EXPERIMENTS

A summary of selected recent laboratory experiments is presented in this section that illustrate the various aspects of current experimental research into fracture flow and transport. The principal publications describing recent laboratory research in fracture flow and transport that were identified in this literature review are listed in Table 1. The reviewed research addresses saturated and unsaturated flow and transport, coupled hydromechanical effects, fracture intersection mixing studies, and fracture network studies. Of the recent laboratory studies identified, all but two address flow in single fractures. Of these two, one addresses fracture intersection mixing, and the other addresses flow in fracture networks. Additional publications describing numerical rather than experimental studies in fracture flow and transport were also reviewed, and are discussed in Section 3.

2.1 Mixing at Fracture Intersections - Chunhong Li

Theoretical and experimental studies of mixing at fracture intersections were performed as part of a Ph.D. thesis by Chunhong Li at the New Mexico Institute of Mining and Technology (Li, 1995).

2.1.1 Experimental Objectives

Perform numerical simulations and physical experiments to investigate the mixing behavior at idealized fracture intersections in the low to middle range of fracture intersection Peclet numbers (1 to 200).

2.1.2 Experimental Approach

Physical experiments were performed with a smooth-wall fracture intersection model fabricated from lucite blocks to test the results of numerical simulations. The model fractures were orthogonal with apertures of 500 microns, depths of 1.85 cm, and lengths of 20 cm. Chlorine and bromine solutions were used as tracers to determine the mixing behavior at the intersection. Concentrations at the outlet fractures were determined using chromatographic methods. The principal experimental variable was the flow velocity, which although varied was maintained the same in both fractures. All experiments were performed using the same fixed-geometry physical model. The experiments were conducted for Peclet numbers ranging from 1 to 170.

2.1.3 Analysis Methods

Detailed studies of advective and diffusive transport within the fracture intersection were studied with numerical simulations using lattice gas automata (LGA) techniques developed by Dr. Li and described in the referenced thesis.

2.1.4 Results Obtained

The results indicate that for Peclet numbers smaller than 1, diffusion dominates the transport process in the intersection and results in complete mixing. For Peclet numbers in the range of 1 to 170, a transition occurs where both diffusion and advection are important. Although Li's experiments did not reach higher Peclet numbers, the experimental results of Hull and Koslow (1986) are considered to demonstrate that for Peclet numbers greater than 200 the mixing will be advection-controlled and streamline routing techniques will be appropriate. Earlier numerical studies of mixing at fracture intersections by Brian Berkowitz et al. (1994) indicated transition occurring at lower Peclet numbers, with diffusion dominating at $Pe < 5x10^{-3}$ and advection control dominating at $Pe > 1x10^{-1}$. This difference may in part result from different definitions of the velocity term in the Peclet number. No other laboratory tests of fracture systems are being conducted at New Mexico Institute of Mining and Technology at this time.

2.1.5 Unresolved Issues

The results of Li's experiments provide good insights into mixing behavior under fairly simple geometric and hydrologic intersection conditions. Remaining unresolved are detailed physical model studies of:

- intersections of fractures of unequal apertures;
- intersections of fractures with unequal flow rates;
- intersections of non-orthogonal or offset fractures; and
- intersections of rough-wall fractures.

2.2 Coupled Hydromechanical Characteristics of Natural Fractures - Derek Elsworth and Andrew Piggott

Experimental studies were conducted on the coupled stress, permeability, and transport characteristics of a natural fracture at the National Water Research Institute in Ontario, Canada (Elsworth and Piggott, 1993).

2.2.1 Experimental Objectives

The experimental studies were conducted to provide experimental support for the body of analytical work in coupled hydromechanical behavior in fractures by providing flow and transport behavior in the presence of both normal and shear displacements.

2.2.2 Experimental Approach

The study was conducted on a single fracture in a 190 mm diameter granite core retrieved from the Underground Research Laboratory of Atomic Energy of Canada Limited in Manitoba. The fracture had a surface area is 190 x 320 mm and was the same fracture studied by Piggott an Elsworth in their laboratory study of equivalent apertures

discussed elsewhere in this review (Piggott and Elsworth, 1993a). The suite of tests was conducted under sufficient control to define the evolution of porosity distributions with displacement, to define the potential for flow and transport through channeling, and to define these characteristics with respect to fundamental knowledge of fracture roughness. Fracture surface roughness was initially characterized on a 5 x 5 mm grid using a large profilometer capable of resolving elevation differences to 0.01 mm. The core was then loaded in a biaxial frame capable of applying a maximum of 20 MPa. Fluid flow and transport were studied over the 320 mm length of the specimen, facilitated by 20 small 4 mm diameter boreholes on a rectangular grid providing access to the fracture surface. Displacements were controlled by studs mounted on the upper and lower halves of the specimen. Tests were performed under applied loads of zero and 5 MPa.

2.2.3 Analysis Methods

Analytical evaluations of test results were performed to determine aperture characteristics inferred from alternative measurement techniques. Experimental results were reported from direct measurement.

2.2.4 Results Obtained

Results from the study define processes rather than absolute magnitudes of parameters and consequently are general to a variety of geological environments. Changes in average aperture are reported for varying normal loads and shear displacements. Application of a 5 MPa normal load was found to decrease average fracture aperture by approximately 30 percent, while a lateral (shear) displacement of the fracture surface increased average aperture by a factor of about 4. Differences between flow-determined apertures and tracer-determined apertures were thought to result from higher-aperture channels in the fracture surface and emphasize the need to characterize the fracture using tests that directly address the process of interest. Application of tests that characterize flow, non-reactive transport, reactive transport, and particle transport in a methodical manner are thought to offer the possibility of providing progressively increasing levels of constraint to the flow and transport system, and therefore render a portrait of the fracture that offers increasing levels of accuracy.

2.2.5 Unresolved Issues

Results obtained were largely observational and addressed phenomenologically rather than parametrically. Additional studies are needed:

- to better relate the observed experimental results to the characteristics of the rock type and fracture properties;
- to provide a basis for validating predictive models of coupled hydromechanical behavior; and
- to extend the results to other rock and fracture types.

2.3 Aperture Characterization and Flow and Transport Calculations in a Natural Fracture - P. Reimus, B. Robinson, and Robert Glass

Experimental and numerical studies were performed for flow and transport in a natural fracture at Los Alamos and Sandia National Laboratories (Reimus et al., 1993). Single phase transport parameters have also been studied by Keller et al. (1995).

2.3.1 Experimental Objectives

Flow through a fracture with mapped surface topography was compared with numerical modeling results.

2.3.2 Experimental Approach

Surface profile data taken with a noncontact laser profilometer were used to determine aperture distribution within a natural fracture in a sample of Bandelier Tuff from Los Alamos, New Mexico. The fracture surface area studied measured 11.6 by 10.4 cm. A coarse resolution profile was taken with 0.5 mm spacing between points, and a fine resolution profile was taken with 0.05 mm spacing. The numerical model was based on aperture data from only one side of the fracture, with the other side modeled as the mirror image. Hydraulic experiments were conducted on the fracture to determine the effective hydraulic aperture.

2.3.3 Analysis Method

Flow fields associated with the statistical aperture distributions deduced from the surface profile data were calculated using an in-house numerical finite difference model based upon the cubic law. Tracer breakthrough curves were then calculated using a particle-tracking method.

2.3.4 Results Obtained

Comparison of the breakthrough curves obtained using both coarse- and fine-resolution aperture data (0.5 and 0.05 mm spacing between points, respectively) over the same subset of the fracture domain suggests that the spacing between the aperture data points must be less than the correlation length to obtain accurate predictions of fluid flow and tracer transport. Hydraulic testing of the fracture yielded a mean aperture varying from 0.024 to 0.049 mm depending on the normal stress applied across the fracture. De-ionized water used in the flow tests eventually resulted in sealing of the fracture, thought to result from mineral dissolution and reprecipitation. For the numerical studies a mean aperture of 0.056 mm was used, which resulted in an 8.5% contact area and a calculated hydraulic aperture of 0.039 mm.

2.3.5 Unresolved Issues

The overall objective of the series of studies of which this is an early part is to conduct tracer-transport experiments in natural fractures with sufficiently well characterized flow fields that the effects of flow field dispersion on observed transport behavior can be separated from the effects of tracer interactions with rock surfaces (adsorption and matrix diffusion). Future experiments are planned to:

- determine how fine the aperture data resolution must be relative to the correlation length to obtain accurate flow and transport predictions; and
- identify the practical limitations in modeling tracer-transport experiments.

2.4 Tracer Transport Properties in Rough- and Smooth-Walled Fractures - I. Ippolito, P. Kurowski, J.P. Hulin, and G. Daccord

An experimental study of tracer dispersion was conducted in France in single model fractures with rough and smooth walls and with different mean apertures (Ippolito et al., 1995). Similar studies are being conducted in Great Britain at Harwell on samples of granite and slate (Braney et al., 1991; Cliffe et al., 1993). Numerical studies of the sensitivity of fracture parameters to transport were also conducted by Yang et al. (1995), Tsang (1995), and Toran et al. (1995).

2.4.1 Experimental Objectives

Determine the effects of fracture wall roughness on radial and radial/parallel flow geometries for tracer injected into a fracture.

2.4.2 Experimental Approach

Smooth-walled fractures were simulated with flat glass plates, and rough-walled fractures were simulated by replacing one of the flat glass plates with a rough surface zinc plate. The plate roughness pattern was generated by a computer and transferred to the zinc plate through a photographic and acid etching process. The individual surface asperities on the zinc plate have a height of 1 mm and a spacing of 1 mm. For the radial flow tests, round plates 30 cm in diameter were used, and tracer was injected at the center. For the radial/parallel flow tests, 10 x 100 cm rectangular plates were used. Fluid was injected at a point located 1 cm from one end of the plate, and flowed down the length of the plate to the open outlet end. Flow was initially radial near the injection point but became parallel as it progressed down the plate. Fracture aperture was varied by placing 0.5 or 1.0 mm thick rubber spacers near the edges of the plate. The three remaining sides of the plate were sealed with silicon.

An echo technique was used in which the tracer was first injected into the fracture and then pumped back through a detector. This technique allows the experimenter to eliminate the effect of the differences in travel time between the macroscopic flow paths in the system and allows one to isolate the effects of smaller scale features such as the

local fracture aperture and roughness. A salt solution was used as a tracer and electrical conductivity measurements were used to determine variations in concentration.

2.4.3 Analysis Methods

Analytical techniques described in the paper were used to evaluate the results of the echo dispersion test method.

2.4.4 Results Obtained

The echo dispersion technique was found to work well for studying the effects of wall roughness on tracer transit times. The results showed that transmission dispersion, which occurs when tracer traverses the length of a fracture system, is generally controlled by macroscopic differences between the flow path lengths.

2.4.5 Unresolved Issues

The echo dispersion technique may be of use in characterizing local fracture aperture and roughness and should be further evaluated as an analysis technique for determining aperture variations within test specimens. Yvonne Tsang at Lawrence Berkeley Laboratory has conducted additional numerical studies of echo dispersion techniques (which she calls the huff-puff test) as well as other test configurations (Tsang, 1995).

2.5 Coupled Hydromechanical Effects in Fracture Flow - Lee Atkinson and John Gale

2.5.1 Experimental Objectives

Design, construct, and test a large diameter concrete cylinder for validating analytical models for radial flow in a single, rough-walled horizontal fracture (Atkinson and Gale, 1990). Research on coupled hydromechanical effects is also being conducted by Elsworth and Piggott (1993) and by Mohanty et al. (1994 and 1995) at the Center for Nuclear Waste Regulatory Analysis under research grants from the U.S. Nuclear Regulatory Agency.

2.5.2 Experimental Approach

A 3 m high by 1.5 m diameter cylindrical test specimen with a single horizontal fracture was designed and constructed out of concrete to study radial fracture flow. The fracture was created by placing a sheet of geotextile between the top and bottom halves of the cylinder during pouring of the concrete. Twenty-eight piezometers were cast in place in the fracture plane and displacement transformers were installed both on the circumference of the cylinder and in the central wellbore to measure fracture

deformation at applied loads of up to 1 MPa. The model also incorporated features designed to allow withdrawal and injection tests to be conducted with different flow boundary conditions, applied loads, and wellbore diameters. This laboratory setup was used to investigate flow and deformation in the immediate vicinity of a vertical well intersecting a single rough, deformable, horizontal fracture at a depth of 100 m or less and for flow rates of approximately 1.0 L/s.

2.5.3 Analysis Methods

Flow in the simulated fracture was studied using a coupled hydromechanical finite element model developed by Atkinson and described in his unpublished Ph.D. thesis (Atkinson, 1987).

2.5.4 Results Obtained

The principal focus of the paper is on describing design and construction of the test specimen. This laboratory investigation was part of a more comprehensive study that included numerical modeling in an attempt to better understand the production-drawdown response of wells completed into aquifers or reservoirs whose primary conduits are horizontal fractures. More than 60 flow/ deformation tests were conducted on the specimen involving variations in constant rate discharge, variable rate discharge, constant rate injection, boundary fluid pressures, applied normal stress, and wellbore diameter. The actual and modeled fluid pressures in the fracture were very similar when the fracture was open with walls not in contact; however, as applied normal loads were increased and put the fracture surfaces in contact, the best matches of actual and modeled fluid pressures were obtained when the modeled aperture was in the range of 0.3 to 0.8 times the value of the best estimate of the true geometric aperture. Detailed experimental results are presented by Atkinson (1987).

2.5.5 Unresolved Issues

The paper focuses on the design and construction of the model and presents little information on experimental results. The extent to which the synthetic fracture and the properties of the concrete mimic the flow and deformation characteristics of natural rock fractures is not addressed and may remain an outstanding issue. This is the only paper identified in our review that addresses Dr. Gale's recent laboratory work in fractured rock. It is our understanding from telephone conversations that he has since been testing 1 to 2 m rock blocks at applied effective stresses up to 10 MPa. Fluid pressures are monitored at 140 ports around the block, 60 ports are dedicated for studying two phase flow, and LVDTs and strain gauges are used for measuring displacement. He has developed procedures for extracting and preparing these large block samples and is currently carrying out experiments to define laws for fracture desaturation/ resaturation, and relationships between aperture structures and flow and transport properties. He is supported by a consortium of oil companies and considers his work proprietary to the supporting companies. He is asking $10,000 to $20,000 per year to join the consortium and have access to his equipment, procedures, and experimental results.

2.6 Aperture Distributions of Rock Fractures - Eva Hakami

Experimental studies of aperture distributions were conducted by Eva Hakami as part of a Ph.D. thesis at the Royal Institute of Technology in Stockholm, Sweden (Hakami, 1995). This work was supported in part by the Swedish Nuclear Fuel and Waste Management Company.

2.6.1 Experimental Objectives

Develop and apply methods for measuring fracture aperture as a parameter to describe fracture void geometries for use in studying the hydromechanical properties of fractures.

2.6.2 Experimental Approach

Fracture apertures were measured using several techniques: transparent replicas of fracture surfaces using silicon rubber and transparent epoxy molds; injection molds of polyurethane; injection molds of cement grout (for fractures with large apertures); manual aperture measurements from photographs or video films of fracture cross sections; and image analysis of photographs of cross sections of a fluorescent epoxy injection mold. For large fractures, photographs of fracture cross sections can be taken from boreholes drilled parallel to the fracture plane.

2.6.3 Analysis Methods

Numerical modeling of fracture flow was not performed as a part of this thesis.

2.6.4 Results Obtained

Different measurement techniques were found to be advantageous for different types of fractures and measurement objectives. For fractures with very large apertures an in-situ injection technique must be applied and the fracture surface area studied should be large. For fractures with smaller apertures in competent rocks, injection and analysis of sectioned cores is recommended. Fractures can be injected in-situ or in the laboratory and a high color contrast between the rock and injected material is very helpful. The use of transparent fracture replicas is recommended when the fracture models are to be used in flow experiments where advantage is taken of the transparency for studying tortuosity and channeling.

Although relatively few different types of fractures were studied, aperture distributions were often found to be bell-shaped with a percentage of very small apertures in contact areas. Apart from the contact areas, aperture frequencies could be fairly well approximated with normal or log-normal distributions. Distributions became more skewed and the coefficient of variation increased for fractures with large average apertures. Results of flow experiments on fractures with known aperture distributions

showed that the ratio between mean aperture and hydraulic aperture ranged from 1.1 to 1.7 for fractures with mean apertures ranging from 0.1 to 0.5 mm.

2.6.5 Unresolved Issues

Although highly detailed results were obtained, relatively few individual fractures were studied. The following unresolved issues were identified by Dr. Hakami and the authors of this review:

- take more aperture measurements on different types of fractures (such as tensile breaks versus shear faults) to provide a broader basis for generalizing results and developing conceptual models of aperture characteristics - in particular there is a lack of data for fractures with average apertures larger than 0.5 mm;
- aperture data for fracture intersections are very limited and should be collected;
- perform additional studies on correlations between fracture aperture and variably saturated flow, transport, and storage (deformability) characteristics; and
- develop conceptual models of fracture aperture characteristics correlated with fracture types that can in turn be related to hydromechanical behavior.

2.7 Flow in a Network of Variably-Saturated Fractures - Ed Kwicklis

Theoretical and experimental studies of flow in a network of variably-saturated fractures were performed by Ed Kwicklis and others at the U.S. Geological Survey (USGS) laboratory in Denver, Colorado. This work has been completed and the results are in internal review and will be presented in journal publications and internal USGS reports. No additional testing of this type is currently planned.

In addition to the USGS experiment, network studies are currently being performed by Peter Vilks at Atomic Energy of Canada Limited's Whiteshell Laboratory in Manitoba. From telephone conversations, these experiments are reported to involve migration in a 1 m granite cube with one horizontal fracture and several vertical fractures. The studies involve the migration of nonreactive tracers and colloids. Nine small boreholes drilled into the horizontal fracture permit tracer migration to be monitored within the fracture. Publications describing this work were not available during the period of this review.

2.7.1 Experimental Objectives

Determine how closely flow could be predicted in a well characterized, variably-saturated, fractured block of welded tuff, in support of the U.S. Department of Energy's Yucca Mountain Project for high-level radioactive waste disposal.

2.7.2 Experimental Approach

Unsaturated flow was studied in the fracture system within a block of welded tuff with approximate dimensions of 0.5 m x 0.5 m x 0.8 m tall obtained at the Nevada Test Site. Eighteen small diameter boreholes were drilled into the initially dry block to intersect and determine the hydraulic characteristics of the principal fracture planes through air injection tests. These holes were then instrumented with psychrometers and water sprayed on a sand bed on top of the block was allowed to percolate through the block under gravity flow and discharge at the bottom. Through the instrumented holes, the relationship between water potential and flow rate was determined.

2.7.3 Analysis Methods

A numerical model of the fracture network was prepared using Golder's FRACMAN and MAFIC codes. Unsaturated flow was simulated by manually adjusting the permeability in the model depending upon the degree of saturation.

2.7.4 Results Obtained.

The modeling results were found to come close to reproducing the experimental results, and the experiment was considered a success.

2.7.5 Unresolved Issues

Because the detailed experimental methods and results were not available for review, a listing of specific unresolved issues cannot be prepared. However, as with many other aspects of fracture flow theory, principal unresolved issues are expected to be:

- methods for generalizing the experimental results for application to fracture systems that are not as well characterized; and
- the accuracy with which unsaturated flow in less well characterized fracture systems can be predicted.

2.8 Influence of Fracture Aperture on Retardation - Christoph Wels, Leslie Smith, and T.T. Vandergraaf

An experimental study of the migration of sorbing and nonreactive tracers in fractures of different apertures was conducted at the University of British Columbia and at the Atomic Energy of Canada Limited's Whiteshell Laboratories Wels, Smith, and Vandergraff, 1996). Another experimental study emphasizing the importance of reactive tracers was conducted by Vandergraaf (1995). Field studies and numerical simulations of the influence of fracture aperture were conducted by Parney and Smith (1995), and a numerical study of sorption effects in fractured media, looking at controlling influences related to network scale geometry, was conducted by Wels and Smith (1994).

2.8.1 Experimental Objectives

Determine the influence of fracture aperture on the transport of a sorbing tracer.

2.8.2 Experimental Approach

Test specimens of granite from the Lac du Bonnet Batholith in Manitoba, Canada, were prepared with dimensions of 10 x 2.5 x 1.25 cm. Machined fractures of known, constant aperture were prepared by placing narrow teflon spacers between two flat, polished surfaces of the specimens, thereby creating smooth-walled fractures of known, constant apertures. A sorbing strontium tracer and a nonreactive tritium tracer were used in the experiments.

2.8.3 Analysis Methods

Numerical analysis of the test results was not performed.

2.8.4 Results Obtained

Strontium was found to be subject to significantly greater dispersion than the nonreactive tritium tracer. This enhanced dispersion was believed to be the result of chemical heterogeneity at the mineral grain scale, hysteresis in sorption, and limited transverse mixing across the fracture aperture. The influence of fracture aperture was found to be much greater than predicted by the commonly used definition of the surface retardation factor based upon the specific surface area of the fracture (the ratio of the fracture surface area to the volume of mobile water in the fracture). Strontium retardation was approximately an order of magnitude greater in a smaller-aperture fracture (450 um) than in a large-aperture fracture (780 um). The authors hypothesize that hysteresis in sorption (with higher surface distribution coefficients for desorption than for sorption), in conjunction with limited transverse mixing across the aperture, caused the apparent increase in the surface distribution coefficient with a decrease in fracture aperture. The results also suggest that the magnitude of hysteresis increases with the residence time of the sorbing solute in the fracture.

2.8.5 Unresolved Issues

Simultaneous, multiple effects have limited the ability to isolate and quanitfy the specific factors causing the observed differences in dispersion and sorption. Additional experiments could be conducted to evaluate the use of:

- reactive tracers other than strontium that would have different hysteretic behaviors to further study the effect of hysteresis in sorption; and
- rough-walled fractures more closely mimicking those found in nature to enhance transverse mixing across the aperture.

2.9 Laboratory Study of Equivalent Apertures - Andrew Piggot and Derek Elsworth

An experimental study of flow and transport in a natural fracture was performed at the National Water Research Institute in Ontario, Canada (Piggot and Elsworth, 1993a).

2.9.1 Experimental Objectives

Compute hydraulic and electrically derived effective aperture values for a natural fracture in a large granite core, and compare predicted versus actual transport characteristics to validate aperture model.

2.9.2 Experimental Approach

A natural fracture surface measuring 190 x 320 mm encountered in a large diameter granite core at Atomic Energy of Canada's Underground Research Laboratory in Manitoba was tested in the laboratory to determine aperture variations. The testing was accomplished by drilling an array of 20 small 5 mm diameter boreholes to intersect the fracture surface at spacings of about 40 mm. Average aperture in the vicinity of each borehole was determined hydraulically through injection testing and electrically by measuring the resistivity of an injected saline solution. A tracer test was conducted across the entire fracture and tracer movement was monitored in the borehole array.

2.9.3 Analysis Methods

Aperture variation on the fracture surface was modeled at three different degrees of refinement, and numerical simulations of tracer transport were performed for each aperture variation model using a parallel plate finite element model. The methods used to characterize the fracture aperture variation is also described in Piggot and Elsworth (1993b).

2.9.4 Results Obtained

The average hydraulic and electrical apertures were found to be similar indicating minimal fracture surface-to-surface contact. The numerical modeling results reproduced in basic form the experimentally derived rates of tracer migration, which was considered to generally validate the aperture variation models. However, the average transport aperture exceeded the average hydraulic aperture indicating that transport was occurring at a lower velocity than would be predicted on the basis of the hydraulic aperture.

2.9.5 Unresolved Issues

The method can be further advanced through additional studies:

- Apply the method to additional fractures and rock types to further check its validity;

- Evaluate alternative experimental techniques to obtain more refined aperture data;
- Evaluate alternative analysis/ techniques to develop aperture variation maps; and
- Extend the method to developing aperture data near boundaries such as fracture intersections.

2.10 Flow Visualization and Permeability Measurements in Natural Fractures - Peter Persoff and Karsten Pruess

Experiments with two-phase flow have been conducted at Lawrence Berkeley Laboratory in California using transparent replicas of natural rock fractures (Persoff and Pruess, 1995). Related work includes similar but earlier studies by Cox et al. (1990) and Persoff et al. (1991), quantitative visualization of entrapped phases by Glass and Nicholl (1995), fracture-matrix interaction studies by Foltz et al. (1993), Glass et al. (1994), and Tidwell et al. (1995), a laboratory characterization of unsaturated flow parameters by Rasmussen (1995), and an analysis of two-phase flow in regionally saturated fractured rock near excavations by Geller et al. (1995).

2.10.1 Experimental Objectives

Obtain a phenomenological understanding of two-phase flow in rough-walled fractures through visual observations of changes in pore occupancy.

2.10.2 Experimental Approach

Experiments were conducted at carefully controlled flow rates and pressures in a natural fracture and three transparent fracture replicas. In all experiments the two phases were nitrogen gas and water. Liquid was injected at a controlled volume flow rate while gas was injected at either a controlled mass flow rate or a controlled pressure. The inlet and outlet pressures of the two immiscible fluids were measured and movement of the multiphase fluids was observed visually. The fracture replicas were cast with a clear epoxy resin from silicone rubber molds of each side of the fracture. The casts were taken from a fracture in granite from the Stripa Mine in Sweden and a fracture in tuff from Dixie Valley in Nevada. The test fractures were approximately 75 mm wide and 81 mm long. Use of transparent replicas allowed not only flow visualization but also a pointwise measurement of aperture using the light attenuation methods of Glass (1993) and Nicholl and Glass (1994). One phase liquid permeability measurements were first made for a range of flow rates and gas flow was then initiated by injecting gas into the fracture. Gas was observed to displace the liquid and create a flow path from inlet to exit. After each experiment reached steady state, the gas pressure was increased and the liquid pressure decreased and a new experiment was performed. Gas-to-liquid flow rates were varied over three orders of magnitude.

2.10.3 Analysis Method

Permeabilities were calculated for each phase using analytical equations given in the text. Effective hydrodynamic aperture was estimated using the cubic law. Numerical modeling of the tests was not performed.

2.10.4 Results Obtained

Two-phase flow exhibited persistent instabilities with cyclic pressure and flow rate variations even under conditions of constant applied boundary conditions. Visual observations of changes in pore occupancy showed that the instabilities could be explained as resulting from in interplay between capillary effects and pressure drops due to viscous flow. Measurements of relative permeabilities indicated strong phase interference, with relative permeabilities reduced to very small values at intermediate saturations for both wetting and nonwetting phases. These results are counter to the conventional view that the relative permeability of each phase in a fracture is equal to its degree of saturation, but the results are consistent with recent models that view fractures as two-dimensional, heterogeneous porous media. Although the average hydrodynamic aperture of the tuff fracture was only 8.5 um, continuous flow paths taken by the gas phase were everywhere 35 to 70 um or greater and most of the fracture pore space was contained in areas where the aperture was on the order of 100 um. The tuff fracture therefore exhibited strong flow channeling. In experiments on the granite fracture no data are available for conditions in which only one phase is mobile.

2.10.5 Unresolved Issues

The method provides good phenomenological insights into two phase flow in fractures and can be extended to detailed studies of transport processes. The data from such models can be used to prepare and validate detailed numerical models of flow in rough-walled fractures. The paper also presents an extensive reference list that can be used to support further investigations of this type.

2.11 Scaling Behavior for Laboratory Research - Vincent Tidwell

Issues associated with the measurement of heterogeneous media properties at one scale and the application at another scale are addressed in an experimental investigation at Sandia National Laboratories in New Mexico (Tidwell, 1994).

2.11.1 Experimental Objectives

Challenge current understanding of property scaling with the aim of developing and testing models that describe scaling behavior in a quantitative manner.

2.11.2 Experimental Approach

Scaling of constitutive rock properties is investigated through physical experimentation involving the collection of gas permeability data measured over a range of discrete scales. The approach is to systematically isolate those factors that influence property scaling and investigate their relative contributions to overall scaling behavior. Factors influencing scaling behavior, such as heterogeneity structure and characteristics of the sampling and analysis approach, were varied in a systematic fashion to isolate relative contributions to overall scaling behavior. Two blocks of rock, each exhibiting differing heterogeneity structure, were examined. Test specimens approximately 1 m in length were saw cut from larger blocks and the heterogeneous permeability of the block was studied on the cut surfaces. Both specimens studied were welded tuff from the Nevada Test Site, and the principal permeability contrasts resulted from imbedded pumice grains.

2.11.3 Analysis Methods

Simple empirical models were fit to the measured scaling behavior. The models for the two rock blocks are of similar functional form but of different magnitude, reflecting the different scaling behavior observed.

2.11.4 Results Obtained

The two rock blocks were found to have different scaling behavior, as exhibited by changes in the distribution functions and semivariograms.

2.11.5 Unresolved Issues

Although this work does not specifically involve fracture flow properties, the experimental approach of selecting and systematically evaluating the scale effects of key physical properties of the system can be adapted to scaling in fracture flow. Further discussion of the philosophy of this approach is presented in Tidwell et al. (1993).

2.12 Inactive Test Facilities

2.12.1 Colorado School of Mines Experimental Mine

A test block was isolated in the 1980s for fracture flow experiments at the Colorado School of Mines Experimental Mine near Denver, Colorado. Studies of fracture flow were conducted by students Parviz Montazer and later by Leslie Gerts and Jim Kunkel. Dr. Kunkel, now an Adjunct Professor at the school, has indicated that there is no further work being performed on the block and the professor and students originally involved with it have left.

2.12.2 Lawrence Berkeley Laboratory Large Core

A fractured granite core approximately 1 meter diameter by 2 meters long was shipped from the Stripa Mine in Sweden to Lawrence Berkeley Laboratory for fracture flow experiments in the 1980s. Although a series of tests was planned for the core, excessive hydraulic pressure dislocated a key fracture plane in early tests, making it unusable for further experiments.

2.13 Summary of Flow Conditions in Recent Laboratory Experiments

A summary of the mean aperture, flow velocity, transport distance, Peclet characteristic length, Peclet Number, and Reynolds Number used in recent laboratory experiments in fracture flow is presented in Table 2. Mean apertures were generally in the range of 100 to 800 um, but apertures as low as 8.5 um and as high as 1,000 um were studied. Flow velocities were reported for only three of the fourteen experiments identified, and ranged from 1E-6 to 1E-3 m/s. The lack of velocity data results in part because many of the reported experiments involved unsaturated flow where mass flux rate is more important than flow velocity. The transport distance is without exception equal to the longest length of the rock sample, and ranged from 81 to 1,000 mm. Peclet characteristic lengths were reported for two of the experiments and were 350 um for the intersection experiment (defined as half the intersection diagonal) and 1,000 um for one of the saturated, single fracture flow tests (defined as the typical grain height on the rough fracture wall). Reported Peclet Numbers ranged from 1 to 1,000 and reported Reynolds Numbers ranged from 0.0005 to 1.0. These experiments were conducted under laminar flow conditions and generally in the transition range where both advective and diffusive transport are important.

3. SUMMARY OF NUMERICAL MODELING TECHNIQUES

3.1 Modeling Techniques Used in Recent Laboratory Fracture Flow Experiments

A summary of the numerical modeling techniques used to analyze recent laboratory fracture flow tests is presented in Table 3. This table also identifies numerical models used in recent theoretical studies of flow in fractured media. Of the 22 studies listed on the table, only twelve used numerical methods to study fracture flow or analyze experimental results. Also, of the 22 studies on the table, only involved fracture systems more complicated than a single fracture. Most current fracture flow laboratory research is focused upon the simpler flow characteristics and geometry of single fractures where analytical solutions alone may be satisfactory for analyzing test results. However, of the seven studies of more complicated fracture systems, all of them used numerical models for data analysis.

In-house codes that were not named in the cited publication were used in most of the studies. Such codes are generally not well documented nor are they verified through rigorous, documented quality assurance reviews and are not appropriate for supporting a high-level radioactive waste repository program that will receive a high degree of technical and public scrutiny. The remaining codes are the following:

TOUGH2: A 2D/3D integrated finite difference code developed at Lawrence Berkeley Laboratory (Pruess, 1991) and used in two-dimensional applications in the cited studies. This code has been widely used and is well documented. It is discussed further in Section 6 of this report.

FRACMAN/MAFIC: A fracture network generation and 2D/3D discrete fracture finite element flow and transport code developed by Golder Associates Inc. (Dershowitz et al., 1991). This code was used by the U.S. Geological Survey to analyze the only recent laboratory fracture network flow and transport experiment identified in this literature review. It has been widely used and is well documented. It is discussed further in Section 6 of this report.

Lattice Gas Automata (LGA): A particle tracking code developed by Chunhong Li (1995) and used in support of his thesis work at New Mexico Institute of Mining and Technology on mixing at fracture intersections. It is a new code and has been used primarily by its author.

FRACTRAN: A 2D finite element code developed by Sudicky and McLaren (1992) for simulating saturated flow and transport in both fractures and matrix. Fractures are represented as line elements in the code that can be located along and interact with any cell boundary. Because it is limited to two dimensions, however, the code could not be used to model the three-dimensional flow fields in the NETBLOCK experiment.

Statistical Continuum Model (SCM): A particle tracking code developed by Frank Schwartz and Leslie Smith (1988) to simulate mass transfer in fractured rock masses. Statistics on particle motion is first collected in a subdomain model using a discrete network simulation, and these statistics are then applied in a continuum model to simulate transport at a larger scale. The intent of the model is to simulate large-scale transport phenomena by extrapolating from smaller-scale, discrete fracture effects. Such capabilities are not expected to be needed for the NETBLOCK experiment, where a capability to discretely model all major fractures will be required.

DISCRETE: A dual permeability finite difference model developed by T. Clemo at the University of British Columbia for studying flow and transport in networks of fractures (Clemo, 1994). This is a new code and has not been widely used.

3.2 Modeling Requirements for the PNC NETBLOCK Experiment

The model or suite of models that will be required for analyzing the results of the NETBLOCK experiment must be capable of evaluating the flow phenomena that will be studied. Although the final plans for the experiment have not yet been completed, it is expected that they will include the following elements.

- Geometry: Codes must be capable of handling up to three dimensions with irregular fracture shapes and orientations.
- Solver: Codes must have efficient solvers to enable multiple simulations and sensitivity studies.
- Porosity: Codes must be capable of addressing both single porosity (fracture or matrix only), as well as dual porosity and dual permeability simulations.
- Flow Processes: Codes must be capable of simulating both laminar and turbulent flow under steady state and transient conditions.
- Transport Processes: Codes must be capable of modeling advection, dispersion, diffusion, matrix diffusion, retardation/sorption, and mixing.
- Rough-Walled Fractures: Codes must be able to model fluid flow and transport in fractures where the geometry of rough fracture walls simulated.
- Fracture Intersections: Codes must be capable of modeling fluid flow and transport through intersections of rough-walled fractures.
- Matrix Diffusion and Sorption: Codes must be capable of modeling interactions of transported solutes with the fracture walls.
- Diffusion into Low Aperture Areas: Diffusion into low aperture areas within fracture planes may be studied as part of the NETBLOCK experiment, and a capability to model such diffusion should be available.
- Coupled Hydromechanical Effects: Coupled stress-flow effects may be studied as a part of the NETBLOCK experiment, and a capability to model such effects should be available.

Recommendations for codes to address these requirements are presented in Section 6.

4. SUMMARY OF KEY UNRESOLVED ISSUES IN FRACTURE FLOW THEORY

Unresolved issues in fracture flow theory have been identified from the literature review in this report, from issues raised in the planning of fracture flow and transport studies by others (see in particular Olsson et al, 1995), and from Golder's basic knowledge of the state-of-the-art in fracture flow and transport. These issues are listed below and have been prioritized to best meet the needs of the NETBLOCK experiment. A brief discussion of each issue follows this list.

First Priority:

- Mixing laws for fracture intersections and effects of preferential pathways
- Preferential pathways in rough fractures
- Laws for transport in rough fractures
  - Diffusion effects in low aperture areas
  - Diffusion into matrix
  - Effects of preferential pathways on sorption

Second Priority:

- Flow dimensions in single fractures and simple fracture networks
- Fluid storage and compliance laws

Third Priority:

- Effects of gas pockets on flow and transport
- Laws for desaturation/resaturation

4.1 Mixing Laws for Fracture Intersections and Effects of Preferential Pathways

Understanding of mixing at fracture intersections is a high priority because of the significant effect such mixing has on transport. The phenomenon has been studied in the laboratory only for simple fracture geometries and has not addressed wall roughness. The degree of mixing depends on the geometry of the intersecting fractures, including aperture and roughness profile at the intersection, the flow velocities in the intersecting fractures, and the Peclet number in the intersection. A comprehensive experimental evaluation of these factors has not yet been conducted.

4.2 Preferential Pathways in Rough Fractures

Higher aperture pathways within individual fractures have been seen to strongly influence transport velocities yet are the subject of debate within the technical community. If channels result only from random locations of asperities on rough fracture walls, their degree of influence will depend upon the direction of fluid movement within the fracture, which in turn will depend upon boundary conditions. This means that a "channel" will not be detected unless there is a significant component of fluid flow in its direction. However, if channels result from other processes such as selective chemical degredation or precipitation within the smaller aperture areas of a

fracture, or from slight shear movement of the opposite sides of an undulating fracture, true geometric "channels" could result. Sorption of migrating radionuclides on fracture walls has been found to be less within higher aperture areas of fractures. Since these are also often the pathways of most rapid flow and transport, retardation in fracture flow may be less than predicted from statically determined partition coefficients. In the NETBLOCK experiment we may be able to detect preferential pathways through partitioned sample collection and by mapping patterns of sorption on the fracture surfaces from dissection following reactive transport experiments.

4.3 Laws for Transport in Rough Fractures

A knowledge of fracture transport laws is key to evaluating the safety of a mined waste repository. Transport in relation to fracture intersections and preferential pathways has already been discussed. Here we will address two additional but related effects: diffusion into low aperture areas, and diffusion into the rock matrix.

As previously discussed, increased sorption may result in low aperture areas where flow velocities are low. In such areas, molecular diffusion will cause solute movement into such areas at a higher rate than would be predicted from advective transport alone. Diffusive processes transporting solutes into low aperture areas, dead fracture porosity, fracture infillings, and the rock matrix would act to reduce the effects of lower sorption in the higher velocity areas, and may be important to overall mass transport rates. Measurements of solute concentration in the NETBLOCK fractures as a function of local fracture aperture and the aforementioned mapping of patterns of sorption on the fracture surfaces from dissection following reactive transport experiments should provide information relative to the importance of molecular diffusion in fracture flow.

4.4 Flow Dimensions in Single Fractures and Simple Fracture Networks

The issue of "channeling" is really the issue of the dimension of flow in fracture planes. Is the flow radial (2D) or pipe-like (1D), or in-between? Does flow dimension vary with Reynolds number (velocity)? How does flow dimension vary with roughness and infilling? The answers to these questions can be a direct input to safety issues, since even a 1D performance assessment code can reflect different flow dimensions by suing different flow and transport equations. The NETBLOCK experiment transient responses can be interpreted to evaluate relationships between fracture and intersection properties and the dimension of flow and transport within that fracture.

4.5 Fluid Storage and Compliance Laws

The relationship between transmissivity and storativity is a key for understanding transient experiments. Compliance is related to the coupling issue of variation of transmissivity with fluid pressure, flow rate, and stress state. Interpretation of transient responses in NETBLOCK depends upon understanding the fundamental fluid storage relationship. We have been using a very simple relationship for storage for most of our

work, based on a very simple theory. NETBLOCK analyses can provide us with a more defensible relationship.

4.6 Laws for Variably Saturated Flow

Variably saturated flow will occur in the unsaturated zone above the water table and in fractures draining into an entry into an otherwise saturated rock mass. Issues include effects of gas pockets on flow and transport, and the laws for desaturation/resaturation of fractures. Such effects are expected to be largely transient in an underground waste repository located below the water table, and have not been identified as an important objective for the NETBLOCK experiment. However, a considerable effort is being placed on research in unsaturated fracture flow, primarily because of the performance assessment needs of the U.S. Yucca Mountain Project where waste is proposed to be placed in unsaturated, fractured tuff. Several recent laboratory experiments in variably saturated flow in fractures are identified in this report. However, because unsaturated flow tests are not being proposed for NETBLOCK, this issue is not addressed further.

5. RECOMMENDED EXPERIMENTAL APPROACHES TO RESOLVING ISSUES

5.1 Introduction

A systematic series of conceptual single fracture, intersecting double fracture, and fracture network experiments is recommended for NETBLOCK in this section to address the unresolved issues in Section 4 that are of primary interest to PNC. Because few experiments of this type have been successfully accomplished on natural fractures, the approach builds from simple, well-controlled studies of single fractures to more complex studies of fracture networks. The approach for all tests involves in overview the following steps:

- Selecting test specimens with simple, clearly-defined, conductive fractures or fracture systems;
- Characterizing the spatial aperture variation in each fracture in the specimen;
- For the single and double fracture specimens, performing flow and tracer tests on each fracture individually to confirm the inferred aperture distributions;
- Proceeding from simple to more complex tests, with flow patterns controlled (to the extent possible) by boundary conditions;
- Analysis of the results with numerical models;
- Following completion of testing, establish the detailed conductive fracture characteristics with fracture casting techniques; and
- Refine numerical model based upon information derived from fracture casts.

An important consideration for all fracture flow experiments is the careful excavation, shipping, and handling of the fractured rock samples. Physical disturbance of the fracture plane can significantly alter the flow and transport characteristics of the fracture because once dislocated, the fragile fracture wall grains and infilling minerals tend to prop the fracture open and attempts to close the fracture and regain its original flow characteristics are often futile. Because of the strong, approximately cubic relationship between aperture and flow in a fracture, even very small aperture increases significantly increase flow conductance. The importance of maintaining a positive compressive stress on the fracture samples to keep the fracture planes from separating is emphasized in the recommendations in Section 7.

5.2 Single and Double Fracture Experiments

5.2.1 Experimental Objectives

The single and double fracture experiments will be used to accomplish the following:

- Establish and refine experimental techniques;

- Test models and methods of data analysis; and
- Determine characteristic test results for the rock type studied.

The single and double fracture experiments are expected to allow resolution of selected unresolved issues under conditions that are sufficiently controlled to yield results that are unambiguous on the scale of the test. Recognizing that control of flow and transport in the fracture network tests is unlikely to be complete, it will be important to first conduct the simpler single and double fracture experiments in the same rock type to check experimental and analytical techniques and determine the behavior characteristics to be expected in the network.

5.2.2 Experimental Approach - Single Fracture Tests

Single fracture tests are tests of rock specimens containing only one fracture. Because these tests are simplest and best controlled, they should be performed first. Depending upon schedule and cost constraints, similar suits of tests should be performed on at least three test specimens as a check on variability.

Selecting Test Specimen. The test specimen should have one clearly defined, conductive planar fracture. The test specimen and fracture should be of the same rock and fracture type as those to be tested in the larger network block. The specimen should be large enough compared to the fractures in the network block that the effects of scale on the experimental results are minimized. Finally, the specimen should be prepared such that flow and tracer tests can be run in reverse and orthogonal directions.

Aperture Characterization. Characterize the spatial aperture variation in the fracture by intersecting the fracture with an array of small diameter (approximately 5 mm) boreholes drilled normal to the fracture surface. The approach is similar to that used by Piggott and Elsworth (1993) in a single fracture in a granite block from Canada's Underground Research Laboratory, and by the U.S. Geological Survey in a block of tuff from the Nevada Test Site (Ed Kwicklis, personal communication). Piggott and Elsworth placed their boreholes in a square array about 4 cm apart. The USGS study has not been published and details of the experiment are not available. Average hydraulic apertures weighted to the vicinity of each hole can then be determined by sequentially performing fluid injection or withdrawal tests in each hole. Alternative analytical techniques can be applied to assign aperture values to the vicinity of each borehole and construct aperture maps of the fracture surface. Complementary aperture information can be obtained by injecting saline solutions and measuring electrical resistivity within the fracture fluid; however, this method may alter the structure of clays that may be present in the fracture and is not recommended without further study.

If the testing times can be made sufficiently long to measure hydraulic transients, flow dimensions may be established from the test results, and fluid storage effects may be evaluated using non-tested boreholes as observation wells. Evaluation of the results of such transient tests will, however, require control of external loads on the specimen

which should be maintained at approximately insitu levels if stresses are not varied in the experiment.

Aperture Confirmation and Tracer Testing. Confirm the spatial aperture variation by tracer testing following the approach of Piggot and Elsworth (1993). Introduce a tracer at one side of the specimen and allow it to migrate to the opposite side while maintaining no flow boundaries on the sides parallel to the direction of flow. Monitor tracer movement through the borehole array. Model tracer migration for various aperture maps and evaluate the most effective data reduction techniques. Repeat in reverse and orthogonal flow directions. Evaluate effects of preferential pathways on tracer migration rates and sorption. Repeat for various flow rates to study advective and diffusive effects focusing on Peclet Numbers in the range of <1 to 200. Repeat, if desired, for point source tracers and study plume migration and growth. Retardation of the tracer may be attributable to matrix diffusion, and records should be kept of tracer concentrations and exposure durations at selected locations in the fracture for later analysis of diffusion into the matrix.

Boreholes located in areas of very low aperture could be used to study the diffusion of tracer into such areas, however the size and shape of the low aperture area are not expected to be well known and the results of such tests in natural fractures could be largely qualitative depending upon the results of the fracture casts discussed below.

Post-Test Analysis. Following the flow and tracer tests, a fracture cast will be made using a low viscosity resin injected into the conductive zones of the fracture. Upon hardening of the resin, the specimen can be opened along the fracture and the resin cast removed. If accurate casts can be made, the variation in fracture aperture can be directly measured and compared with the previous hydraulically inferred variation. Also, sections of the specimen can be cut normal to the fracture and tested for matrix diffusion of the tracer and sorption along preferential flowpaths.

5.2.3 Experimental Approach - Double Fracture Tests

Double fracture tests are tests of rock specimens containing two intersecting fractures. These tests should be performed following the single fracture tests. Depending upon schedule and cost constraints, similar suits of tests should again be performed on at least three specimens as a check on variability.

Selecting Test Specimen. The test specimen should have two clearly defined, conductive planar fractures that intersect at a known angle. The same considerations of rock and fracture type and scale effects as discussed for the single fracture tests should be applied. Also, the specimen should be prepared such that flow and tracer tests can be run in reverse and orthogonal directions.

Aperture Characterization. Characterize the spatial aperture variation in each fracture by intersecting the fracture with an array of small diameter (approximately 5 mm) boreholes drilled normal to the fracture surface. The approach will be the same as described above for the single fracture test.

Aperture Confirmation and Tracer Testing. Confirm the spatial aperture variation by tracer testing generally following the approach described above for single fracture tests. Test each fracture separately through limiting the flow to that fracture alone by establishing no-flow boundaries on the intersecting fracture and on the sides of the specimen parallel to the direction of flow. Monitor tracer movement through the borehole arrays. Model tracer migration for various aperture maps and evaluate the most effective data reduction techniques. Repeat in reverse and orthogonal flow directions to evaluate flow characteristics parallel with the fracture intersection.

Intersection Effects. Evaluate mixing at the fracture intersection by introducing different conservative tracers at each of two inflow sides and measuring tracer mixing at each of two outflow sides. Maintain no-flow boundaries on sides of specimen parallel to flow direction. Monitor tracer movement through borehole array. Vary flow rates and flow directions, achieving Peclet Numbers in the range <1 to 200. Model tracer migration and correlate mixing with flow rates and aperture variations along intersection. Repeat, if desired, for point source tracers and study plume migration, growth, and bifurcation at intersection.

Post-Test Analysis. Following the flow and tracer tests, a fracture cast will be made using a low viscosity resin and analyzed as described above for single fractures. If successful, the cast can be used to obtain accurate measurements of fracture aperture along the intersection as well as the fractures, and can help to support a more refined numerical analysis of the test results.

5.2.4 Expected Results

The single and double fracture tests will provide an analysis of the effects of fracture roughness on flow, transport, and intersection mixing. Preferred flow pathways are expected to be identified, and their effects studied both within the fracture and at intersections.

Experimental and analytical techniques will be developed for identifying aperture variations on fracture surfaces and mixing at fracture intersections, for later application to characterizing fracture networks within a test block. The results will also help to validate numerical models of
flow and intersection mixing in rough-walled fractures.

5.2.5 Additional Tests

Although of lower priority to the PNC, with modifications a similar experimental approach could be used to study unsaturated flow and desaturation/resaturation effects, and the effects of applied mechanical and thermal stresses on increasing or decreasing fracture apertures.

5.3 Fracture Network Experiments

5.3.1 Experimental Objectives

The NETBLOCK fracture network experiments will be used to accomplish the following:

- Apply experimental techniques for single and double fractures to a more complex fracture network;
- Study flow and transport effects in network of fractures;
- Determine accuracy with which a well-characterized fracture network can be modeled;
- Test models and methods of data analysis; and
- Determine characteristic test results for the rock type studied.

The fracture network experiments are expected to indicate the extent to which the experimental and analysis techniques developed for the more simple single and double fracture experiments explained in Section 5.2 can be applied to characterize flow and transport in a more complex fracture network where more than one fracture flowpath may be present between block boundaries. A basic understanding of selected key unresolved issues is expected to be obtained from the more simple experiments. Laboratory experiments on the more fracture network will be a test of the adequacy of that understanding and the ability to extend it to a more complex and less controlled environment. As with the single and double fracture tests, a post-test casting will be made of the conductive fractures to aid in identifying the actual geometry of the fracture network and in refining the numerical analysis of the test results. The capability to extrapolate behavior from simple to more complex fracture geometries will be essential to demonstrating the safety of a nuclear waste repository.

5.3.2 Experimental Approach

Fracture network tests are tests of rock specimens containing multiple fractures with multiple internal flowpaths connecting the various sides of the test block. Because these tests are more complex and difficult to interpret, they should be performed after the single and double fracture tests are completed and the effectiveness of the experimental and analytical methods have been demonstrated. If cost and schedule permit, similar tests should be performed on more than one specimen to better demonstrate the experimental and analytical capabilities.

Selecting Test Specimen. The test specimen is planned to be a rock cube with side dimensions of about 1 m. The conductive fractures in this block should form a relatively simple network with no more than approximately two planar fractures in each fracture set and no more than three fracture sets. The block should be constrained such that fractures do not open during handling and testing. The test block and fractures should

be of the same rock and fracture type as those used in the single and double fracture tests. The specimen should be prepared such that flow and tracer tests can be run in multiple directions.

Aperture Characterization. Characterize the spatial aperture variation in each major conductive fracture in the block by intersecting the fracture with an array of small diameter (approximately 5 mm) boreholes drilled normal to the fracture surface following the same approach used in the single and double fracture tests. This will provide a preliminary, nondestructive characterization of the fracture network in the block that will be used to develop predictive models of flow and transport for studying later, more complex flow tests.

Tracer Testing. During this phase, tracer will be introduced into the test block to study various fracture flowpaths. Although the specifics of these studies will depend upon the actual fracture network configuration in the block that is selected for this test, the objectives of the tests will be to:

- Confirm the spatial aperture variation following the approach of Piggot and Elsworth (1993);
- Determine the flow characteristics and preferred fracture flowpaths within the block through controlling boundary conditions on all six sides of the block;
- Study intersection mixing at various flow velocities (maintaining Peclet Numbers in the range <1 to 200) through simultaneous use of two or more tracers; and
- Evaluate numerical modeling techniques for predicting and analyzing the experimental results.

To the extent possible for the specific fracture network being studied, the network tests will proceed from simple flow paths involving a minimum number of fractures and intersections to more complex flow paths involving parallel flow conduits and multiple intersections. Flow within the test block will be controlled by controlling boundary conditions, and the paths taken by the tracer can be monitored using the array of small diameter fracture-intersecting boreholes. However, if the fracture system cannot be well characterized, it may not be possible to separately distinguish multiple effects occurring simultaneously from fracture roughness, multiple intersections, matrix diffusion, and other influences. Under such circumstances, an accurate understanding of the network's flow characteristics may have to await the results of the post-test fracture casting described below.

If characterization of the fracture system and flow characteristics are reasonably well achieved during flow and transport testing, it may be feasible to attempt more complex experiments such as studying the migration and plume development of a point source tracer, studying diffusion of tracer into the matrix, fracture fillings, or into areas of low fracture aperture, and hydromechanical effects on the network. With the application of an external mechanical stress, fracture planes normal to the direction of loading would be expected to close, while fractures perpendicular to the loading would be expected to open.

Post-Test Analysis. Following the flow and tracer tests, a cast of the conductive fractures will be made as described above for the single and double fracture tests. Analysis of the cast is expected to provide detailed geometric information on the fracture network to support a more accurate modeling of the flow and transport characteristics of the test block.

5.3.3 Expected Results

The fracture network experiments are expected to provide insight into the accuracy with which the flow and transport characteristics can be modeled and possibly predicted within a well-characterized array of natural fractures. The experimental results will demonstrate the effectiveness of both the experimental and the data analysis techniques. It is expected that if the tested fracture system is sufficiently simple, the flow and transport characteristics will be modeled with a degree of accuracy that will enhance confidence in the experimental and analysis techniques. However, natural fracture systems can be highly complex and if uncertainty in the geometry and flow characteristics of the individual fractures is high, it may not be possible to accurately model flow and transport within the block during the tests because of an inability to separately identify the simultaneous effects of multiple influences on fluid movement. Under such circumstances, accurate modeling of the test results may not be attained until more precise geometrical information is obtained from fracture casts made following completion of the tests.

6. ANALYSIS APPROACHES

6.1 Introduction

Analysis approaches for design and interpretation of NETBLOCK experiments should be based on the full range of available technologies. Flow and transport in a single fracture plane is analogous to flow and transport within a planar heterogeneous aquifer. An extensive literature has developed over the past 20 years for stochastic porous media, and these techniques are directly applicable to problems of flow and transport in single fracture planes. The techniques developed include:

- stochastic partial differential equations and analytical solutions (see e.g. Gelhar and Axnes, 1983; Gelhar et al, 1989)
- stochastic continuum modeling (see, e.g.,Follin, 1992)
- percolation theory (see e.g., Dershowitz, 1984; Sahimi, 1994)
- channel theory (see e.g., Moreno et al, 1994).
- fractal approaches (see e.g., Neuman, 1995)

Stochastic continuum approaches provide a method to relate the heterogeneity of aperture, transmissivity, and other fracture properties to effective flow and transport properties such as longitudinal and transverse dispersivity, effective flow, storage, and transport apertures, effective transmissivity anisotropy, and channel properties such as reactive surface area. Thus, the input to a stochastic continuum approach is a description of the heterogeneity within the "confined aquifer", and the output is precisely those parameters of concern for characterizing flow and transport in fracture planes.

Stochastic continuum analysis is therefore a key tool for design and interpretation of NETBLOCK experiments. Within the NETBLOCK experiments, both direct and indirect measurements will be made of the fracture roughness. These measurements can provide a direct input to stochastic continuum approaches. For example, the fracture aperture distribution from resin-injection can be used to develop profiles for fracture transmissivity, storage aperture, and transport aperture field. These fields can then be used in a wide range of stochastic continuum approaches, either by direct simulation within a stochastic continuum model, or by deriving fractal and geostatistical field properties. Solutions from the literature such as Berkowitz and Scher (1995) provide methods to analyze dispersion based on geostatistical or fractal descriptions of the stochastic field of fracture properties.

6.2 Analytical Solutions

A wide variety of analytical solutions relating the properties of stochastic continue to their effective properties have been derived over the past 20 years. One example of these relationships is that of Gelhar and Axnes, 1983 for geostatistical stochastic fields,

$$\alpha_L \approx \lambda \sigma_t^2/\gamma$$

where α_L is the dispersion coefficient, λ is the range or correlation length, σ_t is the natural log of the standard deviation of the transmissivity field, and γ is a shape factor generally set at 1.0.

PNC and Golder have used this relationship successfully for generating appropriate dispersion within the fracture zones of the LPT-2 large scale flow and transport experiment at Äspö (Uchida et al, 1994), and at other sites. The relationship was derived based on a solution for stochastic differential equations, but has been validated by a range of stochastic continuum simulations.

It is recommended that stochastic continuum analytical solutions provide the basis for initial scoping of the expected results from flow and transport experiments in single fractures and simple networks. Stochastic continuum analytical solutions can also be used as the basis for the first order interpretation of experimental results.

6.3 Simulation

6.3.1 General

Stochastic continuum simulation requires the combination of software to generate the heterogeneous field, and software to solve the flow and transport problems. One of the more flexible and powerful stochastic field generator currently available is EdMesh, which can generate a wide range of fractal, geostatistical, empirical, and non-stationary fields. EdMesh can be used in conjunction with any continuum flow and transport model.

Stochastic continuum simulations can be carried out for any heterogeneous field by specifying either a description of the field (fractal or geostatistical), or a direct image of the stochastic field, such as a resin-injection representation of the aperture field. In addition, the stochastic field can be generated by a combination of measurements at specific points and an overall field description, using the projection onto convex sets (POCS) algorithm.

6.3.2 Stochastic Continuum Field Generators

Stochastic continuum field generated for geohydrologic parameters produce the input decks for flow and transport simulators. INFERENS (Geier, 1993), and EdMesh (Lee et al, 1995) are examples of stochastic preprocessors. INFERENS generates geostatistical fields for the SKB Hydrostar flow and transport simulator (Norman, 1992), and EdMesh generates stochastic fields for the MAFIC flow and transport simulator. Other stochastic continuum pre-processors include STOMP (Fennesey, 1988), and Heresim 3D, and ISATIS (Geomath, 1996).

Golder Associates has been directly involved in development of INFERENS, EdMesh, and STOMP, and is familiar with the features of Heresim and ISATIS. Based on our

experience in development and application of stochastic continuum preprocessors, we have identified the key features needed in the PNC stochastic continuum simulator:

a range of stochastic field generation functions, including fractal, geostatistical, and empirical/geological processes,

- local and systematic anisotropy,
- multiple scales of features,
- superposition of local and global spatial correlation structures, and
- conditioning to local measurements.

Of the stochastic field generators available, the vast majority (see, Linville et al, 1993) generate stochastic fields using geostatistical processes such as kriging. This is frequently implemented using the Turning Bands algorithm (Journal, 1973). The problem with these approaches are that they have difficulty incorporating geological information and modeling local structures. This is particularly true of INFERENS, which provides very sophisticated variogram spatial correlation functions, but which generates global fields.

The POCS algorithm in EdMesh is able to meet all of the criteria above, and is both flexible and computationally efficient. It is a relatively new algorithm, but has been implemented for PNC within EdMesh. POCS uses the mathematical technique of projection on convex sets to generate fields consistent with multiple local and global constraints. As implemented in EdMesh, the constraints are:

a global fractal dimension consistent with a geostatistical variogram, and
locally specified values (conditioning)

However, additional constraints can be implemented without changing the fundamental algorithm of solving the constraints in the frequency domain. As a result, we recommend that EdMesh be adapted to provide stochastic continuum preprocessing for whatever continuum flow and transport code is selected by PNC.

6.3.3 Flow and Transport Simulators

Continuum flow and transport simulators which can be used in conjunction with stochastic field generators for stochastic continuum modeling have been surveyed in Section 6.0 of this document. For the purposes of NETBLOCK, relatively simple continuum codes are required. MAFIC includes all of the flow and transport processes being explored within the NETBLOCK experiment:

- advection,
- diffusion
- dispersion
- retardation/sorption

- mixing, and
- decay.

As a result, MAFIC is a good choice for use as a stochastic continuum solver. Other possible 2D and 3D continuum flow codes include SEEP/W (an easy to use 2D finite element model), and MODFLO/MODPATH, the worldstandard 3D flow and transport code for continuous porous media. In addition, custom research codes have been developed which directly implement stochastic partial differential equations (Gelhar et al, 1989). These codes might be considered for some analyses. However, it is expected that for most cases a simple 2D or 3D continuum code solving for a generated or specified stochastic field will be sufficient.

6.4 Percolation Theory

Percolation theory methods provide an approach for characterizing the connected pore space participating in flow and transport within fracture planes (Sahimi, 1994). Percolation methods have an advantage in that they directly address the different types of connected pore spaces related to steady flow, transient flow, transport, absorption/desorption, and diffusion. Examples include the Kozeny-Carmen solution for the relationship between pore size distributions and flow channel development, and the "effective medium approximation" (Kirkpatrick, 1973) for the description of the formation of connected flow channels in two and three dimensional lattices. Another example, "Archie's Law" relates effective transmissivity directly to the porosity for porous media,

$$T/T_0 = \phi^m$$

where T_0 is a reference transmissivity, ϕ is the porosity, and m is an exponent (generally 1.3 to 1.4). This equation can be adapted for flow in fracture planes by replacing ϕ by the percentage of the fracture plane defined by apertures a_t above a given threshold a_{tcrit},

$$\phi = P[a_t | a_{tcrit}]$$

Percolation methods have been applied extensively to evaluation of dispersion in porous media, which is analogous to problems of dispersion in fracture planes. Sahimi et al (1983) have developed relationships between effective hydrodynamic dispersion in 2D heterogeneous aquifers and the geometry of the underlying lattice of conductivity values. For example, Sahimi and Imdakm (1988) develop a relationship from percolation theory between percolation parameters describing the heterogeneous field and the longitudinal dispersion. These were extended by Gist et al (1990) to produce the equation,

$$\alpha_L \approx V^{-4.4}$$

where V is the percentage of the total volume of the heterogeneous aquifer actively participating in flow. An analogous definition of V for fracture panes can be developed using V is the percentage of the fracture surface with aperture greater than a given threshold. Other researchers have developed relationships for the relationship of α_L to Peclet number and to the characteristic length scale, based on Percolation theory.

Percolation theory methods provide a more approximate solution to the problem of relating the geometry of the pores within the fracture plane, and are very useful as such. It is anticipated that the results of the NETBLOCK experiments should be compared against the predictions of Percolation theory. However, percolation theory is necessarily considerably simplified when compared to stochastic continuum simulation methods, and is more an adjunct than a primary tool.

6.5 Channel Theory

Channel theory (Moreno, 1993) requires that flow and transport in fracture networks occur is discrete channels which are independent of the applied boundary conditions. While this may be possible for large scale flow systems in which only small changes to the boundary conditions occur, this is unlikely for fracture planes tested at NETBLOCK.

However, it will be useful to compare the results of NETBLOCK to the predictions of channel theory, to demonstrate the inadequacy of channel approaches for systems with transient boundary conditions. For each NETBLOCK experiment, a simple channel network can be developed and calibrated to the results of the experiment for both flow and transport. This channel network can then be used to predict the results for boundary conditions in which the flow directions are significantly changed.

6.6 Fractal Approaches

Fractals have proven to be a useful mathematical model to describe flow and transport in stochastic porous media. Laboratory experiments involving ideal materials such as glass beads (Chen and Wilkinson, 1985; Måløy et al., 1985) or sand have shown that the development of fingering between two fluids of different viscosities or between air and water is fractal in many respects. These and other experiments have shown that the finger size distribution, roughness, formation rate and number are well-described by fractal geometry. This has also been shown for single phase systems (Måløy et al., 1988). Other experiments (for example, Feder and Jøssang, 1995) that examined invasion percolation and diffusion in stochastic porous media found that the movement and dispersion of tracers in such media exhibit many fractal properties as well. These experiments have shown that the equal concentration contours are self-affine fractals. The dispersion front in such systems also has a fractal geometric structure.

For these reasons, fractal geometry can be used to model flow and transport in single-phase and multi-phase flow systems with considerable realism. Such a system could be used to represent flow in a fracture zone that is envisaged to behave like a stochastic porous medium. Recently, Pyrak-Nolte et al. (1995) found that the percolation

properties of flow along a fracture surface as a function of applied stress could be represented as a random porous medium with strong fractal properties.

Fractal approaches such as those developed by Pyrak-Nolte can be applied directly to interpretation of the NETBLOCK experiments. As a result, fractal dimensions should be calculated for all of the surface profiles and edge profiles collected within the NETBLOCK experiments.

7. RECOMMENDED MODELING TOOLS

During HY-5, Golder Associates carried out a series of surveys of flow and transport codes for PNC. The codes encompass a range of physical processes of flow and transport, and a range of solution methods, including

Geometry: 1-D, 2-D, or 3-D, with Orthogonal or irregular grid triangulation.
Solver Methods: finite element, integrated finite difference ("finite volume"), finite difference, and boundary element

Porosity: Single (Fracture), Single (Matrix), Dual Permeability, and Dual Porosity

Flow Processes: Laminar Flow, Turbulent Flow, Steady State and Transient

Transport Processes: Advection, Dispersion, Diffusion, Matrix Diffusion, Retardation/Sorption, and Mixing

The appropriate numerical modeling code for any given experiment is the simplest, easiest to use code which can solve for the processes of concern for the experiment. a huge array of possible modeling tools are available. However, for the level of complexity of the NETBLOCK experiments, it is not necessary to consider models which are overly complex in the physical processes modeled, can not handle the level of heterogeneity expected in the fracture network, or are too computationally intensive.

The basic codes considered are:

Code	Summary
MODFLO/MODPATH	3D Finite Difference Transient Flow, Particle Tracking Solute Transport
MAFIC	2D/3D Discrete Fracture Finite Element Transient Flow, Particle Tracking Solute Transport with Matrix Diffusion
MOC	Method of Characteristics Solute Transport
SWIFT	2D/3D Finite Difference Flow and Transport/Multiphase/Heat
FEHMN	2D/3D Finite Element Flow and Transport/Multiphase/Heat
TOUGH/VTOUGH/NOUGH	2D/3D Integrated Finite Difference "Finite Volume" Flow and Transport/Multiphase/Heat
SEEP/W + CTRAN/W + SIGMA/W	2D Finite Element Transient Flow and Transport and Coupled Stress
ECLIPSE	2D/3D Finite Difference Flow and Transport/Multiphase/Heat
NAMMU	2D/3D Finite Element Flow and Transport/Multiphase/Heat
SUTRA	2D Finite Element Flow and Transport/Heat, Coupled via Density
HST3D	3D Finite Difference Flow and Transport/Heat, Coupled via Density

7.1 Fluid Flow in Rough-Walled Fractures

A code to model flow in rough walled fractures requires the following features:

- Geometry: Ability to model the 2-D topology of the rough fractures by discretization to a regular grid. This is met by almost all codes. 3-D elements should be used if flow through infillings is to be considered.
- Solver Methods: Because the roughness will be modeled at a fine scale an efficient conjugate gradient or multigrid solver should be used. Boundary element and integrated finite difference ("finite volume") solvers such as TOUGH are generally inefficient.
- Porosity: The model will need to include single (fracture) porosity. Dual permeability may be required if fracture infillings are to be tested.
- Flow Processes: It is contemplated that tests will be modeled primarily in transient laminar flow. Almost all standard groundwater flow models are limited to laminar flow,
- Transport Processes: Not relevant.

It is neither feasible nor appropriate to model the local phenomena of Navier-Stokes flow within the fracture plane. Rather, the processes of concern are at the level of heterogeneity of transmissivity within fracture planes. MAFIC 's conjugate gradient solver is designed specifically for the type of highly heterogeneous flow fields produced inside rough walled fractures. MAFIC can easily be adapted to include a test for Reynolds number within each element, and to correct the fracture transmissivity for turbulent effects, for example according to the method of Schiedeger, 1972. This is much easier to add to a Finite Element code such as MAFIC then to other, more complex codes.

In addition, MAFIC has the unique advantage that it includes both Fracture Flow (2D) and Continuum Flow (3D) elements. This makes it possible for MAFIC to model flow within the fracture planes and flow through fracture infillings simultaneously.

For fully filled fractures, a simple, efficient 3-D continuum code such as MODFLO is recommended. MODFLO has the advantage of a wide range of easy-to-use pre- and post- processors such as Visual MODFLO and ModelCAD. In addition, it is a well established code, and is available at minimal cost for a wide variety of computing platforms.

7.2 Transport in Rough-Walled Fractures

The code used to model flow in Rough-Walled fractures can also be used to model the flow portion of the transport experiment in rough-walled fractures. The transport experiment requires the following additional features:

- Geometry: Ability to model multiple transport pathways within single fracture planes.
- Solver Methods: Transport may be solved most efficiently by particle tracking. The degree of heterogeneity of the advective velocity within the fracture plane is expected to make direct solution of the transport equation impractical due to numerical dispersion effects.
- Porosity: The model will need to include single (fracture) porosity. Dual permeability may be required if fracture infillings are to be tested.
- Transport Processes: The processes modeled should include modeling for (a) multiple advective porosities, (b) multiple diffusion porosities (in fracture plane and matrix), (c) sorption/retardation, (d) diffusion, and (e) mixing effects.

The recommended model for transport in single fracture planes is MAFIC. MAFIC combines an efficient particle tracking transport algorithm with the ability to solve for retardation/sorption, decay, and matrix diffusion. We have developed (but not yet implemented) a new algorithm to allow for modeling and calibration for advective transport through multiple porosities within fracture planes. This will provide all of the processes needed for the experiment. In addition, we recommend adding a flag to MAFIC to provide for adjustment of mixing algorithms and dispersion coefficients based on calculation of local Peclet numbers.

In addition to MAFIC, simple 2D porous media transport solutions can be obtained using User-Friendly packages such as CTRAN/W (Geo Slope International), MOC (USGS), and MODPATH (USGS). These solutions will not treat the heterogeneity of velocities as well as MAFIC, but will provide rapid, accurate solutions for transport treating the fracture as a confined aquifer.

7.3 Fluid flow in Networks of Rough-walled Fractures and Fracture Intersections

The recommendations for modeling of fluid flow in networks of rough walled fractures are the same as those for modeling flow through single, rough-walled fractures. The primary additional influence is the effect of fracture intersections. This can be dealt with by MAFIC without modification, and by MODFLOW for networks of orthogonal fractures.

7.4 Transport in Networks of Rough-Walled Fractures and Fracture Intersections

The recommendations for modeling of transport in networks of rough walled fractures are the same as those for modeling flow through single, rough-walled fractures. The primary additional influence is the effect of fracture intersections. This can be dealt with by MAFIC without modification, and by MODFLOW for networks of orthogonal fractures (MAFIC should be modified to calculate local Peclet numbers and provide for alternative mixing algorithms as described in 6.2 above).

In addition, an enhanced particle tracking algorithm such as Lattice Gas Automata (Chun Li, 1995) can be used to provide a flexible solution for mixing at fracture intersections.

7.5 Matrix Diffusion and Sorption Effects

Although sorption is included in most basic solute transport packages, we did not identify many codes which include matrix diffusion. MAFIC can be used for modeling both matrix diffusion and sorption effects during solute transport in single fractures and fracture networks.

7.6 Diffusion into Low Aperture Areas

We did not identify any codes which include features for modeling diffusion into low-aperture areas of fracture planes. However, we developed an algorithm for modeling this process within MAFIC which will be a simple extension to the current code.

7.7 Fluid Storage and Fracture Compliance Effects

The issue of fluid storage and fracture compliance is primarily related to developing empirical relationships to relate storativity to transmissivity for transient flow under a range of fracture geometries and flow conditions. The appropriate code for this purpose is therefore one which can be adapted to include a range of alternative fluid storage and compliance assumptions. The EdMesh package has been designed to facilitate this for the MAFIC flow and transport code, and can be adjusted to provide this for other codes.

7.8 Coupled Hydromechanical Effects

Coupled hydromechanical effects can be modeled using three basic approaches:

- direct coupling of continuum flow and transport equations using an extension of a generalized coupled code such as FEHM or TOUGH
- indirect coupling between stress and deformation using analytical solutions for stress as in EdMesh/MAFIC, and
- distinct element modeling (UDEC/DDA/3DEC).

For the purposes of NETBLOCK, the stress fields are expected to be relatively simple. As a result, the indirect coupling based on analytical stress solutions approach is recommended.

8. RECOMMENDED TESTING METHODS

An overview of recommended testing methods is provided in this section. The testing methods identified by PNC have been used to develop the overall testing approach, as refined or supplemented by specific recommendations identified from the literature search or from the direct experience of Golder Associates personnel. The sample preparation, equipment design, and testing procedure information provided in this report are necessarily general and are intended to provide a basis upon which the final detailed design can be based and the final detailed operating procedures can be prepared. Similar testing methods should be applied to the smaller samples used for single and double fracture testing and to the larger samples used for the fracture network experiment.

8.1 Sample Preparation

8.1.1 Excavating, Shipping, and Shaping the Sample

The most critical aspect of sample preparation is to maintain the physical integrity of the sample during excavation, shipment, and shaping. Specifically, fractures in the sample should not be allowed to open because once open, subsequent reclosure is likely to result in an imperfect mating of fracture surfaces and an unnaturally large hydraulic aperture. The sample will require shaping to accommodate the 10 x 10 cm flat rubber gaskets that will be used to establish hydraulic boundary conditions. This will require sawing the sample into a rectangular form with relatively smooth, flat sides and dimensioning it to multiples of 10 cm. To simplify instrumentation and analysis, the sample surfaces should be generally orthogonal to the major fracture sets in the sample. To the extent possible, a positive triaxial confining pressure should be maintained on all sample surfaces at all times.

8.1.2 Instrumenting the Sample

The fracture patterns on the sample walls will be mapped and projected into the interior of the sample to prepare a preliminary conceptual model of network geometry. Remote sensing techniques such as those described by Montemagno and Pyrak-Nolte can potentially be used to supplement this information. An array of small diameter (5 mm) boreholes can be drilled normal to each major fracture plane as described in Section 5 to help characterize the spatial aperture variation within the fracture and to monitor tracer movement. The borehole data can be used to develop fracture aperture information and refine fracture network geometry information for subsequent numerical modeling of the tests.

After completing the small diameter boreholes and applying the gaskets, a stainless steel plate will be placed on each side of the sample covering the gaskets to create an array of 10 x 10 cm sealed cells. Cell wall compliance and water storage in the cell are expected to influence system compliance during transient tests and tracer breakthrough concentrations during transport tests. Also, cell walls may provide sorptive surfaces or

otherwise affect the results of the transport tests. Because of these and possible other effects, the sizes of the cells and the cell wall materials should be confirmed for sensitivity to experimental conditions during final test design.

Holes in the plates will be provided for tubes for accessing the small diameter boreholes, for injecting or withdrawing water or tracer into the cell, or for measuring water pressure. Each cell will be similarly instrumented so that any desired boundary condition can be created at any cell in the system. An outer stress frame will surround the steel plates to maintain positive confining pressure on the sample and to simplify sample handling.

8.1.3 Saturating the Sample

The sample will then be placed in a pressure vessel where a vacuum will be created to purge the air in the sample. Deareated water will then be allowed to enter the sample filling the void space. A negative pressure will be maintained on the sample during this process to help remove any remaining air. The process of saturating the sample should proceed slowly because conclusive tests for confirming complete saturation are not expected to be available. The hydraulic pressure inside the pressure vessel will then be increased to seal the rubber gaskets and isolate the 10 x 10 cm cells. The pressure applied by the vessel should exceed the fluid pressure inside the cells to assure maintenance of a tight seal.

8.2 Equipment Design

The major specifications of the NETBLOCK experiment have been identified by PNC as follows:

- Capability to test blocks up to one meter cubes;
- Flexibility in size and shape of the rock block;
- Capability to isolate block surfaces into 10 x 10 cm gasketed panels allowing independent injection/ withdrawal/ pressure measurement at each panel;
- Capability to monitor flow rate simultaneously at 200 panels (on injection and discharge sides of block);
- Capability to monitor pressure simultaneously at 400 panels (on four remaining sides of block); and
- Capability to alternate injection, discharge, and pressure measurement sides of block.

Detailed equipment design issues are identified in the discussion of testing procedures in Section 7.3 and include the following:

- Pins should be firmly attached to the sample for monitoring dilation and contraction, and for use in repositioning the fracture planes should they become dislocated;

- A positive compressive pressure should be maintained on all sides of the sample at all times to keep fracture planes from opening in an uncontrolled manner; the stress on the sample walls should be monitored during all tests;
- Design should consider the effect of cell volume on interpretation of tracer breakthroughs; the volume of the cell should be small; and
- Design should consider the effect of cell compliance on interpretation of pressure transient tests; the volume and compliance of the cell should be small.

8.3 Testing Procedures

8.3.1 Sample Preparation

The samples will be prepared in a manner that accommodates the test equipment for establishing boundary conditions. This is principally expected to involve cutting the sample into a rectangular shape and maintaining a positive confining pressure. Detailed considerations of sample preparation are discussed in Section 7.1.

8.3.2 Aperture Characterization

The spatial variation of aperture will be characterized in each major fracture through hydraulic, electrical, or other testing in arrays of small diameter boreholes as described in Section 5. Specific procedures for these tests will be required and should compare the sensitivity of the procedure with the objective of the characterization tests. The test objective should include consideration of the precision and accuracy needed in characterizing aperture variation, the future use of the boreholes in monitoring tracer movement within the individual fractures, and the disruptive influence of the boreholes and tests on the fracture flow field.

8.3.3 Flow Tests

The detailed objectives of flow tests performed in the fractures and fracture networks should be identified and specific procedures for conducting these tests should be prepared. The flow tests will be used to determine average hydraulic apertures for comparison with the aperture variations characterized by the small boreholes, and the procedures should address methods of flow control and measurement. Additionally, if transient effects are to be studied, the test procedures should provide for separate identification of equipment compliance so that compliance effects due to the fractures and rock matrix can be isolated and quantified.

8.3.4 Tracer Tests

Specific procedures will be required for tracer tests performed in the fractures and fracture networks that address methods of tracer injection, tracer detection in the small

monitoring boreholes, and tracer detection in the discharge cell. To minimize disruption to the flow field, tracers should be used that permit remote, quantitative detection in the small diameter boreholes without sample removal. Radioactive tracers such as strontium and nonreactive tracers such as bromide or chloride have been successfully used and may satisfy these requirements. The means of tracer detection and quantification in the discharge cells should also be carefully addressed because of the dilution that will occur during tracer discharge from the fracture into the cell. To minimize both dilution and the aforementioned compliance effects, the volume of water within the cell and the sampling equipment should be small. To provide a basis for interpreting the test results, the mixing processes of tracer within the discharge cell and sampling equipment should be well understood.

8.3.5 Resin Impregnation.

After completing the suite of tracer tests, PNC is planning to impregnate the rock samples with resin to create castings of the fracture void volume. The sample can then be disassembled and the aperture distribution and fracture network structure can be determined. The actual fracture characteristics will be compared with the hypothesized characteristics and the flow and transport properties of the fracture network can be modeled based upon significantly more accurate and detailed geometric information. The successively increasing information base for the model is expected to lead to increasing accuracy in model predictions and provides an opportunity for increasing refinement in model validation.

9. REFERENCES

Atkinson, L.C., 1987. *A Laboratory and Numerical Investigation of Steady-State, Two-Regime, Radial Flow to a Well from Rough, Horizontal, Deformable Fractures,* Ph.D. Dissertation, Memorial University of Newfoundland, St. John's, Newfoundland, Canada.

Atkinson, L.C. and Gale, J.E., 1990. Design, Construction, and Testing of a Large-Scale, Radial Fracture Flow Model, *Geotechnical Testing Journal,* 13(4), 334-342.

Berkowitz, B. and Scher, H., 1995. On characterization of anomalous dispersion in porous and fractured media. Water Resour. Res., 31(6) pp 1461 -1466.

Berkowitz, B., Naumann, C. and Smith, L., 1994. Mass Transfer at Fracture Intersections: An Evaluation of Mixing Models, *Water Resour. Res.,* 30(6), 1765-1773.

Chen, J. D. and Wilkinson, D., 1985. Pore-scale viscous fingering in porous media. Phys. Rev. Lett. 55, 1892-1895.

Clemo, T., 1994. *Dual Permeability Modeling for Fractured Media,* Ph.D. Thesis, University of British Columbia, Vancouver.

Cliffe, K.A., Gilling, D., Jefferies, N.L. and Lineham, T.R., 1993. An Experimental Study of Flow and Transport in Fractured Slate, *Journal of Contaminant Hydrology JCOHE6,* 13(1/4) 73-90.

Cox, B.L., Pruess, K. and Persoff, P., 1990. *Casting and Imaging Technique for Determining Void Geometry and Relative Permeability Behavior of a Single Fracture Specimen,* Lawrence Berkeley Laboratory Report LBL-28485, Berkeley, California, January.

Dershowitz, W, 1984. Rock Joint Systems. PhD Dissertation, MIT, Cambridge MA.

Dershowitz, W.S., Lee, G. and J. Geier, 1995. *FracMan Version 2.5 User Documentation: Interactive Discrete Feature Data Analysis, Geometric Modeling, and Exploration Simulation,* Golder Associates Inc., Seattle, Washington.

Elsworth, D. and Piggott, A.R., 1993. Experimental Determination of the Stress-Permeability-Transport Characteristics of Natural Fractures, Proceedings International Workshop on Research and development of Geological Disposal, Power Reactor and Nuclear Fuel Development Corporation of Japan (PNC), Tokai Works, Tokai, Japan, November 15-18, pp III-71 - III-80.

Feder, J. and Jøssang, T., 1995. Fractal patterns in porous media flow. Chap 10, Fractals in Petroleum Geology and Earth Processes, C. Barton and P. La Pointe, eds. Plenum Press, New York.

Follin, S., 1992. Numerical Calculations on Heterogeneity of Groundwater Flow, SKB Technical Report 92-12.

Foltz, S.D., Tidwell, V.C., Glass, R.J., and Sobolik, S.R., 1993. Investigation of Fracture-Matrix Interaction: Preliminary Experiments in a Simple System, *Proceedings Fourth Annual International Conference on High Level Radioactive Waste Management*, Las Vegas, Nevada, April 26-30.

Geier, J., 1993. Version 1.0 Users Guide to Inferens 1.1. SKB report AR 93-24. SKB, Stockholm.

Gelhar, L., et al, 1986. Stochastic subsurface hydrology from theory to application, Water Resour. Res., 22(9), pp 135S-145S.

Gelhar, L. and Axnes, C., 1983. Three-dimensional stochastic analysis of macrodispersion in aquifers: Water Resources Res., v. 19, no. 1, pp 161-180.

Gelhar, L., Gutjahr, A. and Naff, R., 1979. Stochastic analysis of macrodispersion in a stratified aquifer, Water Resour. Res., 15(6), pp 1387-1397.

Geller, J.T., C. Doughty and J.C.S. Long, 1995. Two Phase Flow in Regionally Saturated Fractured Rock Near Excavations, *Proceedings of the Sixth Annual International Conference on High Level Radioactive Waste Management*, pp. 209-211, American Society of Civil Engineers, New York,.

GeoMath, 1996. ISATIS Version 2.0 User's Documentation. GeoMath, Avon, France. .

Gist, G., Thompson, A., Katz, A. and Higgins, R., 1990. Phys. Fluids A2, pp 1533.

Glass, R.J. and Nicholl, M.J., 1995. Quantitative Visualization of Entrapped Phase Dissolution within a Horizontal Flowing Fracture, *Geophysical Research Letters*, 22(11) 1413-1416.

Glass, R.J., 1993. Modelling Gravity-Driven Fingering in Rough-Walled Fractures Using Modified Percolation Theory, *Proceedings of the Fourth International Conference on High Level Radioactive Waste Management, Las Vegas, Nevada, April 26-28, 1993*, Vol. 2, pp. 2042-2052, American Society of Civil Engineers, New York.

Glass, R.J., Tidwell, V.C., Flint, A.L., Peplinski, W. and Castro, Y., 1994. Fracture-Matrix Interaction in Topopah Spring Tuff: Experiment and Numerical Analysis, *Proceedings of the Fifth International Conference on High Level Radioactive Waste Management, Las Vegas, Nevada, May 22-26,*.

Hakami, Eva, 1995. *Aperture Distribution of Rock Fractures*, Doctoral Dissertation, Royal Institute of Technology, Stockholm, Sweden.

Hull, L.C., and Koslow, K.N., 1986. Streamline Routing Through Fracture Junctions, *Water Resour. Res.*, 22(12), 1731-1734.

Ippolito, I., Kurowski, P., Hulin, J.P. and Daccord, G., 1995. Tracer Transport Properties of Heterogeneous 2D Structures for Parallel and Radial Flow Geometries, in *Fractured and Jointed Rock Masses*, Myer, Cook, Goodman and Tsang, editors, A.A. Balkema Publishers, Rotterdam, Netherlands.

Keller, A.A., Roberts P.V. and Kitanidis, P.K., 1995. Prediction of Single Phase Transport Parameters in a Variable Aperture Fracture, *Geophysical Research Letters*, 22(11) 1425-1428.

Kirkpatrick, S., 1973. Rev. Mod. Phys. 45, pp 574.

Li, Chunhong, 1995. *Low Peclet Number Mixing Behavior at Fracture Junctions*, Doctoral Dissertation, New Mexico Institute of Mining and Technology, Socorro, New Mexico.

Linville, B., Burchfield, T. and Wesson,T., 1993. Reservoir Characterization III. Proceedings of the Third International Reservoir Characterization Technical Conference, Tulsa OK, Nov. 3-5, 1991. pp 1008.

Måløy et al., 1985. Viscous fingering fractals in porous media. Phys. Rev. Lett. 55, 2688-2691.

Måløy et al., 1988. Fractal structure of hydrodynamic dispersion in porous media. Phys. Rev. Lett. 61, 2925-2928.

Mohanty, S., Chowdhury, A.H., Hsiung, S., and Ahola, M.P., 1994. *Single Fracture Flow Behavior of Apache Leap Tuff under Normal and Shear Loads*, CNRWA 94-024, Center for Nuclear Waste Regulatory Analyses, San Antonio, Texas.

Mohanty, S., Green, R.T. and Meyers-James, K.A., 1995. *Study of Flow in a Fracture under Shear: Progress Report*, CNRWA 96-001, Center for Nuclear Waste Regulatory Analyses, San Antonio, Texas.

Montemagno, C.D. and Pyrak-Nolte,'L.J., 1995. Porosity of Natural Fracture Networks, *Geophysical Research Letters*, 22(11) 1397-1400,.

Moreno, et al, 1988. Flow and tracer transport in a single fracture: A stochastic model and its relation to some field observations, Water Resour. Res., 24(12), pp 2033-2048.

Neuman, S, 1995. On advective transport in fractal permeability and velocity fields, Water Resour. Res., 31(6) pp 1455 - 1460.

Nicholl, M.J., and Glass, R.J., 1994. Wetting Phase Permeability in an Intiially Wet partially Saturated Horizontal Fracture, in *High Level Radioactive Waste Management, Proceedings of the Fifth International Conference, Las Vegas, Nevada, May 22-26, 1994*, Vol. 4, pp. 2007-2019, American Society of Civil Engineers, New York.

Olsson, O., Neretnieks, I. and Cvetkovic, V., 1995. *Deliberations on Radionuclide Transport and Rationale for Tracer Transport Experiments to be Performed at Aspo - A Selection of Papers*, Progress Report 25-95-01, SKB, Stockholm, Sweden.

Parney, R. and Smith, L., 1995. Fluid Velocity and Path Length in Fractured Media, *Geophysical Research Letters*, 22(11) 1437-1440.

Persoff, P., Pruess, K. and Myer, L., 1991. *Two Phase Flow Visualization and Relative Permeability Measurement in Transparent Replicas of Rough-Walled Rock Fractures*, Lawrence Berkeley Laboratory Report LBL-30161, Berkeley, California, January.

Persoff, P. and Pruess K., 1995. Two-Phase Flow Visualization and Relative Permeability Measurement in Natural Rough-Walled Rock Fractures, *Water Resour. Res.*, 31(5) 1175-1186.

Piggot, A.R. and Elsworth, D., 1993b. Characterization of Fracture Aperture by Inverse Analysis, *Can. Geotech. J.* 30, 637-646.

Piggot, A.R. and Elsworth, D., 1993a. Laboratory Assessment of the Equivalent Apertures of a Rock Fracture, *Geophysical Research Letters* 20(13), 1387-1390.

Preuss, K., 1991. *TOUGH2 - A General Purpose Numerical Simulator for Multiphase Fluid and Heat Flow*, Lawrence Berkeley Laboratory Report LBL-29400, Berkeley, California.

Pyrak-Nolte, et al., 1995. Hierarchical cascades and the single fracture. Chap 9, Fractals in Petroleum Geology and Earth Processes, C. Barton and P. La Pointe, eds. Plenum Press, New York.

Rasmussen, T.C., 1995. Laboratory Characterization of Fluid Flow Parameters in a Porous Rock Containing a Discrete Fracture, *Geophysical Research Letters*, 22(11) 1401-1404.

Reimus, P.W., Robinson B.A. and Glass, R.J., 1993. *Aperture Characteristics, Saturated Fluid Flow, and Tracer Transport Calculations for a Natural Fracture*, Los Alamos National Laboratory Report LA-UR-92-4376.

Sahimi, M., 1994. Application of Percolation Theory. Taylor & Francis, New York.

Sahimi, M. and Imdakm, A. 1988. J. Phys A 21, pp 3833.

Sudicky, E.A. and McLaren, R.G., 1992. The Laplace Transform Galerkin Technique for Large-Scale Emulation of a Mass Transport in Discretely Fractured Porous Formations, *Water Resour. Res.*, 38, 499-514.

Tidwell, V.C., and Glass, R.J., 1995. Laboratory Investigation of Matrix Imbibition froma Flowing Fracture, *Geophysical Research Letters*, 22(11) 1405-1408.

Tidwell, V.C., VonDoemming, J.D. and Martinez, K., 1993. Scale Dependence of Effective Media Properties, Fourth International High Level Radioactive Waste Management Conference, Las Vegas, Nevada, April.

Tidwell, V.C., 1994. Laboratory Investigation of Constitutive Property Scaling Behavior, SPE 69th Annual Technical Conference and Exhibition, Society of Petroleum Engineers Paper SPE 28456.

Toran, L., Sjoreen, A. and Morris, M., 1995. Sensitivity Analysis of Solute Transport in Fractured Porous Media, *Geophysical Research Letters*, 22(11) 1433-1436.

Tsang, Y.W., 1995. Study of Alternative Tracer Tests in Characterizing Transport in Fractured Rocks, *Geophysical Research Letters*, 22(11), 1421-1424.

Uchida, M, Doe,T., Dershowitz, W., and Wallman, P., 1993. Simulation of Fracture Flow at the Kamaishi Validation Drift. Proceedings, Fourth Annual International Conference on High Level Radioactive Waste Management, Las Vegas. American Society of Civil Engineers, NY.

Vandergraaf, T.T., 1995. Radionuclide Migration Experiments Under Laboratory Conditions, *Geophyscial Research Letters*, 22(11) 1409-1412.

Wang, J.S.Y., 1991. Flow and Transport in Fractured Rocks, *Rev. Geophys., Suppl.*, U.S. National Report to International Union of Geodesy and Geophysics, 1987-1990, pp 254-262.

Wels, C., and Smith, L., 1994. Retardation of Sorbing Solutes in Fractured Media, *Water Resour. Res.*, 30(9) 2547-2563.

Wels, C., Smith, L. and Vandergraaf, T.T., 1996. The Influence of Specific Surface Area on Transport of Sorbing Solutes in Fractures: An Experimental Analysis, Draft submitted to Water Resour. Res., February.

Wolfram, S., 1986. Cellular Automata Fluids 1: Basic Theory, *J. Stat. Phys.*, 45, 471-526.

Yang, G., Myer, L.R., Brown, S.R, and Cook, N.G.W., 1995. Microscopic Analysis of Macroscopic Transport Properties of Single Natural Fractures Using Graph Theory Algorithms, *Geophysical Research Letters*, 22(11) 1429-1423.

TABLE 1

LIST OF RECENT PUBLICATIONS DESCRIBING LABORATORY FRACTURE FLOW TESTS

Authors	Publication Title	Type of Study	Phenomena Studied
Piggott and Elsworth (1993b)*	Characterization of fracture aperture by inverse analysis	Single fracture	Saturated flow and transport
Ippolito et al. (1995)*	Tracer trasnport properties of heterogeneous 2D structures for parallel and radial flow geometries	Single fracture	Saturated flow and transport
Reimus et al. (1993)*	Aperture characteristics, saturated fluid flow, and tracer transport calculations for a natural fracture	Single fracture	Saturated flow and transport
Wels et al. (1996)*	The influence of specific surface area on transport of sorbing solutes in fractures: an experimental analysis	Single fracture	Saturated flow and transport
Keller et al. (1995)	Prediction of single phase transport parameters in a variable aperture fracture	Single fracture	Saturated flow and transport
Vandergraaf (1995)	Radionuclide migration experiments under laboratory conditions	Single fracture	Saturated flow and transport
Tidwell et al. (1995)	Laboratory investigation of matrix imbibition from a flowing fracture	Single fracture	Unsaturated flow and transport
Persoff and Pruess (1995)*	Two-phase flow visualization and relative permeability measurement in natural rough-walled rock fractures	Single fracture	Unsaturated flow and transport
Foltz et al. (1993)	Investigation of fracture-matrix interaction: preliminary experiments in a simple system	Single fracture	Unsaturated flow and transport
Glass et al. (1994)	Fracture-matrix interaction in Topopah Spring Tuff: experiment and numerical analysis	Single fracture	Unsaturated flow and transport
Glass and Nicholl (1995)	Quantitative visualization of entrapped phase dissolution within a horizontal flowing fracture	Single fracture	Unsaturated flow and transport
Rasmussen (1995)	Laboratory characterization of fluid flow parameters in a porous rock containing a discrete fracture	Single fracture	Unsaturated flow and transport
Atkinson and Gale (1990)*	Design, construction, and testing of a large-scale, radial fracture flow model	Single fracture	Saturated hydromechanical
Li (1995)*	Low Peclet number mixing behavior at fracture junctions	Fracture intersection	Saturated flow and transport
Kwicklis et al. (1996)*	Unpublished	Fracture network	Unsaturated flow and transport

* Publication is summarized in Section 2 of this report

TABLE 2

SUMMARY OF FLOW CONDITIONS IN RECENT LABORATORY EXPERIMENTS

Author Citation	Mean Aperture (um)	Flow Velocity (m/s)	Transport Distance (mm)	Peclet Characteris -tic Length (um)	Peclet Number	Reynolds Number
Piggott and Elsworth (1993b)	270	N/A	320	N/A	N/A	N/A
Li (1995)	500	3E-6 to 5E-4	200	350(1)	1 to 170	.0015 to .26
Ippolito et al. (1995)	500 to 1000	1E-6 to 1E-3	1000	1000(2)	1 to 1000	.0005 to 1.0
Tidwell et al. (1995)	100	(3)	500	(3)	(3)	(3)
Atkinson and Gale (1990)	300 to 800	N/A	750	N/A	N/A	N/A
Persoff and Pruess (1995)	8.5 to 21.7	(3)	81	(3)	(3)	(3)
Reimus et al. (1993)	56 to 138	N/A	116	N/A	N/A	N/A
Wels et al. (1996)	450 to 780	N/A	100	N/A	2 to 100	N/A
Foltz et al. (1993)	100 to 152	(3)	140	(3)	(3)	(3)
Glass et al. (1994)	100	(3)	500	(3)	(3)	(3)
Keller et al. (1995)	380	1.5E-5 to 2.4E-4	200	N/A	N/A	N/A
Glass and Nicholl (1995)	200	(3)	300	(3)	(3)	(3)
Rasmusson (1995)	100 to 800	(3)	925	(3)	(3)	(3)
Vandergraaf (1995)	500 to 800	N/A	900	N/A	N/A	N/A

(1) defined as half the intersection diagonal
(2) defined as typical grain height on rough fracture wall
(3) value not computed for unsaturated flow experiment
N/A value not available from publication

TABLE 3

NUMERICAL MODELS USED TO ANALYZE RECENT LABORATORY FRACTURE FLOW TESTS

Author Citation	Model Name	Model Type	Model Application
Piggott and Elsworth (1993)	Not identified; presumed in-house	Not identified	Single fracture saturated flow and transport
Ippolito et al. (1995)	No numerical model used	--	--
Reimus et al. (1993)	Not identified; presumed in-house	Finite difference	Single fracture saturated flow and transport
Wels et al. (1996)	No numerical model used	--	--
Keller et al. (1995)	No numerical model used	--	--
Vandergraaf (1995)	No numerical model used	--	--
Tidwell et al. (1995)	No numerical model used	--	--
Persoff and Pruess (1995)	No numerical model used	--	--
Foltz et al. (1993)	No numerical model used	--	--
Tsang (1995)	Not identified; presumed in-house	Not identified	Single fracture saturated flow and transport
Yang et al. (1995)	No numerical model used	--	--
Glass et al. (1994)	TOUGH2	Finite difference	Single fracture unsaturated flow and transport
Rasmussen (1995)	No numerical model used	--	--
Geller et al. (1995)	TOUGH2	Finite difference	Single fracture unsaturated flow and transport
Glass and Nicholl (1995)	No numerical model used	--	--
Atkinson and Gale (1990)	Not identified; presumed in-house	Finite element	Single fracture saturated hydromechanical
Li (1995)	Lattice gas automata (LGA), an in-house code	Particle tracking	Fracture intersection saturated flow and transport
Berkowitz et al. (1994)	Not identified; presumed in-house	Particle tracking	Fracture intersection saturated flow and transport
Toran et al. (1995)	FRACTRAN	2D Finite element	Saturated fracture network flow and transport
Parney and Smith (1995)	Stastical continuum model (SCM); an in-house code	Particle tracking	Saturated fracture network flow and transport
Wels and Smith (1994)	DISCRETE	Finite difference	Saturated fracture network flow and transport
Kwicklis et al. (1996)	FRACMAN/MAFIC	Finite element	Unsaturated fracture network flow and transport